

“If a landslide comes as a surprise to the eyewitnesses, it would be more accurate to say that the observers failed to detect the phenomena which preceded the slide”

Karl von Terzaghi (1883-1963)

University of Alberta

Landslide Hazard Assessment, Town of Peace River, Alberta

by

Tai-Hoon Kim

A thesis submitted to the Faculty of Graduate Studies and Research
in partial fulfillment of the requirements for the degree of

Doctor of Philosophy
in
Geotechnical Engineering

Department of Civil and Environmental Engineering

©Tai-Hoon Kim
Spring 2012
Edmonton, Alberta

Permission is hereby granted to the University of Alberta Libraries to reproduce single copies of this thesis and to lend or sell such copies for private, scholarly or scientific research purposes only. Where the thesis is converted to, or otherwise made available in digital form, the University of Alberta will advise potential users of the thesis of these terms.

The author reserves all other publication and other rights in association with the copyright in the thesis and, except as herein before provided, neither the thesis nor any substantial portion thereof may be printed or otherwise reproduced in any material form whatsoever without the author's prior written permission.

Examining Committee

Dr. Peter Steffler, Department of Civil and Environmental Engineering

Dr. C. Derek Martin, Department of Civil and Environmental Engineering

Dr. David M. Cruden, Department of Civil and Environmental Engineering

Dr. Peter Bobrowsky, Simon Fraser University

Dr. David Segó, Department of Civil and Environmental Engineering

Dr. Duane Froese, Department of Earth & Atmospheric Sciences

To my grandmother Yeon-Sik
For a debt I can never repay

To my wife Hyun Sook and daughter Chloé
Who have always been there through the hard times

Abstract

The Town of Peace River is over hundred years old. It was heavily urbanized by the late 1970s. Development extended to the geologically immature valley slopes of the Peace River and its tributaries. Triggered by various agents, landslides caused damage to houses and infrastructure developed on marginally stable slopes. Landslides directly affect the long-term planning and sustainable development of the community.

Landslide related hazards are frequent common and their impact has increased as more developments have been initiated. This study has provided significant progress in analyzing mechanisms and influences of landslides in the present and foreseeable future on the town of Peace River. The main idea of this study was to identify general conditions of the local areas and understand processes initiating those conditions. The temporal and spatial characteristics including geological and geomorphological histories, meteorological variations, economic developments, and demographic distributions over time are also discussed.

Geomorphic and geological characteristics that may impact the landslides in the study area are identified. By analyzing temporal variations in geomorphologic features, major causes that induced landslides in the past can be determined. Recent landslides observed in the study area are analyzed in order to determine overall landslide characteristics that can be used for quantifying the relative contributions of actual landslides. Monitoring surface or subsurface movements of landslides explicitly and directly enables estimates of time intervals to peak landslide velocities. The landslide hazard assessment conducted by geologic and geomorphological methodologies can well delineate the current state of landslide hazards in the study

area by showing with a good feasibility which delineated areas where landslide problems have been continuously reported are consistent with the unstable areas designated by the proposed landslide hazard assessment.

The proposed landslide hazard assessment can be readily adapted to other areas if proper information is provided. Results of this study may be used as a basis for assessing landslide risks and their managements. Appropriate actions or decisions and corresponding countermeasures can also be derived from these outcomes.

Acknowledgments

I would like to thank my supervisors, Dr. Derek Martin and Dr. David Cruden, for their guidance and support during the entire duration of my life at the University of Alberta. Their kindness, patience, and invaluable discussions, both academically and personally, have been always inspiring me.

My thanks are extended to the members of my examining committee, Dr. Peter Steffler, Dr. Peter Bobrowsky, Dr. David Segó, and Dr. Duane Froese, who provided valuable comments to improve my thesis during the final oral examination.

I also acknowledge all the professors of the Geotechnical Engineering Group at the University of Alberta for their great support and wonderful teaching when I was taking coursework. I specifically wish to thank Dr. Dave Chan and Dr. Rick Chalaturnyk. I am deeply indebted to staffs in the Geotechnical Engineering Group. In particular, thanks are due to Stephen Gamble, Christine Hyreygers, and Sally Petaske for their technical and administrative supports.

My work has improved from helpful discussions with my fellow graduate students. I specially thank my officemates: Mehdi Khajeh, Amir H. Hosseini, Reza Moussavi Nik, and Mohamed Mansour. Without their sustainable interactions, my study in Canada would never have been happy.

The financial support provided by the National Science and Engineering Research Council of Canada, NSERC, is gratefully acknowledged. I also wish to thank stakeholders of the Urban Geology and Geohazards Initiatives in the Town of Peace River: Alberta Geological Survey, Alberta Infrastructure and Transportation, Alberta Municipal Affairs, Town of Peace River, CN, ATCO Electric, and ATCO Pipelines. Special thanks go to Corey Froese and James Morgan of Alberta Geological Survey for providing valuable information and advices.

My thanks and appreciations are owed to my friends that I met in Canada: Eunah Lee, Jan Parel, Gyu Sik Kim, Darren Sutton, Lisa Surgenor, Jaeyong Song, Seung-Ji Ha, Kevin Olsen, and Sandy Weatherall. I thank them for the wonderful times I had with them.

I particularly wish to thank my senior Dr. Dugkeun Park for his positive comments and encouragement of my career pursuits while I was at the National Institute for Disaster Prevention and during my time at the University of Alberta. Finally, but definitely not least, I wish to thank my family for their continuous support, encouragement, and love.

Table of Contents

	Page
1 Introduction	1
1.1 Overview and background	5
1.2 Statement of purpose	6
1.3 Approach and methodology	7
1.3.1 Establishing temporal and spatial characteristics	7
1.3.2 Analyzing landslide causal factors	9
1.3.3 Constructing the landslide hazard assessment system	9
1.3.4 Evaluation of the landslide hazard assessment system	10
1.4 Delimitations and limitations	10
1.5 Organization	12
2 Review of landslide hazard assessments	14
2.1 Characteristics of landslide hazard assessments	14
2.1.1 Definition of landslide hazard assessments	15
2.1.2 Framework of landslide hazard assessments	19
2.1.2.1 Scope definition	21
2.1.2.2 Hazard analysis	23
2.1.2.3 Risk analysis	23
2.1.2.4 Risk assessment	23
2.1.2.5 Risk management	24
2.1.3 Fundamental processes for landslide hazard assessments	24
2.1.3.1 Hazard identification in dated and potential land- slides	24
2.1.3.2 Investigation of landslide characteristics	25
2.1.3.3 Implementation of countermeasures for landslide hazard assessments	28
2.2 Landslide hazard assessment analyses	31
2.2.1 Landslide inventory mapping	31
2.2.2 Landslide susceptibility and hazard assessments	33

2.2.2.1	Geomorphological mapping	37
2.2.2.2	Weighting (indexing) method	39
2.2.2.3	Landslide density (isopleth) mapping	43
2.2.2.4	Statistical methods	44
2.2.2.5	Physically based methods	55
2.2.3	Landslide risk assessment	61
2.3	Implementation of the landslide hazard assessment in urban areas . .	63
2.3.1	Landslide costs and impacts on urban areas	63
2.3.2	Approaches to landslide hazard controls	64
2.3.2.1	Restriction or prohibition of further developments in landslide prone areas	67
2.3.2.2	Regulations for excavation, grading, landscaping, and construction	69
2.3.2.3	Implementation of landslide preventing or con- trolling measures	70
2.3.2.4	Development of landslide warning systems	72
2.3.3	Role of landslide hazard assessments	73
2.4	Conclusions	73
3	Landslides in the Peace River Lowland, Alberta	75
3.1	Overview of the study area	75
3.2	Geology of the Peace River Lowland	82
3.2.1	Bedrock formations	83
3.2.1.1	Kaskapau Formation	83
3.2.1.2	Dunvegan Formation	85
3.2.1.3	Shaftesbury Formation	85
3.2.1.4	Peace River Formation	86
3.2.2	Surficial geology	89
3.2.2.1	Buried channel deposits	89
3.2.2.2	Quaternary deposits	90
3.2.2.3	Recent deposits	92
3.2.2.4	Chronological progress for the surficial geology in the study area	92
3.3	Meteorology in the Peace River Lowland	98

3.4	Landslide history in the Peace River Lowland	98
3.5	Conclusions	104
4	Landslide characteristics in the Town of Peace River, Alberta	107
4.1	Recent landslides in the Town of Peace River	107
4.1.1	Mile 47.8 Slide (Ball Park Slide)	110
4.1.2	Mile 47.6 Slide (Judah Hill Slide)	116
4.1.3	Mile 46.5 Slide	122
4.1.4	99/101 Streets Slides	128
4.1.5	Shop Slide	144
4.1.6	Mile 50.9 Slide	153
4.2	Geotechnical characteristics of Peace River landslides	163
4.3	Characteristics of the landslide movement	169
4.3.1	Data compilation and analysis	169
4.3.1.1	Identifying general rupture surfaces	169
4.3.1.2	Movement rates and their characteristics	170
4.3.1.3	Effects of geomorphologic factors	178
4.3.2	Movement characteristics and their behaviours	181
4.3.2.1	Material failure relationships	186
4.3.2.2	Analyzing movement behaviours	196
4.3.3	Discussion and future consideration	203
4.4	Conclusions	206
5	Landslide hazard assessment in the Town of Peace River, Alberta	208
5.1	Major considerations in the landslide hazard assessment	208
5.1.1	Review of landslide induced factors	209
5.1.1.1	Geology	209
5.1.1.2	Geomorphology	212
5.1.1.3	Hydrology and meteorology	212
5.1.1.4	Vegetation	212
5.1.2	Considerations of landslide induced factors in the Town of Peace River	213
5.1.2.1	Geology	213
5.1.2.2	Slope and aspect	216
5.1.2.3	Hydrologic network distribution	222

5.1.2.4	Proximity to transportation	224
5.1.2.5	Anthropogenic distribution	227
5.1.3	Relationship among landslide causal factors in the hazard assessment	229
5.2	Early study on the landslide hazard assessment	238
5.3	Processes of the landslide hazard assessment	241
5.3.1	Identification of geomorphological landslide features	241
5.3.1.1	Texture analysis	246
5.3.1.1.1	Contrast oriented group	247
5.3.1.1.2	Orderliness based group	249
5.3.1.1.3	Descriptive statistic group	249
5.3.1.2	Statistical evaluations of the orientation data	261
5.3.1.2.1	Vector strength and dispersion analysis	261
5.3.1.2.2	Eigenvalue analysis	278
5.3.2	Major principles in determining the landslide hazard	307
5.4	Construction of the landslide hazard assessment	314
5.4.1	Generating geomorphological maps	314
5.4.2	Establishing the degree of the landslide hazard	327
5.4.2.1	Construction of the preliminary landslide hazard	327
5.4.2.2	Anthropogenic considerations	334
5.4.2.3	Evaluation of the landslide hazard enhanced by using landslide controlled features	339
5.5	Results and discussions	345
5.6	Conclusions	357
6	Summaries and conclusions	359
6.1	Summaries	360
6.2	Conclusions	365
6.3	Suggested future research	366
	Bibliography	368
	Appendix A: Detailed borehole data	410

Appendix B: Representative borehole stratigraphy	413
Appendix C: Laboratory tests summary	416
Appendix D: The 2007 Fox Creek landslide, Peace River Lowland, Alberta, Canada	447
Appendix E: Statistical analyses on identified landslide deposits	476

List of Tables

	Page
Table 2.1 Classification of landslide susceptibility and hazard assessments	36
Table 2.2 General steps in constructing the isopleth map	44
Table 2.3 Practical techniques for the landslide hazard reduction	66
Table 3.1 Historical population in the Peace River region	80
Table 3.2 Historical climate records in the Peace River Lowland	103
Table 4.1 Recent landslides in the Town of Peace River	109
Table 4.2 Summary of slope inclinometer measurements at the Mile 47.8 Slide	114
Table 4.3 Instability and mitigation chronology at the Mile 47.6 Slide	120
Table 4.4 Surficial geology distribution at the Mile 47.6 Slide area	120
Table 4.5 Estimated strength properties	121
Table 4.6 Slope inclinometer measurements in borehole 80-7, 8, and 9	127
Table 4.7 Measured groundwater level in the Mile 46.5 Slide	127
Table 4.8 Slope inclinometer measurements at the 99/101 Streets Slides	138
Table 4.9 Summary of slope inclinometer measurements at the Shop Slide	154
Table 4.10 Measured groundwater elevations at the Mile 50.9 Slide	159
Table 4.11 Summary of soil samples for the laboratory test	163
Table 4.12 Atterberg Limits test results	166

Table 5.1	Natural factors causing landslides in San Francisco Bay region	210
Table 5.2	Factors affecting slope movements	210
Table 5.3	Landslide causal factors	211
Table 5.4	Landslide deposits having mean slope angles below the critical slope angle	235
Table 5.5	Degree of the slope stability in the Town of Peace River . . .	242
Table 5.6	Physiographic units in the Town of Peace River	242
Table 5.7	Classification of the second order texture calculations by using the gray level co-occurrence matrix	248
Table 5.8	Type of the spherical distribution based on the distribution of eigenvalues and eigenvectors of the orientation matrix, M	288
Table 5.9	Suggested ranges in eigenvalue ratios of $\ln(S_1/S_2)$ to identify local topographic features	306
Table 5.10	Correlations between the state of the landslide hazard and the landslide activity	310
Table 5.11	Suggested states for landslide hazards based on their specific evolutions	312
Table 5.12	Suggested states of landslide hazards on identified landslide deposits in the study area	331
Table 5.13	Suggested states of landslide hazards which contain uncertainties for the practical application	331
Table 5.14	Modified states of landslide hazards on landslide deposits identified in the study area which are adjusted by landslide controlled features	346
Table 5.15	List of areas where landslide induced problems have been reported	350

List of Figures

	Page
Figure 1.1 Casualties and economic losses resulting from landslide incidents from 1991 to 2005	2
Figure 1.2 Diagram showing mutual relationships among landslide research, mapping, and hazard reduction measures in the United States	4
Figure 1.3 Principal research processes for the landslide hazard assessment in the Town of Peace River	8
Figure 2.1 A process based framework for the landslide risk management	22
Figure 2.2 Comparison of LiDAR and conventional optical images . . .	26
Figure 2.3 Changes in the factor of safety by causal factors	29
Figure 2.4 Landslide inventory mapping in the Peace River area, Alberta	34
Figure 2.5 Diagram showing representative procedures for implementing the weighting method	41
Figure 2.6 Diagram showing representative procedures for implementing the bivariate statistical method	47
Figure 2.7 Diagram showing representative procedures for implementing the multivariate statistical method	50
Figure 2.8 Systematic relationship in the logistic regression method . . .	54
Figure 2.9 Consecutive types of the physically based method for landslide susceptibility and hazard assessments based on the data availability	58
Figure 2.10 Probability density functions	60

Figure 3.1	Location of the study area	76
Figure 3.2	Town of Peace River overview, looking northeast	77
Figure 3.3	Population changes in the Peace River Lowland during 1957 to 1971	79
Figure 3.4	Historical population growth in the Town of Peace River . . .	79
Figure 3.5	Physiography of the Peace River Lowland	81
Figure 3.6	Bedrock geology of the study area	84
Figure 3.7	Geological distribution of bedrock formations	87
Figure 3.8	Table of formations in the study area	88
Figure 3.9	Geological distribution of surficial deposits	93
Figure 3.10	Conceptual diagrams for major geomorphological events . .	95
Figure 3.11	Spatial distribution of meteorological variables in the study area for the 1961 to 1990 normals period	99
Figure 3.12	Temporal distribution of landslides in the Town of Peace River during thirty years (1971-2000)	105
Figure 4.1	Distribution of recent landslides in the Town of Peace River .	108
Figure 4.2	Perspective view of the Mile 47.8 Slide	111
Figure 4.3	Cross section of the Mile 47.8 Slide	112
Figure 4.4	Landslide movements at the Mile 47.8 Slide	115
Figure 4.5	Temporal groundwater distribution at the Mile 47.8 Slide . .	115
Figure 4.6	Meteorological records on the Mile 47.8 Slide	116
Figure 4.7	Perspective view of the Mile 47.6 Slide	117
Figure 4.8	Cross section of the Mile 47.6 Slide	119

Figure 4.9	Landslide movements at the Mile 47.6 Slide	123
Figure 4.10	Temporal groundwater distribution at the Mile 47.6 Slide	123
Figure 4.11	Meteorological records on the Mile 47.6 Slide	124
Figure 4.12	Perspective view of the Mile 46.5 Slide	125
Figure 4.13	Cross section of the Mile 46.5 Slide	126
Figure 4.14	Meteorological records on the Mile 46.5 Slide	129
Figure 4.15	Perspective view of the 99/101 Streets Slides	130
Figure 4.16	Anthropogenic effects on the End of 101 Street Slide	132
Figure 4.17	Cross section of the End of 101 Street Slide	133
Figure 4.18	Cross section of the Transition Zone Slide	134
Figure 4.19	Cross section of the End of 99 Street Slide	136
Figure 4.20	Diagram of the landslide block	137
Figure 4.21	Landslide movements at the End of 101 Street Slide	139
Figure 4.22	Landslide movements at the Transition Zone Slide	140
Figure 4.23	Landslide movements at the End of 99 Street Slide	141
Figure 4.24	Measured groundwater level	143
Figure 4.25	Meteorological records on the End of 101 Street Slide	145
Figure 4.26	Meteorological records on the End of 99 Street Slide	146
Figure 4.27	Meteorological records on the Transition Zone Slide	147
Figure 4.28	Perspective view of the Shop Slide	149
Figure 4.29	Cross section of the Shop Slide	150
Figure 4.30	Landslide movements at the Shop Slide	151

Figure 4.31	Temporal groundwater distribution at the Shop Slide	155
Figure 4.32	Meteorological records on the Shop Slide	156
Figure 4.33	Perspective view of the Mile 50.9 Slide	157
Figure 4.34	Cross section of the Mile 50.9 Slide	158
Figure 4.35	Temporal groundwater distribution at the Mile 50.9 Slide . . .	160
Figure 4.36	Meteorological records on the Mile 50.9 Slide	161
Figure 4.37	Anthropogenic effects on the Mile 50.9 Slide	162
Figure 4.38	Hydrometer test results for soil samples	164
Figure 4.39	Plasticity chart for soil samples	165
Figure 4.40	Direct shear test results for soil samples	167
Figure 4.41	Estimated general rupture surfaces	171
Figure 4.42	Representative moisture contents	172
Figure 4.43	Stratigraphic units on rupture surfaces	173
Figure 4.44	Total movement rates obtained from slope inclinometers . . .	174
Figure 4.45	Movement rates at the Mile 47.8 Slide	175
Figure 4.46	Movement rates at the Mile 47.6 Slide	177
Figure 4.47	Movement rates at the 99/101 Streets Slides	179
Figure 4.48	Movement rates at the Shop Slide	180
Figure 4.49	Geomorphological impacts on landslide movement characteristics	182
Figure 4.50	Rupture surface inclinations with average movement rates . . .	183
Figure 4.51	Ground surface inclinations with average movement rates . . .	184

Figure 4.52 Average movement rates with inclinations of ground and rupture surfaces showing a statistical trend	185
Figure 4.53 Diagrams showing the estimation of the failure time of slopes	189
Figure 4.54 Variation of α values affecting the line length change at the dome of volcano	192
Figure 4.55 Typical material failure modes found in landslides	195
Figure 4.56 Landslide movement patterns at the Mile 47.8 Slide	197
Figure 4.57 Landslide movement patterns at the End of 101 Street Slide .	198
Figure 4.58 Landslide movement patterns at the Transition Zone Slide . .	200
Figure 4.59 Landslide movement patterns at the End of 99 Street Slide . .	201
Figure 4.60 Landslide movement patterns at the Shop Slide	204
Figure 4.61 Formation and propagation of the rupture surface	205
Figure 5.1 Spatial distributions of surficial deposits in the study area . .	214
Figure 5.2 Spatial distributions of bedrock deposits in the study area . .	215
Figure 5.3 Schematic diagram showing how slope (S) and aspect (A) in terrains are defined	217
Figure 5.4 Digital elevation model (DEM) for the study area	218
Figure 5.5 Spatial distribution of slope values	219
Figure 5.6 Spatial distribution of aspect values	221
Figure 5.7 Distribution of the hydrologic channel network in the study area	223
Figure 5.8 Distribution of the road network in the study area	225
Figure 5.9 Distribution of the railway network in the study area	226

Figure 5.10 Land use distribution in the study area	228
Figure 5.11 Spatial distribution of identified landslide deposits	230
Figure 5.12 Spatial distribution of slope values within landslide deposits .	231
Figure 5.13 Mean slope values of landslide deposits	233
Figure 5.14 Geographical distribution of landslide deposits whose mean slope angles are below the critical slope angle	234
Figure 5.15 Geographical distribution of landslide deposits whose mean slope angles are divided by lower and upper limits of the stable state	237
Figure 5.16 Distribution showing the approximate extent of bedrock for- mations in the study area	239
Figure 5.17 Landslide susceptibility map for the Town of Peace River . .	243
Figure 5.18 Contrast texture analysis applied to the study area	251
Figure 5.19 Entropy texture analysis applied to the study area	252
Figure 5.20 Correlation texture analysis applied to the study area	253
Figure 5.21 Spatial distribution of three texture values for the study area .	255
Figure 5.22 Identification of potential rough areas	257
Figure 5.23 Texture analysis on a small scaled multispectral satellite im- agery	259
Figure 5.24 Spatial distribution of the texture analysis within landslide deposits	260
Figure 5.25 Mean texture values of previous landslide deposits observed in the study area	262
Figure 5.26 Geographical distribution of landslide deposits whose mean texture values are over the average value for all landslide deposits . .	263
Figure 5.27 Diagrams representing different surface roughnesses	265

Figure 5.28 Characteristics of distribution and orientation in topographic surfaces	267
Figure 5.29 Decomposition of the unit vector orthogonal to the planar surface	268
Figure 5.30 Spatial distribution of vector dispersion values in the study area	271
Figure 5.31 A closer look at the vector dispersion distribution in the study area	272
Figure 5.32 Spatial distribution of the vector dispersion values for the study area	273
Figure 5.33 Evaluation of the spatial distribution in vector dispersion and texture analyses	275
Figure 5.34 Spatial distribution of the vector dispersion analysis within landslide deposits	276
Figure 5.35 Mean vector dispersion values of previous landslide deposits observed in the study area	277
Figure 5.36 Geographical distribution of landslide deposits whose mean vector dispersion values are over the average value for all landslide deposits	279
Figure 5.37 Definition of a point representing directional data on a spherical surface	281
Figure 5.38 Probability density function representing the Fisher distribution	283
Figure 5.39 Probability density function representing the axial distribution	285
Figure 5.40 Distribution of fabric shapes on a sphere	290
Figure 5.41 Spatial distribution of eigenvalues for the study area	292

Figure 5.42 Spatial distribution of the eigenvalue ratio of $\ln(S_1/S_2)$ in the study area	295
Figure 5.43 Spatial distribution of the eigenvalue ratio of $\ln(S_2/S_3)$ in the study area	296
Figure 5.44 Spatial distribution of the eigenvalue ratios with respect to occupied areas	297
Figure 5.45 A closer look at the part of study area draped by the eigenvalue ratio of $\ln(S_1/S_2)$	298
Figure 5.46 Evaluation of the spatial distribution by the eigenvalue ratio .	301
Figure 5.47 Spatial distribution of the eigenvalue analysis within landslide deposits	303
Figure 5.48 Mean eigenvalue ratios of previous landslide deposits observed in the study area	304
Figure 5.49 Geographical distribution of landslide deposits whose mean eigenvalue ratios of $\ln(S_1/S_2)$ are below the average value for all landslide deposits	305
Figure 5.50 Diagram showing systematic processes for the evaluation of the landslide hazard in the study area	315
Figure 5.51 1949 aerial photographs of the Peace River area	317
Figure 5.52 1949 geomorphological map depicting the Peace River area .	318
Figure 5.53 Delineation of representative symbols used to produce geomorphological maps	319
Figure 5.54 1977 aerial photographs of the Peace River area	320
Figure 5.55 1977 geomorphological map depicting the Peace River area .	321
Figure 5.56 2006 aerial photographs of the Peace River area	322
Figure 5.57 2006 geomorphological map depicting the Peace River area .	323

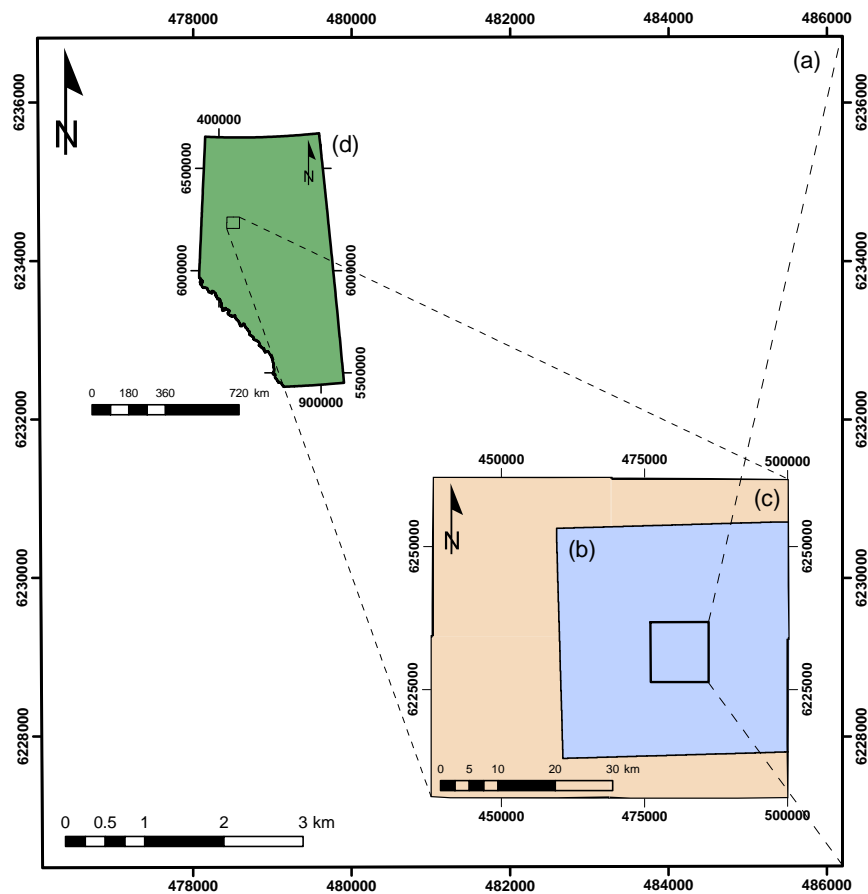
Figure 5.58	1958 aerial photographs of the west bank of the Peace River	325
Figure 5.59	1958 geomorphological map depicting the west bank of the Peace River	326
Figure 5.60	1958 aerial photographs of the east bank of the Peace River	328
Figure 5.61	1958 geomorphological map depicting the east bank of the Peace River	329
Figure 5.62	Distribution showing preliminary landslide hazards derived from geologic and geomorphological factors observed on previous landslide deposits in the study area	332
Figure 5.63	Distribution showing the landslide hazard assessment in the study area derived from geologic and geomorphological parameters observed on previous landslide deposits	333
Figure 5.64	Consideration of the land use in the landslide hazard assess- ment	335
Figure 5.65	Traces of previous drainage systems observed in the west bank of the Peace River and corresponding landslide hazards	337
Figure 5.66	Traces of previous drainage systems observed in the east bank of the Peace River and corresponding landslide hazards	338
Figure 5.67	Relationship between mean texture and slope values on pre- vious landslide deposits	340
Figure 5.68	Relationship between mean vector dispersion and slope val- ues on previous landslide deposits	341
Figure 5.69	Relationship between mean eigenvalue ratio of $\ln(S_1/S_2)$ and slope values on previous landslide deposits	342
Figure 5.70	Relationships of mean values of texture, vector dispersion, and eigenvalue ratio	343
Figure 5.71	Distribution showing modified landslide hazards	347

Figure 5.72 Distribution of occupied percentage areas based on the level of landslide hazards	349
Figure 5.73 Distribution of areas where landslide induced problems have been reported	351
Figure 5.74 Exhaustive examinations for the validation of the proposed landslide hazard assessment with historical landslide evidences in the east bank of the Peace River	352
Figure 5.75 Exhaustive examinations for the validation of the proposed landslide hazard assessment with historical landslide evidences in the west bank of the Peace River	353
Figure 5.76 Evaluation of the proposed landslide hazard assessment . . .	355

Research Extent

Unless mentioned otherwise, the predefined geographic extents covered by this study are as below:

- (a) Main study area. It is generated from the LiDAR imagery
- (b) and (c) Maximum extents where this study may cover. They are defined by the SRTM and Landsat 7 satellite imageries. The area outlined by a black rectangle in (b) is the main study area shown in (a)
- (d) Province of Alberta. The black rectangle provides a closer look at the local area illustrated in (c)



Chapter 1

Introduction

Landslides, reflecting the geomorphological process of the natural landscape, become a threat only when they interfere with lives and properties of people or, more precisely, when people interfere with these ongoing natural processes by various anthropogenic works through massive urbanization (Pestrong 1976).

As the one of several major natural hazards (UNISDR 2009), landslides annually cause the loss of many lives and have enormous economic impact. The casualties and economic losses caused by the landslide incidents from 1991 to 2005 were estimated to be about 12,733 and U.S \$ 3.06 billion (Figure 1.1). In the past, landslides are treated as phenomena, movements of masses of rock, debris or earth down slopes (Cruden 1991b). They drew considerable attention from both economic and engineering points of view since they cause significant casualties and property damages. Increasing costs are closely related to the expansion of population and economic development which results in residential areas being located near slopes where landslides are prone. Aleotti and Chowdbury (1999) noted that increasing awareness of the socio-economic consequence of landslides and growing pressure of urbanization on the environment would attract more global attention than ever before. Moreover, unexpected precipitation caused by climate change will accelerate this awareness.

Urbanization has exposed people and their property to landslides, and therefore more frequent disasters. Through urban expansions, cities transform their surrounding environments and produce new risks (UNDP 2004). Constructing residential developments, industrial structures, transportation routes, and lifelines on hillsides interfere with slope stability. Even though once treated as natural phenomena, landslides can be disastrous events and, in turn, disturb and affect the well being of society. In developing countries, these impacts are even more severe (Schuster and Highland 2007).

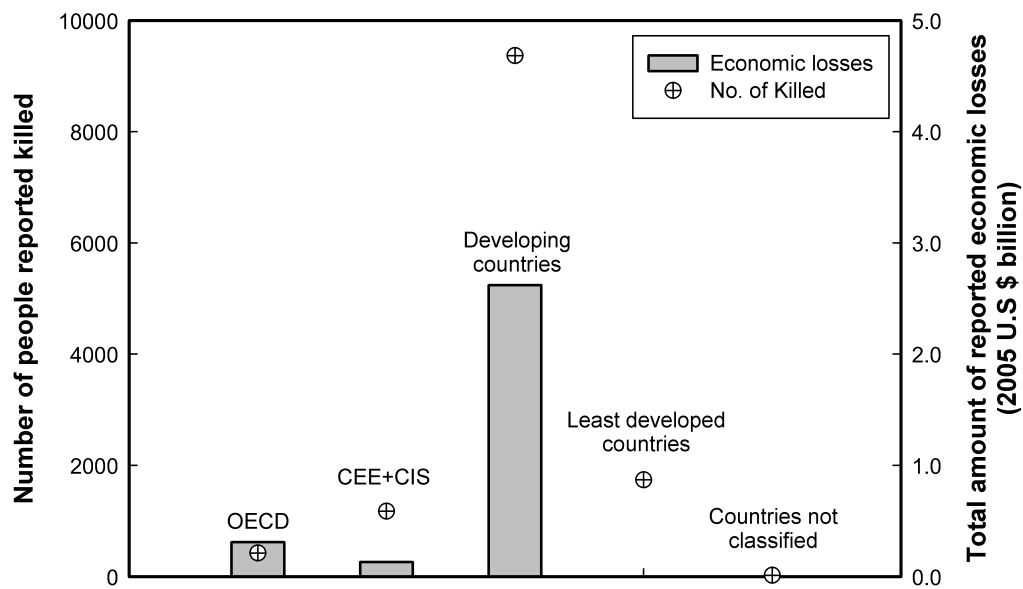


Figure 1.1 Casualties and economic losses resulting from landslide incidents from 1991 to 2005. Reported losses are converted to 2005 U.S currency. Abbreviations used in the plot are as follows: OECD (Organization for Economic Cooperation and Development); CEE (Central and Eastern Europe); and CIS (Commonwealth of Independent States). *Source:* Data from EM-DAT (2011)

Schuster and Highland (2007) reviewed examples of urban landslides from several countries which caused significant damages and casualties. They highlighted socioeconomic impacts of landslides and proposed management of urban landslide hazards. Kjekstad and Highland (2009) indicated the Americas and China have had the highest number of fatalities from landslides, and these were underestimated because of the characteristics of sequential natural hazards following major disasters such as earthquakes or floods. Petley (2008) investigated the numbers of fatalities due to landslides in 2007 and showed that the most affected country (fatalities greater than 100) was China followed by Indonesia, India, Pakistan, Nepal, and Vietnam, all of which are developing countries that have less resources to prevent or reduce such catastrophic disasters. Nadim et al. (2006) identified “hot spots,” which they defined as the highest hazard areas for landslides and avalanche hazards based on global datasets of climate, lithology, earthquake activity, and topography. They also provided a global model for landslide prone areas in descending order: Central America, North-western South America, the Caucasus region, the Himalayan belt, Taiwan, Philippines, Indonesia, Italy, and Japan. Fortunately, social and economic losses caused by the landslides can be reduced by means of effective disaster planning and management.

Until recently, major landslide reduction activities have focused on the principle of mitigation, using civil engineered structures after landslides have occurred. This seemed to work successfully especially in most landslide areas. There is, however, increasing need for more collaborative approaches in order to obtain more comprehensive, structured systems to avoid landslide disasters. This includes a framework which is applicable everywhere with adjustments for factors controlling the landslides. This framework should be balanced with an understanding of the main conditions of landslides, identifying landslide susceptibility, hazard, and risk, and reducing loss of life and property damage (Brabb 1991, Figure 3). Figure 1.2 describes mutual relationships among landslide-related research, mapping, and hazard reduction efforts. The development of the landslide risk management technology is the most advanced type of integrated framework for landslide disasters. With the expansion of Geographical Information Systems (GIS), various modeling and simulation tools have also led to the growth of this trend.

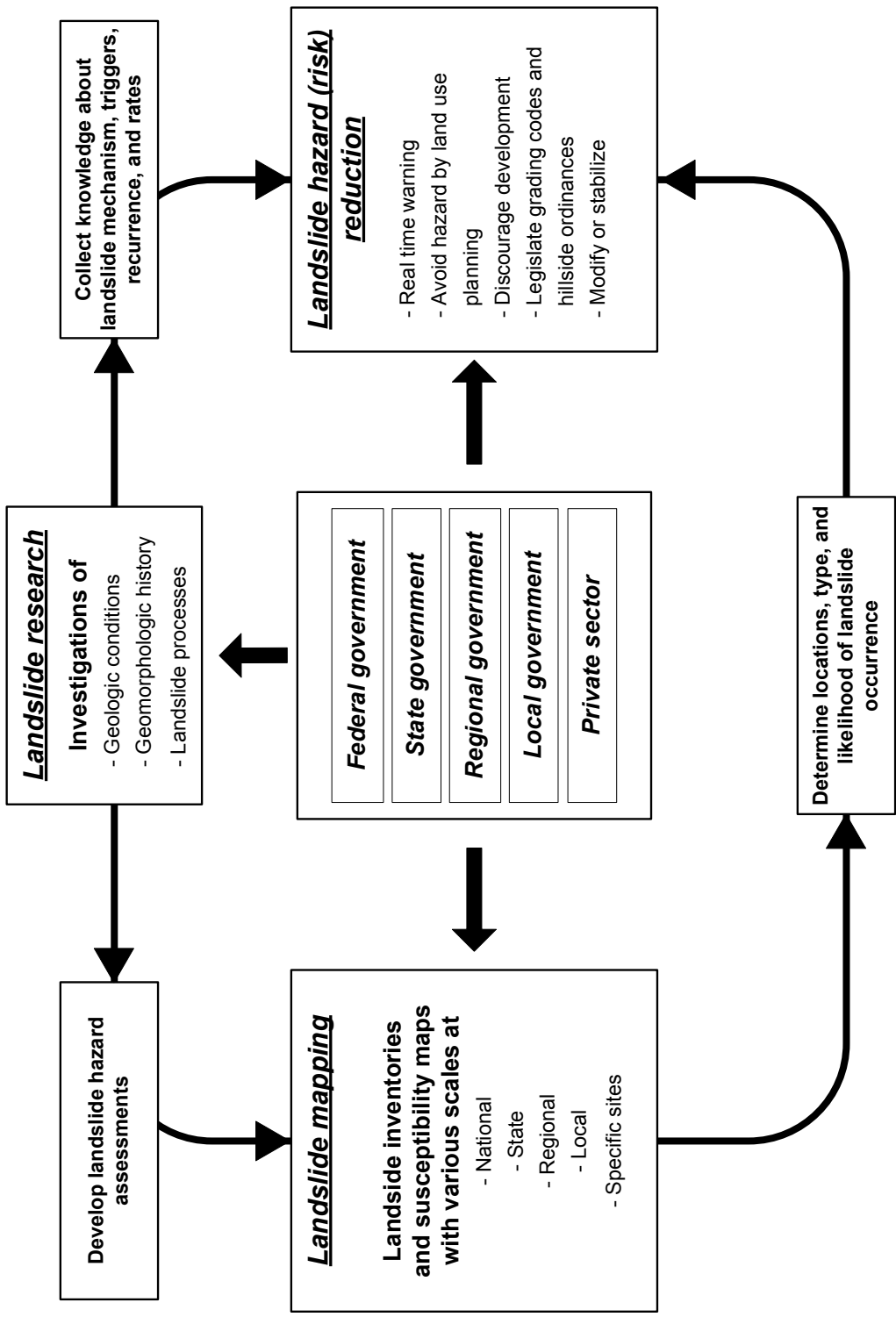


Figure 1.2 Diagram showing mutual relationships among landslide research, mapping, and hazard reduction measures in the United States. Diverse levels of governments and private sectors are involved and support each component

1.1 Overview and background

Canada has experienced numerous landslides which resulted in loss of lives and impacted resources and infrastructures (Cruden et al. 1989). Although the most deadly landslide in Canada occurred at Alberta in 1903, the general geographic distribution of historic landslides that caused casualties is divided into two major parts across Canada (Evans 1997, 1999): (1) Cordillera of Western Canada; and (2) St. Lawrence Lowlands of Eastern Canada. Evans (2001) also collected landslide records (defined as a landslide event or related geotechnical failure with either direct or indirect impact producing at least three casualties) between 1840 and 1998. He documented 43 landslides giving a landslide frequency of one every 3.7 years or an annual landslide frequency of 0.27. The frequency is concentrated during two periods: (1) the late nineteenth to early twentieth century; and (2) the mid 1950s to 1970s (Evans 1997). During these periods the most frequent type of landslide in terms of destructiveness was a rock slide or rock fall with a volume of less than 100,000 m³.

Evans (1997) described landslide characteristics observed in Canada as: (1) some loss of lives are caused by secondary effects of landslides and related geotechnical incidents such as displacement waves and outburst floods induced by landslides; (2) landslides occur where the slope stability is severely affected by the human activity; and (3) landslide related disasters are commonly induced by the human negligence like disobeying regulations. Landslide research in the Canadian Cordillera, the most landslide susceptible region, was carried out by Evans et al. (2002) and Evans and Savigny (1994). Evans et al. (2002) focused on the southeastern Cordillera including compiling a detailed database, developing the hazard assessment of historical events, and providing an approximate regional landslide risk model.

The Town of Peace River, developed in the Peace River Lowland, is a unique municipality because of its location on the flood plain of the Peace, which flows northerly in the Interior Plains of Western Canada. The city has grown substantially since the fifties. Concordant with the economic growth, population increased and led to demand for new space for residences. Several historic landslides occurred, coinciding with the urbanization adjacent to residential developments and transportation corridors. Landslide studies have been limited to these particular situations although Nilson and McCormick (1978) did a broader preliminary risk assessment.

As a part of the Urban Geology and Geohazards Initiatives in the Town of Peace River (Froese 2007), this research would provide important information to estimate the potential landslide occurrence in the study area. It is based on the landslide hazard assessment system proposed by Keegan (2007) and Keegan et al. (2007). Through various geotechnical approaches, characteristics of the area of concern can be determined. The landslide causal factors which may control the mechanism of landslides can be identified and their implications are considered. Finally, the evaluation of the landslide hazard assessment system follows.

1.2 Statement of purpose

This study is mainly concerned with landslide hazard assessment at the municipality scale. It is, therefore, imperative to identify the unique conditions of the local areas and understand the processes causing such conditions. The temporal and spatial characteristics of the study area including geological and geomorphological histories, meteorological variations, economic developments, and demographic distributions over time are also included in these categories.

There are several causal factors, either preparatory or triggering, which affect landslide initiations, their movement patterns, and the degree of damage. Investigating recent landslides in the study area can provide strong correlations between landslides and their causal factors. The second consideration, therefore, is to seek causal agents and evaluate their feasibility within the landslide hazard assessment system.

The third issue is directly related to the technical methodologies for the landslide hazard assessment. In order to get a more accurate and reliable landslide hazard assessment, appropriate methodologies are necessary, which consider geographical, geological, and geomorphological conditions of the study area and proper landslide causal factors indicated earlier. This may start with the generation of the landslide inventory which combines causal factors and environmental conditions previously described. The landslide susceptibility analysis can be carried out after the landslide inventory mapping. A suitable methodology for the landslide hazard assessment should also be provided.

Finally, the evaluation of the feasibility of the landslide hazard assessment created for this study should be completed. From this process a comparison with previous research should be carried out to identify the benefits and costs of the generated system. It is also necessary to indicate the future enhancement of the system for other urban areas which have similar or different components of consideration in building the landslide hazard assessment system based on the spatial and temporal variations. The following questions are closely related to my research goal, which is to estimate the landslide hazards in the study area:

1. What are the temporal and spatial characteristics of the study area?
2. What are the specific causal factors which control landslides and are required in the analysis of the landslide hazard assessment for the study area?
3. How could a landslide hazard assessment system be constructed in order to express the characteristics of landslides in the study area?
4. What is the degree of accuracy of the created hazard assessment system?

1.3 Approach and methodology

Methodologies for this study were employed to determine areas with the most potential for landslide hazards. These, on the other hand, can be subdivided into the following four categories which are consistent with the research questions described in Statement of purpose (Section 1.2). Figure 1.3 gives a schematic overview of the relationship between each methodology needed for solving the research questions and principal components of landslide hazard and risk assessment systems shown in the following section (Section 2.1.3).

1.3.1 Establishing temporal and spatial characteristics

The starting point focuses on the preliminary research of the study area, which include site reconnaissances, aerial photo interpretations, field tests and samplings, laboratory tests, and investigations of the landslide history. Capturing the historic, meteorological, and geological events also occur at this stage. Economic aspects

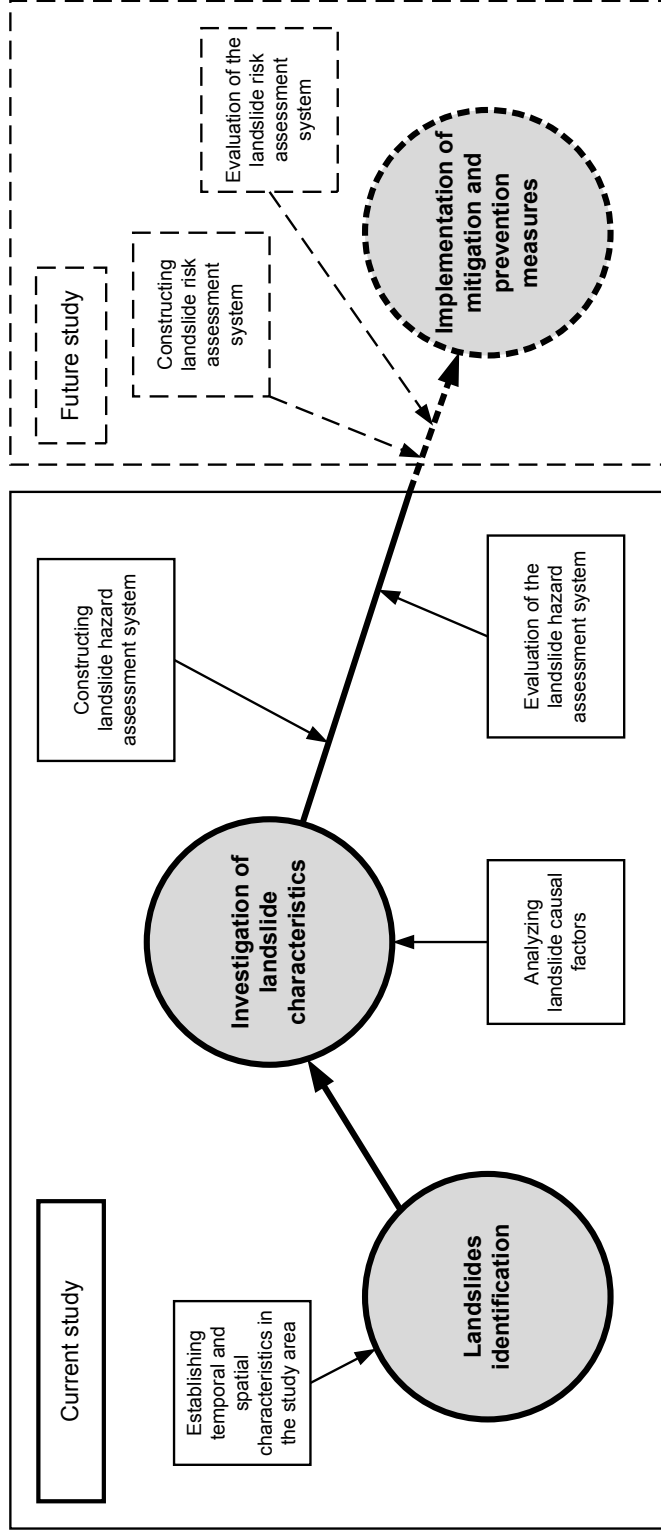


Figure 1.3 Principal research processes for the landslide hazard assessment in the Town of Peace River. Gray shaded circles represent the fundamental procedures of the landslide hazard and risk assessments described in Chapter 2 (Fundamental processes for landslide hazard assessments, Section 2.1.3) and squares indicate typical methodologies employing for this study. The scope of the current and future studies are also differentiated by solid and dashed lines, respectively

would help to understand the development of the study area. High technological landslide identification schemes such as high resolution optical, SAR, and LiDAR imageries can be used to detect the old landslide vestiges which could not be detected by conventional techniques. Topography of the study area, which is essential for identifying the landslide causal factors can be determined by digital elevation models (DEMs) generated from the LiDAR dataset. In this stage it is imperative to find where landslides occurred and establish these data as the form of the inventory system for future research.

1.3.2 Analyzing landslide causal factors

Identifying landslide causal factors is a key for understanding the mechanism of previous landslides and their effects and further provides spatial and temporal estimations on future landslides. Casual factors are various and are spatially and temporally dependent of the geomorphology in the study area because the change of causal factors such as modification of the slope geometry due to the residential development may require the adjustment of landslide hazard assessments. Therefore, it is essential at this stage to prioritize those factors to fit the study area. The GIS technology enables one to visualize those casual factors. Layer based, each casual factor can be used for delineating its own objective or combined to present composite natural phenomena. The selection of causal factors depends on the landslide type, topography, and availability of data (van Westen et al. 2008). Examples of causal factors for this study are geology (bedrock distribution), soil (soil type and depth), topography (terrain units), hydrology (groundwater level, soil moisture, and stream network), anthropogenic aspects (land use, transportation network, and population density), and meteorology (rainfall, snow depth, and temperature).

1.3.3 Constructing the landslide hazard assessment system

In order to get an appropriate landslide hazard assessment, the selection of the analyzing methodology is most important. This depends on the scale and availability of the data accessed. Landslide hazard assessment systems can be broadly divided into two types based on the difference in calculating or weighting landslide causal factors: either qualitative methods using expertise and experience or quantitative meth-

ods using a mathematical calculation. In this study, landslide hazard assessments are carried out by using geologic and geomorphological methodologies which use information for the landslide hazard classification in qualitative or semi-quantitative way to establish the degree of hazard. Information to evaluate landslide hazard is numerous and depends on the objectives of the study, but generally geologic units, slope, and hydrologic distribution, which are believed to be main causal factors for initiating and reactivating landslides, are frequently used. Constructed landslide hazard information is then grouped based on its homogeneous characteristics to illustrate relative degrees of hazard. Guidelines proposed by Keegan (2007) and Keegan et al. (2007) for ground hazards affecting the stability of railway tracks are employed to classify the landslide hazards in the study area. A GIS would also improve productivity in generating various relevant data manipulations with a high accuracy and in a short time.

1.3.4 Evaluation of the landslide hazard assessment system

One of the biggest challenges in landslide hazard assessment research can be the evaluation of the results in order to verify their feasibility. Due to the lack of previous hazard models which enables comparison to current results, only broad ideas or estimated results from similar spatial conditions could be discussed. Comparison with previous outcomes is required to evaluate the validity of the current study.

Landslide hazards in the study area due to urban developments were investigated by Nilson and McCormick (1978). Results of this study can be used to evaluate the validity of the current study even though their results were solely based on the analysis of geomorphological characteristics with limited data and professional experience. Through this process, landslide information for the Peace River area would be updated and provide a valuable practical information about future landslide hazards.

1.4 Delimitations and limitations

Assessing landslide hazard, from identification to response, is quite complex and thus there is no perfect system which is appropriate for all landslide situations. The choice depends on the purpose of an assessment, the nature of the methodology,

and the representation criteria, all of which would affect the final product. A general procedure for the landslide hazard assessment and its implementation has the following components (Fleming et al. 1979).

1. Identify the previous landslide areas and their conditions. If possible quantify the current status and adverse processes which affect the stability in the present and near future.
2. Disseminate the information to responsible agencies as well as to the public in an appropriate form and scale for the policy making, education, and response.
3. Determine actions needed in order to reduce imminent and potential hazards.
4. Operate the landslide hazard reduction measures such as land use control by regulations and codes.

Due to insufficient information on determining proper actions and guidelines to landslide hazard reductions, the extent of this study would be delimited to the first two issues: (1) identify the previous landslide areas and their conditions; and (2) disseminate the information. The former would be accomplished by the landslide inventory and a detailed investigation for the individual landslide and the latter would be completed by the landslide hazard map.

One of the limitations is related to the determination of temporal distribution of historic landslides which can only be identified from degraded landslides features through aerial photo interpretations. The temporal assessment of previous landslides is essential information to construct the landslide inventory and further analyze susceptibility and hazard assessments in which the landslide inventory will be employed as a fundamental component. In this study, recent landslides are limited to those that occurred in the beginning of the 1970s which may not be as effective as other studies carried out by Evans (1997) and Hungr et al. (1999; 2005) that used typical approaches which focused on the relationship between landslide frequencies and their volume.

Another limitation can be found in performing methodologies to determine the landslide hazard in the study area. My current study uses geomorphological mapping which is a relatively subjective method compared to other landslide hazard assessment techniques. However, well-prepared data and systematically organized

aerial photo interpretations will provide reliable results. As indicated earlier, a guideline proposed by Keegan (2007) and Keegan et al. (2007) is used to increase objectivity by classifying obtained landslide hazards depending on their influences on future landslides and impacts on the sustainability of the town.

1.5 Organization

This study is organized in six chapters and each chapter is systematically linked to others and provides an understanding to assess the landslide hazard in the study area. Chapter 1 provides an introduction to the study, i.e., overview and background, statement of purpose, and approach and methodology. In addition, delimitations and limitations of the study are also introduced.

Chapter 2 discusses general ideas about landslide hazard and risk assessments. The fundamental concepts and issues resulting from landslide hazards including distinct nomenclature definition, overall framework, and fundamental processes with regard to the landslide hazard assessments are presented. Relevant research on the landslide hazard assessment systems including comprehensive descriptions of the landslide inventory, susceptibility, hazard, and risk assessments are illustrated with representative examples found in the literature. A summary of socioeconomic impacts of landslides and principles to reduce landslide hazards in urban areas then follows. Finally, the role of landslide hazard assessments in implementing effective landslide hazard reductions is briefly described.

Fundamental information for landslides in the study area is described in Chapter 3. General overviews including geographic and economic backgrounds provide a better understanding of landslides and their impacts on the study area. Geologic and climate settings which comprise indispensable parts for landslide studies are presented to give ideas on various factors that would initiate or reactivate landslides in the study area. Finally, a brief history of recent landslides observed in the study area is presented. This chapter gives an opportunity to look at the general framework of environments in the study area and efforts to reduce the landslide influences. Data obtained from this chapter are used to identify individual landslide and understand their movement characteristics, which are presented in the following chapter.

Based on the comprehensive information described in the previous chapter, Chapter 4 addresses typical landslide characteristics related to the recent slide events in the study area. Recent landslides are analyzed from a geotechnical point of view including identifying the potential rupture surfaces, groundwater distribution, movement behaviours, and possible landslide mechanisms. Efforts to determine strength properties on rupture surfaces materials are also carried out. Displacement records of landslides and possible casual factors are described to show their relationships. Movement patterns observed in landslide displacements are discussed to explain the modes of landslides. Movement characteristics found in this chapter may be used to estimate the future behaviour of unstable slopes and develop a landslide hazard map for the study area.

Chapter 5 illustrates practical procedures to assess landslide hazards in the study area. First major considerations of landslide induced factors are provided to understand the relationship between those factors and landslides. These may include examination of representative factors and determination of their applicability for assessing landslide hazards in the Town of Peace River. By reviewing the previous landslide deposits in the study area, the appropriate approaches and methodologies for this research are discussed. The landslide hazard assessment in the Town of Peace River is achieved by the geologic and geomorphological mapping methodologies and detailed explanations. These include determination of landslide hazard, identification of the geomorphological landslide controlled features, and construction of landslide hazard assessment system, respectively. Finally, results and corresponding discussions related to the practical applications for the landslide hazard assessment follow.

Chapter 6 presents the results of the study, conclusions, limitations, and some recommendations for the future study. References cited for the study are listed thereafter. Supplements are attached in the form of appendices. Detailed borehole data used to identify potential rupture surfaces and determine landslide movements and their behaviours are shown in Appendix A. Appendix B contains the stratigraphic information for representative samples used in laboratory tests. Results of laboratory tests for the representative samples are given in Appendix C. It includes index tests, hydrometer tests, and direct shear tests. Appendix D includes a published paper describing a recent landslide in Fox Creek, Peace River Lowland, which shows an early form of the landslides developed in the study area. Finally, statistical analyses on identified landslide deposits are presented in Appendix E.

Chapter 2

Review of landslide hazard assessments

This chapter covers general ideas for landslide hazard and risk assessments. First, the fundamental concepts and issues regarding landslide hazards including characteristics of landslide hazard assessments are listed. Relevant research for landslide hazard assessment systems including definitions of each nomenclature, comprehensive descriptions on the landslide inventory, susceptibility, and hazard and risk assessments are addressed. Finally, a brief summary of socio-economic impacts of landslides and some implementations for landslide hazards in urban areas are then followed.

2.1 Characteristics of landslide hazard assessments

Brabb (1984) noted that information on landslides which impact people and put their properties at risk should be carried out during landslide hazard and risk assessments. This information may include previous landslide history, containing date, type, volume of landslides, and their induced damages to people and structures. It may also have the estimation of future landslides with vulnerability, elements at risk, and total risk as well as their occurrence time. Therefore, understanding each element comprising landslide hazard assessments can provide an appropriate judgement when dealing with numerous landslide disasters and reducing their impacts.

In practical studies, however, the proper classification of each element and corresponding method seems to be confused and used interchangeably (Brabb 1984). The misuse of landslide assessments could result in an incorrect decision and therefore cause a catastrophe that is similar or even worse if no appropriate assessments or plans had been made. It is, therefore, necessary to clearly define each nomenclature.

ture related to landslide hazard assessments in order to identify and understand its fundamental function.

2.1.1 Definition of landslide hazard assessments

Frequently nomenclature used in disaster related studies have been employed to explain different meanings of the same phenomena and vice versa. Varnes and IAEG Commission on Landslides and other Mass Movement on Slopes (1984) noted a misuse of terms such as “vulnerability,” “hazard,” and “risk” to describe the characteristics of natural disasters and their impacts. According to the United Nations International Strategy for Disaster Reduction (2009), “hazard” and “(disaster) risk” used in disaster related activities generally can be defined as follows:

Hazard *Hazard is a dangerous phenomenon, substance, human activity or condition that may cause loss of life, injury or other health impacts, property damage, loss of livelihoods and services, social and economic disruption, or environmental damage and is described quantitatively by the likely frequency of occurrence of different intensities for different areas, as determined from historical data or scientific analysis (pp. 17-18).*

(Disaster) risk *(Disaster) risk is the potential disaster losses, in lives, health status, livelihoods, assets and services, which could occur to a particular community or a society over some specified future time period and comprises different types of potential losses which are often difficult to quantify but can be broadly evaluated at least if knowledge of the prevailing hazards and the patterns of population and socio-economic development are provided (pp. 9-10).*

More specifically, widely used definitions with regard to landslide hazard assessments were proposed by Varnes and IAEG Commission on Landslides and other Mass Movement on Slopes (1984) under UNDRO (Office of the United Nations Disaster Relief Coordinator) and UNESCO (United Nations Educational, Scientific and Cultural Organization). These are the following:

Natural hazard (H) indicates the probability of occurrence within temporal and spatial boundaries of potential natural event.

Vulnerability (V) means the degree of loss which stands from zero (no possibility to be impacted) to one (absolutely impacted) of element or elements at risk induced by the occurrence of given natural episode.

Specific risk (R_s) represents the supposed degree of loss of a specific element at risk which resulted from a particular natural episode and can be calculated by the product of the specific natural hazard (H) and its vulnerability (V).

Elements at risk (E) indicates components exposed to risk such as population, properties and structures, as well as private and public activities.

Total risk (R_t) can be defined as the supposed degree of loss in each element at risk due to the specific natural event and expressed as:

$$R_t = E \cdot R_s = E \cdot (H \times V) \quad (2.1)$$

Fell (1994) extended the Varnes and IAEG Commission on Landslides and other Mass Movement on Slopes (1984) nomenclature and redefined landslide hazard assessments that especially focused on the clarification of the hazard, dividing it into two sub-elements, the “magnitude” and “probability.” Examples of these modifications are as follows:

Magnitude (M) indicates the volume (m^3) induced by the landslide.

Probability (P) describes the likelihood of occurrence for the specific landslide within given spatial and temporal boundaries. It may be a single value or a summed value comprised of several individual probabilities. For example,

$$P = P_R + P_S + P_H \quad (2.2)$$

stands for a combined probability of P_R = rainfall, P_S = seismicity, and P_H = human disturbance.

Hazard (H) means the product of magnitude (M) times probability (P).

Specific risk (R_s) is the expected degree of loss of specific elements at risk resulting from the particular natural event and can be defined as the product of probability (P) and vulnerability (V).

Total risk (R_t) is, therefore, expressed as the product of elements at risk (E) and specific risk (R_s) in all type of current and future landslides:

$$R_t = \sum (E \times R_s) = \sum (E \times P \times V) \quad (2.3)$$

Studies by Pack et al. (1987) extended landslide hazard assessments using a probabilistic approach. They proposed that the complete risk evaluation should be augmented by combining probabilities that play an important role in trigger, failure, exposure, and consequence perspectives. The final result of the risk evaluation, the risk probability density $P(R)$, can be given by:

$$P(R) = \int \int \int P(T; F; E; C) dT dF dE \quad (2.4)$$

where $P(T; F; E; C)$ is the joint probability density of triggering ($P(T)$), landslide ($P(F|T)$), exposure of elements at risk ($P(E|T; F)$), and consequence ($P(C|T; F; E)$), respectively.

Using the Bernoulli distribution, a discrete probability distribution having a range between one (P) to zero ($Q = 1 - P$), Equation (2.4) can be simplified by the product of the four terms. This results in:

$$P(R) = P(T) \cdot P(F|T) \cdot P(E|T; F) \cdot P(C|T; F; E) \quad (2.5)$$

Equation (2.5) describes well the overall evaluation process for the landslide hazard assessment. In other words, most landslides may be affected by some triggers such as precipitation, snow melt, and earthquake. The possibility of impacts by triggers can be stated by $P(T)$, and Pack et al. (1987) called this term the “landslide opportunity.” These triggers may control the probability of landslide occurrences which is represented by $P(F|T)$, and called the “landslide susceptibility” (Pack et al. 1987). The degree of exposure in people’s lives, properties, and public and private services (which are called elements at risk) may be impacted by the possibility of landslides

given in the degree of trigger occurrences ($P(E|T; F)$). This is equivalent to the “landslide vulnerability.” Lastly, the consequence to elements at risk in terms of number of losses or injured and monetary values (Pack et al. 1987) may be dependent on the vulnerability to those components in a given possibility of landslides due to the extent of triggers ($P(C|T; F; E)$). The total risk, therefore, can be described as the product of four probability terms. The Equation (2.5) is equivalent to Equations (2.1) and (2.3) where $P(T)$ and $P(F|T)$, $P(E|T; F)$, and $P(C|T; F; E)$ are treated as the landslide hazard, vulnerability, and elements at risk, respectively.

Morgan et al. (1992) narrowed the general risk probability approach proposed by Pack et al. (1987) down to the “Probability of Death of an Individual (PDI),” by describing the annual probability of loss of life resulting from large debris flows. The PDI can be expressed as:

$$PDI = P(H) \times P(S|H) \times P(T|H; S) \times P(L|H; S; T) \quad (2.6)$$

where $P(H)$ is the annual probability of landslide, $P(S|H)$ is the probability of death for an individual resulted from spatial impacts of the landslide, $P(T|H; S)$ is the probability of death for an individual due to temporal influences given in spatial impacts of the hazardous events, and $P(L|H; S; T)$ represents the probability of which person would die due to the temporal and spatial impacts in a given hazardous situation. Equation (2.6) only deals with the spatial and temporal considerations of the element at risk (an individual) in a disastrous event. Morgan et al. (1992) noted that the last three terms can be expressed as “severity” for an individual, therefore:

$$PDI = P(H) \times \text{Severity} \quad (2.7)$$

The last three terms of probabilities in Equation (2.6), which combine to generate the severity in Equation (2.7), can be assumed as each discrete vulnerability (V) of a person (E), such as spatial (V_S), temporal (V_T), and loss of life (V_L) vulnerabilities, then the severity can be equivalent to “consequence ($C = V \times E$).” Equation (2.7), therefore like Equation (2.5), corresponds to the Equations (2.1) and (2.3), respectively.

For property damages Dai et al. (2002) proposed the “Probability of Damage in Property (PDP)” in the following relationship:

$$PDP = P(H) \times P(S|H) \times P(P|H;S) \times E \quad (2.8)$$

where PDP is the probability of damage in property, $P(H)$ is the annual probability of landslide, $P(S|H)$ is the spatial probability of property affected by the landslide, $P(P|H;S)$ is the probability of which property would be impacted due to the spatial influences given the landslide situation, and E indicates the type of property. Applying the same concept described above, the probability of property damage can also be expressed as the product of $P(H)$ times severity or consequence which comprises $P(S|H) \times P(P|H;S) \times E$. Therefore,

$$PDP = P(H) \times \text{Severity (or Consequence)} \quad (2.9)$$

A recent study carried out by van Westen et al. (2006) defined the total risk as all the expected consequences (C) of all the landslide hazards (H). Expected consequences means the product of vulnerability (V) described in numerical values (0 to 1) and elements at risk (A) presented by the numbers of losses or injures, and the monetary value of property damages. This relationship gives the following:

$$R_t = \sum (H \sum C) = \sum (H \sum (V \cdot A)) \quad (2.10)$$

2.1.2 Framework of landslide hazard assessments

The landslide assessment framework in this study indicates spatial characteristics of landslide related assessments, either susceptibility, hazard, or risk assessments, in which types and extents of specific assessments are determined and implemented. Although a large number of studies to date on both theoretical and practical landslide assessments have been presented, the ambiguous framework and corresponding misuse of specific assessments would decrease their maximum capabilities down and even cause unexpected consequences. Many authors discuss the roles and interrelationships of each landslide assessment in order to understand

their rigorous responsibilities within the framework (Walker et al. 1985; Pack et al. 1987; Fell 1994; Aleotti and Chowdhury 1999; Lee and Jones 2004; Crozier and Glade 2005; Chacón et al. 2006; van Westen et al. 2006). Efforts by international societies have taken place in recent international conferences, for example, International Union of Geological Sciences Working Group (IUGS Working Group) on Landslides organized the International Workshop on Landslide Risk Assessment (Hawaii, 1997). JTC-1 (Corominas et al. 2008), the joint ISSMGE, IAEG, and ISRM Technical Committee on Landslides and Engineered Slopes, also organized the International Symposium on Landslides (Rio de Janeiro, 2004), the International Conference on Landslide Risk Management (Vancouver, 2005), and the International Forum on Landslide Disaster Management (Hong Kong, 2007). Parts of JTC-1 achievements were published as a special issue of *Engineering Geology* titled “Landslide Susceptibility, Hazard and Risk Zoning for Land Use Planning (Volume 102, pp. 83-256, 2008).” In Alberta the Geotechnical Society of Edmonton organized the second symposium entitled “Risk Assessment in Geotechnical & Geo-Environmental Engineering (Geotechnical Society of Edmonton 1996).”

A recent study by Fell et al. (2005) well described the framework for landslide hazard assessments that show a successful applicability in natural as well as engineered slopes. They noted a framework is augmented by several inter-organized components (in descending order): (1) hazard analysis; (2) frequency analysis; (3) risk estimation; and (4) risk evaluation. They also discussed benefits of recent developments in landslide hazard assessments such as quantitative analyses, enhanced digital technologies, and a thorough understanding of the relationships between rainfall and landslide occurrence, and travel distance and velocity of the slide mass. Picarelli et al. (2005) provided an overview of the landslide hazard analysis, one of the components in landslide hazard assessments. Studies on the post-failure runout models for the sliding mass, which correlates a travel distance to a velocity, are presented by Hungr (1995), and Hungr et al. (1999; 2005).

The Australian Geomechanics Society (AGS) has contributed outstanding achievements in the early establishment of the landslide hazard assessment framework (Australian Geomechanics Society 2000, 2007a, b, c, d, e). The first study published in 2000 improved deficiencies found in previous research and covered fundamental considerations such as terminology unification, framework definition, risk analysis methods, and information on acceptable and tolerable risks for loss of life (Australian Geomechanics Society 2000; Leventhal and Walker 2005). Con-

secutive studies carried out subsequently provided more detailed and practical approaches toward landslide risk management. These focused on the comprehensive geo-guidelines for slope management and maintenance (Australian Geomechanics Society 2007a), landslide susceptibility, hazard and risk zoning for land use management (Australian Geomechanics Society 2007b, d; Fell et al. 2008a, b), and corresponding practical notes for the landslide risk management (Australian Geomechanics Society 2007c, e) in Australia. Practical landslide hazard mappings in various steep terrain residential areas in Sydney and New South Wales were presented by Leventhal and Kotze (2008) for the purposes of regulatory management and land use planning described earlier.

Much relevant research can provide the structure of landslide related assessments. Fell et al. (2005) proposed a general framework of landslide risk management which has the shape of a tiered square based pyramid. The landslide hazard assessment treated in this study is part of the framework (Fell et al. 2005, Figure 3). Figure 2.1 describes similar characteristics of each function comprising the framework proposed by Fell et al. (2005). For example, the landslide characterization covers the top of the framework and has the smallest extent, indicating that this process would be necessary to implement at the beginning of landslide events with limited resolutions. In other words, the framework would work by top-down procedures and each phase may enclose the one above. As the phase progresses down, the more options for reducing the risk are available and more resources for those options are required (Figure 2.1).

The Australian Geomechanics Society (2000; 2007e), Fell et al. (2005), and Leventhal and Walker (2005) also introduced a diagram through which ongoing and potential landslide events can be identified, analyzed, estimated, assessed, and managed. Each process can be briefly summarized as follows:

2.1.2.1 Scope definition

As a starting point, a scope definition covers a broad knowledge about reducing, avoiding, and controlling landslide risks. Objectives and extents of the landslide risk management are usually established at this stage.

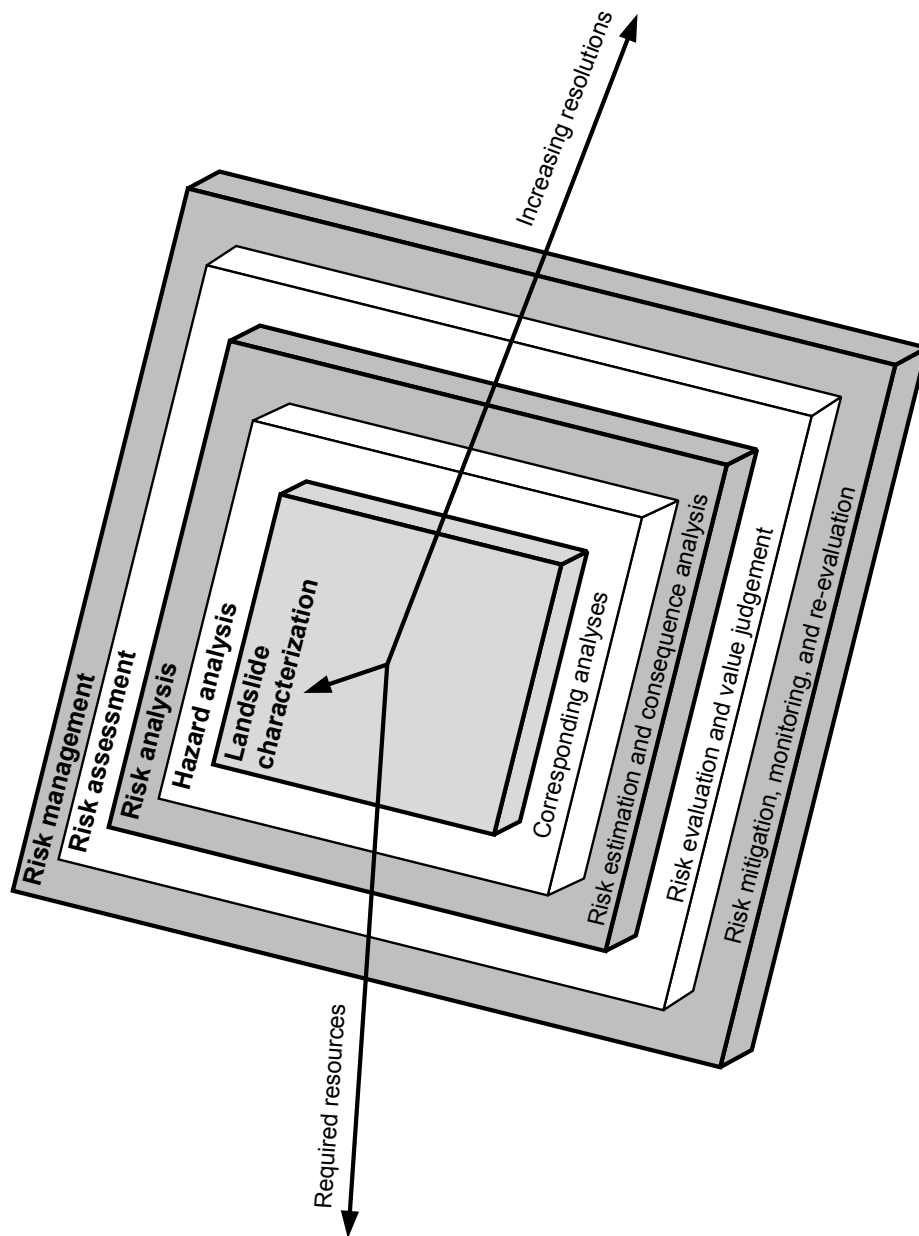


Figure 2.1 A process based framework for the landslide risk management. Each tiered layer indicates an individual component of the framework described in the text. Major schemes of each component are shown in the bottom of the tiered layer. Increasing resolutions and required resources are also described using arrows

2.1.2.2 Hazard analysis

The hazard analysis is the first authentic task in the landslide risk management and consists of landslide characterization and corresponding analyses. The landslide characterization is carried out to gather relevant data from the literature to field investigations and even instrumentations, and determine distinct features such as type, size, occurrence date, and movement mechanism in landslides and their current and future statuses. Corresponding analyses usually include the frequency analysis, which is the study to estimate the annual probability of the landslide occurrence, and the travel distance analysis in order to find the possibility of the spatial impact of landslides against elements at risk.

2.1.2.3 Risk analysis

The main objective of the risk analysis is to estimate the total consequence of elements at risk due to landslides. As mentioned earlier in the section, the risk analysis would include the hazard analysis previously examined and consequence analysis. Consequences can be produced by identifying the elements at risk and their vulnerability, either spatial or temporal, in landslides. Then total risk can be estimated by the product of hazards times consequences (Equations (2.7), (2.9), and (2.10)).

2.1.2.4 Risk assessment

In this process a total estimated risk generated from the previous steps can be compared to the pre-defined tolerance risk criteria for loss of lives and property damage. If the risk is tolerable, risk can be accepted otherwise risk mitigation resolutions are needed to reduce the risk below the tolerable risk criteria. Results of the risk assessment can be completed as a form of risk mapping or zoning.¹ This step is the critical part of the landslide risk management and can require communications between interested parties like owners, engineers, and decision makers (Fell et al. 2005).

¹In this study 'Mapping' is equivalent to 'Zoning' in terms of the fact that they are usually final products of landslide assessment processes for the land use and disaster prevention works even though the exact definition of each other is slightly different. The Australian Geomechanics Society (2007d) defined zoning as "*The division of land into homogeneous areas or domains and their ranking according to degree of actual or potential landslide susceptibility, hazard or risk.*"

2.1.2.5 Risk management

Risk, whether accepted or reduced, is required to monitor its long term behaviour and update its current status by re-evaluation for the appropriate action. In order to reduce the impact of the risk, feasible risk mitigations, either structured or non-structured, are implemented. Major considerations of these methods are based on avoiding the risk, reducing the frequency of landslide occurrence and consequences by the landslide, managing the risk by monitoring, transferring it by insurance, and postponing the decision (Australian Geomechanics Society 2007e).

2.1.3 Fundamental processes for landslide hazard assessments

Methods and procedures to implement landslide hazard assessments such as landslide susceptibility, hazard, and risk assessments are numerous and it is, therefore, difficult to find the best method optimized for specific objectives and conditions because they usually depend on the extent of the problems such as the availability of physical data. Regarding these perspectives, fundamental or practical landslide hazard assessments widely used may broadly require the followings (Soeters and van Westen 1996; Crozier and Glade 2005): (1) Identification of historical and potential landslides in order to develop a detailed landslide inventory; (2) Investigation of behaviours and characteristics of landslides which are connected with environmental conditions; and (3) Implementation of mitigation and prevention plans through constructed landslide hazard and risk assessments.

Each of these processes can be applied independently or collaboratively. Until the 1970s many landslide studies focused on implementing individual techniques, which may be adequate in small landslides whose conditions are local issues only. There is, however, an increasing demand to integrate different technologies in order to reduce the impact due to landslides more effectively and systematically.

2.1.3.1 Hazard identification in dated and potential landslides

In order to make a reliable landslide hazard assessment in an area of concern, it is first necessary to recognize the spatial and temporal information of previous and potential landslides. These may include landslide occurrence dates, size of landslides,

and extent of slide masses, and should be collected and classified properly by internationally accepted landslide classifications because landslides and their impacts frequently depend on their types and processes. Attempts to standardize the classification of landslides and their characteristics have been made by several authors and international organizations (Varnes 1978; Hutchinson 1988; IAEG Commission on Landslides 1990; UNESCO WP/WLI 1993; Popescu 1994; IUGS Working Group on Landslides 1995; Cruden and Varnes 1996; IUGS Working Group on Landslides 2001).

Landslides are usually evident on the ground surface; they can be identified and interpreted by remote sensing techniques from both conventional aerial photography and satellite imagery (Soeters and van Westen 1996). The most conventional and classical method of the landslide identification is the stereoscopic aerial photo interpretation. This type of technique, still popular and mostly used from the practical point of view in the late 1990s, is losing ground to the optical as well as SAR (Synthetic Aperture Radar) imagery techniques. Singhroy (2005) noted that larger than a 3 metre resolution of optical and SAR images are useful for the visual interpretation of large landslides. He also proposed combining optical and SAR images, an image fusion technique, is particularly useful for the landslide inventory mapping in areas of retrogressive slides with low relief. One of the significant developments in the identification of landslides is the use of LiDAR (Light Detection and Ranging) technique. Using photons, rapid pulses of light energy particles, LiDAR can produce more detailed three dimensional models and images. The greatest advantage of the LiDAR technique is the use of shaded relief images created by the bare earth DEM (Digital Elevation Model), which allows more detailed interpretations of the landslide features placed even on heavily forested areas (Figure 2.2).

Reliable landslide hazard assessments are based on the detailed, accurate identification of landslides. Therefore, the use of appropriate identification and mapping technique is the key component for mitigation and prevention strategies in the area at risk.

2.1.3.2 Investigation of landslide characteristics

Identifying the relationship between landslide behaviours and their causal factors, which give an appropriate understanding of potential consequences due to land-



(a)



(b)

Figure 2.2 Comparison of LiDAR and conventional optical images. a. SRTM (NASA Shuttle Radar Topography Mission) satellite image along the Heart River flowing northwest, near Town of Peace River, Alberta. b. LiDAR bare earth image which has the same extent of a. Scale 1:15,000

slides, is the essential part of all landslide studies as well as reliable landslide hazard assessments. The site reconnaissance, sometimes included in the category of the hazard identification as previously described (Crozier and Glade 2005), is often applied to support the identification of previous and potential landslides by detecting subtle landslide evidences which cannot be identified by conventional aerial imageries (Highland and Bobrowsky 2008). During the site reconnaissance, landslide features (scarps, tension cracks, grabens, transformation, and accumulation zones of the landslide debris) can be identified and analyzed. Drilling programs, which determine the subsurface stratigraphy as well as the identified and potential rupture surfaces, and collect representative samples in order to understand mechanical properties of subsurface materials, can support the site reconnaissance in areas of concern which provide significant information about physical characteristics of displaced materials.

Instrumentation can be used to determine the movement mechanism of potential landslides and monitor the possible landslide movement which may transform into a hazard. Mikkelsen (1996) divided instruments in landslide studies into three categories: (1) surface measurement devices for example, tiltmeters, differential GPS (Global Positioning System); (2) ground displacement measurement devices such as inclinometers, extensometers; and (3) groundwater monitoring devices like piezometers. Advances in remote sensing techniques enable the detection of very small ground movements that had not been measured by conventional instruments. The application of satellite-borne or ground interferometric synthetic aperture radar (InSAR) and terrestrial LiDAR has expanded their feasibility for monitoring landslide movement (Morgenstern and Martin 2008). Rott et al. (1999) demonstrated benefits and limitations of the InSAR technique for the long term monitoring of the slope above a hydropower reservoir in the Austrian Alps. Recently Singhroy and Molch (2004) discussed the application of InSAR for the post slide motion of a large rock avalanche in the Canadian Rockies. Martin et al. (2007) demonstrated the evaluation of the rock slope deformation by using the terrestrial LiDAR system and compared with the digital photogrammetry.

When conducting landslide hazard assessments for a specific area, identification of geomorphological and geological conditions exposed in the study area, which may be treated as thresholds for guidelines to the landslide instability, can provide substantial benefits from thorough investigations of landslide characteristics (Popescu 1994). These characteristics are also, in turn, related to remedial measures for mit-

igation and prevention plans. Popescu (1994) discussed these characteristics as landslide causal factors and classified them into the following two categories based on their functions (though such clear separation is not always attained).

“Preparatory causal factors” move slopes from a stable to a marginally stable stage without actual initiation (Ground conditions).

“Triggering causal factors” initiate landslides. Slopes can be transformed from marginally stable to unstable stage (Geomorphological, physical, and man-made processes).

Figure 2.3 shows continuous changes in the factor of safety within a slope due to causal factors described earlier. The temporal distribution of the factor of safety is affected by preparatory as well as triggering factors. It also exerts the first-time or reactivated landslide movements which is dependent on the state of activity (Figure 2.3). Detailed explanations for causal factors are covered by Chapter 5.

2.1.3.3 Implementation of countermeasures for landslide hazard assessments

Most landslide countermeasures applied up to 1990s were focused on remedial measures, mainly by using geotechnical structures, after the landslide occurred. Whereas these are effective in terms of the mitigation, they seem to be insufficient from the prevention and preparation points of view. In other words, socio-economic impacts due to landslides such as human casualties and property damages would increase, or at least maintain the current average, unless the estimation where future landslides occur is performed. In addition, climate change like global warming would make landslide triggering factors occur more frequently than in the past. Therefore, a systematic process that identifies temporal and spatial information from dated landslides, understands the information that will play important roles in future landslide events, and provides appropriate countermeasures based on landslide hazard assessments may become a major interest in landslide studies.

Classical landslide remedial measures were mainly based on geotechnical engineered structures. The International Union of Geological Sciences Working Group on Landslides (2001) discussed four conceptual landslide remedial measures: (1) modifications of slope geometry; (2) drainages; (3) retaining structures; and (4)

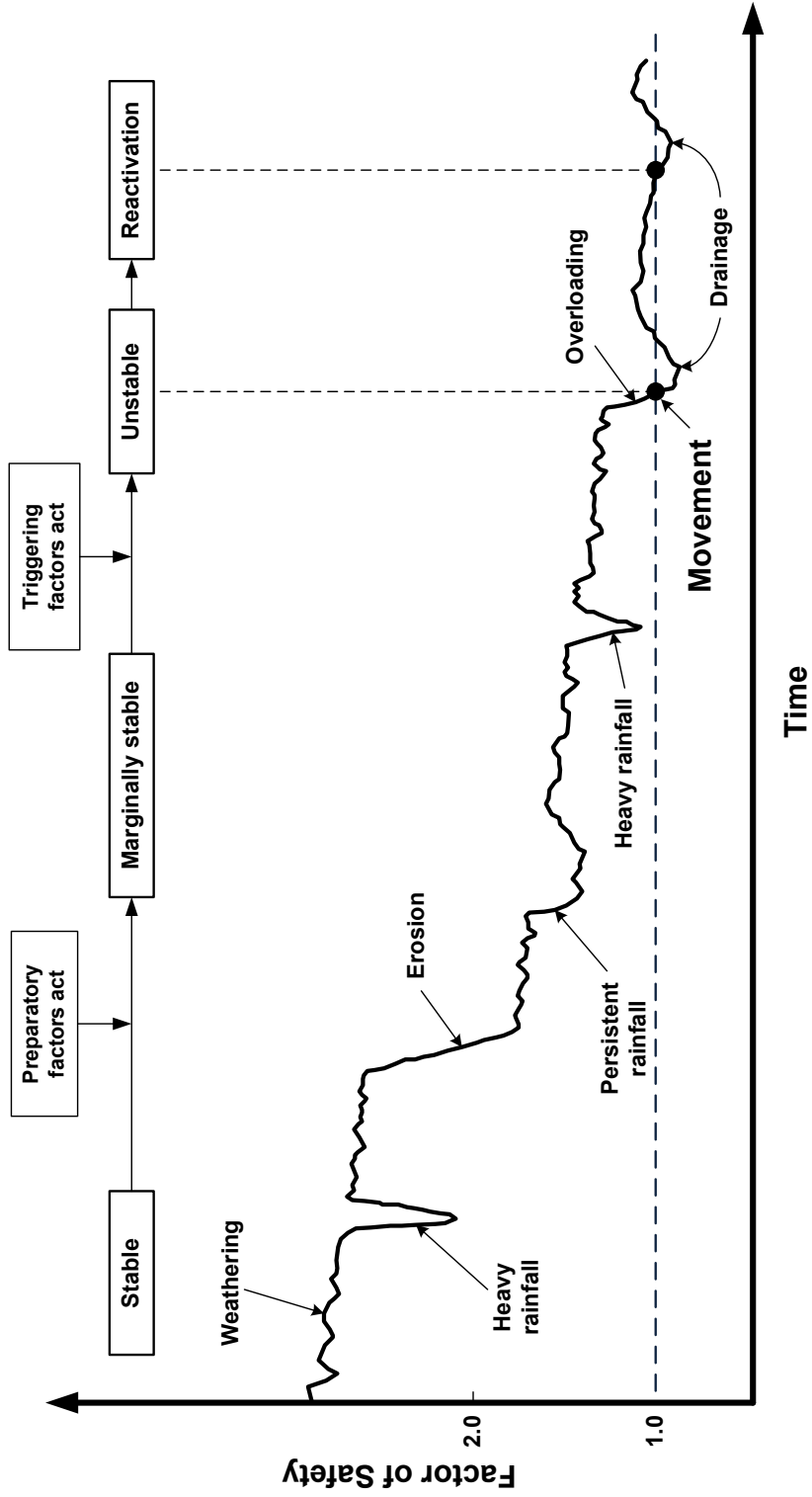


Figure 2.3 Changes in the factor of safety by causal factors. Examples of preparatory and triggering causal factors are also described. *Source:* Popescu 1994, Fig. 1

internal slope reinforcements. Monitoring potential landslides and disseminating early warning signals to areas at risk have been adopted recently in many countries. Besides structural measures, non-structural measures are also applied as landslide remedial measures by the means of zoning districts and regulations or codes (Schuster and Highland 2007). Land use zoning and sewage disposal regulations are common means of landslide remedial measures performed by local governments in the United States. Safety information and education against landslides and landslide insurance program are other indirect non-structural examples of landslide remedial measures. Transitions from structural to non-structural measures tend to increase as landslide hazards have been treated as complex, integrated concerns rather than a single geological disaster.

Landslide assessments, either susceptibility, hazard, or risk assessments, enable this transition more effectively. Ranging from simple inventory maps to complicated analytical methods, landslide assessments have been used as mitigation tools to reduce landslide hazards (Highland 1997). Determining the frequency and magnitude of previous landslides obtained from the landslide inventory can be used as guides to other areas whose environments are similar to the mapped areas. Complex landslide assessment approaches such as probabilistic methods provide not only estimates of upcoming landslide events but also optimized and prioritized directives before and after disastrous situations. Detailed landslide assessment methods are discussed in Section 2.2.

In addition, developments of computing systems and GIS (Geographic Information System) techniques have increased in use for landslide hazard assessments with accurate and rapid responses to landslide conditions that are continuously changing. Integrated into database formats, information embedded in GIS systems can enable more precise estimations for possible upcoming landslide events in both spatial and temporal perspectives (occurrence, date, and location). GIS also supports decisions on mitigation, prevention, and even evacuation plans against landslides.

2.2 Landslide hazard assessment analyses

Identifying landslide prone areas, mapping landslides, and evaluating expected risks to population, property, environment, and other resources are progressive studies which require land use, engineering design work, and emergency planning to reduce impacts by landslides (Hervás and Bobrowsky 2009). These sequential processes generally demand appropriate data collection with proper scale and cost effective methods, and comparable models to produce reliable assessment systems.

Hervás and Bobrowsky (2009) proposed a general sequence implementing landslide hazard assessment systems through four levels: (1) depict the past and current landslides (landslide inventory); (2) identify the area of the spatial probability for future landslides (landslide susceptibility); (3) distinguish the area of the spatial and temporal probability for future landslides (landslide hazard); and (4) estimate damages of future landslides (landslide risk). Hervás (2003) also noted various measures and actions to landslides and corresponding assessment systems in which relevant authorities should cooperate and play roles to implement the effective response.

Recognizing basic concepts and assumptions which are inherent in each landslide assessment methodology would provide a general idea to understand the overall structures and functions of landslide hazard assessment systems and can update or improve the system in case of changes in external environments.

This section, therefore, provides general reviews of representative methodologies for landslide hazard assessment analysis, relying on those widely used in practical exercises. Brief summaries of their basic functions, key approaches, and typical examples are outlined. Discussions on fundamental concepts with regards to landslide hazard assessment analyses are also described. I cover landslide inventory mapping, landslide susceptibility and hazard assessments, and finally, landslide risk assessment, respectively.

2.2.1 Landslide inventory mapping

The objective of the landslide inventory can be defined as “to identify, map and classify areas of natural landslides and to assess their state of activity in order to establish an accurate and complete database of past and present slope movements in

the study area” (Jennings and Siddle 1998). In other words, landslides often occur where previous activity existed. Therefore, the understanding of past and current landslides may provide significant information about future landslides in an area in which landslide hazards are assessed. This information also could be integrated into a system to forecast the impact of future landslide events in areas of residences and transportations. Information on such landslides can be represented as forms of an inventory, which denote areas identified as landslides (Highland and Bobrowsky 2008). Hervás and Bobrowsky (2009) noted that requirements for the landslide inventory are to take the spatial distribution of the past and current landslides and their characteristics, to identify major casual factors and their actions, and to provide reliable assessment systems using volume-frequency analysis. Landslide inventories can be compiled at different temporal and spatial scales as well as based on their different purposes (Galli et al. 2008).

The early landslide inventory study carried out by Pašek (1975) provided a preliminary structure of the landslide inventory which functions in computer-based environments. Another example by Carrara and Merenda (1974; 1976) used an inventory mapping mainly based on the morphometric field investigations for landslides and rapid erosions in southern Italy. This proposed inventory mapping provides standardized working criteria, a basis for further sophisticated landslide assessments, and insights into the soil conservation and land use planning. A study on the nation-wide inventory mapping, as bibliographical and archival forms, for landslides and floods in Italy was carried out by Guzzetti et al. (1994). Over 9,300 historic hydro-geologic events including landslides and floods were identified through this inventory and can be used as a source for future landslide hazard and risk assessments on a regional basis. Other relevant works on the landslide mappings can be found in Jennings and Siddle (1998) who studied landslides in deeply incised valleys in UK and Brardinoni et al. (2003) who discussed how forest canopies usually hamper the correct interpretation of evidence of previous landslides during the landslide inventory mapping by comparison with traditional aerial photo interpretations with field surveys in rugged watersheds located in British Columbia. A recent study by Chau et al. (2004) discussed the application of the landslide hazard assessment which is based on inventory mapping and GIS with various information such as geologic, geomorphologic, and climate data. After establishing previous landslide distributions of 1,448 landslides from 1984 to 1998 by inventory mapping, they noted a relationship between landslide consequences and rainfall.

A global scale landslide inventory was initiated by the International Geotechnical Societies' UNESCO Working Party on World landslide Inventory (deLugt and Cruden 1990). It suggested a framework for the compilation of landslides and also included suggestions how to report and summarize the identified landslides incidences. The World Landslide Inventory had been transferred later to the database management system (Brown et al. 1992).

In Alberta historical landslides was compiled by Cruden et al. (1990a). Spangenberg (1993) proposed the Alberta Landslide Inventory initiated by the Alberta Environment since 1984, to identify areas of concern in the selection of sites for infrastructure such as transportation routes. The compilation of landslides in the Peace River district which had occurred in the Holocene Epoch (Quaternary Period) was carried out by Davies et al. (2005). Using a surficial geology map and aerial photo interpretation, they listed 157 landslides and extensive colluvial sediments deposits in the landslide inventory including their dimensions, material types, and mode of movements (Figure 2.4). Scale issues, however, can emerge when landslide features are represented as points rather than polygon or line features (Davies et al. 2005).

2.2.2 Landslide susceptibility and hazard assessments

Although landslide inventories provide critical information about past and current landslide conditions in an area, they are unlikely to give further knowledge with respect to future evolution of landslides such as spatial and temporal distribution. Landslide susceptibility and hazard assessments may play an important role in establishing the future framework.

However, both terms, 'susceptibility' and 'hazard' of landslides, have been frequently misused even in professional groups. A 'hazard' refers to the probability of landslide occurrence in a specified period of time and within a given area (Guzzetti et al. 1999; Hervás and Bobrowsky 2009; Varnes and IAEG Commission on Landslides and other Mass Movement on Slopes 1984), which includes volume of event and frequency. On the other hand 'susceptibility,' often refers to 'propensity,' indicates the probability of occurrence of a landslide within a given area (Hervás and Bobrowsky 2009). Due to the difficulty of obtaining temporal data, the landslide susceptibility assessment is likely to be a substitute for the hazard assessment.

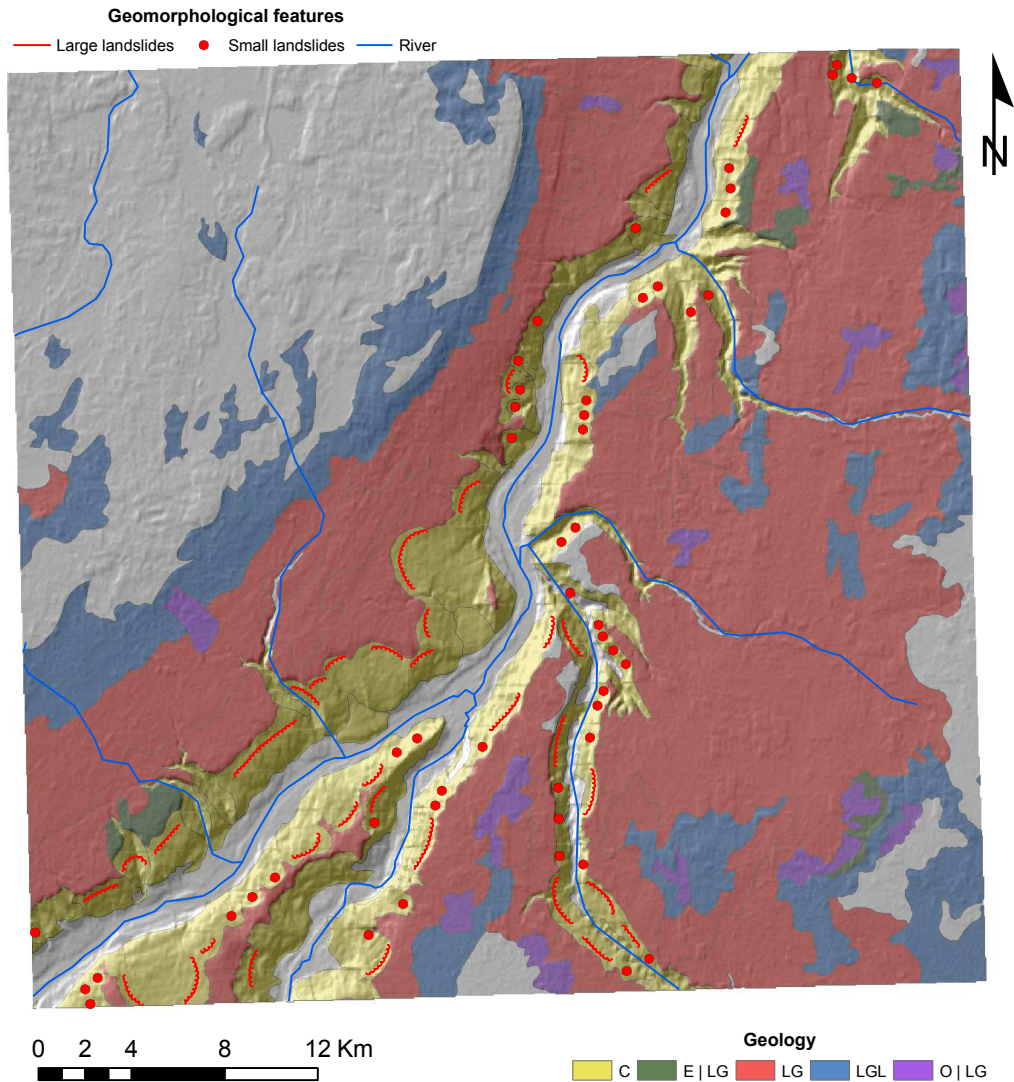


Figure 2.4 Landslide inventory mapping in the Peace River area, Alberta. The location of landslide features is illustrated by red solid lines and circles based on their size. Large landslide symbols indicate the scarp of landslide while small landslide symbols represent the centre of the slide. Major rivers including the Peace, Smoky, and Heart Rivers and their tributaries are also described by blue solid lines. Geologic unit symbols illustrated in this figure are C: colluvial deposits, E|LG: eolian veneer overlying glaciolacustrine deposits, LG: deep water glaciolacustrine deposits, LGL: littoral and near shore glaciolacustrine deposits, and O|LG: organic veneer overlying glaciolacustrine deposits, respectively. A shaded relief image shown in background is obtained from SRTM dataset. *Source:* Data from Davies et al. (2005)

Temporal data such as a volume-frequency relationship, however, enables one to find a correlation between the landslide initiation and triggering factors and relates the spatial frequency to the return period (van Westen et al. 2006). The fundamental concept or assumption with regard to landslide susceptibility and hazard assessments is documented by Varnes and IAEG Commission on Landslides and other Mass Movement on Slope (1984, pp. 10-11) in the following brief statements:

“The past and present are keys to the future” denotes that future landslides are likely to occur where similar geologic, geomorphologic, and hydrologic conditions are present. These features can be recognized and classified by various methodologies.

“The main conditions that cause landsliding can be identified” means that the landslide casual factors, either preparatory or triggering, can be recognized and weighted. Through these processes mechanisms of landslide driving the failure can be understood.

“Degrees of hazard can be estimated” describes that relative contributions to the overall landslide instability which can be estimated.

Most approaches to landslide susceptibility and hazard assessments largely depend on project objectives, landslide processes and their environments including the scale (Hervás and Bobrowsky 2009). But the most important factor to determine appropriate susceptibility and hazard assessments can be the availability of input data.

Many studies have proposed to use different methodologies and have evaluated them by comparing each methodology (Brabb 1991; van Westen et al. 2008). Representative examples can be found in Carrara et al. (1977; 1978), Rib and Liang (1978), Carrara (1983), Brabb (1984), Hansen (1984), Varnes and IAEG Commission on Landslides and other Mass Movement on Slopes (1984), Hartlén and Viberg (1988), Soeters and van Westen (1996), Aleotti and Chowdhury (1999), Guzzetti et al. (1999), Dai et al. (2002), Chacón et al. (2006), van Westen et al. (2006), and Hervás and Bobrowsky (2009). Despite their diversities, major generic characteristics can be classified into two ways, which have considerable differences in calculating or weighting factors, for examples, using either expertise (or experience) - qualitative, or mathematics - quantitative (Table 2.1).

Table 2.1 Classification of landslide susceptibility and hazard assessments. Explanation of each method can be found in the text. *Source:* Data adapted from Hervás and Bobrowsky (2009)

Category		Specific methodology
Qualitative (Heuristic)	Direct	Geomorphological mapping
	Indirect	Weighting (indexing) method (Qualitative map combination [†]) (Numerical rating of contributing factors [‡])
Quantitative	Indirect	Landslide density mapping
		Statistical methods
		Physically based methods (Deterministic approaches [†])

[†] Soeters and van Westen 1996.

[‡] Varnes and IAEG Commission on Landslides and other Mass Movement on Slopes 1984.

Qualitative approaches, often called heuristic methods, are relatively descriptive and subjective, and can be divided into two distinct methods based on the data manipulation processes (Soeters and van Westen 1996). A direct qualitative approach or geomorphological mapping technique would apply geomorphological surveys by experienced geomorphologists to landslide hazard mapping procedures. In contrast to the direct method, indirect or weighting approach employs weighting of factors contributing to landslide occurrences. Results of this method can be produced by combining layers of prioritized factors in which classes are also classified by their relative contribution or priority. These approaches usually require experienced personnel, therefore they are unlikely to maintain the quality of landslide assessments independent of expertise. Carrara (1983) also noted limitations in implementing qualitative landslide assessments as follows: (1) subjectivity; (2) difficulty in extrapolation or extension of models to other areas; and (3) absence of precedent works such as a landslide inventory mapping. Therefore, studies to reduce the subjectivity inherent in qualitative approaches have increased with the addition of new concepts or modification of existing ones. Recent results can be found in Ayalew et al. (2005b), Komac (2006), Yoshimatsu and Abe (2006), Yalcin and Bulut (2007), Boroushaki and Malczewski (2008), and Ercanoglu et al. (2008), all of which employed an analytical hierarchy process (AHP) which is the semi-quantitative model originally proposed by Saaty (1990) who used a multiple criteria evaluation approach that considers both subjective and objective factors (Yalcin 2008).

Qualitative approaches, despite pitfalls, are relatively fast, cost effective, and also suitable for crude estimations of the landslide susceptibility and hazard assessments especially in regional landslide studies (Hervás and Bobrowsky 2009). Brief explanations of qualitative approaches are described in the following sections.

2.2.2.1 Geomorphological mapping

Geomorphological mapping, or the cartographic method, uses information for landslide hazard classification in a qualitative or semi-quantitative way in order to establish the degree of hazard (Varnes and IAEG Commission on Landslides and other Mass Movement on Slopes 1984). Information used to evaluate the degree of hazard varies and depends on the objectives of the study. But closely related factors to landslides like geologic units, slope are frequently used.

The preliminary approach using the geomorphological mapping can be found in Europe (Carrara and Merenda 1974). Carrara and Merenda (1974) established an inventory method for slope instability in southern Italy needed gathering field data and related map symbols. They also noted that the proposed scheme gave benefits for further enhanced methodologies by means of either analyzing or presenting. Another example of an early study was carried out by Mahr and Malgot (1978). The zoning map they provided was based on the degree of stability of slopes which was determined by engineering geological characteristics (geologic, morphologic, and hydrologic conditions) and divided into three zones such as unstable, relatively stable, and stable areas.

Kienholz (1978) carried out a pioneering study on landslide hazards in mountainous regions of Switzerland by using geomorphological mapping techniques. He proposed two basic maps, geomorphological and combined hazard maps which were derived from the geomorphological mapping (Kienholz 1978, Figures 2 and 5). The geomorphological map delineated geomorphologic features containing topography and relief, hydrography, erosion and mass movement, accumulation, anthropogenic activities, and morphographic signatures with their unique codes and colors. The combined hazard map described the degree of hazard based on the degree of danger depending on the influence and frequency of specific landslide processes and the type of dangers of avalanches, rockfalls, landslides, and water. These components are differentiated by using predefined notations (underlined upper case, upper case, and lower case letters).² These techniques were further enhanced to identify landslide hazards in the Colorado Front Range (Dow et al. 1981; Kienholz and Bichsel 1982), mountainous areas of Nepal (Kienholz et al. 1983, 1984; Zimmerman et al. 1986).

Natural hazard mapping using the geomorphological method for land use planning in the northern San Juan Mountains, Colorado was carried out by Ives and Bovis (1978). They made three different maps, geomorphic, snow avalanche, and combined hazards assessments, which were generated by geomorphological mapping with NASA LANDSAT color IR underflight imagery and field investigations. The combined hazard map showed overall impacts of geomorphic and snow avalanche, and provided five different categories of the hazard based on their impacts.

²For example, 'A' is avalanches of degree 3, 'F' is rockfalls of degree 2, and 's' is landslides of degree 1, respectively (Kienholz 1978).

Slope instability hazard zoning exercises induced by earthquakes in the U.S. National Forest areas were carried out by geomorphological mapping (Seeley and West 1990). Detailed stereoscopic analysis with limited field reconnaissance was augmented in order to delineate different hazard zones. The hazard map was based on the mapped slope instability features having either active or potentially active states and corresponding zones of different degrees of the hazard (high, moderate, and low hazard zones). They also noted the significance of the slope instability hazard map which was compared to the other maps such as seismic shaking hazard maps because of its frequent occurrence.

Practical applications of the geomorphological method were implemented on steep topography in Hong Kong. A Geotechnical Land Use Map (GLUM), which comprised the base map, terrain classification map, and engineering geology map, was compared with conventional engineering approaches (mainly calculating the factor of safety) to increase its reliability for landslide hazards (Styles et al. 1984; Brand 1988). A recent study by Devonald et al. (2009) showed the application of geomorphological mapping into a site-specific model to identify characteristics of natural hill slopes and evaluate geomorphological conditions.

2.2.2.2 Weighting (indexing) method

Weighting (indexing) methods, or qualitative map combinations (Soeters and van Westen 1996), have been devised to reduce the subjectivity which is apparent in direct qualitative methods. The principle of this method is the numerical rating of contributing factors (Varnes and IAEG Commission on Landslides and other Mass Movement on Slopes 1984). In other words, landslides usually occur by the combination of various factors and these factors may contribute to the instability of slopes based on the relative degree of influence. Therefore, weights are imposed to factors according to their relative contribution to landsliding. Each factor can be represented as parameter maps: geology, slope, aspect, proximity to drainage, and land use. Each weighted assigned parameter map is divided into a series of classes based on their relative importance which depends on the professionals' expertise. For example, the slope map can be classified as less than 10, 10 to 30, and over 30 degrees, respectively. Identifying weighted values and combining them would lead to the relative potential for the landslide susceptibility and hazard in an area of concern. This method, in turn, would benefit to assess and evaluate the role of

each contributing factor in landslide occurrences (Varnes and IAEG Commission on Landslides and other Mass Movement on Slopes 1984). Figure 2.5 shows the general procedure in implementing weighting methods for landslide susceptibility and hazard assessments, which is similar to those proposed by Soeters and van Westen (1996).

Stevenson (1977) made an early contribution to the weighting method. He devised a simple weighting method to measure the relative risk of landslides for land use planning and insurance purposes. He employed five factors, clay, water, slope angle, slope complexity, and land use. They can be worked as a pair based on the interaction with each other: (1) clay and water factors; (2) slope angle and slope complexity; and (3) land use. The risk results from the product of these three terms is as follows:

$$Risk, R = (P + 2W) \cdot (S + 2C) \cdot U \quad (2.11)$$

where P is clay, W is water, S is the slope angle, C is the slope complexity, and U is land use factors, respectively. Calculated values of 60 or more can be treated as a failed status whereas values of over 50 are used as a warning of possible instability. Varnes and IAEG Commission on Landslides and other Mass Movement on Slopes (1984) indicated Equation (2.11) is equivalent to other equations defining the landslide risk if the first two terms of right hand side of Equation (2.11) are assumed to the hazard (H) and the last term is considered as the vulnerability (V), respectively.

Other examples of the application for this method were carried out by other authors. Krohn and Slosson (1976) defined potential landslide areas in the United States by three principal conditions, topography, type of bedrock, and precipitation. The first two components were used to establish the degree of the landslide potential such as low, low but steep relief, medium, and high. Precipitation data which is represented as a mean annual rainfall was augmented to these ratings to make landslide potential areas influenced by the climate factor. They also discussed the nationwide risk assessment by projecting limited estimations of numerous localized studies. Based on those localized estimations the total risk of casualties due to all type of landslide occurrences can overtake approximately 25 lives per year (Krohn and Slosson 1976). Meneroud (1978) employed a numerical system to determine a risk on a highway route. Various factors such as topography, discontinuity of rock, vegeta-

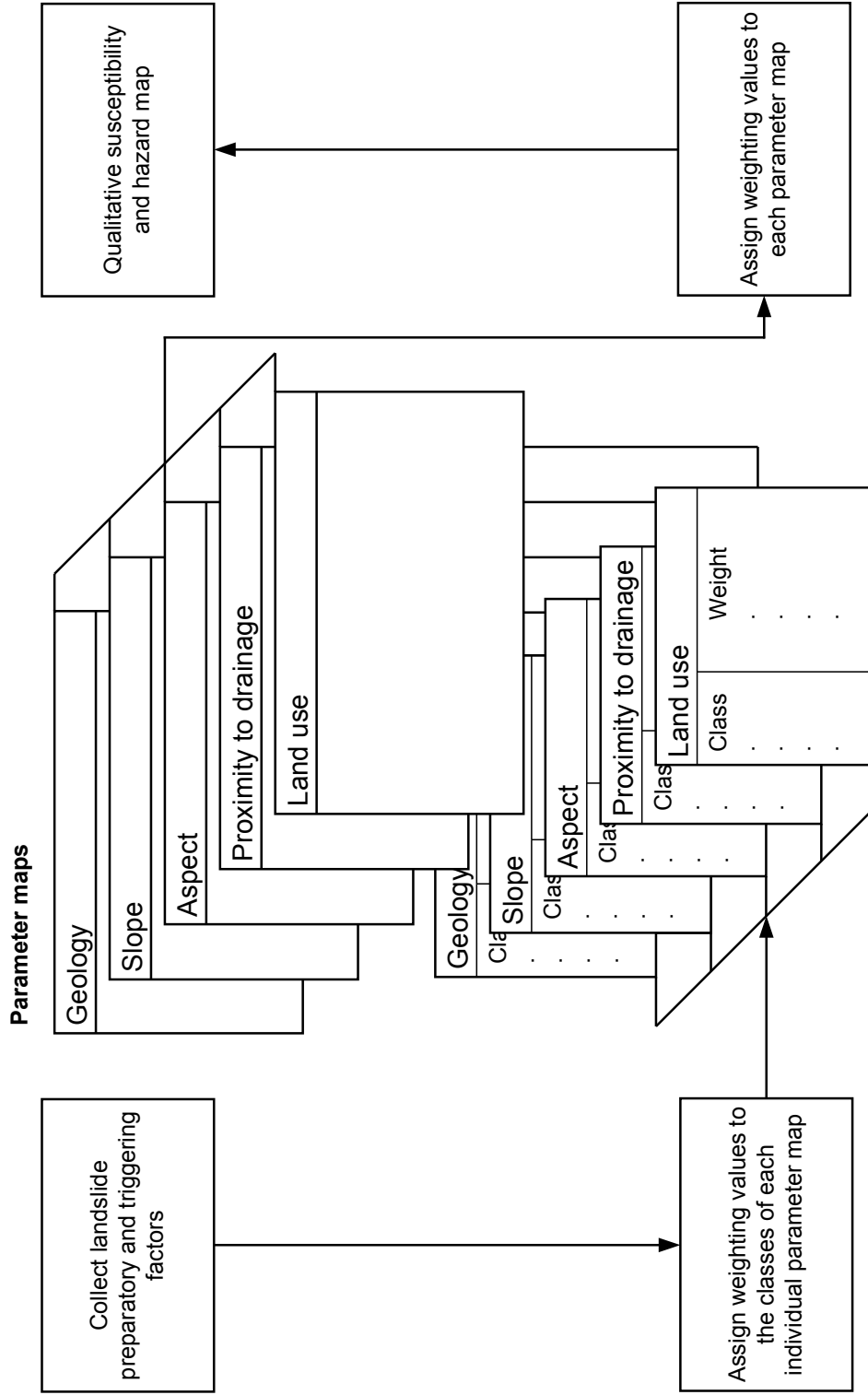


Figure 2.5 Diagram showing representative procedures for implementing the weighting method. Detailed explanations are in the text. *Source:* Soeters and van Westen 1996, Figure 8-16

tion, availability of the protection, previous landslide history, and hydrology were linearly reclassified or rescaled into three numerical values (0, 1, and 2) and added to produce the degree of risk. Vecchia (1978) proposed a terrain index describing the terrain quality of natural hill slopes comprising three different parameters related to: (1) lithology; (2) attitude; and (3) friction (negative values). The terrain index was obtained by simple algebraic sum of these three terms. The terrain index (I_t) with a range between zero (bad) and 100 (favorable) can be used for stability evaluation on hillsides or scarps. Green et al. (1998) made a hazard map which was based on weighted factors believed to be triggers for recent slope movements due to the dissolution of limestones in Durham. Recent studies of this method with the integration of GIS technologies can be found in Blais-Stevens et al. (2010) in two large pipeline corridors in northern Canada.

Although these techniques have proved to significantly reduce the subjectivity compared to other direct methods, it still exists when weights are allocated and then classified into the weighted parameter map. As described earlier, there are many examples to minimize this subjectivity which is inevitable in qualitative approaches. Another example of this effort can be found in Barredo et al. (2000) who compared direct and indirect qualitative methods in determining exact weights of each parameter map. Their study was supported by GIS technology to represent and combine parameter maps for the numerical presentation of landslide susceptibility and hazard.

Other considerations with regard to the proper weighting method are the availability of data used for engineering judgement. Soeters and van Westen (1996) noted that insufficient field investigations and corresponding lack of data would lead to wrong decisions in weighting and classification processes.

Quantitative approaches, mostly indirect, require stepwise procedures, and are subdivided into landslide density, statistical (probabilistic), and physically-based (deterministic) approaches (Hervás and Bobrowsky 2009). The landslide inventory can be analyzed numerically to estimate future landslides where the past and current landslides are abundant. The landslide density usually described by isopleths indicates areas covered by landslides in total area. The mathematical relationship is the core of statistical approaches, which correlates casual factors that may influence landslides with the past and existing landslide distributions obtained through the landslide inventory mapping. Various statistical techniques have been applied to

landslide susceptibility and hazard assessments. Many of them fall into categories of bivariate or multivariate (Soeters and van Westen 1996).

Physically based approaches, deterministic or geotechnical models, apply some physical laws that control the slope stability in an area such as the principle of limit equilibrium which calculates quantitative values like factors of safety. Applications of this method may benefit to understand the mechanism of particular types of landslides such as translational slides, assuming that their rupture surfaces are infinite and specific landslide triggering factors play important roles in the landslide initiation. For instance, a triggering factor such as the pore water pressure ratio which represents a relationship between the groundwater level and the thickness of slope can be repeatedly evaluated to simulate the impact of changes in the input data. The main problem with this approach is a tendency of the high degree of simplification and expensive procedures for the data collection.

2.2.2.3 Landslide density (isopleth) mapping

Landslides commonly occur in areas where previous landslide features can be identified rather than in areas having no such features. Therefore, collecting data for old landslides might be the initial procedure which leads to a possible estimate of type, extent, and consequence of the future landslide activity. The landslide inventory mapping is useful to identify previous landslide information. It can also estimate the extent of potentially unstable areas affected by future landslides. Most landslide inventories, however, simply show the qualitative information related to the existence of the past and current landslides. Therefore, it is necessary to transform the non-quantitative inventory data into a numerical one for use in reliable landslide hazard assessment. Identifying a landslide density within a given area is the one of the methods, which quantifies the aerial distribution of landslide deposits derived from an inventory map (Wright et al. 1974). An isopleth map, connecting equal rates or ratios computed for the unit area by lines (Schmid and MacCannell 1955), makes the discontinuous landslide information into a continuous form. It is prepared by the arithmetic division of landslide deposits within the study area by the area of specific unit (usually circle) and drawn lines (isopleths) through computed points, which represent equal percentages of the land cover occupied by landslides. Early isopleth maps used for landslide studies were prepared for the Point Dume quadrangle, California (Campbell 1973), southern San Francisco Bay region

(Wright and Nilsen 1974), and Washington County, Pennsylvania (Pomeroy 1978). All of these examples indicated advantages of using the isopleth map in order to generalize and quantify the areal distribution of landslide deposits and to combine with other data in preparing derivative maps (Varnes and IAEG Commission on Landslides and other Mass Movement on Slopes 1984). General steps in constructing the isopleth map described by Wright et al. (1974) are summarized in Table 2.2.

Table 2.2 General steps in constructing the isopleth map. Schematic diagrams for each procedure are described in Wright et al. (1974, Figure 2)

Step no.	Description
A	Prepare a landslide inventory
B	Construct a counting circle inscribed with grids
C	Overlap a counting circle on the landslide inventory
D	Record the number of grids covered by landslide deposits within the counting circle
E	Draw isopleths connecting equal percentages of area covered by landslide deposits

Landslide density mapping is a useful means for preliminary landslide hazard assessment in large areas since it only needs a landslide inventory map by site investigation and aerial photo interpretation. It can also compare landslide mechanisms if provided by isopleth maps for different type of landslides, identify changes in landslides over time, and determine landslide hazard zones without other relevant information (DeGraff and Canuti 1988; Bulut et al. 2000). De Graff (1985) used the isopleth map as a tool for timber sale planning in the Sierra National Forest.

2.2.2.4 Statistical methods

Statistical methods, employed by many geologists for data analysis since the late fifties expanded with computers (Davis 2002), and have advanced their capability for landslide hazard assessments since the late seventies. In order to reduce subjectivity which is most restrictive factors in applying qualitative approaches to landslide susceptibility and hazard assessments, these statistical approaches utilize statistical processes in determining the relative contribution of factors which are

believed to occur landslides. The main assumption, therefore, is the same as other direct qualitative hazard assessments described earlier: there is a strong connection between factors and corresponding landslides as identified by landslide inventory or landslide density mappings, and landslide hazard assessments are a step wise effort to find these connections in order to identify potential landslide occurrence in the future. However, the apparent difference can be emerged in determining weights to landslide influencing factors. In qualitative methods, such as a weighting method, experience and expertise of experts are the main tools to allocate weights of each factor whereas statistical methods quantify each weight factor by mathematical calculations. Therefore, statistical methods make landslide hazard assessments irrelevant to the subjectivity but in order to get reliable results acquisitions of large datasets are inevitable (Soeters and van Westen 1996).

Statistical approaches can be divided into two categories which are dependent on the method of correlating each factor to the existing landslide distribution obtained from landslide inventory and density maps: (1) bivariate; and (2) multivariate. The bivariate statistical analysis finds inter-variable relationships between two variables (Carr 2002). Thus in the bivariate analysis how much does each class within each parameter map, for example grass land in the land use map, influence the existing landslides is calculated. The impact of each class on landslides can be represented as a form of density. van Westen (1997) proposed the landslide statistical index method or the information value method, originally introduced by Yin and Yan (1988), which used a bivariate analysis. The mathematical form in determining weighting values of each class within each factor map gives the following equation:

$$W_i = \ln \left(\frac{\text{Densclas}}{\text{Densmap}} \right) = \ln \left(\frac{Npix(S_i)/Npix(N_i)}{\sum Npix(S_i)/\sum Npix(N_i)} \right) \quad (2.12)$$

where W_i is the calculated weight of the i th class within a certain factor map, 'Densclas' is the landslide density covered in the i th class, 'Densmap' is the landslide density for the entire factor map, $Npix(S_i)$ is the number of pixels enclosed by the landslide in the i th class, and $Npix(N_i)$ is the number of pixels in the i th class, respectively. A similar relationship which is called the landslide susceptibility method has been proposed by Süzen and Doyuran (2004b):

$$W_i = 1,000 \left(\frac{Npix(S_i)}{Npix(N_i)} - \frac{\sum Npix(S_i)}{\sum Npix(N_i)} \right) \quad (2.13)$$

where weighting values are represented as a permillage (%). Negative values from Equation (2.13) mean the impact of the calculated class is minor on the stability of the slope and landslide occurrences. Repeated calculations of Equations (2.12) and (2.13) to other parameter maps and then overlaying them provide quantified values which relatively represent the potential of landslide susceptibility and hazards (Figure 2.6). Notwithstanding a quantitative approach, this method still needs an expert's opinion especially when the relative importance to each factor map is assigned (Aleotti and Chowdhury 1999). More data dependent bivariate statistical models to increase the subjectivity induced from professional judgements were carried out by Süzen and Doyuran (2004b). Çevik and Topal (2003) used the weighting factor method to assign a relative contribution on landslide occurrence to each factor map containing weighted classes. Usually the weighting factor for parameter maps has the value of one to 100 for each map and can be determined by the following equation:

$$W_f = \left(\frac{(W_i^{tot}) - (Min_W_i^{tot})}{(Max_W_i^{tot}) - (Min_W_i^{tot})} \right) \times 100 \quad (2.14)$$

where W_f is the weighting factor for each parameter map, W_i^{tot} is the total weighting index value within landslide deposits for each parameter map, $Max_W_i^{tot}$ is the maximum total weighting index value within all parameter maps, and $Min_W_i^{tot}$ is the minimum total weighting index value within all parameter maps, respectively.

Other popular methods based on this bivariate statistical analysis are the certainty factor (CF) method (Chung and Fabbri 1993; Luzi and Pergalani 1999; Lan et al. 2004), probability method (Chung and Fabbri 1999), and weights of evidence modeling (Spiegelhalter and Knill-Jones 1984; Bonham-Carter 1994; Neuhäuser and Terhorst 2007; Thiery et al. 2007), respectively.

An early study by Brabb et al. (1972) showed a simple calculation of the bivariate analysis by using geologic and experimental slope maps with the landslide inventory map to delineate the degree of landslide hazard for the subdivision land planning in San Mateo County, California. During the mapping procedure, they

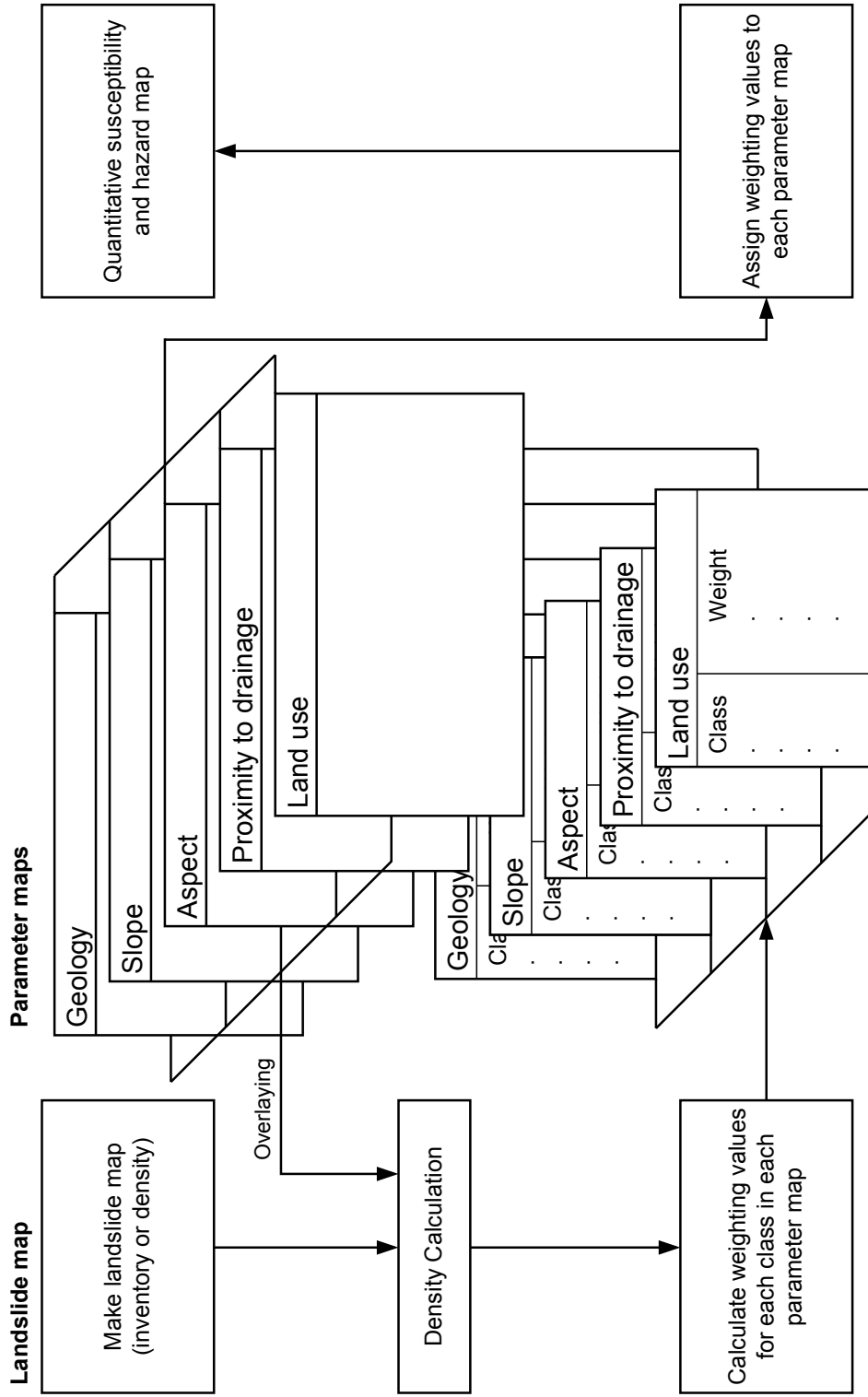


Figure 2.6 Diagram showing representative procedures for implementing the bivariate statistical method. Detailed explanations are in the text.
Source: Soeters and van Westen 1996, Figure 8-17

superimposed the landslide inventory map on the geologic map in order to find geologic units and their areas affected by landslides that are observed from the landslide inventory map. They then superimposed the slope map again on the combined map to evaluate the landslide hazard in each hazard category based on slope intervals. They noted a considerable generalization in small and narrow areas, which indicates a higher landslide potential than shown on the final map. They also mentioned some difficulties in interpreting areas which contain complex geologic units and are adjacent to unstable slopes and sea cliffs.

Most recent studies have focused on the evaluation of various bivariate analyses against other methods. For examples Süzen and Doyuran (2004a) compared the bivariate analysis with the multivariate analysis and discussed its applicability. They noted that in some areas the resultant susceptibility map did not match to existing landslide deposits and believed those areas were influenced by over-weighted classes. Ayalew et al. (2005a; 2005b) used a bivariate analysis as a preceding process for the comparison the results by the analytical hierarchy process (AHP) obtained from the logistic regression. Yalcin (2008) also compared bivariate analyses with the analytical hierarchy process (AHP) and found that the susceptibility map derived by the AHP method could give better results than those by using bivariate analyses especially in very high and high susceptibility classes. van Westen et al. (2003) evaluated the possibility of using the geomorphological information in bivariate analysis environments and noted the combination of direct and indirect methods may increase the overall accuracy of the landslide susceptibility map.

Landslides are the result of complex interactions between numerous elements, internally or externally, that can transform surrounding environments easily for landslides to occur. Davis (2002) also noted that “any observed variable can be considered to be a function of any other variable measured on the same samples.” Based on this statement landslide hazard assessments produced by the bivariate statistical analysis may have a critical pitfall to find the relationship of each factor. The main concept of multivariate statistical analyses employed in landslide hazard assessments is, therefore, that spatially identified phenomena (i.e., potential landslides) are the result of interactions between a large set of inter-related factors that are triggers to landslides (Carrara 1983). In multivariate statistical analyses all relevant factors with the landslide occurrence are sampled by various mapping units such as grid cells, terrain, unique condition, slope, and topographic units (Guzzetti et al. 1999). The availability of the landslide existence or absence is also investigated

(Soeters and van Westen 1996). Then the constructed matrix of sampled factors with landslide deposits as revealed by the landslide inventory or density map is analyzed by various multivariate statistical models such as multiple regression and discriminant analyses. Obtained frequency between zero and one with regard to the presence or absence of the landslide occurrence is represented (Figure 2.7).

Consider the linear polynomial regression which has only one independent variable (Davis 2002):

$$y_i = \beta_0 + \beta_1 x_{1i} + \beta_2 x_{1i}^2 + \cdots + \beta_m x_{1i}^m + \varepsilon_i \quad (2.15)$$

where y_i is a dependent variable at the location i , x_{1i} is an independent variable observed at the location i , and ε_i is a random error which is unique for the location i . β_m are coefficients of the linear equation and can be obtained by the least squares method. If provided with m independent variables, a general linear model for multivariate statistical methods can be presented as the following equation (Guzzetti et al. 1999):

$$y_i = \beta_0 + \beta_1 x_{1i} + \beta_2 x_{2i} + \cdots + \beta_m x_{mi} + \varepsilon_i \quad (2.16)$$

where y_i is a dependent variable at the location i describing the existence (1) or the absence (0) of landslide features or movements in each sampling unit. This value can be represented by the percentage of area covered by landslide deposits (Guzzetti et al. 1999), x_{mi} are independent variables measured or observed at each sampling unit of i and represent the landslide triggering or instability factors. β_m are coefficients of the equation and dependent of specific analysis methods. In multiple regression models, these are called the partial regression coefficients because they would influence dependent variables within a particular independent variable if all other independent variables are remained as constant (Davis 2002). These can also be named as discriminant scores or transformed variables in the discriminant model as the discriminant function would transform a multivariate problem into a one independent variable problem (Davis 2002).

With a mean value of y_i given as (Mendenhall et al. 2003):

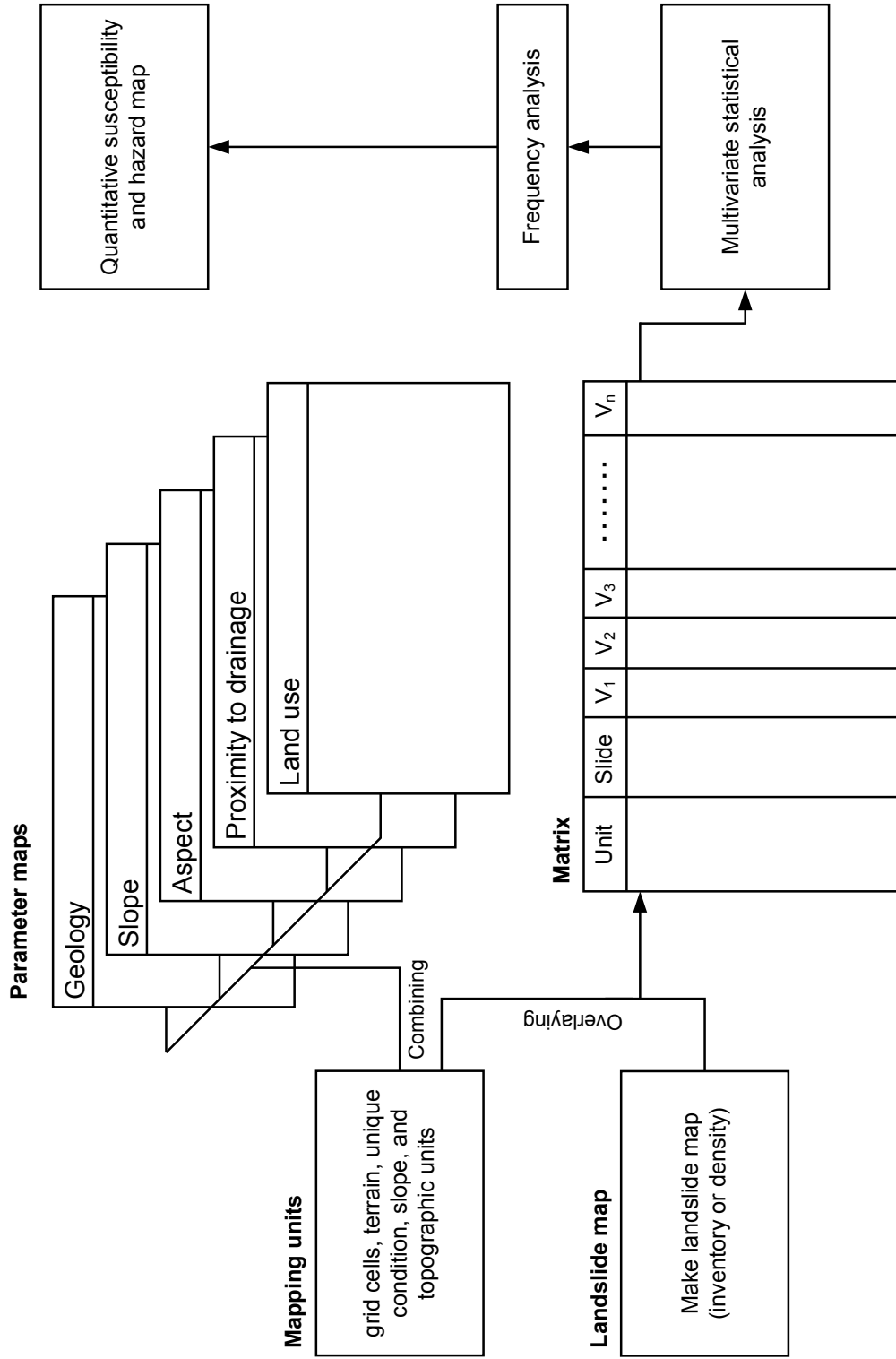


Figure 2.7 Diagram showing representative procedures for implementing the multivariate statistical method. Detailed explanations are in the text. *Source:* Soeters and van Westen 1996, Figure 8-18

$$E(y_i) = \beta_0 + \beta_1 x_{1i} + \beta_2 x_{2i} + \dots + \beta_m x_{mi} \quad (2.17)$$

In the discriminant analysis each cell unit takes values comprising of coefficients and factors of the discriminant function. The discriminant function depends on characteristics of factors within each sampling unit. If the cell unit is related to landslides (cell overlapping with landslide deposits), the resulting value of the dependent variable in Equations (2.15) to (2.17) will approach the value of one (the presence of landslide), in other words the cell unit will be separated from cell units containing no landslide features. Therefore, the coefficient of each variable in the discriminant function could indicate the relative contribution of each factor to the landslide susceptibility and hazard (Santacana et al. 2003).

Early efforts regarding multivariate statistical models are limited to petroleum research on tracing oil traps based on geological and geophysical variables (Carrara 1983; Aleotti and Chowdhury 1999) except for a few studies by Neuland (1976), Carrara et al. (1977; 1978), and Reger (1979) that included landslide hazard assessments. Comprehensive procedures to implement landslide hazard assessments supported by multivariate statistical methods are well described by Carrara (1983). He adapted discriminant and multiple regression models and showed their successful applicability. Guzzetti et al. (1999) attempted to identify the proficiency and limitations of multivariate models employed in central Italy. Santacana et al. (2003) employed discriminant analysis on shallow landslide susceptibility mapping with various parameters obtained automatically from a digital elevation model (DEM). They also mentioned that the inability to make a DEM in all areas would make this analysis difficult to carry out over the entire region since all input data have to be derived from the DEM. With increasing application of remote sensing technology and corresponding decreasing costs this drawback may disappear in the foreseeable future. Landslide susceptibility zoning by multivariate statistical methods was carried out by Ercanoglu et al. (2004). In Japan Tsurumi (2004) estimated the landslide probability along the national highways by the discriminant method. Another study by Pan et al. (2008) discussed a feasibility of multivariate regression analysis on the GIS-based landslide hazard assessment in a regional area of Japan.

Other multivariate statistical models which have gained popularity in recent years are the logistic regression method (Atkinson and Massari 1998; Rowbotham and Dudycha 1998; Dai et al. 2002; Dai and Lee 2003; Ohlmacher and Davis 2003;

Ayalew and Yamagishi 2005), the conditional analysis (Clerici et al. 2002, 2006; Ozdemir 2009; Clerici et al. 2010), and the artificial neural network (ANN) method (Aleotti and Chowdhury 1999; Ercanoglu 2005). The logistic regression or generalized linear modeling (GLM) forms a multivariate regression relationship between the dependent variable and several independent variables (Atkinson and Massari 1998). This analysis allows use of both binary and scalar values for independent variables and the resultant dependent variable can only be represented by two binary values (1 or 0). Therefore, predicted values can be incorporated by the probability form so that interpreted values would fall between one and zero (Dai et al. 2002). The main objective of logistic regression analyses is to find the best fit model to represent the relationship between the landslide occurrence describing the presence and absence and corresponding intrinsic factors (Ayalew and Yamagishi 2005).

This relationship and corresponding variables which influence the probability value are shown by the following equation:

$$P_r = 1/(1 + e^{-Z}) \quad (2.18)$$

where, P_r is the estimated probability related to intrinsic factors of the landslide occurrence, Z is a dependent variable of the linear polynomial regression described in Equations (2.15) to (2.17). The generated curve from Equation (2.18) is a sigmoidal form which is s-shaped and nonlinear (Larose 2006). Therefore, as Z varies between $-\infty$ and ∞ , the P_r value has ranges zero to one. Differentiation of Equation (2.18) will describe the characteristics of the sigmoidal curve. The differential form of Equation (2.18) gives the following result:

$$P'_r = P_r(1 - P_r) \quad (2.19)$$

where,

$$P'_r = \begin{cases} 0 & P_r = 0 \text{ or } 1 \\ \text{Positive} & 0 < P_r < 1 \\ \text{Negative} & P_r < 0 \text{ or } P_r > 1 \end{cases}$$

Through logit transformation, Equation (2.18) can be converted into the ordinary linear regression model where the logistic link function is on the left hand side and the linear regression is on the right hand side (Atkinson and Massari 1998). The logit transformation is carried out by the following procedure:

$$G(x) = \ln \left(\frac{P_r}{1 - P_r} \right) = Z = E(y_j) = \beta_0 + \sum_{i=1}^m \beta_m x_{mj} \quad (2.20)$$

where, $P_r/(1 - P_r)$ is the odds or the likelihood ratio, and the natural logarithm of the odds, $G(x)$, is called a logit. Equation (2.20) is the linear model which has logit values as ordinate and independent variables as the abscissa. This linear model represents a logistic regression of landslide factors and the corresponding probability of the presence or absence of landslides. The logit transformation can provide linearity, continuity, and infinity ranges to logistic functions, which can be found in linear regression models (Larose 2006). Figure 2.8 shows a systematic relationship among the original data distribution, logistic function, and linear logistic regression.

The conditional analysis tries to find the probability of the landslide occurrence given a unique condition unit (UCU), which has a homogeneous domain containing identical characteristics and conditions (Bonham-Carter 1994; Guzzetti et al. 1999), equating the landslide frequency or density determined within each unique condition unit (Carrara et al. 1995). This gives the following relationship:

$$\begin{aligned} P(L|UCU) &= \text{Landslide density in UCU area} \\ &= \frac{\text{Landslide area deposited in UCU area}}{\text{Entire UCU area}} \end{aligned} \quad (2.21)$$

where $P(L|UCU)$ is the conditional probability of a landslide given within the unique condition unit. Descriptive terms in the right hand side can be rewritten by using the joint probability as follows (Bonham-Carter 1994):

$$P(L|UCU) = \frac{P(L \cap UCU)}{P(UCU)} \quad (2.22)$$

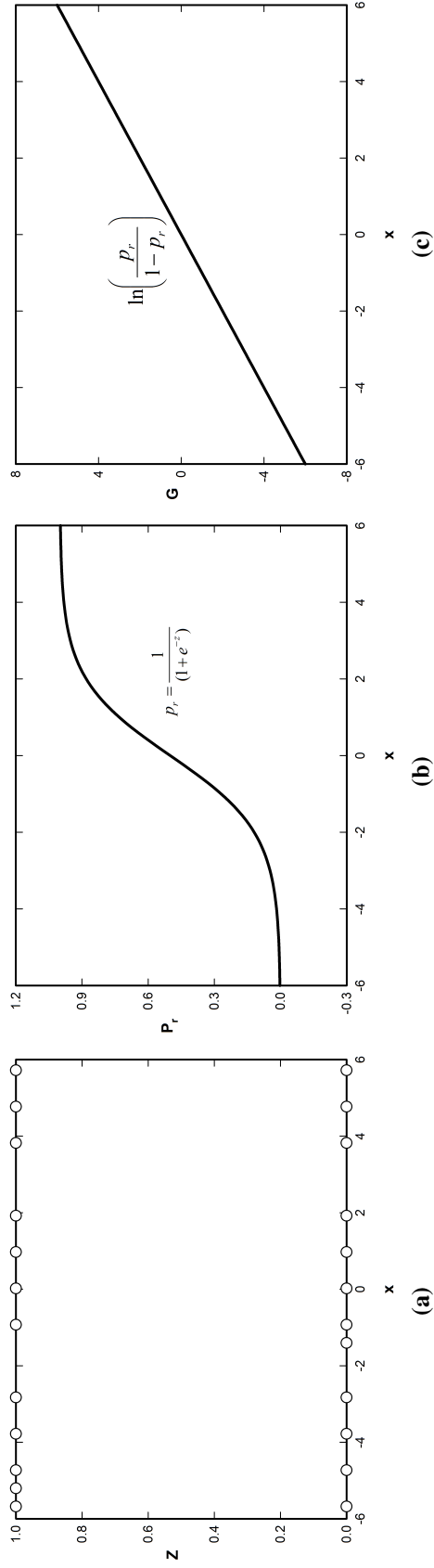


Figure 2.8 Systematic relationship in the logistic regression method. a. Original data distribution. Each individual data is represented by white solid circle, all of which are located on either 0 or 1. Dependent variables (Z) are located in the ordinate while independent variables (x) are shown in the abscissa. b. Logistic function of a . Sigmoidal curve showing the s-shaped and the nonlinear behaviour is delineated by the solid thick line. Estimated probability related to intrinsic factors of landslide occurrence (P_r) is indicated in the ordinate. c. Linear logistic regression of b . The linear trend of the plot is illustrated by solid thick line. The ordinate indicates a logit

where $P(L \cap UCU)$ indicates the joint probability of an area proportional to total area occupied by both L and UCU , and $P(UCU)$ is the probability of the unique condition in the unit area within the total area. Denote $N(T)$ to the count of unit cells in the entire area, Equation (2.22) gives the following result:

$$\begin{aligned}
 P(L|UCU) &= \frac{P(L \cap UCU)}{P(UCU)} \\
 &= \frac{N(L \cap UCU)/N(T)}{N(UCU)/N(T)} \\
 &= \frac{N(L \cap UCU)}{N(UCU)}
 \end{aligned} \tag{2.23}$$

Compared to other multivariate statistical approaches, the major advantage of this conditional method is in its simplicity. It is, however, rather complicated in the operational point of view and necessary to be repeated in the same area. Clerici et al. (2010) also mentioned some pitfalls of the conditional method with regard to the restriction of generating subdivisions with a small size of unique condition units that would lead to little significance of statistical perspectives.

Finally, Soeters and van Westen (1996) noted due to their objective characteristics the use of statistical methods would require painstaking efforts to collect large amounts of data. The advance of computer technologies as well as the increasing concerns for environment, however, encourage one to use these objective statistical methods (Nossin 1975; Matula 1979). Landslide hazard assessments, especially based on statistical analysis, are suitable, cost effective solutions for land use and hazard prevention planning despite their operational and conceptual limitations (Guzzetti et al. 1999).

2.2.2.5 Physically based methods

As previously described the physically based approaches employ physical laws that were conventionally used to solve site specific problems from the engineering point of view. All determined information such as properties of materials involved, hydrologic profile, geometry, and potential rupture surfaces for slope stability models

were incorporated to calculate quantitative values of the factor of safety (Varnes and IAEG Commission on Landslides and other Mass Movement on Slopes 1984; Soeters and van Westen 1996; Dai et al. 2002; Hervás and Bobrowsky 2009). The physically based approaches provide best results where ground conditions are fairly even and simple type of landslides, relatively easy to identify, are abundant over the area (Soeters and van Westen 1996; Dai et al. 2002). Another benefit is the result obtained from this method is ready to use for geotechnical engineering works or another quantitative analyses (van Westen et al. 2006). The advance of GIS helps one to handle large amounts of data that are necessary to obtain reliable quantitative values.

The evaluation of the slope instability which is applicable to a translational slide to determine the factor of safety is based on the infinite slope model (Ward et al. 1982). Main problems with this model are the increasing tendency of over simplification and expensive procedures for data collections. Soeters and van Westen (1996) noted that large scaled, small areas are the only appropriate extent for this method because of reasons described earlier.

An early study contributing to physically based approaches can be found in Klugman and Chung (1976) who extended the site specific factor of safety to the regional based landslide hazard distribution to establish the classification of slope instability for the planning and development guidelines in the regional municipality of Ottawa-Carleton, Ontario where landslides are prevalent in unconsolidated clay deposits along the St. Lawrence and Ottawa River valleys. Based on slope heights, angles, and average soil properties with regard to the strength and groundwater condition, the factor of safety was calculated and results were delineated on maps over the entire study area.

The theoretical basis for the physically based model which controls topographic influences on shallow landslides was provided by Montgomery and Dietrich (1994). They combined soil saturation and an infinite slope stability model with digital terrain data in order to predict a steady state rainfall which may induce landslides and define slope stability classes in the study area. Even further, Wu and Sidle (1995) incorporated a distributed, physically based slope stability model (dSLAM) which is considered by the infinite slope, kinematic wave of groundwater, and continuous change of the vegetation root strength for rainfall induced shallow landslides on steep, forested basins in the Oregon Coast Ranges. By refining the work of Mont-

gomery and Dietrich (1994), the SINMAP (Stability INdex MAPping) methodology which combines a physical infinite slope stability model with the steady state hydrology model to predict a spatial distribution of shallow debris slides was carried out by Pack et al. (1998). Recent studies relevant to physically based approaches can be found in Montgomery et al. (2000) who studied the influence of forest clearing on shallow landslides in the Pacific Northwest. Zaitchik and van Es (2003) employed a SINMAP approach to an agricultural region of Honduras to establish the landslide hazard model, and Moon and Blackstock (2004) used deterministic stability models to identify the size and shape of potential landslides which would impact lifelines and infrastructure in New Zealand for emergency management planning. Evaluation of transient effects by the rainfall infiltration, which represents the near surface pore water pressure distribution and subsequent slope instability for shallow landslides in Seattle, Washington, was conducted by Godt et al. (2008) and Salciarini et al. (2008).

With the aid of GIS technology this method can simulate various possible scenarios which depend on changes of variables mainly affecting the initiation of landslides and can lead to produce more reliable landslide hazard maps and response plans in cases of real landslide events. Based on the data available, the physically based model can be generally grouped into three consecutive types (Aleotti and Chowdhury 1999, Figure 11): (1) simple susceptibility model; (2) susceptibility model with different situations; and (3) hazard model incorporating the probability analysis (Figure 2.9). In the simple susceptibility model, landslide preparatory factors are combined to evaluate the factor of safety. Results are qualitatively grouped into different classes to describe relative potential due to landslides. This model can be upgraded into a more sophisticated one by introducing variable data, which can simulate different possibilities to landslide conditions. The final model would employ the probability analysis to make the complicated landslide hazard model. Aleotti and Chowdhury (1999) also noted these series of transitions would imply a evolution in the methodology from deterministic to probability.

The probability analysis in the physically based method has been firstly proposed to understand temporal and spatial variations of material properties, hydrologic profiles, and corresponding changes of the factor of safety. In addition to these parameter variations, other uncertainties in implementing the system, adopting geotechnical modeling, applying failure mechanisms, and omissions arise (Wu et al. 1996; Aleotti and Chowdhury 1999). In the probability analysis the potential hazard

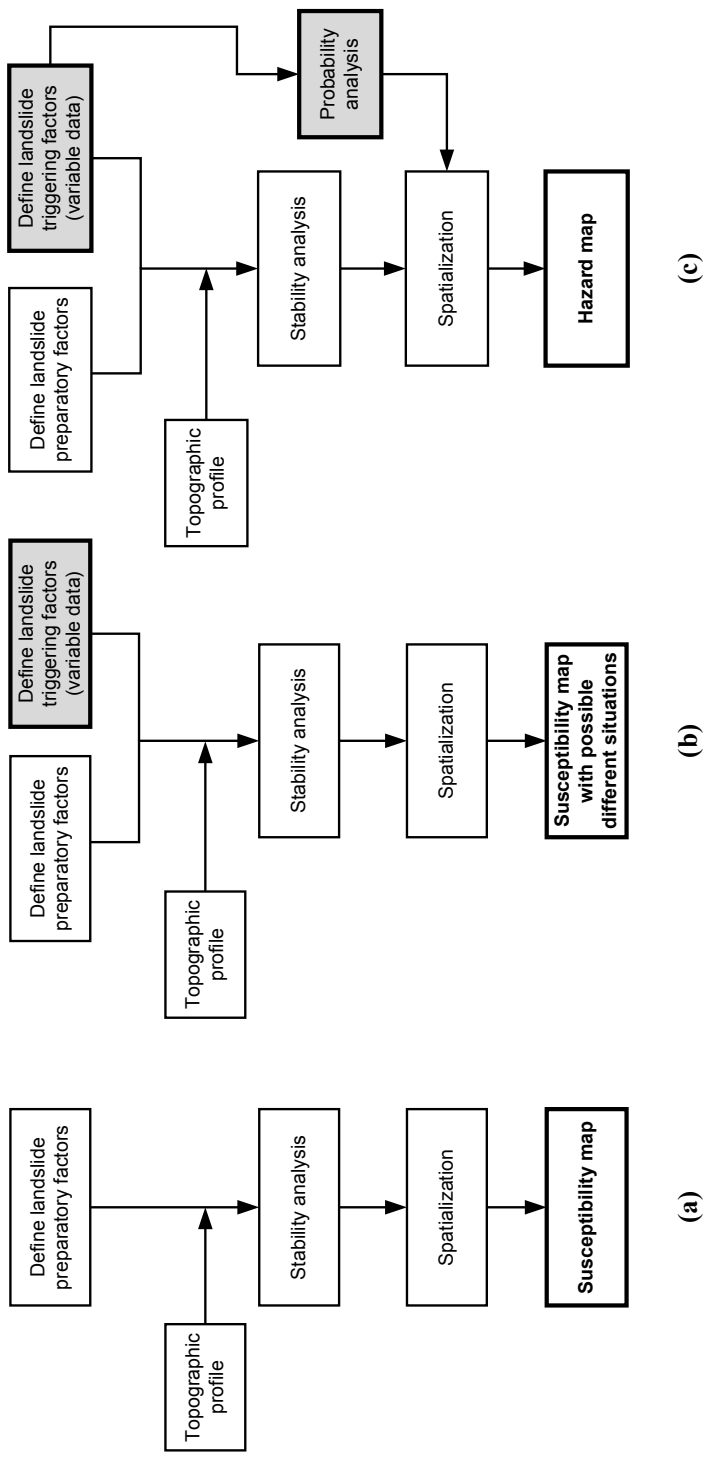


Figure 2.9 Consecutive types of the physically based method for landslide susceptibility and hazard assessments based on the data availability. a. Simple susceptibility model. b. Susceptibility model with different situations. c. Hazard model incorporating the probability analysis. Newly added elements to implement more sophisticated analyses are illustrated by gray shades. Final products are represented by bold letters with thick outlines. *Source:* Aleotti and Chowdhury 1999, Figure 11

which is denoting that the failure probability (P_f) can be estimated by random performance variables of x plotted in a probability density function, $f(x)$, shown in Figure 2.10. Wu et al. (1996) noted that a mean (μ_x) and the standard deviation (σ_x) of the probability density function logically stand for the best guess of true value and uncertainty to the true value, respectively. Most physically based methods take the factor of safety as the random performance variable. The probability of the failure, therefore, can be expressed as the probability of the performance function of the factor of safety where its value is below the designated threshold, mainly one (Figure 2.10). This gives the following relationship (Nguyen and Chowdhury 1985):

$$P_f = P[FS < 1] \quad (2.24)$$

where P_f is the probability of the failure and FS is the random variable of, in this case, the factor of safety, respectively. The probability of success or reliability, P_s , can then be expressed by using the probability of the failure:

$$P_s = 1 - P_f \quad (2.25)$$

The probability density function is then employed to calculate P_f by using the mean or median value and the standard deviation. Mean and standard deviation of random variables can also be combined to denote a reliability index of β (Hasofer and Lind 1974). It gives the following equation:

$$\beta = (\mu_{FS} - 1)/\sigma_{FS} \quad (2.26)$$

where, μ_{FS} and σ_{FS} are the mean factor of safety and the standard deviation of the factor of safety, respectively. The numerator of Equation (2.26) indicates a difference between the mean factor of safety and the threshold value along the abscissa, which describes the safety margin (Hasofer and Lind 1974; Wu et al. 1996). Divided by the standard deviation of the factor of safety, the denominator, Equation (2.26) gives the relative safety margin with respect to the magnitude of uncertainty (Wu et al. 1996).

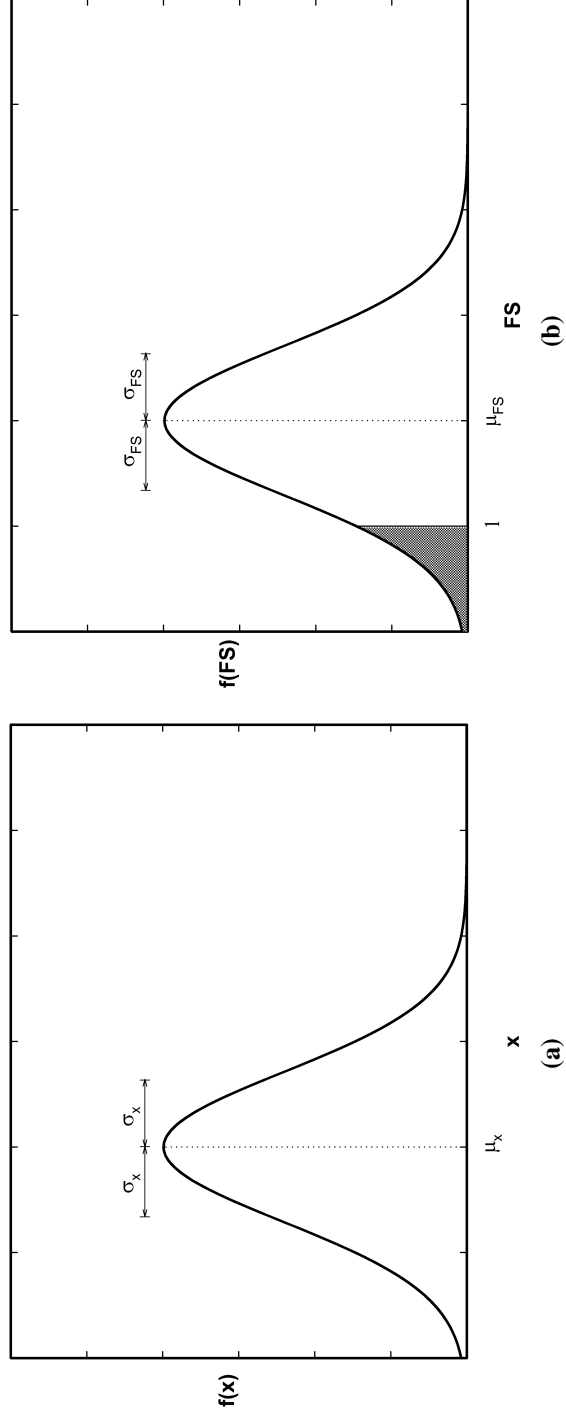


Figure 2.10 Probability density functions. a. Probability density function with a random performance variable of x . b. Probability density function with a determined performance variable of the factor of safety (FS). *Source:* Wu et al. 1996, Figure 6-1

Generally probability analysis methods are grouped into two categories (Aleotti and Chowdhury 1999; El-Ramly et al. 2002): (1) approximate methods including the first order, second moment (FOSM) method and the point estimate method; and (2) Monte Carlo simulation. Among them the Monte Carlo simulation takes a random value for each input variable, then uses this value for building a statistical distribution of the correlated random variable such as the factor of safety (Nguyen and Chowdhury 1985; El-Ramly 2001). Examples of landslide hazard assessments by using the Monte-Carlo simulation can be found in many authors (Nguyen and Chowdhury 1985; Hammond et al. 1992; Davis and Keller 1997; El-Ramly 2001; El-Ramly et al. 2002, 2003; Zhou et al. 2003; El-Ramly et al. 2006).

2.2.3 Landslide risk assessment

Varnes and IAEG Commission on Landslides and other Mass Movement on Slopes (1984) described risk as “the expected number of lives lost, persons injured, damage to property, and disruption of economic activity due to a particular natural phenomenon.” Therefore, dealing with risk one should know relevant components which comprise the risk such as hazard (H), element at risk (E), and vulnerability (V). Generally landslide risk assessment requires one to integrate landslide susceptibility and hazard assessments. Therefore, a reliable risk assessment with incomplete antecedent assessments is unlikely. Despite this practical constraint and limitation the landslide risk assessment has been gaining in popularity and has become the essential tool in emergency management which provides authorities and personnel to implement emergency management activities representing preparedness, response, prevention, and mitigation plans and to establish regulations or codes against various types of landslide disasters.

Practical applications for landslide risk managements including relevant risk, hazard, and susceptibility assessments are well described by Australian Geomechanics Society (2000; 2007a; 2007b; 2007c; 2007d; 2007e). International workshop and conference on landslide risk assessment and management held in 1997 and 2005 presented many beneficial examples, both theoretical and practical, with regard to this subject. Many contributions to risk assessments can also be found in Lee and Jones (2004), Committee on the Review of the National Landslide Hazards Mitigation Strategy (2004), and Glade et al. (2005). One practical example in Canada,

which is related to railway hazards was carried out by Keegan (2007) and Keegan et al. (2007). In this study preliminary analyses involving development and implementation of the risk management methodology for the railway ground hazard along the Canadian railway systems were proposed, which are consistent with the Canadian Standard CSA Q850-97 (1997).

Even though landslide risk assessments are not as more common as landslide susceptibility and hazard, practical landslide risk assessments broadly have a similar classification into qualitative and quantitative approaches, usually representing the possibility of loss of life and the monetary term of damages from landslide occurrences (Hervás and Bobrowsky 2009). Qualitative approach such as a heuristic method which is supported by the expertise of professionals has been applied in many countries because of its simplified and intuitive feasibility. Based on this method the risk can be divided or ranked qualitatively (IUGS Working Group on Landslides, Committee on Risk Assessment 1997; van Westen et al. 2006). Recent studies by Cardinali et al. (2002) and Reichenbach et al. (2005) provided a practical example of using the qualitative risk assessment at a site-specific scale. In order to ascertain landslide hazards they employed a geomorphological mapping method to produce the multi-temporal landslide inventory map. Event based landslide frequency and intensity indexes were used to divide the landslide hazard into a series of classes. Classified hazards are combined with categorized vulnerabilities of elements at risk to generate a specific risk for each element at risk and landslide. The total risk can then be determined based on the largest specific landslide risk in each hazard zone (Reichenbach et al. 2005), which is somewhat different to those imposing the largest specific landslide risk on the entire area (Cardinali et al. 2002).

On the other hand, quantitative approaches including statistical and probabilistic methods would evaluate the probability of landslide susceptibility and hazard as well as the vulnerability of elements at risk and represent the relative probability of the risk as the specific number. As with qualitative methods, the specific risk can be expressed by multiplying the hazard by expected losses for elements at risk, and this can be separated by terms into either loss of life or property damage (Dai et al. 2002). The total risk is then defined as the degree of losses for all different types of elements at risk, determined by each type of landslide (van Westen et al. 2006). Even though numerous theoretical efforts are abundant, practical approaches with regard to the quantitative risk analysis are rare except for a few studies like Bell and Glade (2004), Corominas et al. (2005), Remondo et al. (2008),

and Zêzere et al. (2008). Bell and Glade (2004) proposed a raster based approach in which all available data were converted into the cell derived data. Through the study and the resultant landslide risk map they determined that the debris flow is the highest rank of the landslide risk in both individual and object observed in the BÍldudalur, Iceland. Quantitative risk assessments on rockfalls in Andorra before and after the mitigation measures have been adopted were carried out by Corominas et al. (2005). They analyzed volume, frequency, and release area of rockfall and performed a trajectographic analysis to determine the travel distance and dynamic energy of falling blocks from intact rock slopes. They also noted the risk level at toes of rock cliffs will be dependent on exposed elements and their vulnerability. Remondo et al. (2008) produced risk maps which present the monetary value in the next 50 years for both direct and indirect losses due to landslides. They used a susceptibility model using the statistical method and determined the future landslide frequency based on the past landslide behaviours. They concluded that the total risk can be evaluated as 2.4 million Euros over the next 50 years in northern Spain. Landslide risks impacting roads and buildings in the small study area of Portugal were carried out by Zêzere et al. (2008). Hazards for three different landslides, shallow translational, translational, and rotational slides, were identified based on the probabilistic approach. The return period of rainfall is combined to the landslide hazard assessment to estimate the raster based future influences due to those landslides. Various landslide risk maps for roads and buildings in terms of direct costs induced by three landslides were generated from the statistical combinations of the represented landslide hazard, vulnerability of elements at risk, and estimated values for elements at risk, which is followed by guidelines of the Portuguese Insurance Institute to estimate future reconstruction costs.

2.3 Implementation of the landslide hazard assessment in urban areas

2.3.1 Landslide costs and impacts on urban areas

Landslides affect human lives as well as transportation routes, industrial facilities, and public and private properties. Costs induced by landslides are difficult to estimate especially where they are caused by the combination of other natural disasters

like floods and earthquakes. Early estimates of landslide costs in the United States carried out by Smith (1958) showed hundreds of millions of dollars were required for both direct and indirect landslide damages every year. Jahns (1978) noted at least 75 billion dollars for direct damages from mass related movements, landslides and subsidences, during the years of 1925 to 1975 (1.5 billion dollars per year). He also stressed that significant increases of property damages over the past fifty years contributed to the combination of population growth, mega-structures, and wrong decisions for engineering works toward landslide hazards. Subsequent studies have proved the high increase of costs caused by landslide incidents due to population growth, development in landslide prone areas with the use of large cuts and fills (Fleming et al. 1979; Schuster 1996). Recent surveys for losses due to landslides in the Appalachian, Rocky Mountain, and Pacific Coast regions are well described by Kockelman (1986). Schuster and Fleming (1986) noted growing economic losses and fatalities due to landslides in many countries in the world and stressed the importance of aggregating the socio-economic information to provide priorities to the landslide related research. Schuster and Highland (2007) stressed socio-economic impacts of landslides on urban areas by using the world's case histories. They also noted that a typical pattern, for example, the increasing population, preference for scenic areas, following developments including modifications of natural geometry and drainages, is repeated in developing countries and brings even more serious concerns.

2.3.2 Approaches to landslide hazard controls

All impacts induced by landslides paradoxically accentuate the necessity for effective means against landslide related hazards. The Committee on Ground Failure Hazards (1985) provided two principles to reduce costs due to landslide hazards. These are (1) emergency management; and (2) long-term hazard reduction. Emergency management is a series of actions which respond to ongoing landslide hazard situations as well as predicting and preparing for possible future landslide occurrences. The former may include evacuation and rescue, food and water distributions, and repair and recovery of the transportation, lifelines and public services whereas the identification of landslide prone areas, development of emergency plans, training personnel, and dissemination of relevant information by various media as a warning may belong to the latter. The aim of emergency management is to

minimize the damages or loss of life during landslides and facilitate rehabilitation procedures after landslides (Committee on Ground Failure Hazards 1985). On the other hand, the long term hazard reductions focus more on reducing direct damages resulted from landslides. It may include reducing landslide occurrences and minimizing damages induced by landslides. It is also recommended that the key prerequisite elements are to be integrated within the landslide reduction program (Committee on Ground Failure Hazards 1985; Schuster and Fleming 1986). These are as follows:

1. Land use regulations
2. Building and structure codes
3. Landslide mapping techniques
4. Basic research on landslide mechanisms (initiation and processes)
5. Applied research to identify and control landslide hazards
6. Technology transfer to encourage interdisciplinary cooperations
7. Insurance programs
8. National leaderships for the effective landslide reduction and research
9. Legislation

In fact, numerous measures have been developed and applied to real situations. They include techniques that range from trivial, for example relocating or acquiring private and public properties, to complex techniques such as warning systems. Some techniques proved their capability by dealing with other hazards like floods, earthquakes, and hurricanes. Kockelman (1986) proposed seven practical measures in order to decrease impacts occurred by landslide hazards (Table 2.3).

Later Schuster and Kockelman (1996), and Schuster and Highland (2007) redefined Kockelman's approaches and summarized these into four principal approaches to reduce the risk due to landslide hazards as follows:

Table 2.3 Practical techniques for the landslide hazard reduction. *Source:* Data adapted from Kockelman (1986)

Category	Representative measures
Discouraging new development in hazardous areas	<ol style="list-style-type: none"> 1. Disclosure 2. Posted warnings 3. Utility and public facilities policies constraining development 4. Public information and education 5. Public records containing landslide histories
Removing or converting existing development	<ol style="list-style-type: none"> 1. Acquisition, exchange, and relocation 2. Discontinuance of nonconforming uses 3. Post-disaster redevelopment 4. Removal of unsafe structure 5. Urban redevelopment
Providing financial incentives or disincentives	<ol style="list-style-type: none"> 1. Federal and state financial assistance 2. Legal liability 3. Lending policies 4. Nonsubsidized insurance 5. Tax credits or lower assessments
Regulating new development in hazardous areas	<ol style="list-style-type: none"> 1. Grading ordinances 2. Hillside development regulations 3. Land use zoning districts and regulations 4. Sanitary ordinances 5. Special hazard reduction zones and regulations 6. Subdivision ordinances 7. Rebuilding moratoriums
Protecting existing development	<ol style="list-style-type: none"> 1. Slide and slump controls 2. Mudflow and debris flow controls 3. Rockfall controls 4. Assessment districts 5. Monitoring, warning, and evacuating systems

1. Restriction or prohibition of further developments in landslide prone areas
2. Regulations or codes for excavation, grading, landscaping, and construction
3. Implementation of landslide preventing or controlling measures
4. Development of landslide warning systems

All of these principles will be conducted by policy makers who have a responsibility for controlling landslide hazards. Based on physical characteristics and subsequent impacts of landslides they usually have three possible options (Rossi et al. 1982; Schuster 1991; Schuster and Kockelman 1996; Schuster and Highland 2007):

1. Take no action at all, either before or after a landslide event
2. Take action either during or after a landslide (response, relief, and recovery orientated)
3. Take action before landslides occur (prevention or preparedness dominated)

With advances of relevant technologies and increasing concerns in society toward landslides actions which are included within the third option, i.e., taking action before catastrophic events, are getting their popularity since the late 1950s (Schuster and Kockelman 1996; Schuster and Highland 2007).

2.3.2.1 Restriction or prohibition of further developments in landslide prone areas

Restriction or avoidance of the development in landslide prone areas is the most conservative option (Schuster and Highland 2007) considering the fact that even perfect engineering works are not always done with their right intentions. As pointed out by Kockelman (1986), this practice includes discouraging new developments, removing or converting existing developments, and providing financial incentives or disincentives (Table 2.3). Restricting new development is the most economical measure for landslide hazard reduction if possible and has been successful in the United States (Schuster and Highland 2007). Removal and change of

existing structures and developments is an alternative measure in the case that discouraging of development is not feasible. Table 2.3 shows representative examples belonging to this category.

Kockelman (1986) well described the type and function of financial methods which can be used for discouraging or encouraging the development of landslide prone areas. These methods are somewhat indirect compared with those described earlier. Numerous options for this category are available: (1) federal and state financial assistance; (2) legal liability; (3) lending policies; (4) nonsubsidized insurance; and (5) tax credits or lower assessments (Table 2.3). Among them costs of the landslide insurance can control developments in landslide prone areas by imposing the higher premium where landslide occurrences are evident (Erley and Kockelman 1981). Insurance programs for geologic hazards have been developed as balanced with the advance of related regulations and codes (Arnould 1976). If the area is known to be potential for landsliding, the loss of damages induced by landslides would be deprived of “random nature,” and this leads to a requirement of high premium charges (Erley and Kockelman 1981; Kockelman 1986). In the United States, the National Flood Insurance Program (NFIP) is used to discourage developments in ‘mudslide’ prone areas. It requires people who will develop or acquire areas where potential mudslides have been identified to purchase flood insurance before any kind of federal financial assistance is available (United States Code 2006a, b). However, there were many controversial disputes on applying the NFIP program into landslide hazard areas because of clear differences between floods and landslides in the identification of hazards, experience with hazards, and accommodation of applied mitigations (Olshansky and Rogers 1987). Despite the difficulties in clarifying glossaries and applying these to practical situations, using the insurance program to reduce landslide hazards is one of the attractive solutions. Olshansky and Rogers (1987) noted that some benefits of using insurance are (1) to get an equitable distribution of costs and benefits; (2) to encourage landslide hazard reduction; and (3) to make a balance between private and public interests.

A comprehensive review on international practices to apply insurance to geologic hazard reduction was carried out by Arnould (1976). Olshansky and Rogers (1987) also discussed landslide related insurance programs in New Zealand and France. A recent study by Zêzere et al. (2008) showed a practical use of the insurance program to determine reconstruction costs for elements at risk in landslide risk analysis.

2.3.2.2 Regulations for excavation, grading, landscaping, and construction

Regulations are one of the most effective ways to reduce the damage from landslides. Developments are allowed within stable areas and unstable areas are left as open spaces or developed as low intensity uses (Committee on Ground Failure Hazards 1985). On the other hand, special codes for design and construction in landslide prone areas would provide specific structures to reduce the damages from landslides. In fact, the restriction or prohibition of developments without a regulatory body may not work voluntarily (Schuster and Highland 2007). Therefore, administrative based regulations or codes are essential in urban areas for the landslide reduction program. Representative regulations for the land use which can be applied to landslide prone areas are as follows (Schuster 1991; Schuster and Kockelman 1996; Schuster and Highland 2007): (1) land use zoning regulation; (2) subdivision regulation; and (3) sewage disposal regulations. In Colorado, for example, the House Bill (House Bill 1041) was passed to provide the identification, designation, and administration of areas for the land use and related activities, and assign duties to relative agencies (Rogers et al. 1974).

The best example of implementing regulations and codes in the United States is the landslide hazard reduction effort by the City of Los Angeles (Mayor's Ad Hoc Landslide Committee 1967; Jahns 1969; Slosson 1969; Fleming et al. 1979). During twelve years (1952 to 1963), the landslide hazard reduction program was re-evaluated and refined several times depending on ongoing landslides due to heavy precipitation. Slosson (1969) and Fleming et al. (1979) described the chronological history of the development and efforts of the Los Angeles' landslide reduction program and estimates of damages due to landslides before and after implementing regulations and codes.

According to Slosson (1969), Fleming et al. (1979), and Schuster and Highland (2007), the first regulation which contained a grading ordinance was passed in 1952 after massive damages in many cuts and fills were constructed without any regulation due to heavy rainfall in winter of 1951 to 1952 and the severe storm in January 1952. In 1956 a rainfall event in the city resulted in a change to the ordinance in order to require compaction on the slope face of fills and geologic reports for special landslide problems before getting grading permits. The reactivation of a large, dormant landslide led to the termination of the landslide insurance and the bringing of landslide problems into courts. Legal aspects related to landslide hazards

are well presented by Smith (1958). In the winter of 1957 to 1958 when heavy rainfall triggered significant landslides, the city modified the grading ordinance to fit special landslides within one geologic formation. Concurrently, the Engineering Geologists Qualification Board established by the city devised a guideline and checklist for geologic reports.

Another modification was conducted in the winter of 1961 to 1962 following a rainfall and storm in February, 1962. New ordinance adopted in 1963 focused on the implementation of more severe grading standards and encouragement of participation of geologists and engineers for entire design procedures. The Grading Regulation, which was the result of the 1963 ordinance and landslides that occurred after that ordinance, was evaluated in the winters of 1968 to 1969 and 1977 to 1978, respectively. Damages induced by the 1969 storm were grouped based on the effective date of each grading ordinance: (1) before 1952 (no grading ordinance); (2) 1952 to 1962 (first grading ordinance and revised one); and (3) after 1963 (since the Grading Regulation was adopted). Results showed that total damages under no grading activities (prior to 1952) were 18 times higher than those under the Grading Regulation (after 1963). Within the stringent grading regulation only three percent of total damages were influenced by landslides during the 1969 storms. In 1977 to 1978 more than 93 percent of total damages were related to those before the Grading Regulation was issued. The development of the regulation also was supported by enforcement to conduct regulations, gather information with regard to potential landslide areas, and including the interests of people. Finally, Fleming et al. (1979) indicated three key elements for the successful development and practice of landslide hazard reduction especially by using regulations or codes in other parts of the United States: (1) capability of local governments; (2) information availability and the presence of professional societies who support governments and utilize the landslide hazard information; and (3) citizens who understand the value of grading regulations. Other construction and grading codes which were adopted by local governments in California to control landslide hazards are well described by Schuster and Highland (2007).

2.3.2.3 Implementation of landslide preventing or controlling measures

Landslide prone areas which were developed before any regulation or code went into effect would have a higher potential to landsliding than those developed after

regulations or codes were issued (Schuster and Highland 2007). Therefore, mitigating or controlling ongoing landslides by appropriate measures can be the best effort for the landslide hazard reduction activity. Implementation of countermeasures can be divided into two categories: (1) physically based methods by the engineering profession; and (2) monitoring and warning systems based on the practical enforcement (Erley and Kockelman 1981). Landslide countermeasures can also be grouped into prevent and control categories based on their main objectives. Countermeasures using physical methods are focused on preventing existing landslides which are moving, either quickly or slowly. Characteristics and the applicability of physical measures have been discussed by many authors (Committee on Ground Failure Hazards 1985; Kockelman 1986; Schuster 1991; Schuster and Kockelman 1996; Schuster and Highland 2007).

The most commonly used landslide prevention method in the United States is the control of water, either surface or subsurface, because of its high efficiency compared to installation expenses (Committee on Ground Failure Hazards 1985; Schuster 1991; Schuster and Kockelman 1996). In some states in the United States, such as California, the modification of the geometry of landslide prone terrains is preferred if available (Committee on Ground Failure Hazards 1985). Earth retaining walls or berms are the common form of physical structures in the United States (Committee on Ground Failure Hazards 1985; Schuster and Highland 2007). Usually placed at the toe they contribute to the stability by increasing the resisting force of the slope. More sophisticated countermeasures augmented by anchors, rock bolts, soil nails, piles, and geosynthetics are also regularly applied in those cases that previous options are known to be ineffective (Schuster 1991; Schuster and Kockelman 1996; Schuster and Highland 2007). For particular landslides such as debris flows and mudflows various physical countermeasures are employed in western parts of the United States where such landslides are prevalent (Committee on Ground Failure Hazards 1985).

Physical landslide countermeasures are, however, restricted by costs involved and available space which is necessary for their implementations and corresponding construction equipments. Thus, it is usually recommended to use these where high landslide damages are expected (Schuster 1991; Schuster and Kockelman 1996).

2.3.2.4 Development of landslide warning systems

The main purpose of monitoring and warning systems, another type of landslide countermeasures (Erley and Kockelman 1981), is to control existing landslides and their movements. The control may include monitoring landslide prone areas or on-going landslides, warning residents who live near monitoring areas, so they will be easily influenced once landslides have occurred, and directing the evacuation of residents involved or allowing physical based methods to reduce imminent landslides and increase the long term stability (Erley and Kockelman 1981; Schuster 1991; Schuster and Highland 2007). Monitoring systems may comprise field observations and instrumentation in which numerous data are correlated with landslide mechanisms that are automatically obtained from landslide prone areas and linked to warning systems for real time dissemination of relevant information. High costs were required to achieve these systems but with the advent of relevant technologies including innovative instruments and remote telecommunications, costs have become more reasonable.

One significant progress in monitoring and warning systems is the combination of warning systems with major landslide triggering factors such as rainfall and earthquakes, as determined by the United States Geological Survey (Schuster 1991; Schuster and Kockelman 1996; Schuster and Highland 2007). An early study on relationship between rainfall thresholds and landslides was carried out by Nilsen and Turner (1975). Keefer et al. (1987) developed a real time system in the San Francisco Bay region for the issue of a landslide warning during major storms. The system was comprised of: (1) determination of the relationship between rainfall and landslide initiation, both empirical and theoretical; (2) identification of geologically susceptible areas to landslides; (3) regional network of telemetering rain gages for the real time monitoring; and (4) connection to precipitation forecasts of the National Weather Service (Keefer et al. 1987). They successfully used this system for issuing a warning of landslide in the winter of 1986 when about 800 millimetres of rainfall was produced by storms. Similar studies can be found in Seattle, Washington (Chleborad 2000, 2003; Coe et al. 2004; Chleborad et al. 2006; Godt et al. 2006, 2008; Salciarini et al. 2008), Europe (Cascini and Versace 1988; van Asch et al. 1996; Angeli et al. 2000; Guzzetti et al. 2007), and other parts of the world (Onodera et al. 1988; Guidicini and Iwasa 1977; Brand et al. 1984).

Coe et al. (2003) discussed the application of a global positioning system (GPS) with other instruments on measurements of landslide movements on the Slumgullion landslide, Colorado that was affected by groundwater fluctuation, which is, in turn, influenced by rainfall. Guzzetti et al. (2008) produced a global database containing 2,626 rainfall events which had induced shallow landslides and debris flows throughout the world and noted a possibility for the international level of the landslide warning system which is based on global precipitation measurements. More recent examples of the international attention on landslide early warning have been published as a special issue of *Landslides* (Sassa and Picarelli 2010). Besides, major applications of the aerospace technology into the natural disaster reduction were carried out by Verstappen (1995).

2.3.3 Role of landslide hazard assessments

The Committee on Ground Failure Hazards (1985) noted that “it is essential to know where the landslide-prone areas are and how serious the hazard is.” Better understanding of the landslide hazard and risk in areas, and their corresponding damages are the prerequisite for implementing effective landslide hazard controls and enforcing appropriate decisions. One example of the role of landslide hazard assessments can be found in the early failure in practicing the National Flood Insurance Program (NFIP), which was largely due to difficulties in delineating mudslide hazard zones (Olshansky and Rogers 1987). In addition to these, the term of ‘mudslide’ in the insurance program was not defined clearly. Kockelman (1986) noted the term is legislative rather than engineering in nature. All of these may well present the aspects of landslide hazard assessments to reduce damages induced by landslides in urban area. Landslide hazard assessments performed on numerous theoretical basis described in Section 2.2 and their cartographic representations augmented by GIS technologies provide a fundamental information to help to implementing various approaches to mitigate landslide hazards.

2.4 Conclusions

The general idea to implement landslide hazard and risk assessments provides fundamental concepts and issues with regard to the identification of landslides and their

future activity. From thorough reviews in practical examples of various methodologies it is imperative to identify characteristics of landslides that occurred in the area of concern. Since many factors are linked to form the general characteristic of landslides, choosing the proper methodology can be a major issue in landslide hazard and risk assessment studies. For example, one of the main characteristic observed from landslides is that landslides are reactivated where they usually move along a pre-defined rupture surface. The rupture surface may be generated by previous landslides or other processes. With this circumstance, exhaustive examinations should be focused on physical aspects such as geomorphological, geological, and geotechnical contributions to landslides. In this respect, the geomorphological mapping based on the aerial photo interpretation is the most appropriate method.

Another issue is related to the uniformitarianism in which future landslides are likely to occur under the same geologic, geomorphologic, and hydrologic conditions if no substantial changes are provided. In reality, however, previous landslides have been experienced massive development since they have been formed, which leads to new instabilities on the ground where pre-defined rupture surfaces exist and they may exert force to reactivate landslides. Therefore, the assumption of uniformitarianism will not be in effect where severe modifications of physical attributes are observed. Anthropogenic factors play an important role in the stability of slopes. Finally, understanding socio-economic impacts on landslides can provide insights into appropriate landslide hazard assessments, which helps to determine the priority in implementing landslide hazard controls.

Chapter 3

Landslides in the Peace River Lowland, Alberta

This chapter describes basic information for landslides in the study area. Firstly, general overviews, both geographic and economic backgrounds, are presented for a better understanding of landslides and their impacts on the study area. Geologic and climate settings are also illustrated to give an idea on various factors that would lead landslides to occur in the study area. Finally, a brief history of recent landslides observed in the study area is presented.

3.1 Overview of the study area

The Peace and Slave River Basin is the largest river basin system in Alberta (Alberta Environment 2010). The Peace River originates in the Rocky Mountains, 300 kilometres to the west and flows across the province, through the Town of Peace River, and eventually empties into the Slave River (Figure 3.1). The river flow is controlled by the WAC Bennett dam 175 kilometres upstream of the Alberta-British Columbia border (Cruden et al. 1990b). The Peace River Valley is up to 3.5 kilometre wide at its crest ranging from 600 to 750 metres of elevation and 400 to 800 metres wide at water level and around 275 metres below the upland prairie (Ruel 1988; Lu and Cruden 2000). Tributaries of the Peace such as Heart and Smoky Rivers, and Pat's Creek have steep slopes which are susceptible to landslides by rapid river erosion of their banks (Lu and Cruden 2000).

The Town of Peace River, one of few towns on river terraces of the Peace, is located 485 kilometres northwest of Edmonton on Highway 2 (Figure 3.2). Before the 1900s the area was developed as a commercial waypoint (especially for fur trade) and missionaries along the Mackenzie Highway and Highway 2 (Byfield 1984).

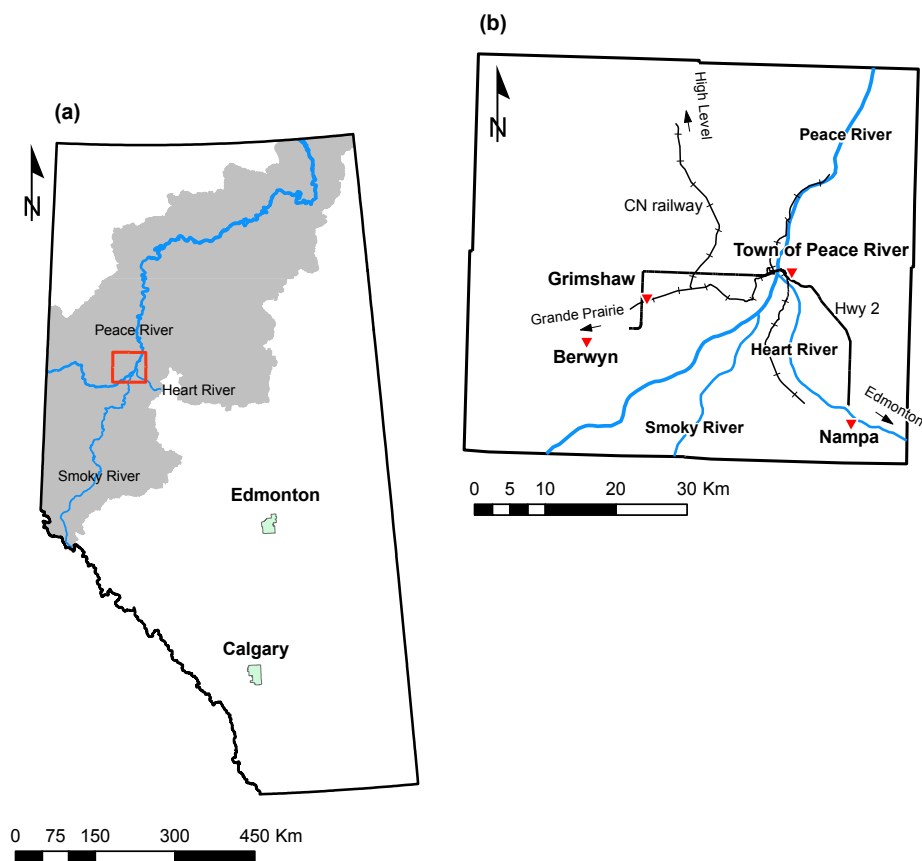


Figure 3.1 Location of the study area. a. Overview map showing the study area. Peace and Slave River Basin is described in the map by a gray shade. Peace, Heart, and Smoky Rivers are also delineated. Area outlined indicates a closed view of the study area in b. b. A closed view over the study area. Adjacent towns and transportations traversing the study area are also shown



Figure 3.2 Town of Peace River overview, looking northeast. Photo was taken near the Shop Slide, one of the recent landslides located on old Highway 2 (Figure 4.1). Peace River flows right to left. Peace River Bridges are in the middle of photo

Since it was incorporated as a village in 1914 and as a town in 1919, the Town of Peace River has contributed to administrative, retail and general service, and distribution to both the region and province (Peace River Regional Planning Commission 1980). An early study by the Peace River Region Planning Commission (1980) noted three economic activities in the region are agriculture, forestry, and oil and gas. Before 1950 the Town of Peace River and its adjacent gently rolling lowland areas (Peace River Lowland) still had more rural characteristics than other areas in the province. After the mid 1950s, however, the Peace River Lowland developed rapidly. Considerable changes in the population ratio between urban and rural areas in the Peace River Lowland during the past twenty years (1951 to 1971) are shown in Figure 3.3.

The population of the Town of Peace River which was growing relatively slowly prior to 1940s significantly increased up to 190 percent in the beginning of 1950s. This might be the result of major economic developments which attracted people from outside of the region. With annexations of adjacent Municipal Districts the town grew larger after the 1960s. Despite minor declines in the late 1970s and 2000s the general population in the Town of Peace River is growing and is higher than other nearby towns (Table 3.1 and Figure 3.4).

As the town grew in the 1970s, terraces were fully packed and development commenced on valley slopes to make more spaces for residents. Many valleys in the Peace River Lowland are relatively young, and consequently unstable. Even small disturbances on valley slopes may cause movements. The general surface topography has three elements: (1) semi-continuous uplands; (2) broad prairies with gentle slopes; and (3) deeply incised river valleys with steep slopes (Sharma 1970). The geometry of the river valley differs based on the aspect of the river banks. The west side of the river bank has longer and gentler slopes down from flat forested uplands compared to steep slopes on the east bank which has uplands with the steep ravines of tributaries of the Peace River (Heart River and Pat's Creek). Uplands and prairies have been used as a crop land but steep slopes retain their original shapes except where cut by major transportation routes. Figure 3.5 shows physiographic characteristics in the study area.

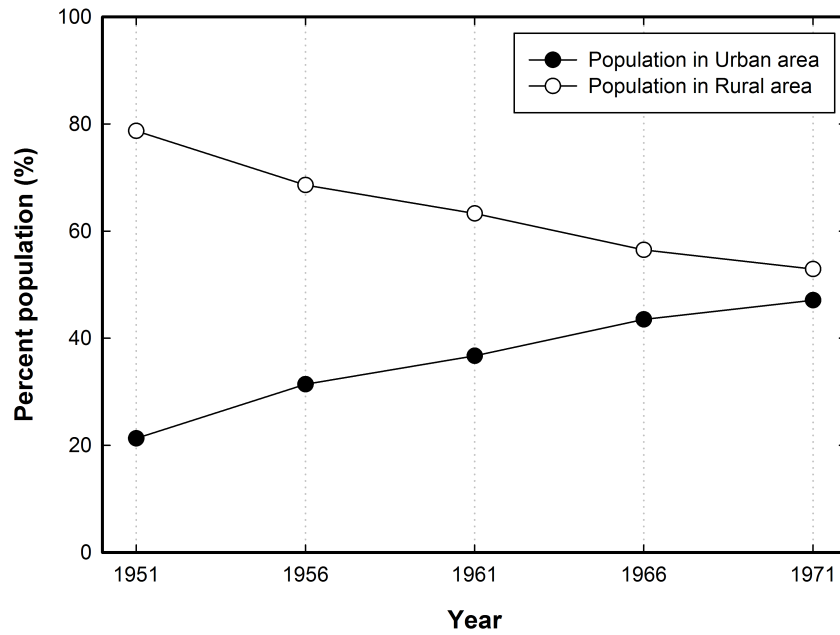


Figure 3.3 Population changes in the Peace River Lowland during 1957 to 1971.
Source: Data from Peace River Regional Planning Commission (1971), Table No. 1

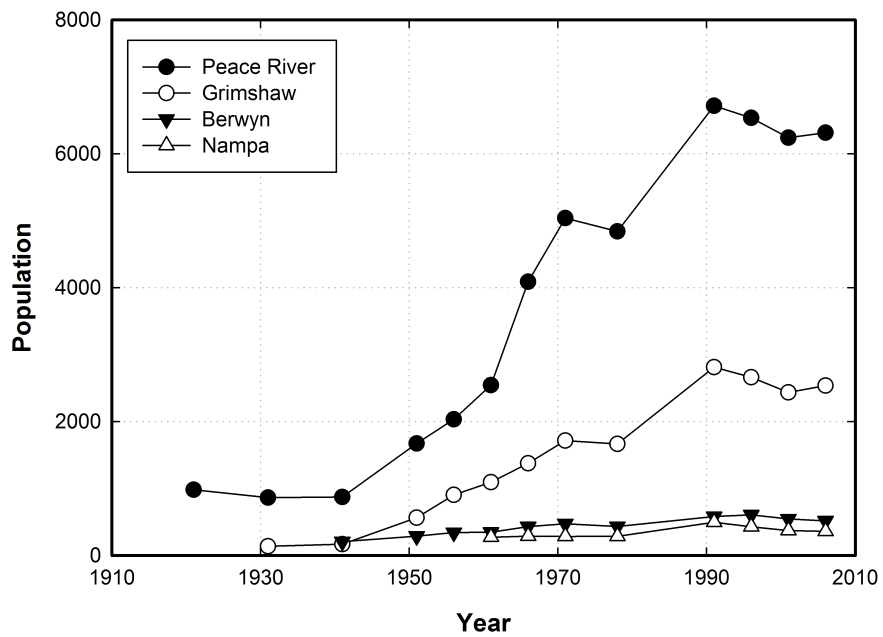


Figure 3.4 Historical population growth in the Town of Peace River. Adjacent towns are also indicated for comparison

Table 3.1 Historical population in the Peace River region. Locations of towns are shown in Figure 3.1

Year	1921 [†]	1931 [†]	1941 [†]	1951 [†]	1956 [†]	1961 [†]	1966 [†]	1971 [†]	1976 [†]	1991 [‡]	1996 [‡]	2001 [‡]	2006 [‡]
Peace River	980	864	873	1,672	2,034	2,543	4,087	5,039	4,840	6,717	6,536	6,240	6,315
Grimshaw	-	137	169	564	904	1,095	1,376	1,714	1,665	2,812	2,661	2,435	2,537
Berwyn	-	-	206	288	342	347	430	474	433	581	606	546	516
Nampa	-	-	-	-	-	271	288	283	286	496	427	372	360

[†] Source: Data from Peace River Regional Planning Commission (1980).

[‡] Source: Data from Statistics Canada (2006).

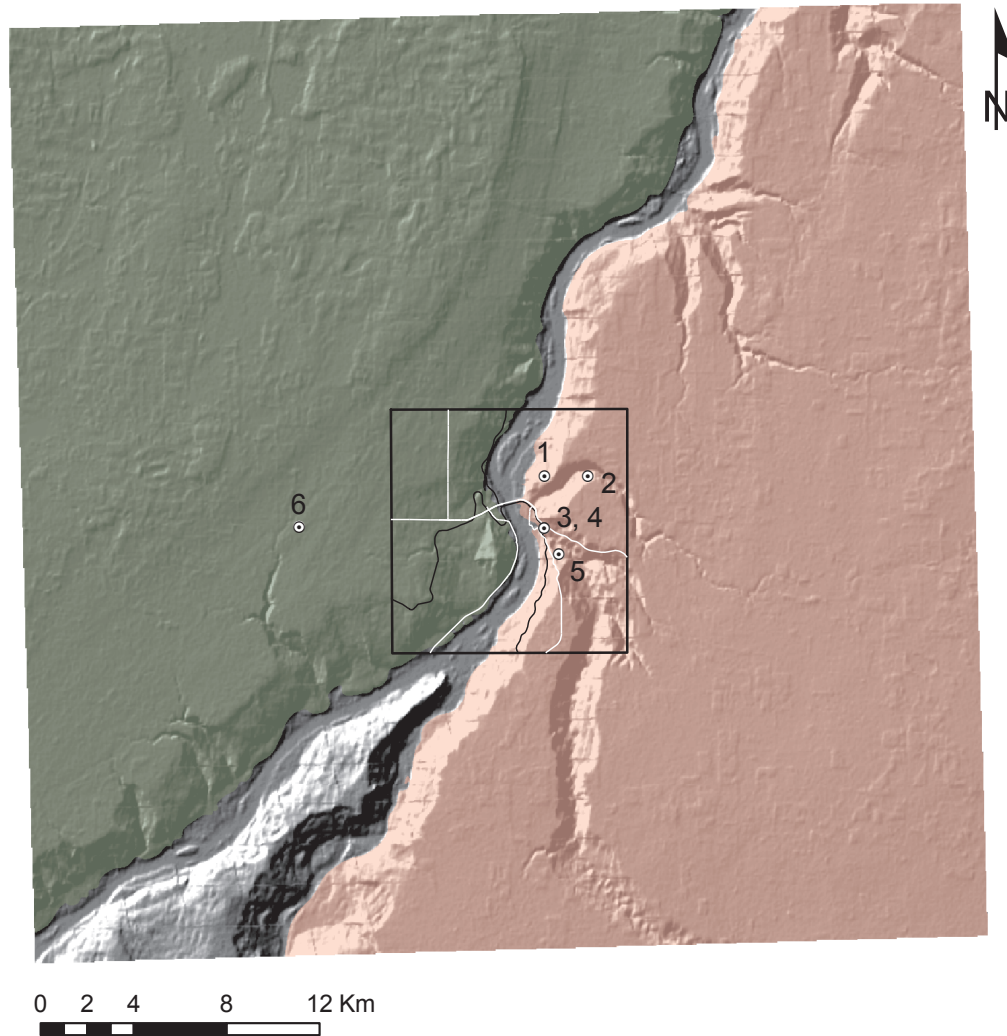


Figure 3.5 Physiography of the Peace River Lowland on which the Town of Peace River is focused. A shaded relief image is obtained from the SRTM dataset. West and east banks are differentiated by colors. White circles indicate weather stations: 1. Peace River; 2. Peace River Crossing; 3. Peace River CKYL; 4. Peace River WRB (same location as No. 3); 5. Peace River Forest HQ; and 6. Peace River A. Major transportation routes are also delineated by white solid line for road and black solid line for railway. Area outlined by the black rectangle illustrates the outline of the study area

3.2 Geology of the Peace River Lowland

The Peace River Lowland, located within the Western Canada Sedimentary Basin (Davies et al. 2005; Morgan et al. 2008) consists of several geological features which result from repetitive erosion and deposition. The area may have experienced several major ice advances (Fenton 1984; Fulton et al. 1986; Liverman et al. 1989; Leslie and Fenton 2001; Fenton et al. 2003; Davies et al. 2005). The present Peace River was incised into a preglacial valley which was wider and shallower than the modern Peace River. Large amounts of sediments accumulated by glacial activities were deposited in the previous valley. Rutherford (1930) described the sequence of surface feature development in the Peace River Lowland in three different stages: (1) preglacial erosion; (2) glacial erosion and deposition; and (3) postglacial erosion and deposition. Major geological features found in the study area are bedrock formations, buried channel deposits, glaciolacustrine and glacial sediments, and lastly, fluvial and eolian deposits.

Although the preliminary geological studies of the Peace River Lowland began in the late 1800s (Dawson 1881; McConnell 1893), McLearn (1918; 1919) first described the Cretaceous geology of the Peace and Lower Smoky Rivers in the beginning of 1900s. Geology and water resources in the Peace River and Grande Prairie areas were carried out by Rutherford (1930). Studies on the Peace River Lowland by various authors (McLearn 1926, 1932; Rutherford 1937; Wickenden and Shaw 1943; McLearn and Henderson 1944; Gleddie 1949; McLearn 1945; Wickenden 1951; Badgley 1952; Alberta Study Group 1954; Gleddie 1954; Henderson 1959; Taylor 1960; Jones 1966; Tokarsky 1967, 1971; Mathews 1980; Borneuf 1981; Fenton 1984; Fulton et al. 1986; Liverman et al. 1989), from government as well as industry, were at a regional scale and provided limited details of the surficial deposits. Leslie and Fenton (2001) reported a complete glacial stratigraphy as well as bedrock formations and surficial sediments of the Peace River area. The Holocene landslide inventory for Peace River area was conducted by Davies et al. (2005). A recent work by Morgan et al. (2008) described updated bedrock topography and Quaternary stratigraphy in the Peace River Lowland generated from multiple data sources.

3.2.1 Bedrock formations

The bedrock in the study area which is underlying poorly consolidated surficial materials is mostly Cretaceous in age (Tokarsky 1971). The regional dip of the Cretaceous bedrock is in a southwesterly direction becoming steeper toward the Foothills near the Alberta-British Columbia border. Cretaceous bedrock in the Peace River Lowland includes the Smoky Group, the Dunvegan Formation, and the Fort St. John Group in base downward (Green 1972; Hamilton et al. 1999). Major bedrock formations surrounding the Town of Peace River are in descending sequence (Leslie and Fenton 2001): (1) Kaskapau Formation (Smoky Group); (2) Dunvegan Formation; (3) Shaftesbury Formation (Fort St. John Group); and (4) Peace River Formation (Fort St. John Group) and their exposures are confined to river banks and occasionally along the road cuts. The spatial distribution of bedrock formations in the study area is shown in Figure 3.6. Figure 3.7 shows the cross section of the study area which shows the geological distribution of the bedrock formations. Chronological distribution of respective geological formations in the study area is illustrated in Figure 3.8. Detailed explanations are presented as follows.

3.2.1.1 Kaskapau Formation

The Smoky Group, renamed from the Smoky River Group (McLearn and Henderson 1944), indicated upper dark shales exposed along the Smoky River (Dawson 1881). The group is Upper Cretaceous in age and marine based. McLearn (1919) divided it into three members, 'Upper shale,' 'Bad Heart sandstone,' and 'Lower shale' and later he redefined the lowest member of the group as 'Kaskapau' instead of Lower shale (McLearn 1926). The Kaskapau Formation is predominantly of marine shales and also has a basal transition zone comprising brackish to marine shale, silty shales, and sandstone (Gleddie 1949). The transition zone conformably overlies Dunvegan Formation which has brackish to fresh water sandstone and shale on top of the formation. Although lithological characteristics of the formation are similar to the Fort St. John Group (Cruden et al. 1990b) in which several mass movements have been reported, the Kaskapau Formation is known to be stable in the study area (Davies et al. 2005). The exposure of the Kaskapau Formation is not common. It appears in small portions to the northwest and southeast of the study area (Figure 3.6).

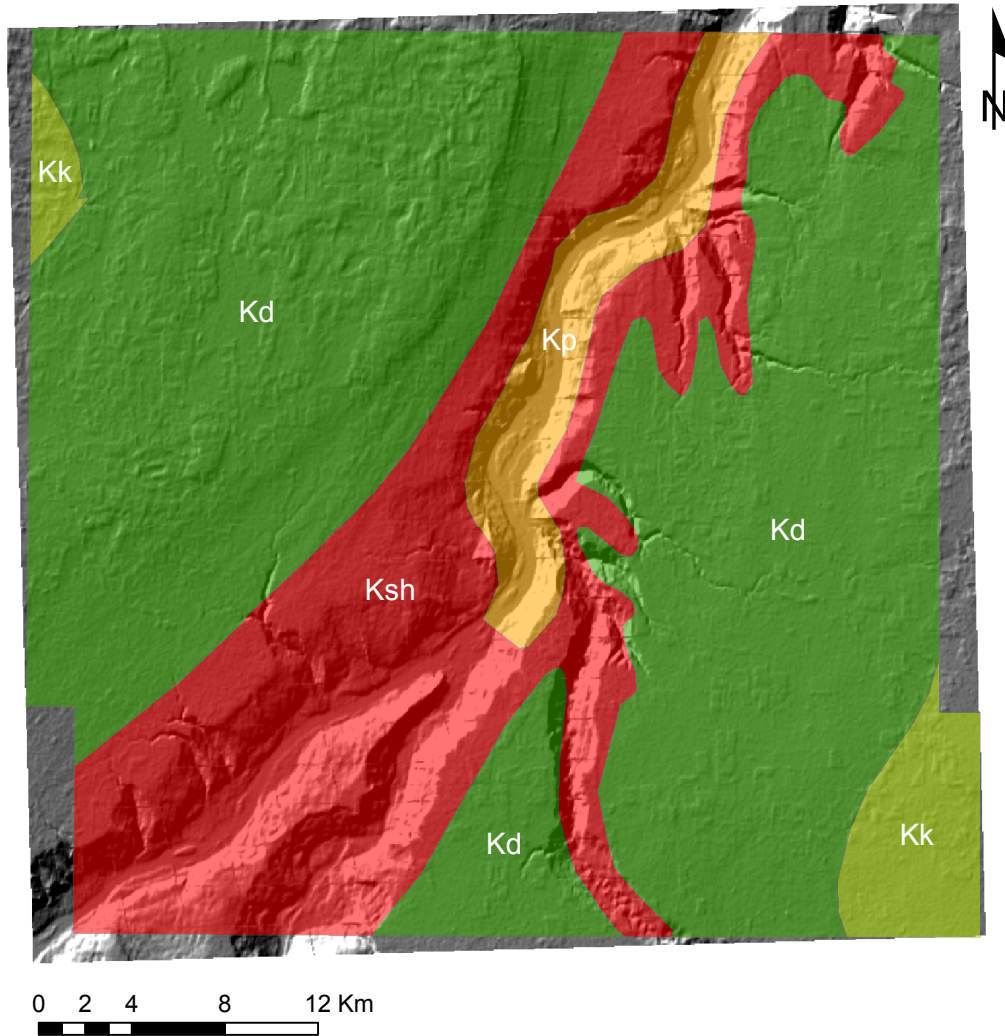


Figure 3.6 Bedrock geology of the study area. Formational units are differentiated by colors. Major formations are as follows: Kk: Kaskapau Formation; Kd: Dunvegan Formation; Ksh: Shaftesbury Formation; and Kp: Peace River Formation. A shaded relief image shown in background is SRTM dataset which is same as in Figure 3.5. The spatial distribution of the formational bedrock units is obtained from Green (1972) and Hamilton et al. (1999)

3.2.1.2 Dunvegan Formation

The Dunvegan Formation consists of a multiple series of depositional cycles, which is dominated by fluvial related processes (Bhattacharya and Walker 1991a, b). This formation, named by Dawson (1881), contains fresh water sandstones and shales, Upper Cretaceous in age, with local coaly beds and some brackish to marine phases (Gleddie 1949). In upper and lower parts of the formation some sandy beds predominate. It overlies marine shales of the Shaftesbury Formation, and the Fort St. John Group as well as underlies the Kaskapau Formation, and the Smoky Group. The Dunvegan Formation can be found in river banks along the tributaries of Peace such as Smoky and Heart Rivers (Figure 3.6).

3.2.1.3 Shaftesbury Formation

The Fort St. John Group, named by Dawson (1881) is a group of shales exposed in Fort St. John along the Peace River in British Columbia, includes all strata lying between the Dunvegan Formation above and the Bullhead Group below (McLearn 1918; Wickenden and Shaw 1943). The Shaftesbury Formation representing marine shales cropping out in the eastern part of the Peace River area (McLearn and Henderson 1944) is the uppermost formation of Fort St. John Group and contains fish-scale bearing, friable, dark marine shale interbedded with concretionary ironstone (Green 1972). This formation lies geologically between Early (Lower) to Late (Upper) Cretaceous in age, thus it can be divided into two members (Gleddie 1954): (1) the uppermost member of Lower Cretaceous, mainly thinly bedded fissile shales containing at least three fish scale zones (Lower Shaftesbury); and (2) the lowermost member of the Upper Cretaceous, silty to sandy and micro-micaceous shales which are relatively clear of fish remains (Upper Shaftesbury). Upper Shaftesbury Formation also contains a few ironstone concretionary bands, transition strata into the overlying non-marine Dunvegan Formation sandstone. Outcrops of the formation have been identified along the Peace and its tributaries (Figures 3.6 and 5.16). Lithological characteristics of the Shaftesbury Formation have induced several mass movements in the study area. Cruden et al. (1990b) noted the significance of lithology in slope stability problems and found that landslides are very common in the Kaskapau and Shaftesbury Formations containing thinly bedded shales.

3.2.1.4 Peace River Formation

The Peace River Formation was designated by McConnell (1893) as the strata lying below the Shaftesbury Formation and above the Spirit River Formation. This unit formerly comprised four members distinguished by Wickenden (1951) but later was redefined into three members, the Paddy, Cadotte, and Harmon Members (Badgley 1952; Alberta Study Group 1954).

The Paddy Member, named from Paddy's Creek (Alberta Study Group 1954) flowing into the Peace River from the east, consists of continental sandstone with some coaly beds. Badgley (1952) interpreted the Paddy Member as non-marine in origin. It contains thin, mixed sandstone layers at its base. He also noted the difficulty of placing the contact between Paddy and Cadotte Members. The Cadotte Member, named by McLearn (1945), is a marine, coarse to fine grained, massively-bedded sandstone (Leslie and Fenton 2001). Cadotte Member sand is generally well sorted and has a salt and pepper appearance which resulted from the grain mixture of colorless quartz, light and dark chert, white clay, and calcite (Alberta Study Group 1954).

Harmon Member indicates shale outcrops exposed in the east bank of Peace River. The name comes from the Harmon River (the present Heart River). The unit includes dark gray shales similar to the Shaftesbury Formation shale and contains some thin lenses of very fine sandstone, fish scales, and bone fragments (Alberta Study Group 1954).

Outcrops of the Peace River Formation, especially Paddy and Cadotte Members, can be seen in valley walls above and below the river level near Peace River Town and downstream (Figures 3.6 and 5.16). The Peace River Formation influences the slope stability of the river banks. It combines with an external factor, toe erosion by river stream, which is a considerably different mechanism commonly occurred in the Shaftesbury Formation.

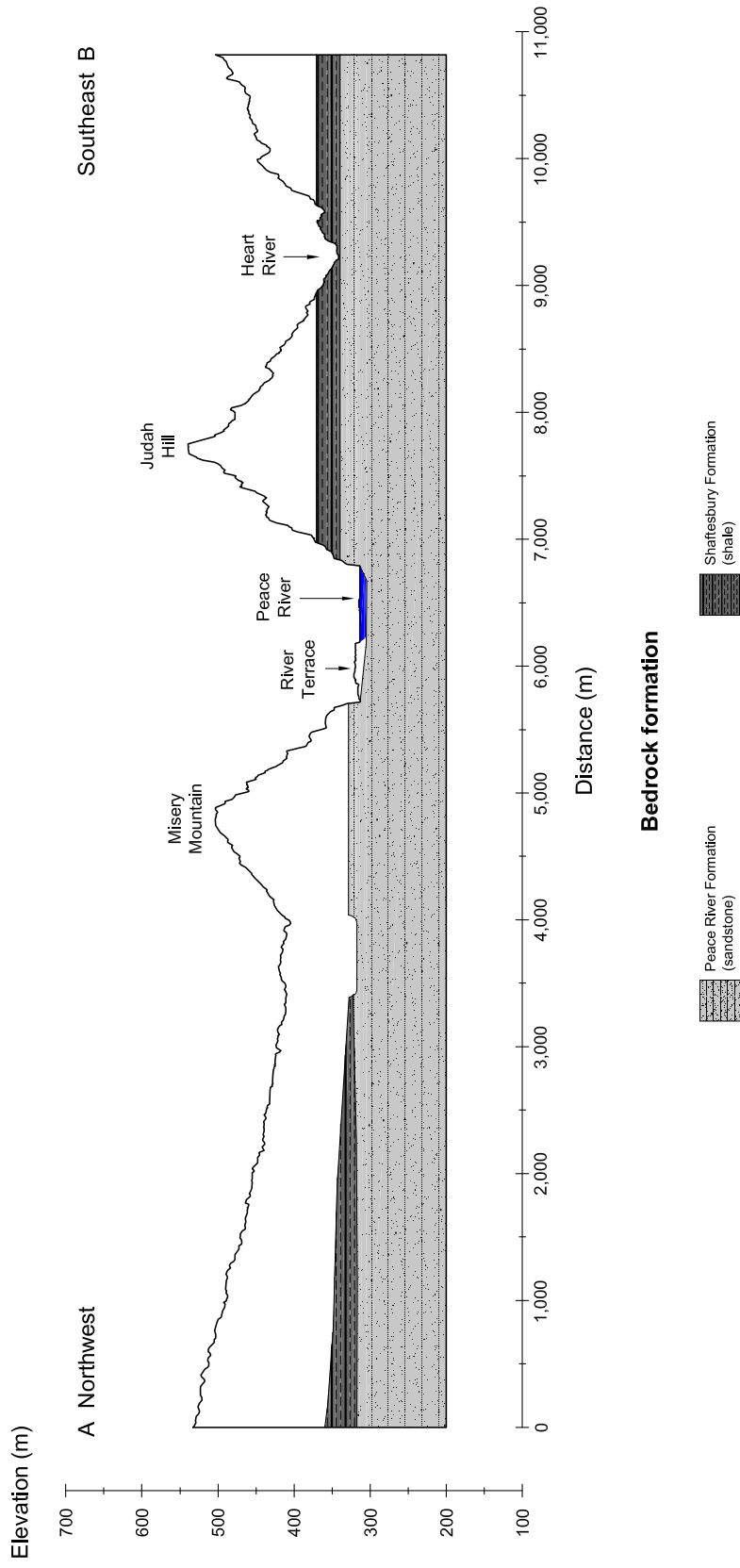


Figure 3.7 Geological distribution of bedrock formations. Surficial stratigraphy as described in Figure 3.9 is voided for the clear presentation. Formational units described in Figure 3.6 are differentiated by colors and symbols. The location of the cross section is presented in Figure 4.1. 6 times of vertical exaggeration is applied to the ordinate. Subsurface profile of the bedrock units is adapted from Morgan et al. (2008)

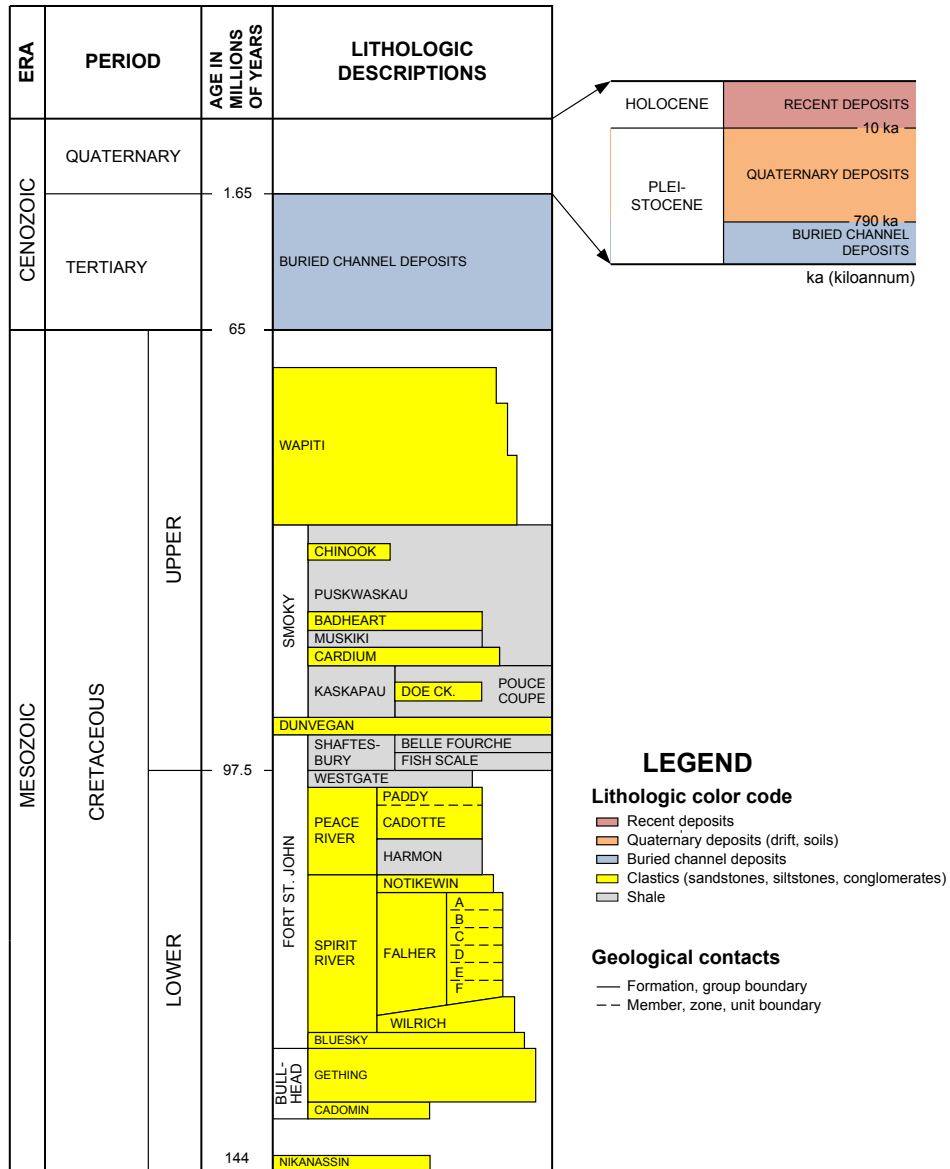


Figure 3.8 Table of formations in the study area. Bedrock formations in Cretaceous Period and the surficial geology in Tertiary and Quaternary Periods are presented. Explanations of each bedrock formation and surficial deposit covered the study area are described in the text. The lithology is differentiated by color codes. Geological contacts are also shown by different symbols. *Source:* Data from Energy Resources Conservation Board (2009). Time-scales shown in the Quaternary geology are obtained from Trenhaile (2004)

3.2.2 Surficial geology

Surficial geology defined in this study indicates sediments which were deposited above the Cretaceous bedrock strata by natural agents since the Cenozoic Era. They are generally divided into three components by their geological provenance: (1) buried channel deposits; (2) Quaternary deposits; and (3) recent deposits in base upward. The general stratigraphy of the surficial geology in the study area is described in Figure 3.9. These informal units are numbered in ascending order.

3.2.2.1 Buried channel deposits

The buried channel deposits relates to those deposits that are mainly of granule to boulder sized, well sorted, gravel interbedded with poor to moderately sorted fine to coarse sand overlying the Cretaceous bedrock and underlying glacial sediment deposits during the Tertiary and early Quaternary Periods (Leslie and Fenton 2001). The buried channel has a similar course to the present river, located northwest of the current Peace River and running parallel to it, and this represents a preglacial phase of the ancestral river system (Tokarsky 1971). The preglacial channel was wider but shallower, consequently less flow constrained, and had flatter slopes. Sediments deposited in the buried channel have been recognized by many studies. Rutherford (1930) mentioned strata of Tertiary age once covered most of the Peace River and Grande Prairie area. These strata were apparently removed by the preglacial fluvial erosion. In some buried channels sand and gravel deposits originated from the glaciofluvial streams of the early Pleistocene age (Henderson 1959). A thin layer of gravel found along the Peace, the Ksituan, and the Badheart and their tributaries overlying the bedrock is the remains of the buried channel deposits during the earliest ice advance (Rutherford 1930). However, Jones (1966) considered that most of the buried channel deposits are preglacial in origin, suggesting that buried channel sand and gravel are the northern equivalent of the Saskatchewan Gravels and Sands in central Alberta which were identified as preglacial sediments in origin (Rutherford 1937). Outcrop of the buried channel deposits are rare in the study area because of the preglacial erosion and the large amount of surficial deposits. Some of these sediments are preserved in preglacial valleys on the upland of the town of Grimshaw, in the floodplain of the Peace River, and the east of Manning area (Tokarsky 1967; Borneuf 1981; Leslie and Fenton 2001; Paulen 2004).

3.2.2.2 Quaternary deposits

Fenton (1984) described five major glacial events of early to middle Pleistocene age and four of the late Pleistocene events on the Canadian Prairies. Before glaciation controlled geomorphological characteristics, western Canada had broad and shallow northeast trending valleys and depressions incised through a gently rolling plain which was underlain by flat lying sedimentary rocks (Fenton 1984). Cycles of glacial and non-glacial events in the Quaternary Period produced a complex sequence of sediment deposits (Figure 3.9). With advances of the Laurentide ice preglacial drainages were blocked and caused the water from the Rocky Mountains to form proglacial lakes around the present town site. Sediments deposited in the lake were glaciolacustrine sediments, whose grain sizes varied by retreat and advance of ice sheets. During the Late Wisconsin glaciations, glacial sediments - usually called basal clay tills - were overlaid on the glaciolacustrine sediments. During the retreat of ice sheet, glaciolacustrine sediments were deposited on the glacial sediments in the postglacial lake which was the result of blocking the drainage by the glacier. Representative sediments can be classified as follows in descending order (Figure 3.9);

1. Glacial Lake Peace sediments (Unit 4)
2. Glacial sediments, mainly tills (Unit 3)
3. Advance phase glaciolacustrine sediments (Unit 2)
4. Glaciofluvial sediments (Unit 1)

Glaciofluvial sediments are mainly gravel, silt, and sand that were outwashed from the ice advance in Middle Wisconsin time (Figure 3.9). Generally meltwater from the ice sheet transported and sorted the glacial drift which was then deposited around the ice margin (Henderson 1959). They contain fluvial, subangular to subrounded, boulder to pebble size gravels with a high percentage of Canadian Shield lithologies, Precambrian in origin (Leslie and Fenton 2001).

The advance phase glaciolacustrine sediments were deposited when the advancing Laurentide ice in the Late Wisconsin age blocked drainage and made large proglacial lakes at or near the ice margin (Henderson 1959). Sediments deposited

in these lakes include fine to coarse sand and gravel with high contents of silt and clay (Leslie and Fenton 2001). Fine sediments of silt and clay were inter-stratified during their accumulation on the lake floor, producing bedding units, which are usually varved from alternating light and dark laminae (Jones 1966). These sediments are sources of high quality soils in the Peace River Lowland (Jones 1966) and the physical characteristics of these deposits give an insight into the landslide mechanisms occurring in Peace River valleys (Morgan et al. 2008).

Glacial sediments, mainly till or diamicton, are unsorted materials derived by erosion and deposition by glacial ice. They contain mainly boulder clays and gravels (Rutherford 1930). A recent study by Leslie and Fenton (2001) noted about 8 to 12 percent of the unit has been taken by clasts which are subangular to well rounded in shape, and have various degrees of weathering. Clay contents in these sediments are generally higher in the study area than those in east-central Alberta (Jones 1966). Pawluk and Bayrock (1969) analyzed physio-chemical characteristics of Alberta tills sampled in the Plains region and found hydrous mica dominated clay fraction of tills in northern Alberta. They also noted the difference of till composition between Laurentide and Cordilleran ice sheets in Alberta. The Laurentide (continental) tills are low carbonate, fine grained materials whereas Cordilleran tills contain high carbonates from the Paleozoic rocks of the Rocky Mountains and have a high percentage of coarse grained materials. These findings support the hypothesis that till constitutions are largely influenced by the local composition of underlying strata even though major typical materials of tills are transported by the glaciers. Glacial sediments deposited in different locations and depth indicate multiple invasions of glaciers throughout the Pleistocene epoch. Henderson (1959) described three different tills which gives a direct evidence of repeated advances and retreats of the Laurentide ice. Burke Lake glacial deposits in the Early Wisconsin age were described by Davies et al. (2005).

Glacial lake Peace, an ice dammed lake restricted to the Peace River basin (Taylor 1958, 1960), had covered most of the area between the Laurentide and Cordilleran ice sheets with water blocked by retreating ice in the Late Wisconsin age (Mathews 1980). A recent study by Leslie and Fenton (2001) indicated glacial lake Peace sediments included two subsequent units of sediments: (1) diamicton deposited as ice-rafted debris or debris flow from the adjacent ice; and (2) laminated silt and clay interpreted as glaciolacustrine sediments. The amount of glaciolacustrine sediments including both advance phase and glacial lake sediments is estimated to

be the higher percentage of Quaternary deposits than those of glacial sediments (Tokarsky 1967). Figure 3.9 shows massive glaciolacustrine sediments in Quaternary deposits.

3.2.2.3 Recent deposits

As the Late Wisconsinan glacier retreated further, major rivers from the Holocene glacial lakes drained and began to erode the complex sediments deposited in the Pleistocene rapidly. They created narrow, deep valleys such as the present Peace River valley. Fast flow of water brought coarse materials to form alluvial terrace deposits in the river bed and encroached through the Shaftesbury Formation and even reached the upper layers of the Peace River Formation (Unit 5 in Figure 3.9). Rapid river erosion was recorded by the different levels of the river terraces (Davies et al. 2005). Downcutting by erosion has produced a veneer of colluvium on the faces of valley slopes (Unit 6 in Figure 3.9). Jones (1966) indicated extensive landslide deposits where present rivers and streams traverse buried channels.

Where sand and silt were abundant, adjacent to the streams and glacial lakes, eolian deposits are developed as dunes (Henderson 1959; Unit 7 in Figure 3.9). Dunes found in the Peace River area were described by Henderson (1959) and Jones (1966). Other recent sediments which can be found in the study area include organic sediments in marshes, swamps, fens and bogs (Leslie and Fenton 2001; Davies et al. 2005), bottomland and beach deposits along lake shores (Jones 1966).

3.2.2.4 Chronological progress for the surficial geology in the study area

Understanding major geomorphic events provides an insight into the mechanism of major landslides in the study area. For example, laminated lacustrine strata can play a significant role in slope movements because of their structural characteristics that had been created during deposition. Layers in the Shaftesbury shale formation pre-sheared by the advancing phase of glaciers also reduce the resistance to slope movements. Valley rebound due to the release of high overburden loads where river valleys are cut into bedrock by postglacial streams can be an intrinsic factor in slope stability (Peterson 1958; Matheson and Thomson 1973; Imrie 1991).

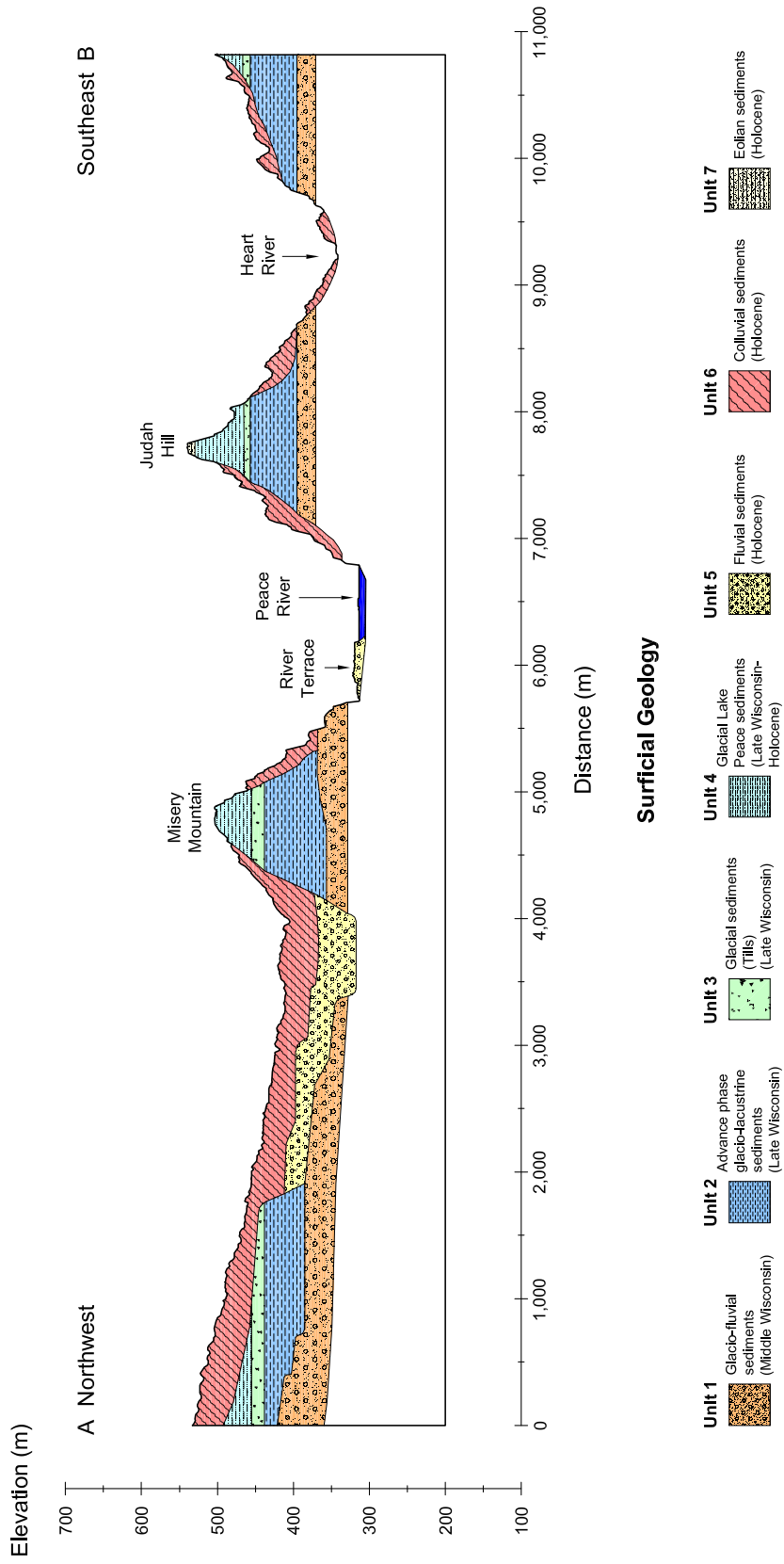
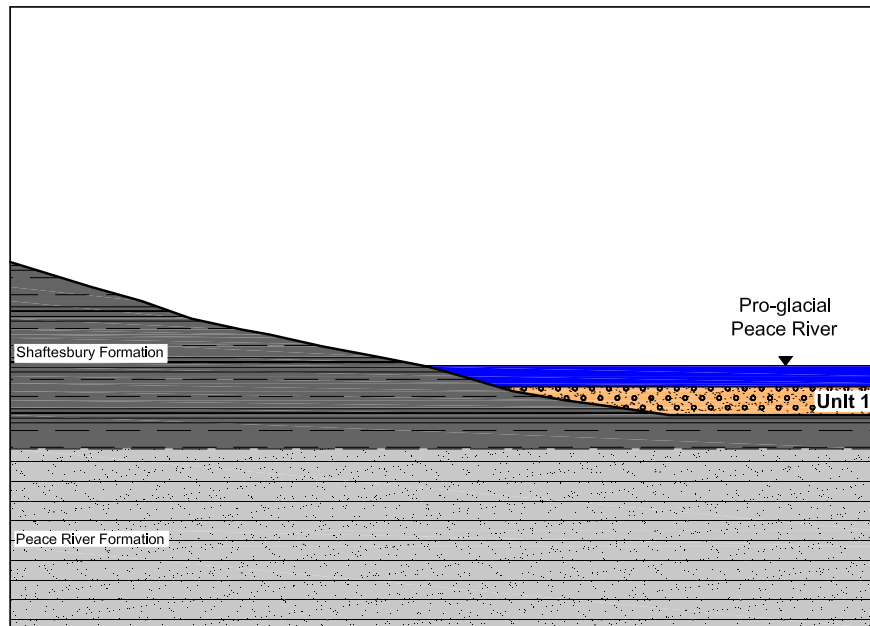


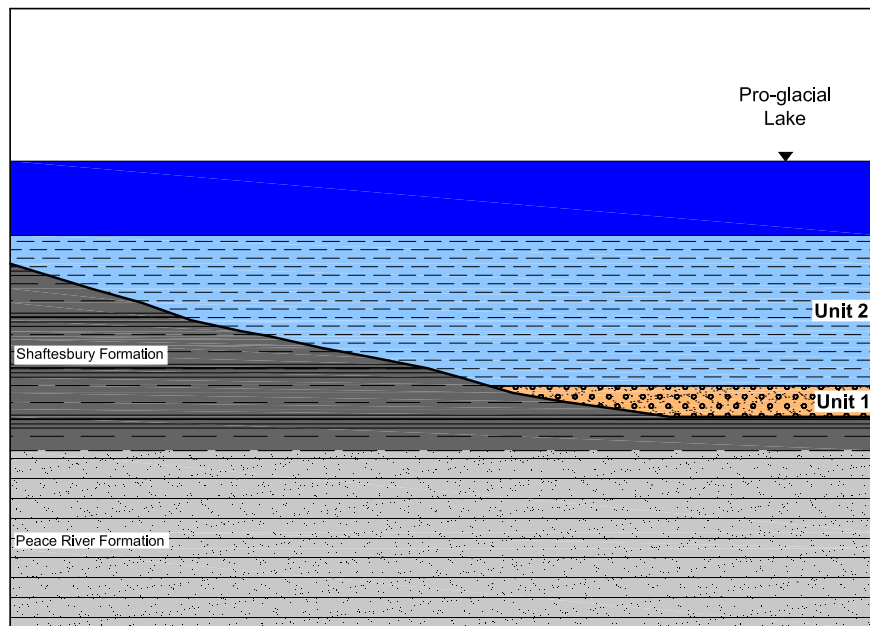
Figure 3.9 Geological distribution of surficial deposits. Bedrock stratigraphy as described in Figure 3.7 is voided for the clear presentation. Representative surficial sediments are described using colors, symbols, and unit numbers. The location of the cross section is presented in Figure 4.1. 6 times vertical exaggeration is applied to the ordinate. Subsurface profile of the surficial deposits is adapted from Morgan et al. (2008)

For descriptive purposes, therefore, major geomorphological events which influenced the surficial geology of the study area are briefly summarized. Summary is based on Henderson (1959) and Nilson and McCormick (1978). Explanations can be shown by conceptual diagrams (Figure 3.10).

- a. Early ice advance (Middle Wisconsin; 64 - 23 ka): Fluvial sediments produced by the advancing glaciers were deposited along the preglacial channels at and near the ice margin.
- b. During ice advance (Late Wisconsin; 23 - 12 ka): Proglacial lakes formed to block the preglacial drainages that originated from the Rocky Mountains. Lacustrine sediments were deposited. Varved layers were constituted by alternating different grain-sized lacustrine sediments deposited seasonally.
- c. Late ice advance (Late Wisconsin; 23 - 12 ka): Glacial sediments carried by Laurentide ice sheet deposited on the glaciolacustrine deposits. Due to the high load of the glacier, the top of the bedrock and glacial sediments were eroded and pre-sheared. The retreat of the glacier (around 12,000 years ago) triggered Glacial Lake Peace, an ice dammed lake, and lacustrine sediments were deposited above the glacial sediments.
- d. Early deglaciation (Holocene; 12 ka - present): As the ice sheet retreated, flow of water began to erode the Quaternary deposits and created the present narrow deep valleys. Fluvial sediments deposited on the river floor resulted in terraces. The present Peace River reached through the Shaftesbury Formation and entrenched within the Peace River Formation. In areas where silt and sand sediments are abundant, eolian deposits were formed.
- e. Post glaciation (Holocene; present): As the water eroded the toe of the river valley, steep slopes, especially outsides of river meanders, slid down and formed colluvium. The downcutting of the slope by river erosion is one of the major causal factors of landslides in the study area.

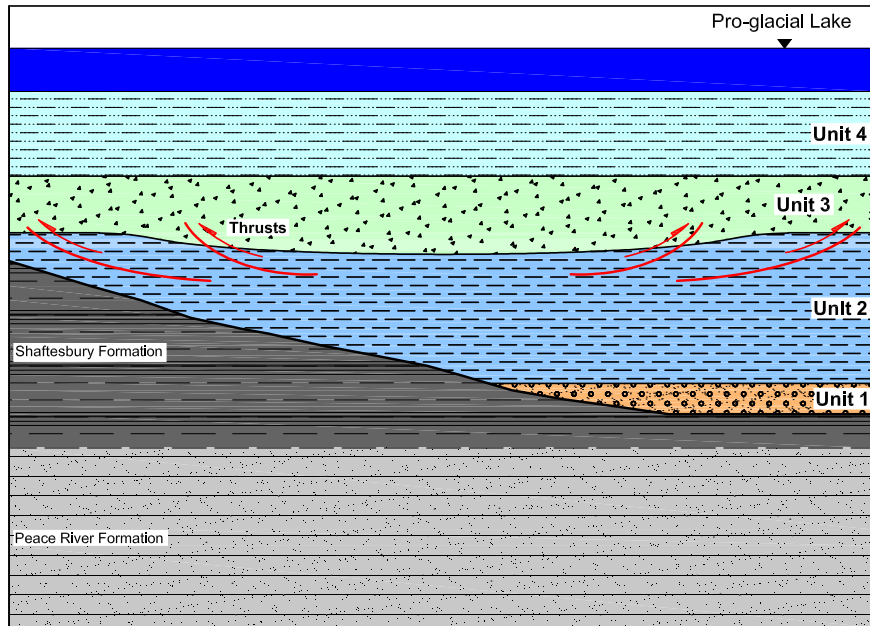


(a)

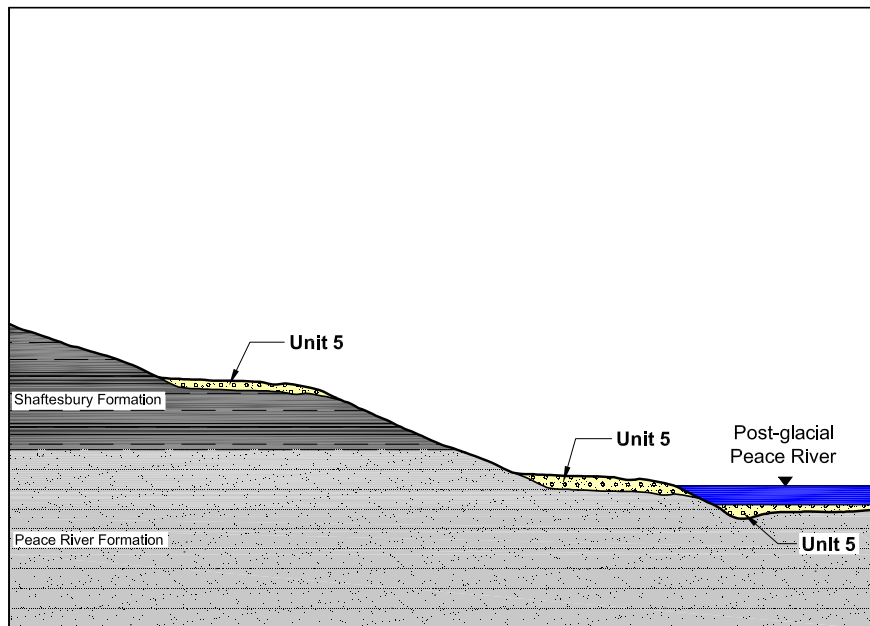


(b)

Figure 3.10 Conceptual diagrams for major geomorphological events. a. Early ice advance. b. During ice advance. c. Late ice advance. d. Early deglaciation. e. Post glaciation. Details of each stage are described in the text. Each surficial deposit is presented and explained in Figure 3.9. No scale is applied

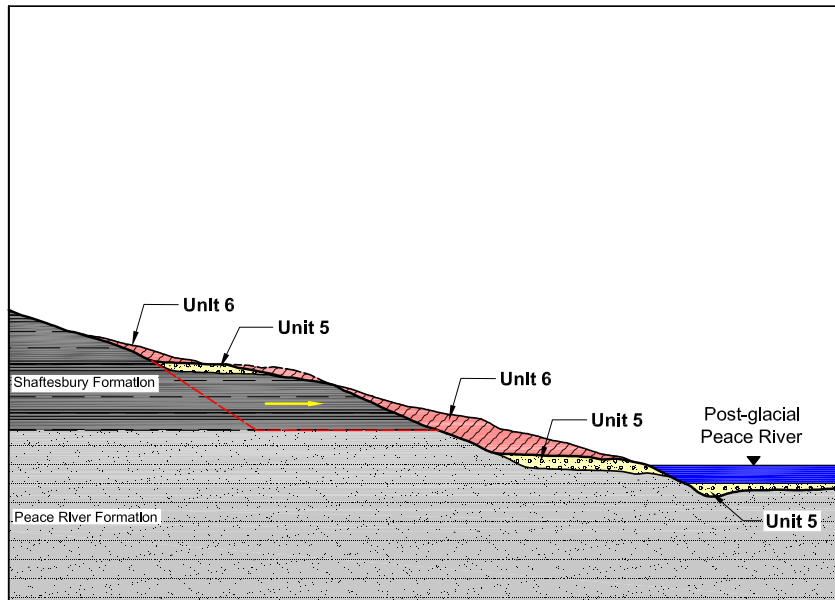


(c)



(d)

Figure 3.10 (Cont'd)



(e)

Figure 3.10 (Cont'd)

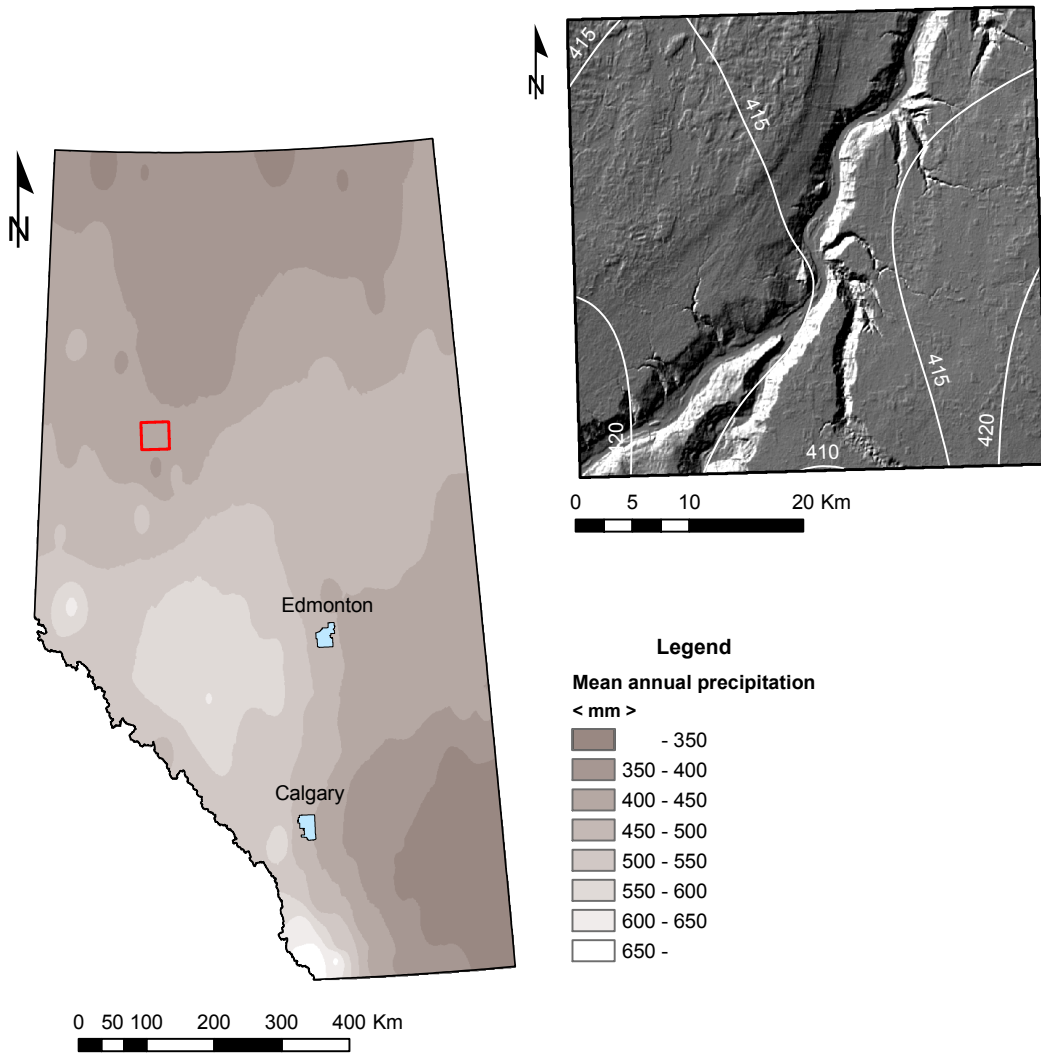
3.3 Meteorology in the Peace River Lowland

The climate characteristics of the Peace River Lowland can be categorized based on the Köppen-Geiger Climate Classification as snow (main climate), fully humid (precipitation), and warm arid (temperature) in the southwest and snow, fully humid, cool summer in other parts (Kottek et al. 2006). Located in the northwest of the forest and parkland region of Alberta, this area has the typical weather of the Western Canada Prairies, a moderately warm summer and a relatively cold winter (Jones 1966). Precipitation increases westward and the majority falls as rainfall in summer. The water equivalent of total snowfall is the larger part of precipitation in winter. Snow that covered the drainage basins melts in spring and causes high infiltration. With heavy rainfall, it raises the groundwater levels. The spatial distribution of the thirty year (1961 to 1990) mean annual precipitation, rainfall, snowfall, and temperature in the study area with those values for the whole province is presented in Figure 3.11, respectively.

Six weather stations are related to the study area (Figure 3.5). The Peace River A (Airport) weather station has the longest meteorological records (since 1955 to current) and provides data having a range of recording intervals down to hourly, although its proximity to the town is not ideal for the study. Other stations, however, have either limited or overlapped records. Records from these stations, therefore, should be used for validating the records obtained at the Peace River A station. The average and historical weather records taken from the Peace River A weather station are shown in Table 3.2.

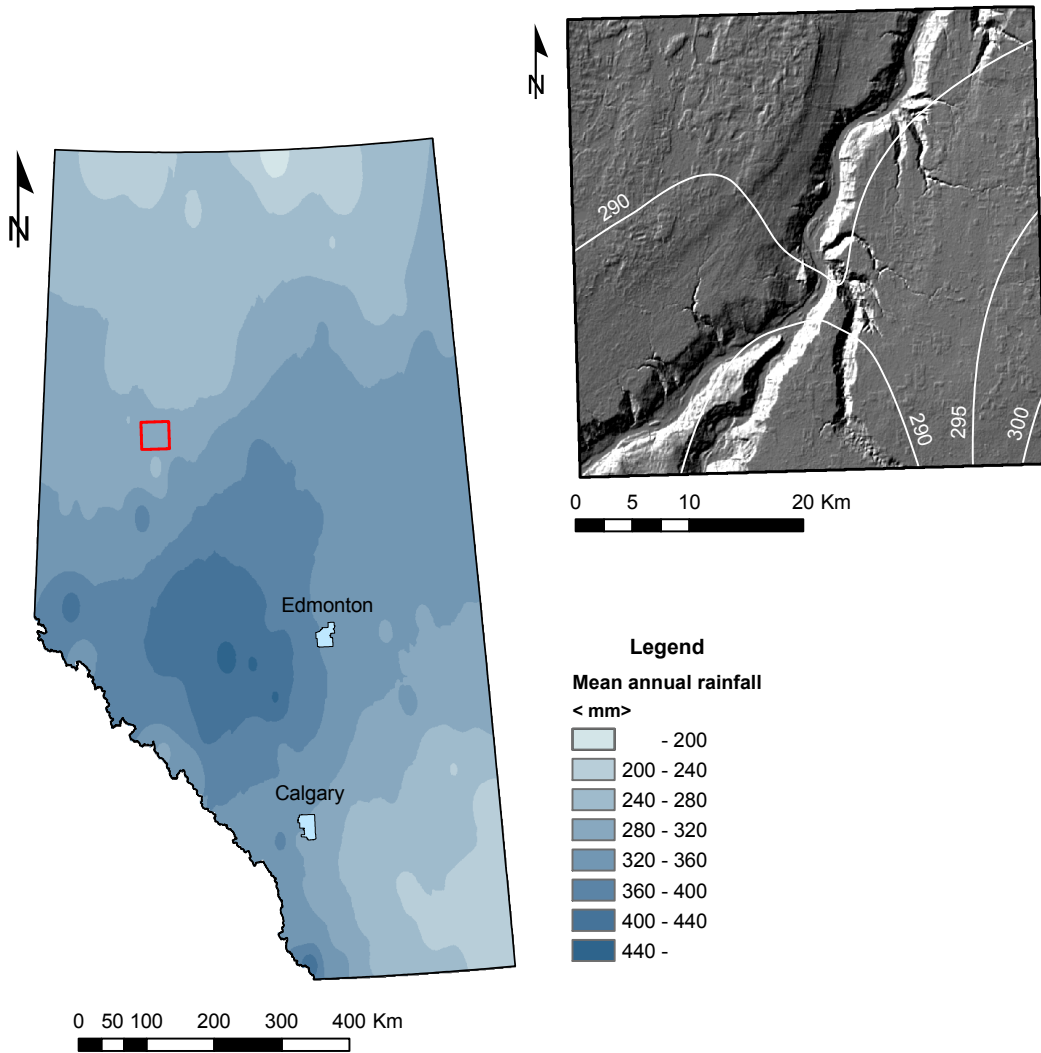
3.4 Landslide history in the Peace River Lowland

Tributaries located adjacent to the preglacial river channel of the Peace River which have experienced landslides are Montagneuse River (Cruden et al. 1997), Saddle River (Cruden 1991a; Keegan 1992; Cruden et al. 1993), Hines Creek (Lu et al. 1998), Eureka River (Miller 2000; Miller and Cruden 2002), Spirit River (Miller 2000; Miller and Cruden 2001), and Fox Creek (Kim et al. 2010a). Although all of these regional studies are useful for understanding the failure mechanism of the landslides which occurred in the Peace River Lowland, they are relatively remote



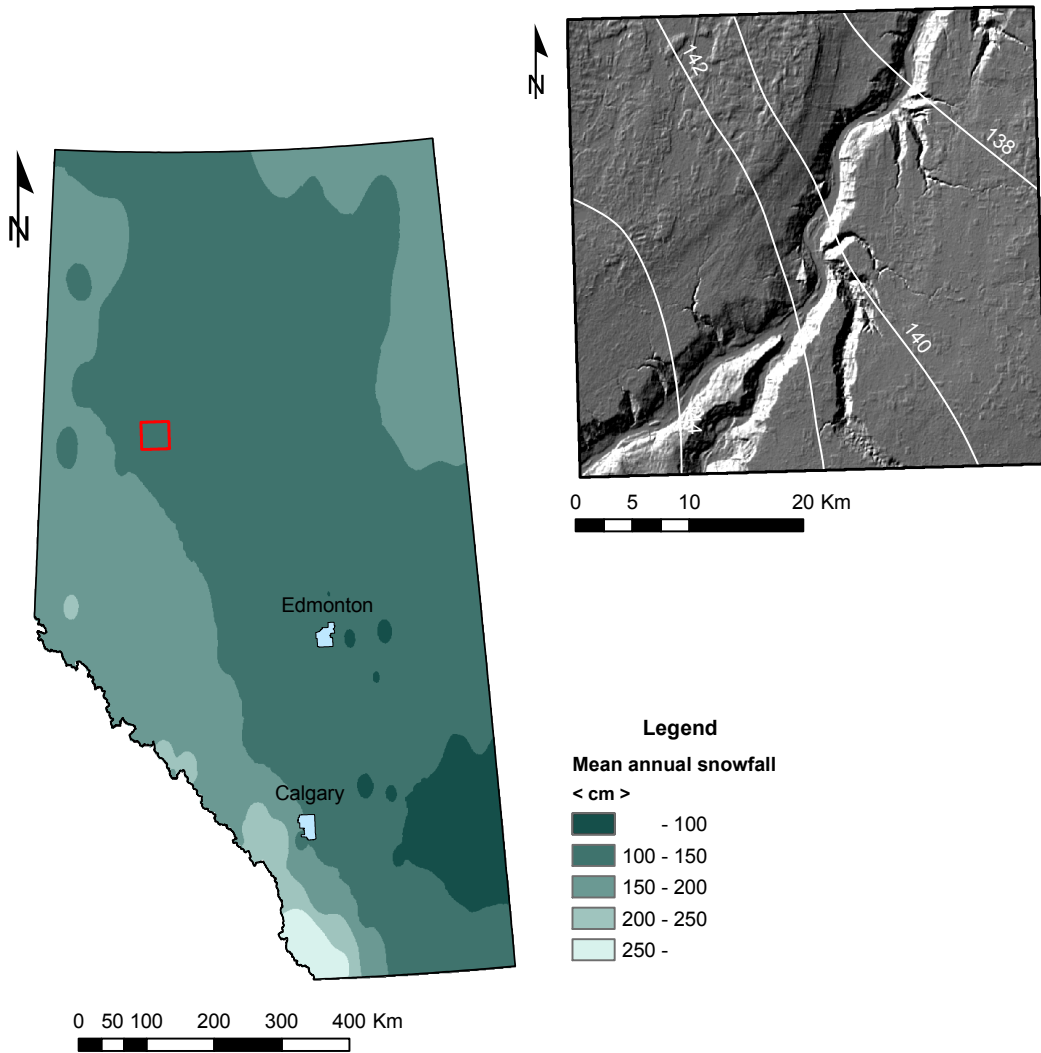
(a)

Figure 3.11 Spatial distribution of meteorological variables in the study area for the 1961 to 1990 normals period. a. Mean annual precipitation. b. Mean annual rainfall. c. Mean annual snowfall. d. Mean annual temperature. The distribution of each variable for the whole province is also shown in the left by using gradational color ramps. The area outlined indicates a boundary of the study area presented in the upper right. The aerial distribution of each climate variable in the study area is delineated by contours and corresponding values. A shaded relief image is derived from the SRTM dataset which has same dimension shown in Figures 3.1, 3.5, and 3.6. *Source:* Data from Agriculture and Agri-Food Canada (2011)



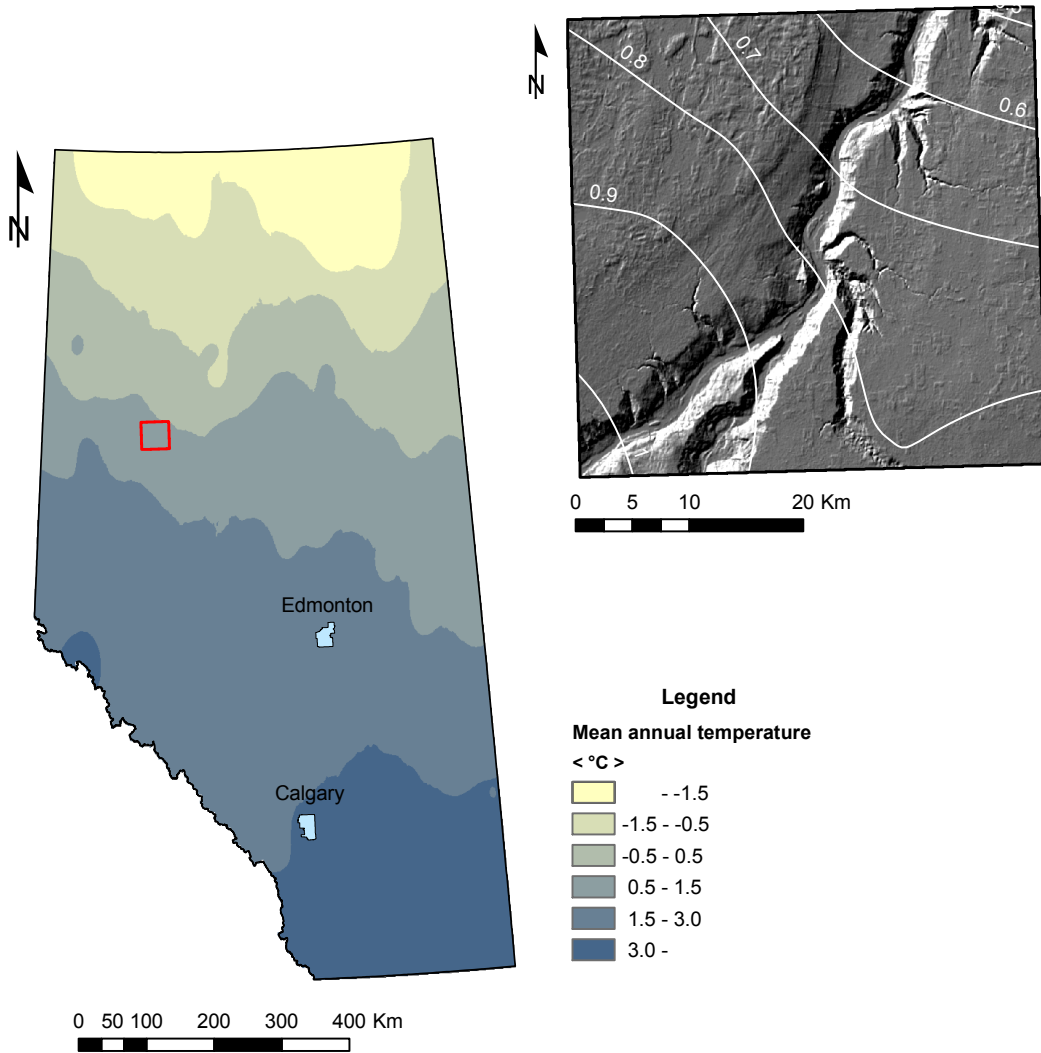
(b)

Figure 3.11 (Cont'd)



(c)

Figure 3.11 (Cont'd)



(d)

Figure 3.11 (Cont'd)

Table 3.2 Historical climate records in the Peace River Lowland obtained from Peace River A. *Source:* Data from Environment Canada (2009). Weather stations are shown in Figure 3.5

Weather station	Average (1971-2000)			Extreme (daily)		
	Temperature (°C)	Precipitation (mm)	Snow depth (cm)	Max. precipitation (mm)	Max. temperature (°C)	Min. temperature (°C)
Peace River A	1.2	402.3	8	53 [†]	36.7 [#]	-49.4 ^{††}

[†] May 4, 2000.

[#] July 13, 1945.

^{††} Jan. 13, 1950.

from the incorporated area. Detailed local studies on the landslides in the Town of Peace River were focused on the instabilities of slopes in residential areas and infrastructure such as highway and railway. An early study by Hardy (1957) described engineering experiences regarding landslides in clay shale along the highway at Pat's Creek. Sharma (1970) described strength properties of the postglacial lake sediments exposed along a portion of Highway 2 near the Town of Peace River. Ruel (1988) and Cruden et al. (1990b) reported a landslide affecting the Canadian National Railway which is located on the Heart River valley. This landslide was also examined to establish the remedial measures for the maintenance of the Secondary Highway 744 parallel to the Canadian National Railway (Diyaljee 1992). Barlow (1990) suggested effective mitigation approaches against the landslides in the residential subdivisions within the east bank of the Peace River. A recent study by Kjelland et al. (2009) examined 14 landslides grouped into seven areas along the Highway 744:04 located on the east bank of the Peace River. They also discussed stabilization measures including drainage, earthworks, retaining structures, and road alignments that applied to landslides and evaluated their effectiveness against stability and cost for maintaining landslide areas.

Figure 3.12 indicates a temporal distribution of recent landslides which had occurred in the Town of Peace River over thirty years against annual precipitation. It also shows annual precipitation at the time of the landslide occurrence is above or near the average value of 402.3 millimetres. Therefore it is expected that landslides in the study area were mostly caused by the unstable slope geometry due to urban developments, one of the preparatory factors, and abnormal precipitation acting as a triggering factor. Comprehensive examinations on recent landslides shown in Figure 3.12 are discussed in Chapter 4.

3.5 Conclusions

Chapter 3 focuses on gathering fundamental information which would help to understand the physical layout of the study area. It included geographic and economic perspectives, geologic, geomorphologic, and meteorological attributes. The Town of Peace River, located on river terraces of the Peace River, has developed in accordance with the population growth since the 1950s. As stable areas were fully packed, development commenced on slopes to make more spaces. Many valley

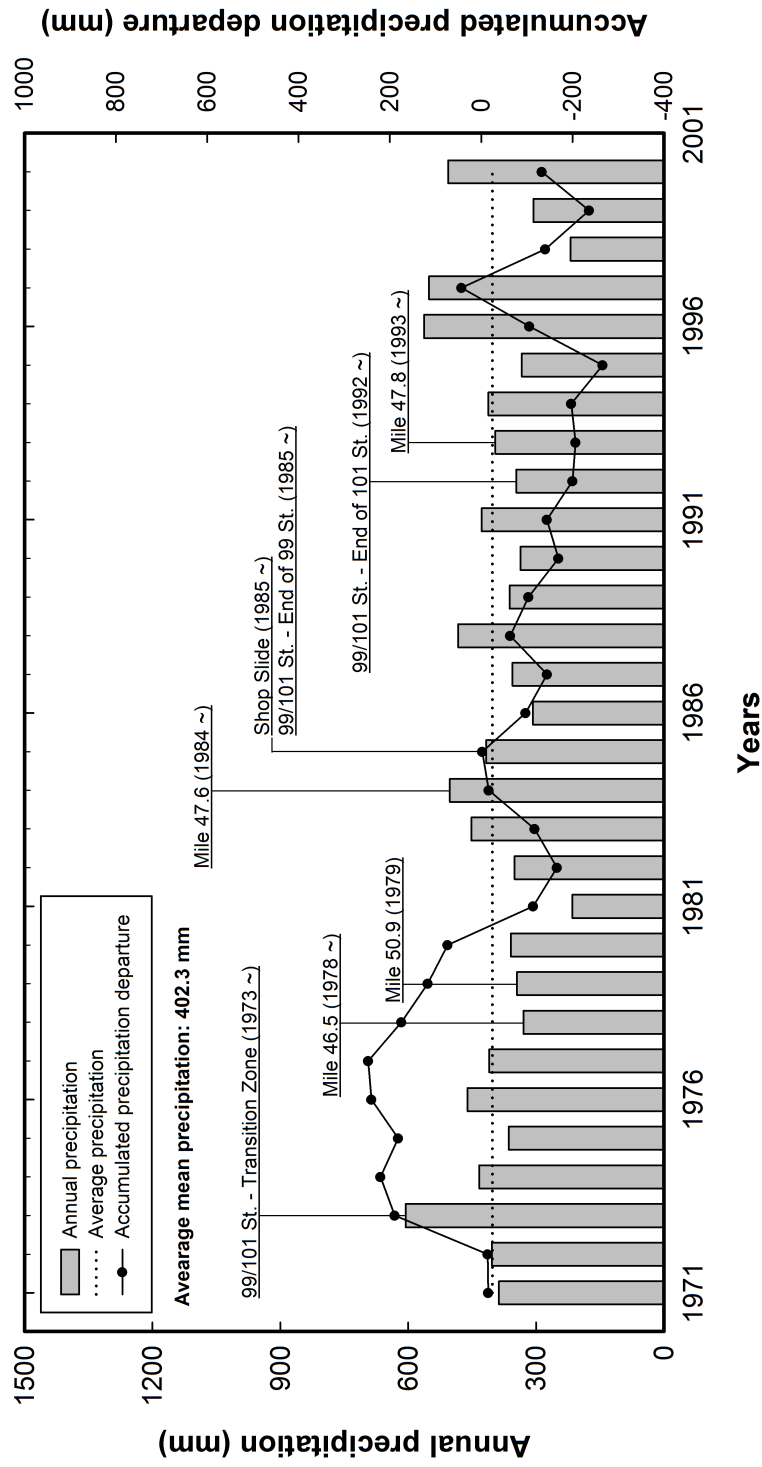


Figure 3.12 Temporal distribution of landslides in the Town of Peace River during thirty years (1971-2000). Vertical bars and the horizontal dotted line show annual and average precipitation, respectively. Landslides in the Town of Peace River since 1970 are also displayed. Accumulated departure of precipitation from mean is shown as black circles with solid line

slopes, however, are relatively young, consequently easy to move as even small disturbances occurred. The subsequent task, therefore, is to identify the geological setting which might be observed in the study area.

The first geological investigations on the study area were conducted in the late 1800s (Dawson 1881; McConnell 1893). Representative geological units are in ascending sequence: (1) bedrock formations; (2) buried channel deposits; (3) glacio-lacustrine and glacial sediments; and (4) fluvial and eolian deposits. These units, combined with major geomorphic events occurred in the Peace River area, would provide valuable information on the development of landslides. For example, laminated lacustrine strata which were created during the ice advance can play a significant role in slope movements observed in the study area. Landslides found in the Shaftesbury Formation mainly moved along the thin, pre-sheared layer induced by the glacial movements. Valley rebounds due to releases of high pressured loads where river valleys are cut into bedrock by postglacial streams can also be an intrinsic factor in slope stability.

In Chapter 3, overviews of landslides in the Peace River Lowlands are focused on the tributaries located adjacent to the preglacial river channel of the Peace River; these regional studies are useful for understanding the mechanisms of the landslides in the Peace River Lowland. A temporal distribution of landslides which had occurred in the study area since the seventies illustrates that the annual precipitation at the time of the landslides is above or near the average value of 402 millimetres. From this observation, it is expected that landslides in the Town of Peace River might be affected by precipitation and this can be used as a landslide triggering causal factor.

Chapter 4

Landslide characteristics in the Town of Peace River, Alberta

This chapter gives typical landslide characteristics observed in the recent landslides. Each recent landslide is analyzed to identify the potential rupture surface, groundwater distribution, movement behaviours, and possible landslide mechanisms. Efforts to determine strength properties on rupture surfaces materials are also carried out. Displacement records measured in these landslides are used to show their typical relationships with landslide causal factors. Movement patterns observed in landslide displacements are discussed to explain modes of landslides.

4.1 Recent landslides in the Town of Peace River

In this study, landslides which have occurred in the Town of Peace River since the 1970s, when developments encroached on slopes for residential subdivisions, are collected for the event-based inventory mapping (van Westen et al. 2008). This event-based inventory mapping helps to identify major triggering causal factors which drive landslides at that time and provides a good understanding of the mechanism for the reactivation of old landslides. Six landslides on the slopes in the Town of Peace River are collected from various technical reports published by either local municipalities or industry. Four landslides are located in the east bank, relatively steep slopes, two are in gentle slopes of the west bank of the river valley (Figure 4.1), all of which are located in residential areas close to roads and railways. Table 4.1 summarizes general information on these landslides and detailed descriptions of individual landslide are given in the following sections.

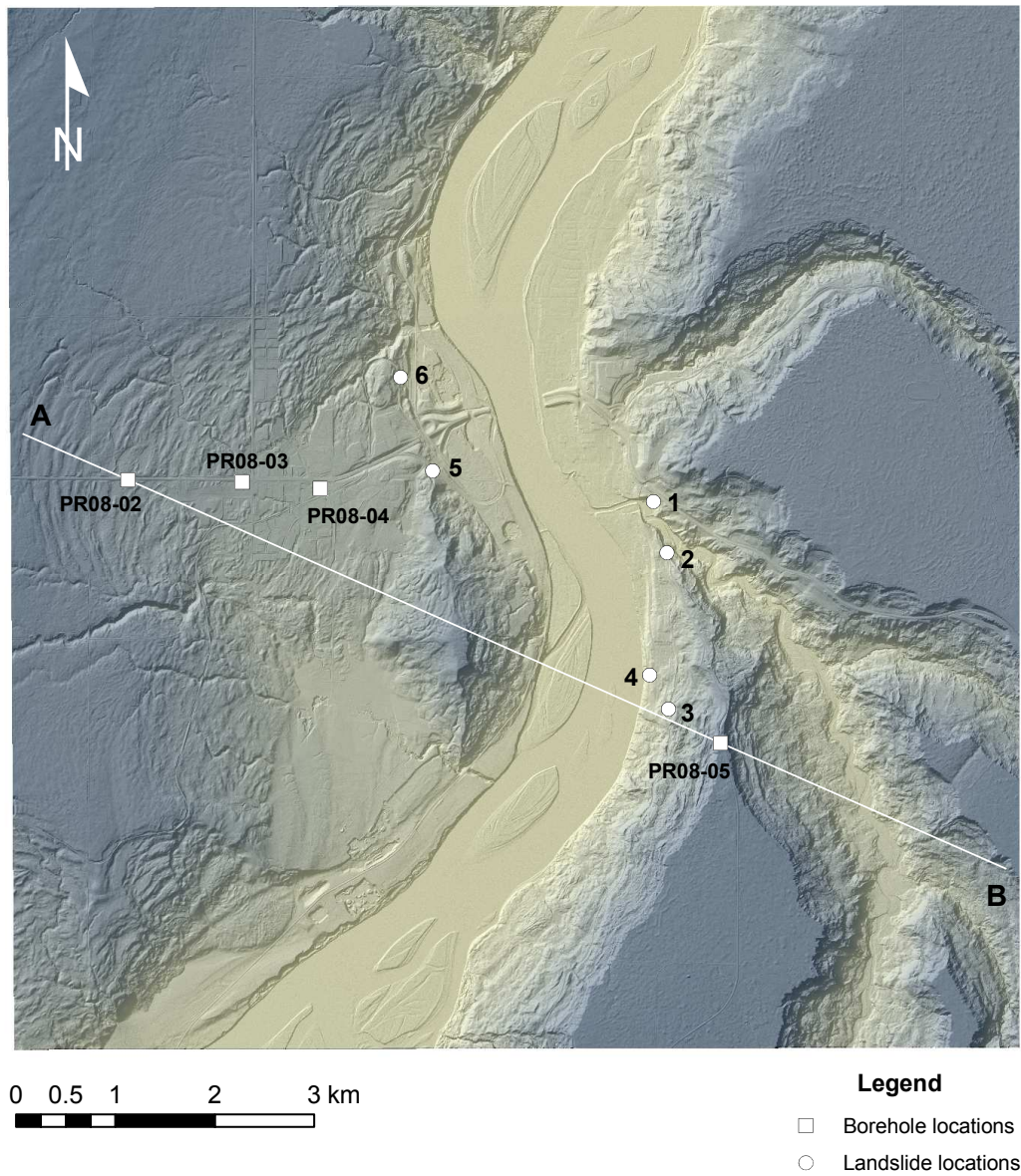


Figure 4.1 Distribution of recent landslides in the Town of Peace River. The Peace River flows northward. Numbers with white solid circles represent the location of each landslide: 1. Mile 47.8; 2. Mile 47.6; 3. Mile 46.5; 4. 99/101 Streets; 5. Shop Slide; and 6. Mile 50.9. A shaded relief image shown in the background is obtained from the LiDAR dataset. Boreholes drilled by the Alberta Geological Survey (Morgan et al. 2009) are shown as white squares. Line A-B shows the cross section indicated in Figure 3.7

Table 4.1 Recent landslides in the Town of Peace River since 1970

ID [†]	Location		Date [‡]	Type	Infrastructures
1	Mile 47.8		1993	Translational block slide / Single rotational slide	Railway
2	Mile 47.6		1984	Translational block slide	Railway / Road
3	Mile 46.5		1978	Translational block slide	Railway
4	99/101 St.	End of 101 St.	1992	Translational block slide	Residential area
		End of 99 St.	1985		
		Transition Zone	1973		
5	Shop Slide		1985	Translational block slide	Road
6	Mile 50.9		1979	Flow	Railway

[†] IDs are shown in Figure 4.1.

[‡] Represents the year when the initial movements (displacements, tension cracks) had occurred.

4.1.1 Mile 47.8 Slide (Ball Park Slide)

The Mile 47.8 Slide is on a slope near a ball park located on the east bank of the Heart River. In late 1993 and early 1994, structures of the Twelve Foot Davis ball park including dugout and fence were distressed by the landslide and a minor derailment took place on the railway track above the ball park. Aerial photos indicated previous instabilities of the study area prior to 1952 (Leir and Savigny 1996). Landslide deposits from prior to 1952 were removed for the development of playground and related facilities. Figure 4.2 shows an oblique view of the Mile 47.8 Slide.

Leir and Savigny (1996) described a geological stratigraphy of the landslide area. The landslide in 1993 to 1994 occurred below the Canadian National Railway (CNR) track which is filled with cinders, ballast, and gravel. This fill is underlain by colluvium and till which are commonly slickensided. Till rests on the coarse gravel near the slope face and on the Shaftesbury Formation clay shale and Peace River Formation sandstone in an eastward direction. Approximate bedrock elevation is around 340 metres and drops off at the lower half of slope (Figure 4.3).

As delineated earlier and in Figure 4.3, bedrock units are stepped eastward and flatten at an elevation of 340 metres. Between the till and bedrock, about 1 to 2 metres of poorly graded, coarse gravel is shown in boreholes 95-2 and 3. This layer is believed to be part of fluvial sediments containing Canadian Shield lithologies (Morgan et al. 2008). This unit is usually found in the floodplain of the Peace and Heart Rivers and is characterized by pre-Late Wisconsin, moderately sorted gravel and poor to moderately sorted fine to coarse sand (Leslie and Fenton 2001).

In the lower half of the slope, near boreholes 95-5 and 7, the colluvium consisting of landslide deposits is underlain by the bedrock. Especially in borehole 95-7, silt sediments including fine sand are found between the colluvium and the bedrock. These are considered as postglacial fluvial sediments after rapid erosion.

Four slope inclinometers (boreholes 95-2, 4, 5, and 7) and three piezometers (boreholes 95-1, 3, 6) were installed in 1995 within seven boreholes drilled to measure ground movements and pore water pressures in the study area. For the slope inclinometers, boreholes 95-2 and 4 are located in the upper half of the slope whereas boreholes 95-5 and 7 are installed in the lower portion of the slope. The first reading was taken in the late 1995 with subsequent data acquisition in 1996 (Table 4.2).

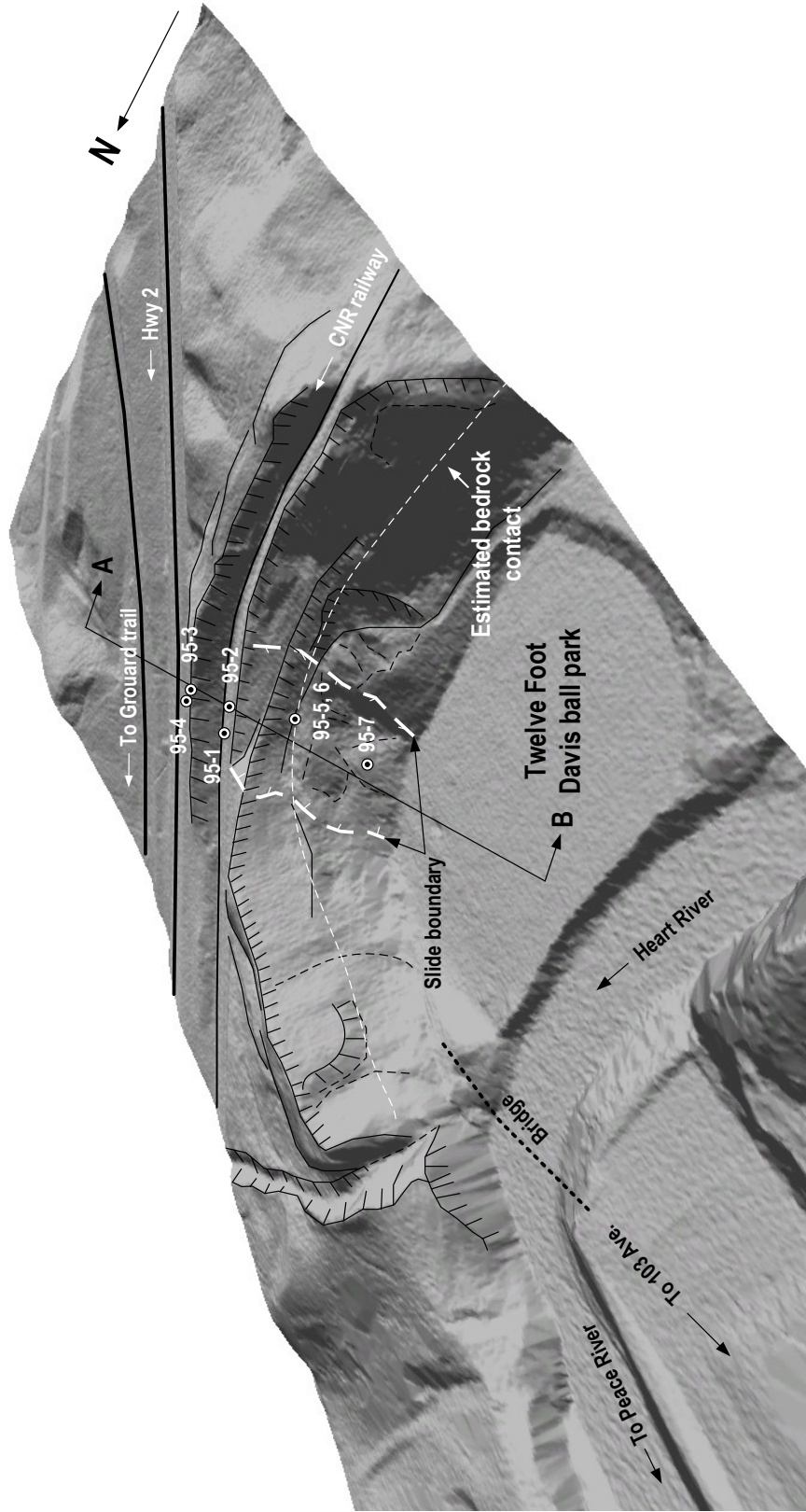


Figure 4.2 Perspective view of the Mile 47.8 Slide. Scale 1:1,500. Looking northeast. Landslide extent and boreholes are also shown. Line A-B shows the cross section of the slide (Figure 4.3). The three dimensional hillshade is derived from the LiDAR dataset obtained in 2007

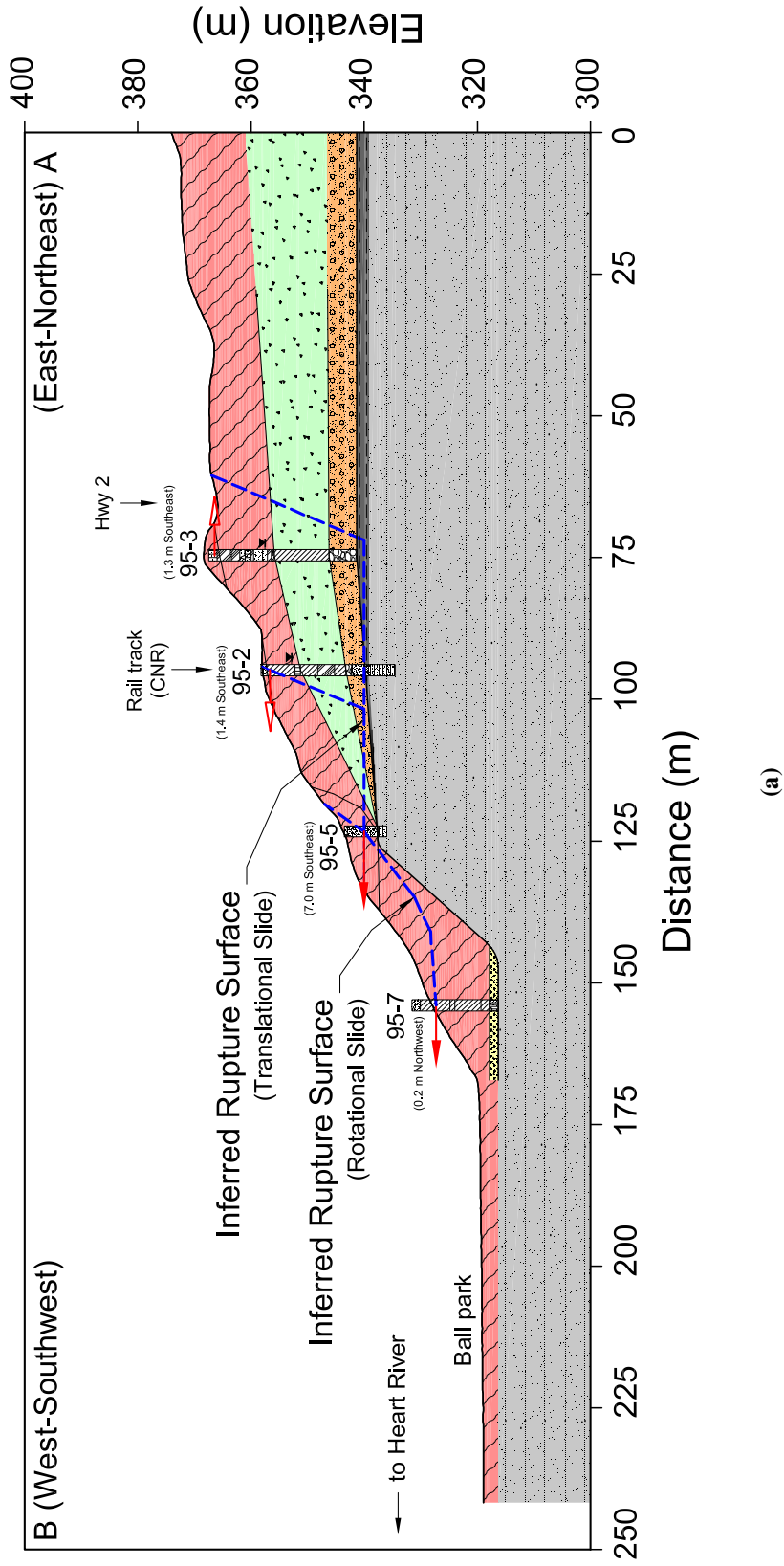
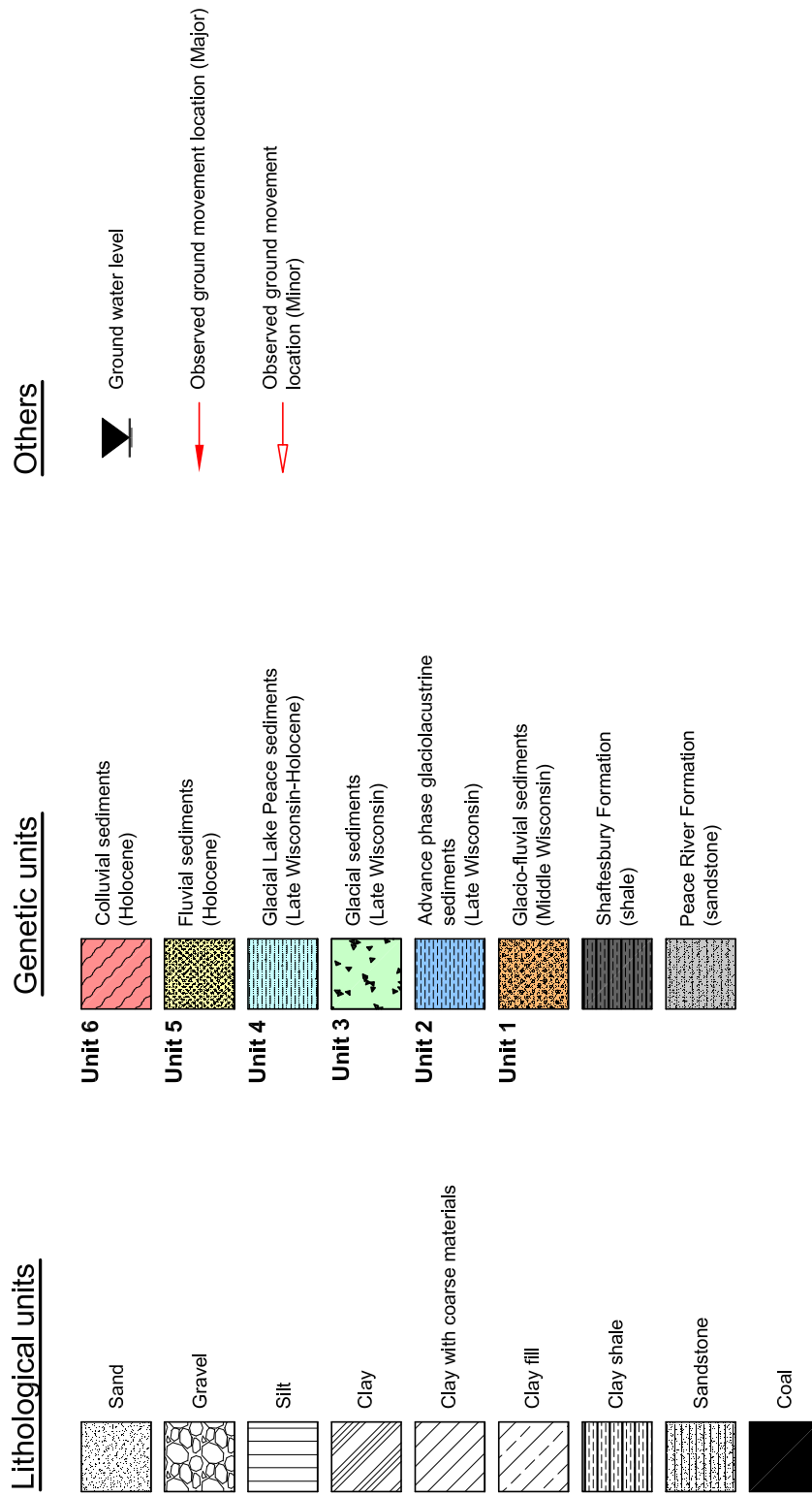


Figure 4.3 Cross section of the Mile 47.8 Slide. a. Cross section of the slide. Boreholes and their proximity to the cross line are indicated. Lithological and genetic stratigraphies are also shown. Observed locations for ground movements are illustrated by red arrows. Ground movement delineated by a red open arrow in borehole 95-3 was imported from borehole 95-4 in which the slope inclinometer was originally installed (Figure 4.2). Inferred rupture surfaces are delineated by thick blue dashed lines. Detail borehole data are also noted in Appendix A. b. Representative symbols for a. Lithological and genetic units are illustrated with their unique symbols and colors. Unit numbers in genetic stratigraphy are equivalent to those shown in Figure 3.9. Other features such as groundwater level and observed locations for ground movements are also presented



(b)

Figure 4.3 (Cont'd)

Table 4.2 Summary of slope inclinometer measurements at the Mile 47.8 Slide

BHs	95-2	95-4	95-5	95-7
Depth of movement (m) [†]	2	2	4	5
Max. displacement (mm)	4	2	47	41
Ave. movement rate (mm/year)	8	-5 [‡]	100	125

[†] Depth below ground surface.

[‡] Upslope direction.

As shown in Table 4.2 slope movements occurred in the lower half of the slope especially around boreholes 95-5 and 7. In the upper slope, however, no significant movement was detected. Two rupture surfaces based on slope inclinometer measurements are estimated in different locations: (1) at the contact between fluvial sediments and bedrock; and (2) within the clay colluvium deposits (Figure 4.3). The former indicates a deep seated translational landslide mechanism whereas the landslide behavior for the lower portion of slope is similar to a rotational slide having a concave rupture surface. Movement behaviors obtained in boreholes are shown in Figure 4.4. Movements at boreholes 95-5 and 7 show that the slope movements in the lower slope increased along with increasing precipitation. Increased infiltration from heavy rainfall and snow melt would cause a rotational movement in the lower slope followed by a deep translational slide above the rotational slide. The upslope movement of boreholes 95-3 and 4 show the depth of the rupture surface is deeper than the length of boreholes which points to a retrogressive behavior.

Groundwater level in the study area was also monitored with slope movement measurements (Figure 4.5). Groundwater level in borehole 95-6 which is near borehole 95-5 (Figure 4.2) showed a dry condition during the measuring periods despite large slope movements at boreholes 95-5 and 7. This may suggest that large movements in the lower slope would make pore water pressure decrease or not change where large movements occurred. Groundwater levels in boreholes 95-1 and 3 are at 352 and 357 metres, respectively, and these may be perched water trapped in sand and silt pockets within colluvial sediments.

One possible cause of the 1993 to 1994 Mile 47.8 Slide is the infiltration of snow melt in spring. Precipitation records compared with the 30 year average value (Figure 4.6) indicate that there was over 40 centimetres of snow in December 1993 and high precipitation in January 1994 which also fell as snow. Infiltration of snow

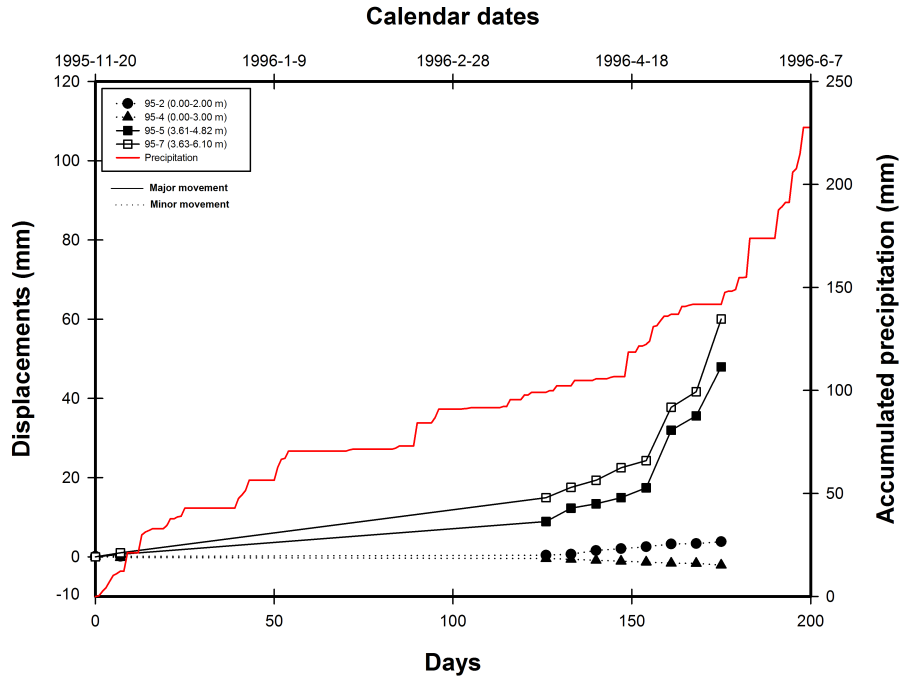


Figure 4.4 Landslide movements at the Mile 47.8 Slide. Precipitation data of the measurement period are also described. Location of boreholes is shown in Figure 4.3. Detailed data are also noted in Appendix A

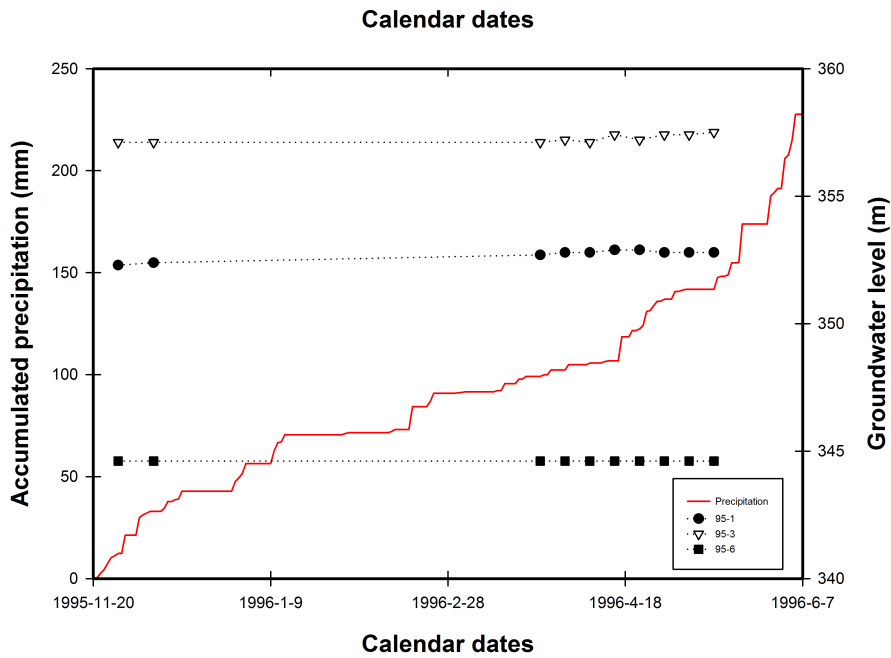


Figure 4.5 Temporal groundwater distribution at the Mile 47.8 Slide. Location of boreholes is shown in Figure 4.3

melt into the slope would initiate landslide movement in the study area by increasing pore water pressure.

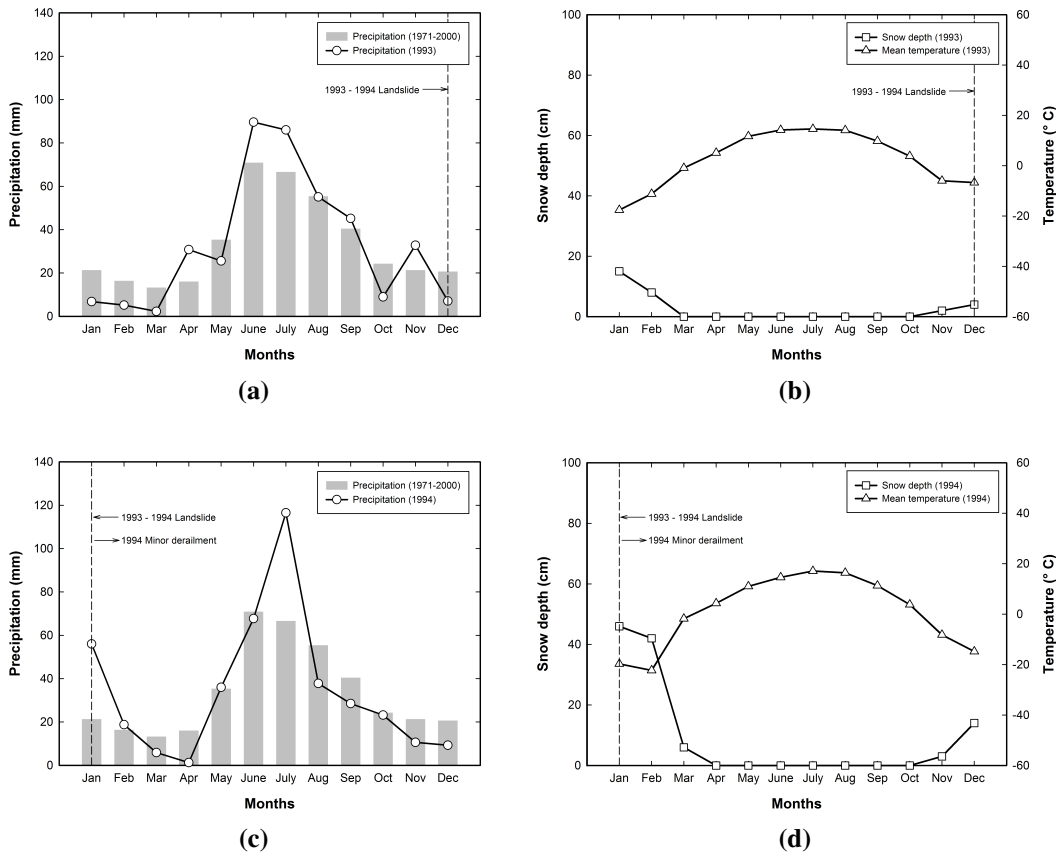


Figure 4.6 Meteorological records on the Mile 47.8 Slide in 1993 and 1994. a and c. Annual precipitation in each year compared with the 30 year average value represented in gray bars. b and d. Mean temperature and snow depth on the ground in each year

4.1.2 Mile 47.6 Slide (Judah Hill Slide)

The Mile 47.6 Slide, or the Judah Hill Slide, occurred 1.1 kilometres upstream of the confluence of the Heart River, one of the tributaries of the Peace River, and the Peace River. The slide is located on the west bank of the Heart River and has a toe about 40 metres above the river level. The Canadian National Railway (CNR) and Alberta Transportation Secondary Highway (SH) cross on the crown of the slide (Figure 4.7). These two transportation routes carry significant freight and commuter traffic into the town of Peace River.

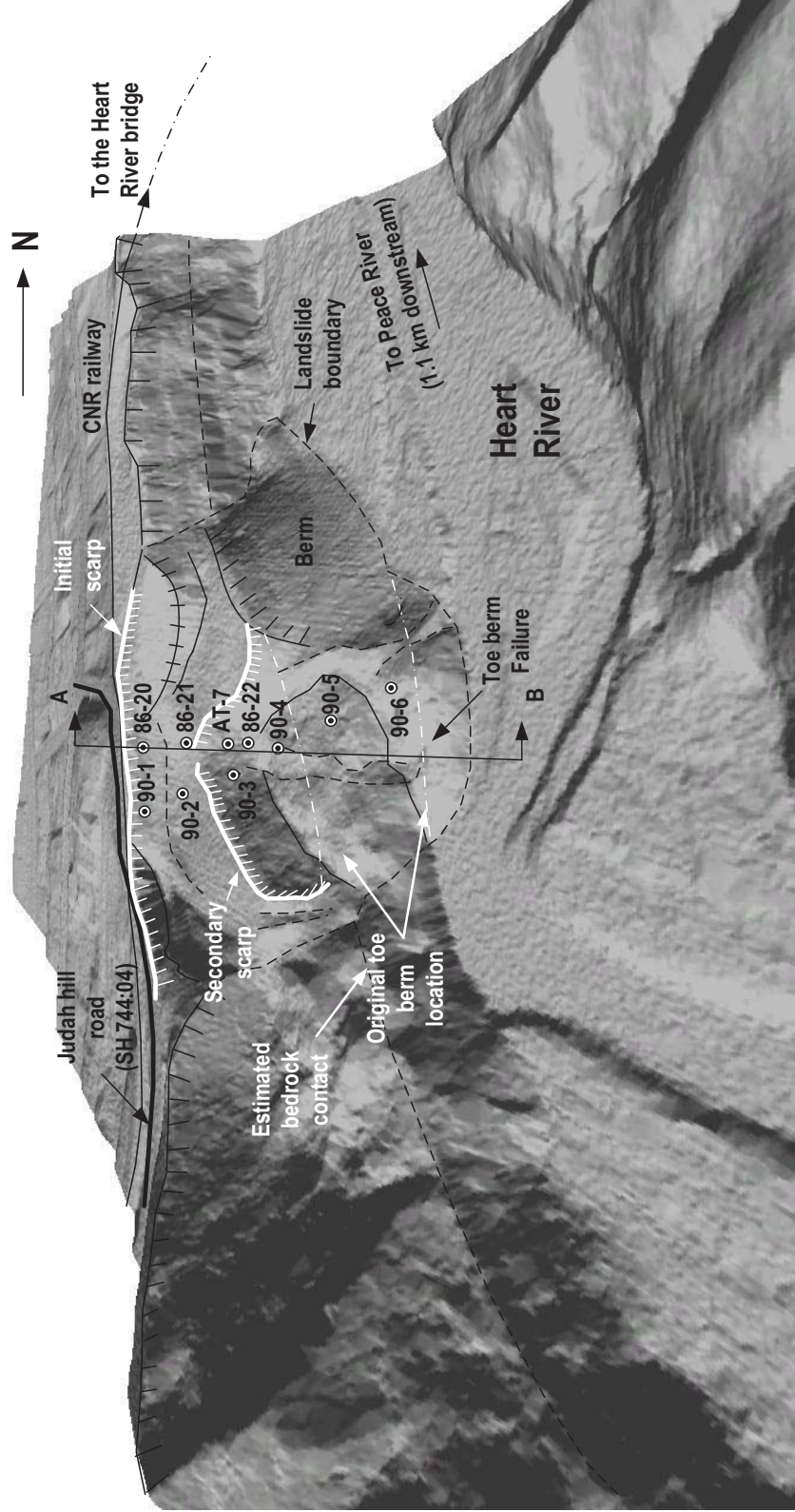


Figure 4.7 Perspective view of the Mile 47.6 Slide. Scale 1:2,000. Looking west. Landslide scarps and boreholes are also shown. Line A-B shows the cross section of the slide (Figure 4.8). The three dimensional hillshade is derived from the LiDAR dataset obtained in 2007

The history of slope movement at the Mile 47.6 Slide is described by Ruel (1988) and Dyaljee (1992). The initial instability of the Mile 47.6 Slide started in June 1984 after the asphalt pavement on the roadway was completed. Less than a metre of railway track subsidence and tension cracks on the road were reported and attempts to place timber piles on the slope to prevent further movements were made. They were not effective because the rupture surface of the slide was located below the timber piles driven to resist the movement. The railway was realigned to the west and the road crossing was also relocated southward. After a few weeks a progression of the movement required the railway track and road crossing to be moved farther west and south, respectively. In July 1984 a toe bulge was observed on the north end of the slide and one year later, in 1985, an accelerated retrogressive slope movement caused a significant settlement on the west bank of the Heart River. This made 25 metres of stabilizing berm at the toe of the slide necessary. Although the berm was designed to provide a factor of safety higher than 1.5, tension cracks were found on the berm and at the head scarp. Surface drainage systems preventing run off and infiltration into the slope were made by the Alberta Transportation. In April 1987, however, portions of the south flank of the berm structure moved, affecting the railway and road. Measures were used to prevent ongoing slope movements. Chronological instabilities and their mitigations are summarized in Table 4.3.

A typical subsurface stratigraphy is shown in Figure 4.8. The dominant bedrock formation in this slide area is the Paddy Member of the Peace River Formation which consists of sandstone with thin shale and coal (Cruden et al. 1990b). The Peace River Formation is located between elevations of 318 to 340 metres in the Mile 47.6 Slide area. At 338 metres Shaftesbury Formation, dark gray, marine, fissured, slickensided clay shale lies over the Peace River Formation. Two distinct river terraces were found at elevations of 315 and 324 metres, which are the result of river erosion after the last glacial retreat. The general surficial stratigraphy in this slide area is mainly clay till deposits consisting of medium-plastic, silty clay with granular material lenses which are believed to be preglacial fluvial sand and gravel. Detailed surficial geology compositions introduced by Savigny and Harris (1988) and Morgan et al. (2008) are described in Table 4.4.

The rupture surfaces inferred from 1986 slope inclinometer data (Figure 4.8) show two distinct movements located in the upper and lower slopes between elevations 329 to 340 and 326 to 329 metres. They represent slope movements in 1984 and 1987, respectively. Rupture surfaces are nearly horizontal and pass through col-

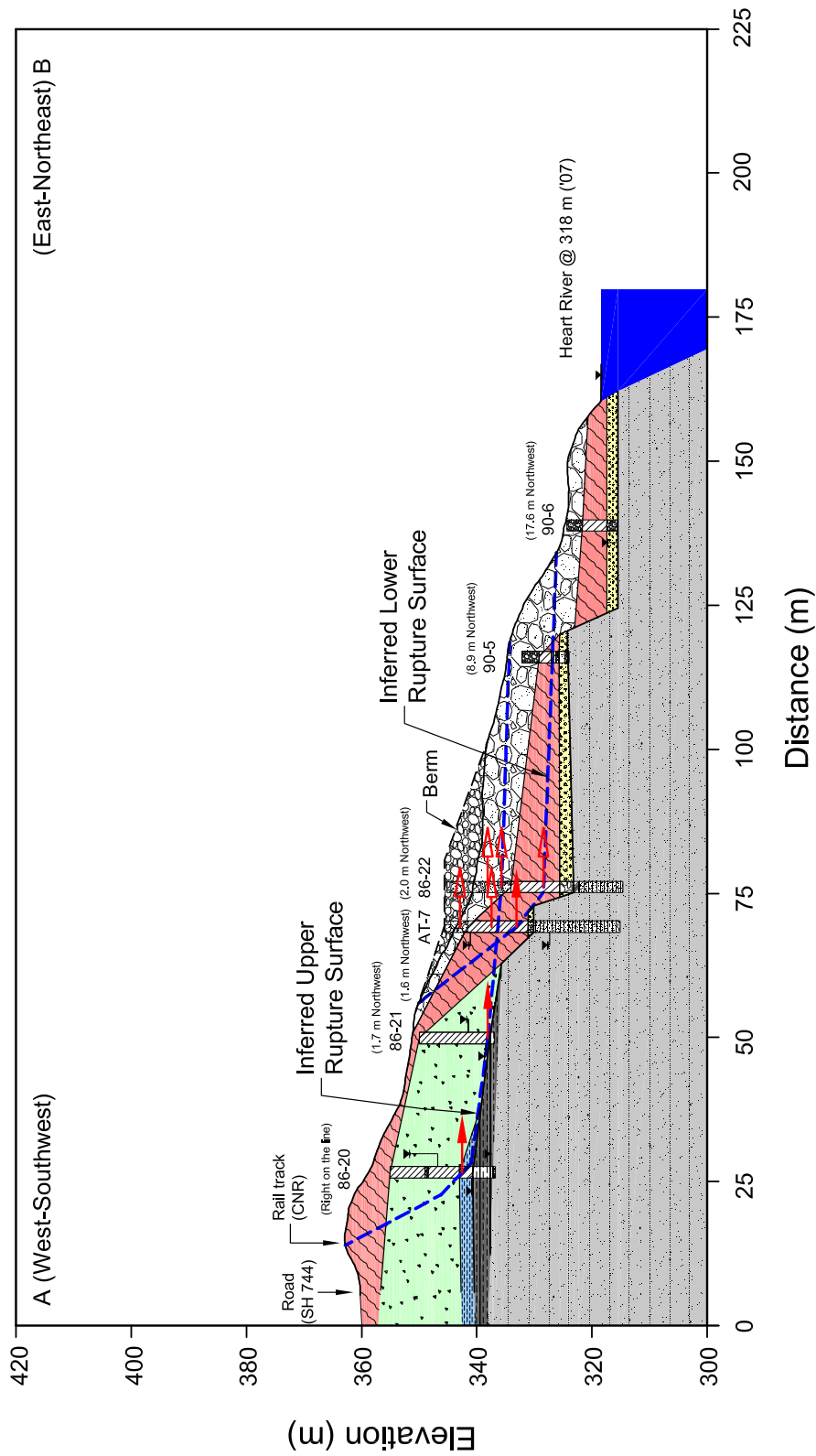


Figure 4.8 Cross section of the Mile 47.6 Slide. Boreholes and their proximity to the section plane are indicated. Lithological and genetic stratigraphies are also shown. Observed locations for ground movements are illustrated by red arrows. Inferred rupture surfaces are delineated by thick blue dashed lines. Representative symbols for lithological and genetic units are also presented in Figure 4.3. Detail borehole data are also noted in Appendix A

Table 4.3 Instability and mitigation chronology at the Mile 47.6 Slide. *Source:* Data adapted from Diyaljee (1992)

Year	Significant instability	Mitigations
1984	Slope movement initiated with subsidence of railway track (June)	Emergency retaining wall Railway track realignment Site investigation (1st.)
1985	Progressive slope movement continued (July to Dec.)	-
1986	Tension cracks on the berm and at the head scarp after completion of berm (May to June)	Toe berm installed Surface drainage installed Site investigation (2nd.)
1987	Toe berm failed (April)	Horizontal drainage installed
1988	Road depression continued	Surface drainage installed Retaining wall installed Preformed cracks established
1989	Slope behind the retaining wall failed (Aug.)	Deep well installed Railway track realignment Tie back wall installed Vertical pile wall installed
1990	Vertical pile wall tilted	Sawdust backfilling Surface drainage rerouted

Table 4.4 Surficial geology distribution at the Mile 47.6 Slide area. Each unit and its description are shown at legend in Figure 4.7. *Sources:* Data from Savigny and Harris (1988) and Morgan et al. (2008)

Unit	Name	Description
1	Silty sand and gravel	Berm material
2	Clay	Colluvial sediments (Holocene)
3	Gravel and sand	Fluvial sediments (Holocene)
4	Glacial lake clay and silt	Advance phase glaciolacustrine sediments (Late Wisconsin)
5	Bedrock and undifferentiated basal till	Shaftesbury Formation (shale) Peace River Formation (sandstone)

luvial sediments, glaciolacustrine sediments, glacially-deformed Shaftesbury Formation, and berm materials (Unit 1, 2, 3 and 5 in Table 4.4). Estimated strength properties mobilized in the initial movement in 1984 are shown in Table 4.5.

Table 4.5 Estimated strength properties mobilized the initial movement in 1984. *Source:* Data from Savigny and Harris (1988)

Unit [†]	Effective cohesion (kPa)	Effective friction angle (°)
1	10	28
3	10	9

[†] Each unit is shown in Table 4.4.

Ruel (1988) concluded that a progressive failure might have occurred in this slide area because shear strength values decreased as the slide progressed. Berm structure which was effective in preventing the upper slide in 1984 may have had an adverse effect on the stability of the lower slope. This could have been a major trigger of the 1987 slide in the lower slope. From the shape of rupture surfaces and mechanism of movement it is inferred that translational block slides occurred on the slope.

The landslide movements measured from the borehole data in 1986 are illustrated in Figure 4.9. It also shows precipitation recorded during the same measurement period. Figure 4.9 notes a clear difference in movement behaviors between the scarp and rupture surface. While slope movements at boreholes 86-21 and 22 representing the movements at the rupture surface show high rate of movements followed by shearing of the boreholes, movements at the back scarp (boreholes 86-20 and AT-7) only illustrate an increasing trend without any failure of boreholes.

Groundwater tables were estimated from several piezometers in boreholes (Figure 4.10). Groundwater varies with subsurface strata. Near the bedrock, the groundwater table is very low due to the sub-drain effect of the Peace River Formation (sandstone) and post glacial fluvial sediments (Unit 1 and 3 in Table 4.4). However, it is occasionally higher in sand and gravel lenses within the clay till and colluvium (Unit 4). High groundwater table is due to the infiltration of surface runoff. Annual and 30 year average precipitation, mean temperature, and snow depth on the ground in 1984, 1985 and 1987 are shown in Figure 4.11. Heavy precipitation was recorded between April and June in 1984. This would lead to a rise of pore water pressure below transportation routes, to cause a subsidence in June 1984. Snow on the ground

during the end of 1984 and early 1985 melted in the spring of 1985. Melting water combined with high precipitation in summer and fall 1985 may cause a progressive slope movement. In 1987, high precipitation during March to April may induce the toe berm failure (Table 4.3). Besides changes of the physical topographic condition due to railway and road constructions, high and sustained infiltration of surface runoff would be a major trigger of the landslide in the Mile 47.6 area.

4.1.3 Mile 46.5 Slide

The Mile 46.5 Slide is situated on the east bank of the Peace River where the railway grade of the Canadian National Railway (CNR) climbs along the valley slope. In the late 1970s, a residential development plan below the slope was established by the Peace River Regional Planning Commission (Peace River Regional Planning Commission 1980). However there were concerns about inadequate slope stability in the proposed area (Thomson 1980). The valley slope in the landslide area has hummocky topography produced by abandoned landslides which were formed by Holocene down-cutting of the Peace River. A large landslide scarp is located above the railway track (Figure 4.12).

Air photos indicate that landslides on the east bank of the Peace River valley appear to overlap each other such that the reactivation of one landslide could trigger the movement of its neighbours (Lindberg and Savigny 1981b). The railway has been realigned due to slope movements in and around the Mile 46.5 since 1966 (Lindberg and Savigny 1981a). Realignments were necessary after earthworks for a residential development in 1977. A tension crack was found in 1978 and the railway realigned again as slope movement occurred in 1980. In a detailed site investigation, five boreholes (80-1, 2, 7, 8, and 9) were installed in the area of concern in order to determine the stratigraphy of the landslide area. Slope inclinometers and piezometers were also introduced to identify rupture surface and groundwater level. Cross section and subsurface stratigraphy in the study area are shown in Figure 4.13.

Major quantities of soil strata making up the area are hard, medium to high plastic clay till and very hard clay shale. In borehole 80-7, however, about 20 metres of a dry, fine silty sand is underlain by clay, which can be interpreted as fluvial sediments from the Holocene epoch when the river flowed freely after glaciers fully retreated. The bedrock surface is almost flat and has a dip of 2 degrees toward the Peace River.

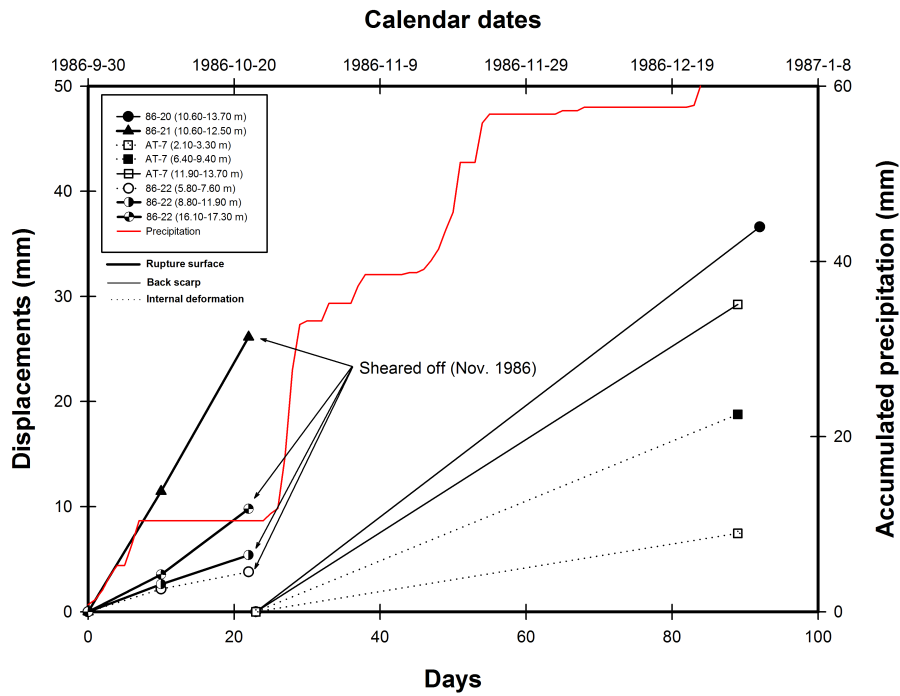


Figure 4.9 Landslide movements at the Mile 47.6 Slide. Precipitation data of the measurement period are also described. Location of boreholes is shown in Figure 4.8. Detailed data are also noted in Appendix A

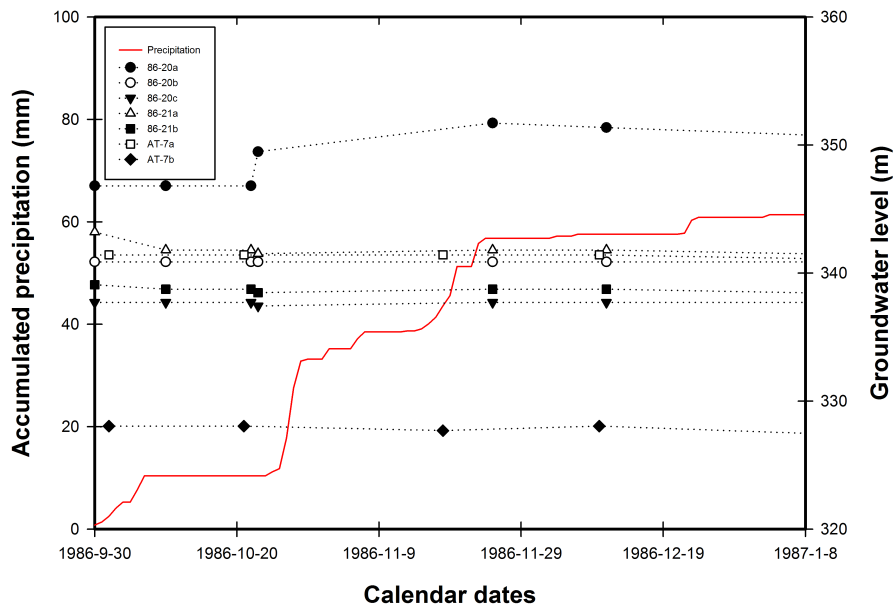
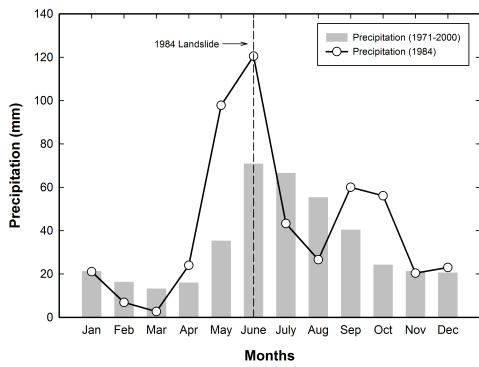
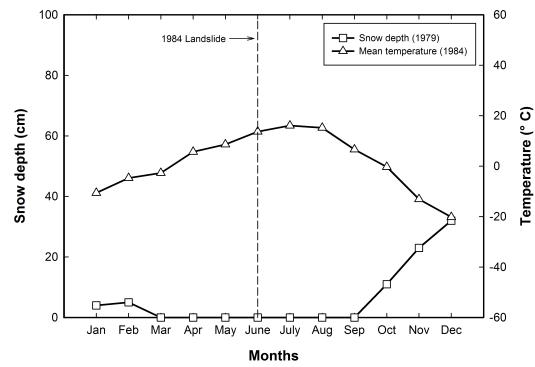


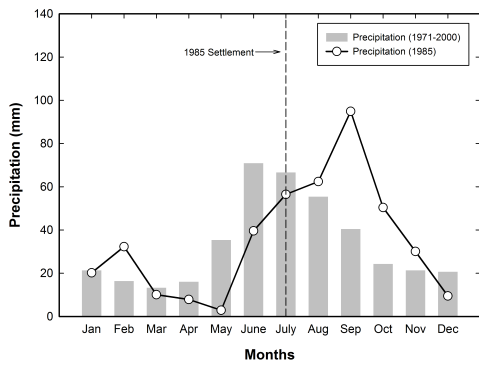
Figure 4.10 Temporal groundwater distribution at the Mile 47.6 Slide. Location of boreholes is shown in Figure 4.8



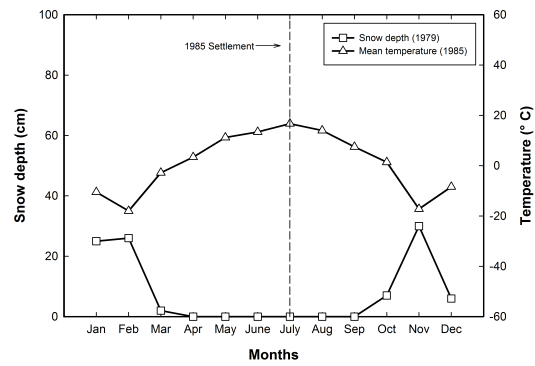
(a)



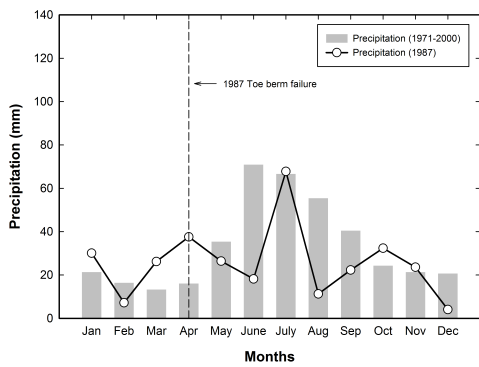
(b)



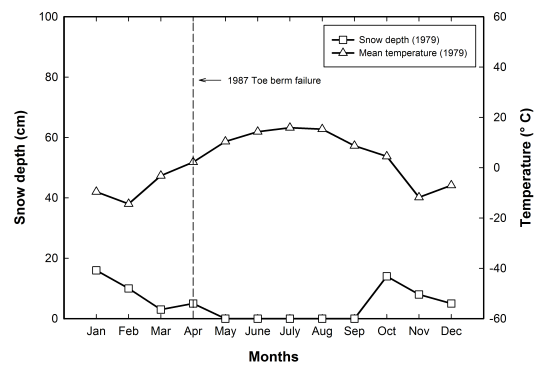
(c)



(d)



(e)



(f)

Figure 4.11 Meteorological records on the Mile 47.6 Slide in 1984, 1985, 1987. a, c, and e. Annual precipitation in each year compared with the 30 year average value represented in gray bars. b, d, and f. Mean temperature and snow depth on the ground in each year

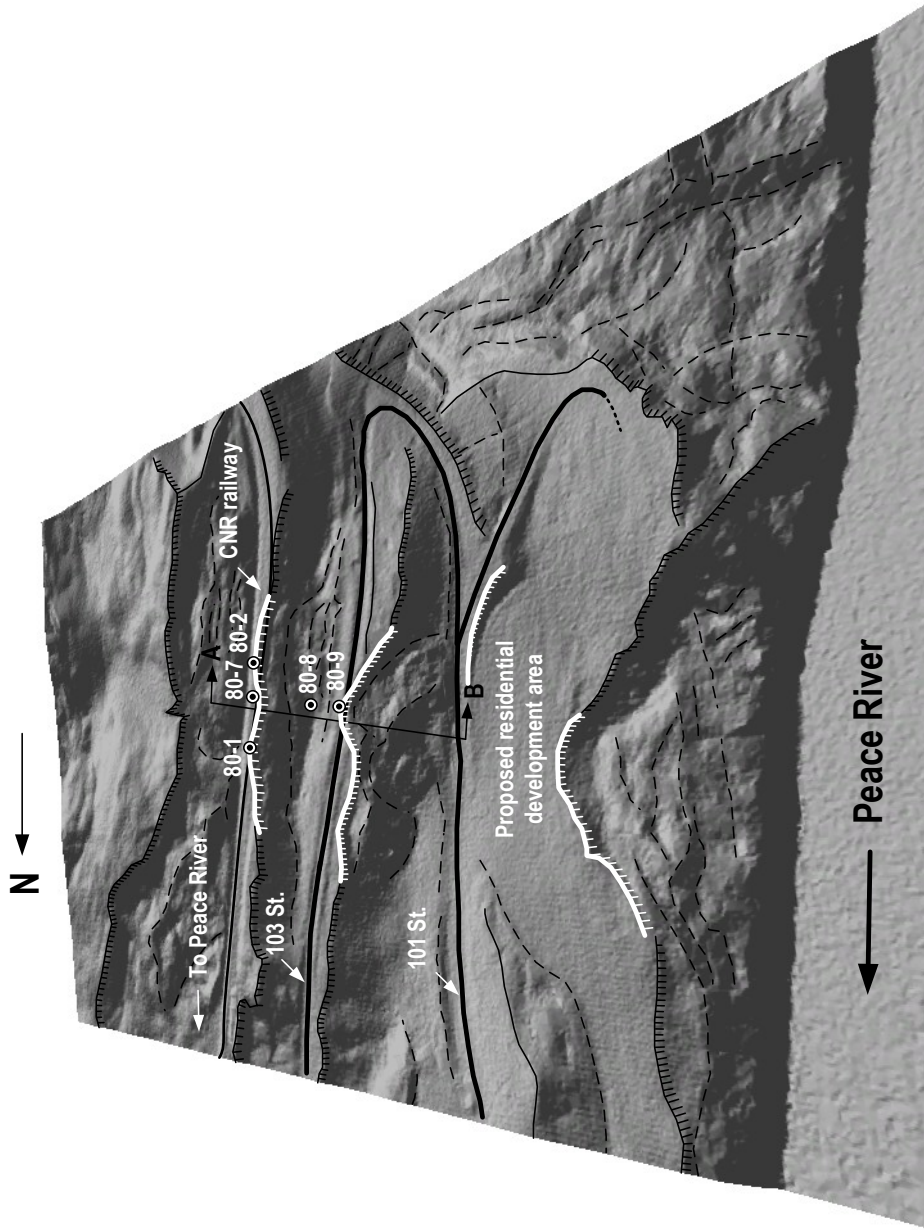


Figure 4.12 Perspective view of the Mile 46.5 Slide. Scale 1:2,000. Looking east. Landslide scarps and boreholes are also shown. Line A-B shows the cross section of the slide (Figure 4.13). The three dimensional hillshade is derived from the LiDAR dataset obtained in 2007

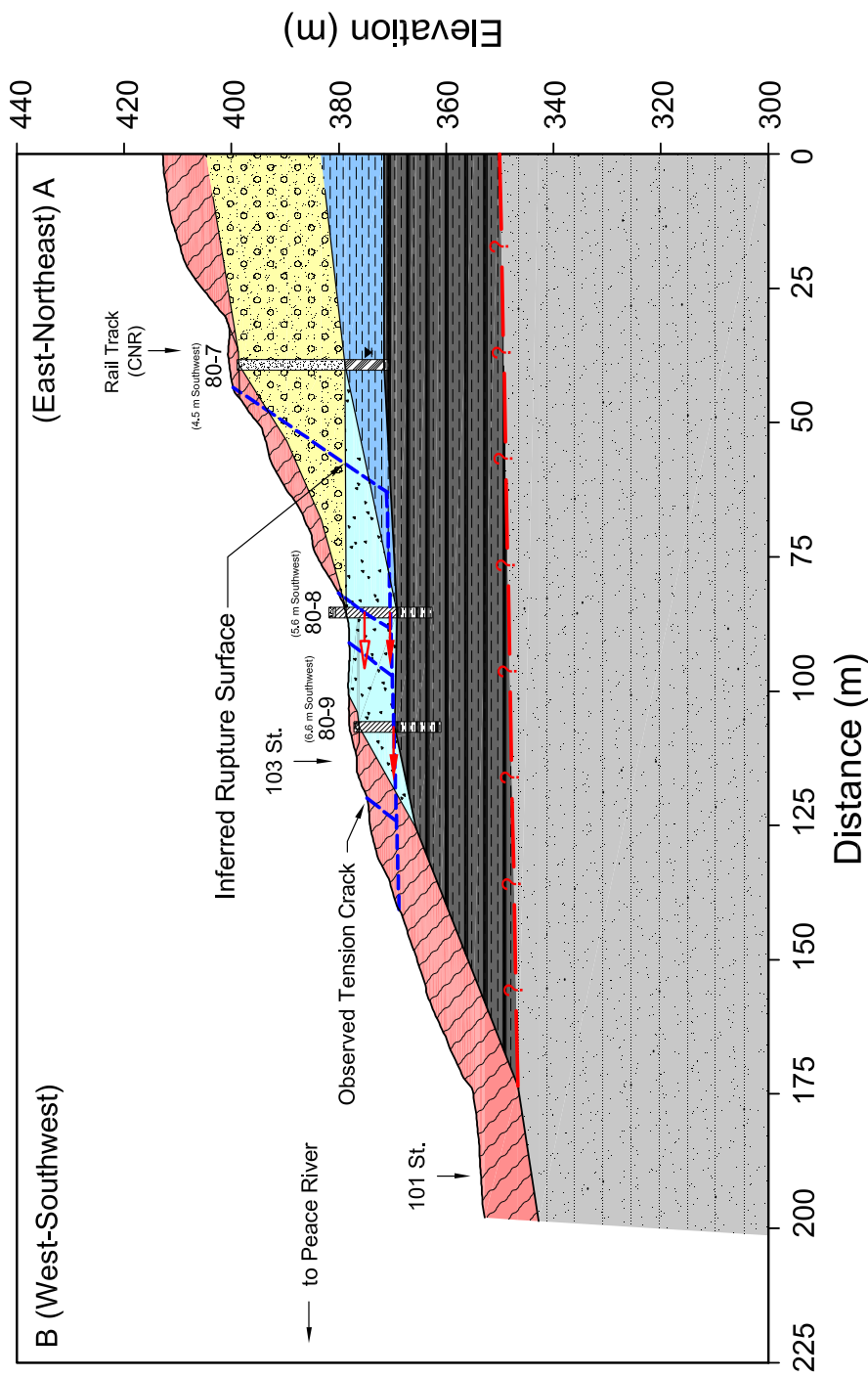


Figure 4.13 Cross section of the Mile 46.5 Slide. Boreholes and their proximity to the section plane are indicated. Lithological and genetic stratigraphies are also shown. Observed locations for ground movements are illustrated by red arrows. Inferred rupture surfaces are delineated by thick blue dashed lines. Representative symbols for lithological and genetic units are also presented in Figure 4.3. Detail borehole data are also noted in Appendix A

Slope inclinometer readings were taken in 1980 and 1981. Table 4.6 shows results of measurements in boreholes 80-7, 8, and 9. Table 4.6 indicates that there were small movements in boreholes 80-8 and 9 of five to six centimetres but no movement was measured in borehole 80-7 during the 1980 reading. However, boreholes 80-8 and 9 were distorted in the 1981 measurement. Borehole 80-7 did not shear off and still showed no movement. Borehole 80-8 also showed a secondary movement at a depth of 7.6 metres. Based on Figure 4.13 and Table 4.6, the anticipated failure mechanism was largely deep seated translational block sliding with a flat lying rupture surface. This is also supported by the slope inclinometer data and back analysis in which a calculated friction angle was consistent with the residual strength along the pre-existing rupture surface (Lindberg and Savigny 1981b).

Table 4.6 Slope inclinometer measurements in borehole 80-7, 8, and 9. Location of boreholes is shown in Figure 4.13. Detailed data are also noted in Appendix A. *Source:* Data from Lindberg and Savigny (1981b)

BHs		80-7	80-8	80-9
Inferred rupture surface elevation (m)		-	370.42	369.79
Movement (cm)	Oct. 17, 1980	0	5 to 6	5 to 6
	April 28, 1981	0	sheared off	sheared off

Groundwater level recorded by piezometers was shown in Table 4.7. Groundwater was found about 25 metres of borehole 80-7 below the ground surface whereas other boreholes were in a dry state.

Table 4.7 Measured groundwater level in the Mile 46.5 Slide. *Source:* Data from Lindberg and Savigny (1981b)

BHs	80-7	80-8	80-9
Elevation (m) [†]	373.93	dry	dry

[†] Measured on April 28, 1981.

Figure 4.14 shows precipitation in 1978 and 1980, compared with the 30 year average value. Precipitation in 1978 and 1980 indicate that there was no significant rainfall prior to or after the landslide event. Snow depth on the ground also seems to have had little impact to initiate the tension crack in 1978 only. It is, therefore, expected that an increase in pore water pressure produced by precipitation was not a major factor in the Mile 46.5 Slide. Considering that there were earthworks in this

area, changes in topographic geometry due to residential developments may have been a trigger in reactivating these inactive landslides in this area.

4.1.4 99/101 Streets Slides

The east bank of the Peace River valley is more developed than the west due to the existence of large terrace deposits and convenient transportation access. An early study by Pestrong (1976) noted that many residences are ironically established on old landslide deposits or terraces because they are relatively flat, clear of vegetation, and close to ponds and springs. Since 1950, when the first community was established on these terraces, development for residential subdivisions was extended to the valley wall (Cruden et al. 1990b). Expansion of the development have reached farther southward together with 99, 101, and 103 Streets. Developments in these areas with the hummocky terrain which is related to the previous landslides caused several slope instability problems such as foundation settlements, distresses of retaining walls and road pavements. An aerial view of 99 and 101 Streets with locations where major slope movements occurred is shown in Figure 4.15.

Landslide movements in the 99/101 Streets started in 1973 (Harris 1973) below the junction of 99 and 101 Streets and the first major slide occurred in 1985 on 99 Street (Plewes and McCormick 1985). During 1988 and 1989, when houses damaged by the 1985 landslide were removed, a cut slope located north of the 1985 slide moved downward. Houses located on the cut slope were eliminated during the period of 1990 to 1991. Movements at the intersection of 99 and 101 Streets activated in 1992 (Barlow and McRoberts 1992; Hofmann and Barlow 1992) and accelerated in 1993. Stabilization projects on this area have been initiated since 1993 (Küpper et al. 1994) and monitoring programs have also been maintained (Barlow and McRoberts 1999; Barlow and Küpper 2001).

The area affected by the slope instability is divided into three sections (Küpper et al. 1994) from south to north (Figure 4.15): (1) End of 101 Street (A-B); (2) Transition Zone (C-D); and (3) End of 99 Street (E-F). The End of 101 Street located on the southern end of the residential subdivision. This area was graded in 1974 and 1975 with a large placement of fills. According to Barlow and McRoberts (1992) there was a gully on the present lookout and water which had flown into this gully was blocked by fills. This impeded water, therefore, might have caused an increase in

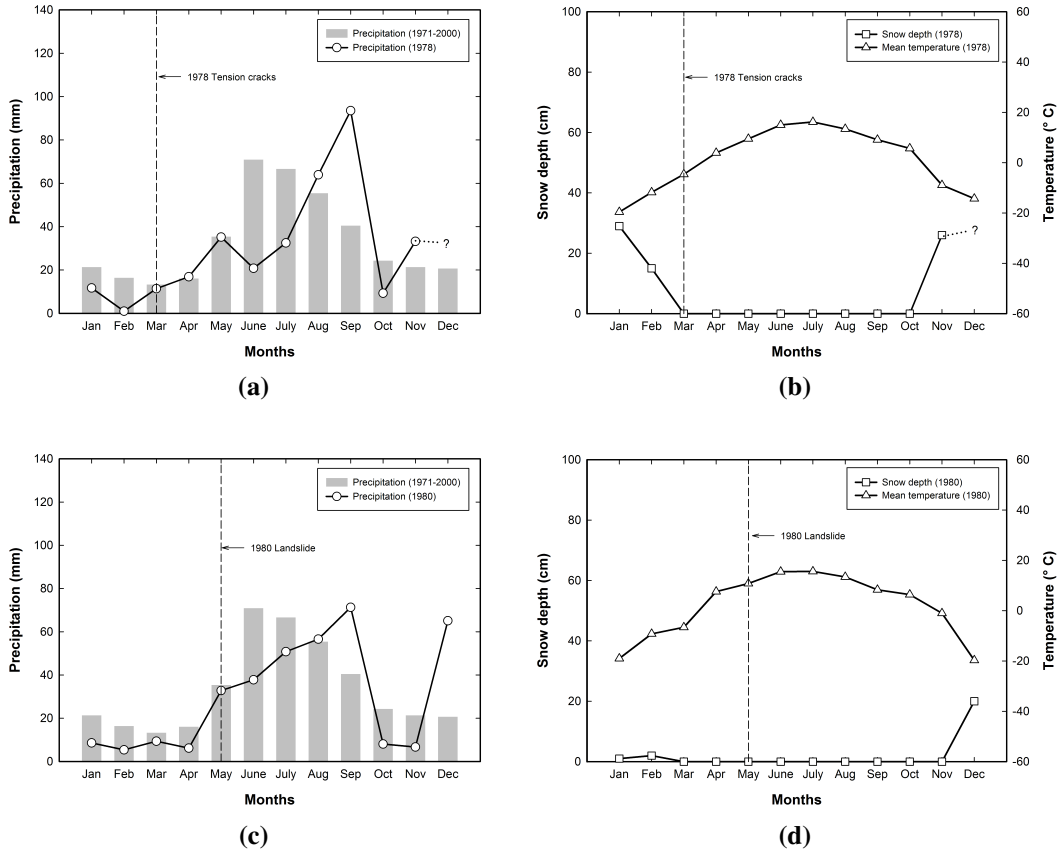


Figure 4.14 Meteorological records on the Mile 46.5 Slide in 1978 and 1980. a and c. Annual precipitation in each year compared with the 30 year average value represented in gray bars. b and d. Mean temperature and snow depth on the ground in each year. Precipitation and snow depth in December 1978 are missed and shown by dashed line with question mark

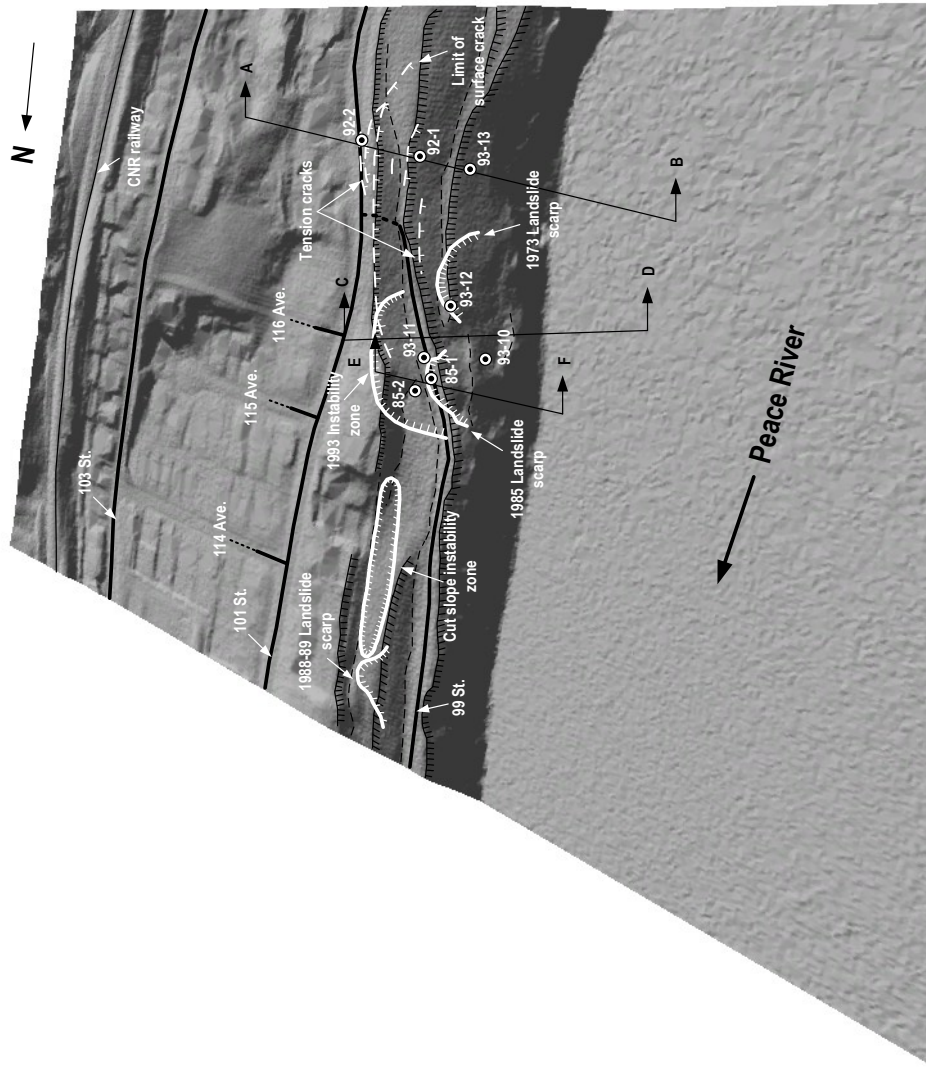


Figure 4.15 Perspective view of the 99/101 Streets Slides. Scale 1:2,000. Looking northeast. Historical landslide scarps and boreholes are also indicated. Lines with alphabets (A-B, C-D, and E-F) show cross sections of the slides (Figures 4.17 to 4.19). The three dimensional hillshade is derived from the LiDAR dataset obtained in 2007

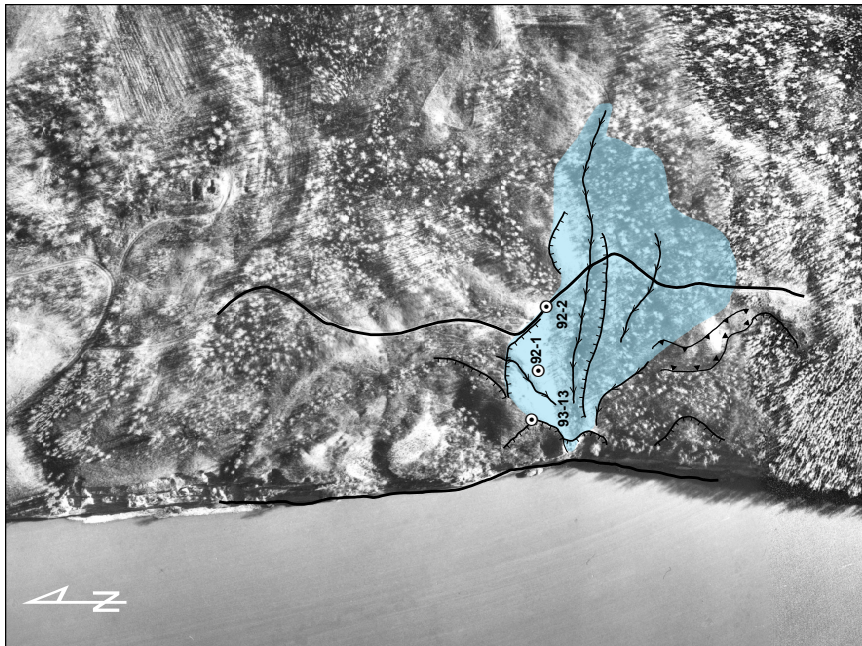
pore water pressure and reduced the stability of slopes in the area. Figure 4.16 shows distinct changes in the ground surface profile in the study area from this anthropogenic activity.

There were no obvious signs of the slope movement in this area after grading. In January 1992 several tension cracks appeared (Figures 4.15 and 4.16). The distress directly affected three houses to the west located on the south End of 101 Street. Typical stratigraphy of the End of 101 Street Slide is shown in Figure 4.17.

Figure 4.17 shows a descending sequence of fill, colluvium, clay till, sand and gravel lenses, a disturbed clay shale, and clay shale and sandstone. These sequences are similar to the conventional succession in the Town of Peace River which Morgan et al. (2008) mentioned. Figure 4.17 also indicates that inferred rupture surfaces are located around 332 and 336 metres representing major and initial slope movements respectively. From the observations in boreholes 92-1, 92-2, and 93-13, it can be seen that the slope movement at this area gradually progressed. Besides amounts of fills can be estimated from the original ground surface delineated in Figure 4.17.

The Transition Zone is located a little farther north from the End of 101 Street Slide. The movement of the slide was observed in 1992 and accelerated in 1993. Figure 4.18 shows stratigraphy of the Transition Zone in which preglacial gravel deposits overlie clay shale and sandstone bedrock. Three boreholes, the 93-10, 11, and 12, indicate ground movements caused by the landslide, which shows typical characteristics of a translational block slide. The lower rupture surface in Figure 4.18 which boreholes 93-11 and 12 did not reach, may adjoin rupture surfaces of End of 101 and 99 Streets (Figures 4.17 and 4.19).

The End of 99 Street Slide is located north from the intersection of 99 and 101 Streets (Figure 4.15). The initial ground movement occurred in 1985. Instabilities in 1985 related to this area consist of a shallow surficial slide on the slope face and a shallow translational slide below the 99 Street which affected the road pavements and concurrently occurred with the surficial slide (Figure 4.19). Because the storm sewer outfall was located above these slides, a leakage from the sewer line is considered one of the causal factors which initiated slides. The other slide appeared to have a deep translational slide mechanism whose rupture surface is located in the clay shale bedrock and is considered to link to rupture surfaces of adjacent slides. It is also believed to be related to the accelerated ground movement in 1993. A gen-



(a)



(b)

Figure 4.16 Anthropogenic effects on the End of 101 Street Slide. a. 1958 air photo (Alberta Photo: AS26-162) b. 2007 Quickbird imagery. Scale 1:2,000. Approximate boundary of gully is delineated by a blue shade. Symbols of air photo interpretation in a are consistent with Dearman et al. (1972) and Federal Geographic Data Committee (2006). Landslide scarps and tension cracks are shown in b by white dashed line. Detail borehole data are also noted in Appendix A

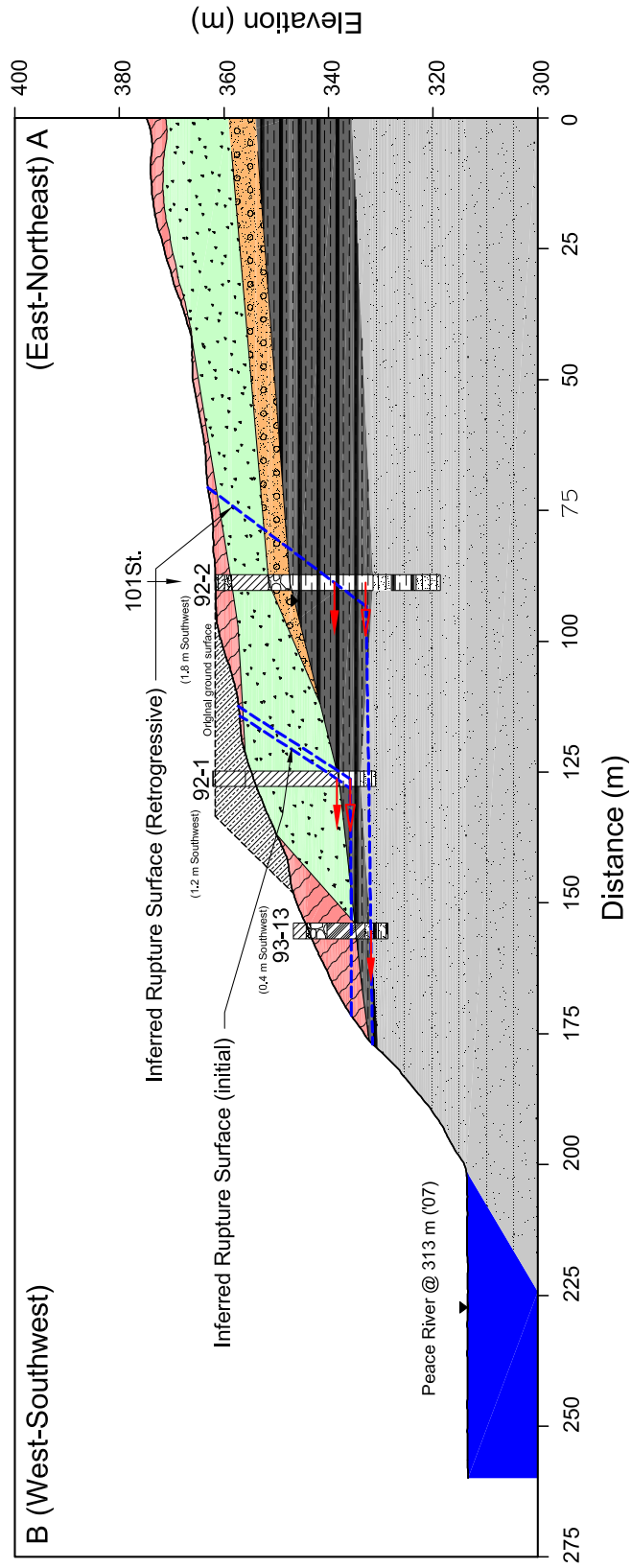


Figure 4.17 Cross section of the End of 101 Street Slide (A-B). Boreholes and their proximity to the section plane are indicated. Lithological and genetic stratigraphies are also shown. Observed locations for ground movements are illustrated by red arrows. Inferred rupture surfaces are delineated by thick blue dashed lines. Representative symbols for lithological and genetic units are also presented in Figure 4.3. Detail borehole data are also noted in Appendix A

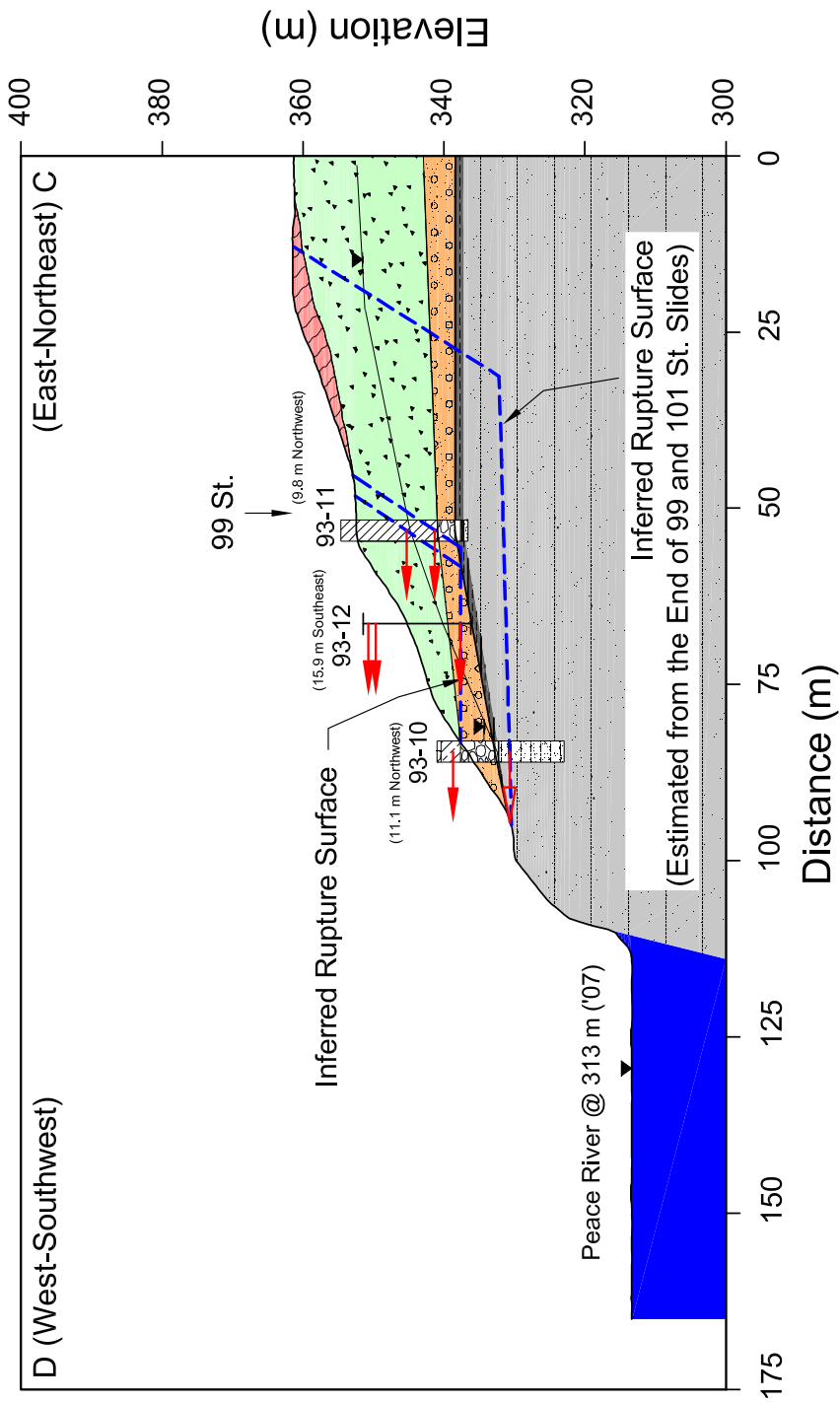


Figure 4.18 Cross section of the Transition Zone Slide (C-D). Boreholes and their proximity to the section plane are indicated. Lithological and genetic stratigraphies are also shown. Observed locations for ground movements are illustrated by red arrows. Inferred rupture surfaces are delineated by thick blue dashed lines. Representative symbols for lithological and genetic units are also presented in Figure 4.3. Detail borehole data are also noted in Appendix A

eral sequence of the subsurface stratigraphy in this area which is shown in Figure 4.19 indicates clay fills, colluvial deposits, clay till, preglacial gravel, and clay shale and sandstone bedrock, which are similar to those at the Transition Zone. Rupture surfaces based on measurements of boreholes 85-1 and 2 are located at elevations of 332 and 349 to 350 metres for deep and shallow rupture surfaces respectively.

It is evident from the subsurface stratigraphy and borehole data that there is a general rupture surface controlling the translational movement mechanism in the 99/101 Streets Slides area (Figure 4.20). It has an elevation of 330 to 333 metres, which lies on the Shaftesbury Formation. In addition to the general rupture surface, the slide area also has at least one isolated surficial slope movement caused by local weakening of the soil due to the concentrated infiltration of water. Reactivation of a major slide block along the pre-existing rupture surface in the Shaftesbury Formation has resulted in significant changes of the natural topography, forming landslide scarps, tension cracks, and subsidence.

Landslide movement rates obtained from slope inclinometer data at the 99/101 Streets Slides are shown in Table 4.8 and Figures 4.21 to 4.23 show movement rates for each slide area together with precipitation recorded during the measurement period. In Table 4.8 the overall average movement rate has a range from 0.7 to a maximum of 320 mm/year except borehole 85-1 which was sheared off by the extremely large movement over two days. Movement rates in borehole 92-1 ranges between 119 and 320 mm/year, which is relatively high compared to other boreholes. They are detected at depths of 24 and 26 metres below the ground surface respectively. These unusual rates appeared to result from the relatively short measurement period (less than two months).

Movement rates and precipitation during measurements are strongly correlated especially at the End of 101 Street and Transition Zone Slides. Data from borehole 92-1 shows a spontaneous increase of the movement rate in a short period of time with increasing precipitation. Movement rates at the depth of 23 metres of borehole 92-2 and 15 metres of borehole 93-13 showed a gradually increasing trend between January 1993 to January 1997. These increased in accordance with heavy rainfall in 1997 (Figure 4.21). The ground movement at the depth of 29 metres in borehole 92-2 was recorded at less than 1 mm/year.

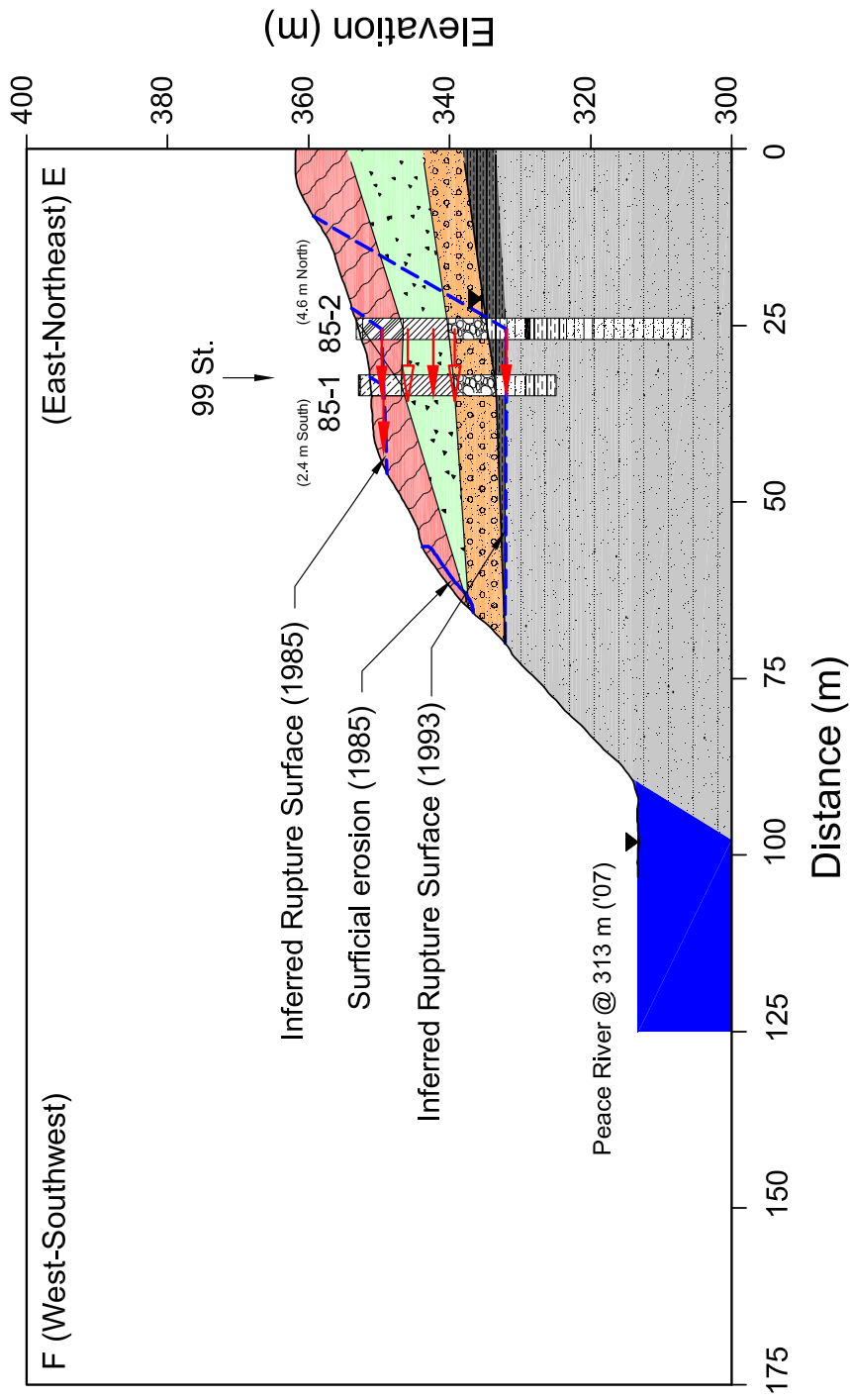
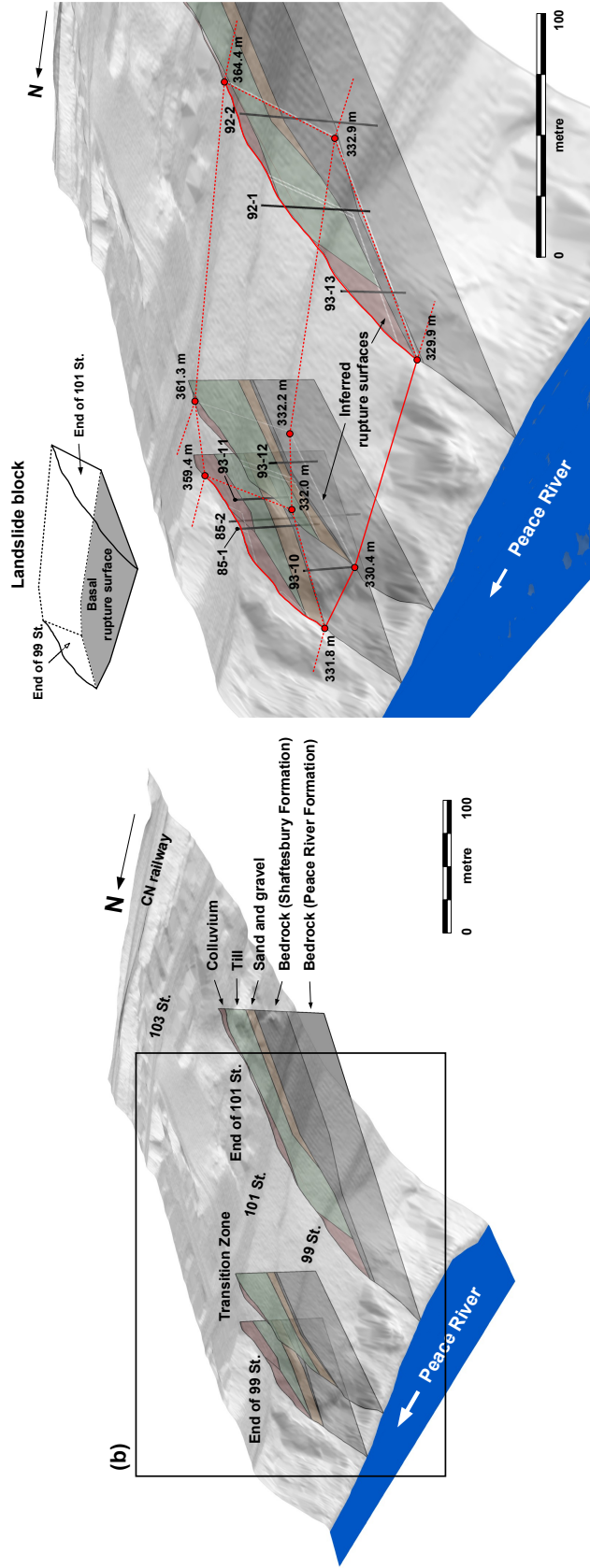


Figure 4.19 Cross section of the End of 99 Street Slide (E-F). Boreholes and their proximity to the section plane are indicated. Lithological and genetic stratigraphies are also shown. Observed locations for ground movements are illustrated by red arrows. Inferred rupture surfaces are delineated by thick blue dashed lines. Representative symbols for lithological and genetic units are also presented in Figure 4.3. Detail borehole data are also noted in Appendix A



(a)

(b)

Figure 4.20 Diagram of the landslide block controlling a translational movement mechanism in the 99/101 Streets area. a. Distribution of three cross sections (Figures 4.17 to 4.19) in the study area. Looking northeast. The subsurface stratigraphy is also described. The rectangular area provides a closer look at the general landslide block shown in b. b. Close view of a. Boreholes and inferred rupture surfaces with their elevations are indicated. The boundary of a general landslide block is shown by red solid and dashed lines. The diagram of the landslide block is delineated at upper left of b

Table 4.8 Slope inclinometer measurements at the 99/101 Streets Slides. Location of boreholes is shown in Figures 4.17 to 4.19. Detailed data are also noted in Appendix A

Slide name	BHs	Measuring periods (days)	Elevation of rupture surface (m)	Average movement rate (mm/year)
End of 101 Street	92-1	40	338	320
		40	336	119
	92-2	3,253	339	8
		3,253	333	1
	93-13	2,564	332	5
Transition Zone	93-10	296	339	130
		296	331	5
	93-11	3,376	345	13
		3,376	341	2
	93-12	2,994	350	10
		2,994	351	26
2,994		338	1	
End of 99 Street	85-1	2	349	17,902
	85-2	2,555	350	3
		2,555	346	0
		2,555	342	1
		2,555	339	1
	2,555	332	5	

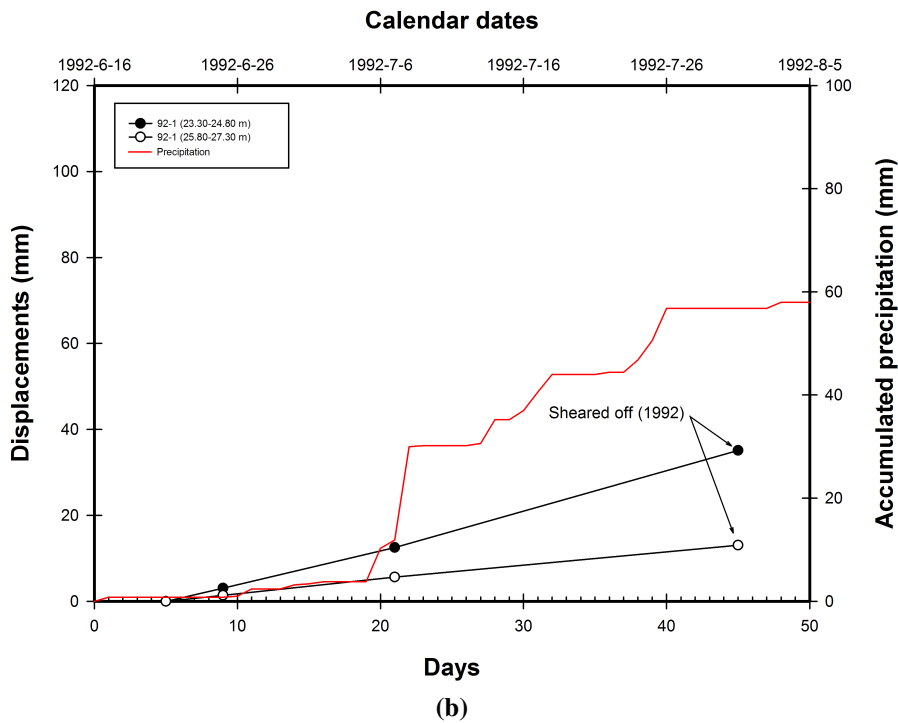
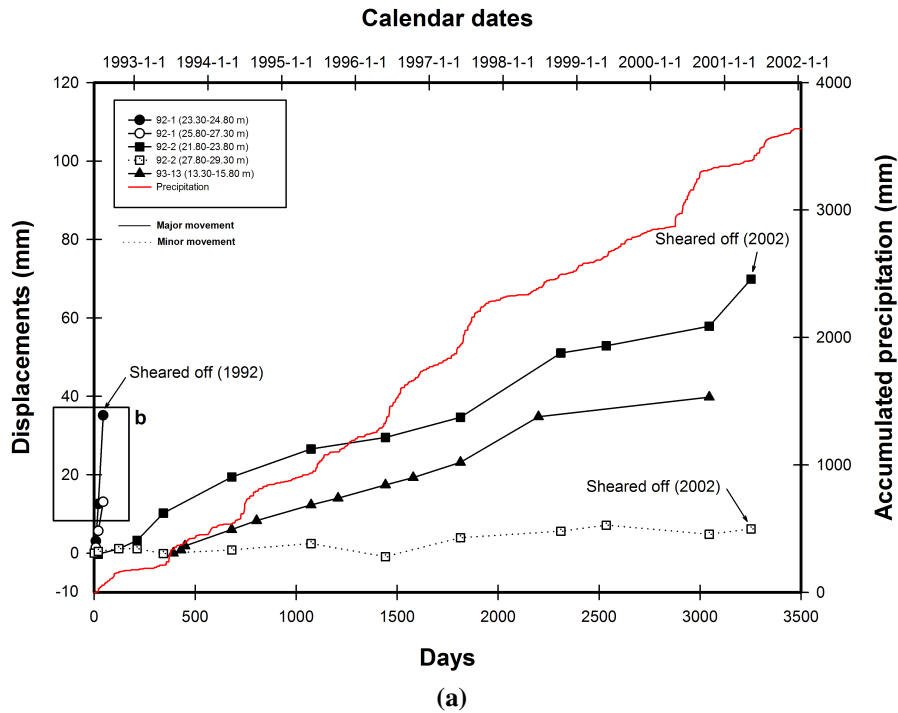


Figure 4.21 Landslide movements at the End of 101 Street Slide. a. Total movement rates in the slide area. b. Specific movement rates in which boreholes were sheared off in short duration. Area is described by rectangular shape in a. Precipitation data of the measurement period are also described. Location of boreholes is shown in Figure 4.17. Detailed data are also noted in Appendix A

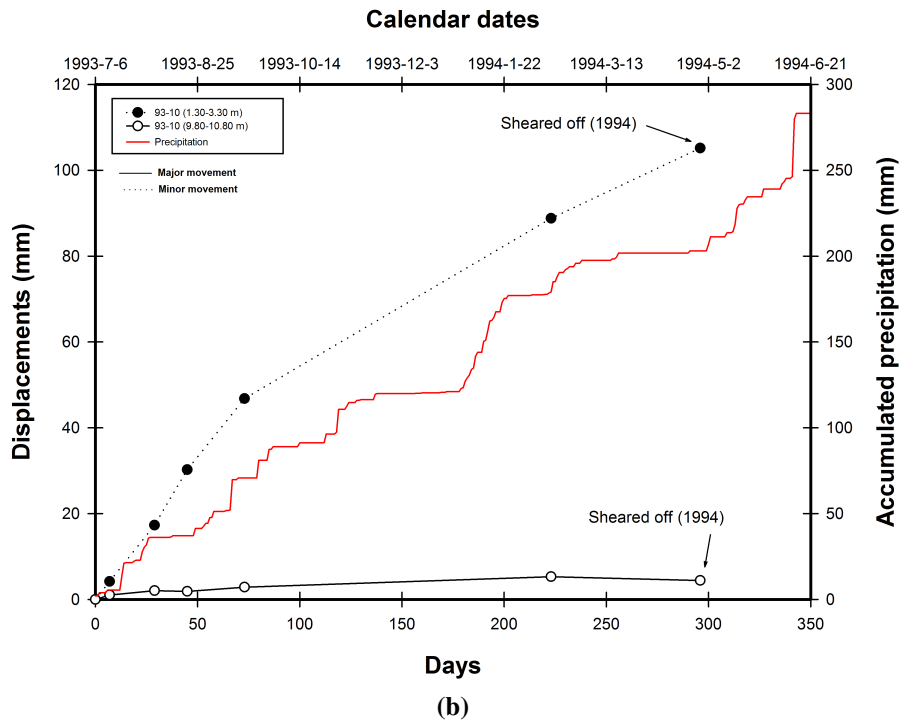
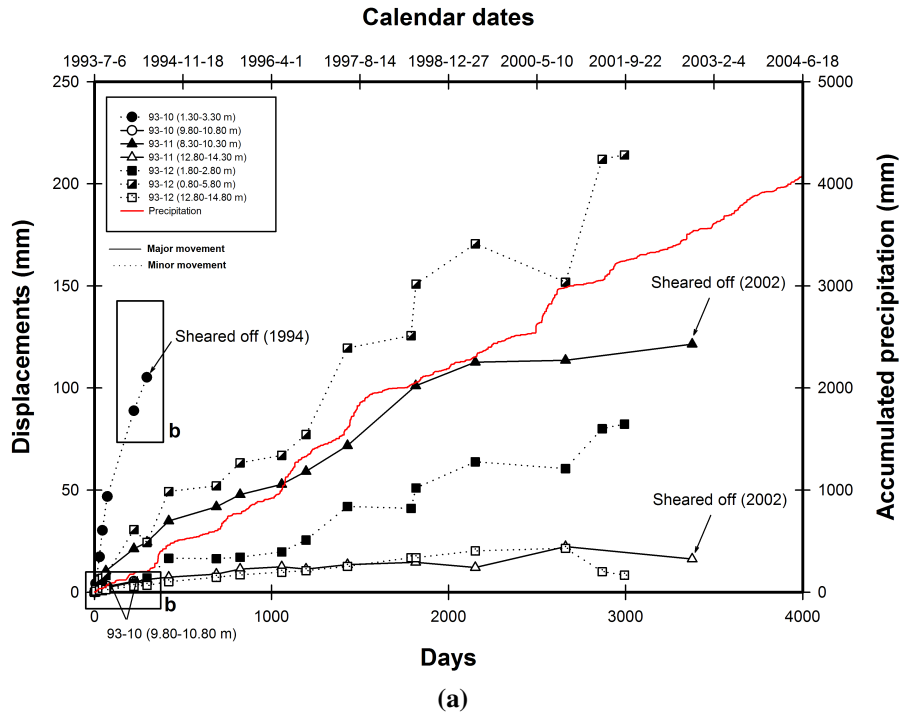


Figure 4.22 Landslide movements at the Transition Zone Slide. a. Total movement rates in the slide area. b. Specific movement rates in which boreholes were sheared off in short duration. Area is described by rectangular shape in a. Precipitation data of the measurement period are also described. Location of boreholes is shown in Figure 4.18. Detailed data are also noted in Appendix A

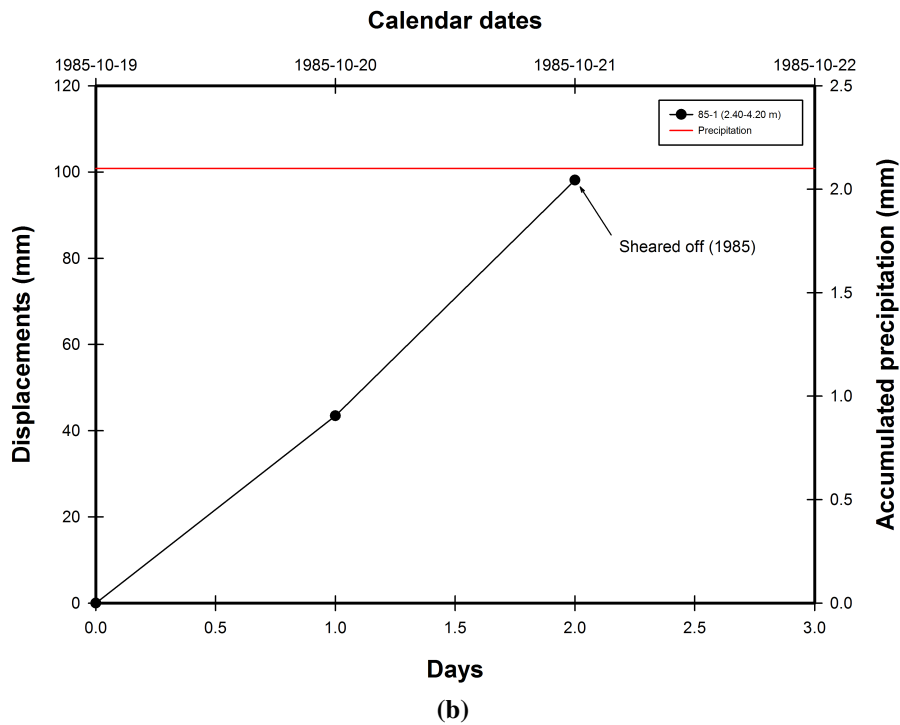
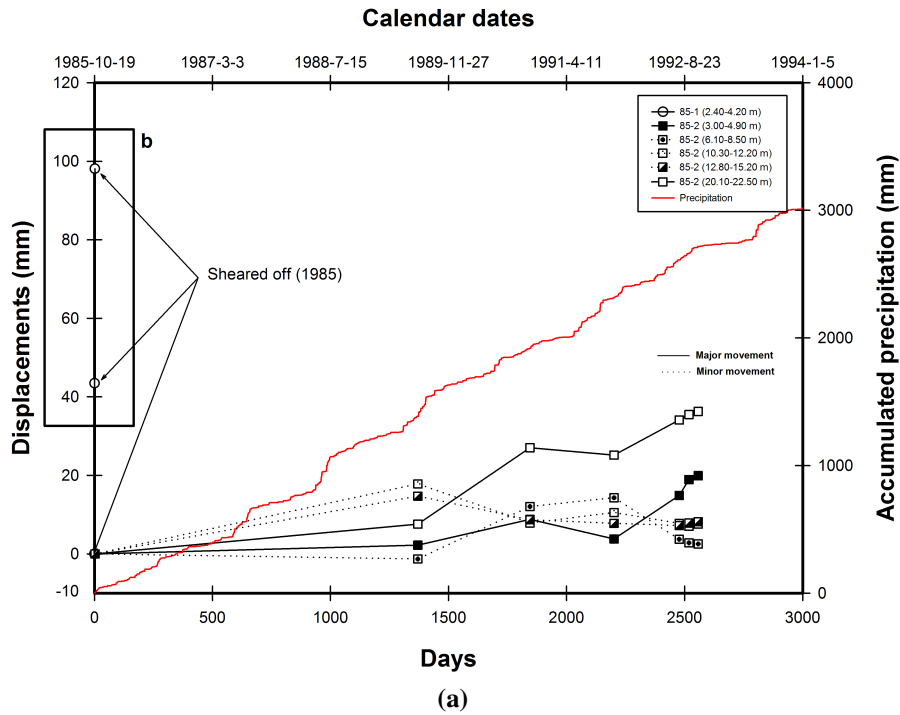


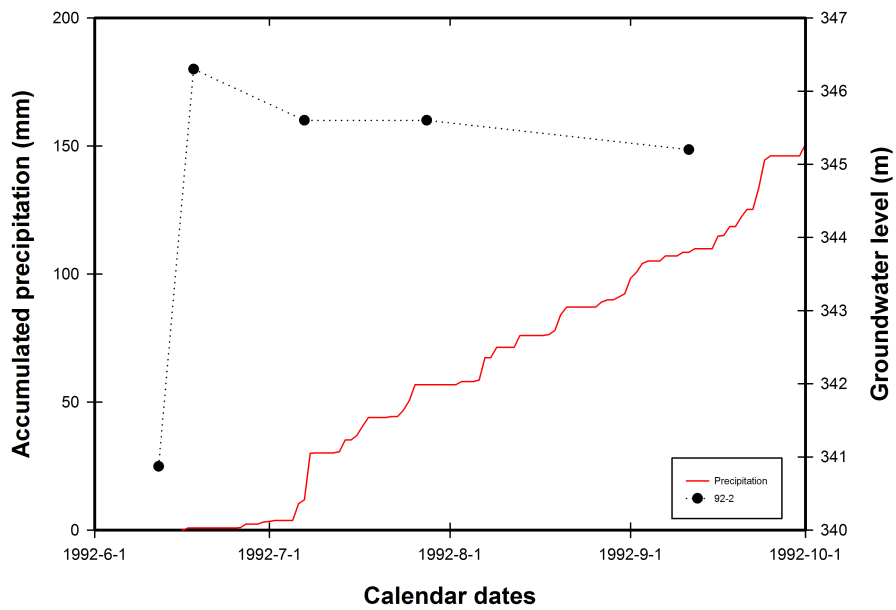
Figure 4.23 Landslide movements at the End of 99 Street Slide. a. Total movement rates in the slide area. b. Specific movement rates in which boreholes were sheared off in short duration. Area is described by rectangular shape in a. Precipitation data of the measurement period are also described. Location of boreholes is shown in Figure 4.19. Detailed data are also noted in Appendix A

Ground movements in the Transition Zone are shown in Figure 4.22. Borehole 93-10 showed a significant increase of the movement rate (maximum 295 mm/year) at a depth of 2.3 metres and sheared off in April 1994. Movement at borehole 93-10 was measured for a relatively short time interval (296 days), and this movement does not represent the overall trend of this slide area. Boreholes 93-11 and 12 show gradual increases during the measuring period especially at depths of 0.8 to 1.8, and 9.3 metres, respectively. One interesting point is that the overall behaviour of movements obtained from the borehole 93-11 was little influenced by the periodic variation of precipitation. By contrast borehole 93-12 shows that the movement rate correlated with the change of annual precipitation and fluctuated throughout time. This suggests that movement of borehole 93-11 is induced by the constant stress rather than changes in pore water pressure by precipitation or snow melting water. At the lower depth of about 13 metres both boreholes showed average movement rates of 1.76 and 1.02 mm/year indicating extremely slow movements.

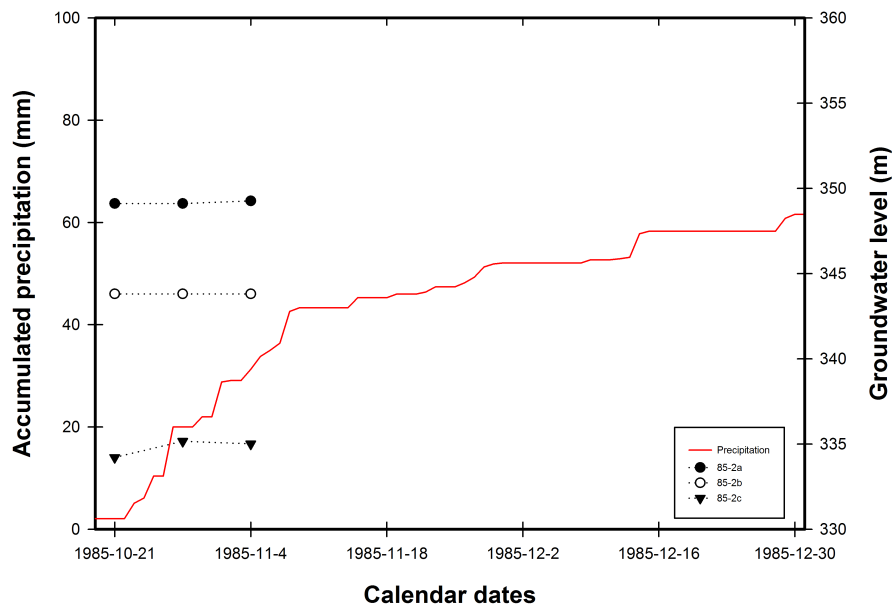
Figure 4.23 shows ground movements at the End of 99 Street Slide area. Movement rates at borehole 85-2 showed a gradual increase of 2.8 and 5.2 mm/year at depths of 4 and 21 metres, respectively. There were movement rates in those depths during November 1990 to October 1991 which showed suspended or decreasing behaviors. This suggests a characteristic of groundwater level changes which usually related to precipitation and snow melting water. Movement rates at other elevations in borehole 85-2 showed a reverse behavior since 1990. High movement rates at borehole 85-1 indicate a destruction of the borehole.

Groundwater measurements from slide areas are shown in Figure 4.24. Due to the limited number of measurements, a comprehensive groundwater regime was unattainable. In Figure 4.24, however, a groundwater level in borehole 92-2 and 85-2 was located in clay shale bedrock and gravel deposits, respectively. Locations of high groundwater level can be supported by the fact that the clay shale bedrock is relatively impermeable even though the upper portion of clay shale is weathered or fissured. There is no obvious information in the Transition Zone to determine groundwater level but it can be assumed that the groundwater is located between fluvial sediments and Shaftesbury Formation (Figure 4.18).

Figures 4.25 to 4.27 show precipitation which may induce several slope instabilities in the 99/101 Streets area. 30 year average precipitation, mean temperature, and snow depth on the ground are also plotted in order to find inter-relationships.



(a)



(b)

Figure 4.24 Measured groundwater level. a. End of 101 Street Slide. b. End of 99 Street Slide. Location of boreholes is shown in Figures 4.17 and 4.19

Precipitation and snow depth shown in Figure 4.25 can explain slope movements that occurred at the End of 101 Street, which began in 1992 and accelerated in 1993. Precipitation in June and July 1993 were 126 and 129 percent of the 30 year average value, which facilitated the acceleration of ground movements. The ground movement can also be initiated from precipitation in November and December 1991 that caused a distress in January 1992 (Figure 4.25).

Precipitation which is related to the occurrence of the slide at the End of 99 Street is shown in Figure 4.26. Mean annual precipitation in 1985 and 1988 were 34.73 and 40.25 millimetres, respectively, which are 104 and 120 percent of the 30 year average (33.52 mm). In 1989, however, precipitation in August is 212 percent higher than the 30 year average. A shallow surficial slide which occurred at the slope face in October 1985 may have initiated after heavy precipitation. Figure 4.27 also shows precipitation in 1973 in which the first major slide at the Transition Zone occurred. Heavy precipitation and large snow melting water were generated prior to the landslide.

Considering all information which related to instability problems at the 99/101 Streets, rises in pore water pressure due to high precipitation and large snow melts can be major factors. However, residential subdivision developments often become factors for landslides in urban areas. Developments may induce expansions of communities by large cuts and fills which would change the natural topography. Changed ground profiles may block natural groundwater flows and cause pore water pressures to increase. With other adverse effects of developments such as leakage from utilities and lawn watering, heavy rainfall and snow melting water finally trigger landslides.

4.1.5 Shop Slide

The Shaftesbury Trail which traverses the west bank of the Peace River, has experienced several slope stability problems since it was constructed in 1982 (Lau 1986; Gassen and Barlow 2003). One of the recent landslides, the Shop Slide, is located along the old Highway 2 where it is climbing valley walls of the Peace River. The highway has a 4:1 slope inclination from south to north. Figure 4.28 shows a general outline of the slide area. In Figure 4.28, Canadian National Railway (CNR) runs along the toe of the slide. Standing water due to seepage was found around the toe.

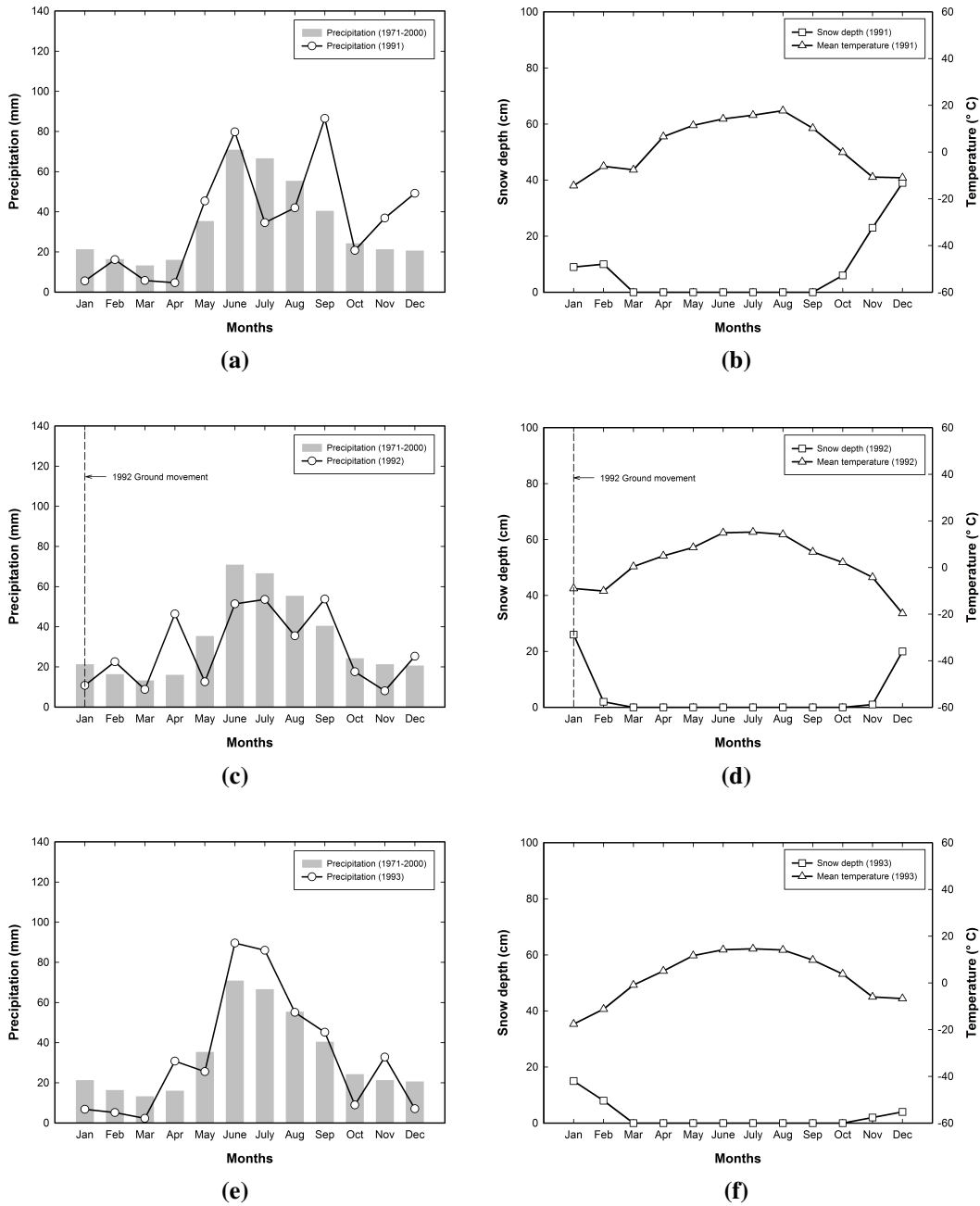


Figure 4.25 Meteorological records on the End of 101 Street Slide in 1991, 1992, and 1993. a, c, and e. Annual precipitation in each year compared with the 30 year average value represented in gray bars. b, d, and f. Mean temperature and snow depth on the ground in each year

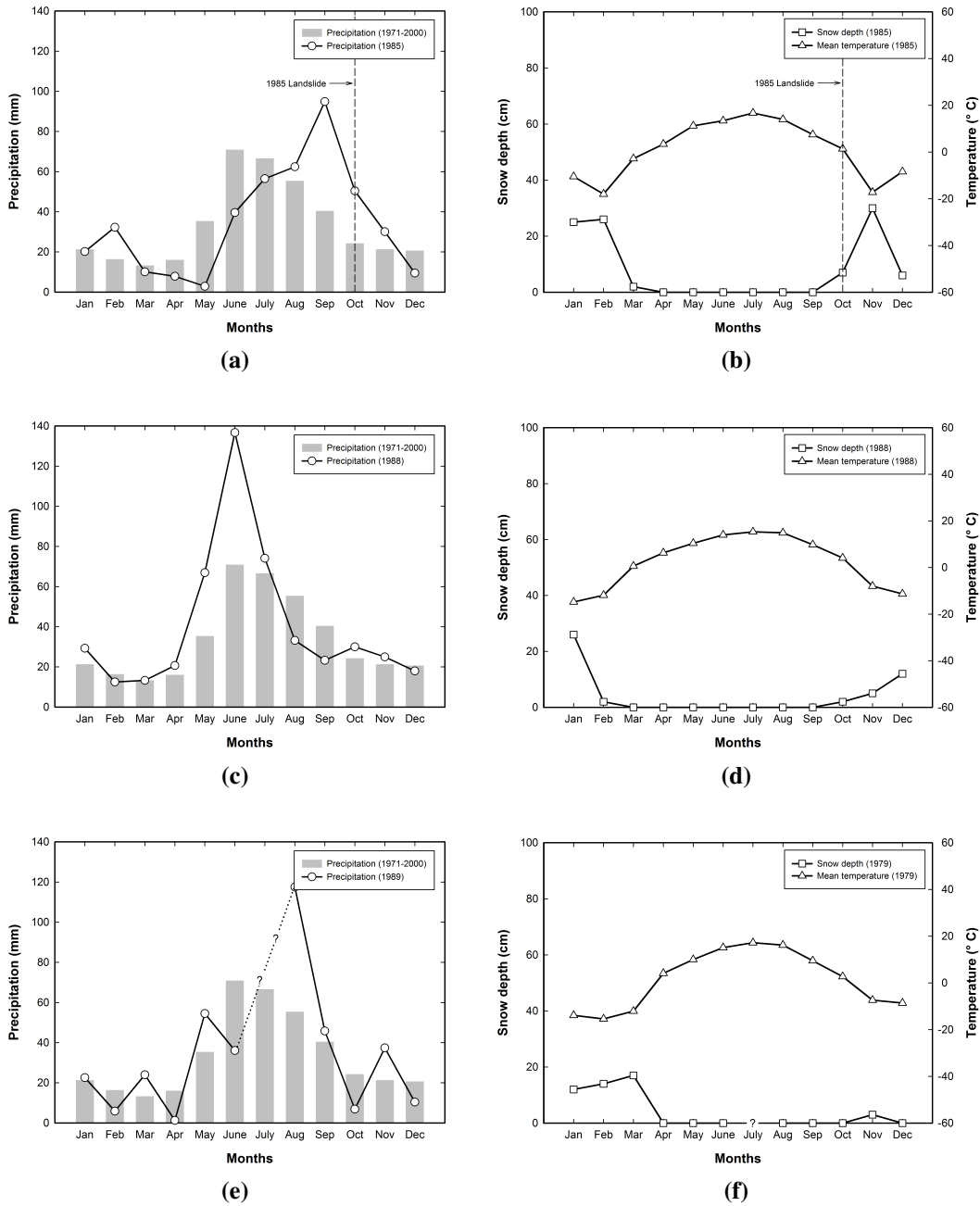


Figure 4.26 Meteorological records on the End of 99 Street Slide in 1985, 1988, and 1989. a, c, and e. Annual precipitation in each year compared with the 30 year average represented in gray bars. b, d, and f. Mean temperature and snow depth on the ground in each year. Precipitation and snow depth in July 1989 are missed and shown by dashed line with question marks

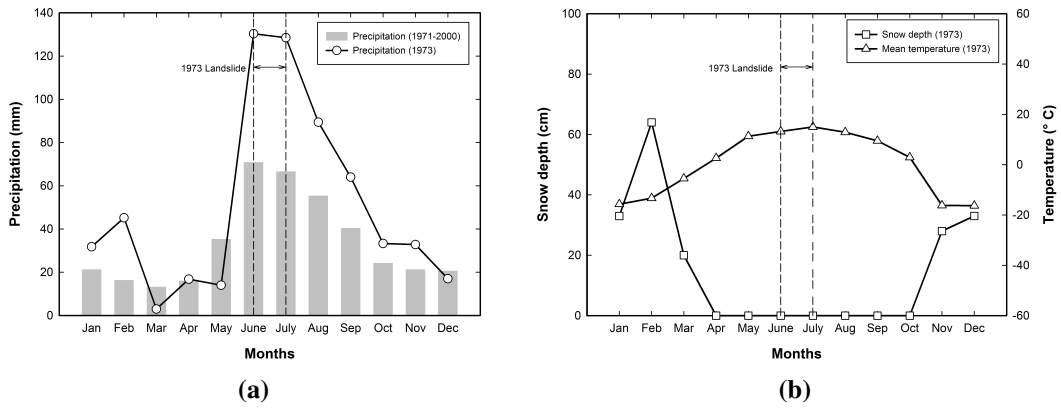


Figure 4.27 Meteorological records on the Transition Zone Slide in 1973. a. Annual precipitation in each year compared with the 30 year average value represented in gray bars. b. Mean temperature and snow depth on the ground in each year

A subtle bulge and old landslide scarps were also seen in the middle and bottom of the slide, respectively. These relicts are the proof of previous landslide movements which may have happened in the study area. The evidence of the current slope movement is more obvious on the road. The initial vertical offset across the road pavement occurred in 1985 and 1986 (Proudfoot and Cullum-Kenyon 2006). In 1987 mitigations including gridlocks and gabion baskets were implemented. Some telegraph poles along the highway were tilted toward the road (adjacent to TH05-1 in Figure 4.28). The width of slide on the road was approximately 200 metres.

The general subsurface stratigraphy of the Shop Slide consists of a sequence which is similar to other Peace River areas, is shown in Figure 4.29. Some clays which covered the slope surface might be an embankment fill for road constructions. Beneath the clay fill, the postglacial lacustrine clay is underlain by clay till sediments. The difference between these layers is not clear. The Shaftesbury clay shale bedrock was encountered in the lowest part of the borehole TH05-1. Some coarse materials such as sand and gravel were found in boreholes TH05-4 and 5 which are located below the CNR track (Figure 4.29).

The approximate rupture surface can be estimated by the location of ground movements generated from slope inclinometer measurements established in boreholes (Figure 4.29). The rupture surface is located on clay sediments with the maximum depth of 17 metres below the ground surface adjacent to borehole TH05-3. Based on slope inclinometer measurements, the rupture surface of the Shop Slide can be divided into two parts: the first, which is located on the upper slope and above the old Highway 2, appears inactive; and the second, located on the lower slope and above the CNR track is active and directly affects roads. A deep seated translational slide can be estimated in the slope.

Movement rates obtained in three boreholes (TH05-1, 3, and 4) indicated in Figure 4.29 are shown in Figure 4.30. Slope inclinometers were installed in 2005 (Proudfoot and Bijeljanin 2005). Since then, movements shown by the three slope inclinometers appear to have increased gradually. This behavior is correlated with precipitation during monitoring periods (Figure 4.30).

In Figure 4.30, the slope inclinometer in borehole TH05-1 showed a stable movement rate of less than 1 mm/year in the 2007 measuring period. Movement rates in other boreholes, however, increased and had an average value of 9 mm/year at depth

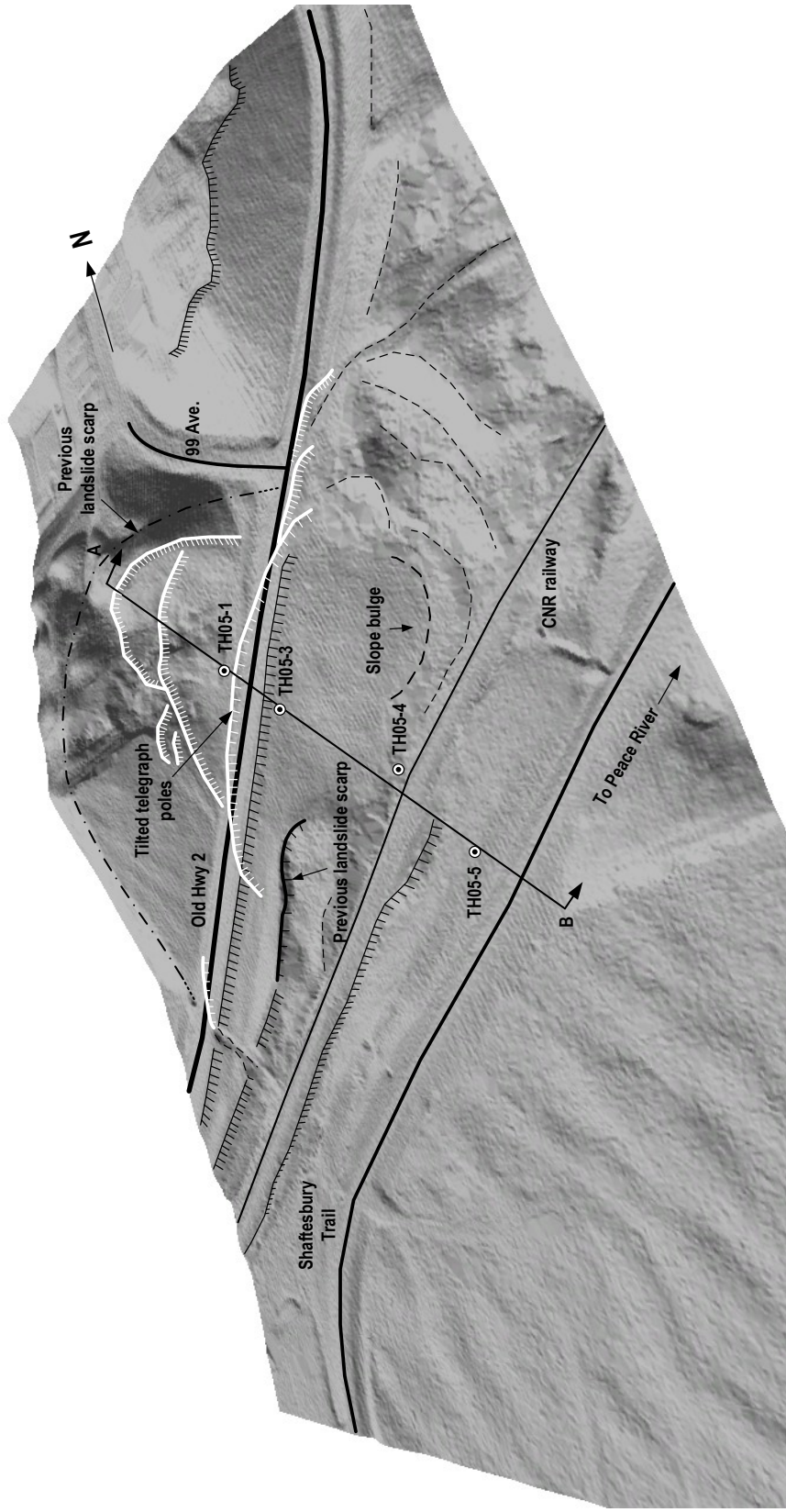


Figure 4.28 Perspective view of the Shop Slide. Scale 1:1,900. Looking northwest. Landslide scarps and boreholes are also shown. Line A-B shows the cross section of the slide (Figure 4.29). The three dimensional hillshade is derived from the LiDAR dataset obtained in 2007

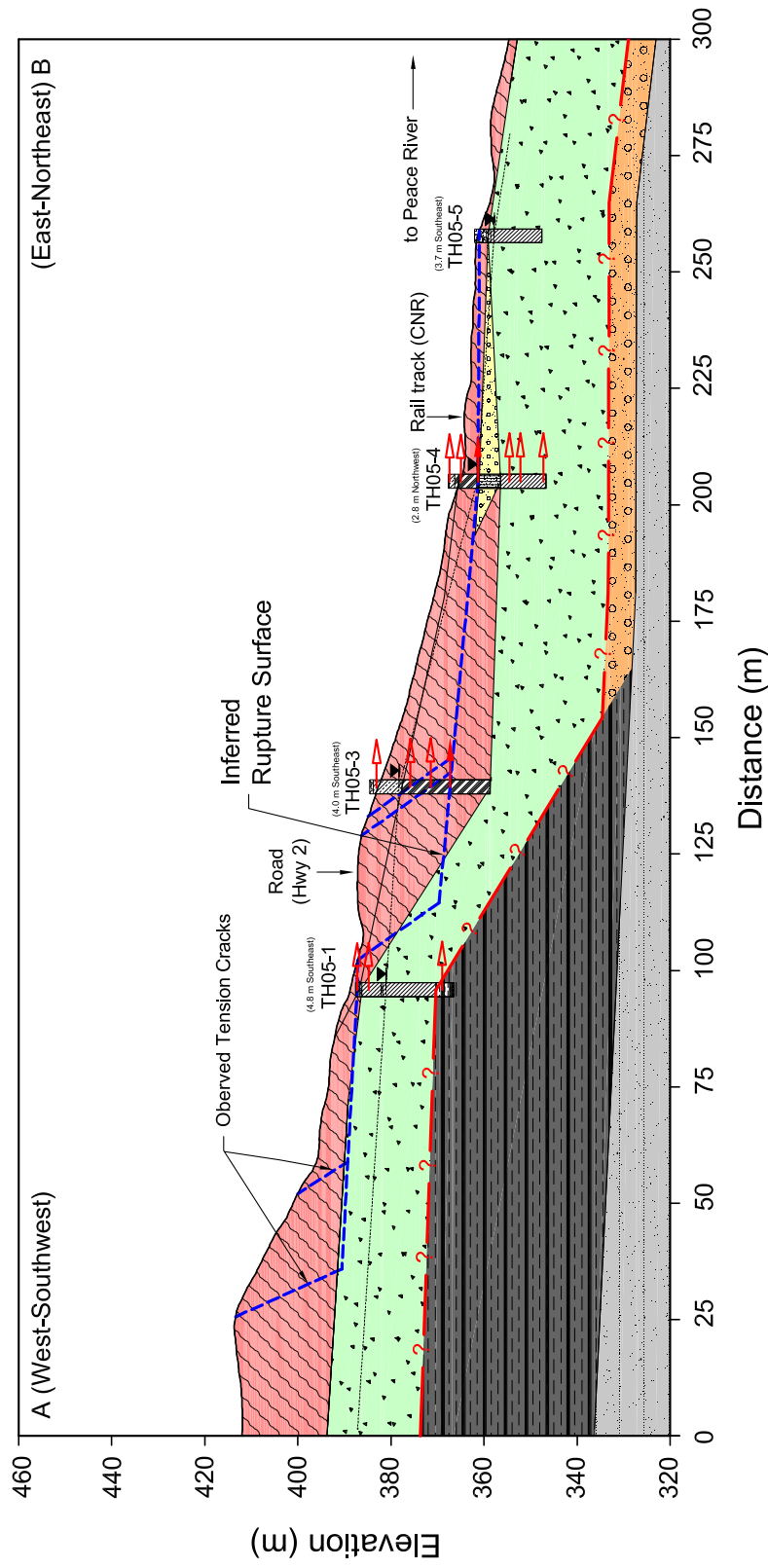


Figure 4.29 Cross section of the Shop Slide. Boreholes and their proximity to the section plane are indicated. Lithological and genetic stratigraphies are also shown. Observed locations for ground movements are illustrated by red arrows. Inferred rupture surfaces are delineated by thick blue dashed lines. Representative symbols for lithological and genetic units are also presented in Figure 4.3. Detail borehole data are also noted in Appendix A

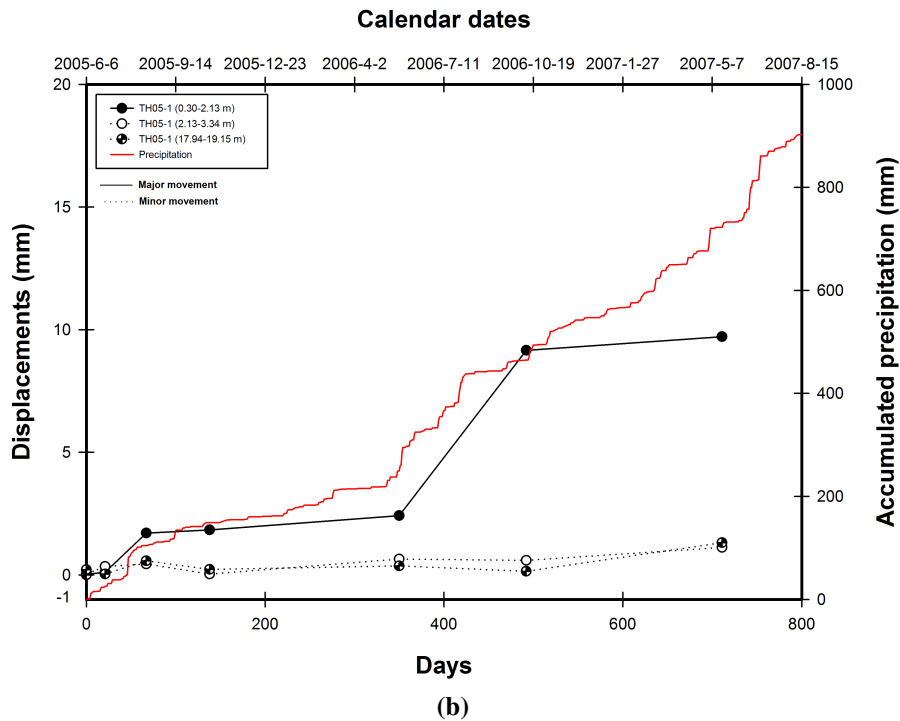
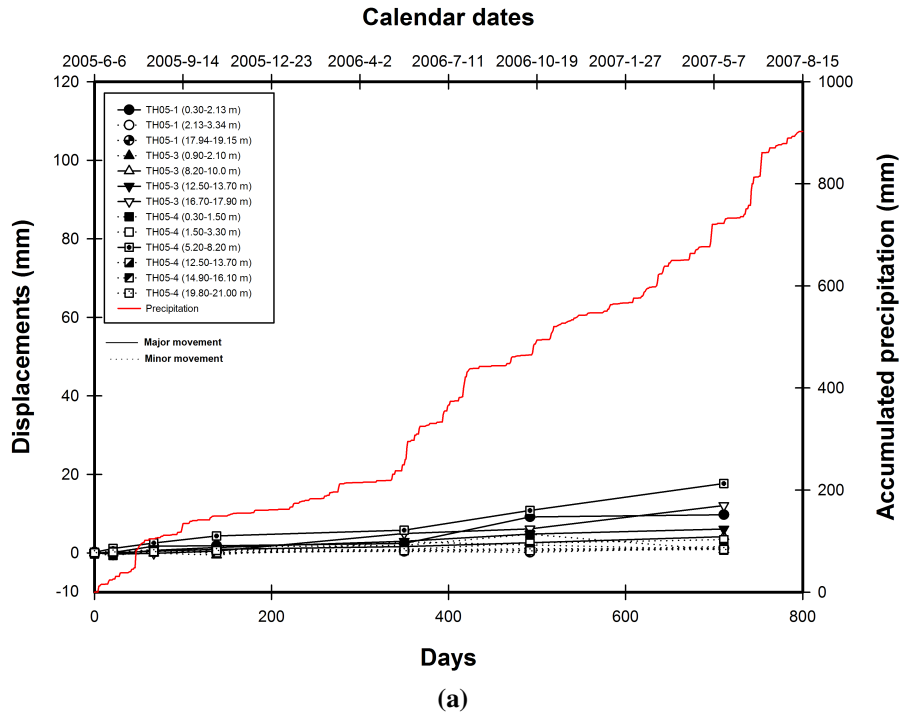


Figure 4.30 Landslide movements at the Shop Slide. a. Total movement rates. b. Movement rates at Borehole TH05-1. c. Movement rates at Borehole TH05-3. d. Movement rates at Borehole TH05-4. Precipitation data of the measurement period are also described. Location of boreholes is shown in Figure 4.29. Detailed data are also noted in Appendix A

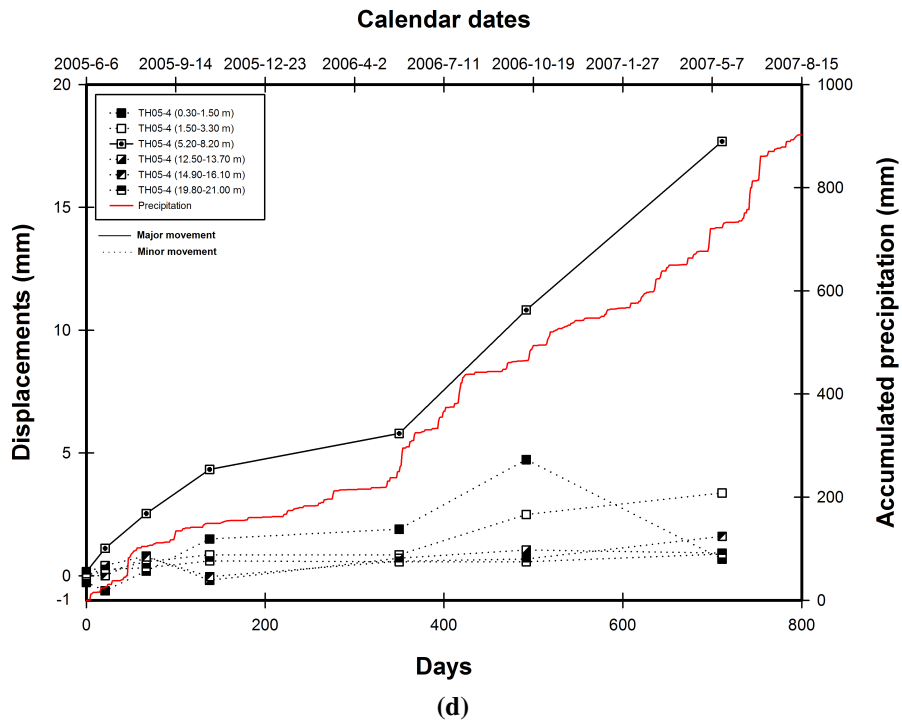
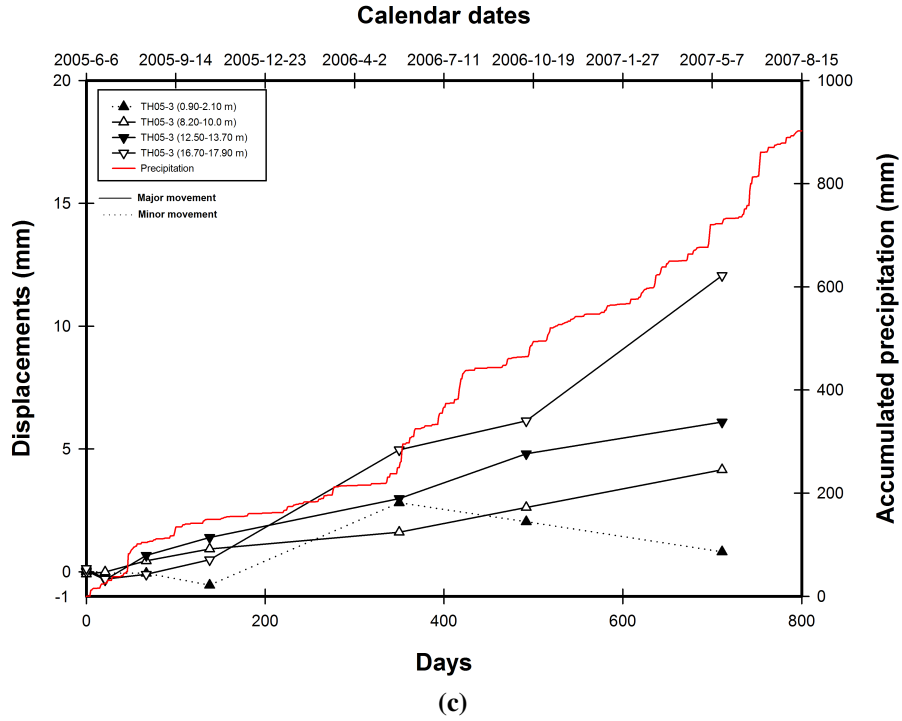


Figure 4.30 (Cont'd)

of 6.4 metres in borehole TH05-4. This suggests the upper portion of the slide may reach its stable condition whereas the lower part of slide may need more movement to stabilize. Table 4.9 summarizes movement characteristics of the individual slope inclinometer.

Groundwater is also recorded for the same monitoring period as slope inclinometer measurements (Figure 4.31). The variation of the groundwater level is due to the seasonal fluctuation of precipitation and impacts the rate of the slope movement.

Figure 4.32 shows precipitation which may induce the slope instability in the study area. A 30 year average precipitation, mean temperature, and snow depth on the ground are also plotted to determine inter-relationships. The Shop Slide initiated in 1985 and 1986, and accelerated during 2005 through 2007 (Figure 4.30). Precipitation in the first half of 2007 was much higher than the 30 year average value. Early precipitation in 2007 was snow. Together with snow melt, heavy rainfall in April to June raised pore water pressure in the slope and drove a movement in the area.

4.1.6 Mile 50.9 Slide

The landslide, at the Mile 50.9 of the Peace River subdivision of the Canadian National Railway, is located on the west bank of the Peace River above the river terrace. Trailer courts have been constructed on steep slopes and it is expected that substantial cuts and fills were made during construction. Trailer courts have two different levels and the upper trailer court is adjacent to steep slopes (Figure 4.33). Initial movement was detected by court residents on May 3, 1979 and the size of the landslide was about 24 to 30 metre wide and 58 metre long.

Boreholes were installed to determine the subsurface stratigraphy and groundwater distribution. Figure 4.34 shows the cross section of the landslide where borehole 80-1, 2, and 4 were drilled through the east-west direction along the line A-B.

In Figure 4.34, borehole 80-1, which is near the scarp of the slide, the stratigraphy of slide generally consists of top soil, fine sand, laminated clay and silt. The sequence of the stratigraphy is underlain by a stiff to very stiff medium plastic silty clay dominating glacial till deposits which have water contents of 17 to 22 percent (Lindberg and Savigny 1980). It is, however, not consistent to the borehole 80-4,

Table 4.9 Summary of slope inclinometer measurements at the Shop Slide

BHs	Depth of movement (m)	Ave. movement rate (mm/year)
TH05-1	0.3	5
	2.7	0.6
	18.5	0.7
TH05-3	1.5	0.4
	8.8	2.1
	13.1	3.1
	17.3	6.2
TH05-4	0.3	0.4
	2.7	1.7
	6.4	9.1
	13.1	0.5
	15.5	0.8
	20.4	0.5

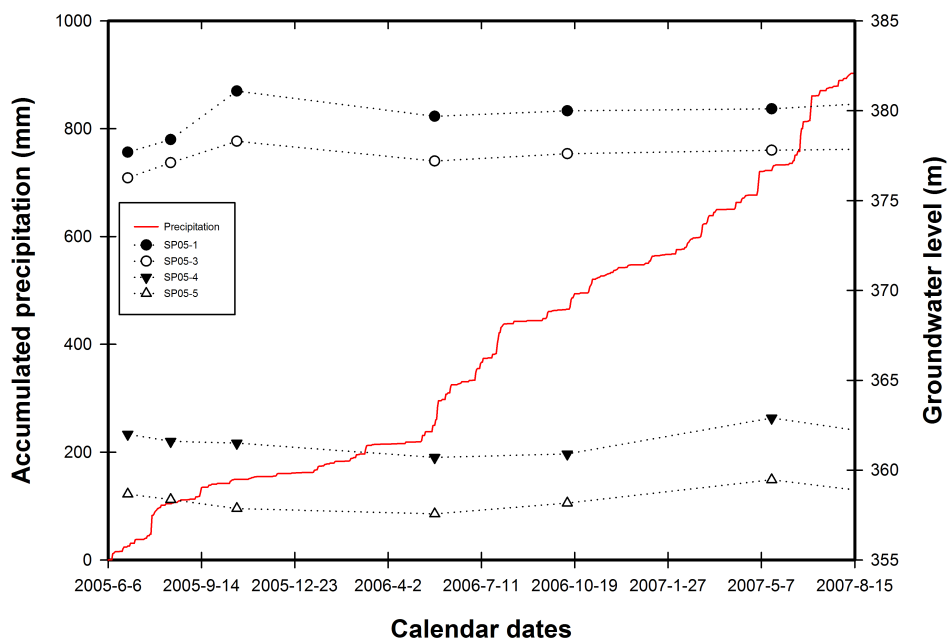
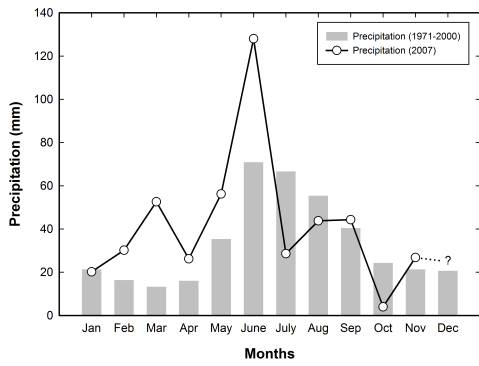
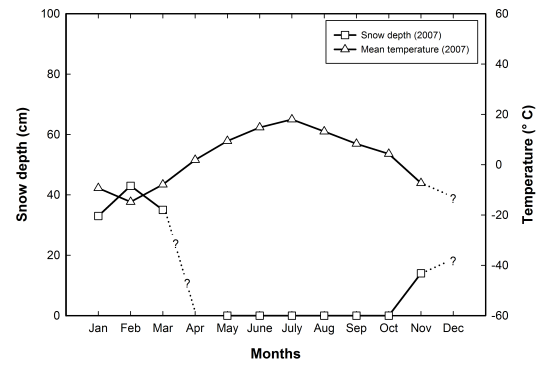


Figure 4.31 Temporal groundwater distribution at the Shop Slide. Location of boreholes is shown in Figure 4.29



(a)



(b)

Figure 4.32 Meteorological records on the Shop Slide in 2007. a. Annual precipitation in each year compared with the 30 year average value represented in gray bars. b. Mean temperature and snow depth on the ground in each year

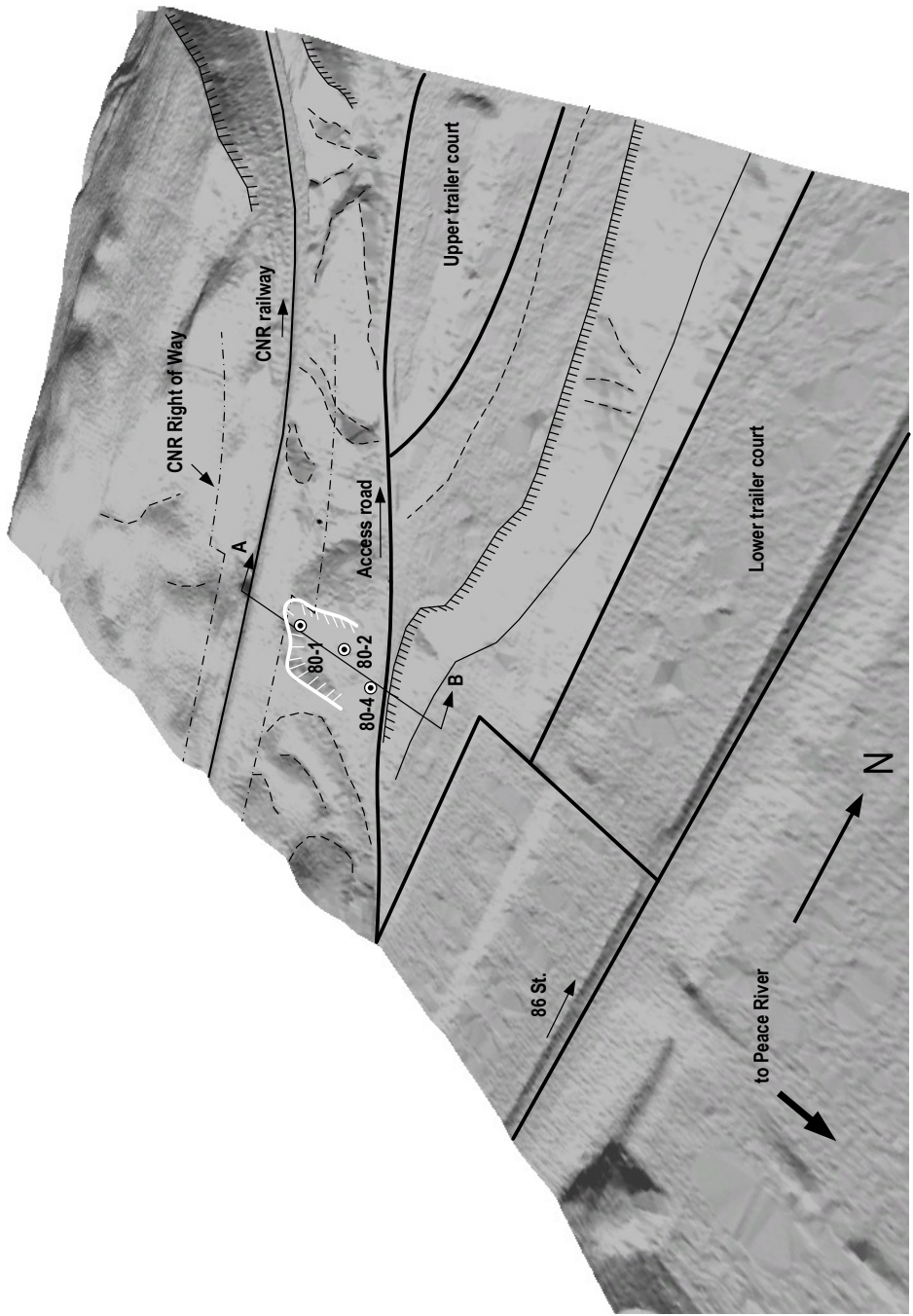


Figure 4.33 Perspective view of the Mile 50.9 Slide. Scale 1:1,500. Looking northwest. Landslide boundary and boreholes are also shown. Line A-B shows the cross section of the slide (Figure 4.34). The three dimensional hillshade is derived from the LiDAR dataset obtained in 2007

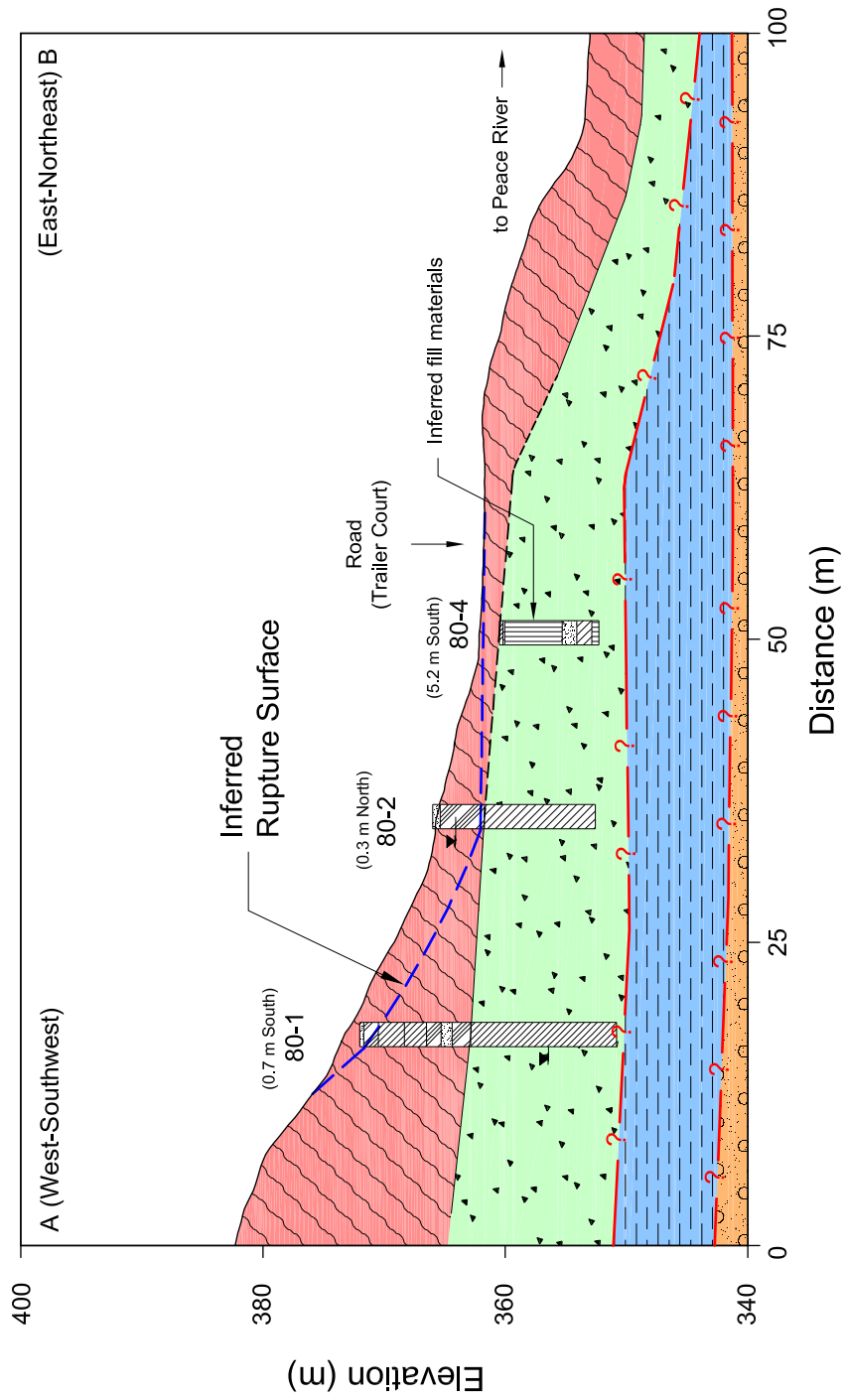


Figure 4.34 Cross section of the Mile 50.9 Slide. Boreholes and their proximity to the section plane are indicated. Lithological and genetic stratigraphies are also shown. Observed locations for ground movements are illustrated by red arrows. Inferred rupture surfaces are delineated by thick blue dashed lines. Representative symbols for lithological and genetic units are also presented in Figure 4.3. Detail borehole data are also noted in Appendix A

which is established in the toe of the slide. Lindberg and Savigny (1980) noted about 5 metres of clayey silt deposits, which were interpreted as fill materials used in the access road construction, with a condition of high water content close to the liquid limit were found at borehole 80-4. The cross section also shows the rupture surface of the slide and measured groundwater elevations at boreholes 80-1 and 2 (Table 4.10). Groundwater elevations indicate that the pore water pressure in silt deposits was built up at the toe of the slope and interfere with the natural subsurface drainage system due to the relatively impervious condition of the fill materials (Figure 4.35). Increased pore water pressure may cause the initial slide when blocks of silt deposits lose their strength are exposed to a small amount of groundwater change. Based on this hypothesis and the observation of wet silt materials which covered the access road at the toe, the landslide can be classified as a moderately slow, very wet, earth flow (Cruden and Varnes 1996).

Table 4.10 Measured groundwater elevations at the Mile 50.9 Slide. *Source:* Data from Lindberg and Savigny (1980)

Borehole No.	Groundwater level (m) [†]
80-1	17.33 [‡]
80-2	4.26 ^{††}

[†] Below the ground surface. [‡] Measured on Oct. 17, 1980.

^{††} Sheared off prior to Oct. 17, 1980.

Precipitation, mean temperature, and snow depth on the ground were also recorded to determine effects of hydrologic and meteorological factors of the landslide (Figure 4.36). Figure 4.36 shows precipitation during March and April which was similar to the 30 year average. Data in February, however, indicate precipitation 285 percent of the 30 year average and may have fallen as snow. The snow depth on the ground measured in February had a similar trend with precipitation. As temperature increases, snow melts and infiltrates into the ground and causes a rise in pore water pressure at the toe. Therefore, snow melting water may be a main trigger of the landslide on the Mile 50.9 after the low precipitation period prior to the landslide.

Another possible trigger is a loss of support due to anthropogenic factors. Significant cuts on toes of slopes for the access road in the trailer court made slopes steeper than their natural conditions. As noted in Figure 4.37, the construction which did not appear on 1958 aerial photographs has encroached on toes of the slopes and removed materials acting as lateral supports, which therefore decreased their stability.

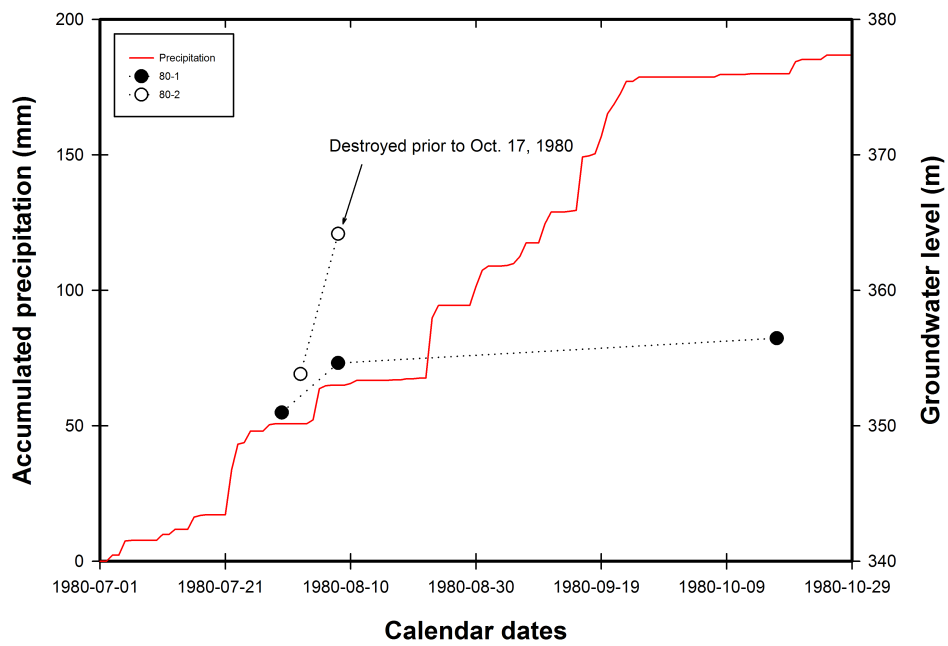


Figure 4.35 Temporal groundwater distribution at the Mile 50.9 Slide. Location of boreholes is shown in Figure 4.34

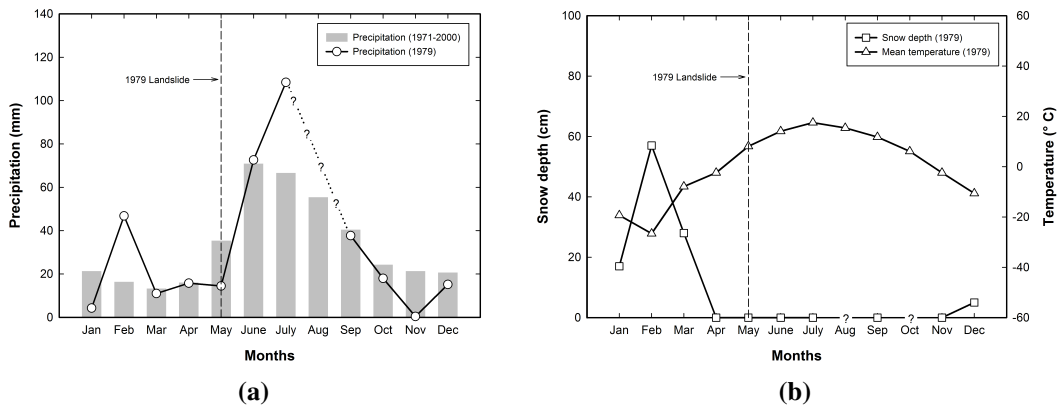
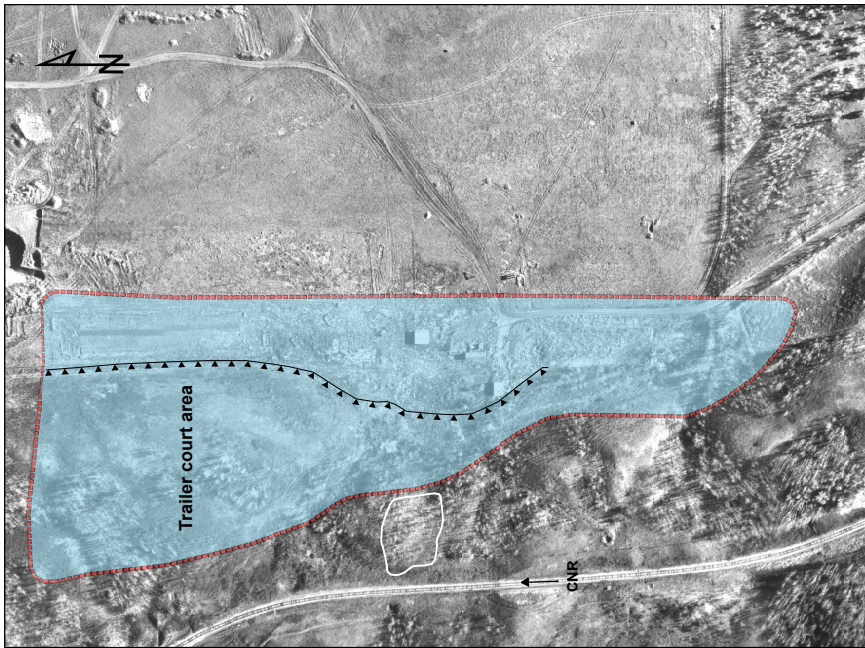


Figure 4.36 Meteorological records on the Mile 50.9 Slide. a. Annual precipitation in 1979 compares with the 30 year average value represented in gray bars. b. Mean temperature and snow depth on the ground in the year of 1979. Precipitation in August and snow depth in August and October in 1979 are missed and shown by dashed line with question marks



(a)



(b)

Figure 4.37 Anthropogenic effects on the Mile 50.9 Slide. a. 1958 aerial photograph (Alberta Photo: AS26-100) b. 2007 Quickbird imagery. Scale 1:2,000. The Mile 50.9 Slide is delineated by white line. The boundary of the trailer court is shown by a blue shade and red dashed line. Symbols of air photo interpretation are consistent with Dearman et al. (1972) and Federal Geographic Data Committee (2006)

4.2 Geotechnical characteristics of Peace River landslides

In order to determine geotechnical characteristics of landslides which were found in the Town of Peace River, I carried out laboratory tests on representative soil samples located at elevations of general rupture surfaces because they usually govern the entire stability of the slope. Boreholes for soil sampling were implemented by the Alberta Geological Survey (Morgan et al. 2009) by using mud-rotary and sonic rigs. Desired samples were taken except for certain depths of the east bank because the entire length of the borehole drilled on the east bank by the Alberta Geological Survey could not reach the depths where the expected rupture surface is located. Therefore, samples which represent general stratigraphic units were obtained for the east bank. Sampling points are indicated by Figure 4.1 and briefly described in Table 4.11. Detailed borehole logs with general stratigraphy and sampling elevations are also described in Appendix B.

Table 4.11 Summary of soil samples for the laboratory test

Sample ID	Elevation (m)	Depth (m)	Typical soil type	Borehole No. [†]
a	517.01-515.49	21.34-22.86	Diamicton (Till)	East (PR08-05)
b	459.10-457.58	79.25-80.77	Silt and Clay	
c	450.44	87.91	Silt and Clay	
d	381.75	63.65	Diamicton (Till) [‡]	West (PR08-03)
e	381.50	63.80	Diamicton (Till) [‡]	
f	364.71	80.59	Diamicton (Till) [‡]	
g	360.67	84.63	Silt (Till) [‡]	

[†] Locations of borehole are shown in Figure 4.1. [‡] Colluviated tills.

Atterberg Limits (ASTM 2005) and hydrometer tests (ASTM 2007b) were carried out to characterize soils on rupture surfaces. Results of these tests are given in Table 4.12 and Figure 4.38 respectively and Atterberg Limits of each soil sample are displayed by using the plasticity chart which shown in Figure 4.39. Liquid limits of colluviated glacial sediments samples (Samples d, e, f, and g) have a large extent on the plasticity charts in terms of the soil classification (from CL to CH), which are correlate to their disturbed characteristics. Advance phase glaciolacustrine sediments (Samples b and c) indicate high plasticity whereas glacial sediments (Sample a) show medium plasticity, respectively.

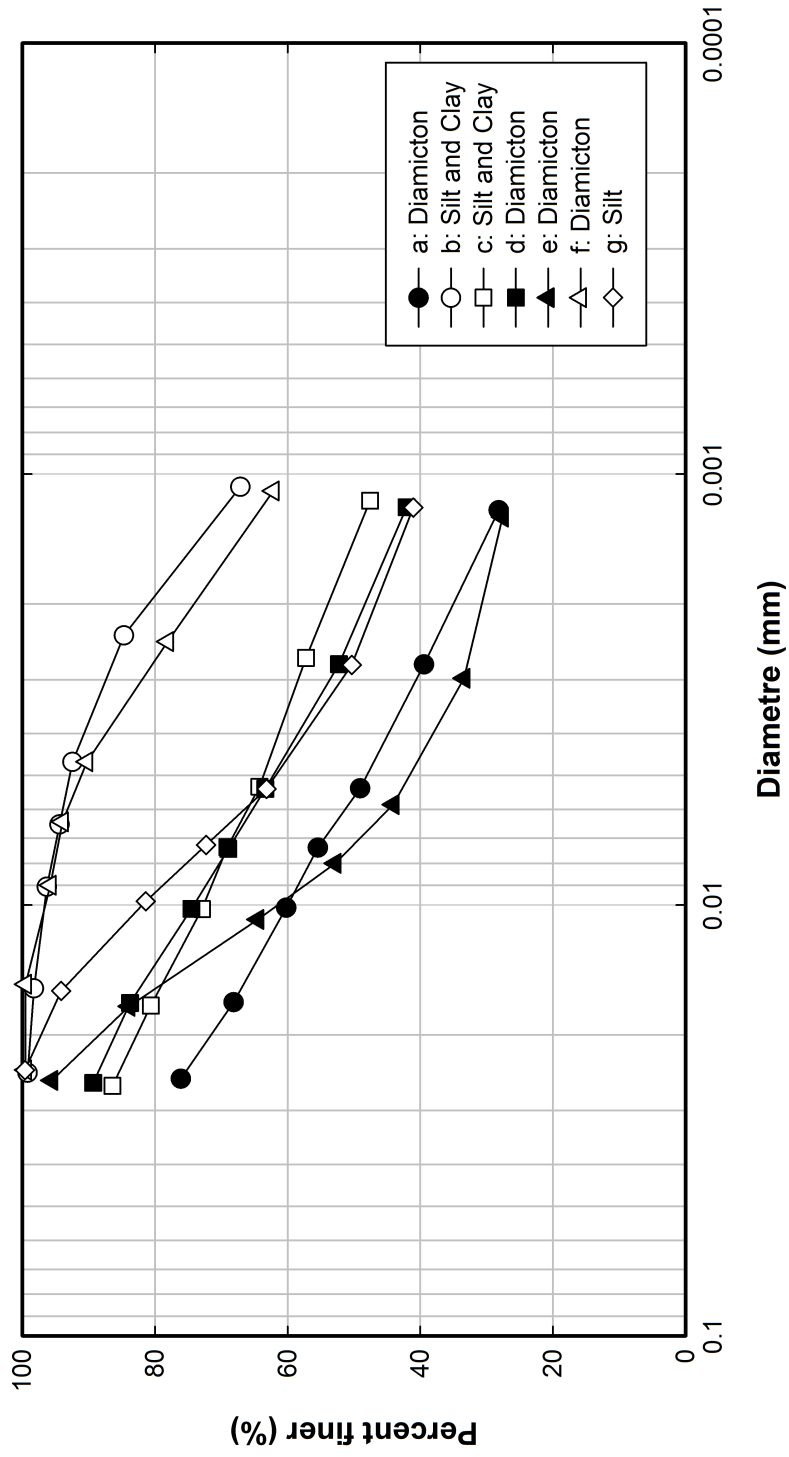


Figure 4.38 Hydrometer test results for soil samples. The general description of each sample is described in Table 4.1.1. Soil samples are differentiated based on their representative types (diamicton type soil: black solid symbol; silt or silt and clay: white solid symbols)

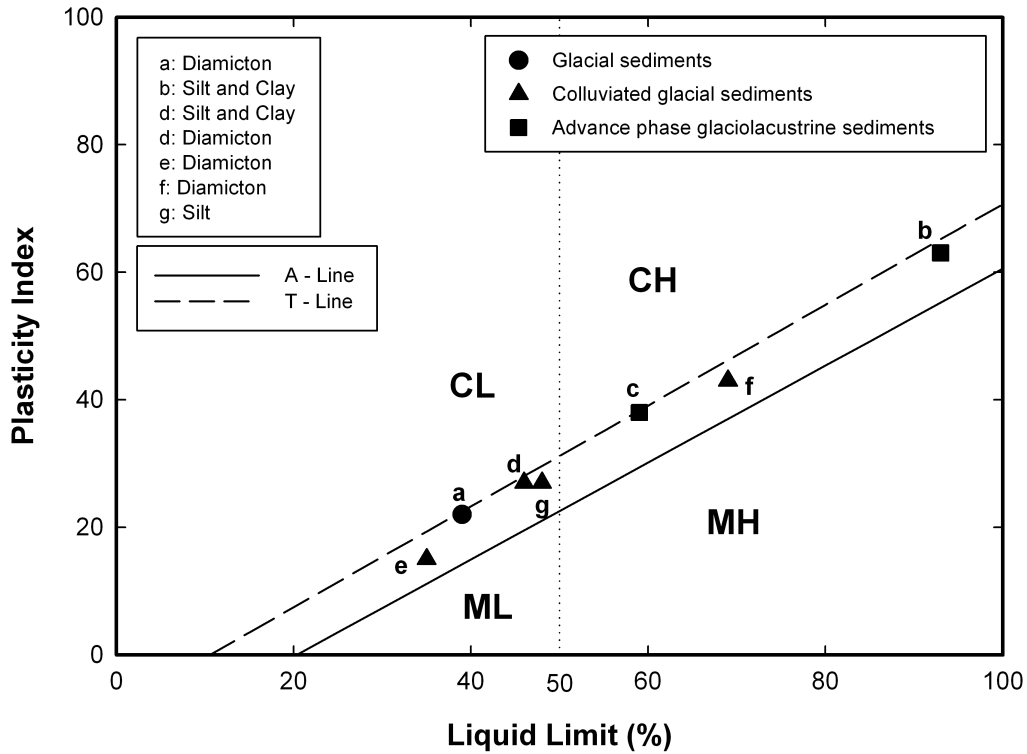


Figure 4.39 Plasticity chart for soil samples. Soils are classified by the Unified Soil Classification System (USCS) that identifies engineering properties of soils based on particle-size characteristics with liquid limit and plasticity index (ASTM 2010). Representative soils shown in the figure are as follows: Inorganic clays of high plasticity, fat clays (CH); Inorganic clays of low to medium plasticity, gravelly clays, sandy clays, silty clays, lean clays (CL); Inorganic silts, micaceous, or diatomaceous fine sandy or silty soils, elastic silts (MH); and Inorganic silts and very fine sands, rock flour, silty or clayey fine sands with slight plasticity (ML). Soils are also differentiated by geological stratigraphic units by using solid symbols (glacial sediments: circle, colluviated glacial sediments: triangle, and advance phase glaciolacustrine sediments: square). The A-line represents a constant relationship between liquid limit and plasticity index for sedimentary clays and acts as an empirical boundary which separates inorganic clays from inorganic silts and plastic soils containing organic components (Casagrande 1948). The T-line reflects changes of the grain size distribution of tills by sorting processes and mixtures of other sediments (Boulton and Paul 1976)

Table 4.12 Atterberg Limits test results

Location	East (PR08-05)			West (PR08-03)			
Sample ID [†]	a	b	c	d	e	f	g
Liquid limit (%)	39	93	59	46	35	69	48
Plastic limit (%)	17	30	21	19	19	26	21
Plasticity Index	22	63	38	27	15	43	27
Soil classification [‡]	CL	CH	CH	CL	CL	CH	CL

[†] General description of each sample is noted in Table 4.11.

[‡] Soils are classified by the Unified Soil Classification System (USCS) shown in Figure 4.39.

Shear strengths for each stratigraphic unit are determined by direct shear tests (ASTM 2007a). Four soil samples previously described were used for these tests (Samples a, b, e, and f) to find both peak (or fully softened) and residual strengths. Obtained shear strength parameters are shown in Figure 4.40 and comprehensive direct shear test results are also described in Appendix C.

Figures 4.40a and 4.40b which illustrate colluviated glacial sediments show similar shear strength parameters of both fully softened and residual values. Although the difference between their sampling locations is about 17 metres, both samples show similar characteristics of the colluviated sediments. On the other hand in sample a, Figure 4.40c, internal friction angles of fully softened and residual values are higher than those obtained from samples e and f. This high shear strength value was postulated by the relatively intact characteristic of the glacial sediment even though both are same till materials. The shear strength of the advance phase glaciolacustrine sediment (sample b, Figure 4.40d) showed high peak and low residual values which are typical behavior for clay and within ranges obtained from Sharma (1970) and Ruel (1988). A recent study carried out by Kim et al. (2010a) showed similar results of low residual friction angles in the advance phase glaciolacustrine sediment obtained from Fox Creek, a tributary of the Saddle River in the Peace River Lowland (Appendix D). The obtained peak internal friction angle (19.3 °) in sample b is identical to the fully softened value (19.2 °), indicating that this advance phase glaciolacustrine sediment sample had already been sheared over time. The elevation of the sample located in the transition zone between glacial and advance phase glaciolacustrine sediments, which was tremendously affected by the glacier movement, would support the decrease of the peak strength value toward the fully softened one.

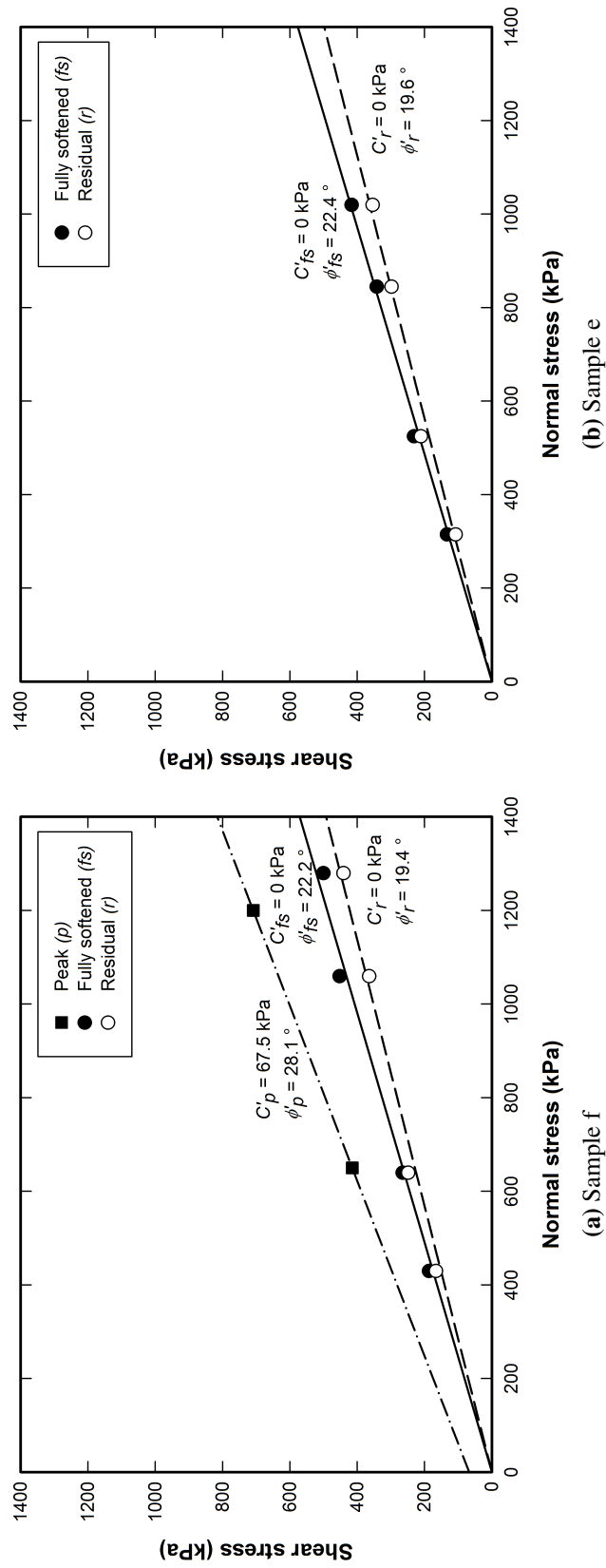


Figure 4.40 Direct shear test results for soil samples. a, b, and c. Diamiction. d. Silt and clay. Each sample shows peak (or fully softened) and residual strength properties with cohesions. Peak strength parameters obtained by Sharma (1970) are also noted in d for a comparison with current results

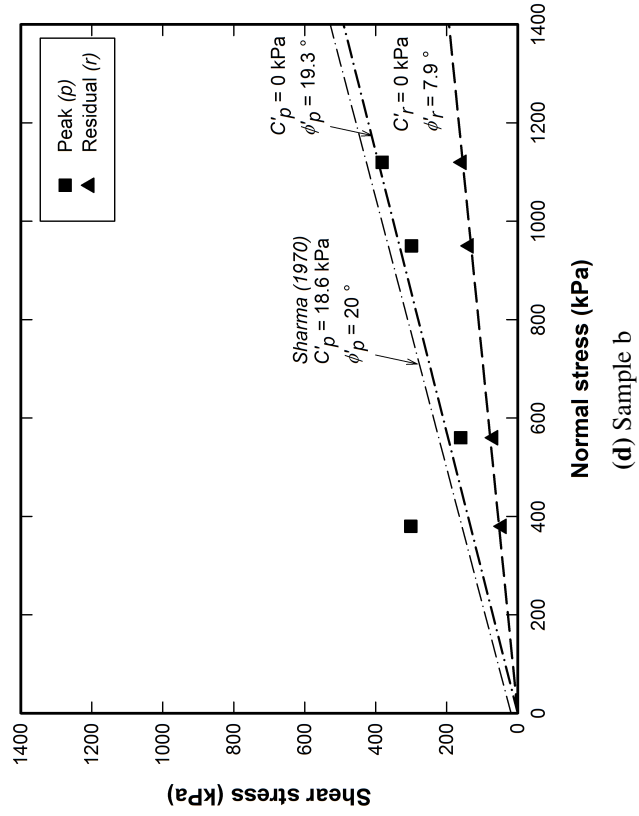
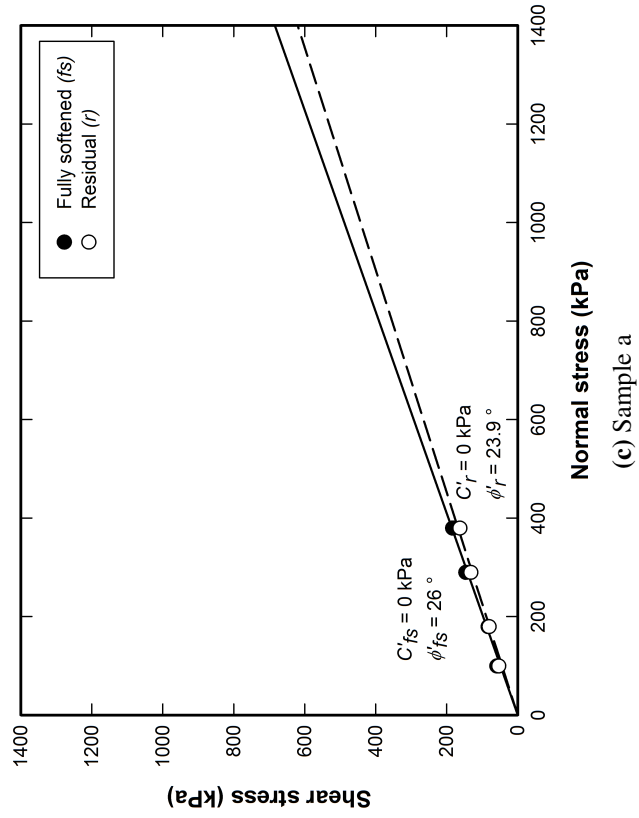


Figure 4.40 (Cont'd)

4.3 Characteristics of the landslide movement

In this section movement data are processed in various ways to represent characteristics of landslides. Analyzed data on the landslide movement would help to identify the general rupture surface which controlled landslides in the study area. The rate of movements may indicate the state of current landslides and give an indication of their classification type. Geomorphological features can also affect the landslide movement displacements.

Movement patterns are discussed to explain modes of landslide kinematics. Observations of movement patterns from recent landslides showed different movement behaviours which indicate the evolution of the landslide activity. Movement characteristics observed may be used to estimate the future behaviour of unstable slopes and develop a landslide hazard map for the Peace River area (Kim et al. 2010b).

4.3.1 Data compilation and analysis

Boreholes installed in six landslides are used to identify their movement characteristics during the progress of each landslide. A total of 23 boreholes in which slope inclinometers were installed since the initiation of movements were compiled for the study, 48 points within boreholes were identified to have moved. Measuring points which represent movements within the boreholes were classified as either horizontal rupture surfaces or back scarps based on their elevations and approximate geometry of displaced landslide masses. Appendix A describes detailed boreholes information. From these borehole data the general rupture surface was evaluated by combining general characteristics of rupture surfaces in recent landslides.

4.3.1.1 Identifying general rupture surfaces

The common rupture surfaces which may control recent landslides in the Town of Peace River can be classified by the type of rupture surfaces, such as horizontal rupture surfaces or back scarps and calculated the basal rupture surface by averaging elevations of horizontal rupture surfaces obtained from each landslide (Figure 4.41). Elevations of general rupture surfaces are 365 and 386 metres in the west bank,

330, 338, and 370 metres in the east bank, respectively. These general elevations of rupture surfaces can be used in landslide hazard and risk assessments as one of the preparatory casual factors.

Moisture contents of the rupture surface of each landslide are shown in Figure 4.42. As indicated in Figure 4.41, available moisture contents were displayed and divided by the type of rupture surfaces. Displayed moisture contents were averaged following the soil type such as clay fill, clay, clay till, and shale and sandstone. Calculated representative moisture contents for each soil type lying on basal rupture surfaces are also indicated in Figure 4.42.

One useful finding which can be obtained from these analyses is the soil type comprising rupture surfaces. Figure 4.43 shows the soil type lying on the rupture surface of each landslide. As shown in Figure 4.43, most rupture surfaces, both horizontal rupture surfaces and back scarps, are within colluvial sediments (33 %) and till deposits (31 %), respectively. A few rupture surfaces were located within bedrock formations (15 %). It is interesting to note that some rupture surfaces were observed in fill materials (15 %), which indicate shallow landslides occurred near the ground surface.

4.3.1.2 Movement rates and their characteristics

Figure 4.44 shows total movement rates obtained from 48 points in 23 boreholes installed in the recent landslides of the study area. Results of analyzing movement rates show that most movement rates are in the very slow (1,600 to 16 mm/year) and extremely slow (less than 16 mm/year) classes (IUGS Working Group on Landslides 1995). Under these conditions, structures may be undamaged or have manageable damages if such as cracks.

Both maximum and average movement rates in the recent landslides are presented in Figures 4.45 to 4.48. Movement rates of the Mile 47.8 Slide is described in Figure 4.45. Average movement rates at boreholes 95-5 and 7 showed up to 1,500 percent faster movement rate than at borehole 95-2, which indicate the Mile 47.8 Slide moved along the lower half of the slope (Figure 4.3). The difference would be larger when considering the maximum movement rate.

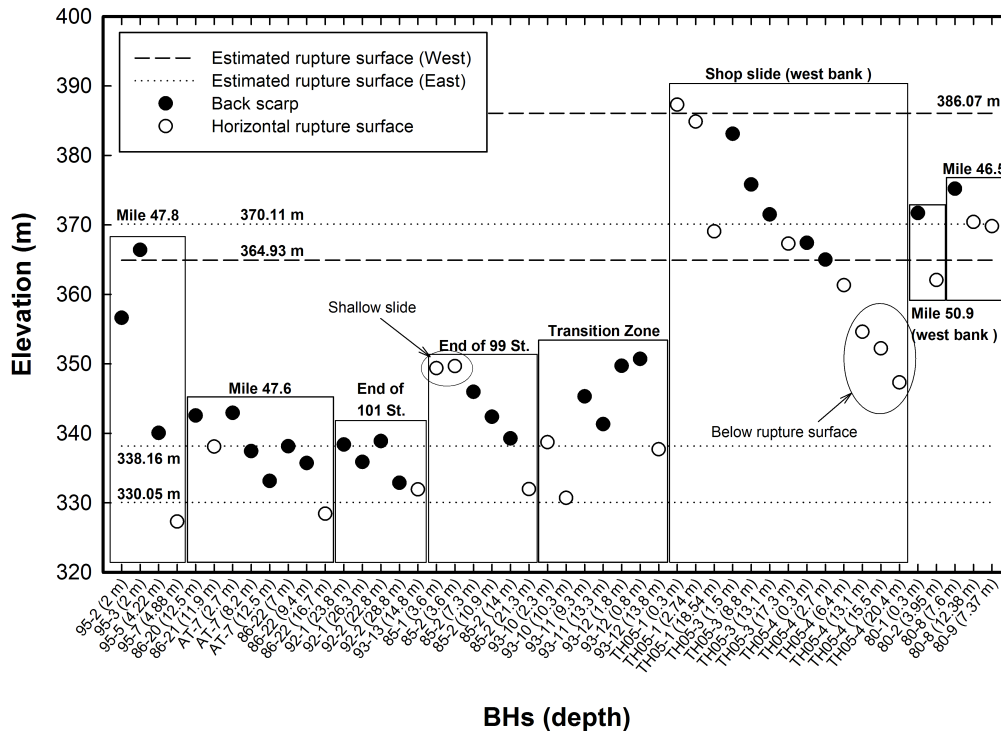


Figure 4.41 Estimated general rupture surfaces. Elevations on rupture surfaces obtained from boreholes within each landslide are described. Boreholes presented in the abscissa are divided based on each recent landslide by using rectangular areas. Rupture surfaces on basal surfaces are presented by white circles and those located on back scarps are shown by using black circles. Estimated general rupture surfaces on the west bank are delineated by dashed lines and those on the east bank are indicated by dotted lines

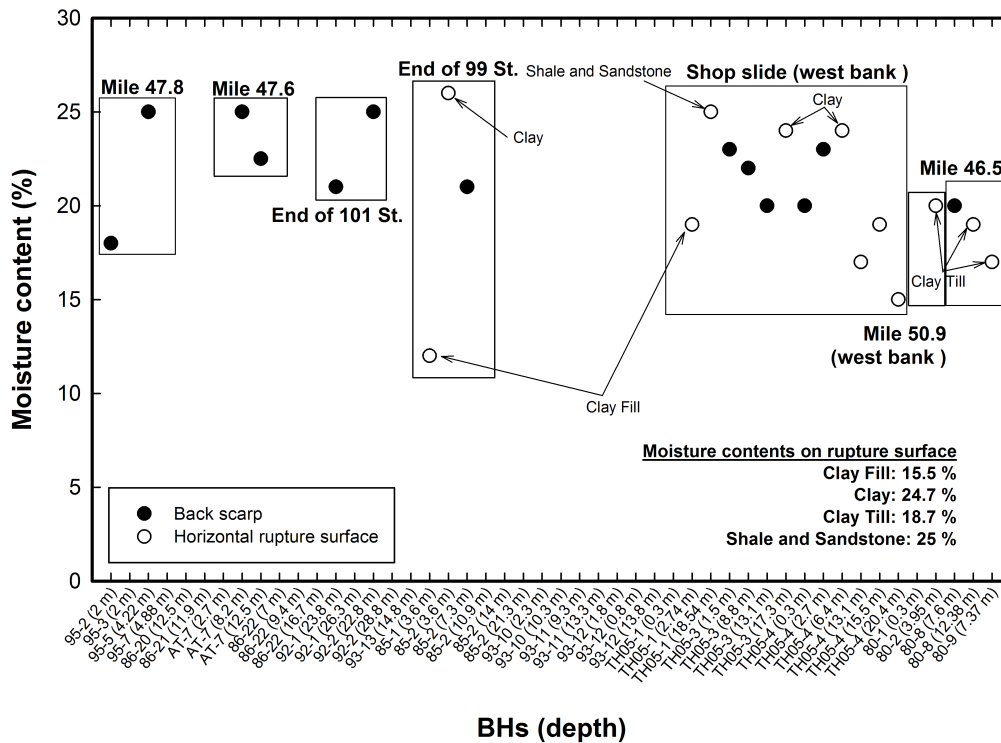


Figure 4.42 Representative moisture contents. Boreholes containing moisture contents are presented. Boreholes in the abscissa are divided based on each recent landslide by using rectangular areas. Rupture surfaces on basal surfaces are presented by white circles and those located on back scarps are shown by using black circles. Soils on horizontal rupture surfaces are classified based on soil type. Overall moisture contents of each soil on horizontal rupture surfaces are shown on lower right of the plot

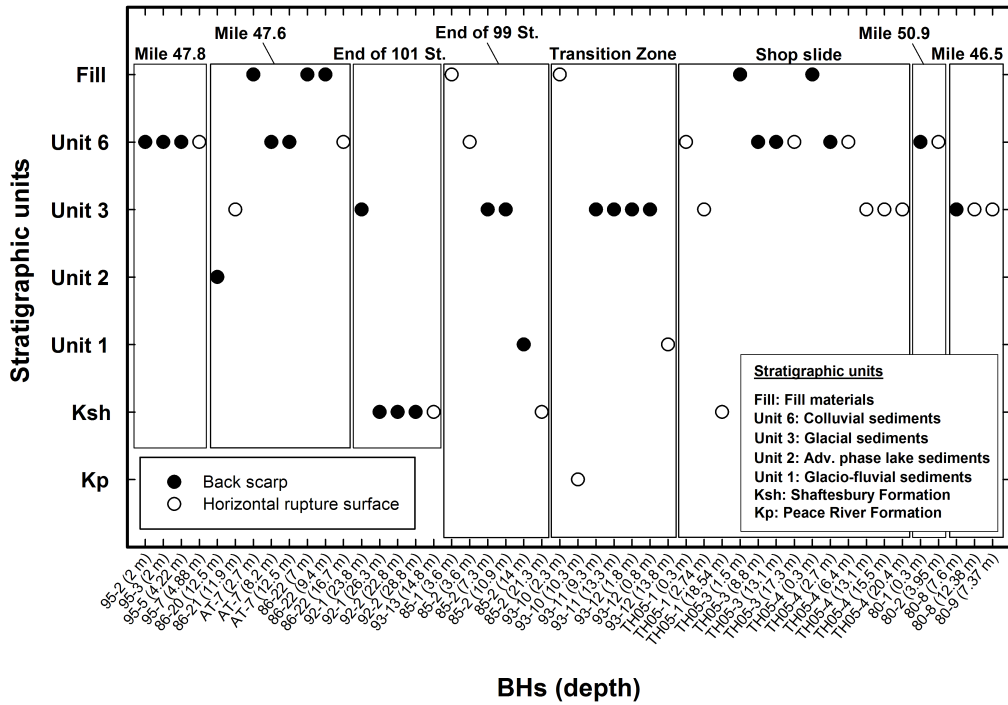


Figure 4.43 Stratigraphic units on rupture surfaces. Observed rupture surfaces are divided by stratigraphic units shown in the ordinate. Each stratigraphic unit described in Figure 3.9 is briefly explained in lower right of the plot. Presentations of boreholes with their symbols follow Figures 4.41 and 4.42

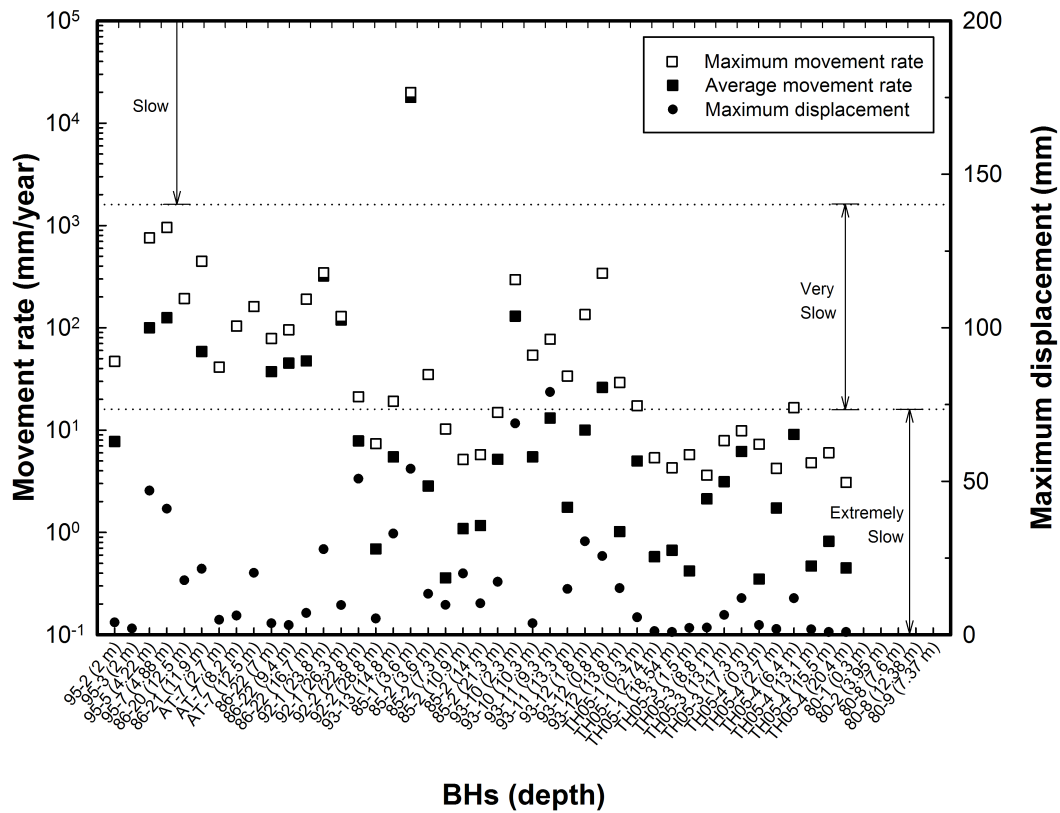


Figure 4.44 Total movement rates obtained from slope inclinometers. Maximum and average values of movement rates are described on the logarithmic ordinate using white and black squares, respectively. Maximum displacement of each slope inclinometer during the monitoring periods is shown using black dot. Landslide movement classes proposed by the IUGS Working Group on Landslides (1995) are also presented in the plot

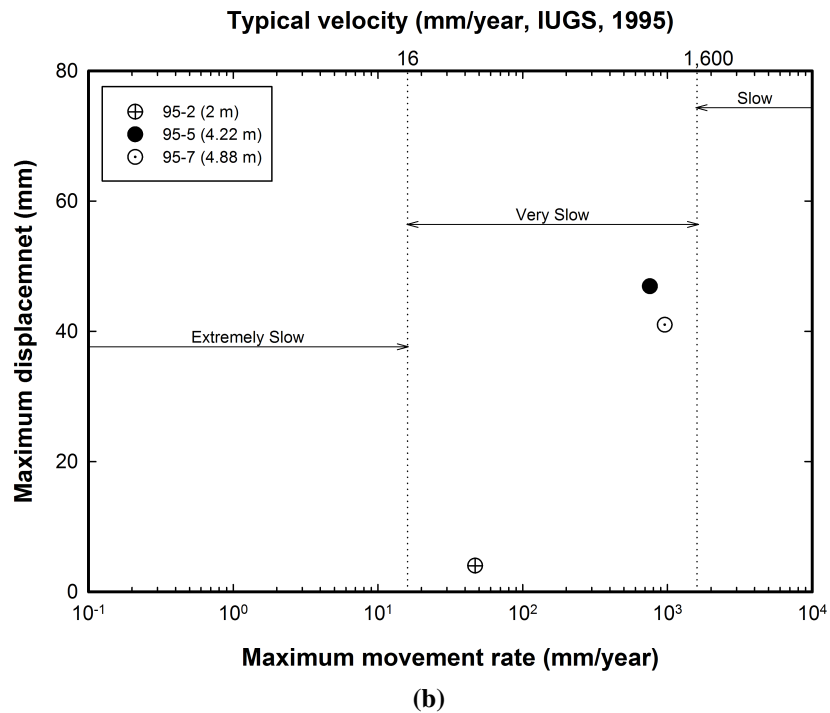
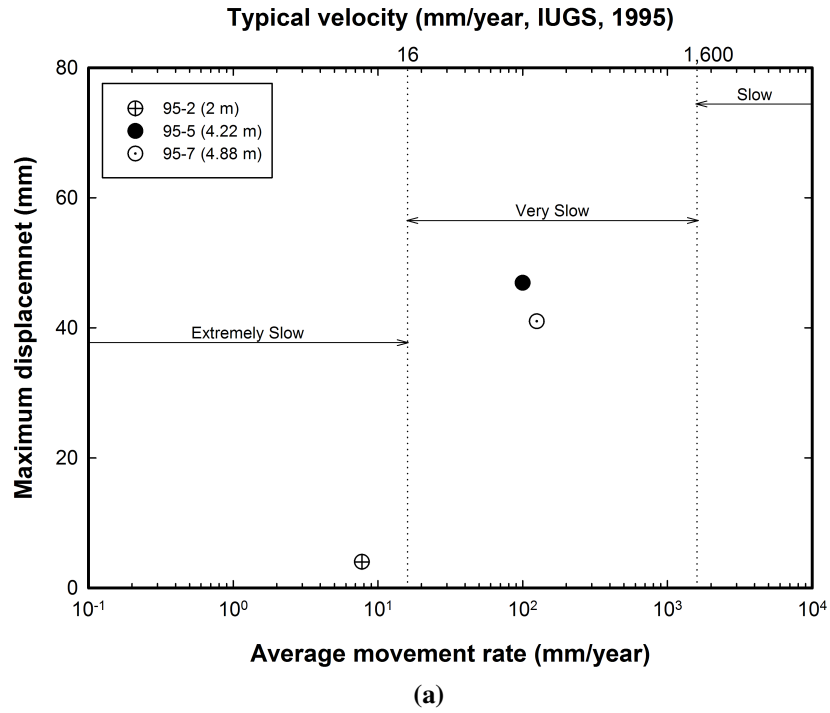


Figure 4.45 Movement rates at the Mile 47.8 Slide. a. Average movement rates. b. Maximum movement rates. Location of boreholes is shown in Figure 4.3. Landslide movement classes proposed by the IUGS Working Group on Landslides (1995) are presented by using the logarithmic abscissa on top of the plot. Maximum displacements of each slope inclinometer are also indicated

Movement rates from the Mile 47.6 Slide presented in Figure 4.46 show significant increases of the slope movement at basal rupture surfaces. Three boreholes of 86-21 and 86-22 (9.4 and 16.7 m, respectively), located on horizontal rupture surfaces of the upper slope, have high maximum movement rates compared to average values. Due to the insufficient data availability for maximum movement rates at back scarps, boreholes 86-20 (12.5 m) and AT-7 (12.5 m), are same as average values. Large displacements, however, were found in both boreholes. From these, it is postulated where the most influenced areas on the slope by slope movements are located.

Figure 4.47 shows movement rates obtained in the 99/101 Streets Slides area. For the End of 101 Street Slide, inferred rupture surfaces can be divided into two based on movement rates: (1) a relatively shallow slide in which borehole 92-1 is located; and (2) a retrogressive slide that has a boundary including boreholes 92-2 and 93-13 (Figure 4.17). Relatively rapid movements are detected on the shallow slide and these shear off the borehole at the beginning of the monitoring period (Figure 4.21). Movement rates on the lower rupture surfaces show an extremely slow movement behaviour. Measured values at boreholes 92-2 (28.8 m) and 93-13 (14.8 m) have similar average movement rates of 8 and 5 mm/year, respectively, which represent slope movement on the same rupture surface. Figure 4.21 shows cumulative movements at these boreholes which show a comparable behaviour.

Consistent movement rate characteristics, for both shallow and retrogressive slides, can be found in the Transition Zone Slide. Boreholes 93-10 (2.3 m), 93-11 (9.3 and 13.3 m), and 93-12 (13.8 m) comprise the shallow slide (Figure 4.18) and significant movements are found at toe and backscarp of the shallow slide (Figure 4.22). Movement rates obtained at lower rupture surface have the extremely slow movement. Measured values near ground surface, boreholes 93-12 (0.8 and 1.8 m) show a comparable behaviour each other which indicates the same movement.

Movement rates at the End of 99 Street Slide indicate a less consistent behaviour compared to the End of 101 Street and Transition Zone Slides in the fact that no potential slope movements are found at the middle of the slide (Figure 4.19). Average movement rates at this area are less than 1.2 mm/year showing internal deformations without constructing distinct rupture surfaces. The movement rate obtained at the top of the borehole 85-1 shows the highest value of 18,000 mm/year and this represents a shallow slide near ground surface (Figure 4.23). The movement rate

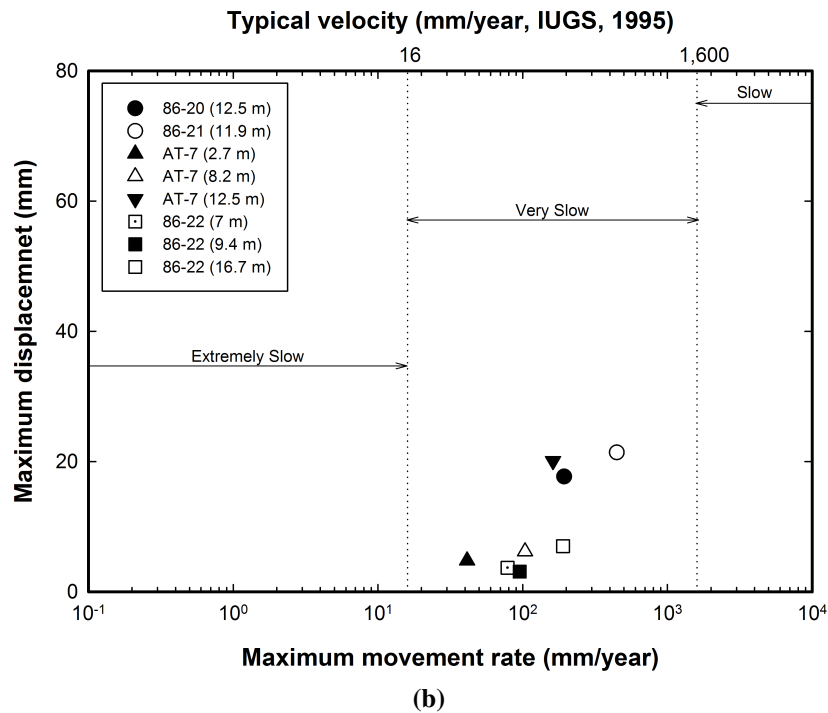
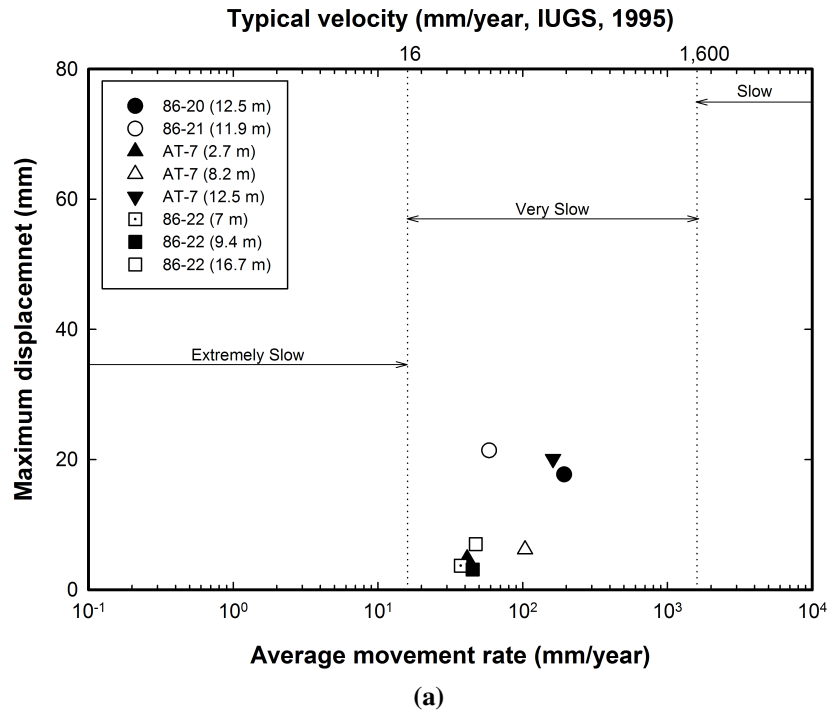


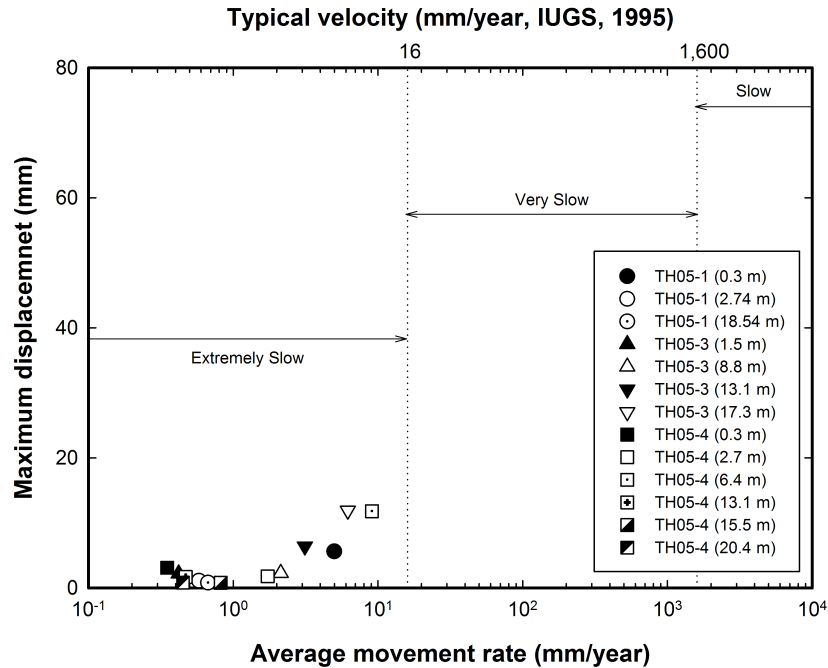
Figure 4.46 Movement rates at the Mile 47.6 Slide. a. Average movement rates. b. Maximum movement rates. Location of boreholes is shown in Figure 4.8. Landslide movement classes proposed by the IUGS Working Group on Landslides (1995) are presented by using the logarithmic abscissa on top of the plot. Maximum displacements of each slope inclinometer are also indicated

at the deepest point of borehole 85-2 shows an extremely slow behaviour but greater than those at the middle of the slide. Considering the relative location of the End of 99 Street Slide to the other slide areas, the rupture surface in colluvium sediments is not fully generated at the End of 99 Street Slide area yet whereas the rupture surface near bedrock (mainly the Shaftesbury shale Formation) may create a general form through the entire 99/101 Street Slides area. (Figure 4.20).

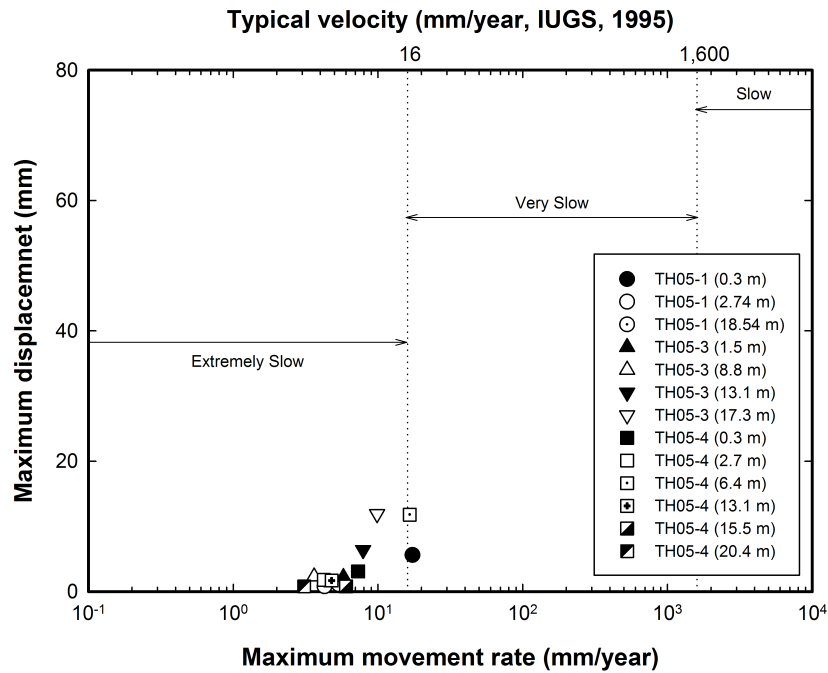
Movement rates recorded at the Shop Slide are described in Figure 4.48. Majority of obtained values are within the extremely slow category. However those can be divided by the average movement rate of 1 mm/year. Movement rates above 1 mm/year comprise rupture surfaces which shown in Figure 4.29. Movements at boreholes TH05-3 (17.3 m) and TH05-4 (6.4 m) representing the basal rupture surface on lower slope show a rapid movement between 6 and 10 mm/year. Borehole TH05-1 (0.3 m) located at the toe of the upper slide has a movement rate around 5 mm/year. Other locations forming rupture surfaces have values up to 3 mm/year. Boreholes whose locations are outside of rupture surfaces have movement rates less than 1 mm/year which indicates the internal deformation of the slope. This information would provide benefits in case movements occurred in the slope are similar therefore, movement characteristics of each borehole are difficult to identify.

4.3.1.3 Effects of geomorphologic factors on landslide movement rates

The configuration of physical ground geometries can affect movement characteristics of landslides. Generally rapid movements of the sliding mass would be accelerated when they pass through steep ground surfaces. The initiation of landslides is also easily activated in steep slopes. Glastonbury and Fell (2002; 2008) proposed a general relationship between ground surface slope angles and movement rates in mudslides. They also noted no obvious relationships in translational debris flows were found between ground surface angles and movement rates or rupture surface inclinations and displacement rates if differences between average and maximum displacement rates on the ground surface are small. Unfortunately most recent landslides in the study area are translational block slides (Table 4.1), which have similar movement mechanisms to 'Translational rock slides,' 'Internally sheared compound slides,' and 'Block type movement' which are referenced in Glastonbury and Fell (2002; 2008). It is, therefore, necessary to identify the influence of the geomorphological factor, especially the slope, on recent landslides in the study area.



(a)



(b)

Figure 4.48 Movement rates at the Shop Slide. a. Average movement rates. b. Maximum movement rates. Location of boreholes is shown in Figure 4.29. Landslide movement classes proposed by the IUGS Working Group on Landslides (1995) are presented by using the logarithmic abscissa on top of the plot. Maximum displacements of each slope inclinometer are also indicated

Results of analysis in determining a relationship between geomorphological feature and movement rates are shown in Figures 4.49 to 4.51. Figure 4.49 describes rupture surface inclinations obtained at each movement elevation in slope inclinometers installed in recent landslides of the study area with their average movement rates. Given that the geometry of slide rupture surfaces, they have distinct inclinations comprising basal rupture surfaces and back scarps. Figure 4.49 also shows a relationship between ground slopes that are measured on top of each borehole and corresponding average movement rates. No obvious differences between basal rupture surfaces and back scarps are found in the plot.

Figure 4.50 shows a relationship between average movement rates and rupture surfaces based on their locations. Average values of inclinations measured at horizontal rupture surfaces and back scarps are 3 and 55 degrees, respectively. Some basal rupture surfaces are completely horizontal. Ground surface angles with average movement rates recorded at the top of boreholes, including basal rupture surfaces and back scarps that are 19 and 18 degrees, respectively, which also show comparable values (Figure 4.51).

General correlations between inclinations of ground and rupture surfaces, and average movement rates presented in Figures 4.50 and 4.51 are shown in Figure 4.52. From the general point of view obtained in Figure 4.52 there is a positive correlation between slope angles and movement rates, which is adequately consistent to findings of Glastonbury and Fell (2002; 2008) in mudslides. It is, however, very difficult to arrive at any valid conclusion for this correlation by judging only from the available dataset without further detailed analysis.

4.3.2 Movement characteristics and their behaviours

Monitoring of landslide movements causing instability has become common practice in most slope related projects. Movements characteristics or patterns could indicate relationships with factors affecting their behaviours. With the development of instrumentation, we can capture reliable behaviours which would explain actual landslide mechanisms. Therefore, movement characteristics expressing displacement, velocities and accelerations in landslides could give insights during and even prior to hazardous situations.

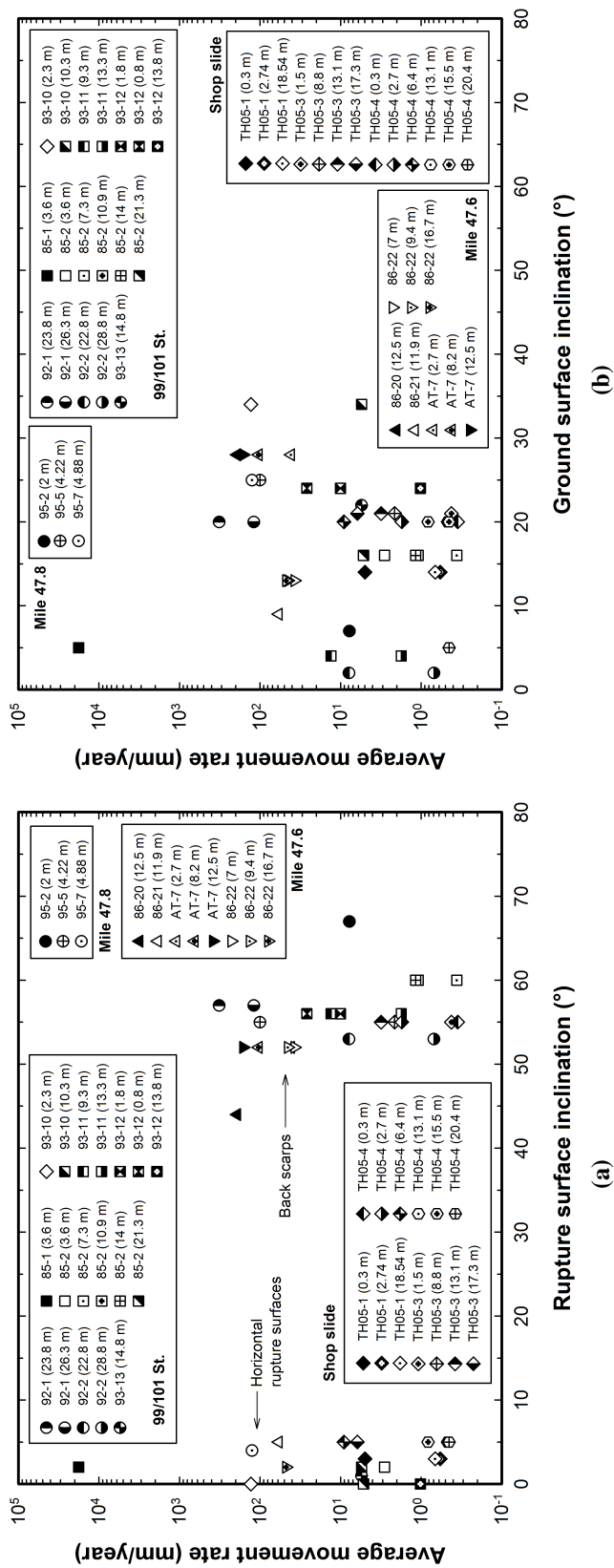


Figure 4.49 Geomorphological impacts on landslide movement characteristics. Average movement rates obtained from slope inclinometers in recent landslides of the study area with: a. Rupture surface inclinations. b. Ground surface inclinations. Rupture surfaces can be divided into basal and back scarp parts which are specifically described in Figures 4.50 and 4.51, respectively. Location of each boreholes is shown in Figures 4.3, 4.8, 4.17, 4.18, 4.19, and 4.29

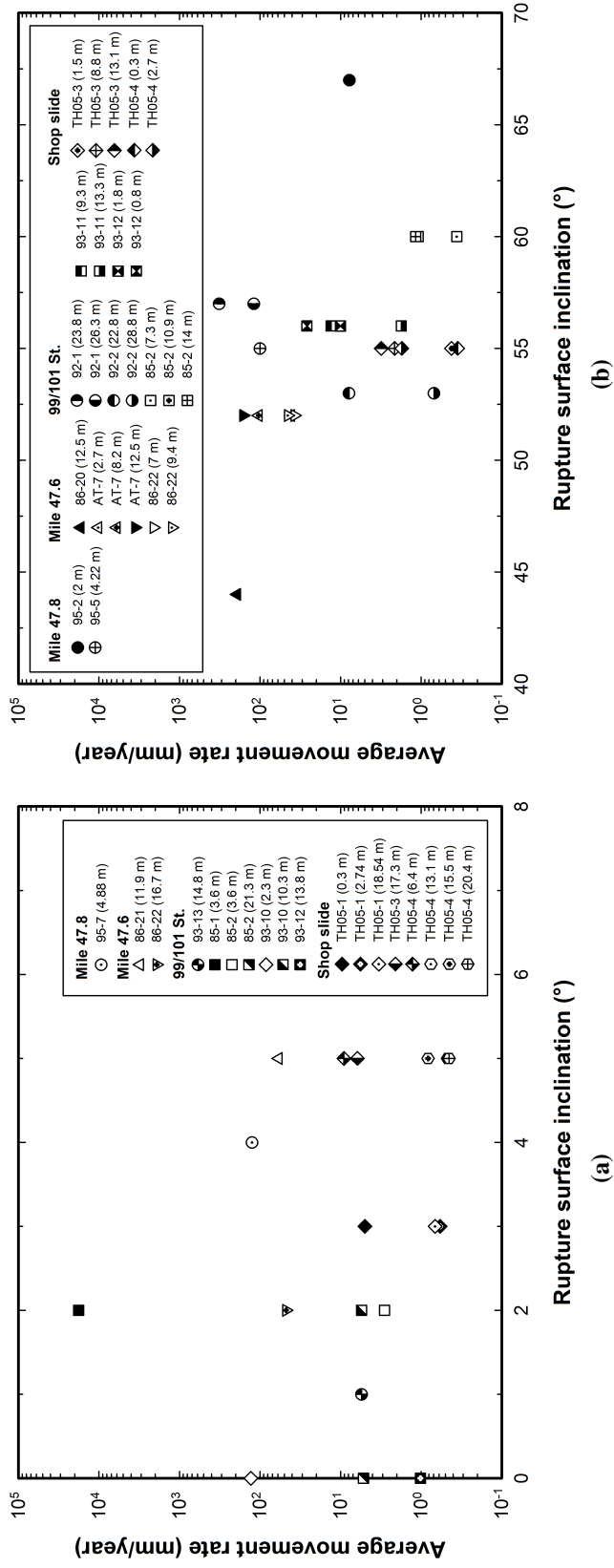


Figure 4.50 Rupture surface inclinations with average movement rates. a. At basal rupture surfaces. b. At back scarps

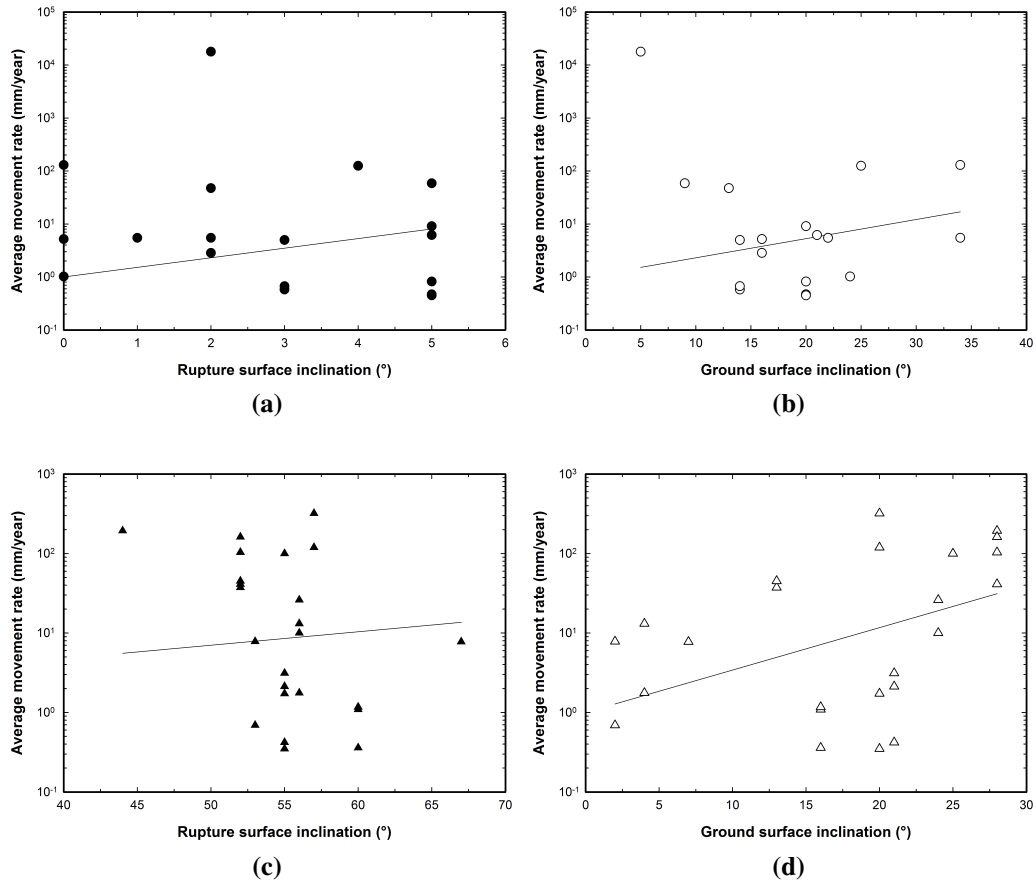


Figure 4.52 Average movement rates with inclinations of ground and rupture surfaces showing a statistical trend. Inclinations are at: a. Basal rupture surfaces. b. Ground surfaces in which basal rupture surfaces are located. c. Back scarps. d. Ground surfaces in which back scarps are located. Boreholes are notified in Figures 4.50 and 4.51, respectively

4.3.2.1 Material failure relationships

Theoretical studies for the rate-dependent material failure was proposed by Saito and Uezawa (1961) indicating that there is a close relationship between creep induced rupture and strain rate. They noted a possibility of estimating the slope failure by measuring the surface strain in slopes. Based on the simple compression and triaxial compression tests on various soils, Saito and Uezawa (1961) suggested a simple relationship of the creep rupture related to the steady-state strain rate as follows:

$$\log_{10} t_r = 2.33 - 0.916 \log_{10} \dot{\epsilon} \pm 0.59 \quad (4.1)$$

where t_r is a creep rupture (min) and $\dot{\epsilon}$ is a strain rate ($10^{-4}/\text{min}$), respectively. This simply leads to the following equation:

$$t_r \cdot \dot{\epsilon} = 214 \quad (4.2)$$

From Equations (4.1) and (4.2) the creep rupture is inversely proportional to the strain rate and independent of the type of soils and testing methods.

Saito (1965) also noted examples applying the creep rupture-strain rate relationship to actual slope failures. Later the extent of creep inducing rupture was furthered into the tertiary creep ranges, in which strain rate is gradually increasing, and previous equations can be redefined to the following form (Saito 1969, 1970, 1980):

$$\log(t_r - t) = \log a - \log \dot{\epsilon}_t \quad (4.3)$$

or, simply rearranged by:

$$\dot{\epsilon}_t = \frac{a}{t_r - t} \quad (4.4)$$

and, denoted by the strain or displacement:

$$\Delta l = a \log \frac{t_r - t_0}{t_r - t} \quad (4.5)$$

where Δl is a displacement, t is the observed time in the tertiary creep stage, t_0 is the time of no displacement, $\dot{\varepsilon}_t$ is the strain rate at the time t , and a is a constant. Therefore, the creep rupture life in soils can be estimated for the entire range of creep.

Many consecutive researches focused on estimating the time of slope movements have been made by theoretical, experimental, and practical perspectives since Saito and Uezawa (1961) first proposed the availability of their experimental work on the creep rupture-strain rate relationship. Relevant studies can be found in Fukuzono (1985; 1990), Hayashi et al. (1988). Varnes (1982) noted the time-deformation observation by Saito (1969; 1970; 1980) can be utilized by many experimental creep curves using various functions and is equivalent to those usually found in fracture mechanics. Azimi et al. (1988) employed graphical methods that are similar to those of Saito (1969) in estimating the time of failure in the tertiary creep stage on the rock slide in France which consist of gypsum. Studies on the future application to alarm systems by using critical velocity and acceleration which were recorded by field observations at recent landslides in New Zealand were carried out by Salt (1988) and Smith and Salt (1988). In both studies, they proposed suggested critical limits of downslope velocity and acceleration on local bedding planes of schist as 50 mm/day and 5 mm/day/day, respectively.

Fukuzono (1985; 1990) used experimental slope models in order to identify the failure time of slopes. He noted a relationship between surface displacement and slope failure induced by rainfall. The relationship can be expressed as follows:

$$\frac{d^2x}{dt^2} = a \left(\frac{dx}{dt} \right)^\alpha \quad (4.6)$$

where x is a surface displacement, t is time, and a and α are constants. Differentiation forms of Equation (4.6) refer acceleration and velocity of downward surface displacements with respect to time. Equation (4.6) indicates that the increment of the logarithm of acceleration is proportional to the velocity of surface displacement prior to significant movements of slopes changing their previous geometry (Fukuzono 1990). By integrating Equation (4.6) in the range of $a > 0$, then:

$$\text{for } \alpha < 1 \quad \frac{dx}{dt} = \{a(1 - \alpha)\}^{1/(1-\alpha)} \cdot (t_1 + t)^{1/(1-\alpha)} \quad (4.7)$$

$$\text{for } \alpha = 1 \quad \frac{dx}{dt} = \exp\{a(t_2 + t)\} \quad (4.8)$$

$$\text{for } \alpha > 1 \quad \frac{dx}{dt} = \{a(\alpha - 1)\}^{-1/(\alpha-1)} \cdot (t_r - t)^{-1/(\alpha-1)} \quad (4.9)$$

where t_1 , t_2 , and t_r are constants of the integral and can be used as observations time. As seen in Equations (4.7) to (4.9), the velocity of surface displacement has three distinct forms with respect to the time of t : a positive power function when $\alpha < 1$; an exponential function if $\alpha = 1$; a negative power function when $\alpha > 1$. The α is a dimensionless value and controls the sensitivity of acceleration of the displacement (Cornelius and Scott 1993). Based on experimental rupture tests on soils α is in the range of 1.5 to 2.2 (Fukuzono 1985). Voight (1989) compiled experimental results of various materials and suggested approximate values of 1.7 to 2.0 and 1.9 to 2.1 for alloys and metals, and soils, respectively. Equation (4.9) can be rewritten as follows:

$$\begin{aligned} \frac{dx}{dt} &= \{a(\alpha - 1)\}^{-1/(\alpha-1)} \cdot (t_r - t)^{-1/(\alpha-1)} \\ &= \frac{\{a(\alpha - 1)\}^{-1/(\alpha-1)}}{(t_r - t)^{1/(\alpha-1)}} = \frac{C}{(t_r - t)^n} \end{aligned} \quad (4.10)$$

where $C = \{a(\alpha - 1)\}^{-1/(\alpha-1)}$ and $n = 1/(\alpha - 1)$. Equation (4.10) is, therefore, a general form of the material failure relationship presented by Saito (1969; 1970; 1980) and Equation (4.4) is a special form of Equation (4.9) in case of $n = 1$.

Fukuzono (1985; 1990) proposed a simple estimation for the failure time of slopes by using the inverse rate of displacement based on experimental studies of Equation (4.9). He showed a linear behaviour when $\alpha = 2$ in reciprocal of velocity and time space (Figure 4.53). For the case of $\alpha \neq 2$, either convex or concave, graphical interpretations on Equation (4.9) by using tangent lines at each point would give a satisfiable result (Fukuzono 1985).

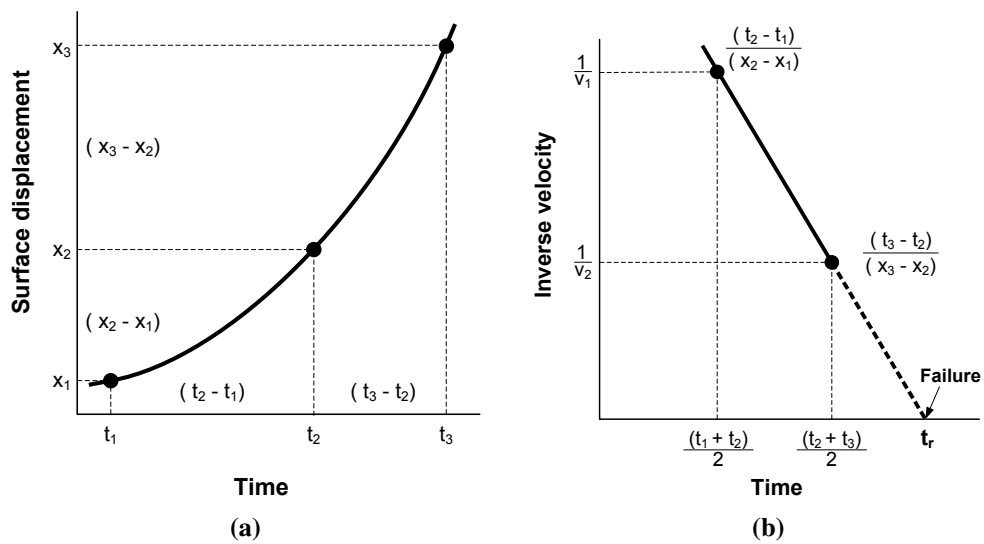


Figure 4.53 Diagrams showing the estimation of the failure time of slopes. a. Surface displacement b. Inverse velocity. A failure time can be calculated by extending the straight line of b described by a dashed line to meet the abscissa. *Source:* Fukuzono 1990, Figure 2

Voight (1988a; 1988b; 1989; 1991) and Cornelius and Voight (1995) further generalized this experimental correlation with monotonic load increases (Fukuzono 1985, 1990) in order to reflect a general law governing the material failure including from the natural (rock, soil, ice) to artificial bases (metal, plastic, concrete), at the terminal stage under conditions of constant stress and temperature in various loading conditions. The basic equation he suggested can be written as follows:

$$\dot{\Omega}^{-\alpha}\ddot{\Omega} - A = 0 \quad (4.11)$$

where Ω is arbitrary observable quantities which are suitable for explaining numerous behaviours of the material such as tension and compression induced by displacement or stain, a tilting due to the angle change, a seismic energy release, and a gas emission (Voight 1988b). A and α are empirical constants and can be found as a plot of the logarithms of creep acceleration and rate (Voight 1989). A represents the proportionality in the acceleration-rate relation and is dependent of α (Cornelius and Scott 1993; Cornelius and Voight 1995). Differentiation with respect to time can be described by dot. Equation (4.6) proposed by Fukuzono (1985; 1990), therefore, is a special case for Equation (4.11) provided by monotonic loading conditions on soils (Voight 1988a).

In order to estimate the time of landslide occurrences, usually Ω in Equation (4.11) can be treated as displacement. For the initial condition of $\dot{\Omega} = \dot{\Omega}_0$ at $t = t_0$, the integration of Equation (4.11) gives following forms depending on the value of α :

$$\text{for } \alpha = 1 \quad \dot{\Omega} = \dot{\Omega}_0 e^{A(t-t_0)} \quad (4.12)$$

$$\text{for } \alpha \neq 1 \quad \dot{\Omega} = [A(1 - \alpha)(t - t_0) + \dot{\Omega}_0^{1-\alpha}]^{1/(1-\alpha)} \quad (4.13)$$

for $\alpha > 1$, Equation (4.13) gives the following result:

$$\dot{\Omega} = [A(\alpha - 1)(t_f - t) + \dot{\Omega}_f^{1-\alpha}]^{1/(1-\alpha)} \quad (4.14)$$

where t_f is the failure time and $\dot{\Omega}_f$ indicates the velocity of displacement at failure.

Considering $\dot{\Omega}_f$ is infinite, thus can be ignored from the Equation. It is, therefore, identical to the equations of Fukuzono (1985; 1990) and subsequently to those of Saito (1969; 1970; 1980). α determines the shape of curvature in velocity and time relationship which show a linear behaviour for $\alpha = 2$, a convex shape for $\alpha > 2$, and a concave trend for $\alpha < 2$. As previously noted the α ranges in 2 ± 0.3 and near two is most practical for volcanoes (Voight 1988b). Figure 4.54 shows how the variation of α values could affect the curvature of the rate and time relationship in volcano eruption.

Predicting the time of material failure, t_f , can be calculated by rearranging Equation (4.14). For an arbitrary rate $\dot{\Omega}_*$ at the time of t_* , Equation (4.14) is:

$$\begin{aligned}\dot{\Omega}_* &= [A(\alpha - 1)(t_f - t_*) + \dot{\Omega}_f^{1-\alpha}]^{1/(1-\alpha)} \\ \dot{\Omega}_*^{1-\alpha} &= A(\alpha - 1)(t_f - t_*) + \dot{\Omega}_f^{1-\alpha} \\ A(\alpha - 1)(t_f - t_*) &= \dot{\Omega}_*^{1-\alpha} - \dot{\Omega}_f^{1-\alpha}\end{aligned}\tag{4.15}$$

Therefore, the remaining time to failure is,

$$t_f - t_* = \frac{\dot{\Omega}_*^{1-\alpha} - \dot{\Omega}_f^{1-\alpha}}{A(\alpha - 1)}\tag{4.16}$$

Since $\dot{\Omega}_f$ is assumed infinite,

$$t_f - t_* = \frac{\dot{\Omega}_*^{1-\alpha}}{A(\alpha - 1)}\tag{4.17}$$

Disregarding the velocity at failure, $\dot{\Omega}_f$, would make a non-conservative estimation and lead to improper decisions for emergency situations (Voight 1988a).

For the special case of $\alpha = 2$, Equation (4.17) can be simplified to:

$$t_f - t_* = \frac{1}{A\dot{\Omega}_*}\tag{4.18}$$

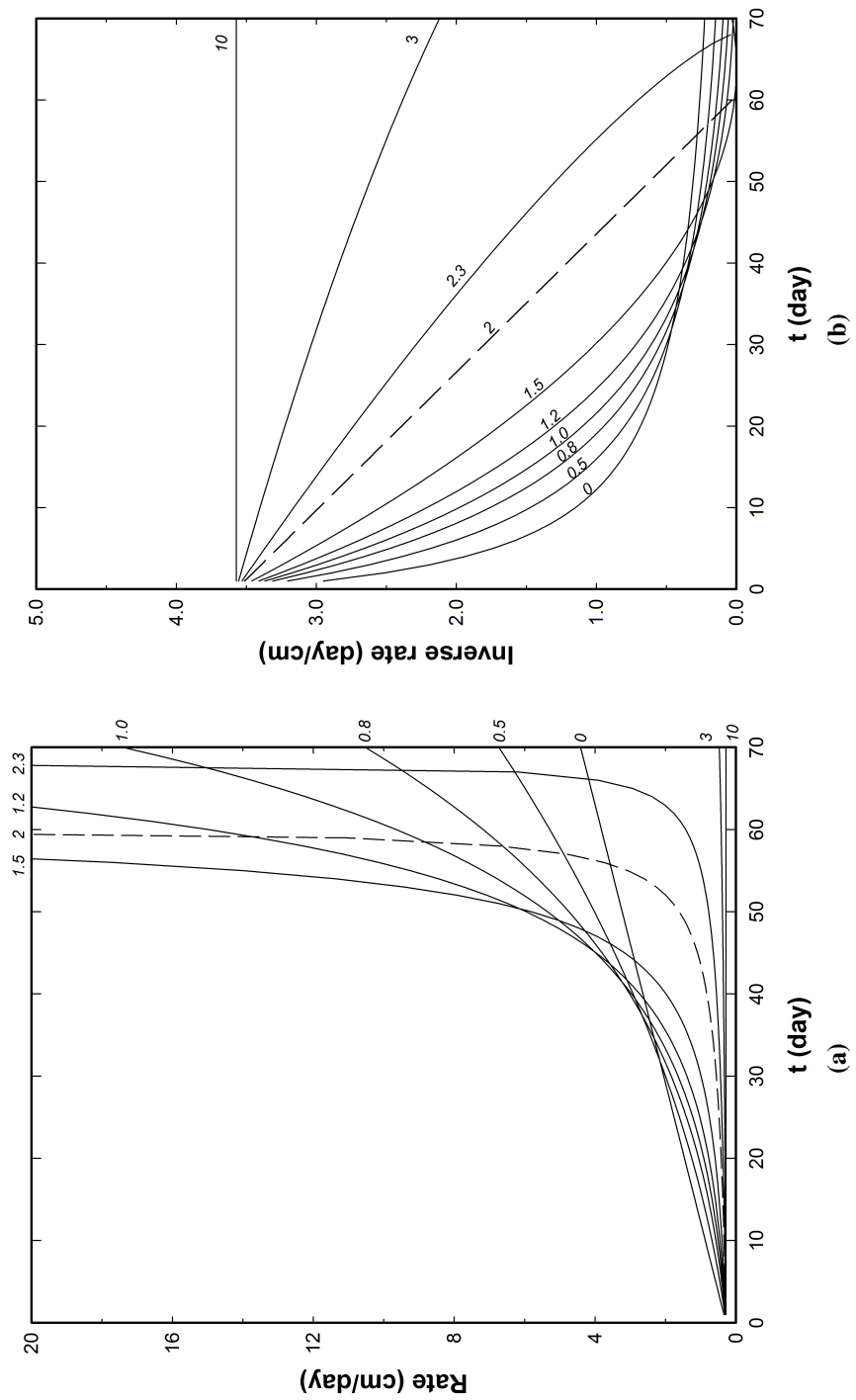


Figure 4.54 Variation of α values affecting the line length change at the dome of volcano. a. Velocity b. Reciprocal of a. α values ranging from 0 to 10 are presented in the plot. α of 2 is delineated by a dashed line. Initial conditions of $A=0.059$, $\Omega_0=0.28$ cm/day, and $t_0=0$ are applied. Source: Voight 1988b, Figure 2

One may also find the solution for forecasting the time of material rupture graphically, using the inverse rate of displacement against time. The reciprocal of the velocity can be obtained from Equation (4.14):

$$\begin{aligned}\dot{\Omega}^{-1} &= [A(\alpha - 1)(t_f - t) + \dot{\Omega}_f^{1-\alpha}]^{-1/(1-\alpha)} \\ \dot{\Omega}^{-1} &= A(\alpha - 1)^{-1/(1-\alpha)} \cdot (t_f - t)^{-1/(1-\alpha)} \\ \dot{\Omega}^{-1} &= A(\alpha - 1)^{1/(\alpha-1)} \cdot (t_f - t)^{1/(\alpha-1)}\end{aligned}\tag{4.19}$$

Therefore, by equating $\dot{\Omega}^{-1} = dt/dx$, $A = a$, and $t_f = t_r$, Equation (4.19) is identical to the reciprocal of Equation (4.9) of Fukuzono (1985; 1990).

Even though the fundamental theory of the material-deformation relation, continued deformation under sustained load (Varnes 1982), can be used for many engineering studies, early applications seemed to be very limited and results were often doubted given inaccurate data due to poor instrumentation. It is relevant that the advance of modern technology of instrumentation would promote understanding of material-deformation relations (Cruden and Masoumzadeh 1987). Voight (1988a) stressed the importance of accurate data, regularly obtained, and the responsibility of interpreters for better understanding of the material-failure relation. One of major fields adopting this relation is volcanology. Voight (1988b) discussed its possibility of estimating the eruption time by measuring length changes on a crater floor, tilting, and fault activations at Mount St. Helens. He also noted other characteristics of volcanic eruptions such as seismic energy release can be explained by this material failure relationship. In further studies some possibilities were discussed about the conjunction with the real time seismic amplitude monitoring system for volcano eruption prediction (Voight and Cornelius 1991). Computer based graphical presentations of the surface deformation, tilt, and seismicity for forecasting the volcanic eruption were also carried out by Cornelius and Voight (1995).

The material-deformation relationship that had been started from the creep-induced rupture in soils has achieved results in landslide researches. Zovodni and Broadbent (1980) discussed continuous surface displacements which estimate the movement behaviour of rock slides in open-pit mine. They noted the importance of gradual evolution of few tension cracks that would control a major slope instability.

Some comparisons on existing accelerating creep laws imposing slope movements in open-pit coal mine were carried out by Cruden and Masoumzadeh (1987). They evaluated four different creep laws, Saito laws (1969; 1970; 1980), exponential and power laws (Varnes 1982), and modified exponential law (Zavodni and Broadbent 1980), and discussed their applicabilities based on separate accelerating creep stages. The generalized material-deformation relation proposed by Voight (1988b) was also evaluated and its practical applicability was compared with various existing relations for material failures (Voight 1989; Cornelius and Scott 1993).

Recent practical approaches to landslides by using the material-deformation relationship as previously described above can be found in De la Cruz-Reyna and Reyes-Dávila (2001), Crosta and Agliardi (2002), Kilburn and Petley (2003), Petley (2004), Crosta et al. (2004), and Petley et al. (2002; 2005). Studies by Kilburn and Petley (2003), Petley (2004) and Petley et al. (2002; 2005) indicated typical material failure modes based on different movement behaviours. From a large number of landslide movement records, they postulated that a linear behaviour of the reciprocal of velocity (Λ) against time represented a brittle failure mechanism where landslides occur on a discrete rupture surface. Ductile movements within shear zones or bedding planes would form an asymptotic or non-linear tendency. In other words, rupture surfaces that are newly-generated by crack formation and propagation mainly show linear behaviours whereas non-linear trends are usually found on existing rupture surfaces or bedding planes (Figure 4.55). Different movement behaviours, therefore, become indicators of both current and future activity of landslides. Additionally this approach which is consistent with damage mechanics does explain some ambiguous questions in which the conventional stress-strain relation could not give clear answers (Petley et al. 2005). Petley (2004) also demonstrated the applicability of the subsurface movement information from slope inclinometers to estimate the landslide occurrence. He noted the understanding of subsurface movements is also beneficial for estimating the time of slope failure as ground surface movements do.

In order to identify movement characteristics in recent landslides in the study area, material-deformation relations in each landslide are analyzed. Landslide movements that were measured from slope inclinometers are refined to fit the purpose of the analysis. Procedures for relating the inverse movement rate to time follow Fukuzono (1985; 1990).

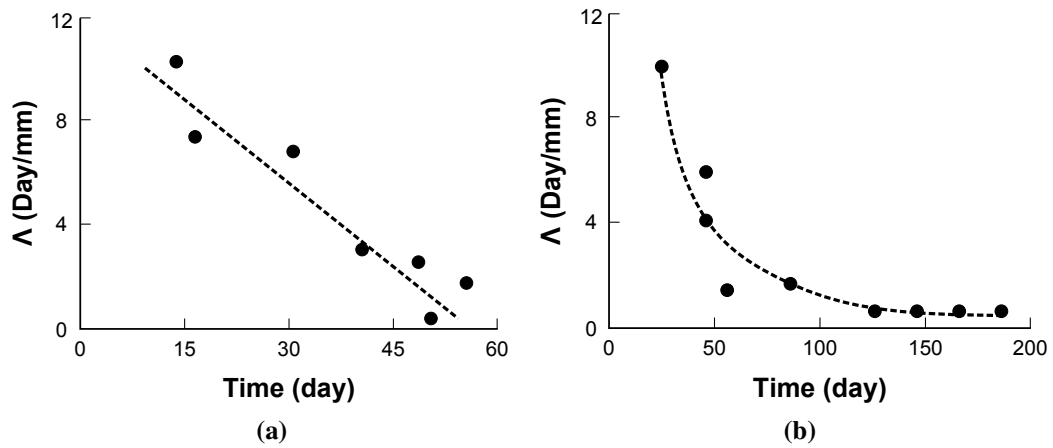


Figure 4.55 Typical material failure modes found in landslides. a. Linear trend. b. Non-linear or asymptotic trend. Failure modes are presented in reciprocal of displacement rate (Λ) and time space. *Source:* Petley et al. 2002

4.3.2.2 Analyzing movement behaviours

Figure 4.56 shows several movement records obtained from the Mile 47.8 Slide. Landslide movements were taken from slope inclinometers installed in the slide. Locations of each borehole holding slope inclinometers are indicated in the cross-section (Figure 4.3). Figure 4.56a shows movement behaviours obtained from boreholes 95-5 and 7. From the linear behaviour, it is postulated that the landslide movement within this part of the slope occurred on a newly-generated rupture surface. Specifically, movements had started from several fractures and when these fractures exceeded a threshold indicated in Figure 4.56a, fractures combined to form a general rupture surface which then propagated. Linear behaviours beyond the threshold could be explained by the crack propagation along the rupture surface.

On the other hand, the movement pattern at borehole 95-2 (Figure 4.56b) showed an asymptotic trend. Unlike the behaviour on existing rupture surfaces or bedding planes identified in Figure 4.56a, this non-linear trend seemed to be affected by landslide movements in front of borehole 95-2. After a significant movement, the adjacent slope had undergone either a decrease in driving force (perhaps by drainage) or an increase in resisting force (perhaps by friction with velocity) which resulted in this non-linear behaviour. The behaviour found in borehole 95-2 is related to the regressive stage of Zovodni and Broadbent (1980) stating slopes are re-stabilized if any modification is imposed on them.

Movement patterns at the End of 101 Street Slide shown in Figure 4.57 indicate two distinct slides, shallow and deep retrogressive ones. The shallow slide bounded by borehole 92-1 showed that the movement pattern at the elevation of the maximum displacement, which is referred to the 'movement controlled elevation,' is a linear and progressed toward the instability (Figure 4.57a) during the monitoring period. Unfortunately the borehole was sheared off therefore further movement patterns were not detected. Movement patterns measured at the lower retrogressive slide showed a fluctuation indicating the internal deformation influenced by seasonal changes of the groundwater level (Figure 4.57b).

In the middle of the 99/101 Streets Slides, movement patterns are relatively complex. Figure 4.58a shows movement behaviours at the upper shallow slide encroaching the upper portions of boreholes 93-10, 93-11, and 93-12. Boreholes 93-11 and 93-12 show a consistent manner of the internal deformation. However,

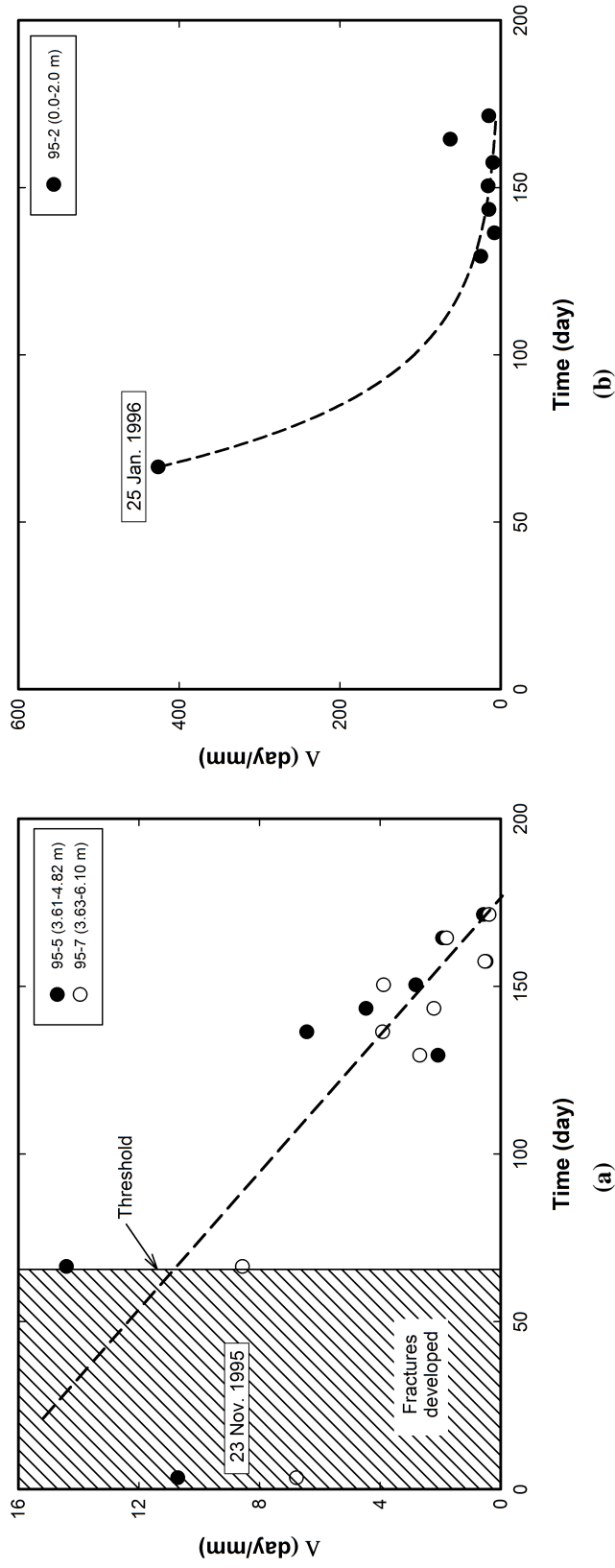


Figure 4.56 Landslide movement patterns at the Mile 47.8 Slide. a. Movement behaviours obtained from boreholes 95-5 and 7. Area including micro-cracks and fractures is delineated by hatches. b. Movement behaviour at borehole 95-2. Linear and asymptotic trends of movement pattern are shown by thick dashed regression lines. Initiation dates of the monitoring are also presented. Location of the boreholes in the slide is shown in Figure 4.3

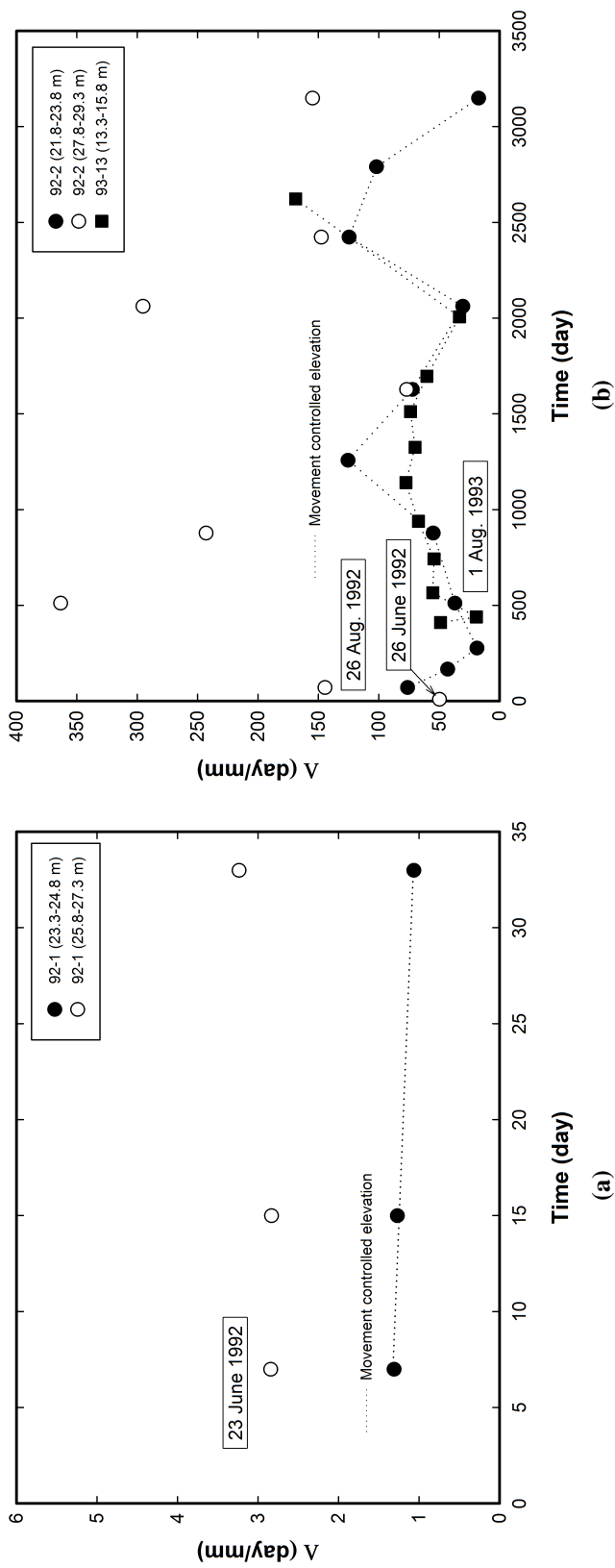


Figure 4.57 Landslide movement patterns at the End of 101 Street Slide. a. Movement patterns obtained from the borehole 92-1. Linear trend of movement pattern is shown by the thick dashed regression line. b. Movement behaviour at boreholes 92-2 and 92-13. The movement controlled elevations which referred to the elevation that has the maximum displacement are also presented by using dot lines. Initiation dates of the monitoring are also presented. Location of the boreholes in the slide is shown in Figure 4.17

one unique pattern is detected during the monitoring period of 2,400 to 3,010 days (Feb. 6, 2000 to Oct. 10, 2001). A sharp drop of movement patterns at those boreholes indicates the instability of slopes. Such behaviour might be connected to high rainfall during the rainy seasons. The toe of the shallow slide experiences a slight instability at 37 days after the start of monitoring but immediately recovers its stability (Figure 4.58b). Other movement patterns at the upper part of borehole 93-12 (0.8 and 1.8 m), representing ground surface movements, shows the comparable behaviour to the lowest elevation of the borehole (Figure 4.58c).

The last example of the 99/101 Streets Slides is shown in Figure 4.59, which presents movement behaviours obtained from the End of 99 Street Slide, located in the northern boundary of the 99/101 Streets Slides. Movement obtained from the top of borehole 85-1 (Figure 4.59a) shows a linearity possibly caused by the rupture surface propagation. It can also forecast the approximate time to rupture by extending the linear trend to meet the abscissa of the plot (Fukuzono 1985, 1990). Because the uncertainty and lack of data for the estimation are apparent, the estimate of the time to rupture seems to be inconsistent with the time of the actual rupture.

Figure 4.59b shows the movement behaviour of the top of borehole 85-2 showing a non-linear trend similar to movements presented in Figure 4.56b which describes the regressive stage (Zavodni and Broadbent 1980). The movement pattern obtained at the lowest point in borehole 85-2 (Figure 4.59c), however, represents the movement on existing rupture surfaces or bedding planes. It can be reasonably postulated that the elevation of this movement is consistent with the Shaftesbury Formation, which has undergone the glacial disturbance and become sheared in the past. Movements occurred at intermediate elevations in the borehole 85-2 (Figure 4.59d) produced an internal deformation due to seasonal fluctuations.

Movement patterns at the Shop Slide are presented in Figure 4.60. Borehole TH05-1 locating the toe of the upper slide seems to have experienced slope instability in 421 days after the monitoring started (Figure 4.60a). Figure 4.60a also shows that the movement rate of the slide, however, has decreased and the slope has gained its resisting forces again. A drastic decrease of the movement pattern is identified at the lowest elevation of borehole TH05-1. But it does not affect the entire stability of the upper slide due to the magnitude of its displacement and the relatively deep location with respect to the rupture surface.

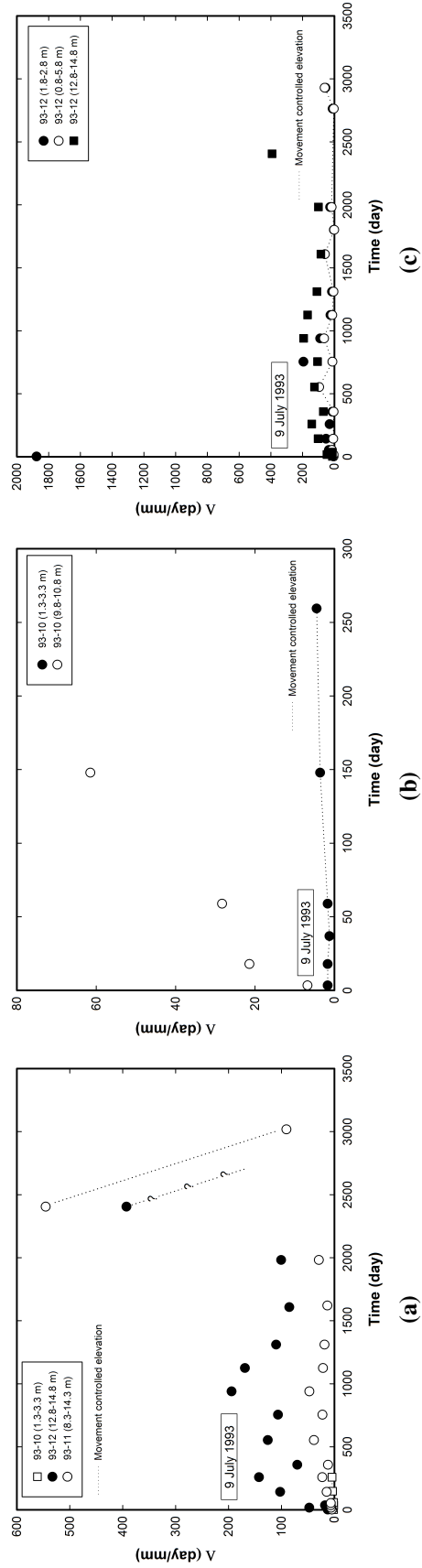


Figure 4.58 Landslide movement patterns at the Transition Zone Slide. a. Movement patterns of the upper shallow slide. Sharp drops of linear trend are shown by the thick dashed regression lines. Question symbols are added to the approximate linear trend. b. Movement behaviour at borehole 93-10. c. Movement patterns representing the behaviour near the ground surface. The movement controlled elevation which referred to the elevation whose has the maximum displacement is also presented. Initiation dates of the monitoring are also presented. Location of the boreholes in the slide is shown in Figure 4.18

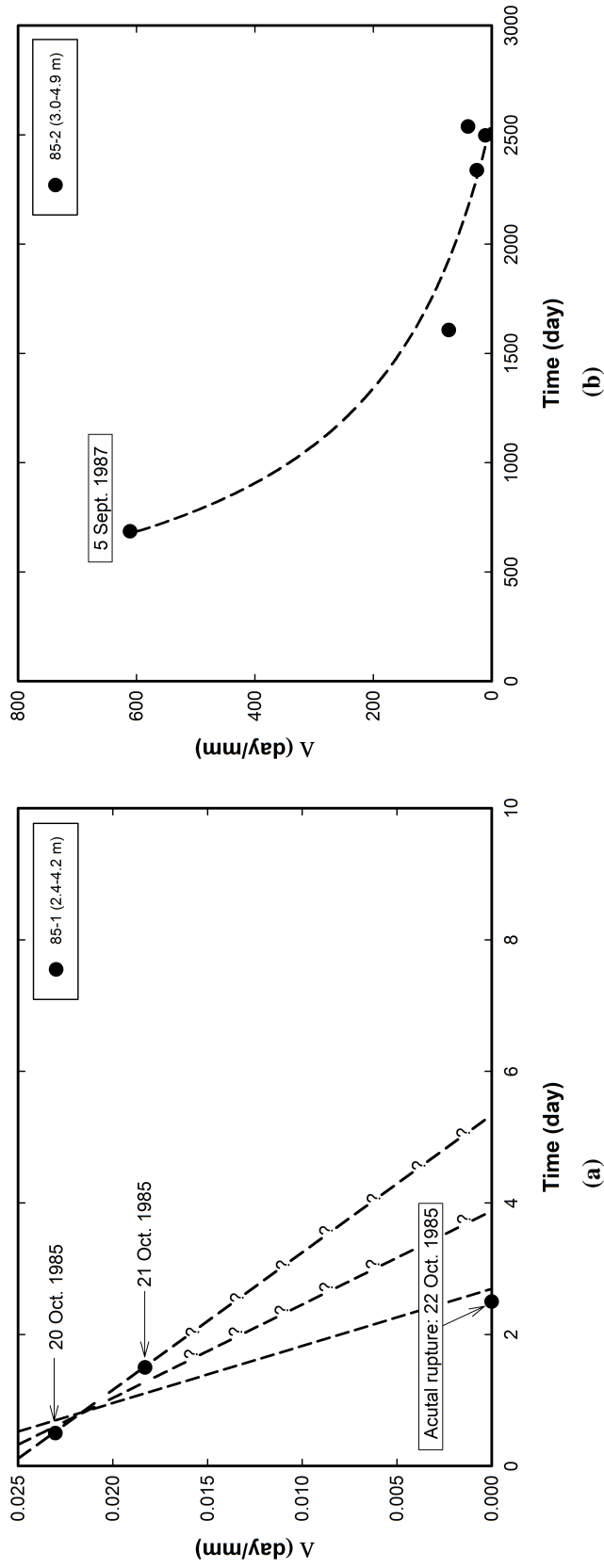


Figure 4.59 Landslide movement patterns obtained at the End of 99 Street Slide. a. Movement behaviours obtained from the borehole 85-1. b. Movement behaviour obtained from the top of borehole 85-2. c. Movement behaviour obtained from the bottom of borehole 85-2. d. Movement behaviours in the middle of borehole 85-2. Linear and asymptotic trends of movement pattern are shown by thick dashed regression lines. Initiation dates of monitoring are also presented. Location of slide is indicated in Figure 4.19

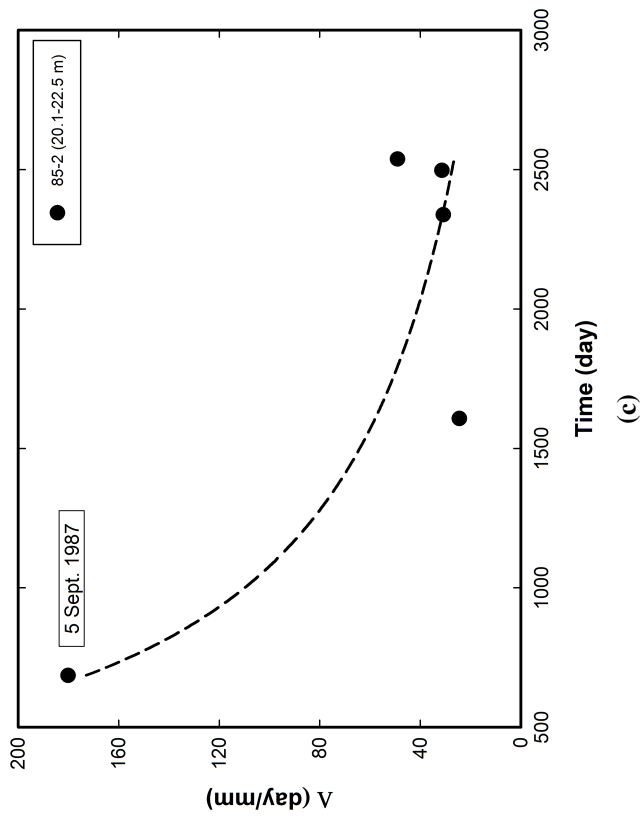
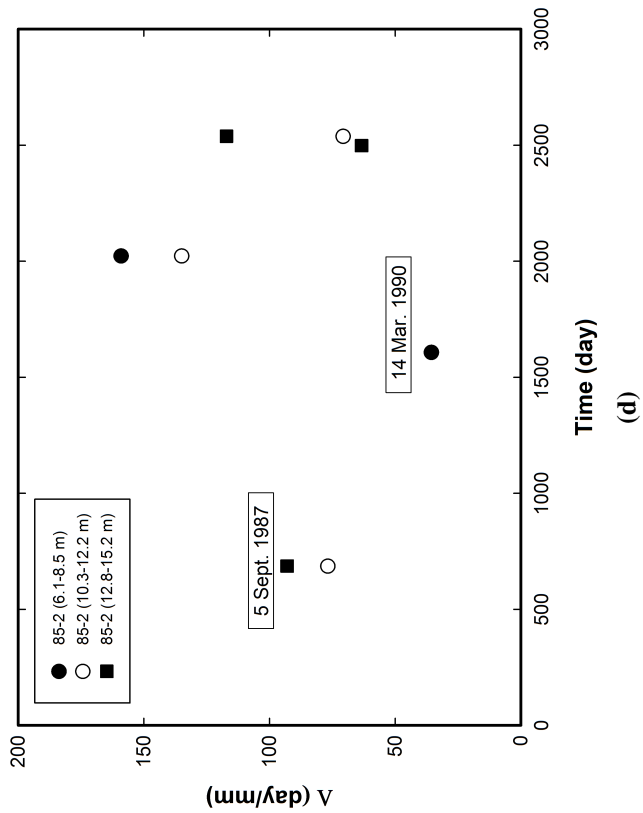


Figure 4.59 (Cont'd)

Figure 4.60b shows a movement pattern at the bottom of borehole TH05-3. It is postulated that this non-linear trend is a ductile movement within a shear zone or bedding and looks similar to the behaviour in Figure 4.59c and somewhat different to those shown in Figures 4.56b and 4.59b even though they all have similar patterns. An asymptotic behaviour identified in borehole TH05-3 does not have any significant geometry change adjacent to the borehole which causes a stress redistribution in the slope. Movement patterns at the toe of the lower slide in which borehole TH05-4 is installed show an internal deformation of the movement pattern due to seasonal changes of the groundwater fluctuation (Figure 4.60c).

4.3.3 Discussion and future consideration

Empirical approaches based on monitoring surface or subsurface movements explicitly and directly estimate time intervals to peak landslide velocities if provided with sufficient, reliable movement observations. However, these do not consider the kinematics of the rupture or properties of materials which are being deformed. The uncertainties in determining movement patterns, whether linear or non-linear, make the estimation of the time to peak velocity difficult. As Heim (1932) showed, the internal deformation due to seasonal fluctuations can be often misunderstood as an accelerating movement leading to a forecast of a catastrophic landslide. One well-known pitfall of this method is that few reports of the successful prediction of time of rupture of a landslide exist (Hungr et al. 2005). Therefore, it seems to take more studies of mechanisms, rupture surface developments and deformations within slopes to achieve reliable results predicting the ruptures of landslides.

Practically, however, these can provide insights into formation and propagation of rupture surfaces. Figure 4.61 shows an internal deformation measured at the Shop Slide. Movements from boreholes TH05-3 and 4 have initiated in different patterns, but present consistent behaviours about 600 days later which mean that they are in the same displacing mass and move along the general rupture surface formed within the slope. Another application is as a warning threshold. Because of the lack of precise estimates of the time of rupture, this can be used only as a warning alert (Salt 1988). Together with the consideration of external conditions (such as precipitation or earthquake) and zonation of potential areas by the landslide hazard assessment it would be a powerful tool for managing landslides in the future.

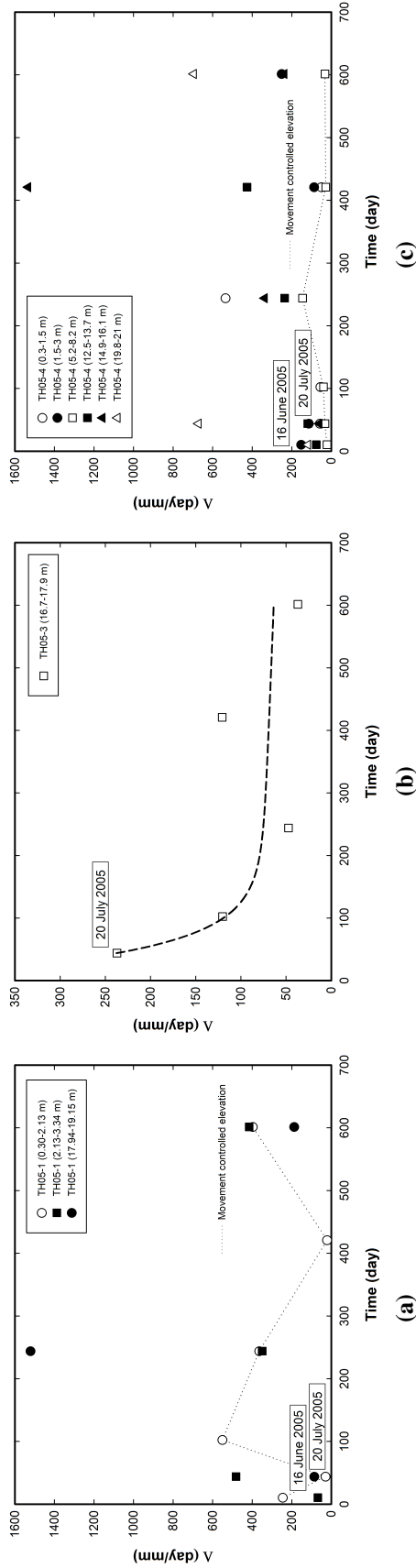


Figure 4.60 Landslide movement patterns at the Shop Slide. a. Movement patterns at the toe of the upper slide. b. Movement behaviour at the lowest points of borehole TH05-3. An asymptotic trend of the movement pattern is shown by a thick dashed regression line. c. Movement patterns representing the toe of the lower slide. The movement controlled elevation which referred to the elevation whose has the maximum displacement is also presented. Initiation dates of the monitoring are also presented. Location of the boreholes in the slide is shown in Figure 4.29

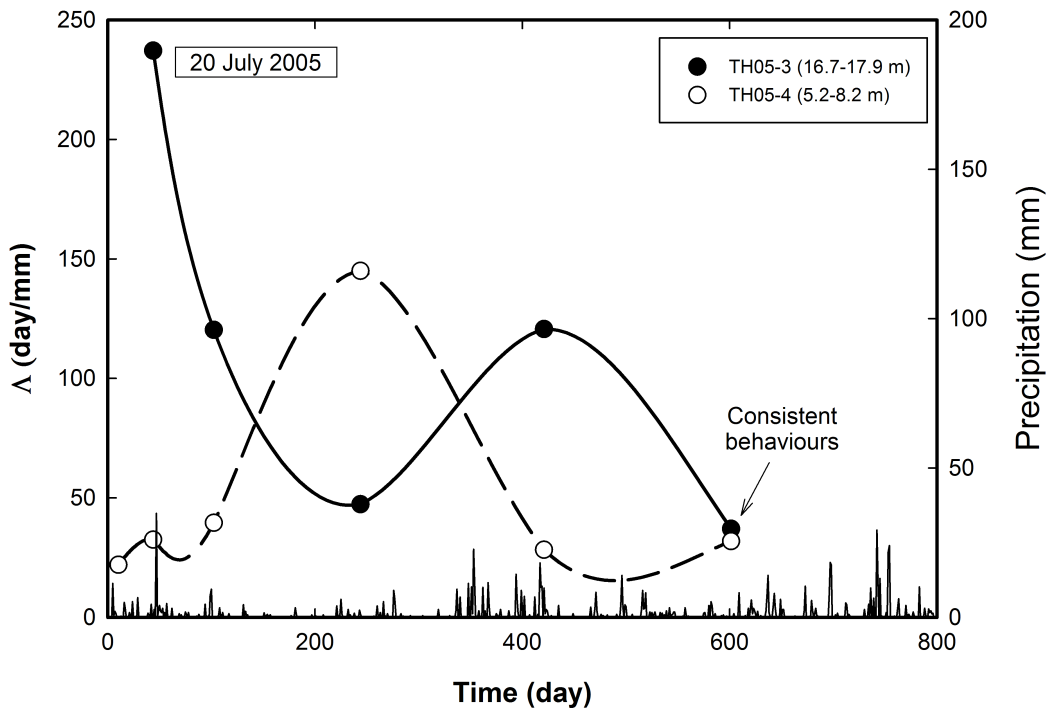


Figure 4.61 Formation and propagation of the rupture surface. Landslide movement patterns obtained at the Shop Slide. Precipitation data recorded during the monitoring period are also presented. Location of slide is indicated in Figure 4.29

4.4 Conclusions

In Chapter 4, I covered characteristics observed at recent landslides from a geotechnical point of view. Features that I found include the identification of potential rupture surfaces, groundwater distribution, movement behaviours, and possible landslide mechanisms. All of these can be used to find general characteristics inherent in landslide mechanisms found in the study area.

A total of six landslides on slopes in the Town of Peace River were examined from various sources in order to generate a landslide inventory. Most landslides were identified as translational block slides and some landslides showed a complex form in which landslides were the combination of or initiated by other forms of sliding. A relationship between human activities, developments of residences or infrastructures such as roads and railways, and landslide occurrence was observed. This indicates that developments on slopes would be a main cause of landslides. I have also discovered that increasing pore water pressures due to precipitation or ice melting would exert destabilizing forces on landslides in unstable slopes.

Efforts to determine strength properties on rupture surfaces materials were also carried out. I performed laboratory tests on representative soil samples located at elevations of general rupture surfaces in order to understand their contributions to the stability of slopes. From index and direct shear tests, I found that colluviated glacial sediments have a wide range on the plasticity chart with similar shear strength parameters to both fully softened and residual values. Although sampling elevations are different, geotechnical characteristics observed in colluviated sediments show a consistent behaviour. Shear strength parameters obtained from glacial sediments illustrate some discrepancies that are based on the degree of the disturbance in samples at sampling elevations. Finally, advance phase glaciolacustrine sediments show high plasticity, and high peak and low residual values which are typical behaviours of clay. I also found that the elevation of the sample located in the transition zone between glacial and advance phase glaciolacustrine sediments, which was tremendously affected by the glacier movement, would support the decrease of the peak strength toward the fully softened value. All of these findings are consistent with those from previous studies (Sharma 1970; Ruel 1988).

Other findings that I observed in Chapter 4 are the identification of characteristics in landslide movements. By observing displacements of landslides they are corre-

lated to a typical relationship between landslides and their causal factors. Obtained information of movements from recent landslides was processed in various ways to represent characteristics of the landslide. For example, it would help to understand the existence of a general rupture surface which controls the landslides in the study area. The elevations of general rupture surfaces in the study area are determined around 365 and 386 metres in the west bank, 330, 338, and 370 metres in the east bank, respectively and they are placed in both glacial and colluvial sediments. This information can be used in landslide hazards assessments as a landslide preparatory causal factor.

Rates of landslide movements may indicate the state of current landslides and give insights into their classification types. I found that most movement rates are in the very slow and extremely slow classes. Under these conditions, structures may be undamaged or have manageable damages such as cracks. Geomorphological features can also affect these landslide displacements. Results of the analysis of a relationship between geomorphological features and movement rates showed there is a positive correlation between slope angles, either on the ground or at the rupture surface, and movement rates.

Different modes of landslide kinematics were also shown by movement patterns. I observed movement patterns from recent landslides and showed distinct movement behaviours which would indicate the evolution of landslide activities. Observed movement characteristics may be used to estimate the future behaviour of unstable slopes and develop a landslide hazard map for the study area. Results of movement patterns can provide insights into formation and propagation of rupture surfaces even though they do not clearly explain the kinematics of the rupture or properties of materials which are being deformed.

Chapter 5

Landslide hazard assessment in the Town of Peace River, Alberta

This chapter illustrates practical procedures to assess landslide hazards in the study area. Firstly, major considerations of landslide induced factors are provided to understand relationships between those factors and landslides. By reviewing the early landslide hazard assessment performed in the study area, appropriate approaches and methodologies for this research are discussed. The landslide hazard assessment in the Town of Peace River is achieved using geomorphological mapping method with detailed explanations. Finally, results and corresponding discussions related to the practical applications for the landslide hazard assessment follow.

5.1 Major considerations in the landslide hazard assessment

Landslides are geomorphological processes having complex connections to the terrain, surface and subsurface materials, and climate conditions where they occur, therefore, landslides can be affected by the numerous elements which make landslide environments stable or unstable (Crozier and Glade 2005). These elements sometimes influence the stability individually but usually combine with each other to give a complexity for understanding to their movement mechanism. In this section major landslide causal factors are reviewed and some representative factors applied to the study area are discussed to delineate the potential landslide hazard areas. These would provide a basis for understanding the relationship between landslides and their environments and for the landslide hazard assessment system which will be described in Sections 5.3 and 5.4.

5.1.1 Review of landslide induced factors

There are a variety of studies on landslide causing elements and their relationship to the landslide occurrence. Pašek (1974) early showed on natural conditions causing slope movements and the importance of understanding those conditions for the application of effective measures. Pestrong (1976) noted natural factors which would promote landslides in San Francisco Bay region (Table 5.1) and these can combine within limited areas to initiate landslides. Jahns (1978) divided natural conditions into indigenous and superimposed factors, respectively, which generally weaken resisting forces of materials in the slope and introduce an unfavourable status. Varnes and IAEG Commission on Landslides and other Mass Movement on Slopes (1984) identified a similar classification for inherent or basic conditions affecting slope stability. Representative factors affecting landslides can be shown in Table 5.2. As described in Chapter 2, a recent work by Popescu (1994), supported by the International Geotechnical Societies' UNESCO Working Party on World Landslide Inventory provided more detailed landslide causal factors which were divided into preparatory causal factors and triggering causal factors (Table 5.3).

Indigenous (inherent or internal) factors connect physical and chemical properties of slope forming materials and can remain constant over time (Jahns 1978). They are briefly described as follows.

5.1.1.1 Geology

Geological information, which can be used in a variety of ways in landslide hazard assessments, is one of the important factors related to slope stability. This information simply shows the distribution of geological units like conventional geological maps or can be grouped by lithology and structure, then their susceptibility evaluated against landslides. The lithology, such as composition, fabric, and texture of rocks and soils, is the major influencing factor in determining material properties of slope forming materials. Physical and chemical processes alter the original structure of materials, which in turn provide an initial momentum to the slope movement. The structure, like stratigraphic sequences, faults, and folds in geological units, is often heterogeneous with discontinuous characteristics in materials which represent potential weaknesses within rocks and soils and can lead to a susceptibility

Table 5.1 Natural factors causing landslides in San Francisco Bay region. *Source:* Data adapted from Pestrong (1976)

Factor	Unfavorable condition to landslides
Rock type	Rupture surfaces in Serpentine
Slopes	Steep, irregular faces
Accumulation of soils	Expansive soils containing high percentage of clay
Heavy rainfall	During winter periods
Long, dry summer	Leads to forest fires
Slopes undercut	By streams and sea waves
Ground shaking	By earthquakes

Table 5.2 Factors affecting slope movements. *Sources:* Data adapted from Jahns (1978) and Varnes and IAEG Commission on Landslides and other Mass Movement on Slopes (1984)

Category	Factor affecting slope movement	
Indigenous	Geology	Lithology
		Structure
	Geomorphology (topography)	
	Hydrology (moisture content)	
	Meteorology (climate condition)	
Superimposed	Vegetation	
	Material deterioration	
	Change of subsurface groundwater regime	
	Overloading	
	Removal of support	
	Vibration of ground	
Others (volcanic eruption)		

Table 5.3 Landslide causal factors. *Source:* Data from Popescu (1994), Table 1

Origin	Landslide causal factors	Type
Ground condition	Problematic materials [†] Adversely oriented mass discontinuities (bedding) Adversely oriented structural discontinuities (faults) Contrast in permeability and its effects on groundwater Contrast in stiffness [‡]	Preparatory causal factors
Geomorphological processes	Tectonic uplift Glacial rebound Fluvial erosion of slope toe Wave erosion of slope toe Glacial erosion of slope toe Erosion of lateral margins Subterranean erosion (solution, piping) Deposition loading of slope or its crest Vegetation removal (by erosion, forest fire, drought)	
Physical processes	Intense, short-period rainfall Rapid melt of deep snow Prolonged high precipitation Rapid drawdown following floods, high tides or breaching of natural dams Thawing of permafrost Freeze and thaw weathering Shrink and swell weathering of expansive soil	Preparatory or Triggering causal factors
Man-made processes	Excavation of slope or its toe Loading of slope or its crest Drawdown (of reservoirs) Defective maintenance of drainage systems Water leakage from services (water supplies, sewers) Vegetation removal (deforestation) Mining and quarrying ^{††} Creation of dumps of very loose waste Artificial vibration (including traffic, pile driving)	

[†] Weak, sensitive, weathered, sheared, and jointed or fissured.

[‡] Stiff, dense material over plastic material.

^{††} Open pits or underground galleries.

for landslides. Krohn and Slosson (1976) noted certain rock types which are more susceptible to landslides than other rock types in the United States. These are as follows:

1. Younger (Mesozoic and Cenozoic) igneous and metamorphic rocks: Intense fractured and weathered (western United States).
2. Mesozoic and Cenozoic sedimentary rocks: Containing large portions of clay.
3. Cenozoic volcanic rocks: Highly fractured and weathered. Containing montmorillonite zones (western United States).
4. Serpentinite (magnesium-rich silicate minerals) rocks.

5.1.1.2 Geomorphology

Configurations of the ground surface is the key for landslide hazard research. Early studies emphasized relationships between geomorphological features and their contributions to landslides (Kienholz et al. 1983, 1984; Zimmerman et al. 1986). Characteristics of the topography such as previous landslide deposits, slope, and aspect are significant constituents in determining the degree of landslide activity.

5.1.1.3 Hydrology and meteorology

Understanding current status and distribution of the drainage system is important because it significantly influences the slope stability by breaking the equilibrium of forces within the slope by changing the weight of materials and pore water pressure, removing cohesive components, and lubricating weak zones within slope materials (Krohn and Slosson 1976). Climate conditions, temperature and precipitation, contribute to the recognition of hydrological perspectives to landslides.

5.1.1.4 Vegetation

There are two different opinions regarding the effect of vegetation on slope stability. Vegetation promotes the stability of the slope by protecting the ground surface

from climate agents. On the other hand, vegetation acts as a weight on the ground and the mechanical action of wind on tree trunks widens ground cracks and leads to high infiltration which may increase susceptibility to landslides. Prandini et al. (1977) discussed different aspects of the consequence of vegetation in terms of the slope stability and stressed beneficial impacts of vegetation even though questionable issues still existed.

Superimposed (external or active) factors accompany significant changes which affect the stability of slopes by increasing shear stresses or decreasing shear strengths. Superimposed factors shown in Table 5.2 can be activated by the change of external conditions due to humans and natural input. Duncan and Wright (2005) noted explanations for causes of slope instability in terms of limit equilibrium analysis.

5.1.2 Considerations of landslide induced factors in the Town of Peace River

Factors which are believed to cause landslides are examined for their influences on the study area. As pointed out in Section 5.1.1, these would be grouped into geology, geomorphology, hydrology and meteorology, and vegetation. It is, however, difficult to arrive at any valid conclusion for the landslide hazard by judging only those factors, known as major factors, without comparing them with other minor ones. A landslide has a complex nature requiring numerous interactions of various factors. Even trivial factors may lead to a catastrophe if they exert small amounts of force to exceed thresholds of quasi-stable slopes.

5.1.2.1 Geology

As described in Chapter 3, major geological characteristics in the study area can be divided into bedrock formations and surficial deposits. Recent landslides described in Figure 4.43 indicate that estimated rupture surfaces of six recent landslides mainly occur in colluvial sediments followed by till deposits, bedrock formations, and fill materials. Therefore, areas containing those geologic units would have a higher potential of future landslides. The spatial distributions of surficial deposits and bedrock formations are presented in Figures 5.1 and 5.2.

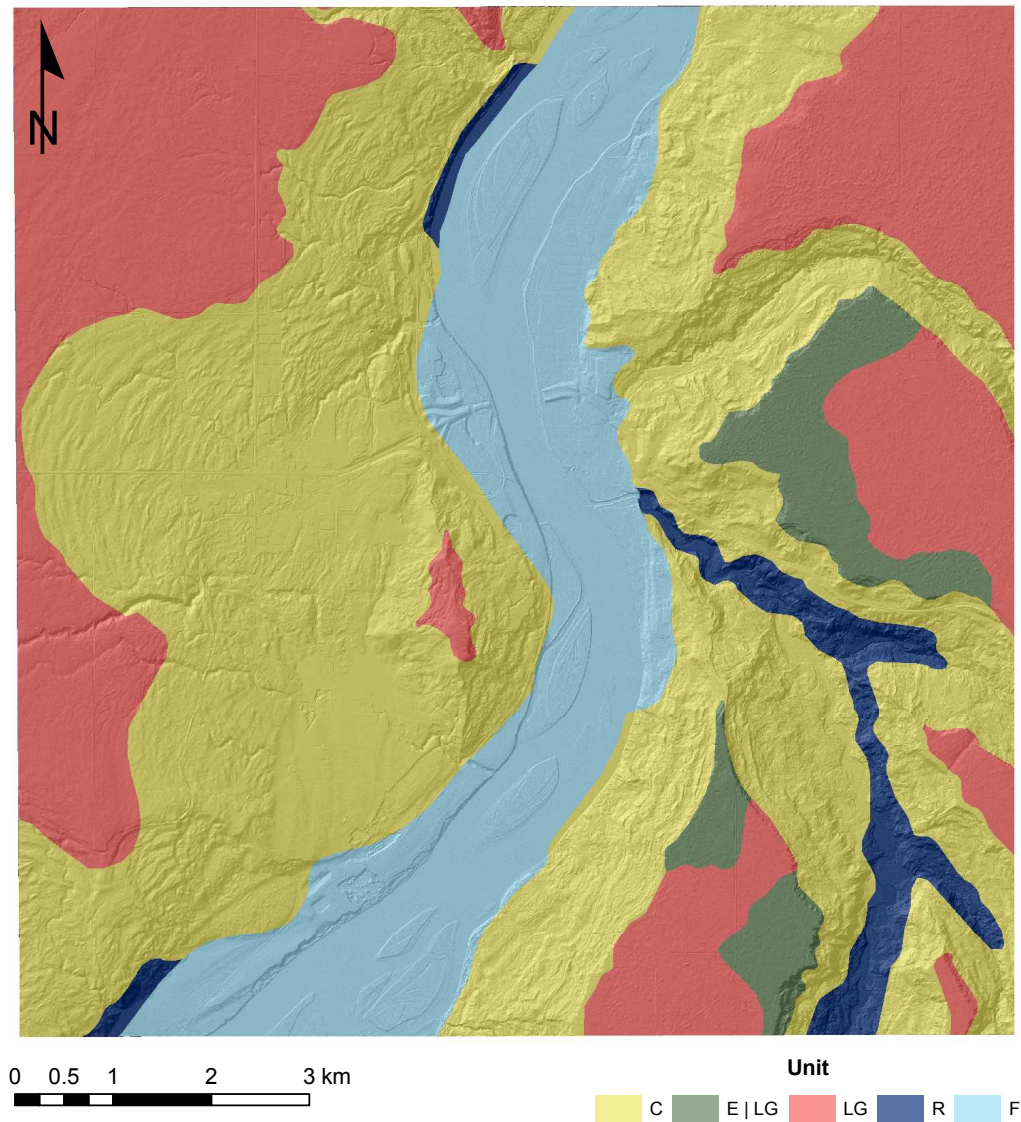


Figure 5.1 Spatial distributions of surficial deposits in the study area. Surficial unit symbols illustrated are as follows: C: colluvial deposits; E|LG: eolian veneer overlying glaciolacustrine deposits; LG: deep water glaciolacustrine deposits; R: bedrock; and F: fluvial deposits. A shaded relief image shown in background is generated from the LiDAR dataset. *Source:* Data adapted from Paulen (2004)

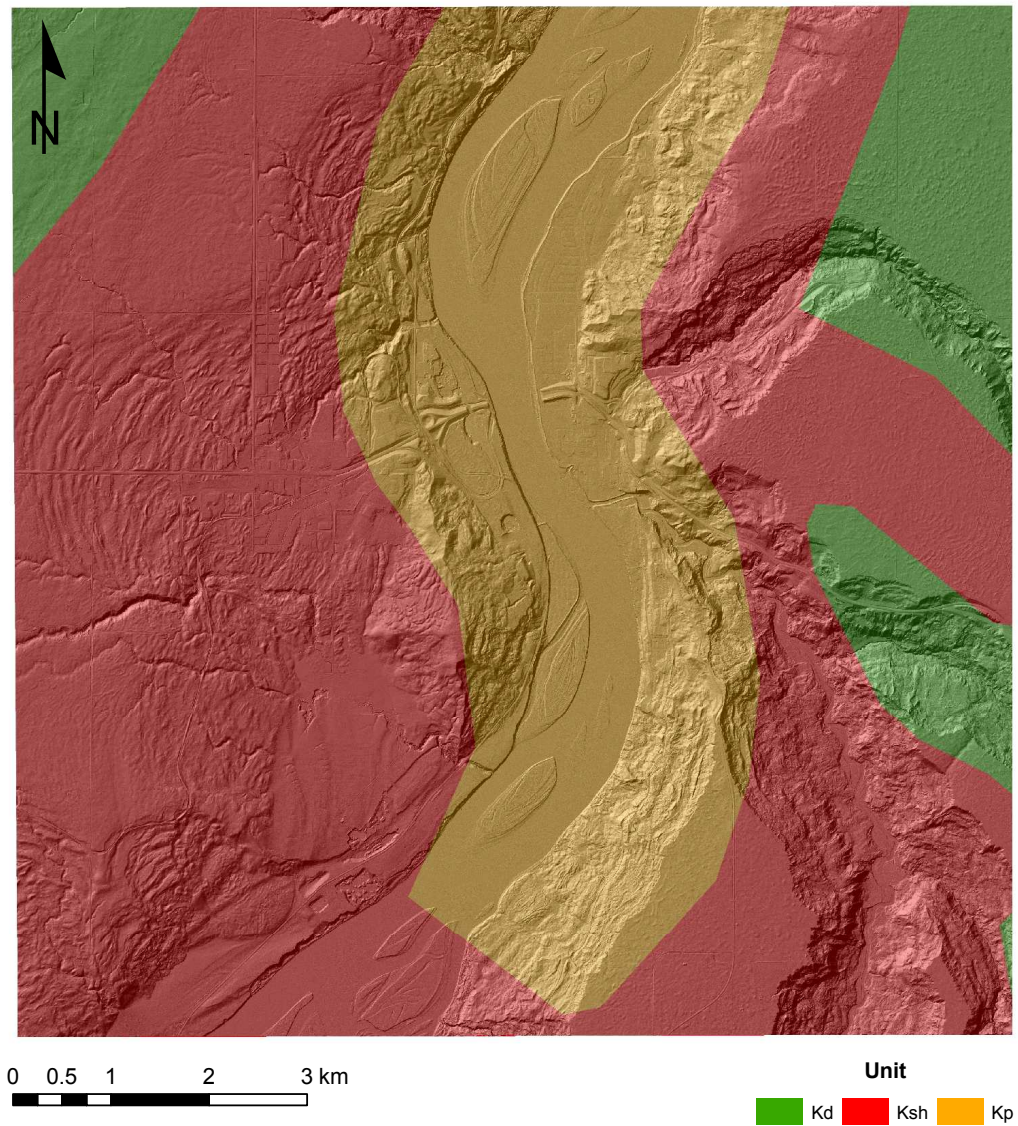


Figure 5.2 Spatial distributions of bedrock deposits in the study area. Formational units are differentiated by colors. Major units are as follows: Kd: Dunvegan Formation; Ksh: Shaftesbury Formation; and Kp: Peace River Formation. A shaded relief image shown in foreground is the LiDAR dataset. Formational bedrock units boundaries are obtained from Green (1972) and Hamilton et al. (1999). They are approximated

5.1.2.2 Slope and aspect

Geomorphological factors, such as slope and aspect, are frequently used elements for landslide hazard assessments because they involve the physical profile of the landslides. Figure 5.3 shows a diagram in which slope and aspect are defined. The slope or gradient can be defined as a derivative of a surface in which the maximum rate of changes in surface values (elevation) is calculated (Davis 2002). The spatial distribution of slopes in the study area can be obtained from the following equation in degrees (Ritter 1987; Zevenbergen and Thorne 1987; Hunter and Goodchild 1997; Burrough and McDonnell 1998; de By et al. 2001; Zhou and Liu 2004; Kasai et al. 2009):

$$S = \arctan \sqrt{f_x^2 + f_y^2} \quad (5.1)$$

where S is a slope value, f_x and f_y are rates of elevation changes in horizontal and vertical directions in east-westward and north-southward, respectively. Because of the proportional relationship between slope values and the possibility of landsliding, slope values are the critical factor in determining landslide hazards (Yalcin and Bulut 2007). In this study, slope values are calculated from a digital elevation model (DEM), which was originally generated from the LiDAR dataset acquired in 2007. The geographic representation is helped by ArcGIS (version 9.2), a commercial GIS software of the Environmental Systems Research Institute, Inc. DEM and spatial distribution of slope values in the study area are illustrated in Figures 5.4 and 5.5, respectively.

Based on the results shown in Figure 5.4, the elevation of the study area ranges from 310 to 579 metres. Lower elevations include river level and adjacent terraces whereas upland areas cover the higher elevations. River valleys have intermediate values showing drastic elevation changes. Figure 5.5 shows slope values which are grouped by designated classes represented in degrees. Slope values from zero to five degrees cover 47 percent of calculated slope values in the study area. Steep slopes are placed on the river valleys, some cuts and fills in residential areas, and transportation routes.

The aspect is a direction of the slope value and represented by the azimuth angle. It is closely related to the degree of exposure to external circumstances such as

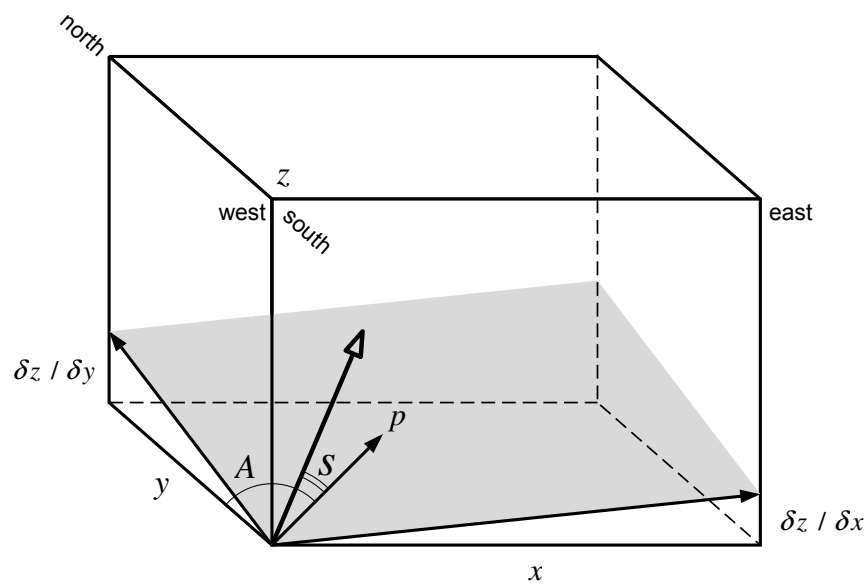


Figure 5.3 Schematic diagram showing how slope (S) and aspect (A) in terrains are defined. p is a horizontal path having the maximum elevation changes. A tangent space consisting of rates or gradients of elevation changes in x (east-westward) and y (north-southward) directions is also illustrated in a gray shade

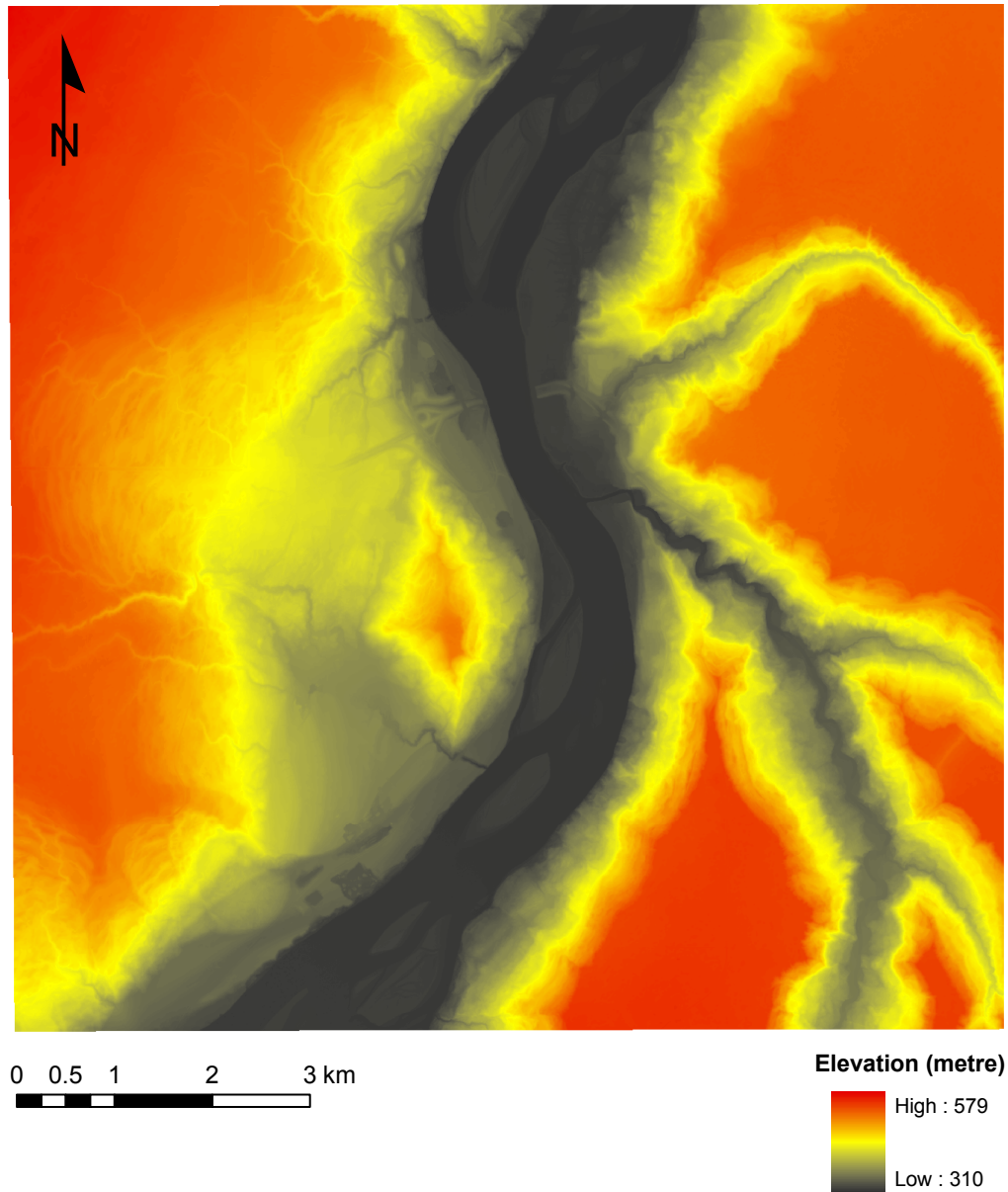


Figure 5.4 Digital elevation model (DEM) for the study area. The cell size is 0.5 by 0.5 metres. It is generated from the LiDAR dataset

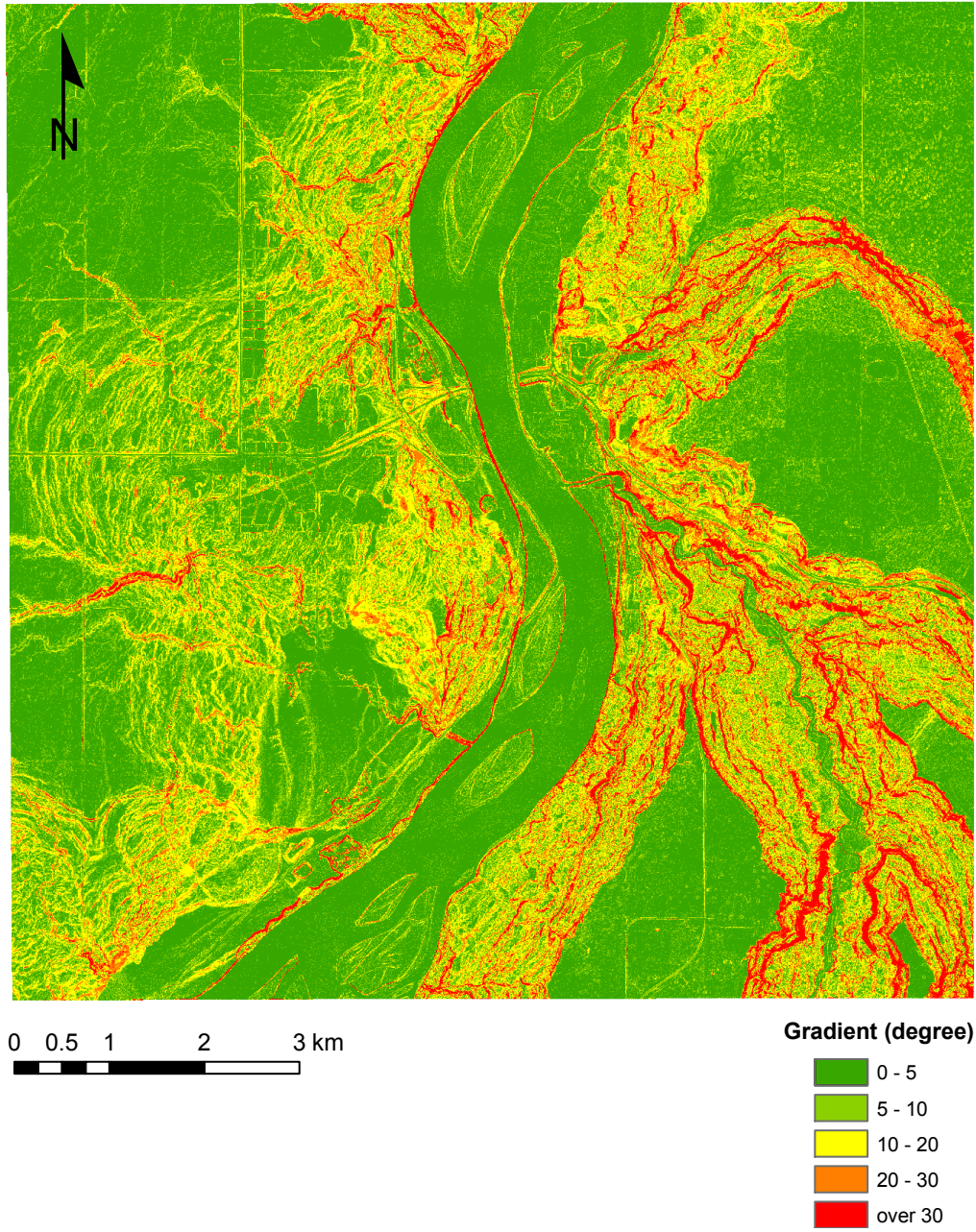


Figure 5.5 Spatial distribution of slope values. The cell size is 0.5 by 0.5 metres. It is generated from the digital elevation model (Figure 5.4)

rainfall, wind, and sunshine (Yalcin and Bulut 2007). Based on Figure 5.3 the aspect (A) can be defined by the following equation (Ritter 1987; Zevenbergen and Thorne 1987; Hunter and Goodchild 1997; Burrough and McDonnell 1998; de By et al. 2001):

$$\tan(A) = \frac{f_x}{f_y} = \frac{\delta z / \delta x}{\delta z / \delta y} \quad (5.2)$$

However, implementing Equation (5.2) for aspect calculation would lead to problems to derive a correct aspect value. Major problems are characteristics of the arctangent function and the division by zero as a denominator (Ritter 1987). Therefore, modifications were introduced to overcome these problems. Ritter (1987) proposed a modified aspect calculation of a cell surrounded by four adjacent cells as the following equation:

$$\text{for } (e_1 - e_3) > 0, \quad A = 90 - 57.296(\arctan(\frac{e_4 - e_2}{e_1 - e_3})) \quad (5.3)$$

$$\text{for } (e_1 - e_3) < 0, \quad A = 270 - 57.296(\arctan(\frac{e_4 - e_2}{e_1 - e_3})) \quad (5.4)$$

where e_n is the surface value (elevation) of each surrounding cell. A value of 57.296 is used as a factor of transformation between radian to degree values. A recent study by Zhou and Liu (2004) also showed a generalized form of the aspect calculation which avoided mathematic pitfalls inherent in Equation 5.2. It gives the following:

$$A = 270^\circ + \arctan(\frac{f_y}{f_x}) - 90^\circ(\frac{f_x}{|f_x|}) \quad (5.5)$$

In this study, the aspect of the study area is produced to identify the overall distribution. As with the slope analysis aspect values are obtained from the digital elevation model (DEM) and classified into four representative compass directions: northeast (0 to 90 °); southeast (90 to 180 °); southwest (180 to 270 °); and northwest (270 to 360 °). Results are shown in Figure 5.6.

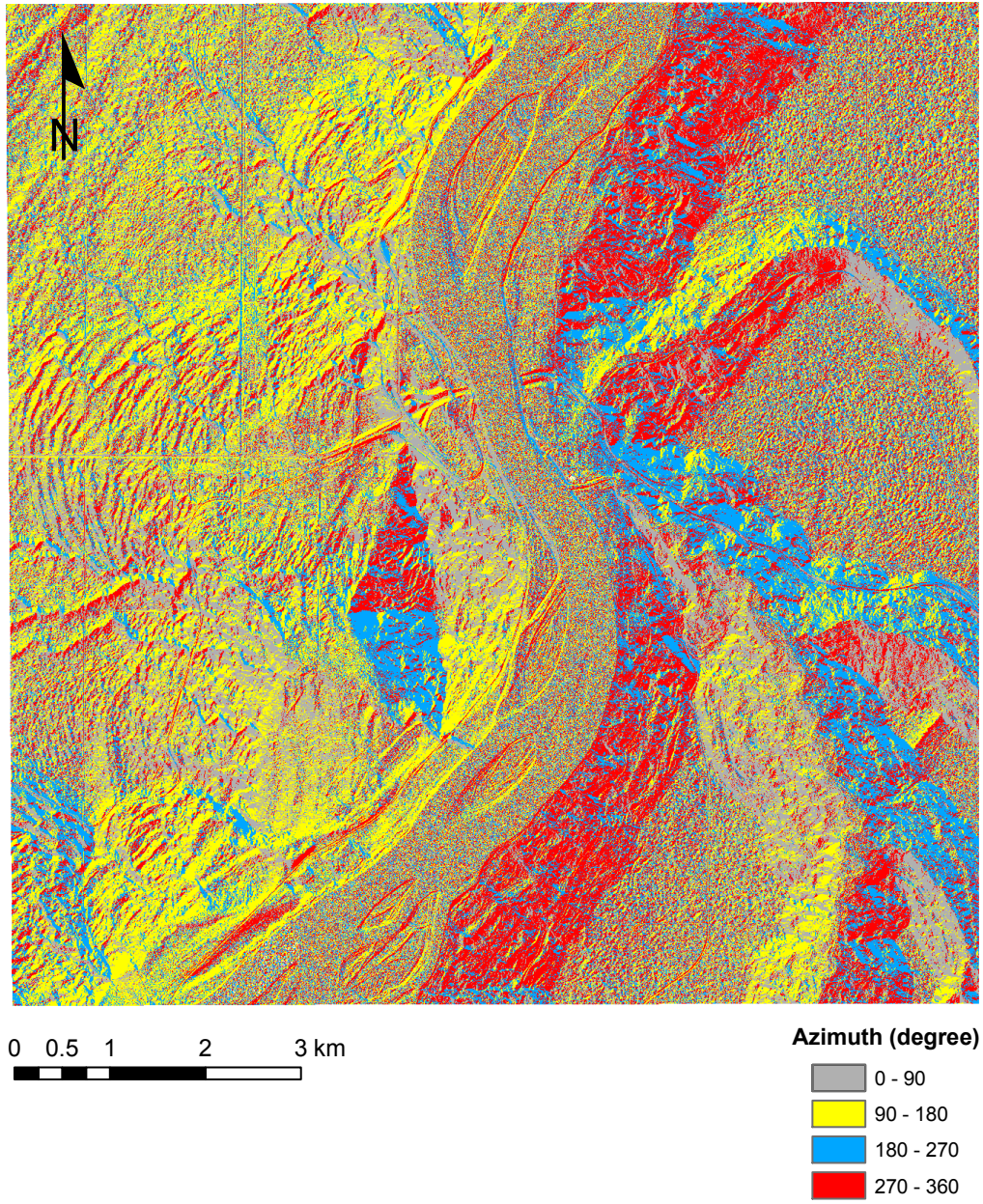


Figure 5.6 Spatial distribution of aspect values. The cell size is 0.5 by 0.5 metres. It is generated from the digital elevation model (Figure 5.4)

The spatial distribution of aspect values shown in Figure 5.6 is similar in four directions. About 28 percent of calculated values are covered by the southeast aspect, which is the largest portion in the study area. The southerly aspect would play an important role in the slope stability to control the snow depth on the ground since the degree of sunshine exposure is greater than other aspects. Snow accumulated in winter may melt rapidly in daytime and lead to increase pore water pressure in subsurface by infiltrating water.

5.1.2.3 Hydrologic network distribution

Understanding of the hydrologic channel network distribution in the study area would give useful information on landslides. Generally stream flows would influence the slopes in two different ways: (1) they erode the toe of the slope and decrease the stability (direct impact); and (2) they infiltrate and increase pore water pressure within the slope (indirect effect). Therefore, identifying current stream flows and measuring their proximity can be a valuable factor to delineate the landslide hazard assessment in the study area.

In this study, major stream flows surrounding the Town of Peace River are identified. By using the Spatial Analyst Tools embedded in ArcGIS the digital elevation model (DEM) is examined for the presence of pits, sinks, or voids which might produce an unwanted complexity (Greenlee 1987; Jenson and Domingue 1988; Tarboton et al. 1991). These pits should be removed to produce a depressionless DEM. The course of water in a cell can be defined by the flow direction (Greenlee 1987; Jenson and Domingue 1988). By using a three by three matrix the orientation of flow direction in eight cells are assigned to unique values depending on the relationship of the neighboring cells. Finally a flow accumulation is calculated in a cell where the number of cells flowing from upstream is recorded to delineate the drainage network (Jenson and Domingue 1988). A designated number of cells or a threshold can be used to isolate the major drainage channels from small streams located in slopes. Jenson and Domingue (1988) also noted the density of computed drainage network would decrease by increasing the threshold value. In this study a value of 50,000 is used to determine the threshold for major stream channels. These channels are illustrated in Figure 5.7. It also shows the distance from major streams, which is useful to identify the influence of water on landslide hazard.

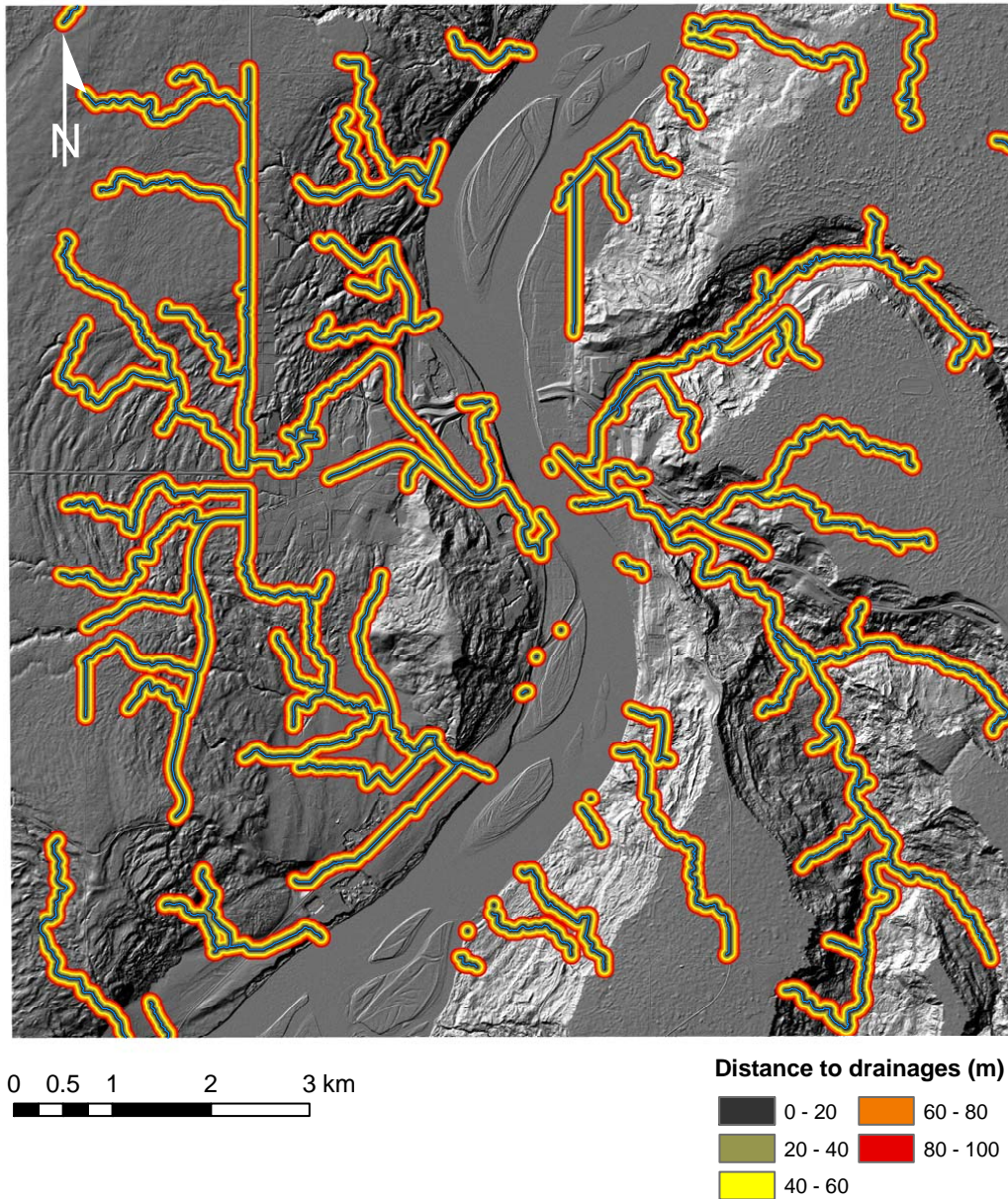


Figure 5.7 Distribution of the hydrologic channel network in the study area. The cell size is 2.5 by 2.5 metres. Calculated streams are delineated by blue solid lines. The distance to drainages is presented by different colored extents which are shown in the legend. A shaded relief image shown in background is obtained from the digital elevation model (Figure 5.4) having a cell size of 0.5 by 0.5 metres

5.1.2.4 Proximity to transportation

Transportation routes, roads or railways, are one of the vulnerable objects impacted by either direct or indirect influences of landslides. Landslides would cause movements of natural slopes adjacent to transportation routes or cuts and fills which have allowed transportation construction. Displaced materials may induce loss of life and property damage, block the routes, and interrupt their services. The construction of transportation routes usually changes the topography of the ground surface and natural drainage systems, with adverse effects on the slope stability. Therefore, identifying the degree of modification on the geomorphological profile and the extent of changes can provide to understanding of causes of landslides induced by anthropogenic factors.

As pointed out in Chapter 4, recent landslides observed in the Town of Peace River are all located near roads and the railway and would provide detrimental influences. A recent study by Kjelland et al. (2009) well described the efforts in preventing landslide impacts on the highways in the study area.

In this study it is hypothesized that constructing major transportation routes may affect initiation and reactivation of landslides by changing the physical geometry of the ground surface. In order to determine its influence on landslides, the proximity to major roads and railway are analyzed. Highway 2 and Secondary Highways 684, 743, and 744 are employed for the analysis on the effect of roads to landslides. Canadian National Railway is selected for the same analysis on the influence of railway.

In each transportation route, five different extents are assigned based on the distance from the routes. Figures 5.8 and 5.9 show results of the distance analysis on highways and the railway which traverse the study area.

Both Figures 5.8 and 5.9 also present the extent of influence on landslides by the construction of major transportation routes. Figures also show the majority of roads and railway are placed on previous landslide deposits comprising colluvial sediments. Landslide movements on these deposits are relatively active and easily recur with small changes of ground profiles or internal stability conditions.

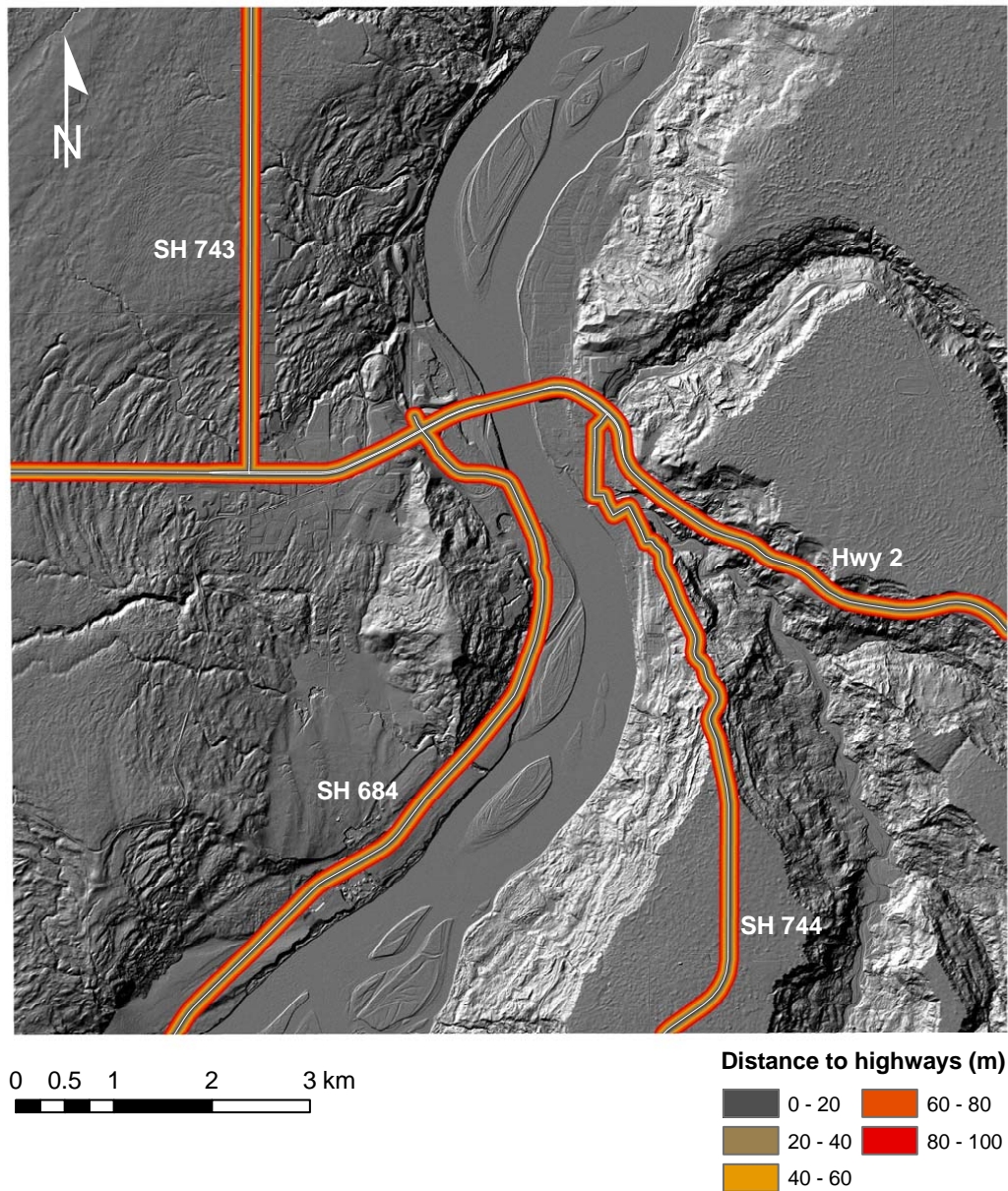


Figure 5.8 Distribution of the road network in the study area. The cell size is 2.5 by 2.5 metres. Roads are delineated by white solid lines. Each road is named in the figure. The distance to roads is illustrated by different colored extents which are shown in the legend. A shaded relief image shown in background is obtained from the digital elevation model (Figure 5.4) having a cell size of 0.5 by 0.5 metres

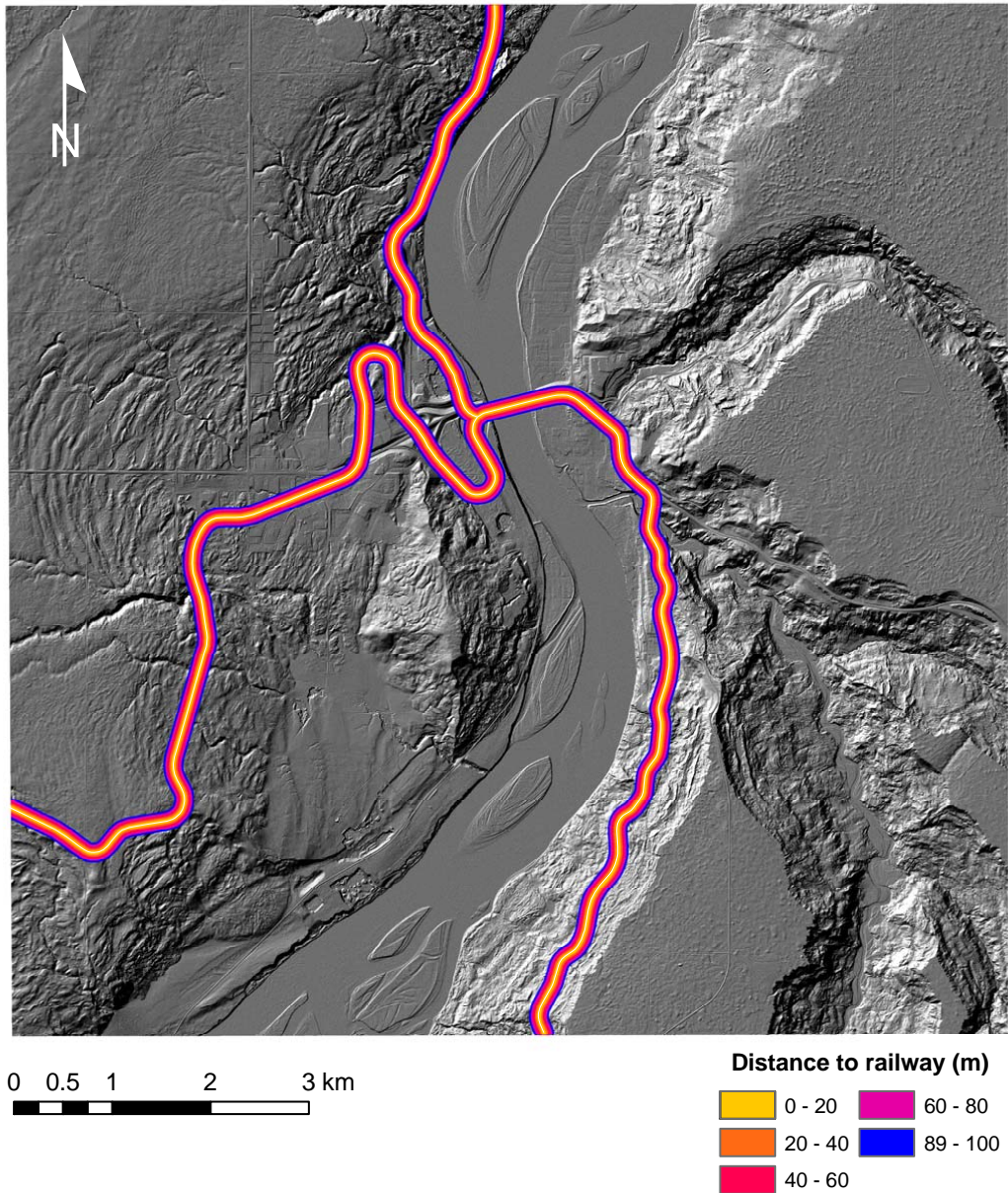


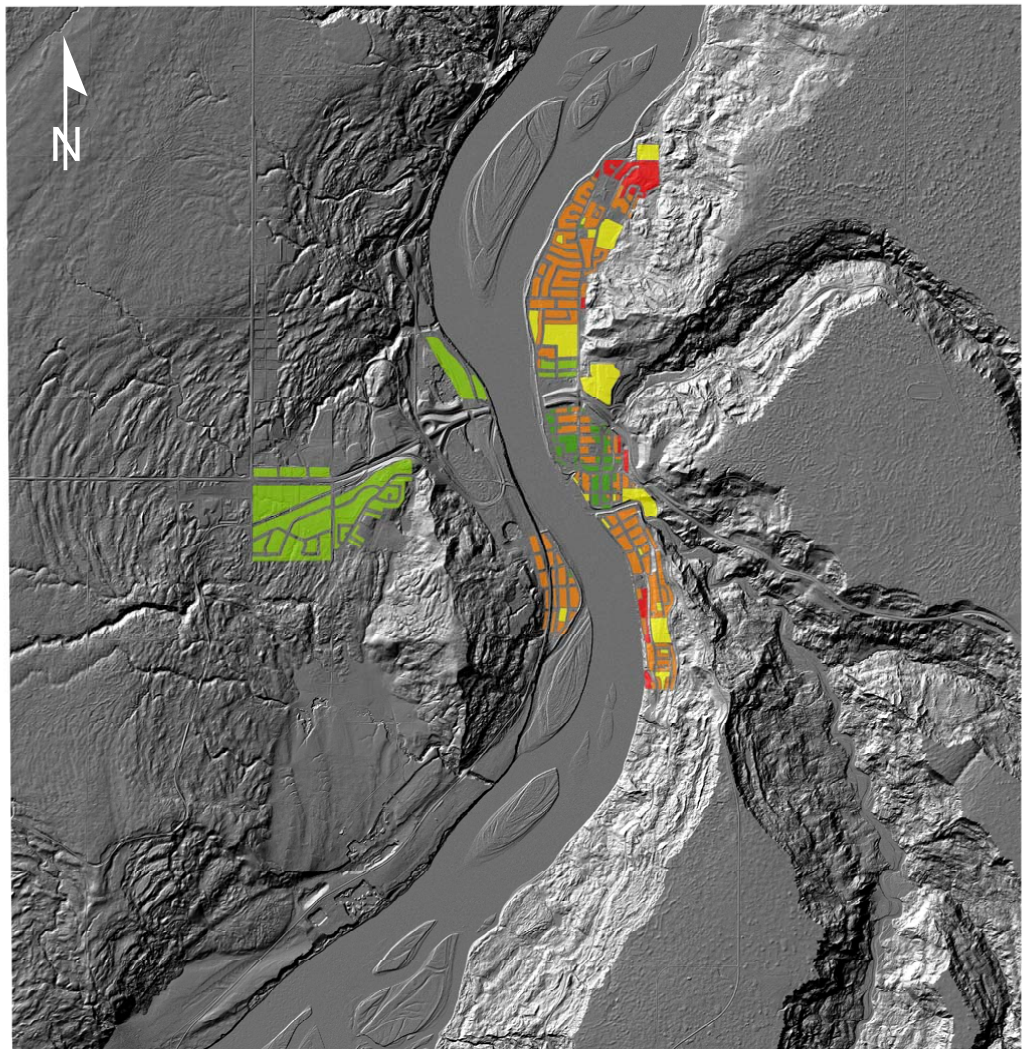
Figure 5.9 Distribution of the railway network in the study area. The cell size is 2.5 by 2.5 metres. The railway is illustrated by a white solid line. The distance to a railway is delineated by different colored extents which are shown in the legend. A shaded relief image shown in background is obtained from the digital elevation model (Figure 5.4) having a cell size of 0.5 by 0.5 metres

5.1.2.5 Anthropogenic distribution

As similar to transportation construction, landslides initiated by human activities are usually account for the majority of events. Human related activities can include as follows: (1) grading for the residential spaces and other facilities followed by water mains, sewer, and gas lines; (2) lawn and plant watering; and (3) recreational usages such as a swimming pool. These activities can physically modify ground surface profiles and decrease the stability of slopes by raising the groundwater level within slopes. Therefore identifying the anthropogenic distribution in the study area in forms of the land use and evaluating the landslide hazard based on the susceptibility of elements at risk may provide a priority in implementing countermeasures against landslides and a basis for landslide risk management plans.

In this study the anthropogenic distribution can be illustrated by the land use. Figure 5.10 shows the spatial distribution of land use. Data for the analysis are based on by Byfield (1984). All the types of the land use are grouped into five different classes: (1) commercial; (2) industrial; (3) park, school, or playground; (4) residential; and (5) undeveloped or partially developed. It is determined that the residential class takes the largest area of 36 percent in total evaluated areas followed by industrial (35 %), park, school, or playground (17 %), and undeveloped or partially developed areas (7 %). The commercial area has the smallest portion, five percent. Due to the relatively inferior type of elements at risk, expected responses of elements at risk at the time of the landslide occurrence, and surrounding environments, the degree of vulnerability in residential areas is generally known to be higher than industrial areas to landslide events even though their percentages are similar in the study area.

As previously described in Chapter 3, Figure 5.10 shows that all evaluated areas are located in the terrace deposits and toes of previous landslides. Without considering potential floods, the threat of landslides seems likely the major concern for anthropogenic activities in the study area.



0 0.5 1 2 3 km

Land use

- Commercial
- Industrial
- Park, school or playground
- Residential
- Undeveloped / partially developed

Figure 5.10 Land use distribution in the study area. The cell size is 2.5 by 2.5 metres. The distribution is grouped by using the land use. Each class is differentiated by specific colors shown in the legend. A shaded relief image shown in the background is obtained from the digital elevation model (Figure 5.4) having a cell size of 0.5 by 0.5 metres

5.1.3 Relationship among landslide causal factors in the hazard assessment

In this section a more detailed relationship among landslide causal factors is examined based on the combination of the influence from each landslide causal factor identified in the study area. This can provide an understanding of the complex nature of landslides and give estimates of landslide hazard and activity. I focused on a relationship between geologic and geomorphological factors, which are represented by surficial deposits and slopes. Identified landslide deposits are used to delineate the extent of this relationship. Results of laboratory tests are also employed to add their geotechnical characteristics to surficial deposits.

Figure 5.11 shows landslide deposits that are identified from consecutive geomorphological maps and LiDAR dataset. Geomorphological maps were generated from aerial photo interpretations which are described in Section 5.4.1. A total of 148 previous landslides were identified and their extent was also delineated. 110 landslide deposits are placed on the east bank of the Peace River, which is equivalent to 74 percent of the total. Appendix E presents detailed information on identified deposits such as locations, dimensions, data sources, and statistical calculations.

Figure 5.11 also gives the extent of colluvial deposits that were obtained from the spatial distribution of surficial deposits (Figure 5.1). From Figure 5.11 it can be postulated that most previous landslide deposits are placed on colluvial deposits. A few exceptions are also found where toes of landslide deposits were located on bedrock formations and fluvial deposits.

The spatial distribution of slope values within the landslide deposits is shown in Figure 5.12. Calculated slope values range from zero to 86 degrees and have 17 degrees as their average. The standard deviation of all landslide deposit slopes can be calculated as 9.3 degrees. Subsequent values related to each landslide deposit are also presented in Appendix E. Landslide deposits showing the high standard deviation usually indicate wide ranges in slope values on the ground. In the study area, the east bank of the Peace River has an average value of the standard deviation 134 percent of the mean value in the west bank.

The mean slope angle of each landslide deposit is presented in Figure 5.13 with the mean slope angle obtained from all landslide deposits. Figure 5.13 clearly shows

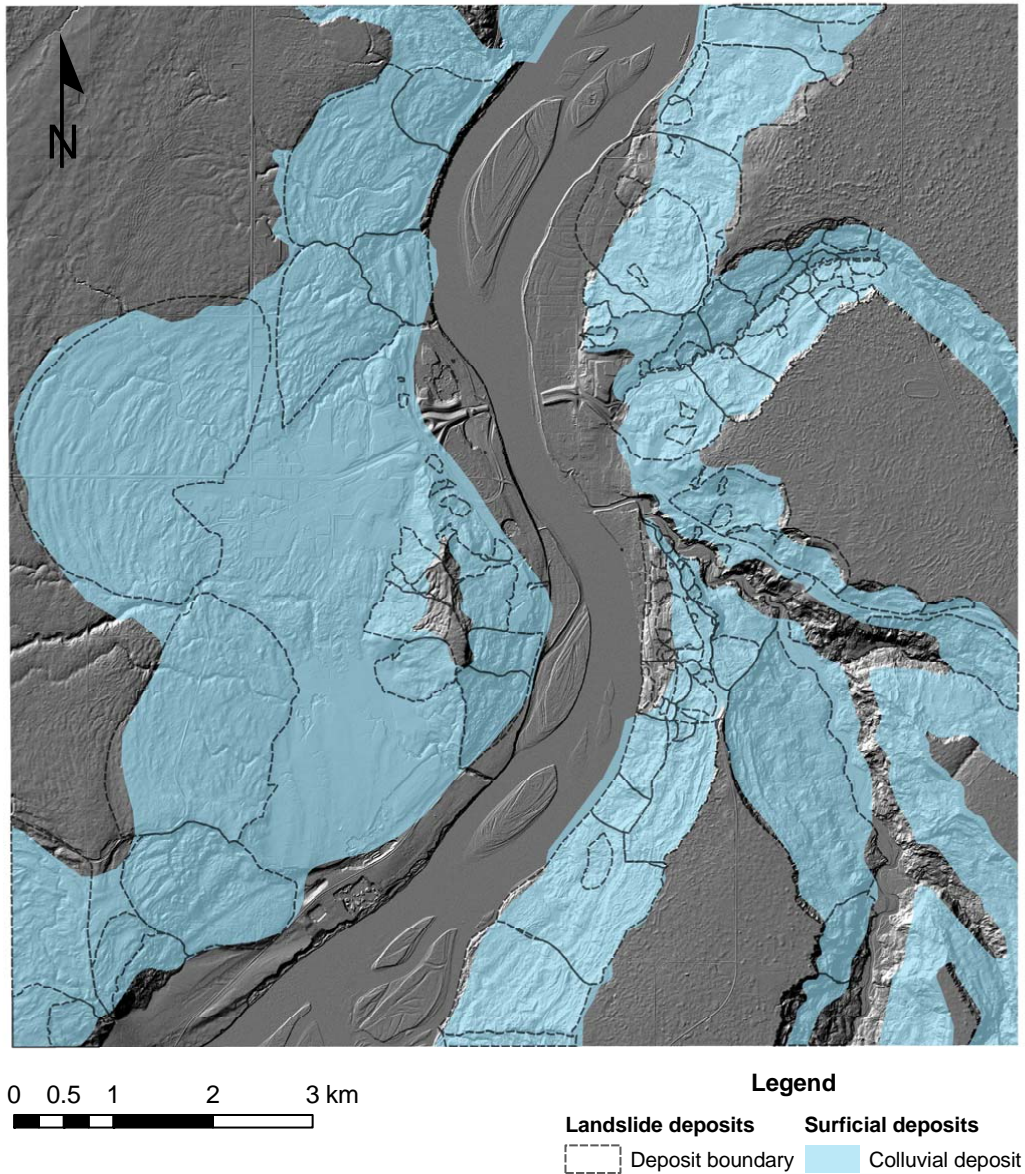


Figure 5.11 Spatial distribution of identified landslide deposits. Previous landslide deposits are delineated from geomorphological maps and LiDAR dataset. Detailed information on each landslide deposit is presented in Appendix E. Colluvial deposits which are underlying landslide deposits are captured from the distribution of surficial deposits shown in Figure 5.1. A hillshade imagery presented in the background is obtained from the digital elevation model (Figure 5.4) with the spatial resolution of 0.5 by 0.5 metres

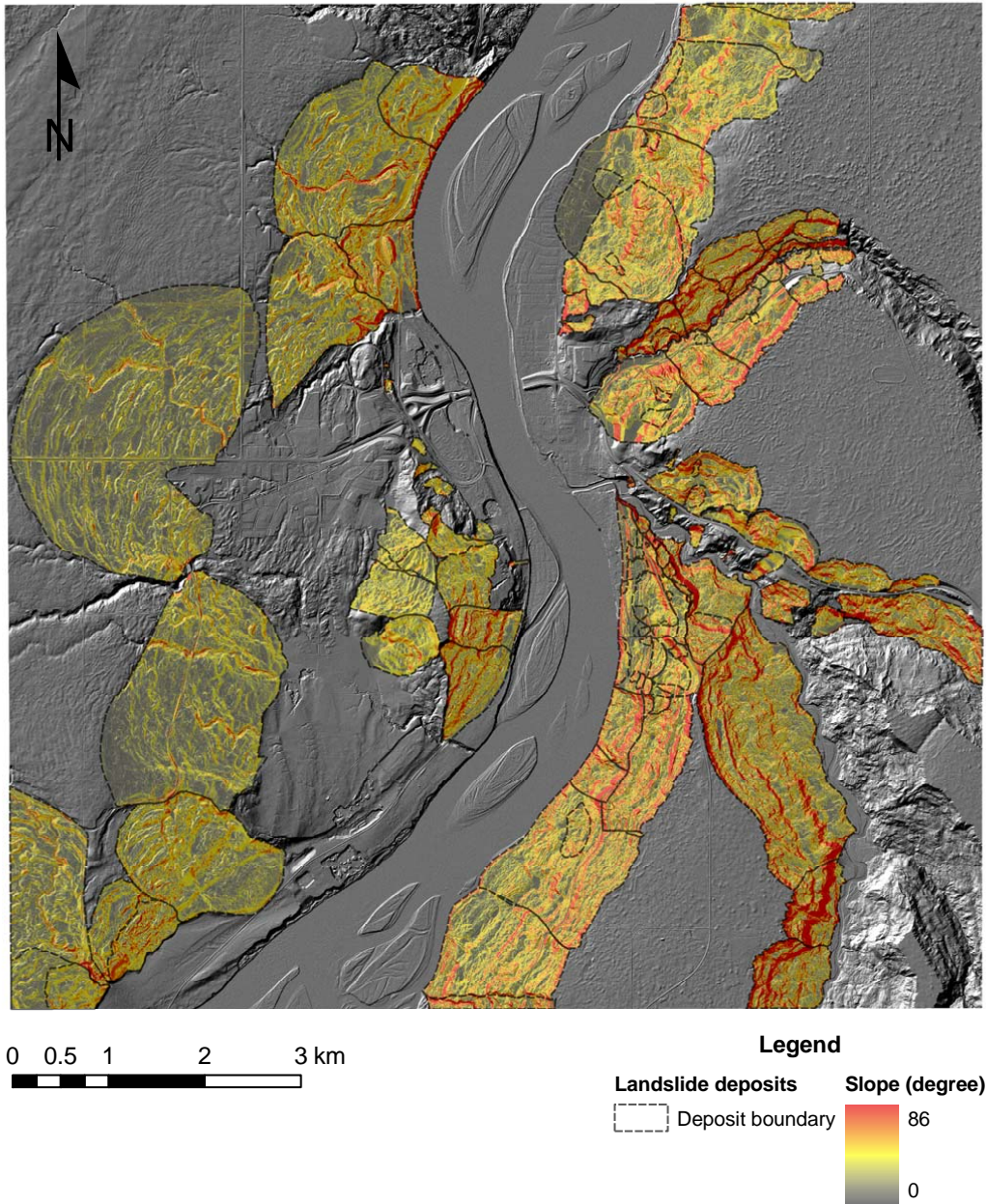


Figure 5.12 Spatial distribution of slope values within landslide deposits. The variation of slopes is presented by the legend. Slope values are obtained from Figure 5.5 with a cell size of 0.5 by 0.5 metres. A hillshade imagery presented in the background is obtained from the digital elevation model (Figure 5.4) with the spatial resolution of 0.5 by 0.5 metres

the mean slope angle of landslide deposits observed on the east bank of the Peace River is higher than those on the west bank. Based on the average value of slopes in all landslide deposits (17°), landslide deposits on the east bank which have the mean slope angle higher than the average value are 59 percent whereas only 13 percent of landslide deposits on the west bank exceed the average value. Most landslide deposits on the east bank that have slopes over the average can be found on valley slopes along Pat's Creek and the Heart River, which are relatively young compared to those on the Peace River. The stream degradation in those areas is, therefore, more severe than other areas. This also made the mean slope angle over 30 degrees in some portions of valley slopes along tributaries of the Peace River (Figure 5.13). On the other hand, only five landslide deposits on the west bank have mean slopes over the average value. These are located at the toe of Misery Mountain and near the Canadian National Railway.

Figure 5.13 also illustrates the critical slope angle which is based on the assumption of groundwater reaching to the ground surface of an infinite slope (Skempton and Delory 1957). By applying the result of laboratory tests in Section 4.2, the critical slope angle for colluvial deposits where previous landslide deposits were concentrated can be calculated as 10 degrees ($\pm 1.2^\circ$ for the error propagation which considers the 95 % confidence ranges in the residual friction angle and the uncertainty of the unit weight of colluvial sediments, Figure 5.13) by assuming the unit weight of 19.5 kN/m^3 (Thomson and Hayley 1975). This value can be used as a threshold to determine the landslide hazard state in the study area. A total of 13 landslide deposits are observed below the critical slope angle and 69 percent of them are in the west bank of the Peace River. The low slope angles of some landslide deposits, Deposit ID of 1, 2, and 24 in Appendix E, were mainly affected by the weathering process over time since they have formed colluvial deposits. For other landslide deposits, all on the east bank, however, their low slope angles were produced by anthropogenic factors such as urban developments. Especially landslide deposits of 62, 91, 96, and 113 show low slope angles due to the modification of ground profiles by human activities. Table 5.4 shows a list of landslide deposits whose mean slope angles are below the critical slope angle and the corresponding spatial distribution is presented in Figure 5.14.

To determine the lower limit of the stable state within which landslides may initiate or reactivate, a simple geometry of the infinite wedge or block which is sliding along the horizontal bedding is applied to understand the landslide mechanism of

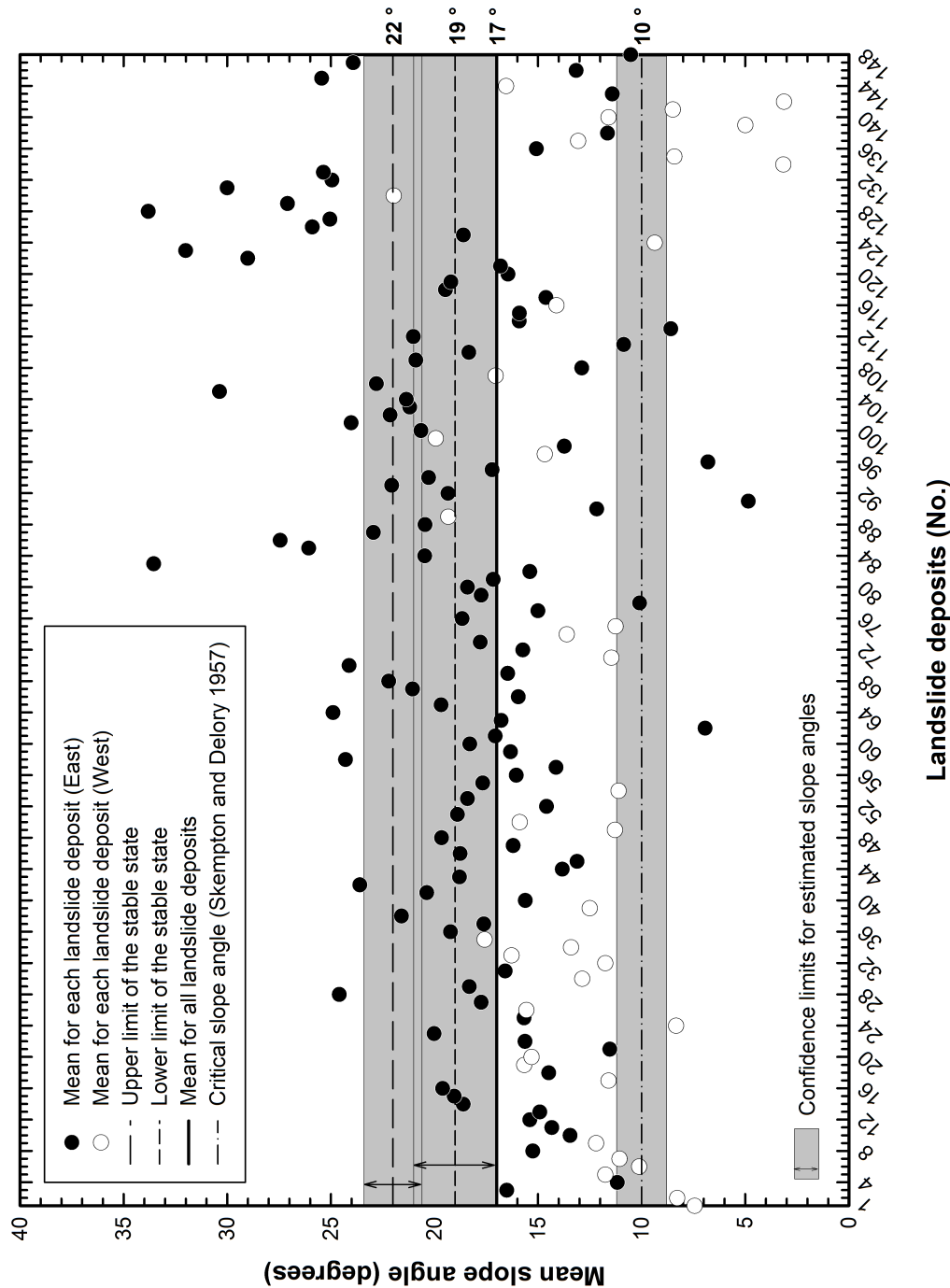


Figure 5.13 Mean slope values of landslide deposits observed in the study area. Landslide deposits denoted by the unique number are presented in the abscissa while corresponding average slope angles are shown in the ordinate. Landslide deposits are grouped, either the west or east, based on the location where they were identified. Horizontal lines represent the critical slope angle, average slope angle for all landslide deposits, and lower and upper limits of the stable state, respectively. Gray shaded areas also illustrate the 95 percent confidence intervals with respect to friction angles and the uncertainty of the unit weight of colluvial sediments, which described in the text. Detailed information for landslide deposits are also presented in Appendix E

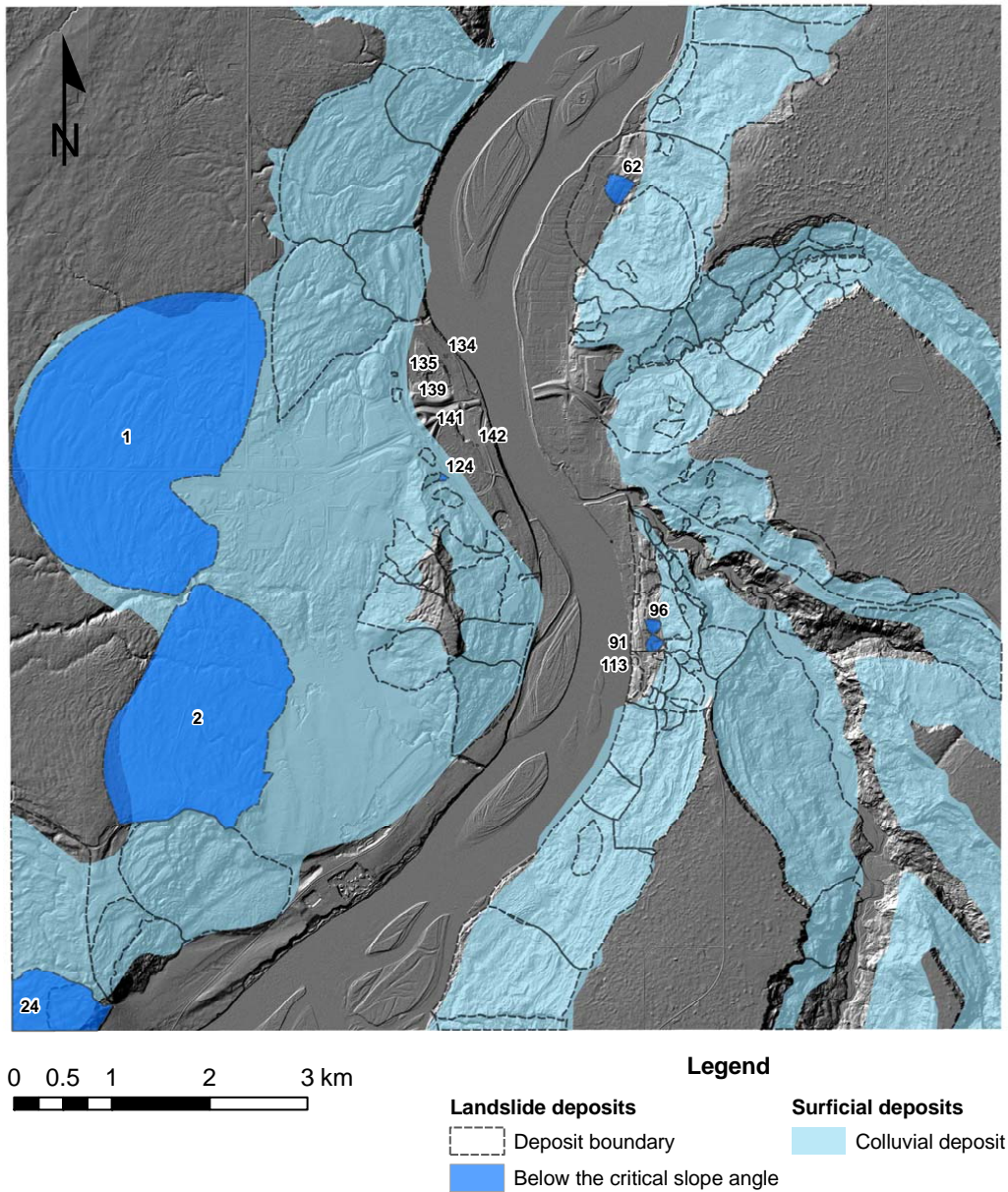


Figure 5.14 Geographical distribution of landslide deposits whose mean slope angles are below the critical slope angle. Illustrated landslide deposits are listed in Table 5.4. A hillshade imagery presented in the background is obtained from the digital elevation model (Figure 5.4) with the spatial resolution of 0.5 by 0.5 metres

Table 5.4 Landslide deposits having mean slope angles below the critical slope angle. Location and corresponding coordinates of each landslide deposit is described in Appendix E. The geographical distribution of listed deposits is shown in Figure 5.14

Deposit ID [†]	Location	Mean slope (°)	Cause of low slope values
1	West	7.4	Degradation
2		8.3	
24		8.3	
62	East	6.9	Human activity
91		4.8	
96		6.8	
113		8.6	
124	West	9.4	Human activity
134		3.1	
135		8.4	
139		5.0	
141		8.5	
142		3.1	

[†] Individual landslide deposit ID is denoted in Appendix E.

translational block slides mainly observed in the study area (Table 4.1). Based on simplifying assumptions such as no distance between crests and tension cracks, and groundwater that fills tension cracks to the ground surface (O'Brien et al. 2011, Eq. 7), the lower limit of slope angle can be calculated as 19 degrees ($\pm 2^\circ$ for the error propagation which considers the 95 % confidence ranges in the residual friction angle and the uncertainty of the unit weight of colluvial sediments, Figure 5.13). Only three landslide deposits on the west bank, landslide deposits of 89, 99, and 130, exceeded the designated slope angle and give six percent of landslide deposits over 19 degrees. This leads to the fact that 94 percent of landslide deposits over 19 degrees are placed on the east bank (Figure 5.15). This finding, the concentration in the distribution of landslide deposits with slopes over 19 degrees on the east bank, is in contrast to the distribution of slope values below the critical slope angle. The discrepancy between distributions in slope values can lead to different landslide activity in the study area.

Next, the fully softened friction angle of 22.2 degrees, which was obtained from direct shear tests on colluvial sediments (Section 4.2), is used to differentiate the upper limit from the lower limit of the stable state. The result shows that a required angle for the slope to move under the fully softened circumstance is calculated as 22 degrees ($\pm 1.4^\circ$ for the error propagation which considers the 95 % confidence ranges in the fully softened friction angle and the uncertainty of the unit weight of colluvial sediments, Figure 5.13). This value, which reflects the limit of material transport in colluvial deposits, can be used as the upper limit of the stable state of the landslide activity within which most landslides are in the 'Marginally stable' state unless any other landslide causal factor increases the instability of the slope.

The identification of slope angles observed in landslide deposits can be a useful approach to classify the activity state of landslide hazards. It is also a good indicator to differentiate between unstable and stable areas even though it cannot provide the information on temporal changes in the ground surface. In this study the landslide hazard and corresponding activities are grouped based on representative slope values described in Figure 5.13. The specific condition of the landslide hazard is taken from recent studies by Keegan (2007, Table 4-4) and Keegan et al. (2007, Table 4). Sections 5.3.2 and 5.4 describe the major principles in determining landslide hazard and the construction of the landslide hazard assessment by using slope gradients.

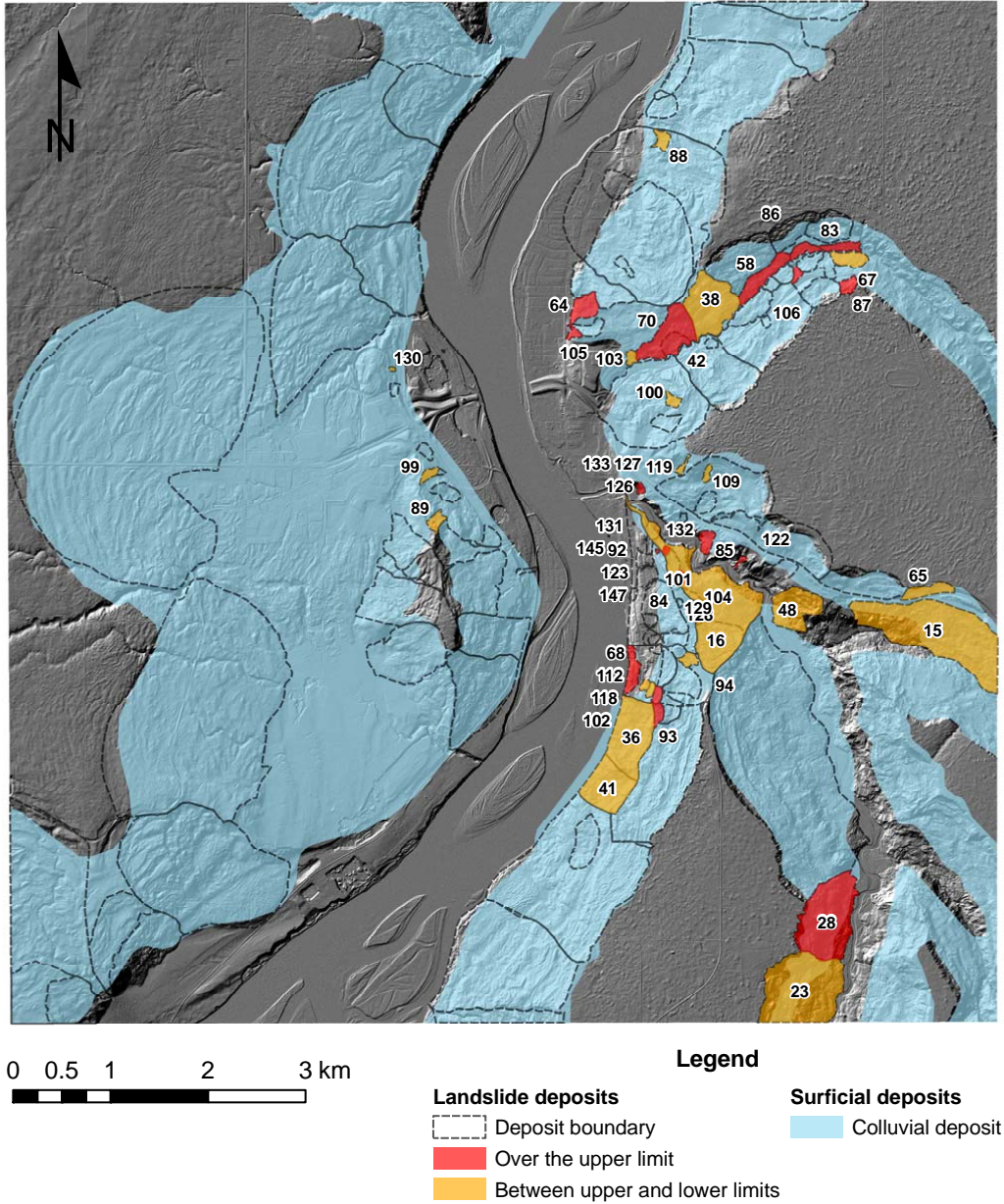


Figure 5.15 Geographical distribution of landslide deposits whose mean slope angles are divided by lower and upper limits of the stable state. A hillshade imagery presented in the background is obtained from the digital elevation model (Figure 5.4) with the spatial resolution of 0.5 by 0.5 metres

One limitation found in this analysis is that it focuses on the ground surface and does not have any consideration of the subsurface stratigraphy. Most landslides observed in the study area have translational characteristics (Table 4.1) and therefore, estimated rupture surfaces follow the bedding in colluvial and glacial sediments, or sometimes even in bedrock formations (Figure 4.43). With these complex conditions, analyzing geomorphic characteristics without any consideration of the subsurface stratigraphy does not provide the useful information with regard to the state of landslide hazards. Therefore, it is imperative to relate geomorphological factors to various geological ones in order to delineate correct mechanisms inherent to the landslides in the study area.

One example relating geologic properties to the landslide hazard assessment is shown in Figure 5.16. It illustrates approximate extent of bedrock formations especially exposed on the ground surface. These bedrock outcrops can be found on the bottom of valley slopes along the Peace and Heart River, and the downstream of Pat's Creek. The presence of bedrock formations within landslide deposits may influence the state of the landslide activity especially when they are placed on the toe of slopes. They may increase stability unless the existing rupture surface is observed along the bedding in bedrock formations. However, bedrock outcrops which contain pre-sheared rupture surfaces should be considered carefully when they are included in modifications of ground surfaces for developments. The analysis of bedrock exposures shown in Figure 5.16 indicates the bedrock located above 300 metres is the Shaftesbury Formation which mainly consists of shale. The existence of the shale bedrock may contribute to the instability of slopes in the study area by forming a distinct rupture surface along the bedding plane, which is the typical property of the translational block slide determined in Chapter 4.

5.2 Early study on the landslide hazard assessment

Most studies regarding landslides and their impacts in the Town of Peace River were limited in their extent to how infrastructures such as road, railway, and residential areas would be affected by landslides. In other words, the main purposes of the studies were to identify the mechanism of individual landslides and to propose appropriate remedial measures to remove or prevent future threats. There was no systematic approach for the overall slope stability in the study area until the

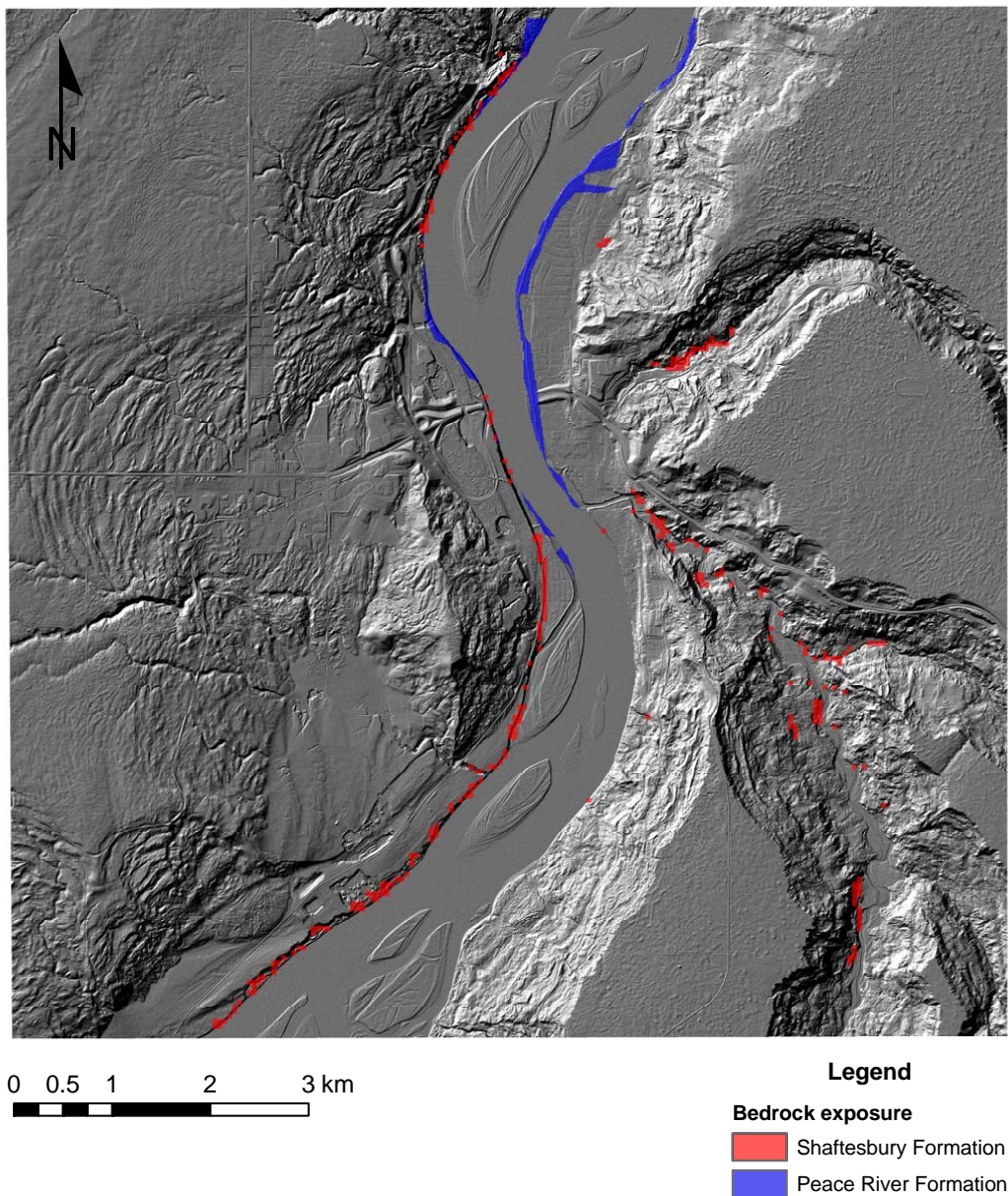


Figure 5.16 Distribution showing the approximate extent of bedrock formations in the study area. The spatial distribution of bedrock formations exposed on the ground surface is draped on the topographic hillshade imagery. Exposed bedrocks which denote Shaftesbury and Peace River Formations are illustrated by red and blue areas, respectively. The original dataset for the bedrock distribution is obtained from Borneuf (1981) and Morgan et al. (2008, Figure 3). A hillshade imagery presented in the background is obtained from the digital elevation model (Figure 5.4) with the spatial resolution of 0.5 by 0.5 metres

1970s. Since 1970, as the urbanization encroached on the steep areas, the pinpoint of the landslide studies has converted into the preparation to the future landslides especially when the municipality would develop the valley slope for residential areas. One of the case studies of this comprehensive landslide hazard assessment was conducted by Nilson and McCormick (1978).

Under an agreement with the Peace River Regional Planning Commission (1980), the purpose of their study was to identify the areas in which the slope stability could create serious problems if they are developed. That is, the objective was to differentiate whether slopes in the study area are gentle enough to be stable or require high remedial costs for future developments. Contour maps, aerial photographs, published reports accompanied the study for determining major landslide causal factors that may influence the slope stability. These included slope geometry, strength property, moisture contents, and time for exposure. Landslides were grouped into two, either retrogressive translational landslides or shallow landslides, which were denoted as a representative slope degradation process.

Finally they divided the study area into several physiographic units using letters and combined them with four separated roman numerals which represent the degree of the possibility of landslides. Results of the study showed the degree of landslide susceptibility for classifying areas whether developments are available or not. Based on the feasibility of the development, river terraces and the west upland of the Peace River were identified as the possible development areas without landslide problems. Areas placed on previous landslide deposits were also accepted to be developed if provided more detailed geotechnical information. Other areas were assumed to be improper for further developments (Nilson and McCormick 1978). Tables 5.5 and 5.6 show the degree of the slope stability and physiographic units, respectively. The landslide susceptibility map is illustrated in Figure 5.17.

Despite their contributions to the early landslide hazard assessment in the study area, the authors overlooked key issues for the landslide susceptibility model. For example, the division of physiographic units (Table 5.6) was not clearly differentiated. In other words, terrain and process units were combined to present these physiographic units. Terrain units such as upland plateau (A), terraces (D, F, and T), hill (G), previous channel (H) should be presented by separating from large slide mass (B), slide scarp (K), slide toes (M and P), and other slides (Q and R) comprising process units. The latter can be shown by the landslide inventory.

The other pitfall is the lack of the geologic information. As pointed out in the previous section, the geological information is a significant factor for landslide hazard assessments (Krohn and Slosson 1976; Pestrong 1976). Selected geological units which are believed to influence the slope stability are then overlaid with the historical landslide information representing the landslide inventory and define their degree of susceptibility and hazard from landslides.

5.3 Processes of the landslide hazard assessment

An early study by Pestrong (1976) showed that landslides would become a hazard when they intersect human activities. A similar concept was introduced by Mahr and Malgot (1985) in which landslides would be a problem when the 'natural landscape' is converted into the 'cultural landscape.' Therefore, identifying both interests of humans and natural processes of landsliding in ground surface is a prerequisite function for the landslide hazard assessment. In the previous section several activities by humans which might induce slope stability were discussed. Landslide related natural processes are examined in this section. Advanced landslide identification schemes are employed to detect landslide related natural processes. This information will be integrated to evaluate the degree of hazard induced by landslides. Finally landslide hazard assessments are implemented by mapping.

5.3.1 Identification of geomorphological landslide features

Once landslides occur, they usually leave related features such as scarps, cracks, flanks, and displaced materials on the ground and these are distinct from areas without landslides. Identifying these features provide invaluable information on building the landslide hazard assessment as it would help to determine potential landslide areas based on historical evidences. This is the main purpose of landslide inventory mapping that gathers information from various sources such as aerial photographs and archives. These classical methods in identifying remnants of previous landslides have several limitations. First of all, such sources have only limited time spans of no more than hundred years compared to the longevity of landslide that ranges at least thousand years. Although ancient documents that successfully recorded previous landslide events that occurred hundred years ago, their value as

Table 5.5 Degree of the slope stability in the Town of Peace River. The distribution of results is shown in Figure 5.17. *Source:* Data adapted from Nilson and McCormick (1978)

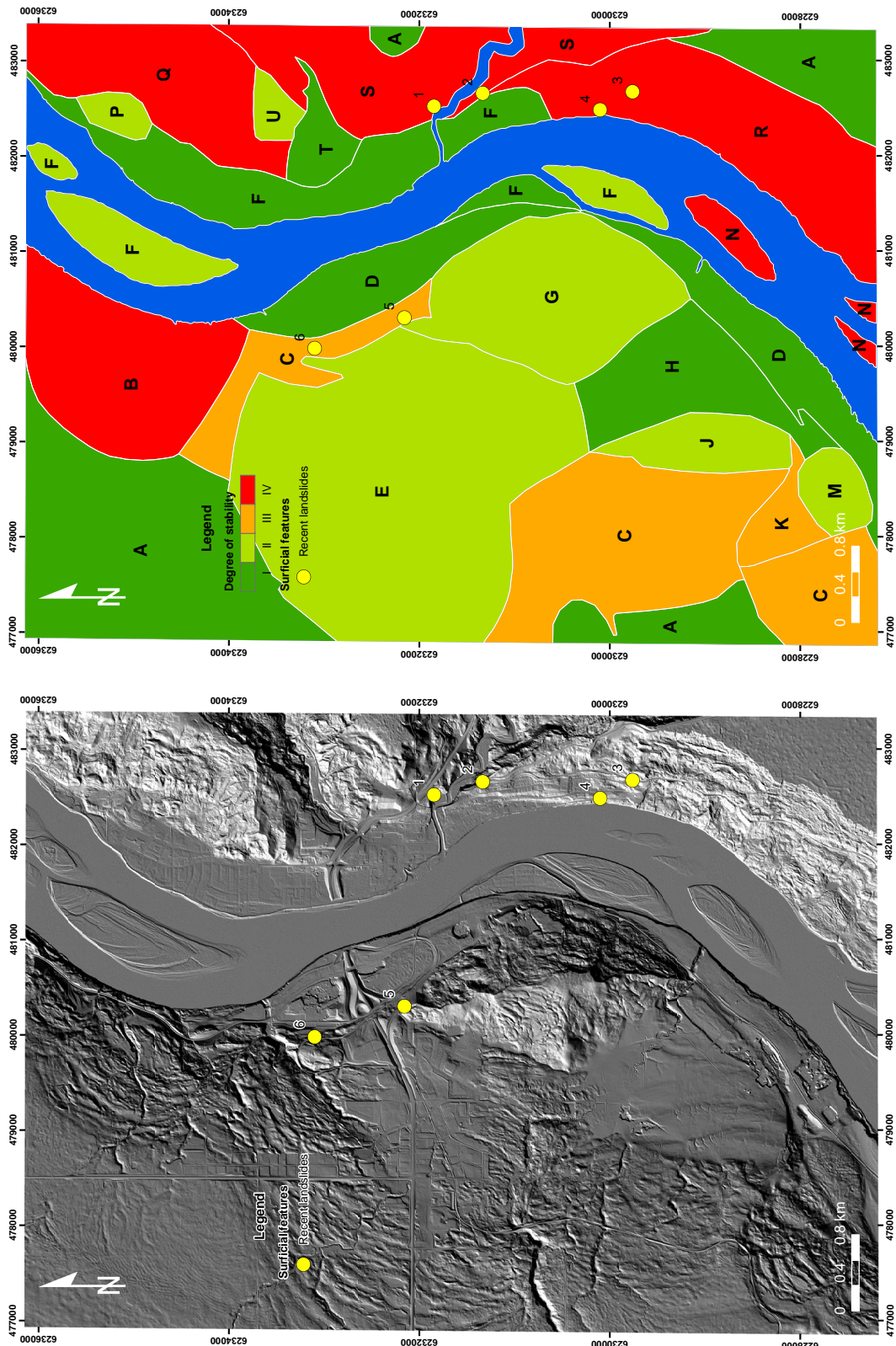
Degree of slope stability	Description
I	Unaffected by any slope failure
II	Possible slope failure [†]
III	Probable slope failure [‡]
IV	Presently unstable

[†] Areas of old landslides.

[‡] Areas which are stable, but would be unstable when they are developed.

Table 5.6 Physiographic units in the Town of Peace River. The distribution of results is shown in Figure 5.17. *Source:* Data adapted from Nilson and McCormick (1978)

Unit	Description
A	Upland plateau. Covered by lacustrine sediments
B	Large slide mass on outside of the river meander
C	Original slumped bank
D	Upper terrace of the river
E	Major slides blocked original course of the Peace River
F	Most recent terraces and islands
G	Large hill in the center of the study area (Misery Mt.)
H	Abandoned course of Preglacial river channel
J	Transition between the terraces and up-slopes
K	Scarp of a rapid slope failure
M	Toe a rapid slope failure
N	Smaller islands at the confluence of the Peace and Smoky Rivers
P	Toe of the shallow slide
Q	Severe shallow sliding
R	Deep seated sliding
S	Slopes in the tributaries
T	Upper level terraces
U	Old slumped areas



(a)

(b)

Figure 5.17 Landslide susceptibility map for the Town of Peace River. a. A shaded relief image obtained from LiDAR dataset. b. A landslide susceptibility map showing combinations of physiographic units and degree of slope stability shown in Tables 5.5 and 5.6, respectively. Recent landslides described in Figure 4.1 are also indicated in both a and b. The distribution of the landslide susceptibility which is illustrated in b is digitized from Nilson and McCormick (1978)

sources for the landslide inventory mapping may not be significant in the engineering perspective. Rather they would only provide crude information such as approximate occurrence dates, imprecise locations, and rough extents (McLearn 1918; McConnell 1893).

Another issue with conventional methodologies in identifying previous landslides can be related to the evolution of topography by natural processes. Newly generated landslide features usually have distinct characteristics compared with those in non-landslide areas. When they are exposed on the ground surface over time, however, natural processes such as weathering, stream erosion, and vegetation would transform materials consisting of landslide features into those similar to adjacent stable areas which would lead to incorrect results in the landslide inventory mapping. Identifying dormant landslide features concealed by vegetation is difficult using conventional methodologies (McKean and Roering 2004). Various approaches were examined to overcome these limitations (Shih and Schowengerdt 1983; Hervás and Rosin 1996; Kimura and Yamaguchi 2000; Norheim et al. 2002; Rodriguez et al. 2002; Coe et al. 2003; Guth 2003; Rowlands et al. 2003; Yamaguchi et al. 2003; McKean and Roering 2004; Catani et al. 2005; Corsini et al. 2005; Smith and Clark 2005; Whitworth et al. 2005; Chacón et al. 2006; Glenn et al. 2006; Kaplan 2006; Delacourt et al. 2007; Sappington et al. 2007; Schulz 2007; van Den Eeckhaut et al. 2007; Teza et al. 2008; Grohmann et al. 2009; Kasai et al. 2009). One distinct characteristic of those studies is utilizing recent remote sensing technologies. For example, Kimura and Yamaguchi (2000) used a synthetic aperture radar interferometry (InSAR) with precipitation data for modeling landslide movements in northern Japan. They noted that the model powered by InSAR technology can account for the complex landslide movements showing either shallow or deep seated landslide behaviours when ground surface measurements observed at the same location are difficult to recognize the overall movement mechanisms. Catani et al. (2005) also discussed the capability of the SAR interferometry technique for quantifying landform attributes.

Identifying geomorphological landslide controlled features by using the global positioning system, or GPS, also has gained its popularity especially in observing landslide movements and their behaviours with other instrumentations. Coe et al. (2003) employed GPS surveys combined with extensometer measurements to monitor movements and velocities of the Slumgullion landslide in Colorado over 3.5 year periods. Similar studies for the application of GPS on landslide movements

were carried out at Japan (Yamaguchi et al. 2003) and Italy (Corsini et al. 2005). Yamaguchi et al. (2003) used GPS measurements as a verification scheme for monitoring landslide movements by using SPOT HRV and ADEOS AVNIR panchromatic images. Landslide monitoring by GPS and other instruments showed the evolution of landslides in terms of magnitude and frequency, and would enable the assessment of the landslide hazard for the study area and apply to the early warning system (Corsini et al. 2005).

While InSAR and GPS technologies are focused on the recognition of dynamic behaviours of geomorphological landslide controlled features on ground surfaces in order to identify landslide movement mechanisms, the static quantification of landslide control attributes are carried out by a high resolution topographic information, which is obtained from LiDAR (Light Detection and Ranging) technique (Glenn et al. 2006). As pointed out in Chapter 2, LiDAR can generate high resolution models which differentiate distinct landslide features such as steep scarps at the top, fan shaped lobes at the toe, and an irregular hummocky topography between top and bottom (Pestrong 1976). These features can be evaluated based on their evolution by natural processes over time. The landslide inventory mapping enhanced by the LiDAR derived digital elevation model (DEM) can provide not only the exact boundary of previous landslides but also an insight on the internal deformation of the landslide body (McKean and Roering 2004).

By selecting pulses of light reflected from the objects the generated DEM does contain the ground surface beneath vegetation and other obstacles (Figure 2.2). The bare earth DEM derived from LiDAR is the most promising functionality for the landslide inventory mapping dealing with remnants of previous landslides degraded by the weathering process or ongoing features of current landslides covered by dense vegetation (Schulz 2007; van Den Eeckhaut et al. 2007). Schulz (2007) pointed out the landslide identification augmented by LiDAR technique has increased its capability by detecting four times more landslides observed in Seattle than those using conventional methodologies such as aerial photo interpretation. The terrestrial LiDAR technique, an alternative application of the airborne laser altimetry, would allow an objective and detailed topographic modeling with fast data processing and least efforts of operators (Rowlands et al. 2003). Norheim et al. (2002) evaluated a suburban terrain in eastern Seattle by using LiDAR and InSAR derived DEMs and found LiDAR derived DEM gave more suitable results with less bias and variance than those obtained from InSAR DEM. They also noted both tech-

niques are capable in less vegetated and flat areas whereas LiDAR DEM showed a high accuracy especially in heavily vegetated areas.

In this study, therefore, some efforts to delineate the status of geomorphological landslide controlled features observed in the Town of Peace River area are discussed. The representation of the landslide controlled features is based on the high resolution DEM derived from LiDAR technique and evaluated by the following analyses: (1) texture analysis; and (2) statistical evaluation of the orientation data. The latter can be divided into two components: (1) vector strength and dispersion analysis; and (2) eigenvalues analysis. Spatial distributions of those features may indicate distinct characteristics between stable and unstable domains in the study area.

5.3.1.1 Texture analysis

The texture, in terms of image processing and classification fields, can be defined as the spatial distribution of gray tones whereas the tone can be stated as the change of gray shades of the cell in images (Haralick et al. 1973). Based on the concept of texture and tone, all surfaces obtained from the image data can be explained by texture and tone.¹

From the geomorphic perspective, a texture on the ground surface can be interpreted as either rough (turbulent) or smooth in which the physical elevation changes between a cell (the reference cell) and neighbouring cells are simulated by tonal changes of each other. Differences in brightness (tonal change) of a reference cell, either gray levels (GL) or digital numbers (DN), can be evaluated (Hall-Beyer 2007). In the process of landslide identification, it is assumed that the rough topography may stand for irregular surfaces such as hummocky terrain comprising landslide features. On the other hand areas without any landslide history may be shown by smooth texture. Applications of the texture in geomorphic studies such as area classification and landslide mapping were carried out by many authors (Shih and Schowengerdt 1983; Hervás and Rosin 1996; Whitworth et al. 2001, 2005; Kaplan 2006; Whitworth et al. 2006).

¹According to the definition by Haralick et al. (1973) that the texture and tone are dependent concepts and their relationship are similar to 'particle' and 'wave.' In other words, the texture is the part of the tone. This relationship, however, may depend on the size of image and size and number of tonal features to identify.

Haralick et al. (1973) noted significant information on structural distribution of surface and connection to surrounding environments are included in texture and tone. Obtaining textural or tonal features is carried out by the Gray-Tone Spatial-Dependence Matrix (Haralick et al. 1973) or Gray Level Co-occurrence Matrix, or GLCM, (Hall-Beyer 2007) in which directions and distances between a cell and neighbour cells are determined. It is imperative to transform the gray tone spatial-dependence matrices into symmetrical ones to eliminate gray level differences in the diagonal direction and normalize them before texture calculations in order to represent them as probability terms. Symmetrical matrix can be obtained from summing GLCM matrices in opposite directions (Hall-Beyer 2007). Dependent of the relationship between the reference cell and neighbouring cells, texture calculations can be divided into three groups (Kaplan 2006; Hall-Beyer 2007):

1st order texture calculation indicates a simple texture calculation without the pixel interrelation. It would include mean, variance, and standard deviation calculations.

2nd order texture calculation which the GLCM texture measurements usually indicate. It considers the relationship of a reference cell and one neighbouring cell at a time.

3rd and higher order texture calculation take into account for relationships between the reference cell and more than two neighbouring cells at a time.

The second order texture calculation can be classified again into three types based on differences in applying weights to the normalized Gray Level Co-occurrence Matrix. Table 5.7 lists examples of the most widely used second order texture measurements using the GLCM texture measurements and a brief description for each method is as follows:

5.3.1.1.1 Contrast oriented group

The texture calculation methods included in this category maximize the difference in pixel values. It is assumed that the pixel values located in the diagonal of the gray-tone spatial-dependence matrix are the same and distinctness in values is increased as pixels to identify are away from the diagonal (Hall-Beyer 2007). Depending on the way of considering weights for contrasting, pixel value differences

Table 5.7 Classification of the second order texture calculations by using the gray level co-occurrence matrix. Commonly used components in equations are shown in the notation column. *Sources:* Data from Haralick et al. (1973), Haralick (1979), and Hall-Beyer (2007)

Category	Method	Equation	Notation
Contrast	Contrast	$f = \sum_n n^2 \left[\sum_{\substack{i,j \\ i-j =n}} p(i,j) \right]$	$p(i,j)$ (i,j) th pixel in a normalized gray level co-occurrence matrix,
	Dissimilarity	$f = \sum_n n \left[\sum_{\substack{i,j \\ i-j =n}} p(i,j) \right]$	$\frac{P(i,j)}{R}$
	Homogeneity [†]	$f = \sum_i \sum_j \frac{1}{1 + (i-j)^2} p(i,j)$	where, R is the normalizing constant
Orderliness	ASM	$f = \sum_i \sum_j (p(i,j))^2$	N_g Number of gray levels in an image to evaluate
	Maximum probability	$Max_{i,j} p(i,j)$	
Descriptive statistics	Entropy	$f = - \sum_i \sum_j p(i,j) \log(p(i,j))$	\sum_n
	Mean [‡]	$\mu_i = \sum_i \sum_j ip(i,j), \quad \mu_j = \sum_i \sum_j jp(i,j)$	\sum_n
	Variance [‡]	$\sigma_i^2 = \sum_i \sum_j p(i,j)(i - \mu_i)^2, \quad \sigma_j^2 = \sum_i \sum_j p(i,j)(j - \mu_j)^2$	\sum_i
	Standard deviation [‡]	$\sigma_i = \sqrt{\sigma_i^2}, \quad \sigma_j = \sqrt{\sigma_j^2}$	\sum_j
	Correlations	$f = \sum_i \sum_j p(i,j) \left[\frac{(i - \mu_i)(j - \mu_j)}{\sqrt{(\sigma_i)^2(\sigma_j)^2}} \right]$	

[†] Also known as Inverse Difference Moment. [‡] Depends on the reference (i) or neighbouring cells (j).

can be increased exponentially (contrast), linearly (dissimilarity), or decreased exponentially (homogeneity) as involved pixels are apart from the diagonal (Table 5.7). The contrast method has ranges of zero to q^2 , where q is the length of the gray-tone spatial-dependence matrix (Honeycutt and Plotnick 2008). For a single constant pixel the contrast value would be zero. Ranges of the homogeneity can be defined as zero to one (Honeycutt and Plotnick 2008), where one is for a constant pixel value observed in the diagonal of the gray-tone spatial-dependence matrix, and this indicates an inverse relationship between contrast and homogeneity texture calculations.

5.3.1.1.2 Orderliness based group

The orderliness in texture calculations would help find a regular trend in images (Hall-Beyer 2007). The degree of regularity is then determined by the number of paired pixels having a same value and weights are, therefore, assigned based on the degree of orderliness. Examples that are based on this orderliness texture calculation would include the angular second moment (ASM), maximum probability, and entropy methods (Kaplan 2006; Hall-Beyer 2007). The angular second moment (ASM) technique, also known as the energy or uniformity, utilizes the gray-tone spatial-dependence matrix as its own weights (Table 5.7) and measures the homogeneity in images (Tahir et al. 2005). It shows the higher ASM values, the more orderly or regularly arranged location variation in pixel values of the image. The ranges in values computed by the ASM method are zero to one, where one represents a single constant image (Honeycutt and Plotnick 2008). Maximum probability finds the largest value in gray level co-occurrence matrix (Table 5.7). Hall-Beyer (2007) noted despite its simple idea, the actual calculations are relatively difficult to make suitable results, which compared to other orderliness based texture measures. The entropy method, which is shown in Table 5.7, is inversely related to ASM (Tahir et al. 2005), and calculates the disorder of the local distribution of paired pixel values in images. This, paradoxically, can explain the orderliness.

5.3.1.1.3 Descriptive statistic group

Similar to the first order texture calculations, major statistic descriptors can be used for the second order texture calculation within the gray-tone spatial-dependence

matrix (Hall-Beyer 2007). Hall-Beyer (2007) mentioned that under the GLCM texture measurements, the statistic descriptor should consider the frequency of paired pixel values. As previously pointed out, the relationship of paired pixels is represented by the gray-tone spatial-dependence matrix. The major statistic or probabilistic descriptors may include mean, variance or standard deviation, and correlation (Kaplan 2006; Hall-Beyer 2007) and are illustrated in Table 5.7. The correlation can be used as an index to identify a linear dependency of a reference pixel to the neighbouring pixels along designated direction and distance over the whole image (Hall-Beyer 2007; Honeycutt and Plotnick 2008; Bremananth et al. 2009). According to the Hall-Beyer (2007), the texture calculation by the correlation method is relatively different, thus it can be used as a verification tool for other texture measures. The range of values obtained from this method is from negative one to one (Honeycutt and Plotnick 2008; Bremananth et al. 2009), where zero is uncorrelated whereas one represents completely correlated (Hall-Beyer 2007).

In this study, texture analysis is employed to identify the geomorphological landslide controlled features and evaluate the efficiency for the landslide inventory mapping by using texture characteristics. Among various texture measures introduced in Table 5.7, one representative texture method in each group is utilized as follows: (1) contrast; (2) entropy; and (3) correlation. Texture calculations are helped by the texture module (Antoniol et al. 2008) integrated in the GRASS (Geographic Resources Analysis Support System) GIS. The module can enable texture calculations by following procedures: (1) importing a raster data from the DEM if the DEM is not a raster format; (2) reclassifying the imported image if it has values over 255; and (3) calculating textures in four directions (north-south, east-west, and two diagonals). Size of the moving window and distance between two pixels can be selected by a user. A LiDAR derived DEM having a cell size of 2.5 by 2.5 metres is exploited for the input raster imagery. Reasons for using a relatively small scaled DEM are mainly due to the computing limitation and difficulty to present the overall view of texture in large scaled area. A total of eight neighbouring cells are exploited for the moving window (3×3) and value of one for the distance between pixels is selected for the analysis. Calculated four texture values are then averaged to show a general view of roughness and smoothness of the study area. Same procedures are applied to the Landsat 7 orthoimages which has multi-spectral bands in order to evaluate the applicability of the LiDAR derived DEM comprising a single spectral band. Following images illustrate results of the texture analysis in the study area.

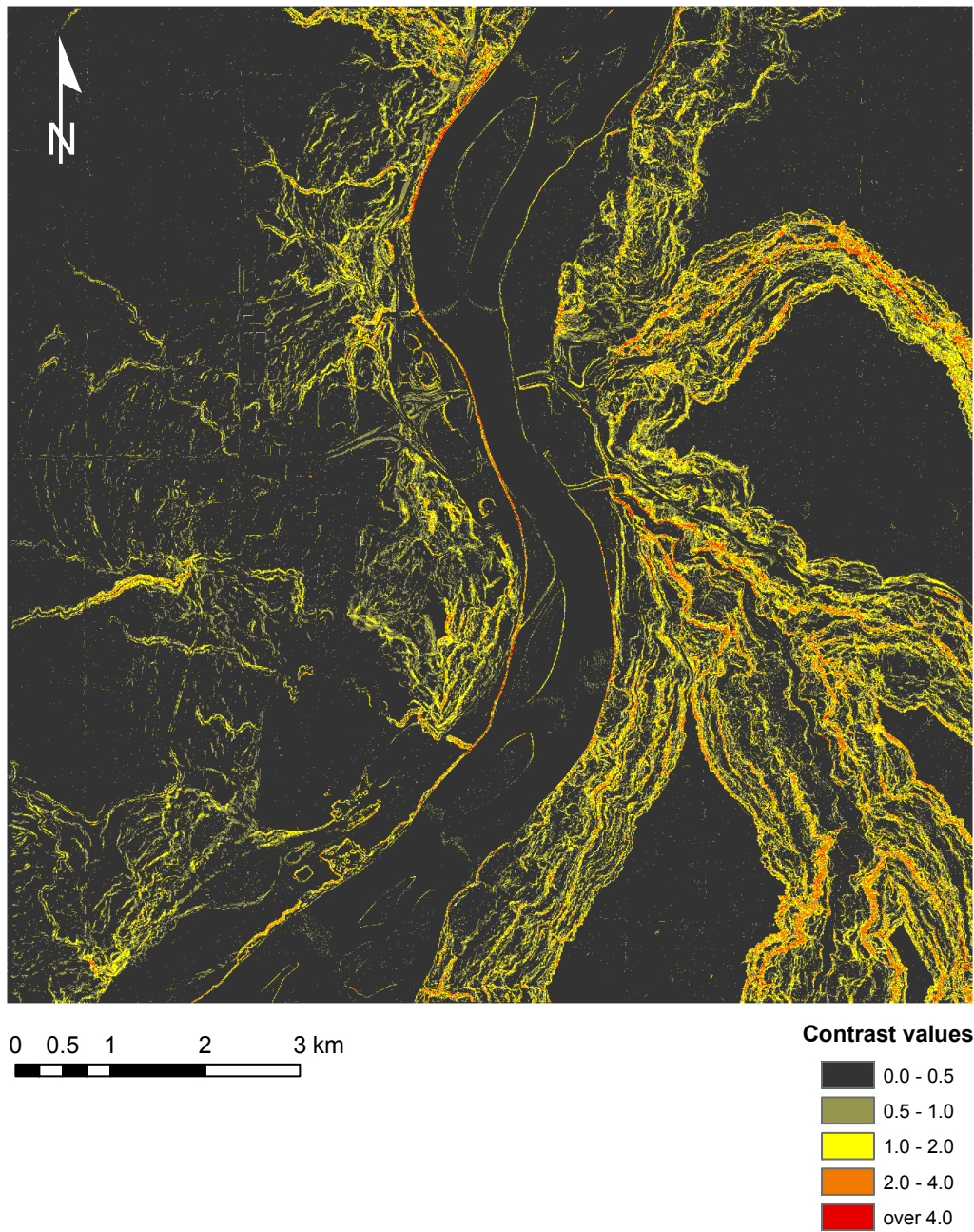


Figure 5.18 Contrast texture analysis applied to the study area. The cell size is 2.5 by 2.5 metres. The degree of contrast values are illustrated in the legend. Contrast values are generated from the digital elevation model shown in Figure 5.4, which is modified to a 2.5 by 2.5 metre resolution for the texture analysis

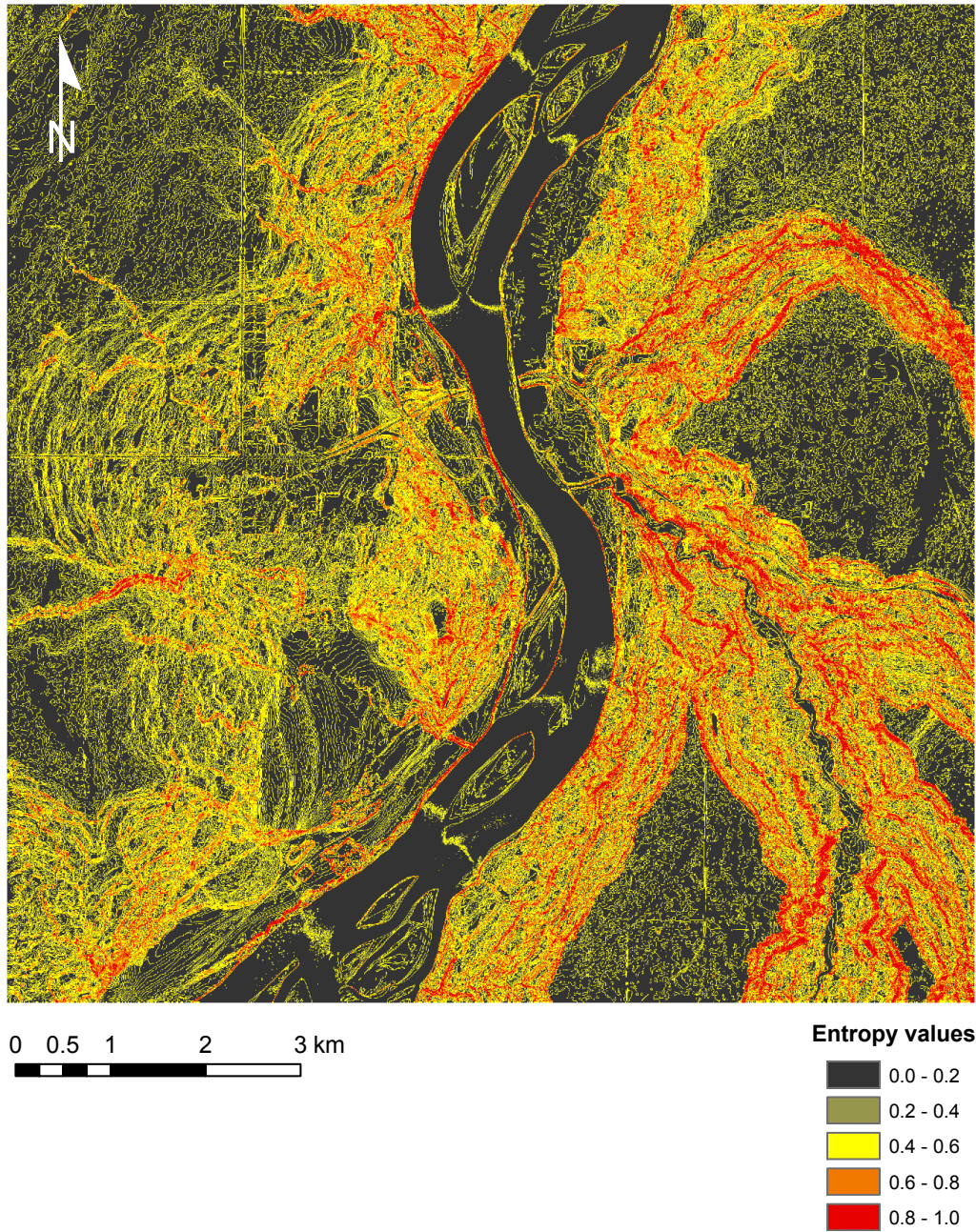


Figure 5.19 Entropy texture analysis applied to the study area. The cell size is 2.5 by 2.5 metres. The degree of contrast values are illustrated in the legend. Contrast values are generated from the digital elevation model shown in Figure 5.4, which is modified to a 2.5 by 2.5 metre resolution for the texture analysis

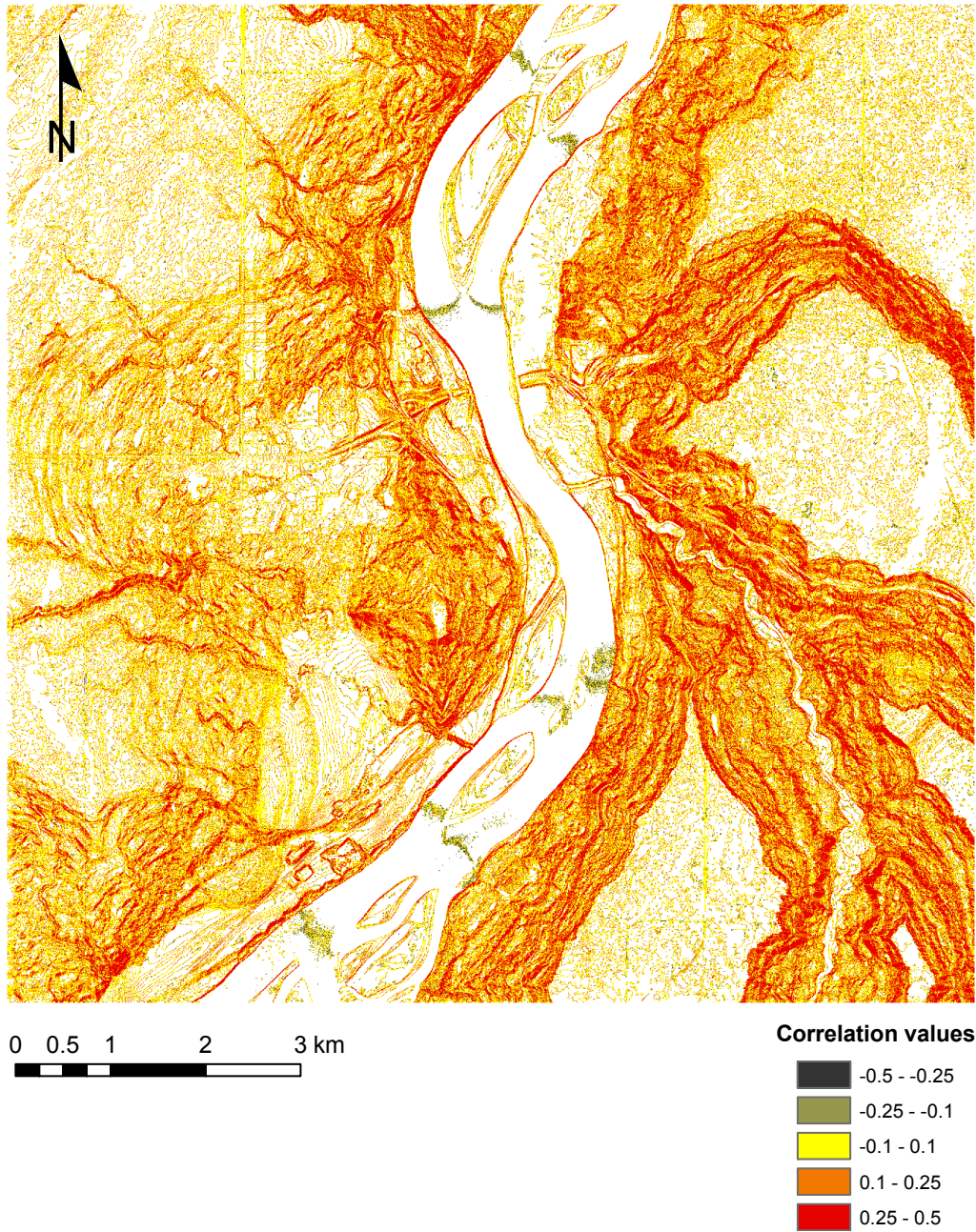
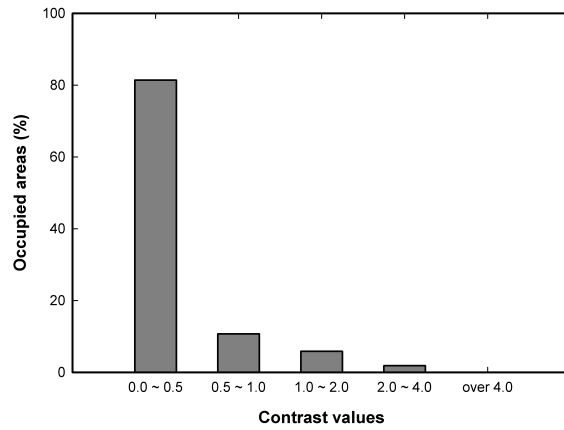


Figure 5.20 Correlation texture analysis applied to the study area. The cell size is 2.5 by 2.5 metres. The degree of contrast values are illustrated in the legend. Contrast values are generated from the digital elevation model shown in Figure 5.4, which is modified to a 2.5 by 2.5 metre resolution for the texture analysis

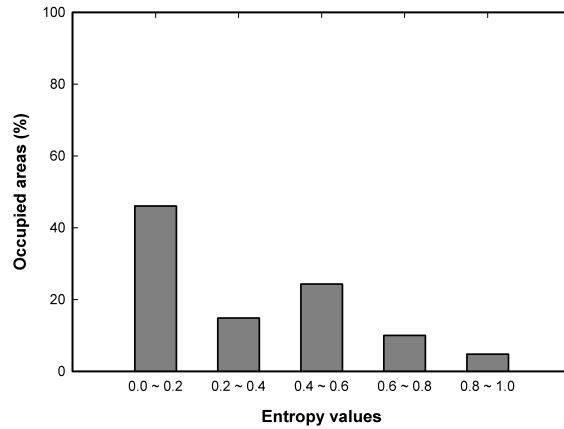
The texture value distribution for the study area based on the contrast method is shown in Figure 5.18. As previously described in the text, the difference of pixel values are increased exponentially in the contrast method, therefore the discrepancy of gray levels in pixels are well illustrated by this method. Areas of low contrast values of zero to 0.5 mean that constant pixel values are estimated on those areas and consequently indicate as flat areas (81 % of the evaluated areas). Most uplands in east and west banks of the Peace River are included. On the other hand, areas adjacent river valleys show high contrast values of over two in contrast values which represent significant gray level differences and rough surfaces (2.1 % of the evaluated areas). Especially lower margins of the west bank of the Peace River and slopes of deeply incised river valleys along the Heart River and Pat's Creek show the highest values (contrast values of over four). The spatial distribution of contrast values and their occupying areas in the study area is presented in Figure 5.21a.

Figure 5.19 shows the spatial distribution of the texture calculation by the entropy method (Table 5.7). An entropy can identify the disorder, or randomness, in the local distribution of paired pixel values. Having the range of zero to one, the higher entropy values would indicate the more considerable random distribution in gray levels on the areas. High entropy values over 0.6 occupied about 15 percent of the evaluated study area and can be observed on valley slopes along tributaries of the Peace River, easterly aspect of Misery Mountain, toes of the west bank along the Peace River, and some surficial drainages on the west bank of the Peace River of the study area (Figure 5.19). Identified relatively rough surfaces by the entropy method would happen to correspond to those obtained from the contrast method. However the clear distinction between rough and smooth surfaces may seem to be difficult compared to the results by the contrast method. One possible explanation can be stated that this may be due to characteristics raised by the entropy method itself, whose objective is to identify the arrangement rather than the contrast or comparison. Figure 5.21b describes the spatial distribution of entropy values where values between zero and 0.2 have the largest portions (46 %) in the evaluated area followed by those ranged from 0.4 to 0.6 (24 %).

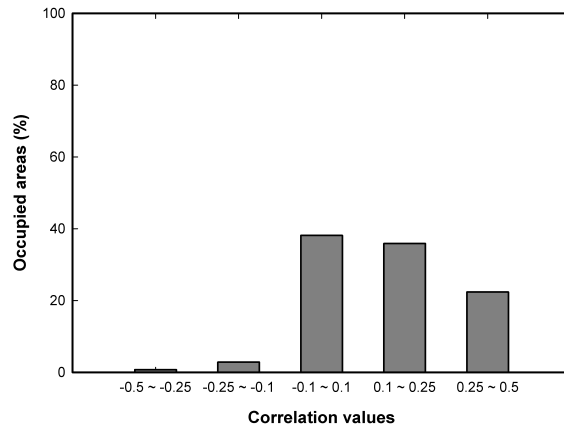
The other texture analysis is performed by the correlation method and illustrated in Figure 5.20. As previously pointed out, a linear relationship of paired pixels can be identified by this method. As resulting values are approach one, the probability of having constant values (black to black or white to white pixels) in paired pixels is increased (positively correlated). On the contrary, paired pixels would have oppo-



(a)



(b)



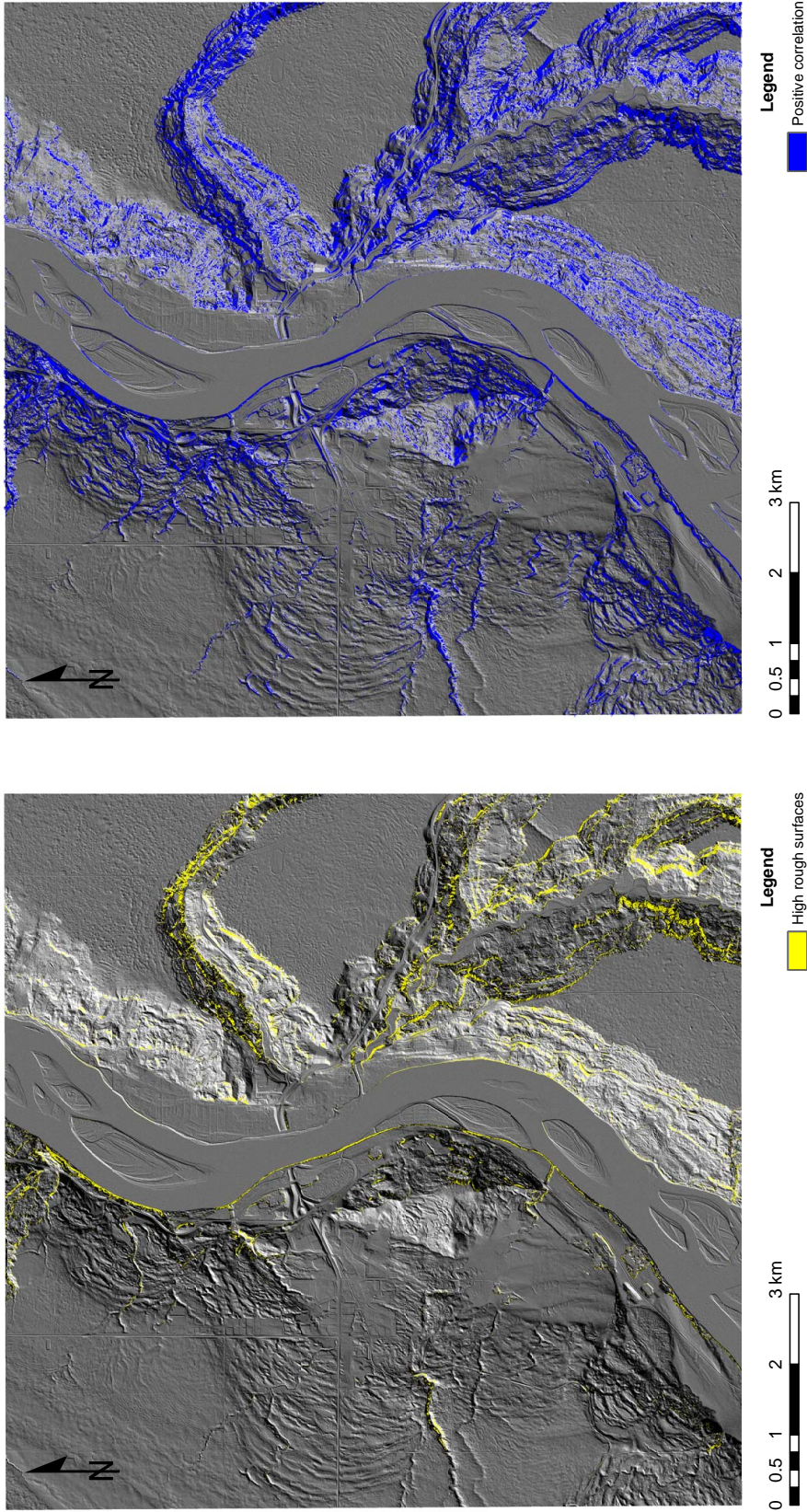
(c)

Figure 5.21 Spatial distribution of three texture values for the study area. a. Contrast. b. Entropy. c. Correlation. Percentage areas occupied by each texture value are located in the ordinate while classes of texture values presented in Figures 5.18 to 5.20 are shown in the abscissa

site pixel values (black to white or white to black pixels) when they are closed to negative one (negatively correlated). As indicated in Figure 5.20, calculated correlation values are within ranges between -0.5 and 0.5. The uncorrelated value of zero is observed in the study area occupying very small portions (0.02 %) in correlation values. The spatial distribution of correlation values is presented in Figure 5.21c. The spatial pattern generated from positive correlation values (0 to 0.5) shows a similar rough surface distribution to those obtained by both contrast and entropy methods (Figure 5.22b). From this observation it is postulated that there is a close relationship between surface texture and positive correlation. The spatial distribution of negatively correlated values (-0.5 to 0), however, has no distinct pattern especially in the study area.

Combining information with regard to rough surfaces that obtained from both contrast and entropy methods would provide a practical guideline for determining the potential high rough areas which may represent geomorphological landslide controlled features in the study area. Values for the contrast over two and for the entropy over 0.8 are used for the clear differentiation of relatively high potential rough areas from others. Figure 5.22a illustrates some efforts on this practice. The identified areas cover two percent of evaluated study area and are concentrated along the major river valleys: (1) toes of the easterly aspect Peace River valley (west bank); (2) southeast valley slopes of the westerly aspect Peace River valley (east bank); and (3) valley slopes along tributaries of the Peace River. The spatial pattern obtained from correlation values shown in Figure 5.22b well indicates the influence of the linear dependency of paired pixel values to the evolution of the surface texture.

It is generally known that the textural information based on multispectral imageries is more acceptable than those in a single band (Kaplan 2006). Based on results of this study, however, a single band imagery which is derived from the high resolution DEM also generated suitable results for identifying geomorphological landslide controlled features that can be seen in landslide areas if provided with a high resolution imagery data. One possible issue is the limited use of high resolution multispectral imageries. Examples of the texture analysis on a small scaled multispectral satellite imagery are presented in Figure 5.23. Comprising three bands of multispectral imageries which are adapted from the Landsat 7 orthoimages, it showed a slightly different distribution field of the textural surface based on each spectral band after analyzing with the contrast method. Due to the low resolution of imageries (cell size: 15 by 15 metres, scale: 1:50,000), the result could not present



(a)

(b)

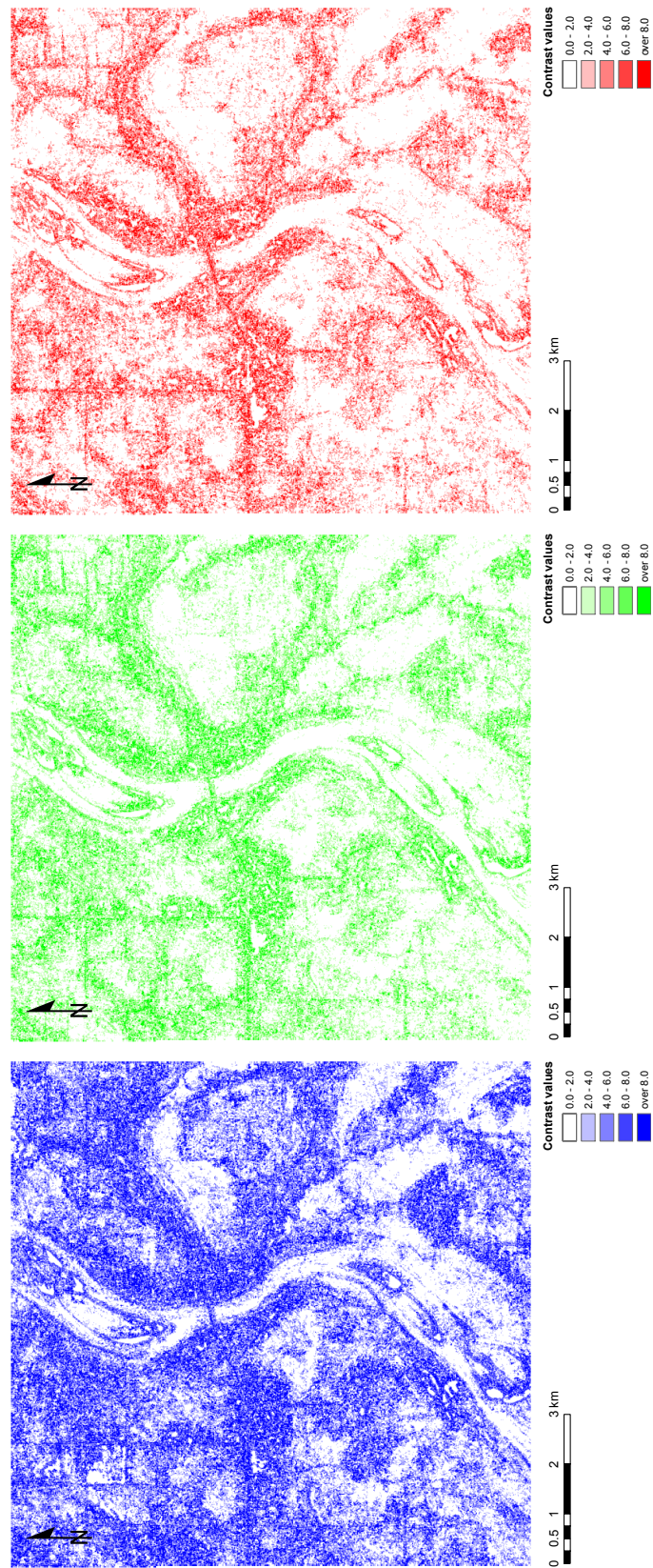
Figure 5.22 Identification of potential rough areas. a. High roughness areas generated by intersecting specific texture values from contrast (over 2) and entropy (over 0.8) methods presented in Figures 5.18 and 5.19. b. Spatial pattern obtained from positive (0 to 0.5) correlation values shown in Figure 5.20. A shaded relief image shown in background is obtained from the digital elevation model (Figure 5.4) having a cell size of 0.5 by 0.5 metres

a clear distinction between rough and smooth surfaces. The texture analysis by using a high resolution single band imagery would provide more accurate information rather than those from low resolution multispectral imageries.

The texture analysis is a simple and versatile method to support a geomorphologic surface classification for the land use. It can make significant results directly from almost all pixel based remote sensing imageries (Kaplan 2006). It also enables one to evaluate overall roughness and smoothness of an image based on distribution and frequency of gray levels contained in the pixel (Whitworth et al. 2005). Differentiating rough and smooth areas can be utilized to identify previous landslide features placed on the ground surface and moreover provide valuable information for the landslide inventory mapping in which conventional methods cannot recognize.

I carried out a similar analysis to slopes on landslide deposits (Section 5.1.3) by using the texture analysis. Results of the texture analysis confined to previous landslide deposits are shown in Figure 5.24. As described in the slope analysis in Section 5.1.3, identifying distinct characteristics observed on landslide deposits by texture parameters can support the slope model proposed in the study and lead to more reliable results in understanding landslide hazards and their states. From the spatial distribution of texture values, the mean texture value using the contrast method (Table 5.7) for all landslide deposits is calculated as 0.72. Mean texture values are different when landslide deposits are grouped by locations such as the east and west. For example, the mean texture value for landslide deposits on the east bank is 179 percent of the mean texture value observed on the west bank. The standard deviations of texture values within landslide deposits are also calculated as 0.67 in the east bank which is 175 percent of the value on the west bank (0.38). Appendix E shows the detailed information with regard to the texture analysis on previous landslide deposits.

The difference of distributions in mean texture values based on their locations clearly shows geomorphological characteristics observed in the study area. Only four landslide deposits which are over the mean texture value of 0.72 are on the west bank whereas 61 landslide deposits are observed on the east bank (Figure 5.25). These make 11 and 55 percent of landslide deposits on each bank. Four landslide deposits found on the west bank, Deposit ID 35, 89, 99, and 130, are concentrated on slopes in Misery Mountain and the Mile 50.9 Slide area. These are consistent with landslide deposits whose slope values are above the mean slope



(a)

(b)

(c)

Figure 5.23 Texture analysis on a small scaled multispectral satellite imagery. a. Band 1 (blue-green). b. Band 2 (green). c. Band 3 (red). The contrast texture method is used to determine the surface texture. The satellite imagery is adapted from the Landsat 7 orthoimages (cell size: 15 by 15 metres, scale: 1:50,000). *Source:* Data from GeoGratis (Natural Resources Canada 2010)

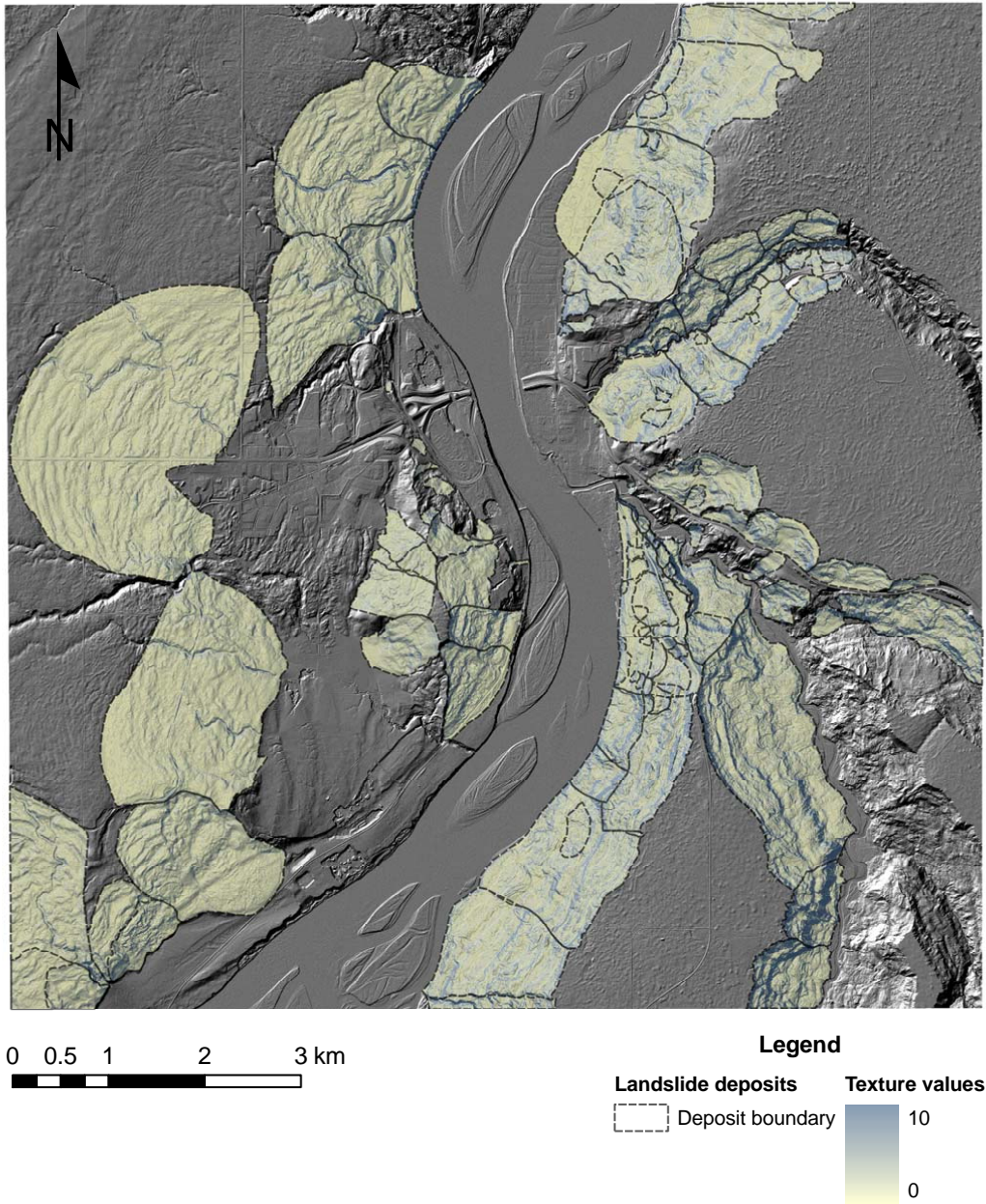


Figure 5.24 Spatial distribution of the texture analysis within landslide deposits. The variation of texture values is presented by the legend. Texture values are obtained by using the contrast method (Table 5.7) and generated from the digital elevation model shown in Figure 5.4, which is modified to a 2.5 by 2.5 metre resolution for the texture analysis. A hillshade imagery presented in the background is obtained from the digital elevation model (Figure 5.4) with the spatial resolution of 0.5 by 0.5 metres

values of 17 degrees (Figure 5.13), especially they are within boundaries between slopes which are obtained from fully softened and residual friction angles (19 to 22 °). The spatial distribution of landslide deposits whose mean texture values are over the average value of 0.72 is presented in Figure 5.26.

From the geomorphic perspective, analyzed texture values can support the postulation that ground surface profiles on the east bank of the Peace River are apparently rougher than those observed on the west bank based on the distribution of mean texture values. This finding is consistent with results obtained from the slope analysis (Section 5.1.3). Therefore, the texture analysis using tonal changes on the ground surface might provide useful information for constructing the landslide hazard assessment proposed in this study even though the procedure in this methodology for acquiring concrete results is apparently different from the slope analysis.

5.3.1.2 Statistical evaluations of the orientation data

Another methodology for determining geomorphological landslide controlled features is the statistical exploitation of axial orientation data in a three dimensional space. Firstly, the vector strength and dispersion analysis is discussed here and eigenvalue analysis is reviewed later.

5.3.1.2.1 Vector strength and dispersion analysis

Analyzing a terrain, whether rough (random) or smooth (even), is an important part for many scientific studies, in which understanding a terrain is essential for further explorations (Sappington et al. 2007). Many methodologies, therefore, have been proposed and the texture analysis described above is one of them. The roughness or ruggedness analysis is another methodology for quantifying the evolution of the terrain. It describes geomorphological features derived from DEM by relating the surface roughness to surface characteristics such as elevation, slope, and aspect. It is unlike texture analysis, which uses differences in gray tones and sometimes requires converting DEM to rescaled raster data.

The status of the terrain geometry is also a essential component for biologists in identifying appropriate habitats for many wildlife species (Beasom et al. 1983). One preliminary approach for analyzing the surface ruggedness used by biologists

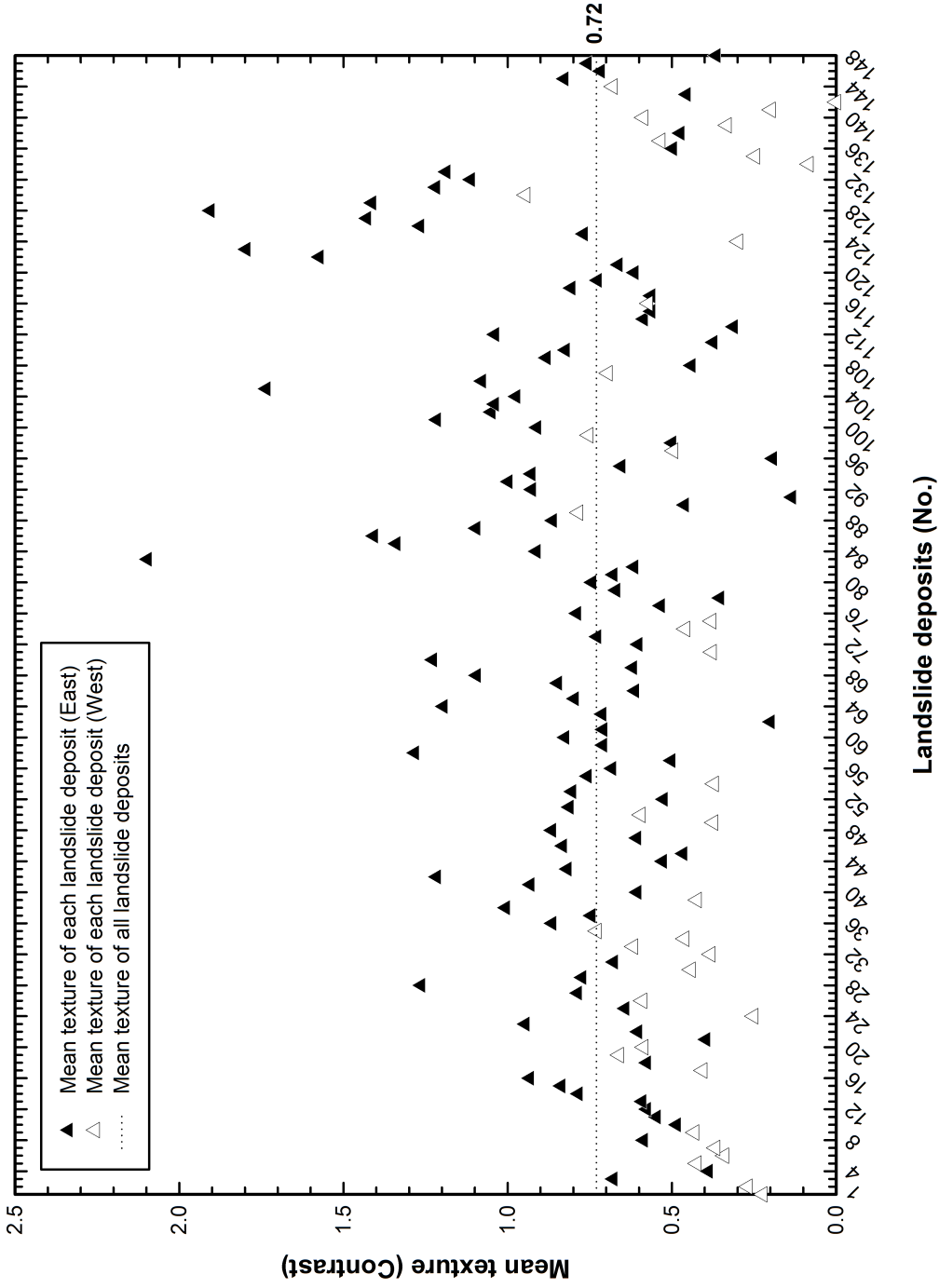


Figure 5.25 Mean texture values of previous landslide deposits observed in the study area. Landslide deposits denoted by the unique number are presented in the abscissa while corresponding average texture values are shown in the ordinate. Landslide deposits are grouped, either the west or east, based on the location where they were identified. The horizontal line represents the average texture value for all landslide deposits. Detailed information for landslide deposits are also presented in Appendix E

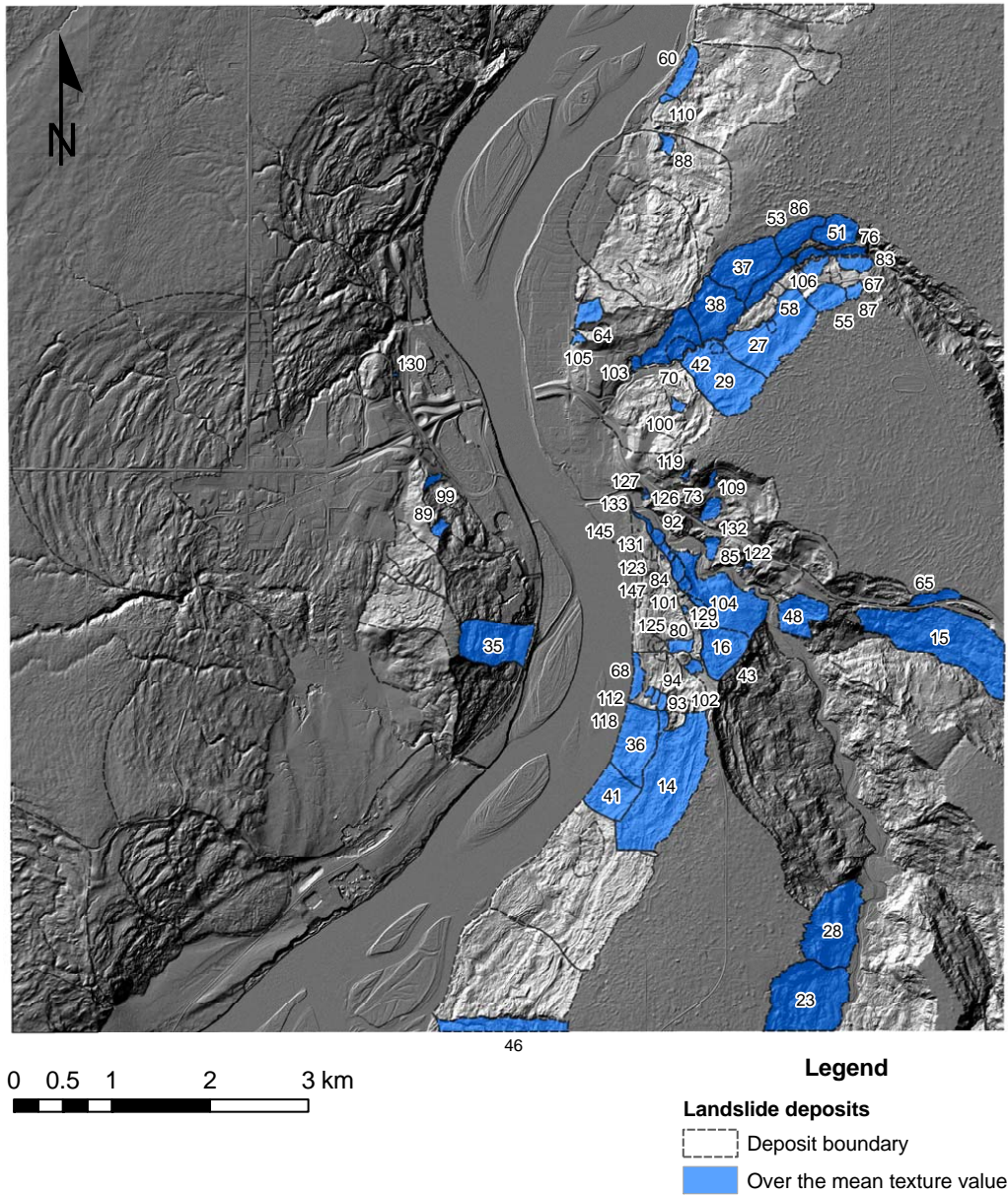


Figure 5.26 Geographical distribution of landslide deposits whose mean texture values are over the average value for all landslide deposits. A hillshade imagery presented in the background is obtained from the digital elevation model (Figure 5.4) with the spatial resolution of 0.5 by 0.5 metres

is the land surface ruggedness index, or LSRI, developed by Beasom et al. (1983). Relating the terrain roughness to the total length of contour lines, which in turn are the function of the number of contour lines, they classified the degree of the terrain roughness into three groups: (1) flat; (2) rolling; and (3) rugged areas (Figure 5.27). LSRI values are low in flat areas whereas they are higher when terrains transform from flat to rolling, and rugged areas. The greatest disadvantage of this method is in the unproductive, time-consuming procedures calculating the total length of contour lines within the study area if study areas are too large (Riley et al. 1999).

Another method to quantify the topographic heterogeneity is the terrain ruggedness index (TRI) developed by Riley et al. (1999). The TRI values are derived from the USGS DEM and calculated by summing squared differences in elevation changes between a reference cell of a square kilometre and eight neighbouring cells. Taking a square root for these summed values provides TRI values. The following equation well explains the concept of the TRI method (Riley et al. 1999):

$$TRI = \sqrt{\sum (x_{ij} - x_{ref})^2} \quad (5.6)$$

where, x_{ij} is the elevation values stored in cells surrounding a reference cell, x_{ref} . Similar to LSRI values, TRI values are low for flat terrains whereas steep and rugged regions would present relatively higher TRI values. Based on the degree of TRI values, Riley et al. (1999) grouped a TRI value distribution in seven classes: (1) level; (2) nearly level; (3) slightly rugged; (4) intermediately rugged; (5) moderately rugged; (6) highly rugged; and (7) extremely rugged. Their ranges of TRI values are from 0 to 4,367 metres. Major issue which might come from implementing the TRI method is that TRI values, as with those obtained from the LSRI method, are highly dependent of elevation values only. Recent studies revealed that a high inclination to one factor, especially the elevation and following slope values, may mislead in differentiating steep, low ruggedness terrains from steep, high ruggedness terrains (Sappington et al. 2007).

Based on sophisticated mathematical procedures for determining surface roughness parameters, Hobson (1972) described various methods in order to identify parameters which stand for the terrain roughness and introduced their computational approaches using FORTRAN languages. These are as follows: (1) comparison of actual surface and corresponding planar areas; (2) identification of the bump fre-

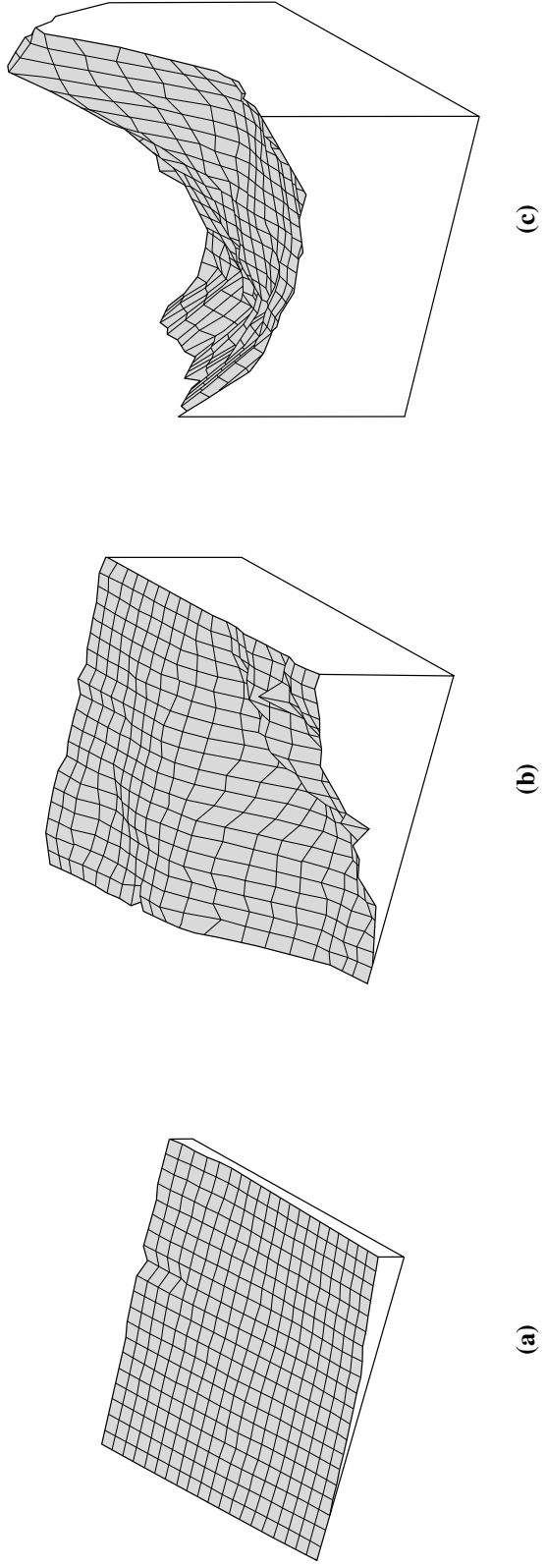


Figure 5.27 Diagrams representing different surface roughnesses. a. Flat area (western Texas). b. Rolling hill (western Texas). c. Rugged area (central Colorado). A grid of each diagram represents one hectare, therefore, the total area amounts 400 hectares, respectively. *Source:* Beasom et al. 1983, Figure 1

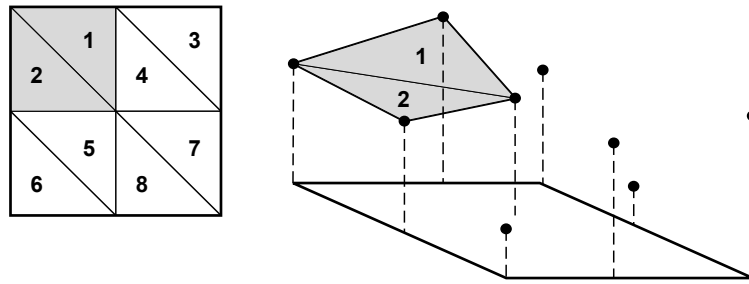
quency distribution by measuring changes of the topographic elevation; and (3) analyzing distribution and orientation of topographic surfaces. Among them the third method is investigated further to determine the surface roughness for this study.

Hobson (1972) hypothesized the geomorphologic surface in a domain can be divided into a set of planar surfaces connecting one after another. The orientation of those planar surfaces is then calculated in the form of unit vectors normal to the planar surface. He then speculated that if the geomorphologic surface is rough or random, the sum of the magnitude of unit normal vectors is small but their dispersion is severe, whereas for a smooth geomorphologic surface their magnitude is high and the dispersion of their orientation is low (Figure 5.28). Therefore, corresponding relationships between these unit vectors and the surface roughness can be established by using two vector geometries such as the strength, also known as the magnitude, and the dispersion of vectors which were evaluated by many authors (Fisher 1953; Watson 1956; Watson and Irving 1957; Watson 1965, 1966). Defining the orientation of the vector is accomplished by direction cosines (Watson 1966; Groshong, Jr. 2006). Decomposing the unit vector normal to the planar surface into their three components, x , y , and z , is presented in Figure 5.29. By using direction cosines, each component of the unit normal vector can be expressed as follows (Sappington et al. 2007):

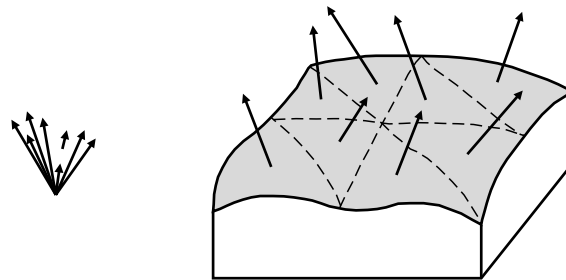
$$\begin{aligned}
 z &= 1 \cdot \cos \alpha = \cos \alpha \\
 xy &= 1 \cdot \sin \alpha = \sin \alpha \\
 x &= xy \cdot \sin \beta = \sin \alpha \sin \beta \\
 y &= xy \cdot \cos \beta = \sin \alpha \cos \beta
 \end{aligned}
 \tag{5.7}$$

The vector strength is the index of the surface roughness and equivalent to the length of the resultant sum of unit vectors normalized by the number of unit vectors (Fisher 1953; Pincus 1956; Watson 1966; Hobson 1972). In a mathematical form the vector strength can be presented as follows:

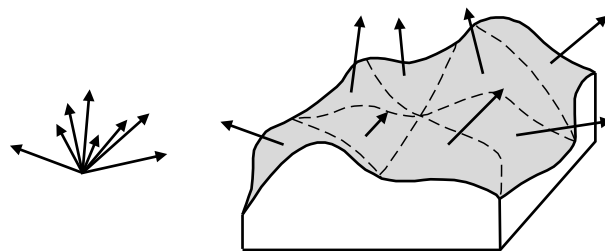
$$\text{Vector strength} = \frac{R}{N} = \frac{\sqrt{(\sum x)^2 + (\sum y)^2 + (\sum z)^2}}{N}
 \tag{5.8}$$



(a)



(b)



(c)

Figure 5.28 Characteristics of distribution and orientation in topographic surfaces. a. Plan view of planar surfaces (left) depicting geomorphologic surfaces (right). b. Distribution of unit vectors normal to geomorphic smooth surfaces. Normal vectors (right) on the smooth planar surface would have a preferred orientation (left). c. Distribution of unit vectors normal to geomorphic irregular surfaces. Normal vectors (right) on the rough planar surface would have a non-preferred orientation (left), and showing a scattered trend. *Source:* Hobson 1972, Figure 8.3

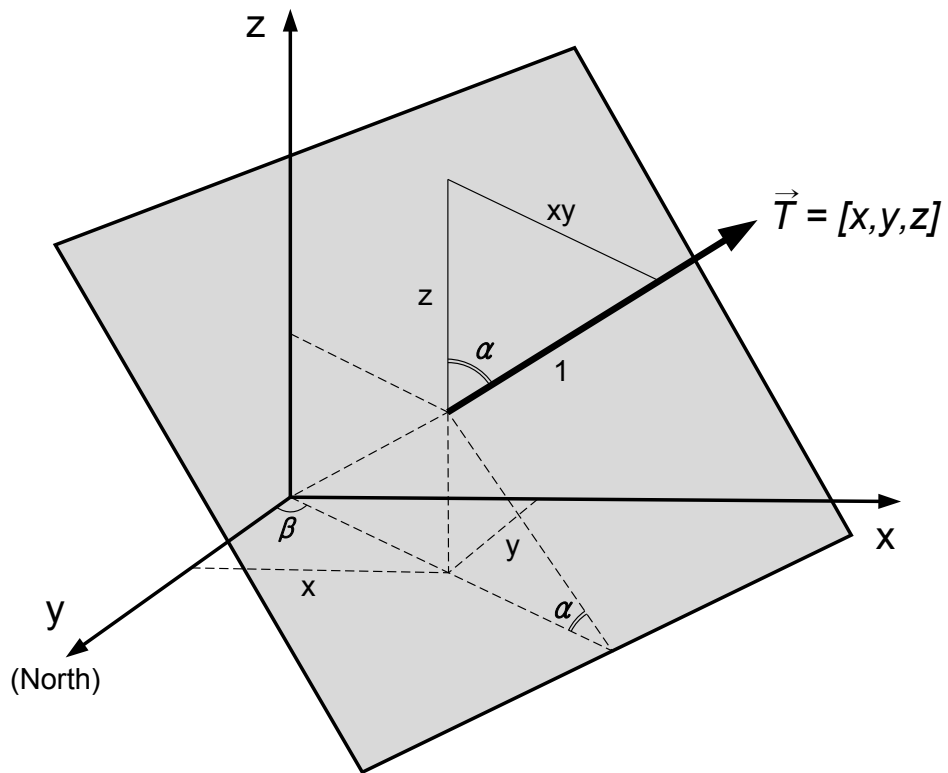


Figure 5.29 Decomposition of the unit vector orthogonal to the planar surface. A planar surface is illustrated by using a gray shade. The unit vector can be disassembled into three components, x , y , and z . Dashed lines in the figure are assumed to be located beneath the planar surface whereas solid lines are treated as to be placed above the surface. Each component is presented by directional cosines which include slope (α) and aspect (β). *Source:* Sappington et al. 2007, Figure 2

where R is the length of the resultant sum of unit vectors and N is the number of unit vectors. Hobson (1972) noted that the range of the vector strength has values of zero (no preferred orientation) to one (preferred orientation). The vector dispersion indicates the degree of scattering in unit vectors and is equivalent to the standard deviation in normal density functions, either linear (Gaussian) or circular (von Mises) (Pincus 1956). The vector dispersion ranges from zero, where uniform surface is chosen, and increases depending on the degree of the surface irregularity (Fisher 1953; Watson 1966). This gives the following equation (Watson 1966):

$$\text{Vector dispersion} = N - R \quad (5.9)$$

Equation 5.9 indicates that as the R approaches N , the unit vectors tend to be clustered, or have a preferred orientation and consequently leads to decrease in values of the vector dispersion. On the other hand, the vector dispersion increases as the R is decreased by scattering the orientation of unit vectors. Therefore, the vector strength and dispersion values are inversely correlated.

Examples of using these sophisticated mathematical procedures can be found in Grohmann et al. (2009) and Sappington et al. (2007). The former evaluated various surface roughness methods in the Midlands Valley in Scotland at different resolutions of digital elevation models and different sets of moving windows (Grohmann et al. 2009). The latter introduced the vector ruggedness measure (VRM) in which resulting values are obtained from subtracting vector strength from one in order to represent a hemispherical variance (Hodgson and Gaile 1999). Under this relationship one indicates a rough surface whereas zero denotes a smooth area. They used this method to simulate a suitable habitat for Bighorn Sheep living in the Mojave Desert, south western United States.

The three dimensional distribution of vector strength and corresponding vector dispersion over the study area is carried out by the following procedures. First slope and aspect values are calculated from the digital elevation model with the spatial resolution of 2.5 by 2.5 metres. Obtained slope and aspect values are converted to a radian unit then used to calculate direction cosines which described in Figure 5.29 and Equation 5.7. After getting x , y , and z component in form of direction cosines, sums of each component are proceeded by a three by three moving-window. The magnitude of the resultant vector, R , is then obtained by using Equation 5.8. Fi-

nally the vector dispersion is obtained by subtracting the R divided by N , the vector strength, from one, as following Sappington et al. (2007). All cell-based (raster based) calculations and their geographical representations are augmented by ArcGIS. The Python programming language is also used to script the entire processes for implementing same procedures to other particular areas. Figures 5.30 and 5.31 illustrate the spatial distribution of vector dispersion values.

Calculated values for the vector dispersion have ranges from zero to 0.43 which would cover the lower bound of ordinary vector dispersion values (0 to 1). Figure 5.32 shows percentage areas occupied by different vector dispersion values. About 80 percent of the study area has vector dispersion values of less than 0.002. Relatively higher values of over 0.02 only have less than one percent of the study area. They are concentrated on cut banks along the Peace River, point bar areas beneath Misery Mountain, river valleys along tributaries of the Peace River, and areas near surface drainage and transportation routes. These locations are consistent with results obtained from the texture analysis (Figure 5.22). One area having a high value of the vector dispersion is the river valley along the Heart River. A closer look at this area is illustrated in Figure 5.31. Relatively rough areas are observed on lower banks along the Heart River where the river stream erodes the toe of slopes. Higher values are visible especially at cut banks rather than point bars. A high roughness in that area may show the previous status of the Peace River before the massive erosion by the ice melting water right after the ice retreat. Large variations in vector dispersion values are found in the landslide deposits located at lower middle parts of the figure whereas the consistent vector dispersion variations are detected on the uplands and residential areas which may represent a smooth ground surface.

The feasibility of the roughness analysis comparing to the texture analysis is illustrated in Figure 5.33. Figure 5.33 clearly shows differences between two approaches in depicting potential areas containing geomorphological landslide controlled features. While the texture focuses on the two-dimensional attributes of landslide controlled features, the roughness would concentrate on linear aspects of them. These distinct characteristics might be come from the way of controlling input values. In other words, the texture analysis evaluates the degree of gray levels within the extent of the cell or pixel, whereas the vector dispersion deals with the normal vector representing the linear features on the cell or grid. Results of combining these are beneficial especially when landslides features are to be classified based on their components such as main scarps and displaced materials. Therefore,

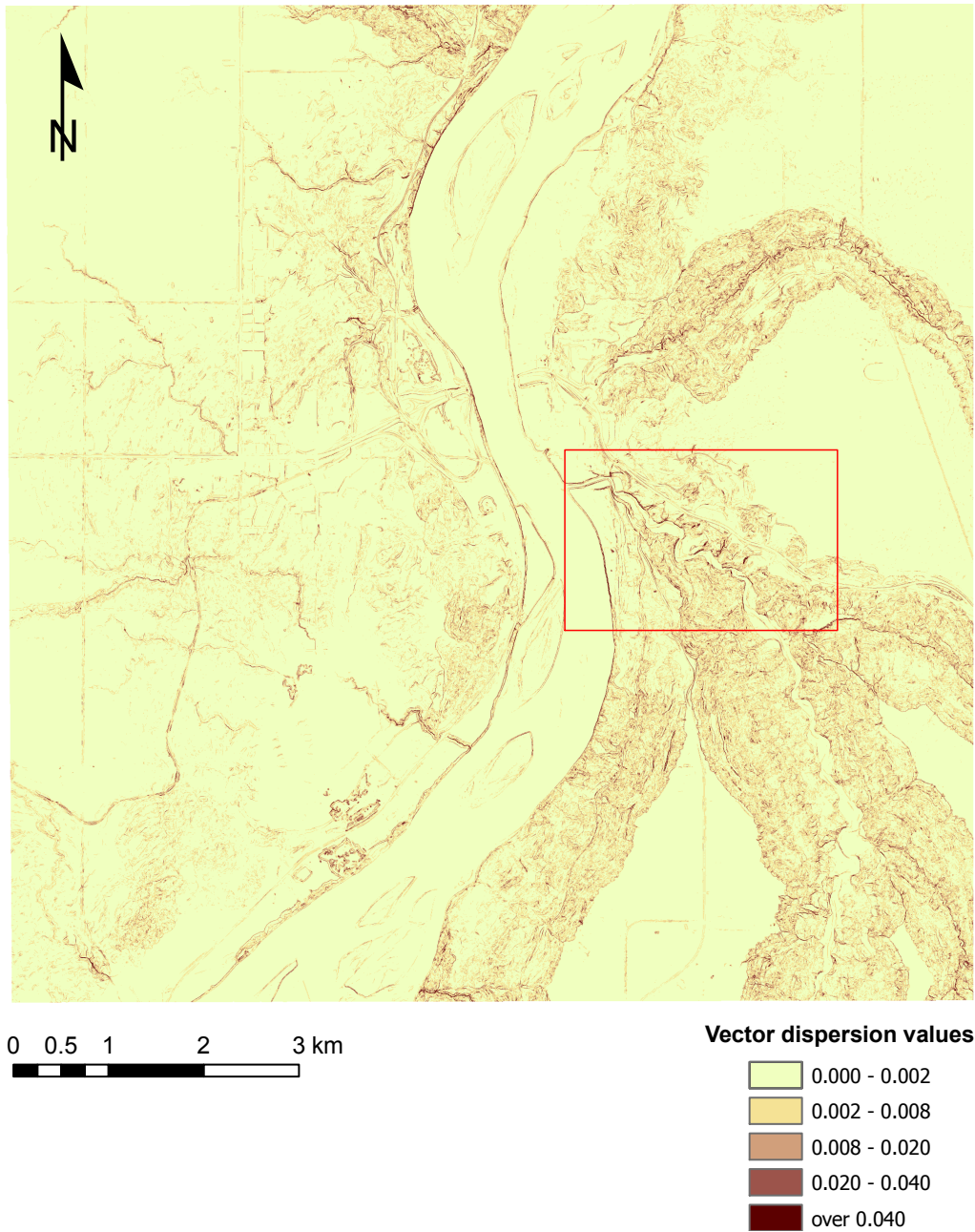


Figure 5.30 Spatial distribution of vector dispersion values in the study area. The cell size is 2.5 by 2.5 metres. Variations of the vector dispersion are shown in the legend. Vector dispersion values are generated from the digital elevation model shown in Figure 5.4, which is modified to a 2.5 by 2.5 metre resolution for the analysis. The area outlined by the red rectangle is illustrated in Figure 5.31

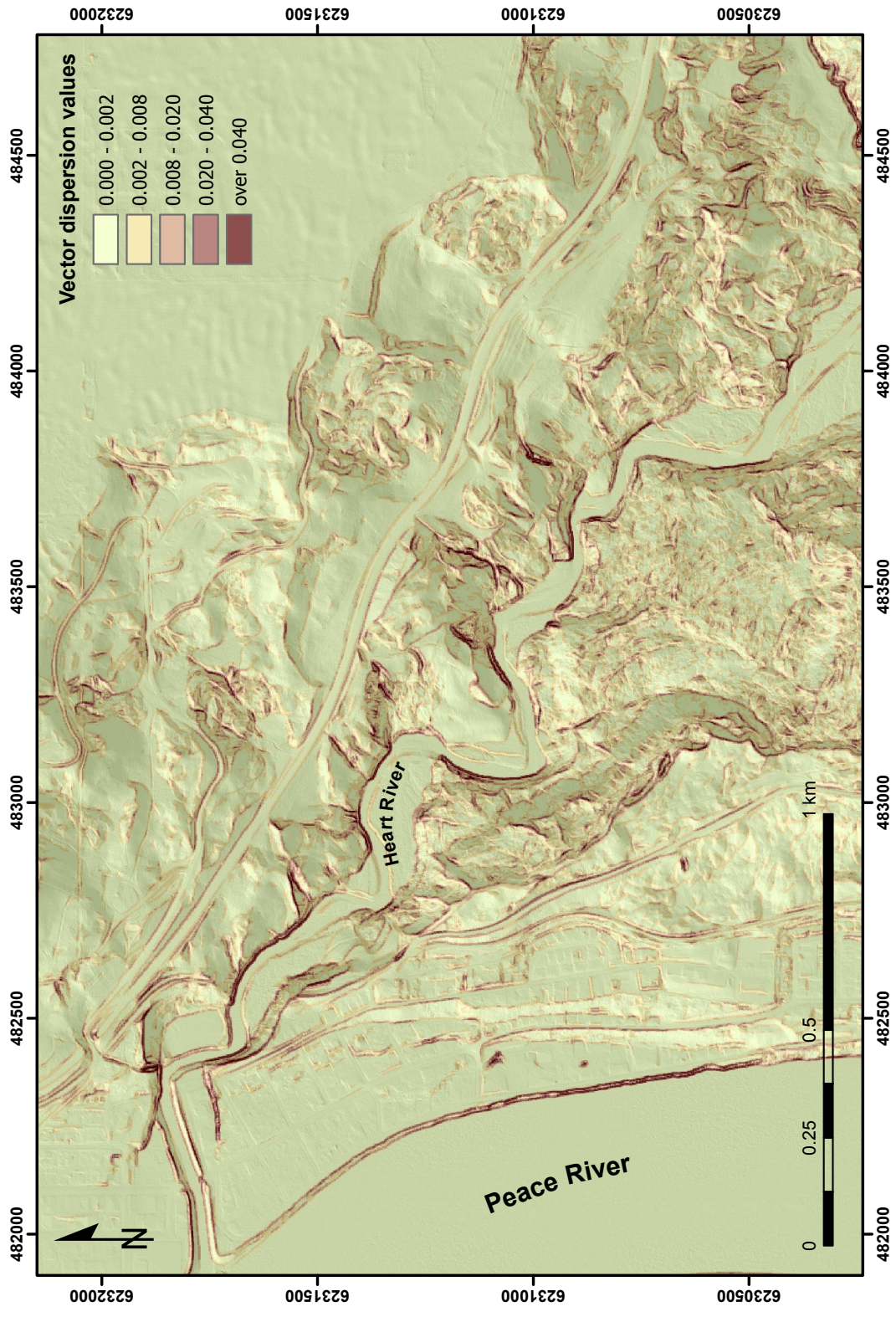


Figure 5.31 A closer look at the vector dispersion distribution in the study area. The location is illustrated in Figure 5.30. Vector dispersion variations are presented by the legend. Peace and Heart Rivers flow northward, northwestward, respectively. A hillshade imagery presented in the background is obtained from the digital elevation model (Figure 5.4) with the spatial resolution of 0.5 by 0.5 metres

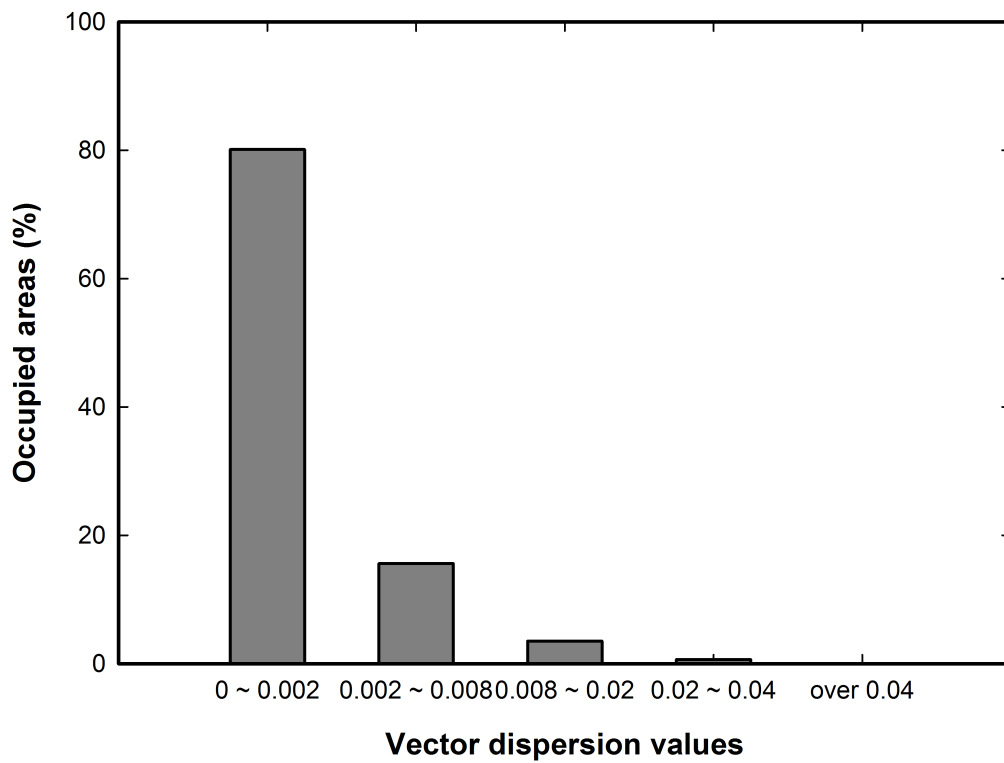


Figure 5.32 Spatial distribution of the vector dispersion values for the study area. The percentage areas occupied by different vector dispersion values are placed in the ordinate while classes of vector dispersion values presented in Figures 5.30 and 5.31 are shown in the abscissa

combining these two methods would provide more accurate delineations for landslide controlled features and produce an appropriate landslide inventory mapping.

Finally, I also carried out the analysis applied to identify the variation of slope (Section 5.1.3) and texture (Section 5.3.1.1) values on landslide deposits in order to determine characteristics of vector dispersion values on them. The distribution of vector dispersion values within identified landslide deposits is shown in Figure 5.34. Obtained values range from zero to 0.24 and they are smaller than those that considered to the entire study area. The calculated mean value of the vector dispersion for all landslide deposits is 0.0038. Mean values by considering the locality of observed landslide deposits can be identified as 0.0043 (for the east bank) and 0.0025 (for the west bank), respectively. Consequently, the standard deviation on the east bank is 170 percent of the value obtained in the west bank (0.0031). The distribution of mean vector dispersion values of each landslide deposit is illustrated in Figure 5.35 and also presented in Appendix E with detailed statistical parameters.

Figure 5.35 shows numbers of landslide deposits whose mean vector dispersion values are over the average value. For example, there are only seven landslide deposits in the west bank of the Peace River whose mean values are higher than the average value of 0.0038. These make 18 percent of landslide deposits located on the west bank of the Peace River. These are mainly placed on slopes of Misery Mountain (landslide deposits of 35 and 89), adjacent to railway (landslide deposits of 137, 139, 140, and 144), and on the Mile 50.9 Slide area (landslide deposits of 130). Moreover, landslide deposits near the railway track even show vector dispersion values which are exceeding 0.01 (landslide deposits of 137 and 144). It is noted that some landslide deposits showing high texture values over 0.7, Deposit ID 35, 89, and 130, also have high vector dispersion values (less than 0.0053) though those of other landslide deposits are much higher.

In the east bank of the Peace River, on the other hand, 59 percent of identified landslide deposits have values over the average and some of them are higher than 0.01 (landslide deposits of 122, 132, 146, and 148). They mainly occupy areas in valley slopes of the Heart River (landslide deposits of 122, 132), the cut bank of the east Peace River valley where bedrock formations are exposed due to the river erosion (landslide deposits of 146), and slope movements adjacent to the road in the town (landslide deposits of 148), which have relatively small extent compared to those whose vector dispersion values are lower than the average. Figure 5.36

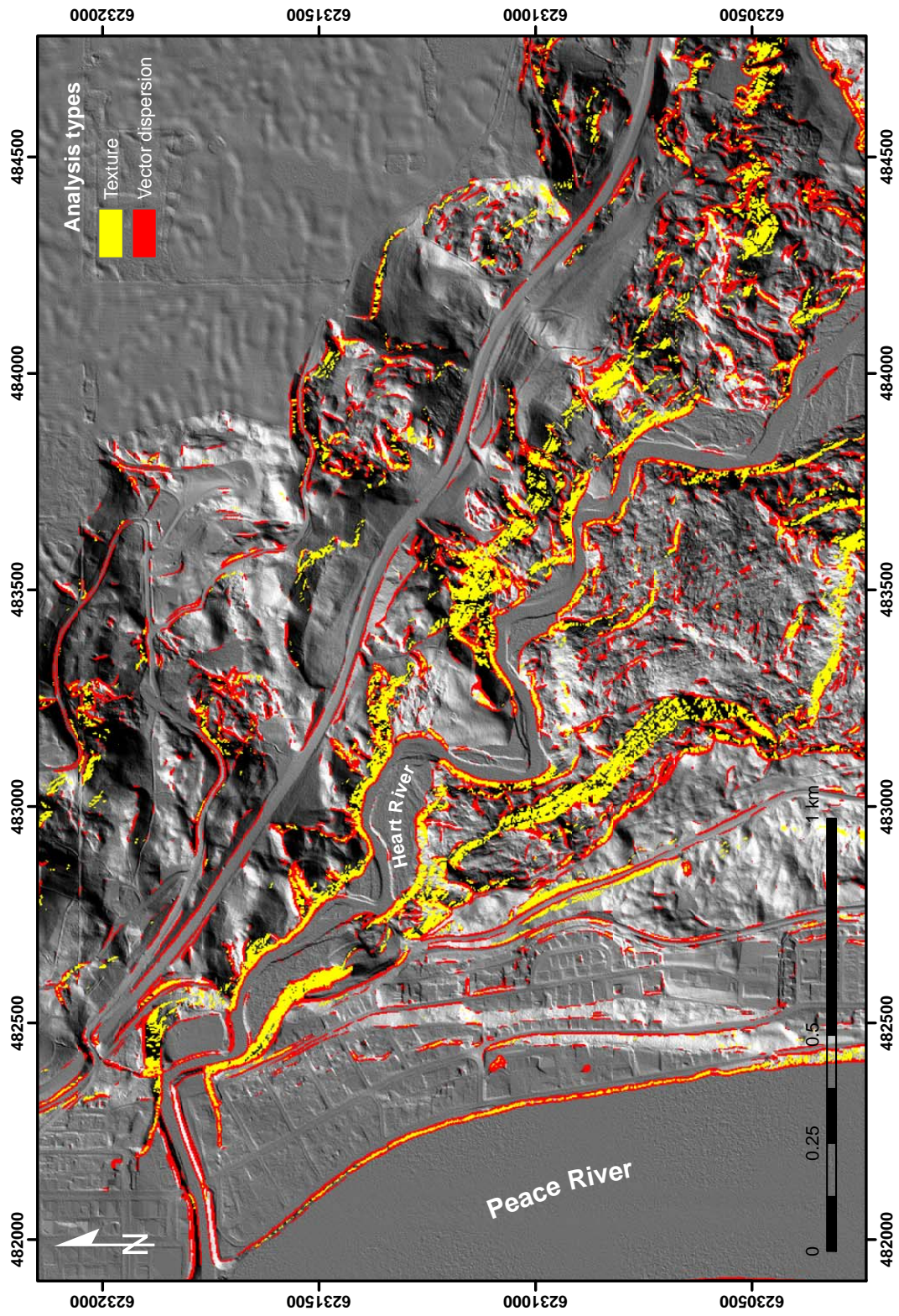


Figure 5.33 Evaluation of the spatial distribution in vector dispersion and texture analyses. High vector dispersion values over 0.008 are illustrated. Texture values represented on high rough areas are generated by intersecting the contrast (over two) and entropy (over 0.8) methods presented in Figure 5.22. The extent of areas depicted in this figure is identical to those shown in Figure 5.31. A shaded relief image shown in the background is obtained from the digital elevation model (Figure 5.4) having a cell size of 0.5 by 0.5 metres

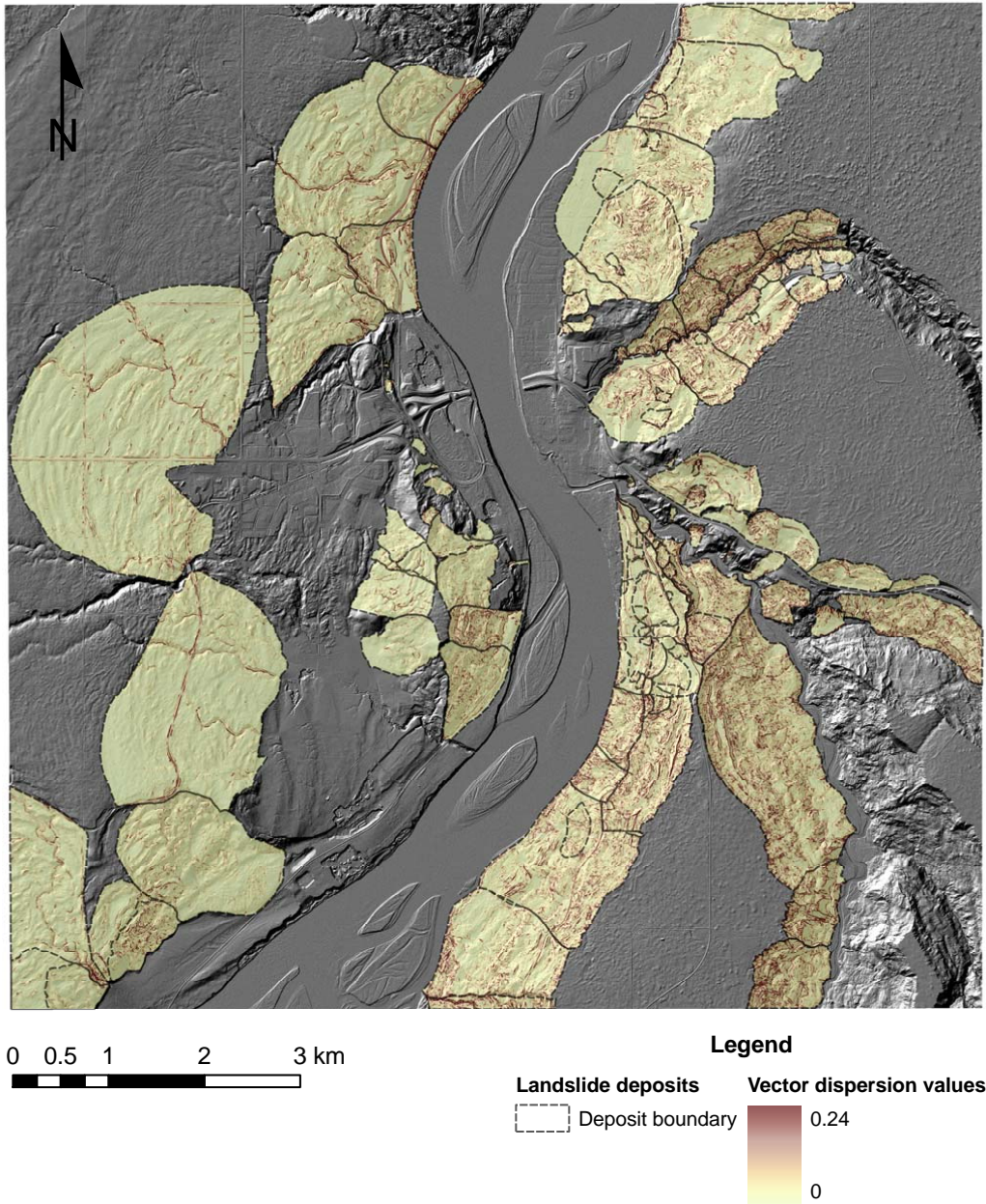


Figure 5.34 Spatial distribution of the vector dispersion analysis within landslide deposits. The variation of vector dispersion values is presented by the legend. Vector dispersion values are generated from the digital elevation model shown in Figure 5.4, which is modified to a 2.5 by 2.5 metre resolution for the vector dispersion analysis. A hillshade imagery presented in the background is obtained from the digital elevation model (Figure 5.4) with the spatial resolution of 0.5 by 0.5 metres

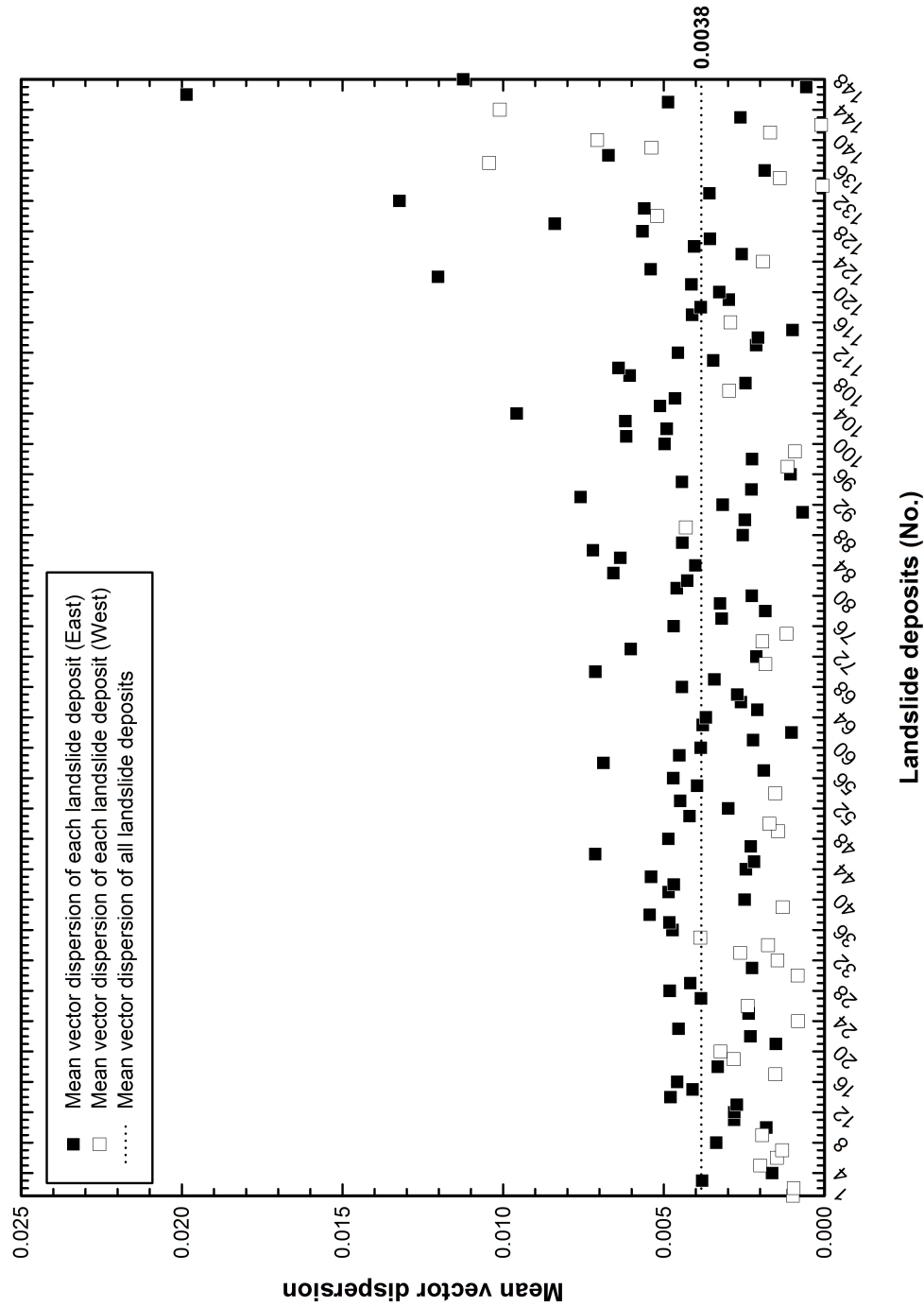


Figure 5.35 Mean vector dispersion values of previous landslide deposits observed in the study area. Landslide deposits denoted by the unique number are presented in the abscissa while corresponding average vector dispersion values are shown in the ordinate. Landslide deposits are grouped, either the west or east, based on the location where they were identified. The horizontal line represents the average vector dispersion value for all landslide deposits. Detailed information for landslide deposits are also presented in Appendix E

shows the geographical distribution of landslide deposits in which their mean vector dispersion values are over the average value.

From the vector strength and dispersion analysis which uses orientation data, it is expected that the presence of preferred directions, representing a smooth surface profile, seems to be relatively small on the east bank compared to those on the west bank of the Peace River. In geomorphological perspectives, in other words, the east bank is rougher than the west bank. This finding is consistent with previous results by using slope (Section 5.3.1) and texture analyses (Section 5.3.1.1). The vector strength and dispersion analysis is, therefore, useful to verify the landslide hazard model and provides insights into the determination of each landslide hazard level based on the degree of the dispersion in orientation data.

5.3.1.2.2 Eigenvalue analysis

Another statistical evaluation of orientation data is using eigenvectors and eigenvalues. Obtained from the orientation tensor, they are useful to analyze the randomness in three dimensional directional data (Woodcock 1977; Woodcock and Naylor 1983).

The early applications on this method to the earth sciences have appeared since the 1960s. An early study on exploiting eigenvalues in order to evaluate directions of the tectonic motion in fault planes due to earthquakes was carried out by Fara and Scheidegger (1963) and Scheidegger (1964; 1965) even though Fisher (1953), Watson (1956; 1960; 1965; 1966), and Breitenberger (1963) introduced a theoretical basis for the distribution of orientation data on a sphere. A test for evaluating the randomness of directions in unit vectors on the spherical surface was devised by Anderson and Stephens (1972) and Woodcock and Naylor (1983). Practical applications by using eigenvalues can be found in Mark (1973; 1974) in which the axial orientation data which represent the fabrics of till materials were correlated to their types and forming processes. Woodcock (1977) also used eigenvalues as a fabric shape indicator. He introduced three different graphical methods for the distribution of eigenvalues and their relative relations in which the fabric shapes and strengths are well delineated.

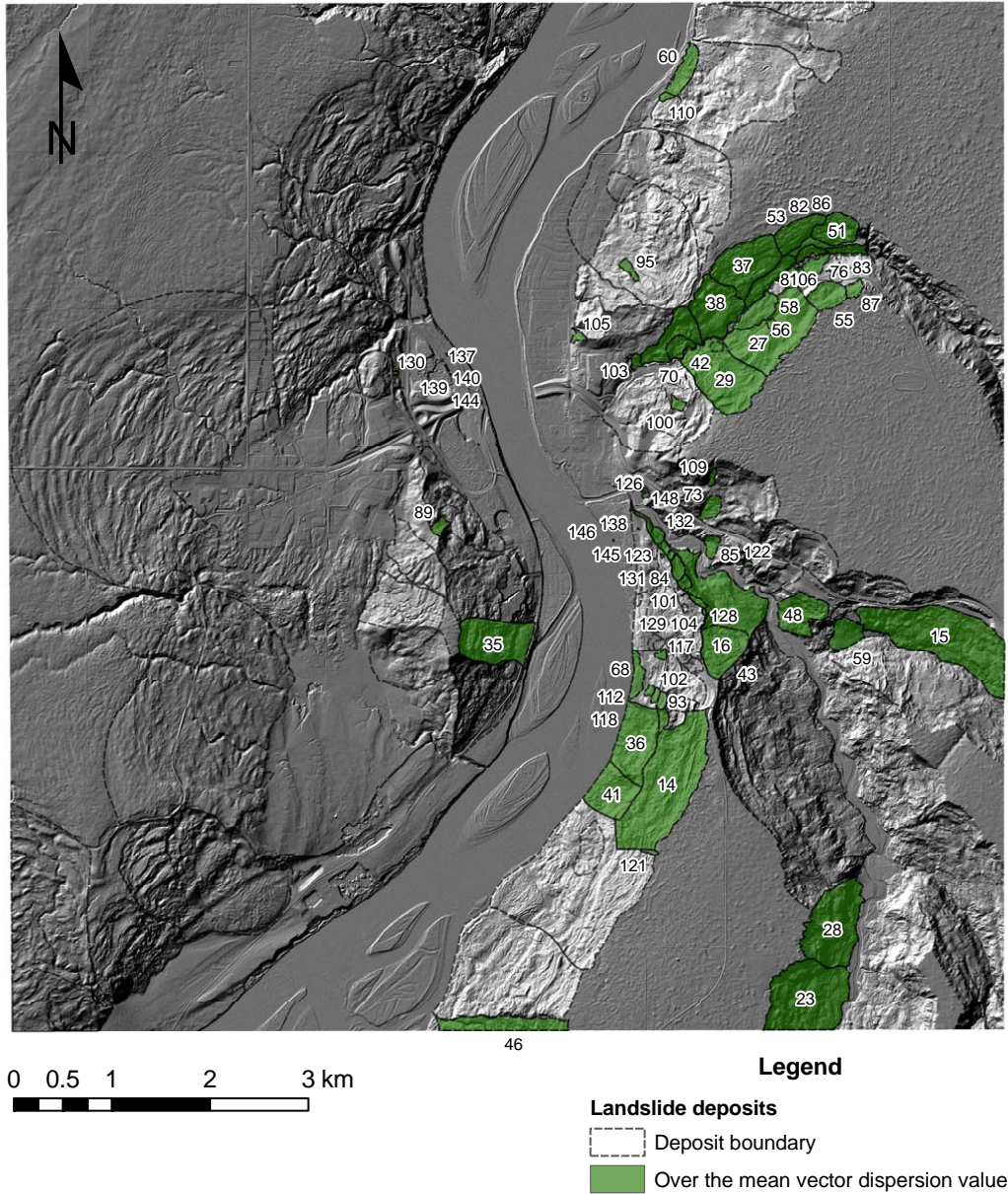


Figure 5.36 Geographical distribution of landslide deposits whose mean vector dispersion values are over the average value for all landslide deposits. A hillshade imagery presented in the background is obtained from the digital elevation model (Figure 5.4) with the spatial resolution of 0.5 by 0.5 metres

Even though analytical explanations of using the eigenvalue analysis for the distribution of axial orientation data are already reviewed by authors mentioned above, some important aspects for understanding their physical meaning related to the distribution in a three dimensional space are briefly summarized here.

Fisher (1953) first drew a proposition for distributing directional data on a spherical or a three dimensional space as angular errors. With this space, data on the spherical surface should be shown on the great circle by using the polar coordinates and the projecting technique (Figure 5.37). He hypothesized that the probability distribution of angular errors on the surface over the unit sphere is proportional to (Fisher 1953):

$$e^{\kappa \cos \theta} \quad (5.10)$$

By using the constant C , Equation (5.10) can be rewritten as the ‘spherical normal’ or ‘Fisher distribution’ (Watson 1956, 1960, 1966; Mardia 1972; Stephens 1974; Fisher et al. 1987):

$$f(\theta, \phi) = C e^{\kappa \cos \theta} \sin \theta \quad (5.11)$$

And the constant C is equivalent to the following relationship:

$$C = \frac{\kappa}{4\pi \sinh \kappa} \quad (5.12)$$

where θ is the angle between the true or preferred direction (in this case, the north) and an observation vector, ϕ is the angle between the true direction and the projection of an observation, and κ is a non negative accuracy parameter which controls the degree of scatter (Watson 1966). Fisher (1953) noted the physical meaning of Equation (5.11) that the maximum probability density can be obtained where θ goes to zero. The variation of κ would influence the shape of density distribution, that is the larger the value of κ , the more the distribution is confined to the observation, which is equivalent to the von Mises, a two-dimensional distribution (Fisher et al. 1987). The uniform probability distribution over the spherical surface is attained if κ is zero. Equation (5.11) also indicates that it is dependent only on the value of

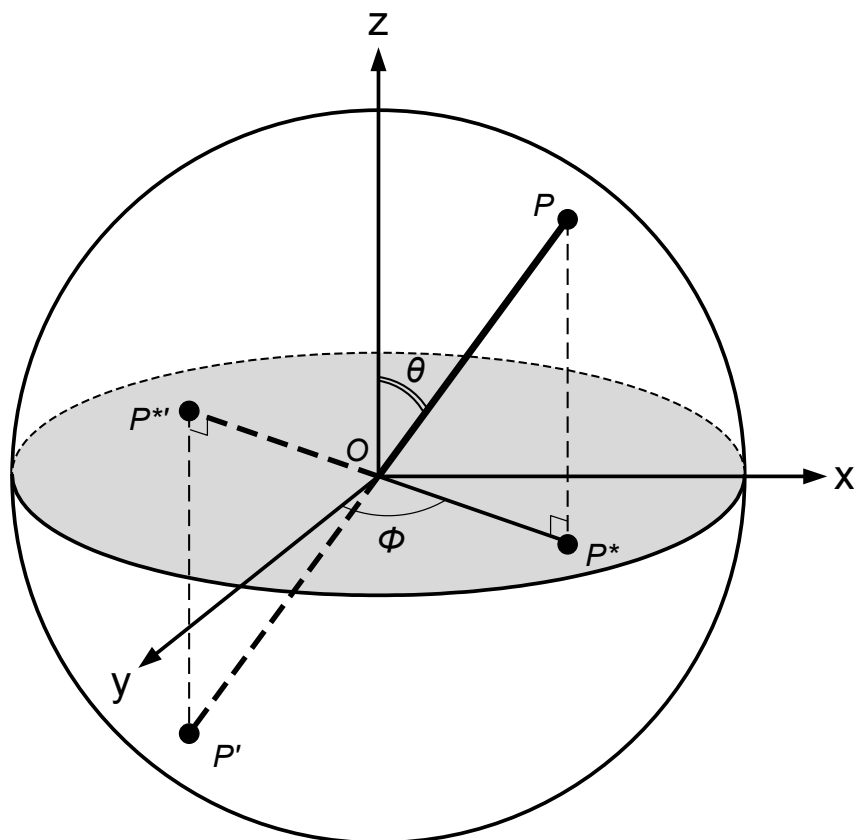


Figure 5.37 Definition of a point representing directional data on a spherical surface. The sphere has a unit radius of one and centered at O which indicates the point P as a unit vector OP . The location of the point P , therefore, can be represented by the colatitude θ and the longitude ϕ . The colatitude is the angle between z axis and the unit vector OP while the longitude is the angle between y axis and OP^* , the projection of OP on $x - y$ plane. The available angles for the colatitude and the longitude range from zero to π and 2π , respectively. Unit vectors OP' and its projection OP'^* can be used to show the point P' for P if provided with the lower hemisphere only. In this case the colatitude and the longitude have ranges of $\pi - \theta$, $\phi + \pi$, respectively. If vectors OP and OP' are not distinguished, vectors are undirected and can be treated as axial data. *Source:* Fisher et al. 1987, Figure 2.1

θ not ϕ which representing the rotational symmetry (Watson 1966). The graphical probability density function based on the Fisher distribution is illustrated in Figure 5.38. It is clearly shown that the unimodal distribution of directional data can be well explained by the Fisher distribution (Mardia 1972).

Assigning direction cosines of preferred and observation vectors to (λ, μ, ν) and (l, m, n) , respectively, Equation (5.11) is given by (Watson 1956, 1966):

$$f(\theta, \phi) = C e^{\kappa \cos \theta} \sin \theta = C e^{\kappa(\lambda l + \mu m + \nu n)} \sin \theta \quad (5.13)$$

Under the unimodal model, the density of the observation vector (l, m, n) is the greatest when the direction is (λ, μ, ν) , which is called the mode, whereas the density is the least at $(-\lambda, -\mu, -\nu)$, the antimode (Mardia 1972; Fisher et al. 1987). This can be explained from Figure 5.37 which shows the standardized form of the Fisher distribution. The Fisher distribution of the observation vector \mathbf{OP} is referred to the true direction of the north pole (positive z axis) with the deviation of the angle of θ . If \mathbf{OP} has the maximum value its direction should be comparable to the north pole, while at the position of $(0,0,-1)$, \mathbf{OP}' would have the minimum value along the negative z axis. The positive z axis is, therefore, the mode and the negative one can be the antimode. Same conclusions can be found in Figure 5.38.

Contrary to the vectorial data described above, the observation of the direction may not be important in some data such as the direction of the tectonic stress normal to the motion direction in the fault plane (Scheidegger 1964), the direction of normal to surfaces of the corrugated roof (Watson 1965), and the direction of normal to a cleavage plane (Mardia 1972). These directions do not distinguish the diametrically opposite vectors (e.g., $\mathbf{OP} = \mathbf{OP}'$ in Figure 5.37). This distribution, also known as the ‘axial distribution’ or ‘Watson distribution’ (Fisher et al. 1987), would lead to assign the same probability density to diametrically opposite positions (Mardia 1972), and thus the probability density distribution can be concentrated on a hemisphere with either bipolar or girdle form. The axial distribution over the unit sphere can be written as follows (Watson 1965; Anderson and Stephens 1972; Mardia 1972; Stephens 1974):

$$f(\theta, \phi) = C(\kappa) e^{-\kappa \cos^2 \theta} \sin \theta \quad (5.14)$$

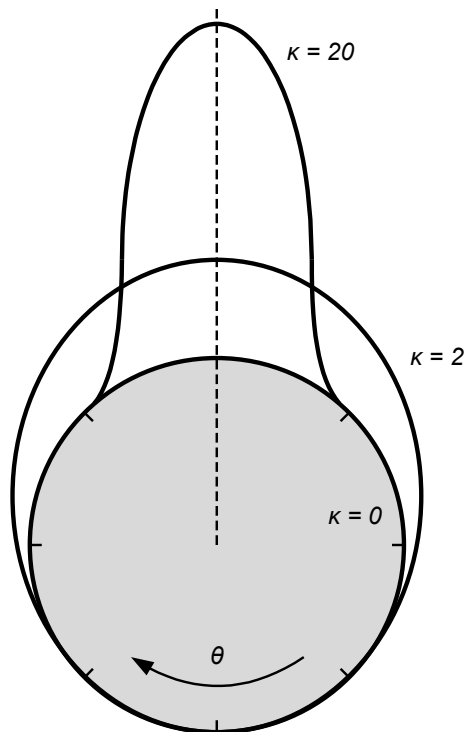


Figure 5.38 Probability density function representing the Fisher distribution. The variation of κ values is also illustrated (0, 2, and 20). θ indicates the angle between the true or preferred direction and observation vectors. The mean direction of the directional data is presented by the dashed line. *Source:* Fisher et al. 1987, Figure 4.6

where,

$$C(\kappa)^{-1} = 4\pi \int_0^1 e^{-\kappa t^2} dt \quad (5.15)$$

and,

$$\cos \theta = \lambda l + \mu m + \nu n \quad (5.16)$$

where the notation is the same as in descriptions for vectorial equations. Watson (1965) noted the most distinct characteristic is that the density of any point over the sphere is identical to the point located at the diametrically opposite position. For example, (λ, μ, ν) goes to $(-\lambda, -\mu, -\nu)$ and/or (l, m, n) turns to $(-l, -m, -n)$ because of the cosine squared term in Equation (5.14). If the shape parameter of κ is positive, the density is greatest at $\theta = \pi/2$, which located around the great circle normal to the preferred direction, (λ, μ, ν) . If provided the rotational symmetry, this distribution on the equator of the sphere is called a symmetric girdle or equatorial distribution (Anderson and Stephens 1972; Mardia 1972). The girdle distribution is similar to the shape of ellipsoid and would become to concentrate on smaller areas as the κ increases. Figure 5.39 illustrates the shape of girdle distribution when the κ value has 0, 2, and 20, respectively.

On the other hand, if κ is negative the density has maximum values at $\theta = 0, \pi$, which are along the preferred direction. This describes a bimodal distribution and bipolar distribution if provided the rotational symmetry along the preferred direction (Anderson and Stephens 1972; Mardia 1972). Obviously the density shows a uniform distribution over the sphere when κ goes to zero. Figure 5.39 also shows the bimodal distribution when κ values are 0, -2, and -20, respectively.

Equation (5.14) can also be presented as follows (Scheidegger 1964; Mark 1973; Fisher et al. 1987):

$$f(\theta, \phi) = C(\kappa) e^{\kappa \cos^2 \theta} \sin \theta \quad (5.17)$$

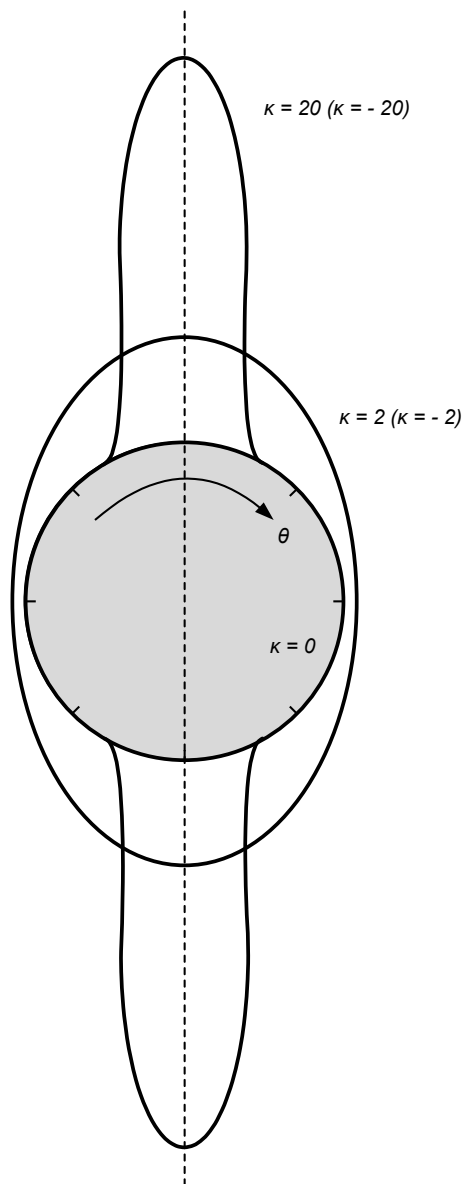


Figure 5.39 Probability density function representing the axial distribution. The variation of κ values is also illustrated (0; 2, and 20 for the girdle distribution; -2 and -20 for the bipolar distribution). θ indicates the angle between the true or preferred direction and observation point. The dashed line represents the principal axis for the bipolar distribution and the equatorial plane for the girdle distribution, respectively. *Source:* Fisher et al. 1987, Figure 4.7

In this case the condition determining density distributions are opposite when comparing with Equation (5.14). In other words, the girdle distribution can be obtained at κ is negative while the bipolar distribution can be described when κ is positive, respectively.

Based on the spherical distribution of directional and non-directional data it is shown that typical characteristics of the spherical distribution are equivalent to the determination of eigenvalues and eigenvectors especially from a symmetric three by three matrix which comprises direction cosines (Fara and Scheidegger 1963; Scheidegger 1964; Watson 1966; Mark 1973). Consider N points of the unit mass of (l_i, m_i, n_i) , where $i = 1, 2, \dots, N$ and suppose that \mathbf{u} is a true or preferred direction through the centre of the sphere, the moment of inertia I of the set of N points of unit observation data about \mathbf{u} can be described as follows (Watson 1966; Mardia 1972):

$$I = N - \mathbf{u}' \mathbf{M} \mathbf{u} = N - \sum_{j=1}^3 \sum_{k=1}^3 u_j M_{jk} u_k \quad (5.18)$$

where \mathbf{M} is a orientation matrix, a three by three matrix consisting sums of the cross products of direction cosines of the unit mass, (l_i, m_i, n_i) . It is given by:

$$\mathbf{M} = \begin{pmatrix} \sum l_i^2 & \sum l_i m_i & \sum l_i n_i \\ \sum m_i l_i & \sum m_i^2 & \sum m_i n_i \\ \sum n_i l_i & \sum n_i m_i & \sum n_i^2 \end{pmatrix} \quad (5.19)$$

The eigenvalues of \mathbf{M} are calculated from the characteristic equation. Therefore:

$$\det(\mathbf{M} - \lambda \mathbf{I}) = 0 \quad (5.20)$$

where \det is the determinant of \mathbf{M} , \mathbf{I} is the identity matrix. Roots of the characteristic equation are the eigenvalues, λ_i ($i = 1, 2, 3$; $\lambda_1 > \lambda_2 > \lambda_3$), and corresponding vectors are the eigenvectors, \mathbf{v}_i ($i = 1, 2, 3$). Three eigenvalues are always positive and add to N while three eigenvectors are always perpendicular to each other (Watson 1966). Normalized form of the eigenvalues can be obtained from dividing by the number of unit observation points, N . So that:

$$S_j = \lambda_j/N, \quad j = 1, 2, 3, \quad \text{thus, } S_1 + S_2 + S_3 = 1 \quad (5.21)$$

The physical meaning of eigenvalues as an indicator for the spherical distributions of directional and non-directional data was well described by Watson (1966). From Equation (5.18), it is shown that the greatest moment of inertia would require the least value of $\mathbf{u}'\mathbf{M}\mathbf{u}$, which leads to a minimum eigenvalue of the orientation matrix of \mathbf{M} and associated minimum eigenvector of \mathbf{u} . Likewise maximum eigenvalue and eigenvector result from the greatest value of $\mathbf{u}'\mathbf{M}\mathbf{u}$ causing the least moment of inertia. If the greatest moment of inertia is observed around the great circle based on the change of shape due to κ values shown in Figure 5.39, which indicate the girdle distribution, the axis perpendicular to the great circle would have small values of both eigenvalue and corresponding eigenvector. Other two moments of inertia along the diameter of the great circle have the least values and they cause large eigenvalues and eigenvectors both of which have similar values. In other words, the girdle distribution is generally indicated by one small eigenvalue with two large eigenvalues in similar values.

If the unit observation mass are clustered at both ends of the diameter in a sphere (Figure 5.39), indicating either unimodal and bimodal distributions, the moment of inertia along this axis would be small and therefore large eigenvalue and eigenvector are induced from the small value of the moment of inertia. Two other small values of eigenvalue and eigenvector are comparable and located along the diameters of the great circle. Obviously fairly equal eigenvalues would represent no preferred direction which having the uniform distribution in observation data. For the clustered distribution, therefore, one large eigenvalue and other two small and compatible eigenvalues are usually observed. Similar discussion was carried out by Mardia (1972) who demonstrated a clear distinction between unimodal and bimodal distributions (Table 5.8).

The spherical distribution of directional or non-directional data can also be used for identifying the shape of fabric on materials. As pointed out by Mark (1973; 1974), eigenvalues of axial orientation data obtained from till samples are directly related to the type of fabrics and their forming processes. Woodcock (1977) and Woodcock and Naylor (1983) used relative significance between eigenvalues to express shapes and strengths of the fabric (Figure 5.40). Figure 5.40 shows two independent ratios between three normalized eigenvalues, S_1/S_2 and S_2/S_3 , are plotted on the orthog-

Table 5.8 Type of the spherical distribution based on the distribution of eigenvalues and eigenvectors of the orientation matrix, M . The order of eigenvalues is $\lambda_1 > \lambda_2 > \lambda_3$. R is the length of the resultant vector. *Source:* Data adapted from Mardia (1972), Table 8.3

Eigenvalue distribution	Spherical distribution	Eigenvector distribution	
$\lambda_1 \simeq \lambda_2 \simeq \lambda_3$	Random	No preferred orientation	
	$\lambda_2 \neq \lambda_3$	Unimodal if R is large Bimodal otherwise	Concentrated at one end of v_1 Concentrated at both ends of v_1
$\lambda_1 > \lambda_2, \lambda_3$	$\lambda_2 \simeq \lambda_3$	Unipolar if R is large Bipolar otherwise	Rotational symmetry about v_1
	$\lambda_1 \neq \lambda_2$	Girdle	Girdle plane containing v_1 and v_2
$\lambda_1, \lambda_2 > \lambda_3$	$\lambda_1 \simeq \lambda_2$	Symmetric girdle	Rotational symmetry about v_3

onal axes. For the proper delineation of ratios with large values, natural logarithmic scales are adopted on both axes. Woodcock (1977) noted that axially symmetric clustered orientation data can be found where the eigenvalue of S_2 is identical to S_3 , in other words, they are located along the ordinate. The rotational symmetric girdle distribution on the great circle of a sphere indicates that orientation data are placed along the abscissa where the eigenvalue of S_1 is equal to S_2 . The relative distribution is, therefore, the function of both clustered and girdle preferences. The degree of the relative distribution can be quantified by the shape parameter, K (Woodcock 1977). It gives the following equation:

$$K = \frac{\ln(S_1/S_2)}{\ln(S_2/S_3)} \quad (5.22)$$

The physical meaning of K is the slope of the $\ln(S_1/S_2)$ and $\ln(S_2/S_3)$ plot and indicates the equal clustered and girdle distribution of orientation data can be located where K value is a unity (Figure 5.40). Snapshots of typical fabric shapes shown in Figure 5.40 also illustrate the degree of distribution strength. The uniform, isotropic distribution of orientation data is concentrated on the origin and as the distribution is far from the origin, a preferred direction would come to dominate the overall distribution (Figure 5.40). Woodcock (1977) also defined the strength parameter, C to quantify the partial contribution to the preferred direction. Therefore:

$$C = \ln(S_1/S_3) \quad (5.23)$$

The evaluation of eigenvalues and their ratios is especially beneficial when large amounts of field data, either geological or geomorphological, containing the fabric characteristic of materials are acquired and compared. Woodcock (1977) noted that the eigenvalue analysis would illustrate a relationship between the change of fabric shape and associated strain progression, which Mark (1974) provided using similar results from till fabrics. In other words, the spherical distribution of orientation data would provide an insight for the relative progression of the landslide controlled features on ground surface correlating their characteristics with typical fabric shapes. Woodcock (1976; 1977) showed that fold axes and axial microfold lineations form a girdle distribution within slump sheets, which indicates evidence of slope movements while the undisturbed bedding forms clusters representing stable areas.

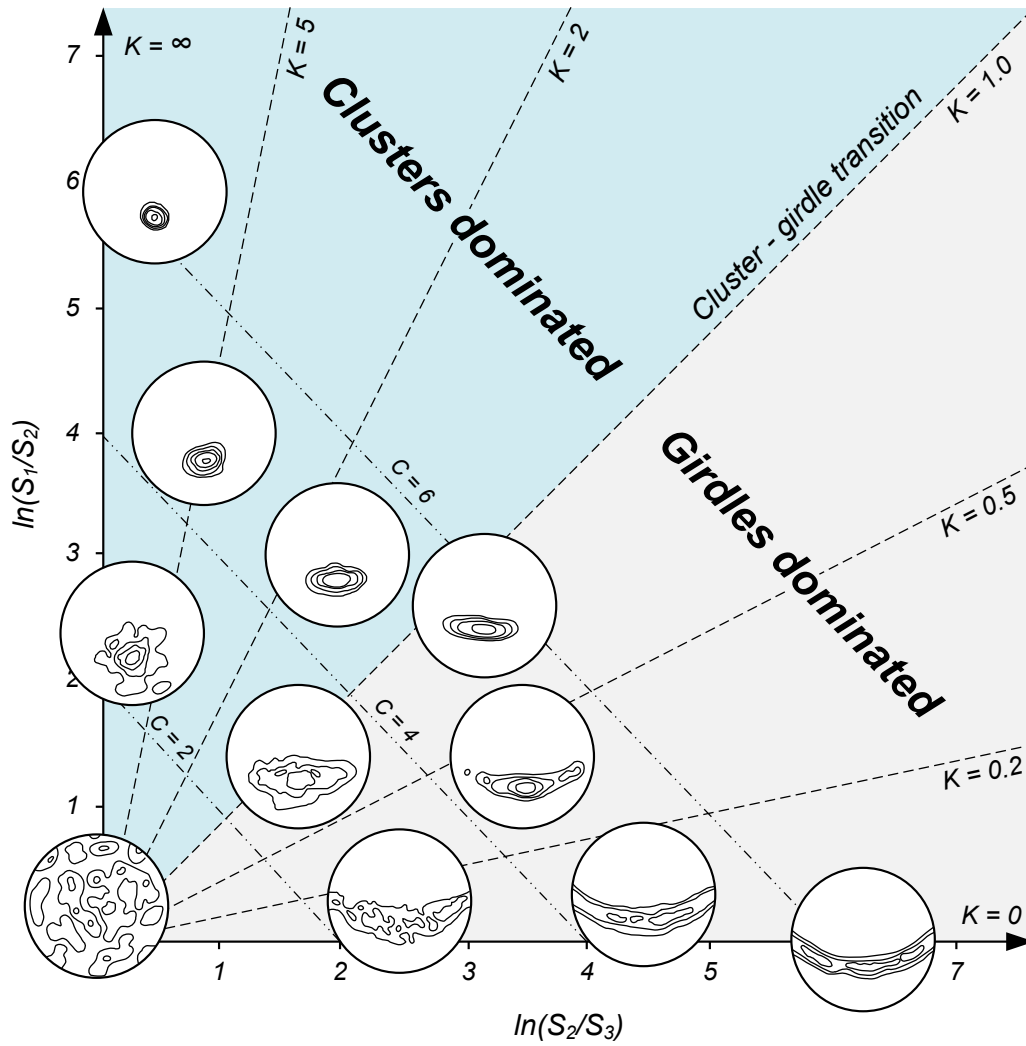
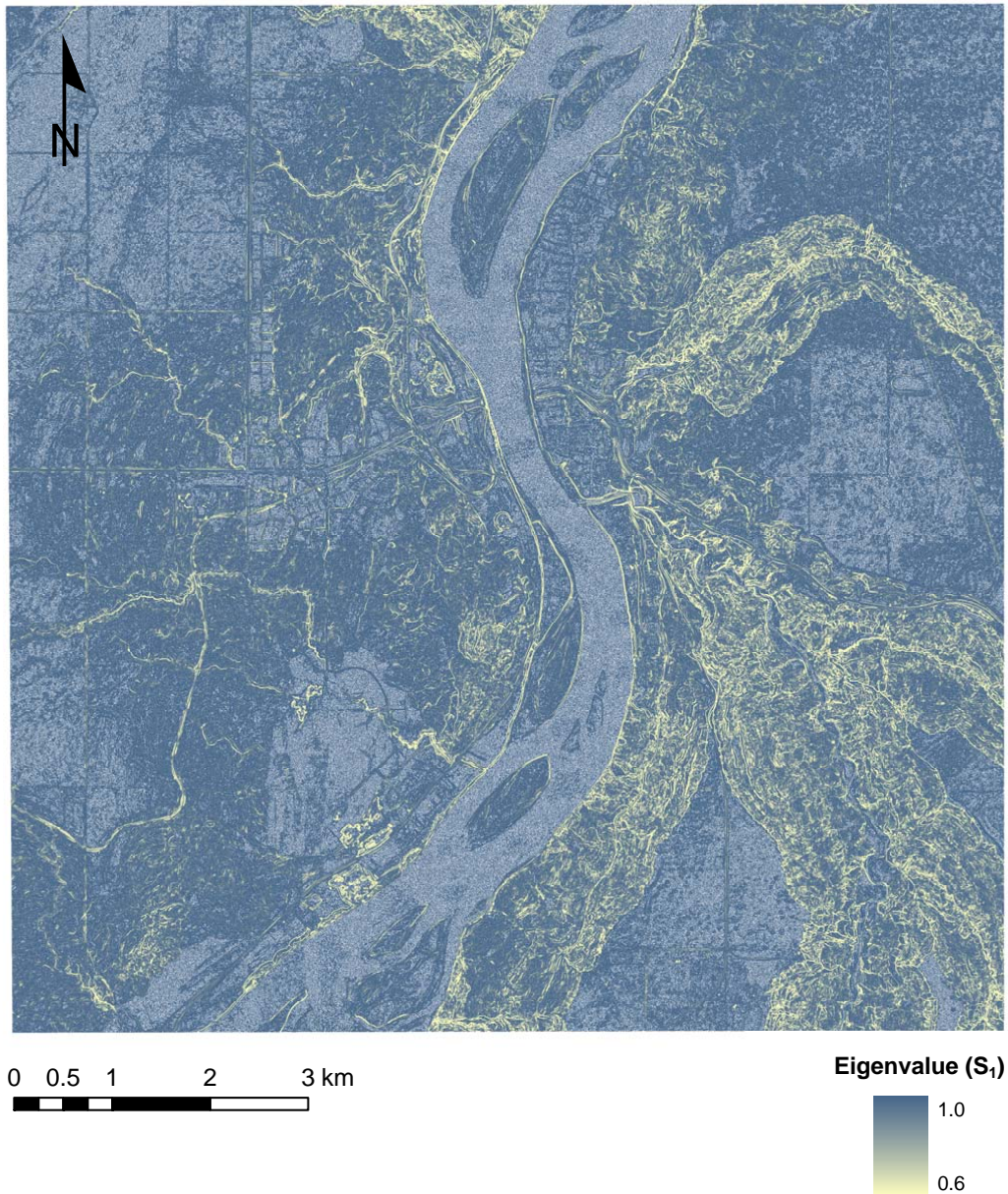


Figure 5.40 Distribution of fabric shapes on a sphere. The relative significance of eigenvalues is illustrated as a normalized form of ratios on the two-axis logarithmic plot. Representative fabric shapes which are corresponding to the values observed in the plot are presented. Shape and strength parameters, K and C , are also described. *Source:* Woodcock 1977, Figure 1

Landslide studies using the characteristic of eigenvalues have been recently developed by Rodriguez et al. (2002), Guth (2003), McKean and Roering (2004), Teza et al. (2008), and Kasai et al. (2009), all of which mainly focused on the recognition of topographic information to identify landslide characteristics and their kinematics. For example, Rodriguez et al. (2002) used the polarimetric eigenvalue decomposition and the scattering matrix to determine the landslide induced hill slopes from the polarimetric SAR imagery. Application to the terrestrial laser scanning technique for obtaining the strain field in order to find the ground surface kinematics that might be observed in landslide deposits was carried out by Teza et al. (2008). Eigenvalue ratios introduced by Woodcock (1977) and Woodcock and Naylor (1983) are also used to differentiate between rough and smooth surfaces based on shape and strength of the distribution in orientation data (Guth 2003; McKean and Roering 2004; Kasai et al. 2009).

The identification of previous landslide controlled features in the study area by using the eigenvalue analysis is performed as follows. Similar procedures are employed in calculating slope and aspect values, which are shown in the vector strength and dispersion analysis. The digital elevation model of 2.5 by 2.5 metre spatial resolution is used for these calculations. Direction cosines are then calculated from slope and aspect values which were converted into the radian unit. Each element of the orientation matrix shown in Equation (5.19) is then represented by direction cosines. All cell-based (raster based) calculations such as summation of elements in the orientation matrix using moving window (3×3) and their geographical representations are followed by the Spatial Analyst tool embedded in the ArcGIS. A cubic equation is introduced into Equation (5.20) in order to determine three eigenvalues. Obtained eigenvalues are then normalized by the N total cells draping the study area. Finally eigenvalue ratios introduced by Woodcock (1977) and Woodcock and Naylor (1983) are calculated to distinguish the landslide controlled features from the study area. I coded the entire processes using Python programming language for later use in other particular areas. High eigenvalue ratios of $\ln(S_1/S_2)$ represent smoother ground surface because of high clustered unit vectors which indicating a preferred direction (McKean and Roering 2004; Kasai et al. 2009). Following figures (Figures 5.41 to 5.45) are the results of eigenvalue analysis for the study area.

The spatial distribution of the three eigenvalues, S_1 , S_2 , and S_3 , are shown in Figure 5.41. Although the sum is always one, ranges of each eigenvalue tend to show



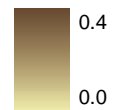
(a)

Figure 5.41 Spatial distribution of eigenvalues for the study area. a. S_1 . b. S_2 . c. S_3 . The cell size is 2.5 by 2.5 metres. Variations of each eigenvalue are illustrated in the legend. Eigenvalues are calculated from the orientation matrix which shown in Equations (5.19) and (5.20), then normalized by the total grids of N (Equation (5.21)). The orientation data of each cell is generated from the digital elevation model shown in Figure 5.4, which is modified to a 2.5 by 2.5 metre resolution for the analysis



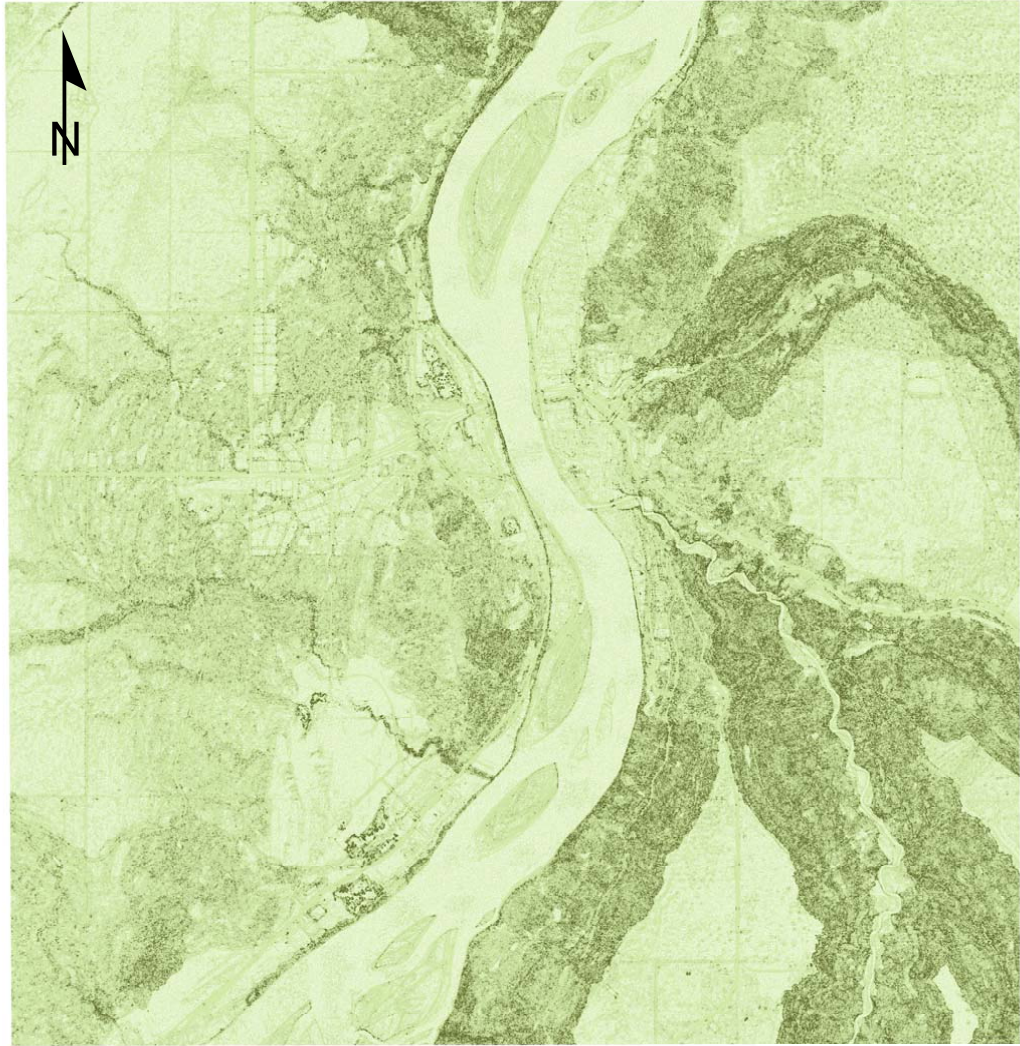
0 0.5 1 2 3 km

Eigenvalue (S_2)



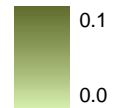
(b)

Figure 5.41 (Cont'd)



0 0.5 1 2 3 km

Eigenvalue (S_3)



(c)

Figure 5.41 (Cont'd)

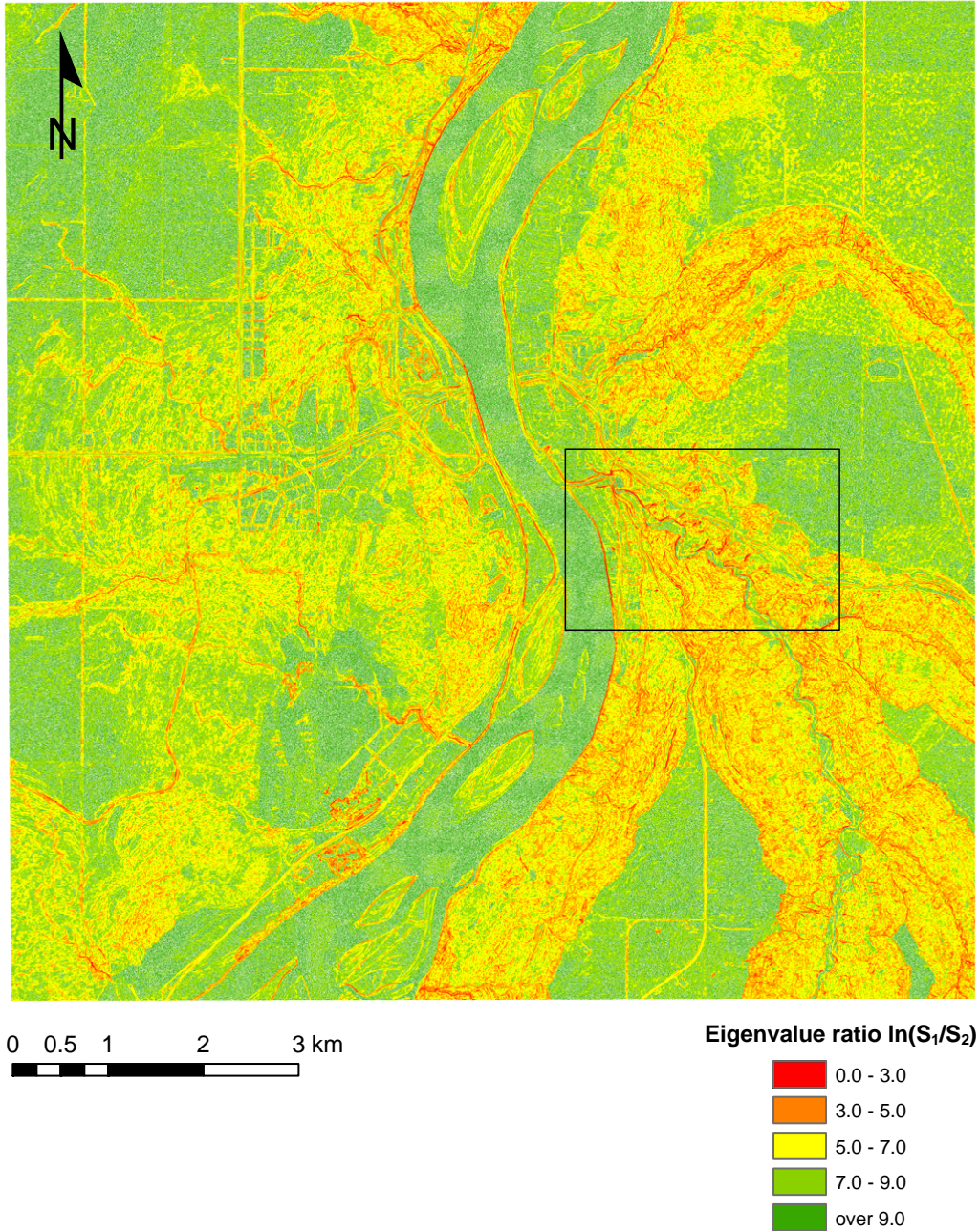


Figure 5.42 Spatial distribution of the eigenvalue ratio of $\ln(S_1/S_2)$ in the study area. The cell size is 2.5 by 2.5 metres. Variations of the eigenvalue ratio are shown in the legend. The eigenvalue ratio is generated among three individual values illustrated in Figure 5.41. Obtained ratios can be represented by the natural logarithmic scale. The area outlined by the black rectangle is also shown in Figure 5.45



0 0.5 1 2 3 km

Eigenvalue ratio $\ln(S_2/S_3)$

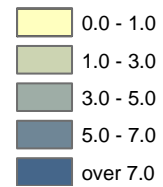
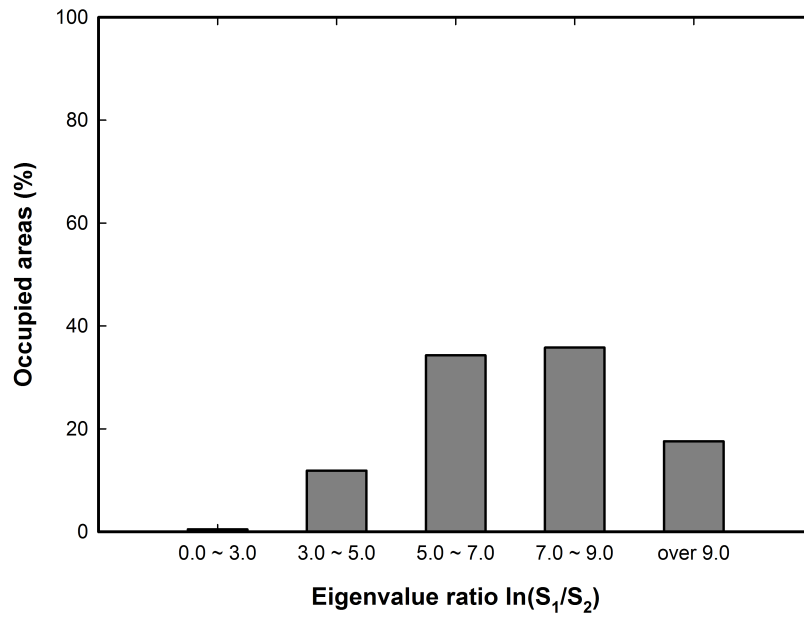
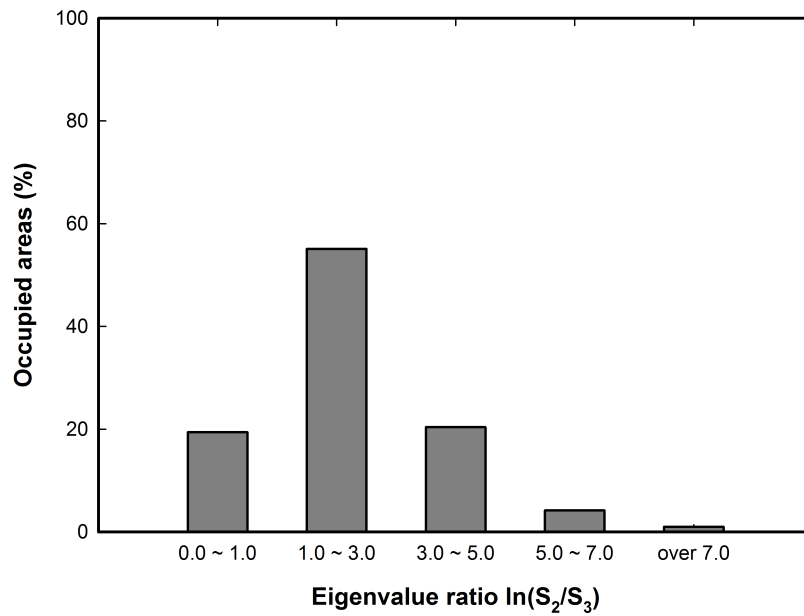


Figure 5.43 Spatial distribution of the eigenvalue ratio of $\ln(S_2/S_3)$ in the study area. The cell size is 2.5 by 2.5 metres. Variations of the eigenvalue ratio are shown in the legend. The eigenvalue ratio is generated among three individual values illustrated in Figure 5.41. Obtained ratios can be represented by the natural logarithmic scale



(a)



(b)

Figure 5.44 Spatial distribution of the eigenvalue ratios with respect to occupied areas. a. Eigenvalue ratio $\ln(S_1/S_2)$. b. Eigenvalue ratio $\ln(S_2/S_3)$. The percentage areas occupied by each eigenvalue ratio are located in the ordinate while classes of eigenvalue ratios presented in Figures 5.42 and 5.43 are shown in the abscissa

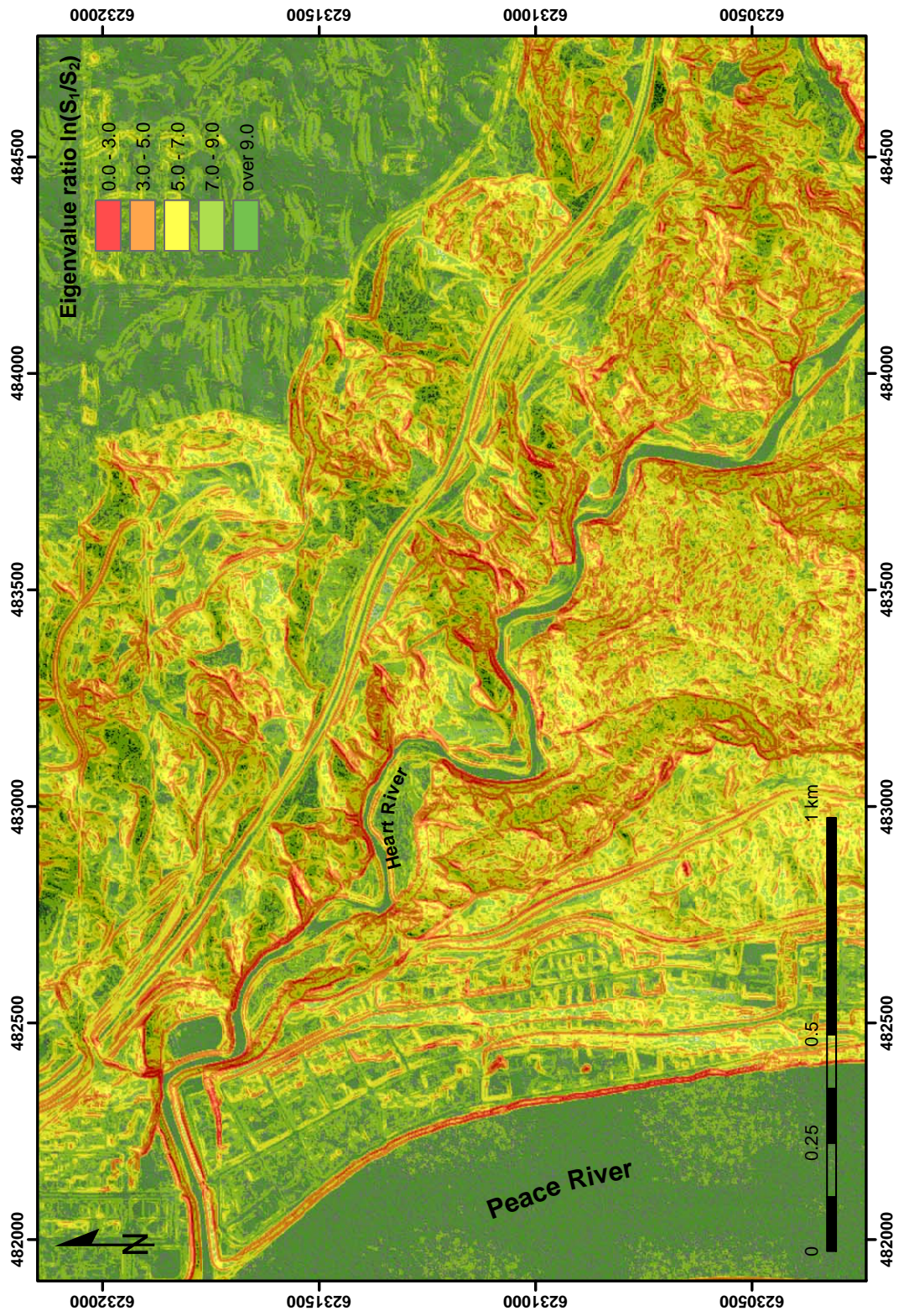


Figure 5.45 A closer look at the part of study area draped by the eigenvalue ratio of $\ln(S_1/S_2)$. The location is illustrated in Figure 5.42. The same variation of the eigenvalue ratio shown in Figure 5.42 is also presented in the legend. Peace and Heart Rivers flow northward, respectively. A hillshade imagery presented in the background is obtained from the digital elevation model (Figure 5.4) with the spatial resolution of 0.5 by 0.5 metres

dispersion in values. For the value of S_1 ranging from 0.6 to a unity, lower values can be found in the valley slopes along the Peace River and major tributaries. On the other hand, higher eigenvalues of S_2 and S_3 , which ranged from zero to 0.4 and 0.1, respectively, tend to be observed on the same valley walls. Based on observed ranges of three eigenvalues, it is postulated that unimodal and bimodal (or bipolar) spherical distribution, or clusters dominated distribution can be anticipated in the study area. These distributions also make the eigenvector v_1 the principal axis normal to the ground surface (Table 5.8).

The variation of the cluster dominated spherical distribution of the orientation data is illustrated in Figure 5.42. The eigenvalue ratio of $\ln(S_1/S_2)$ which represent the ordinate of the distribution of fabric shapes on the sphere (Figure 5.40) ranges from 0.4 to 17. Low values of $\ln(S_1/S_2)$ would represent a rough ground surface because of less clustered unit vectors which indicate non preferred direction (Figure 5.40), and those areas may reflect previous landslides containing landslide controlled features such as scarps, tension cracks, and displaced materials (McKean and Roering 2004; Kasai et al. 2009). In Figure 5.42, high values of $\ln(S_1/S_2)$ are concentrated on the uplands, river surfaces, and river terraces of the study area where surfaces are relatively flat whereas lower values are observed in the valley slopes along the river. The lowest values of eigenvalue ratio (less than three) can be found downstream of the Peace River (easterly aspect cut banks), valley slopes along the Pat's Creek and Heart River, and westerly aspect valley slope of the Peace River, which provide consistent results shown by other methodologies previously discussed (Figures 5.22 and 5.30). The portions of these areas would take less than one percent (0.5 %) of the total evaluated study area (Figure 5.44a).

Another eigenvalue ratio, $\ln(S_2/S_3)$, is illustrated in Figure 5.43. It shows the girdle dominated distribution in the study area in which higher values shows more distinct girdle distribution. Lower values of this eigenvalue ratio covers upland areas, which are relatively uniform distribution of unit vectors in terms of girdles dominated distribution. Since the major spherical distribution of the study area is the clusters dominated based on the variation of the three eigenvalues (Figure 5.41), the contribution of the girdle distribution on identifying the landslide controlled features is less significant compared to the cluster distribution shown in Figure 5.42. One possible application of the girdle distribution, however, is to detect artificial structures. As illustrated in Figure 5.43, the highest eigenvalue ratio clearly indicates the transportation routes such as roads and railway. Unlike the natural slopes man-made

structures usually have the sharp edges near the breaks of slope and therefore orientation vectors would concentrate on these ground profiles as a form of the girdle distribution. Similar behaviours can be found at the toe of the valley slopes along the Peace River which showing sharp edges due to the river erosion. Percentage areas by the variation of eigenvalue ratio for the girdles dominated distribution are shown in Figure 5.44b. Highest value in eigenvalue ratio of $\ln(S_2/S_3)$ takes one percent of the evaluated study area.

More detailed clusters dominated eigenvalue distribution of $\ln(S_1/S_2)$ for the study area is well delineated in Figure 5.45. Rough ground surfaces are clearly shown by the lower eigenvalue ratio of less than three. Typical areas may include the toe of valley slopes along the Peace and Heart Rivers where Peace River sandstone formation is exposed, sharp scarps on top of slopes, courses of surface streams, and some irregular ground profiles observed in displaced materials. These areas are then superimposed to the results obtained from other methodologies illustrated in Figure 5.33 to show the feasibility of the eigenvalue ratio for identifying previous landslide controlled features and potential unstable areas. This effort is shown in Figure 5.46. It clearly shows that areas occupied by the clusters dominated eigenvalue ratio are consistent to those from vector dispersion values, which can describe the potential landslide controlled features. This similarity is believed to come from the control of orientation data which are using the direction of unit vectors. As pointed out by the vector dispersion values in Figure 5.33, the eigenvalue ratio also well describes the linear attributes of the landslide controlled features such as landslide scarps, tension cracks, and stream courses. Although results are similar in use, feasibilities of using the eigenvalue ratio are more practical than those from vector dispersion values because the variation of vector dispersion values differs by thousandth to hundredth orders of magnitude, which is somewhat difficult to differentiate each class of the vector dispersion value compared to the eigenvalue ratio which is varying one to ten orders of magnitude.

Results of identifying the orientation data in forms of eigenvalues and eigenvectors are beneficial in case of the absence of information regarding historical landslides which are the basis for constructing the landslide inventory mapping. Combining with other methodologies such as aerial photo interpretation, the determination of the previous landslide controlled features can be enhanced and this would lead to understand the fundamental landslide mechanisms and finally provide appropriate mitigation measures.

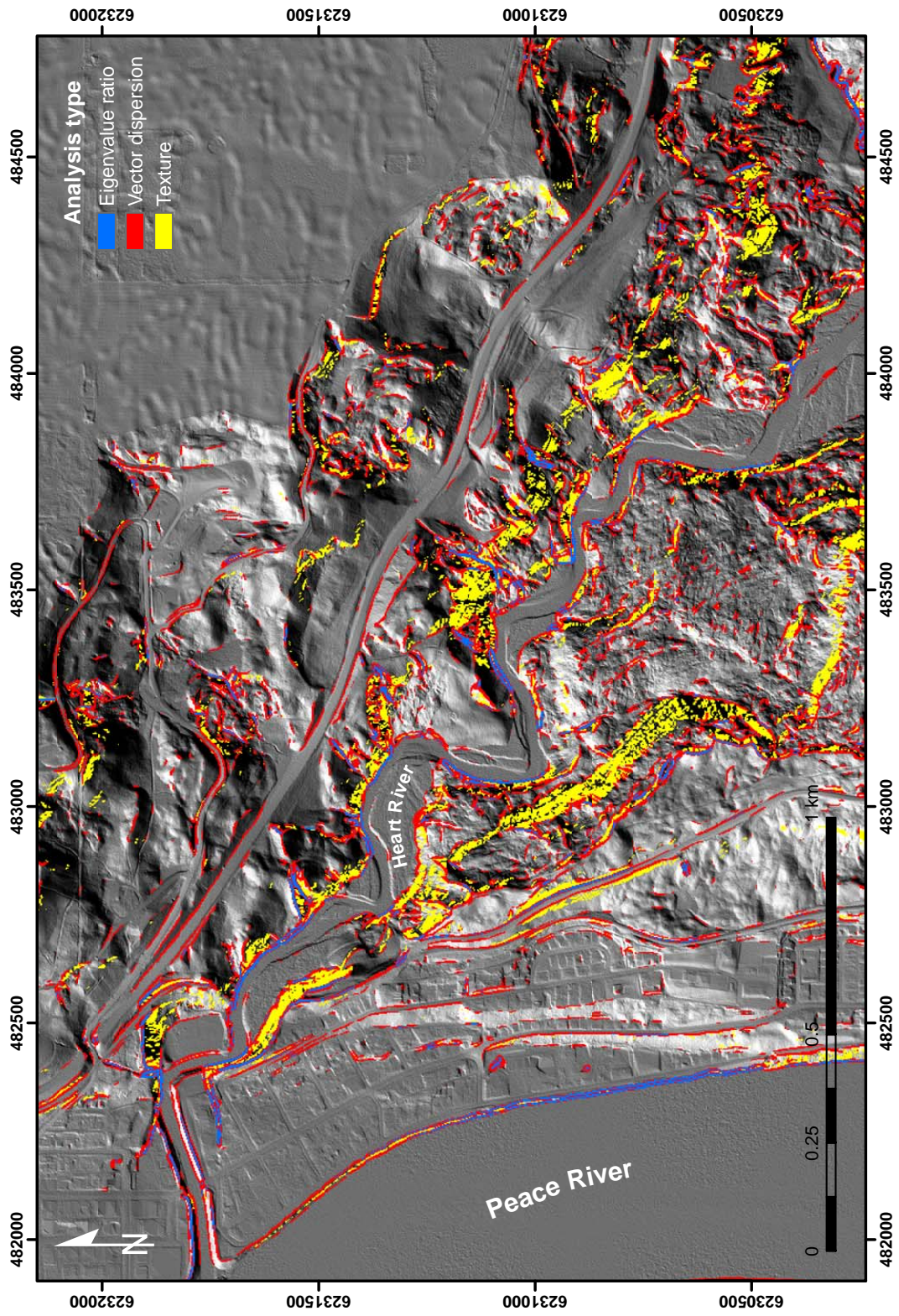


Figure 5.46 Evaluation of the spatial distribution by the eigenvalue ratio. The eigenvalue ratio of $\ln(S_1/S_2)$ less than three is overlaid on the vector dispersion and texture values which illustrated in Figure 5.33. Areas where the figure depicted are identical to those shown in Figure 5.45. A shaded relief image shown in background is obtained from the digital elevation model (Figure 5.4) having a cell size of 0.5 by 0.5 metres

As similar to earlier analyses by using slope, texture, and vector dispersion values, I carried out the spatial distribution of eigenvalue ratios in previous landslide deposits in order to identify the state of landslide activities and their corresponding hazard levels in the study area. Figure 5.47 shows the distribution of eigenvalue ratios representing $\ln(S_1/S_2)$, which are confined to landslide deposits. The distribution of eigenvalue ratios ranges from 0.4 to 17 and the average value for all landslide deposits is calculated as 5.88. Different mean values are obtained based on the locality of landslide deposits. The mean eigenvalue ratio for landslide deposits observed on the east bank is 5.69, which is 89 percent of the value in the west (6.43). The standard deviation value obtained from the east bank is calculated as 1.2 and this also makes 95 percent of the observed value on the west bank (1.26).

The distribution of eigenvalue ratios on each landslide deposit are illustrated in Figure 5.48 with their average and other representative values. Appendix E also presents detailed statistical information which the text did not cover. Figure 5.48 clearly shows the difference of eigenvalue ratios between the east and west banks. Based on the average eigenvalue ratio of 5.88, 70 landslide deposits placed on the east bank are below the average and they make 64 percent of landslide deposits observed on the east bank. Some of them are listed below the eigenvalue ratio of 4 (landslide deposits of 146 and 148), which also have high vector dispersion values over 0.01.

On the contrary to conditions on the east bank, there are only six landslide deposits whose eigenvalue ratios are below the average value of 5.88 (landslide deposits of 35, 89, 130, 137, 140, and 144). These make 16 percent of landslide deposits identified in the west bank. They are located on slopes of Misery Mountain, adjacent to the railway, and on the Mile 50.9 Slide area. All of which indicate the similar landslide deposits whose mean vector dispersion and texture values are higher than the average values. Results of the vector dispersion analysis are almost identical to those from their eigenvalue analysis. This similarity is caused by the use of same orientation data in the analyzing processes. Figure 5.49 shows the geographical distribution of landslide deposits in which their mean eigenvalue ratios of $\ln(S_1/S_2)$ are below the average value and provides a consistency with different methodologies shown in Figures 5.26 and 5.36 in selected landslide deposits.

Understanding the meaning of eigenvalue ratios which represents typical topographic features based on their geomorphologic characteristics is useful to under-

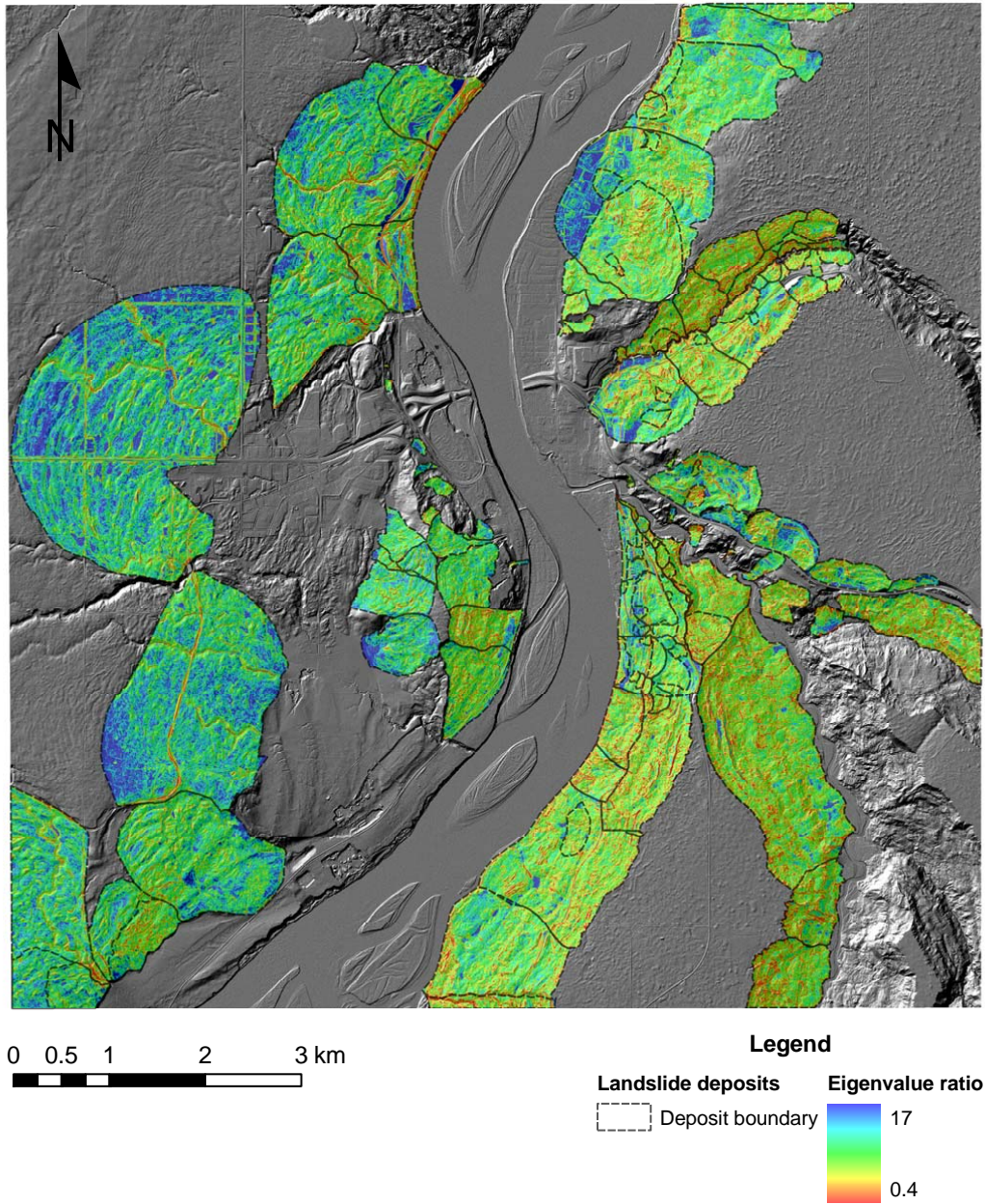
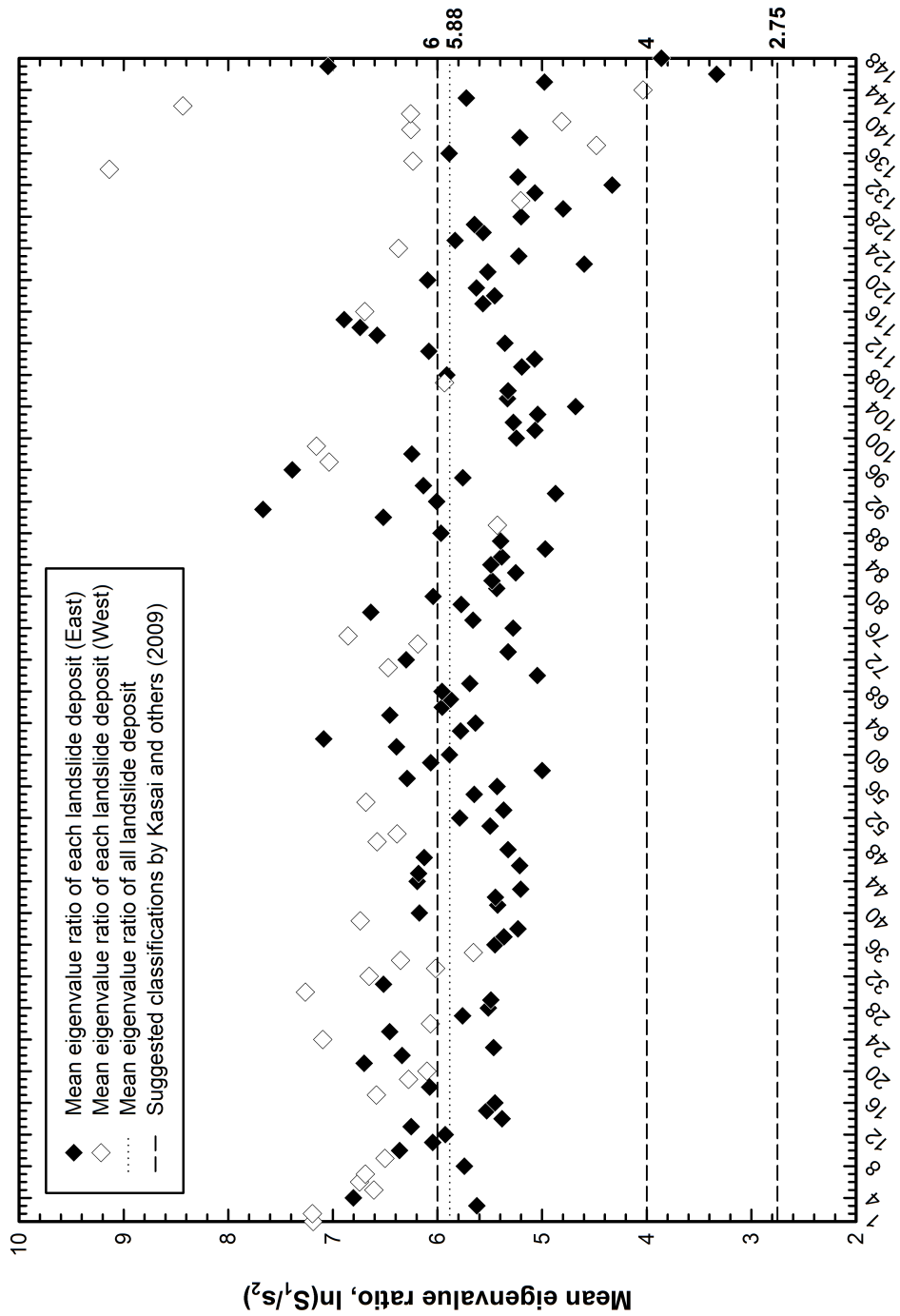


Figure 5.47 Spatial distribution of the eigenvalue analysis within landslide deposits. The variation of eigenvalue ratios of $\ln(S_1/S_2)$ is presented by the legend. The eigenvalue ratios are generated from the digital elevation model shown in Figure 5.4, which is modified to a 2.5 by 2.5 metre resolution for the eigenvalue analysis. A hillshade imagery presented in the background is obtained from the digital elevation model (Figure 5.4) with the spatial resolution of 0.5 by 0.5 metres



Landslide deposits (No.)

Figure 5.48 Mean eigenvalue ratios of previous landslide deposits observed in the study area. Landslide deposits denoted by the unique number are presented in the abscissa while corresponding average eigenvalue ratios of $\ln(S_1/S_2)$ are shown in the ordinate. Landslide deposits are grouped, either the west or east, based on the location where they were identified. Horizontal lines represent the average eigenvalue ratio for all landslide deposits and suggested eigenvalue ratios for the classification of topographic variations in the study area (Table 5.9). Detailed information for landslide deposits are also presented in Appendix E

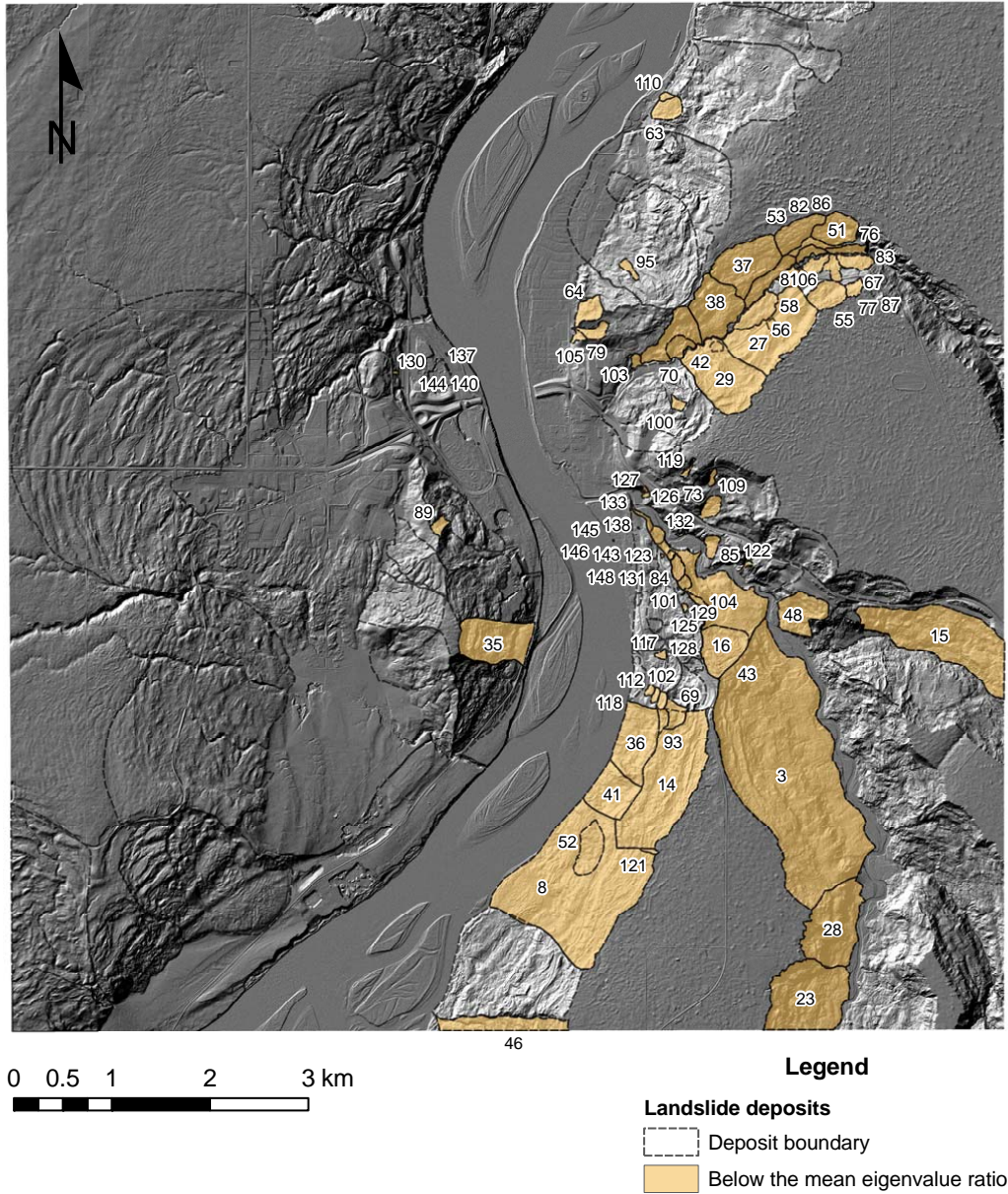


Figure 5.49 Geographical distribution of landslide deposits whose mean eigenvalue ratios of $\ln(S_1/S_2)$ are below the average value for all landslide deposits. A hillshade imagery presented in the background is obtained from the digital elevation model (Figure 5.4) with the spatial resolution of 0.5 by 0.5 metres

stand the state of landslide activities and their corresponding hazards. Recent studies by McKean and Roering (2004) and Kasai et al. (2009) provided a conventional guideline in interpreting eigenvalue ratios for landslide mechanisms and relevant geomorphological features on ground surface based on their observations. Table 5.9 indicates approximate ranges of eigenvalue ratios to delineate the topographic features observed in landslide deposits.

Table 5.9 Suggested ranges in eigenvalue ratios of $\ln(S_1/S_2)$ to identify typical topographic features. Landslide deposits observed in the study area are also classified as percentage values based on the range of eigenvalue ratios. *Source:* Data adapted from Kasai et al. (2009)

Eigenvalue ratio [†]	Topographic features	Landslide deposits (%) [‡]
< 2.75	Cracked bedrock outcrops Sharp slope rises	-
2.75-4	Coarse colluvial deposits Gently undulating surfaces	1.4
4-6	Gently undulating surfaces	55.4
> 6	Smooth surfaces	43.2

[†] $\ln(S_1/S_2)$.

[‡] Mean value for each landslide deposit is presented in Figure 5.48 and Appendix E.

From Figure 5.48 and Table 5.9, the eigenvalue analysis can provide useful information in dividing topographic characteristics observed in landslide deposits based on their ratios. Most landslide deposits located in the study area can be identified as the ‘Gently undulating surfaces’ and this amounts to 55 percent of all landslide deposits. Within this range, the proportion of landslide deposits which the east bank of the Peace River takes is 91 percent whereas the west bank has nine percent only. In the category of the ‘Smooth surfaces’ which makes 43 percent of all landslide deposits, proportions of landslide deposits in the east and west banks are comparable to each other, which is 52 and 48 percent, respectively. Only 1.4 percent of all landslide deposits are included in the range of the ‘Coarse colluvial deposits and gently undulating surfaces.’

However, using this classification based on topographic features shown in Figure 5.48 and Table 5.9 has a limitation in delineating them in the study area since they usually reflect the locality where landslide features are observed. Therefore, it is imperative to determine specific relationships between various parameters based on their localities in order to represent a suitable model for the study area. Discussions

regarding relationships between slope values and other parameters earlier described are presented in Section 5.4.

5.3.2 Major principles in determining the landslide hazard

As pointed out by Popescu (1996), it is necessary to establish a realistic hazard zoning for the effective land management practice which provides numerous sources of information on proper actions against landslide hazard related problems. Identifying the state of the landslide hazard, either simply stable or unstable, is of primary importance to recognize through landslide hazard assessments. In Section 5.1, the state of the landslide hazard can be objectively determined by various causal factors which may influence the stability of slopes in internal and external ways. These factors can also be combined with each other to contribute to the landslide hazard in the area of concern. Descriptive nomenclatures are finally denoted to represent the state of the landslide hazard in the assessed areas. Representative examples of these descriptions of the degree of the landslide hazard based on their activities can be found in Crozier (1986), Popescu (1994; 1996), Vaunat et al. (1994), Cruden and Varnes (1996), Leroueil et al. (1996), Leroueil (2001), and the references quoted therein. Crozier (1986, pp. 32-33) divided the degree of the landslide hazard into three states based on the physical relationship between driving and resisting forces. These are as follows:

Stable indicates that “the margin of stability is sufficiently high to withstand all transient forces.”

Unstable (marginally stable) means that “slopes will fail at some time in response to transient forces attaining a certain level of activity.”

Actively unstable represents that “transient forces produce continuous or intermittent movement.”

Classifying states of the landslide hazard in terms of the factor of safety is useful to determine the amounts of the contribution of causal factors to activate and accelerate landslide movements. These factors can be grouped into three based on their independent functionalities affecting landslides (Crozier 1986, pp. 35-36): (1) preparatory; (2) triggering; and (3) controlling factors. Studies by Popescu (1994;

1996) on the first two factors, preparatory and triggering, were illustrated in Figure 2.3 and Table 5.3, respectively.

The identification of these distinct states may require historical information on the evolution of landslides. As described by Crozier (1986, p. 33), separating the marginally stable status from stable conditions is difficult unless a long period of observation about effects of triggering factors such as precipitation and earthquakes are provided. Because historical records are often difficult to obtain, a study may use a probabilistic approach to overcome a deficiency which was met about by using incomplete historical records.

The state of the landslide hazard can be frequently expressed by the landslide activity. The determination of the state of landslide hazard which is dependent of the landslide activity, either active or inactive, is given by Cruden and Varnes (1996). They described more detailed explanations on each state of the landslide hazard by the activity. Their descriptions about various landslide activities can be briefly listed as follows:

Active indicates a condition where landslides are “currently moving.” It can be subdivided into the first time and reactivated.

Suspended represents a condition in which landslides “moved within the last annual cycle of seasons” but are currently stopped.

Inactive means a condition in which landslide movement ceased in the past. It can be regrouped by the degradation of geomorphological expression and human intervention: (1) dormant; (2) abandoned; (3) stabilized; and (4) relict.

Keegan (2007, Table 4-4) discussed a correlation of the state of the landslide activity to the degree of the landslide hazard. He argued that suspended and dormant activity states defined by Cruden and Varnes (1996) are consistent with the marginally stable and stable-monitoring required states, respectively.

There was an effort to append geotechnical perspectives on landslides to the conventional two dimensional matrix of the landslide classification in which material and movement types are placed at ordinate and abscissa, respectively (Varnes 1978; Hutchinson 1988). Since geotechnical aspects would have distinct characteristics corresponding to the evolution of landslides, it is appropriate to illustrate different

movement states conforming to the progress of landslides. The different movement states suggested by Vaunat et al. (1994), Leroueil et al. (1996), and Leroueil (2001) are described as follows:

Pre-failure means that slopes in this state are competent to the internal deformations generated mainly from creep and progressive failures due to stress changes.

Onset of failure indicates that slopes are moving along the rupture surfaces developed by the deformation which exceeded the resistance of soil materials.

Post-failure represents a state between the initiation of landslides and the end of their movements. In this state landslides would have distinct characteristics dependent of their materials and movement types.

Reactivation of failure shows recurred landslide movements along pre-existing rupture surfaces which are formed in the first onset of landslides.

As with the state of the landslide activity introduced by Cruden and Varnes (1996) the classification defined by Vaunat et al. (1994), Leroueil et al. (1996), and Leroueil (2001) can be used to determine the degree of the landslide hazard. In this case the onset of failure and reactivation of failure is equivalent to the actively unstable state in the landslide hazard delineated by Crozier (1986). The 'Pre-failure' can be included in both stable and marginally stable states based on the magnitude of deformations. Similarly the 'Post-failure' can be contained in both unstable and marginally stable states, respectively. Keegan (2007) summarized these relationships by the following table (Table 5.10).

In order to determine a specific condition of the landslide hazard in the study area the following classification is proposed. It is based on the review of previous methodologies described above and recent studies by Keegan (2007) and Keegan et al. (2007) who established a practical approach to assess the stability states on a railway track due to landslide hazards. Landslide hazard states are subjectively determined by the presence and absence of identified landslide causal factors, either preparatory or triggering, in order to differentiate each landslide hazard state. The landslide hazard state is subdivided into four different categories and each state has a characteristic feature comparable to the counterpart of the landslide hazard.

Table 5.10 Correlations between the state of the landslide hazard (Crozier 1986) and the landslide activity (Vaunat et al. 1994; Cruden and Varnes 1996). *Source:* Data adapted from Keegan (2007)

Crozier (1986)	Cruden and Varnes (1996)	Vaunat et al. (1994) [†]
Stable	Inactive	Pre-failure
Unstable (marginally stable)	Suspended	Pre-failure Post-failure
Actively unstable	Active	Onset of failure Post-failure Reactivation of failure

[†] Also found in Leroueil et al. (1996), and Leroueil (2001).

Recommended actions for each state are also required, which can be used for administrative bodies that manage ongoing or future landslide hazards and related problems. Table 5.11 shows the landslide hazard states applied to this study.

If the state of landslide hazard is equivalent to the 'stable' condition, there is no adverse effect on the area of concern due to landslide hazards. Possible activities which can be found in landslides at this state are classified as: (1) relict; (2) stabilized; and (3) abandoned. Definitions of each activity condition in terms of landslide causal factors are as follows:

Relict "where there is only remnant evidence of a previous activity and the process causes of the activity are no longer apparent."

Stabilized "where artificial remedial measures have stopped activity and more than one cycle of seasons has passed."

Abandoned "where the process causal factors of the activity are no longer apparent."

The recommended action that might be economically appropriate is the acceptance of those hazards. The next state, 'stable with monitoring required,' ensures their stabilities against the landslide hazard with a questionable margin of them. The ambiguity can be solved by monitoring landslide causal factors, or instrumentation. The assumption of this state is the presence of landslide causal factors, either preparatory or triggering ones. Related landslide activities with this state are the following:

Preparatory "where no activity has occurred but preparatory process causal factors are apparent."

Repaired or recently stabilized "where artificial remedial measures have stopped the activity but less than one cycle of seasons has passed."

Dormant "where the causes of the activity remain apparent but last moved more than one annual cycle of seasons ago."

For the monitoring required stable condition, repairing and maintaining landslide causal factors as necessary as well as accepting hazards can be introduced for the landslide hazard management planning.

Table 5.11 Suggested states for landslide hazards based on their specific evolutions. The related landslide activity observed in specific landslide hazard state is also described. *Sources:* Data adapted from Keegan (2007) and Keegan et al. (2007)

Landslide hazard state	Relevant landslide activity
Stable	Relict
	Stabilized
	Abandoned
Stable (monitoring required)	Preparatory
	Repaired or recently stabilized
	Dormant
Marginally stable	Marginal
	Suspended
Unstable	Reactivated
	Active

The third condition with respect to the landslide hazard is ‘marginally stable.’ This state describes the presence of landslide causal factors, both preparatory and triggering. Based on the experience of landslides it can be grouped into two landslide activities: (1) marginal; or (2) suspended. These are as follows:

Marginal “where no activity has occurred but preparatory and triggering casual factors are apparent.”

Suspended “ground hazards that have moved in the last annual cycle of seasons but are not active at present.”

With this condition, administrative bodies may prepare the repairing and maintaining plans for the causes which increase potential landslide hazards and even in the worst situation they consider to incorporate mechanical engineered measures to correct and control the expected ongoing landslide hazards.

The last state of the landslide hazard is ‘unstable’ where destabilizing forces caused by landslide causal factors are dominated the area of concern and slopes are continuously moving. This state gives the following landslide activities dependent of previous landslide incidents:

Reactivated “ground hazard that is again active after being inactive.”

Active “ground hazard that is currently active.”

For the unstable state of landslide hazard, the consideration of economic perspectives is of primary importance in selecting required actions. For example, avoidance and relocating people and their properties from ongoing landslides can be the best strategy to minimize the impact of landslide hazards. However, except in special cases, these actions would lead to the adoption of over-expansive, less appropriate measures than mechanically engineered remedial ones.

The suggested states of the landslide hazard, as illustrated in Table 5.11, are then used as a fundamental threshold in order to assess the landslide hazard in the Town of Peace River. By combining identified landslide causal factors, as described in Section 5.1, with analyzed landslide controlled features from the airborne laser altimetry described in Section 5.3.1 as well as information on previous landslides obtained from aerial photo interpretations, assessments of the landslide hazard which

might control the urban development in the study area are constructed and classified by tolerable classes based on the observed landslide hazard. Detailed procedures and explanations are well described in the following section.

5.4 Construction of the landslide hazard assessment

In this section, a practical and systematic methodology to assess landslide hazards in the Town of Peace River is introduced. Based on proposed thresholds indicating different landslide hazard levels, landslide causal factors illustrated in the earlier section are analyzed and delineated against their impacts on the susceptibility of future landslides. In addition, a detailed aerial photo interpretation which provides a temporal variation of previous landslide deposits and information on the anthropogenic impact in the study area is introduced. All employed data are evaluated and classified as tolerable classes that indicate relative landslide hazards readily adaptable to the study area. These steps are systematically connected as shown in Figure 5.50.

5.4.1 Generating geomorphological maps

Generally, geomorphological maps based on cartographic expressions provide insights into various geomorphological features, processes, and their extents which would affect the human activity (Varnes and IAEG Commission on Landslides and other Mass Movement on Slopes 1984). Those features are also pursued in this study, even though I have focused major efforts on the identification of the temporal alteration of previous landslide features in order to analyze their evolution over time. As shown in Figure 5.50, relative contributions to landslide hazards by various causal factors and controlled features can be shown by superimposing them on geomorphological maps showing temporal variations of landslide features placed in the study area. The presence of landslides deposits over time would give an index for determining reactivated and suspended states of the landslide hazard at present. Tracing previous streams that have been disappeared or removed due to the urban development would also provide an indication for the potential landslide hazardous areas due to anthropogenic effects. The identification of landslide controlled features can be used to validate and improve the results.

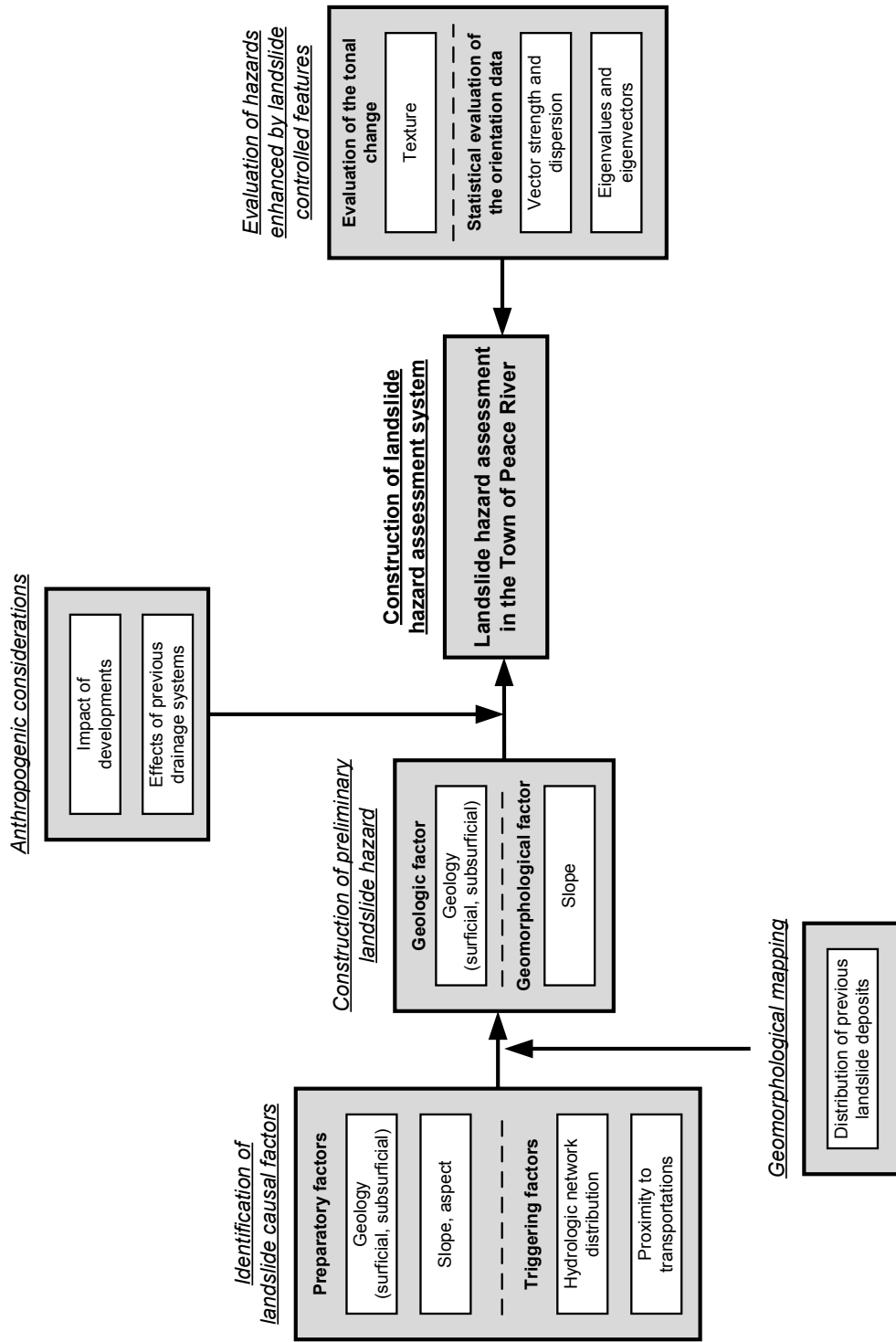


Figure 5.50 Diagram showing systematic processes for the evaluation of the landslide hazard in the study area. Detailed descriptions on the identification of landslide causal factors can be found in Section 5.1. The aerial photo interpretation for the study area is augmented to generate detailed geomorphological maps. Anthropogenic factors are considered to improve the landslide hazard assessment. Examinations of landslide controlled features described in Section 5.3.1 also illustrated to suggest possible enhancements in the landslide hazard assessment system

In this study four sets of aerial photographs are used for producing geomorphological maps to identify evidence of landslide features. Aerial photographs are from: (1) 1949 (1:40,000); (2) 1977 (1:31,680); and (3) 2006 (1:30,000). Each time period indicates the three distinct economic developments in the Town of Peace River (Chapter 2). Aerial photographs of 1958 (1:4,600) are also used for a detailed aerial photo interpretation in areas where six recent landslides occurred. The interpreted geomorphological information is then imported into ArcGIS for a unified representation and stored as a database for further landslide hazard assessment. Following consecutive figures (Figures 5.51 to 5.61) illustrate results of time series geomorphological mappings.

The 1949 aerial photographs and its corresponding geomorphological map cover the western portion of the study area (Figures 5.51 and 5.52). According to geomorphological features shown in Figure 5.52, previous landslide deposits observed in the west bank of the Peace River are relatively large and isolated, representing a maximum 5.6 km² of occupied area. These are all colluvial sediments that slid down in Holocene as the water eroded the toe of the ancient Peace River valley (Figure 3.9). In the east bank, drastic geomorphological changes due to landslides are found. Areas of the east bank of the Peace River as far north as the mouth of the Heart River and valley walls along the Heart River and Pat's Creek are all landslided. Some of them are located adjacent to highways that are parallel to tributaries, which might have affected the road safety (Hardy 1957; Sharma 1970).

Recent geomorphological conditions are illustrated in aerial photographs taken in 2006 (Figure 5.56). Due to the extent of aerial photographs and the relatively large scale, small landslide deposits are easily observed especially along the tributaries of the Peace River (Figure 5.57).

Studies of the variation of geomorphological impacts on recent landslides are best done with large scaled geomorphological maps shown in Figures 5.59 and 5.61. Figure 5.59 shows geomorphological features of the west bank of the Peace River taken in the 1958 aerial photographs prior to the massive development in the study area (Figure 5.58). Extent of recent landslides in the west bank such as Mile 50.9 and Shop Slides clearly show the evidence of a single or multiple surface drainages placed in current landslide displaced materials. For the Mile 50.9 Slide a large surface drainage is found above the landslide scarp near railway track (Figure 5.59) and this drainage feature is also observed in 1949 and 1977 geomorphological maps

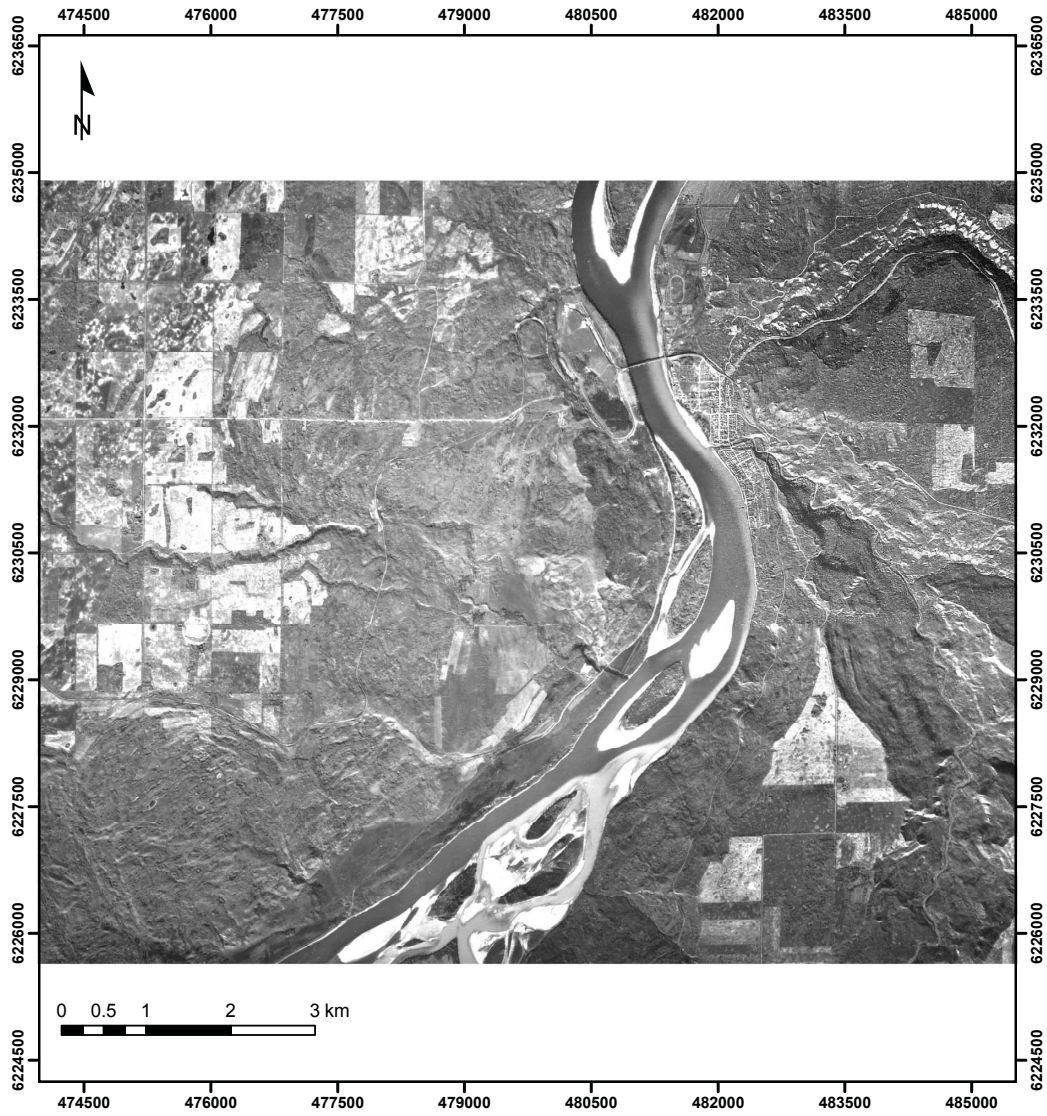


Figure 5.51 1949 aerial photographs of the Peace River area, scale 1:64,000 (Alberta photo: AS 95 5604 266 to 268)

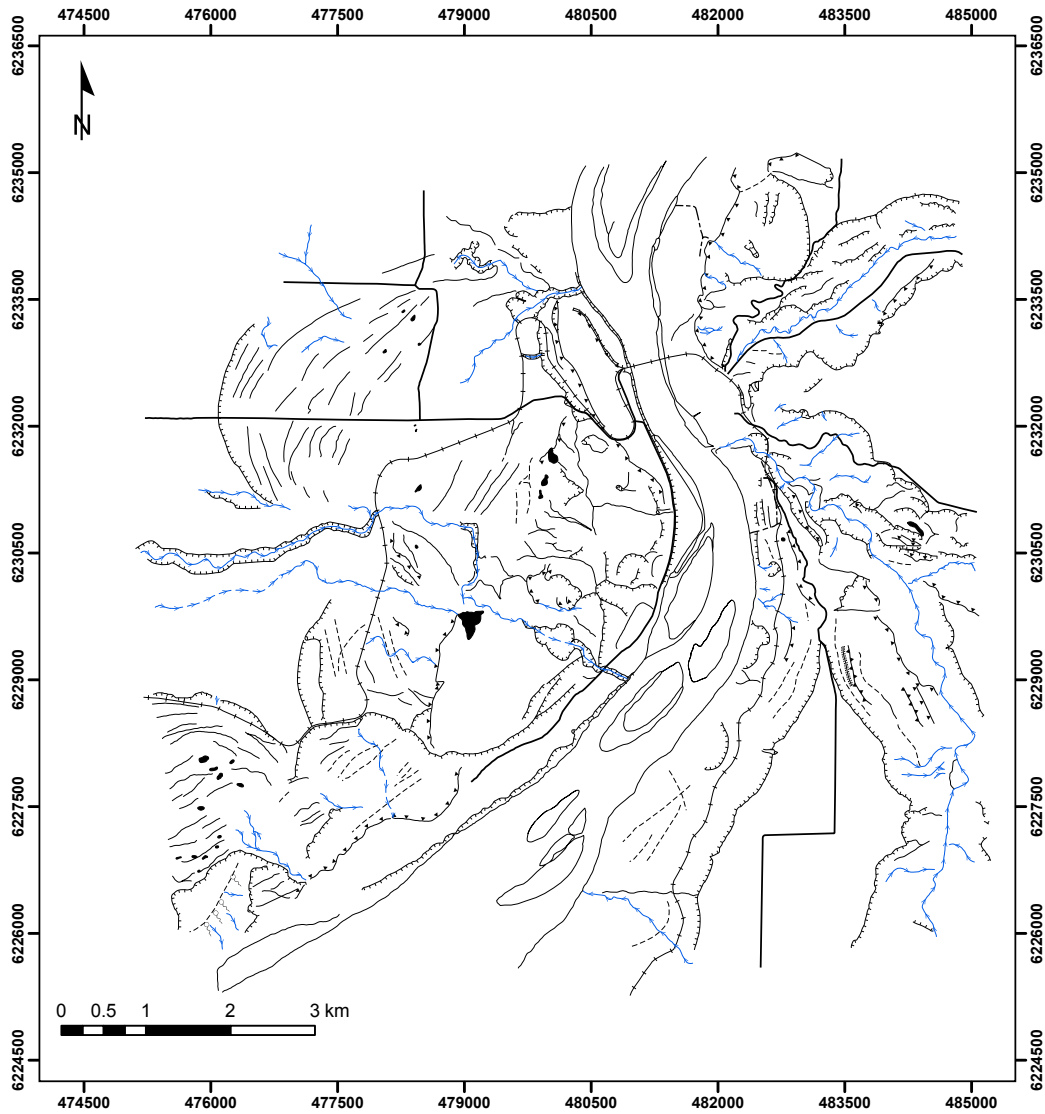


Figure 5.52 1949 geomorphological map depicting the Peace River area. The geomorphological map was implemented by the aerial photo interpretation on consecutive aerial photographs presented in Figure 5.51. Identified streams are delineated by the blue arrow along their flowing directions. Detailed descriptions of other landslide features and anthropogenic structures are illustrated in Figure 5.53












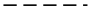
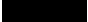




	River outline
	Stream (confirmed)
	Breaks of slope (sharp, concave)
	Breaks of slope (round, concave)
	Breaks of slope (sharp, convex)
	Breaks of slope (round, convex)
	Breaks of slope (sharp, ridge)
	Main scarp (sharp)
	Main scarp (round)
	Minor scarp (confirmed)
	Minor scarp (inferred)
	Sag ponds or depressions
	Spring
	Tension crack
	Residence boundary
	Road
	Railway

Figure 5.53 Delineation of representative symbols used to produce geomorphological maps that are shown in Figures 5.51 to 5.61. Geomorphological (breaks of slopes and scarps), hydrological (streams), and anthropogenic (roads and railways) features are illustrated with their unique symbols. Presented symbols are from Dearman et al. (1972) and Federal Geographic Data Committee (2006)



Figure 5.54 1977 aerial photographs of the Peace River area, scale 1:51,000 (Alberta photo: AS 1575 240 to 242)

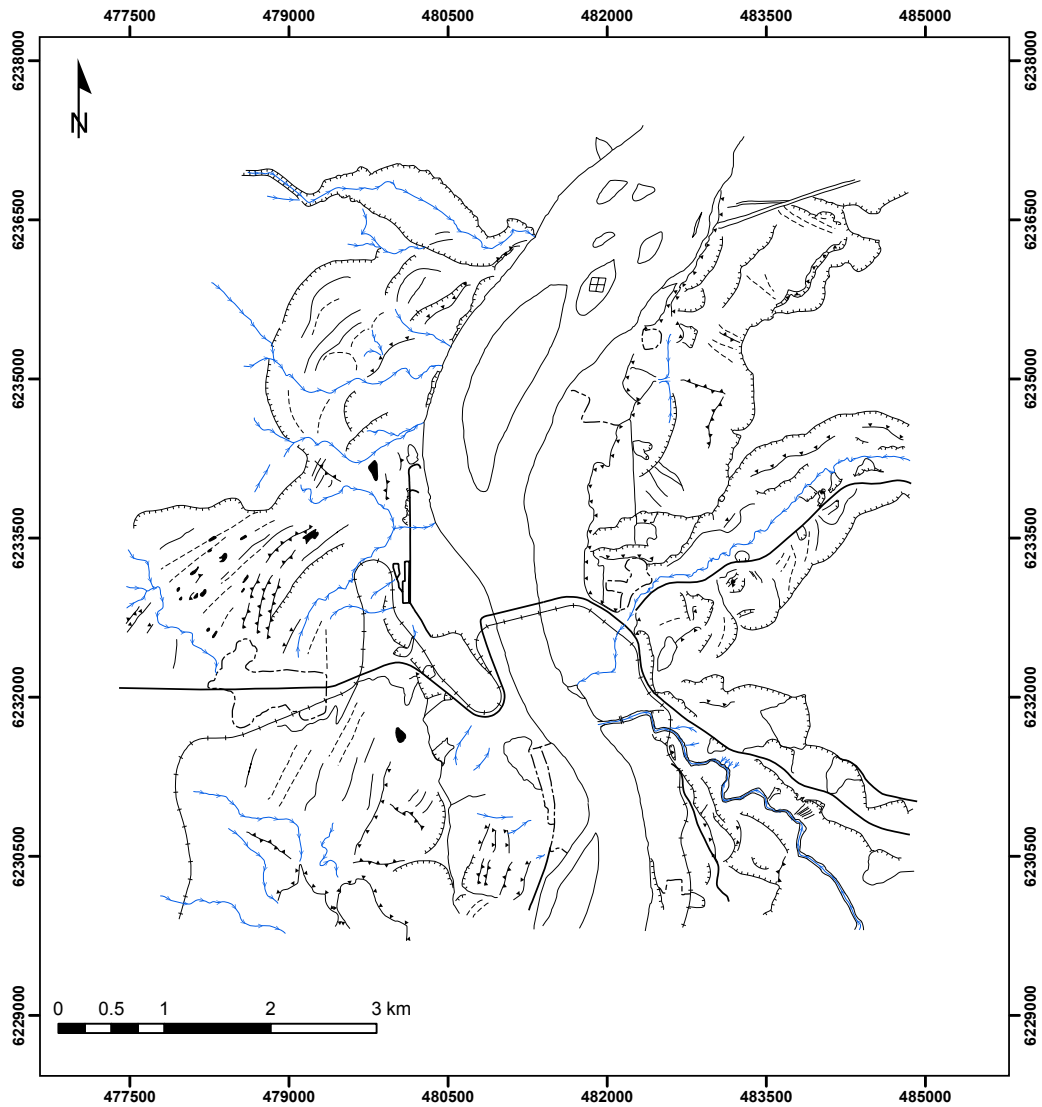


Figure 5.55 1977 geomorphological map depicting the Peace River area. The geomorphological map was implemented by the aerial photo interpretation on consecutive aerial photographs presented in Figure 5.54. Identified streams are delineated by the blue arrow along their flowing directions. Detailed descriptions of other landslide features and anthropogenic structures are illustrated in Figure 5.53

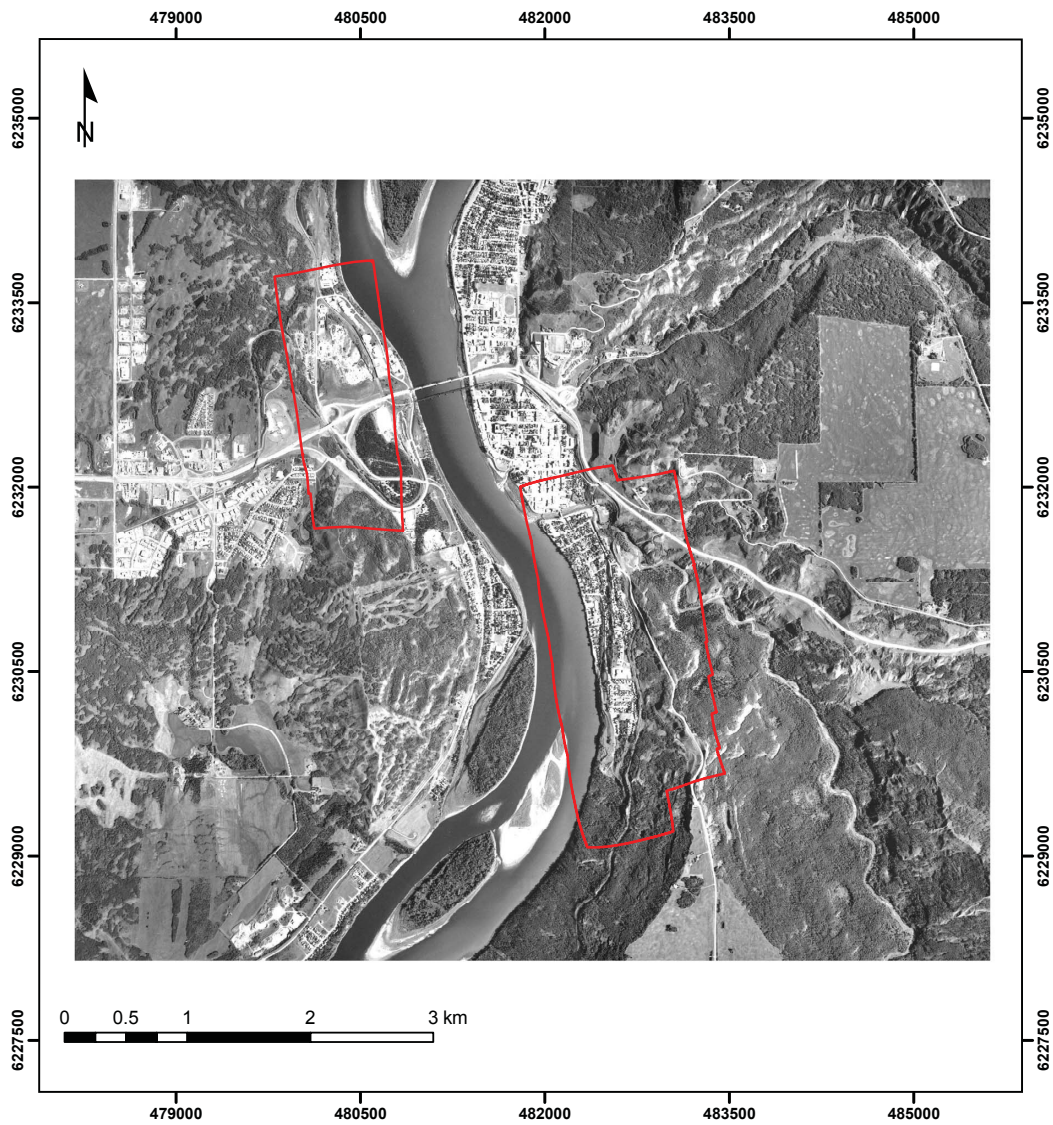


Figure 5.56 2006 aerial photographs of the Peace River area, scale 1:44,000 (Alberta photo: TRS G0602-32-2357 and 2358). Areas outlined by red solid lines represent extents of 1958 aerial photographs depicting the west (Figure 5.58) and east (Figure 5.60) banks of the Peace River where recent landslides are placed

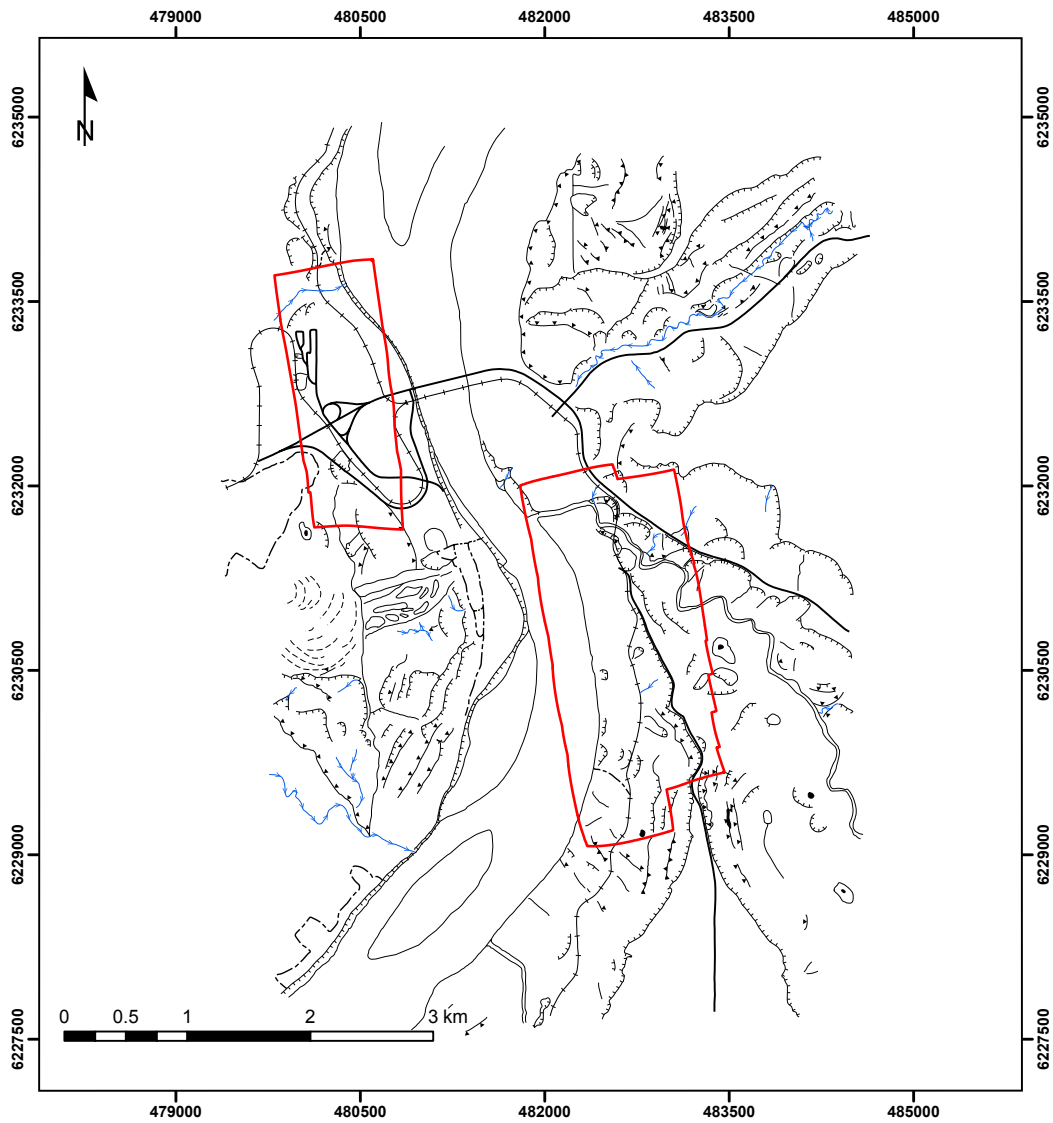


Figure 5.57 2006 geomorphological map depicting the Peace River area. The geomorphological map was implemented by the aerial photo interpretation on consecutive aerial photographs presented in Figure 5.56. Areas outlined by red solid lines represent extents of 1958 geomorphological maps depicting the west (Figure 5.59) and east (Figure 5.61) banks of the Peace River where recent landslides are placed. Identified streams are delineated by the blue arrow along their flowing directions. Detailed descriptions of other landslide features and anthropogenic structures are illustrated in Figure 5.53

(Figures 5.52 and 5.55). This is supported by the presence of a culvert in this location for a surface drainage (Lindberg and Savigny 1980). As pointed out in Chapter 4, the main trigger of the Mile 50.9 Slide is the significant cuts and fills for the construction of the trailer court at the toe of the slope which may have blocked the drainage, either surface or subsurface, by placing of fill materials and led to the interference on the natural surface and subsurface drainage system.

Although the major significant displacement was recorded since 1985 (Proudfoot and Cullum-Kenyon 2006), the approximate extent of the Shop Slide was observed even in the 1977 geomorphological map. Because the old Highway 2 was constructed along the valley wall by extensive earthworks, major drainage systems might have been interfered. Major instabilities were found at the crown and the toe of the slope in forms of tilted telegraph poles and toe bulging (Figure 4.28) whose locations are identical to the outlets of the surface drainage (Figure 5.59).

A correlation of recent landslides in the east bank of the Peace River with previous geomorphological features taken in 1958 (Figure 5.60) is illustrated in Figure 5.61. Extent of three recent landslides, Mile 47.8, Mile 46.5, and 99/101 Streets Slides, are placed in old landslide deposits detected in the 1958 geomorphological map, indicating the reactivated state. While the Mile 47.8 Slide occurred in an isolated location, Mile 46.5 and 99/101 Streets Slides are placed within the margin of large landslide deposits inter-connected with each other, denoting that a landslide would be a trigger to another one (Lindberg and Savigny 1981b). The Mile 47.6 Slide has no apparent active landslide features based on the 1958 geomorphological map, indicating a reactivated state. This is supported by the fact that the first significant movement was reported in 1984 after completing the road pavement (Table 4.3).

The identification of the surface drainage within extents of recent landslides would show the impact of the modification in ground surface profiles on the stability of slopes in the study area. For example, massive short surface drainages can be found in the main scarp of the Mile 47.6 Slide. In the 99/101 Streets Slides several long surface drainages flowed toward the Peace River. Residential developments which had blocked these drainage systems by filling the gullies, might have increased pore water pressures within slopes (Barlow and McRoberts 1992). These anthropogenic effects on 99/101 Streets Slides are well illustrated in Figure 4.16. Observed surface drainages located above the Mile 47.8 and Mile 46.5 Slides may provide large amounts of water from railway drainage systems and bring stability problems.

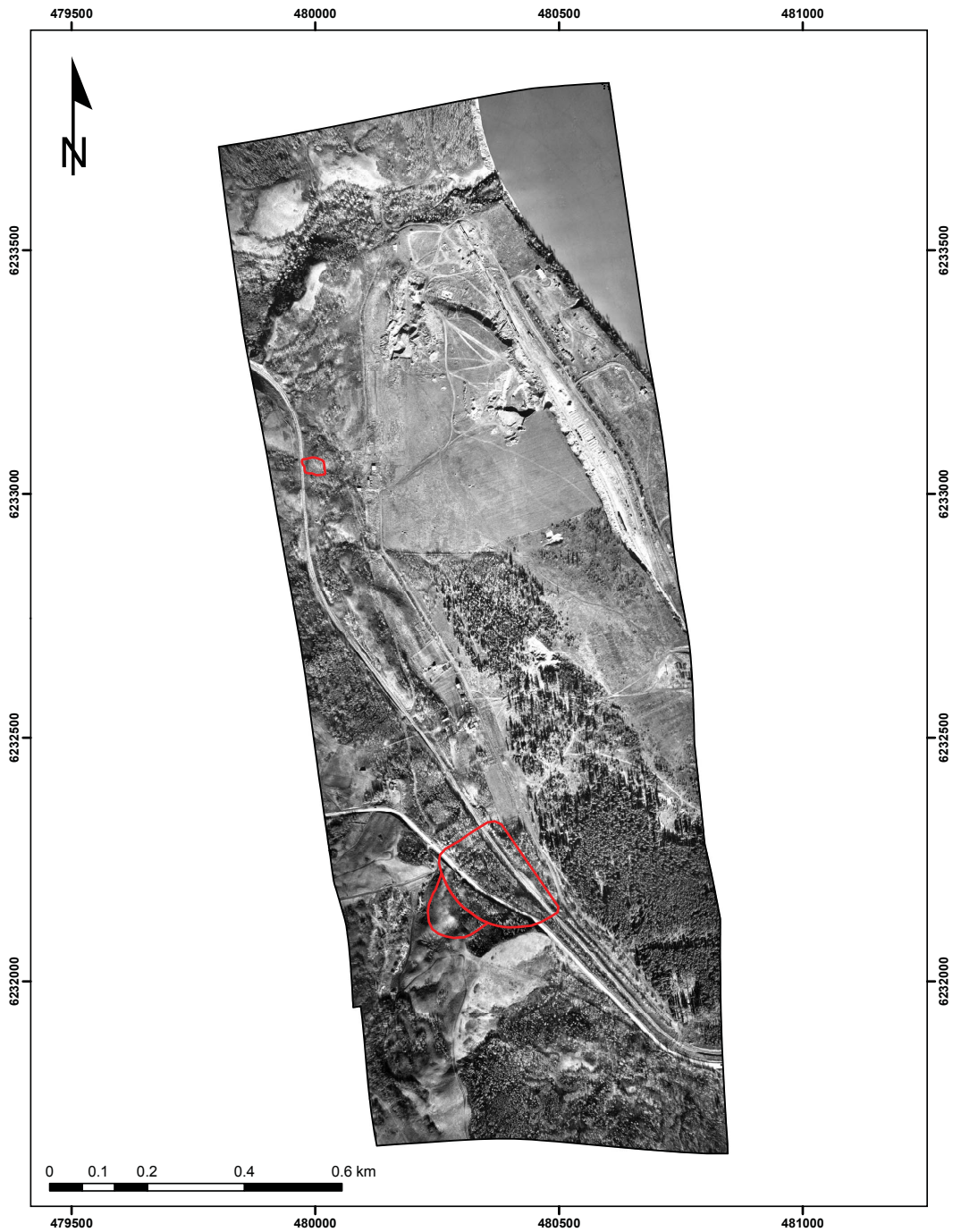


Figure 5.58 1958 aerial photographs of the west bank of the Peace River, scale 1:9,000 (Alberta photo: AS 26-99 to 103). Areas enclosed by red solid lines represent recent landslides occurred in the west bank of the Peace River, which are Mile 50.9 and Shop Slides (Figure 4.1)

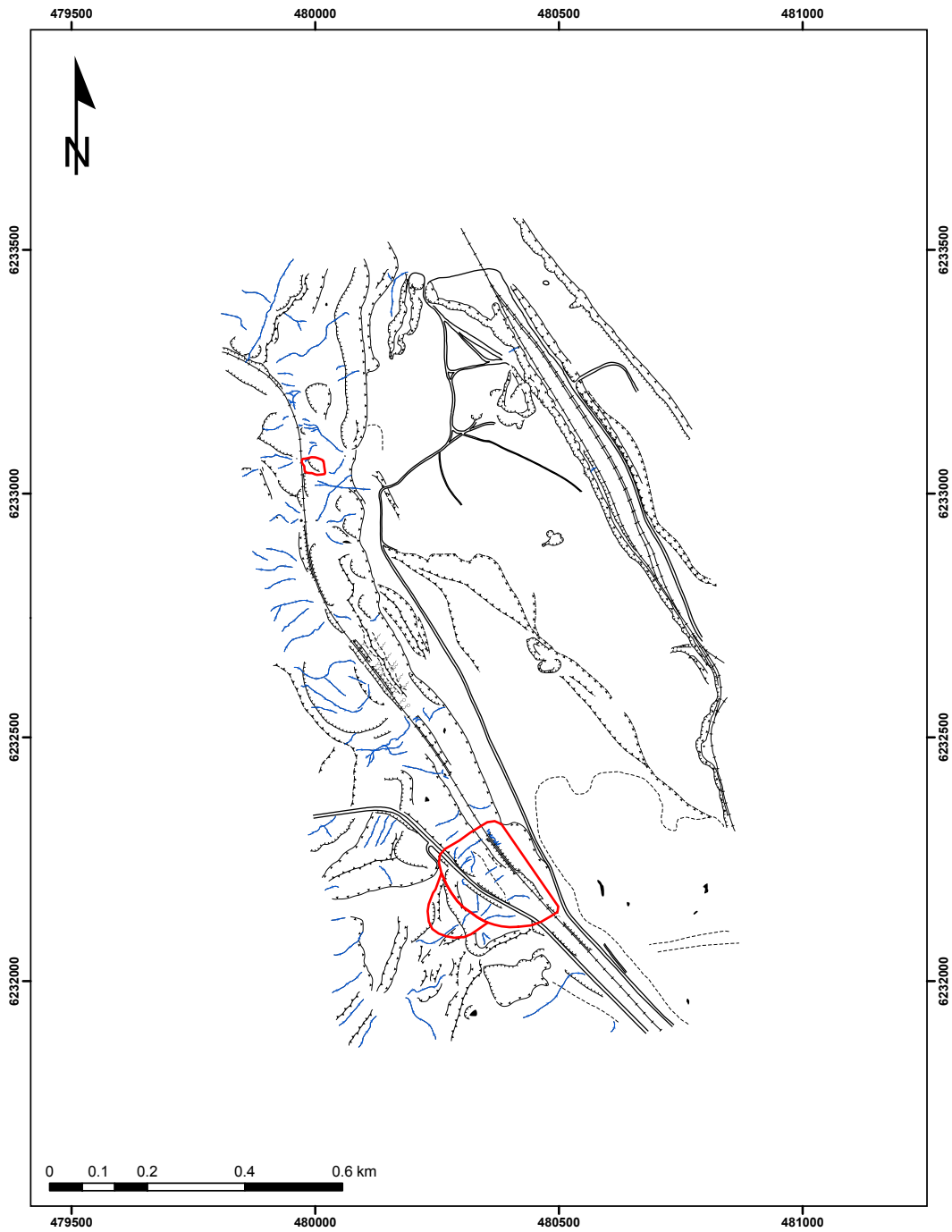


Figure 5.59 1958 geomorphological map depicting the west bank of the Peace River. The geomorphological map was implemented by the aerial photo interpretation on consecutive aerial photographs presented in Figure 5.58. Areas enclosed by red solid lines represent recent landslides occurred in the west bank of the Peace River, which are Mile 50.9 and Shop Slides (Figure 4.1). Identified streams are delineated by the blue arrow along their flowing directions. Detailed descriptions of other landslide features and anthropogenic structures are illustrated in Figure 5.53

Despite difficulties in determining the proper scale, it is worth noting that analyzing temporal geomorphological maps may provide the extent of previous landslides and insights on their occurrences. This information can be used to differentiate fundamental characteristics of the landslide. In this study, therefore, major contributions of temporal geomorphological variations observed in geomorphological maps for the landslide hazard assessment are the identification on previous landslide deposits. This differentiates the active state such as the first time and reactivated one and recognizes the effects of the interference on previous surface drainages due to anthropogenic activities. This finding may also improve the quality of landslide hazard assessments (Figure 5.50).

5.4.2 Establishing the degree of the landslide hazard

In this section the landslide hazard is constructed by two consecutive methodologies. Firstly, results of the slope analysis, combining geological and geomorphological factors, are used to determine levels of the preliminary landslide hazard. Some considerations obtained from geomorphological maps are described to refine the existing landslide hazard, which can delineate influences in landslide hazards due to anthropogenic factors. Finally, correlation analyses between slope values and other parameters such as texture, vector dispersion, and eigenvalue ratios are followed to provide an idea for the enhancement of the landslide hazard assessment applied to the study area.

5.4.2.1 Construction of the preliminary landslide hazard

The preliminary landslide hazard focuses on the identification of typical characteristics observed in landslide causal factors in order to quantify their relative contributions on actual landslides. The major objective for performing the preliminary landslide hazard assessment is, therefore, to get prevailing states or conditions that triggered previous landslides in the study area. This information may also suggest various landslide states in other areas. Table 5.12 shows proposed states of landslide hazards on previous landslide deposits, which are based on geologic and geomorphological factors representing as slope values and colluvial deposits. Each specific condition of landslide hazards is employed from recent studies by Keegan

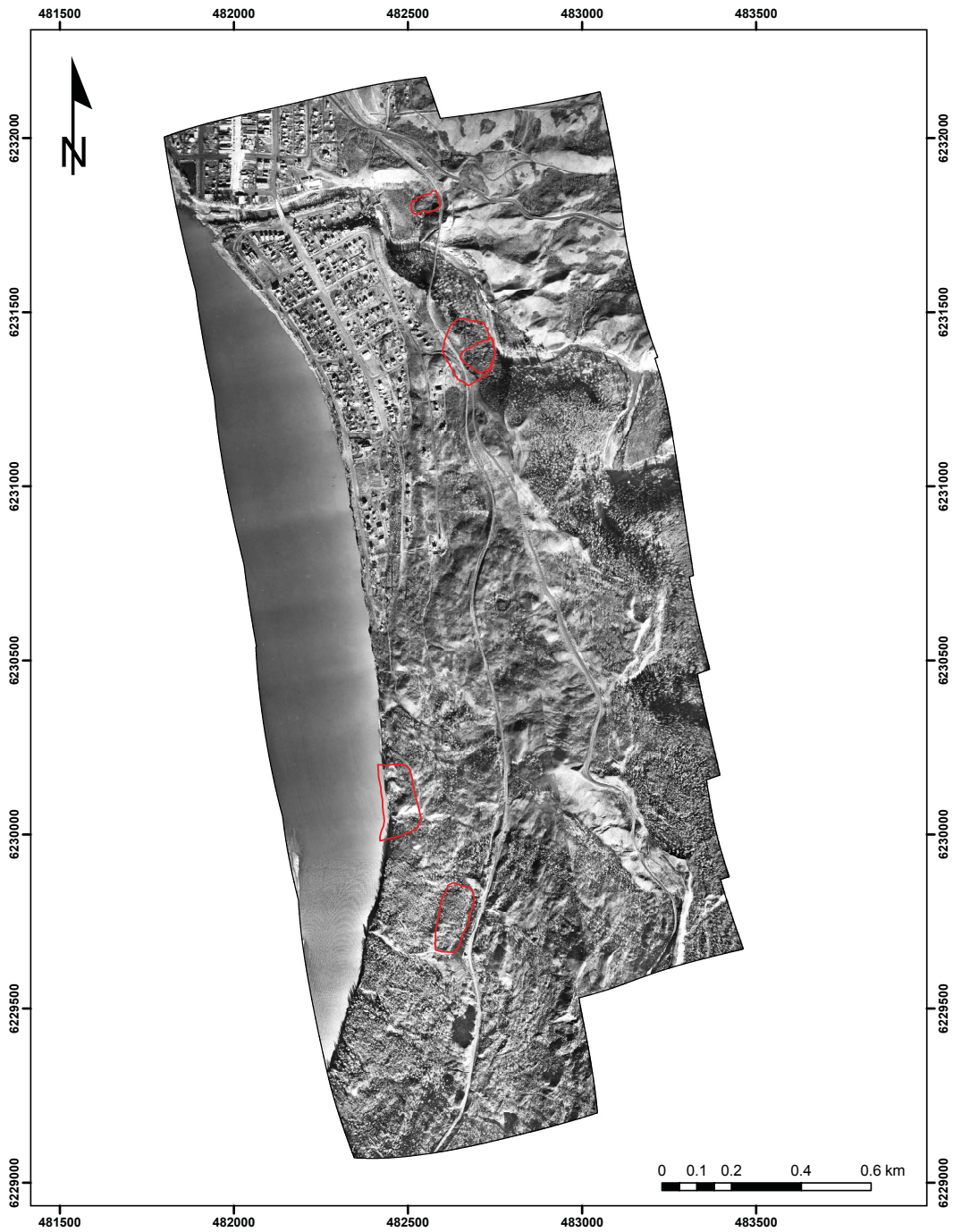


Figure 5.60 1958 aerial photographs of the east bank of the Peace River, scale 1:12,600 (Alberta photo: AS 26-157 to 103; AS 26-175 to 181). Areas enclosed by red solid lines represent recent landslides occurred in the east bank of the Peace River, which are Mile 47.8, Mile 47.6, Mile 46.5, and 99/101 Streets Slides (Figure 4.1)

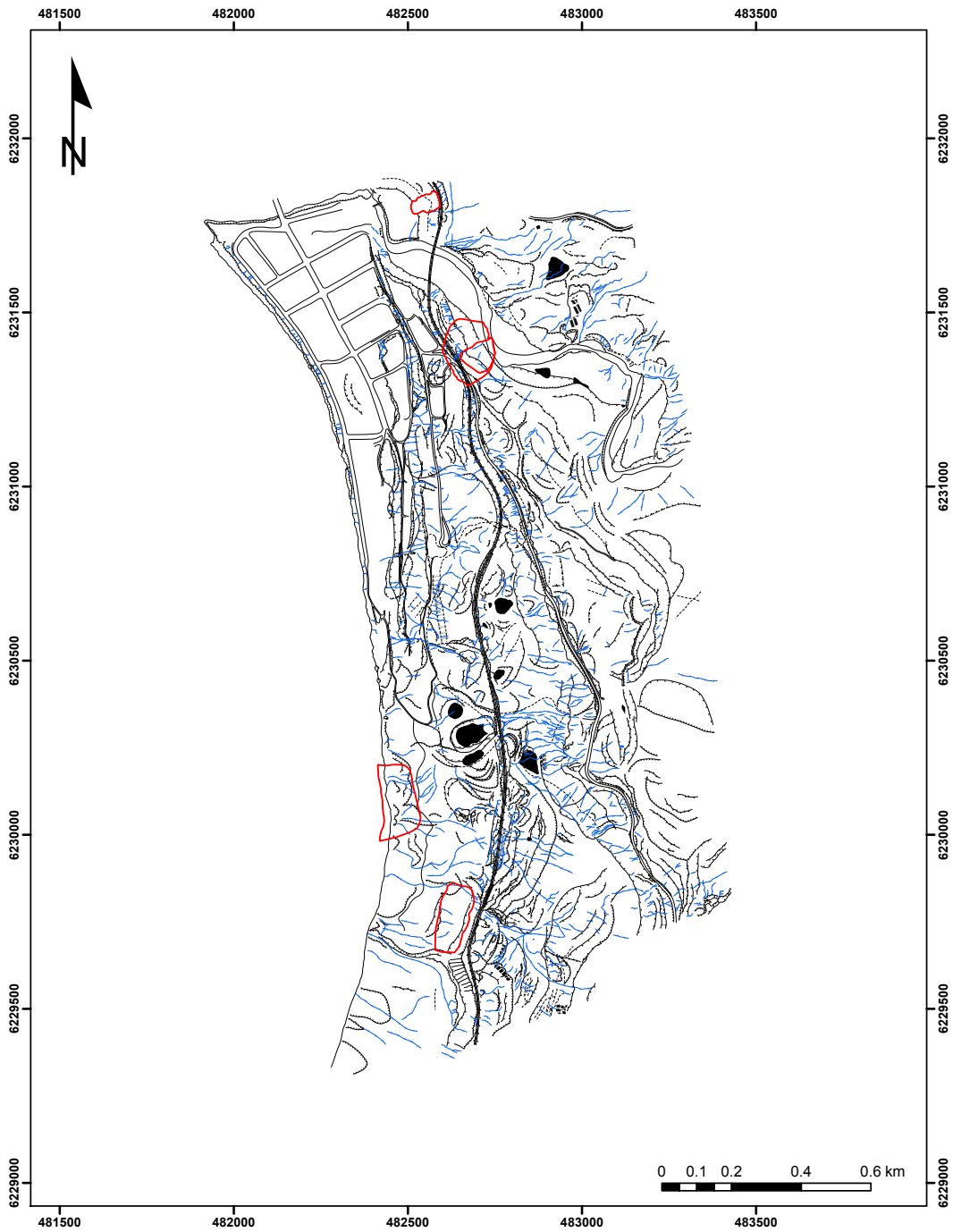


Figure 5.61 1958 geomorphological map depicting the east bank of the Peace River. The geomorphological map was implemented by the aerial photo interpretation on consecutive aerial photographs presented in Figure 5.60. Areas enclosed by red solid lines represent recent landslides occurred in the east bank of the Peace River, which are Mile 47.8, Mile 47.6, Mile 46.5, and 99/101 Streets Slides (Figure 4.1). Identified streams are delineated by the blue arrow along their flowing directions. Detailed descriptions of other landslide features and anthropogenic structures are illustrated in Figure 5.53

(2007, Table 4-4) and Keegan et al. (2007, Table 4) and is also summarized in Table 5.11. The spatial distribution of landslide hazards observed on previous landslide deposits is illustrated in Figure 5.62.

For practical points of view such as the land use planning, however, the safety margin should be incorporated to values in Table 5.12. In other words, suggested states shown in Table 5.12 usually contain uncertainties with regard to determining the state of landslide hazards and these are emphasized on the boundary of each state. In order to reduce the uncertainty inherent to the proposed guideline, therefore, a 95 percent confidence limit should be considered to each landslide hazard state though a five percent of incorrect decision is still existed. Table 5.13 shows suggested states of landslide hazards for the practical problems.

Figure 5.62 shows that unstable areas (the 'Unstable') in the proposed landslide hazard system which are identified from the preliminary landslide hazard map make 17.6 percent of landslide deposits evaluated and can be found in areas on valley slopes along the Heart River and Pat's Creek, the eastern entrance to the town, and the small portion of residential areas in the east bank of the Peace River where transportation routes are located nearby. This finding is reasonable as historical records on the occurrence of landslides in the study area have indicated many landslides which had occurred on and along transportation routes (Kjelland et al. 2009; Alberta Transportation 2011). Unstable areas are enclosed by marginally stable areas (the 'Marginally stable') which are in the quasi-stable state around the unstable zones. These make 15.5 percent of observed landslide deposits. Other landslide hazard levels, 'Stable - Monitoring required' and 'Stable,' make 58.1 and 8.8 percent of landslide deposits and cover westerly aspect slope of the east bank of the Peace River and old landslide deposits located in the east bank of the Peace River, respectively.

Results of the landslide hazard assessment analyzed here can be used as a reference to extend the landslide hazard assessment into the entire study area. In this case same representative values of slope and surficial deposit factors shown in Table 5.12 (or Table 5.13) are consistently employed to delineate the overall landslide hazard on the study area. Figure 5.63 shows the landslide hazard assessment in the study area which is based on geologic and geomorphological factors previously described.

Table 5.12 Suggested states of landslide hazards on identified landslide deposits in the study area based on geologic and geomorphological factors. Distributions of geologic and geomorphological factors on landslide deposits are shown in Figures 5.11 and 5.12. The distribution of mean slope values by using the state of landslide hazards is described in Figure 5.13. States of landslide hazards and their corresponding activities are presented in Table 5.11

State of landslide hazards	Geomorphological factor (Slope, degrees)	Geologic factor (Surficial deposit)
Stable	$< 10^{\dagger}$	Colluvial deposit
Stable - Monitoring required	10-19 [‡]	
Marginally stable	19-22 ^{††}	
Unstable	> 22	

[†] Critical slope angle (Skempton and Delory 1957).

[‡] Lower limit of stable state.

^{††} Upper limit of stable state.

Table 5.13 Suggested states of landslide hazards which contain uncertainties for the practical application. A 95 percent confidence interval of each state is delineated in the Section 5.1.3 and Figure 5.13. States of landslide hazards and their corresponding activities are presented in Table 5.11

State of landslide hazards	Suggested slope angle [†]
Stable	< 8.8
Stable - Monitoring required	8.8-17
Marginally stable	17-20.6
Unstable	> 20.6

[†] Lower bound of the 95 % confidence limit in each landslide hazard state.

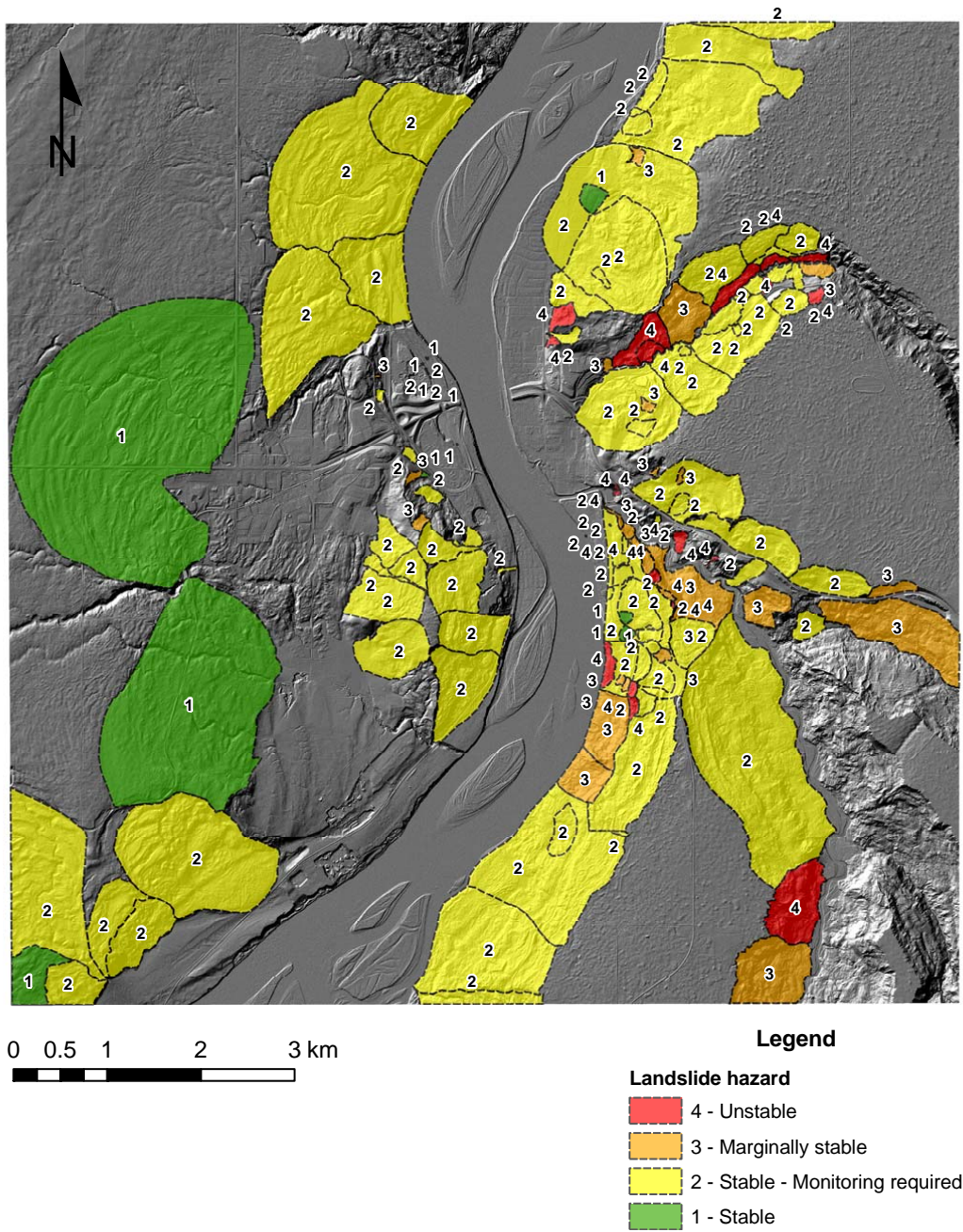


Figure 5.62 Distribution showing preliminary landslide hazards derived from geologic and geomorphological factors observed on previous landslide deposits in the study area. Four levels of landslide hazard are delineated by different colors and numbers. A hillshade imagery presented in the background is obtained from the digital elevation model (Figure 5.4) with the spatial resolution of 0.5 by 0.5 metres

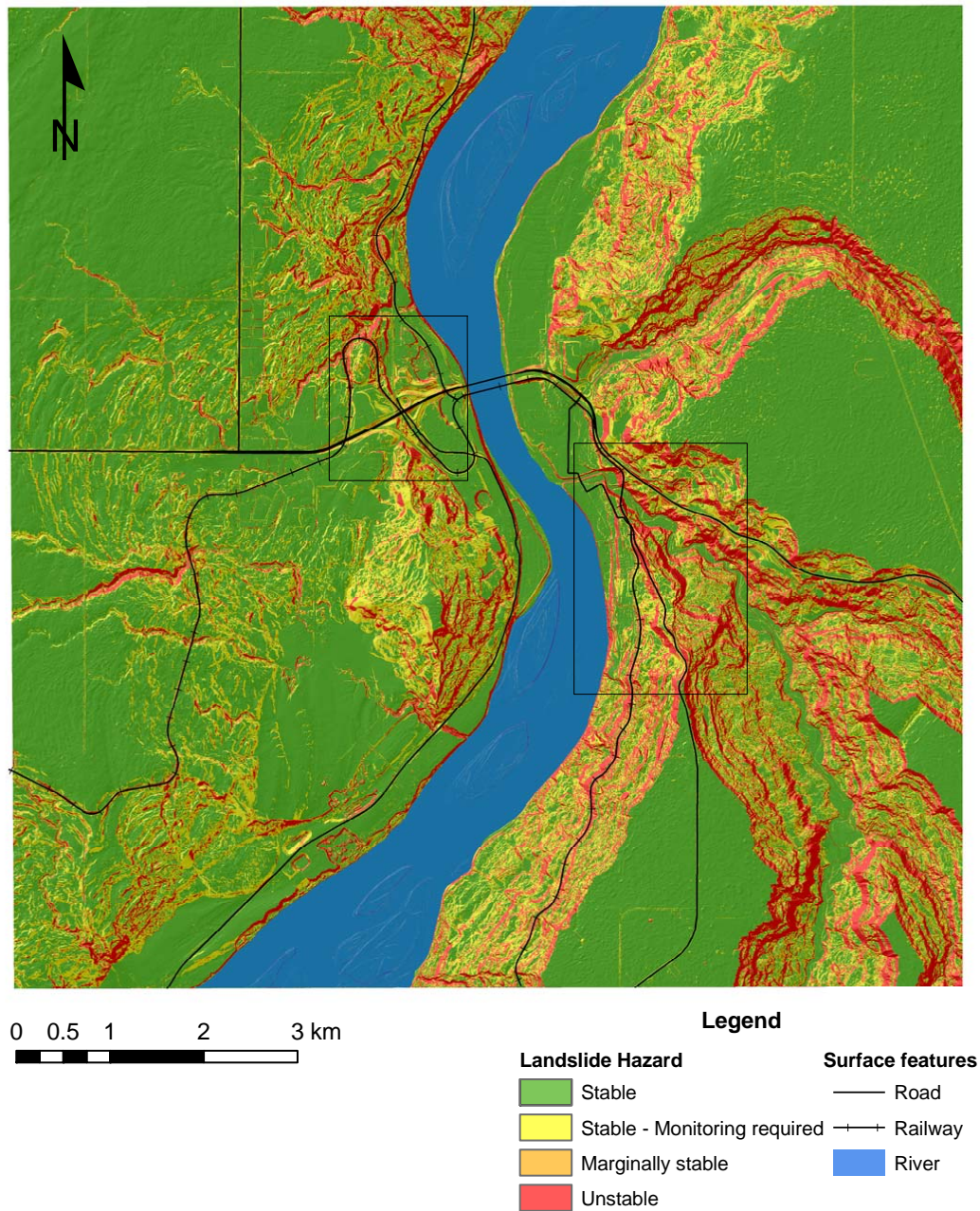


Figure 5.63 Distribution showing the landslide hazard assessment in the study area derived from geologic and geomorphological parameters observed on previous landslide deposits. Representative values which determine the state of landslide hazard are shown in Table 5.12. Four levels of landslide hazard are delineated by different colors. Surface features such as road, railway, and river are also presented. Areas delineated by black solid lines are extents of a closer look shown in Figures 5.64 to 5.66. A hillshade imagery presented in the background is obtained from the digital elevation model (Figure 5.4) with the spatial resolution of 0.5 by 0.5 metres

5.4.2.2 Anthropogenic considerations

In this study two anthropogenic aspects are considered to provide a better understanding of human interferences to the landslide hazard assessment. These elements, the identification of the land use adjacent to slopes and previous drainage systems, are closely related to the urban development for the community. Earthworks to acquire space for residential, commercial, and industrial purposes often generate large cuts and fills in naturally stabilized or nearly-stabilized ground. Making cuts at toes of slopes decreases resisting forces and putting weight on tops of slopes or blocking previous drainages by filling gullies also increases driving forces within slopes. The identification of these aspects from geomorphological maps, therefore, provides more intuitive understanding on causes of landslides and their actual mechanisms.

The land use distribution, one of the anthropogenic aspects, which is usually applied to the landslide risk assessment as a vulnerability factor, the element at risk from the landslide hazard, is used in this study in order to define the degree of landslide hazard by comparing the proximity of its components to the landslide hazard. In other words, developing lands for various purposes usually leads to the disturbance of potentially unstable areas and thus accelerates their instability. In refining landslide hazards, three elements among the five components of the land use distribution shown in Figure 5.10 are recognized, located at toes of slopes, which indicate that developments on those areas may affect the stability of adjacent slopes. These are as follows: (1) park, school, or playground; (2) residential areas; and (3) undeveloped or partially developed areas, all of which are relatively less limited to construct on elevated areas than commercial and industrial areas that may require easy access to resources and transportation routes. The consideration of typical land use which is located near slopes and susceptible to landslides would make the state of the landslide hazard on those areas more precise (Figure 5.64).

Figure 5.64 shows that state of landslide hazards along the toes of slopes located on the east bank should be influenced by anthropogenic considerations, for example, raising the landslide hazard one level above if they met a specific land use such as residential and partially developed areas. Similar issues on the land use can also be found in some areas under Misery Mountain on the west bank of the Peace River where similar land use components are placed.

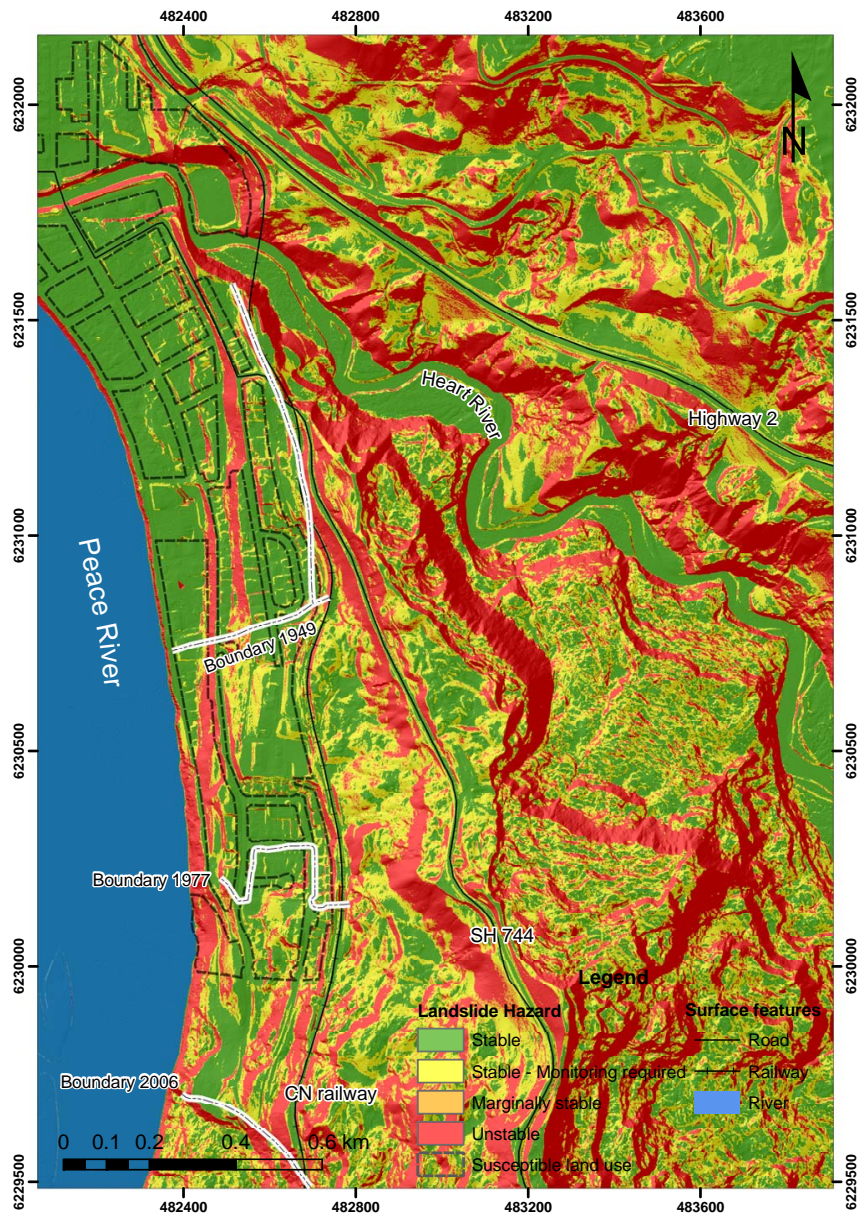


Figure 5.64 Consideration of the land use in the landslide hazard assessment which focuses on the east bank of the Peace River including town centre and adjacent residential areas. The location of the figure is indicated in Figure 5.63. Selected land use components which might affect the slope stability on the study area are delineated to represent extent of anthropogenic impacts. Same colors used in Figure 5.63 are introduced to classify each state of the landslide hazard. The extent of residential boundaries showing the progress of developments is obtained from consecutive geomorphological maps of 1949, 1977, and 2006. A hillshade imagery presented in the background is obtained from the digital elevation model (Figure 5.4) with the spatial resolution of 0.5 by 0.5 metres

The second consideration for the improvement of the landslide hazard is related to geomorphological changes in drainage patterns. Interrupting natural drainages causes changes in pore water pressure within slopes and increases possibilities of future landslides. Causes of this impact are various but human induced factors can be considered as a main agent for this geomorphological alteration.

In this study currently blocked or disappeared drainages are investigated from the subsequent geomorphological maps shown in Figures 5.51 to 5.61. The study also assumes that areas where streams had flowed in the past are more susceptible to landslides because of the blocking of drainages than those where streams are currently flowing. The identification of these areas is then used to modify the landslide hazard where it is located along the course of previous drainages. Figures 5.65 and 5.66 illustrate traces of previous drainage systems that disappeared at present due to urban development and construction of transportation routes.

Figure 5.65 shows that distinct changes in previous drainage systems on the west bank of the Peace River are closely related to the construction of major transportation routes and other nearby structures such as Highway 2, Shaftesbury Trail, and trailer courts under the Canadian National Railway. Especially the construction of Highway 2, which did not appear on the 1977 aerial photograph, is considered to impose tremendous impacts on modifying natural courses of drainage systems in the study area. Effects of human induced factors in changing previous drainages are also found in the east bank of the Peace River along the current course of Highway 2 and the south end of residential areas (Figure 5.66).

By adapting considerations of the land use near slopes and previous drainage systems, landslide hazards in the study area can provide practical perspectives especially where this information is available. Since landslides evolve into a hazard only when they interact with people and their properties (Pestrong 1976), the analysis based on the relative importance to landslide hazards can be a suitable approach and provide an efficient way to construct the overall degree of landslide hazards in the study area.

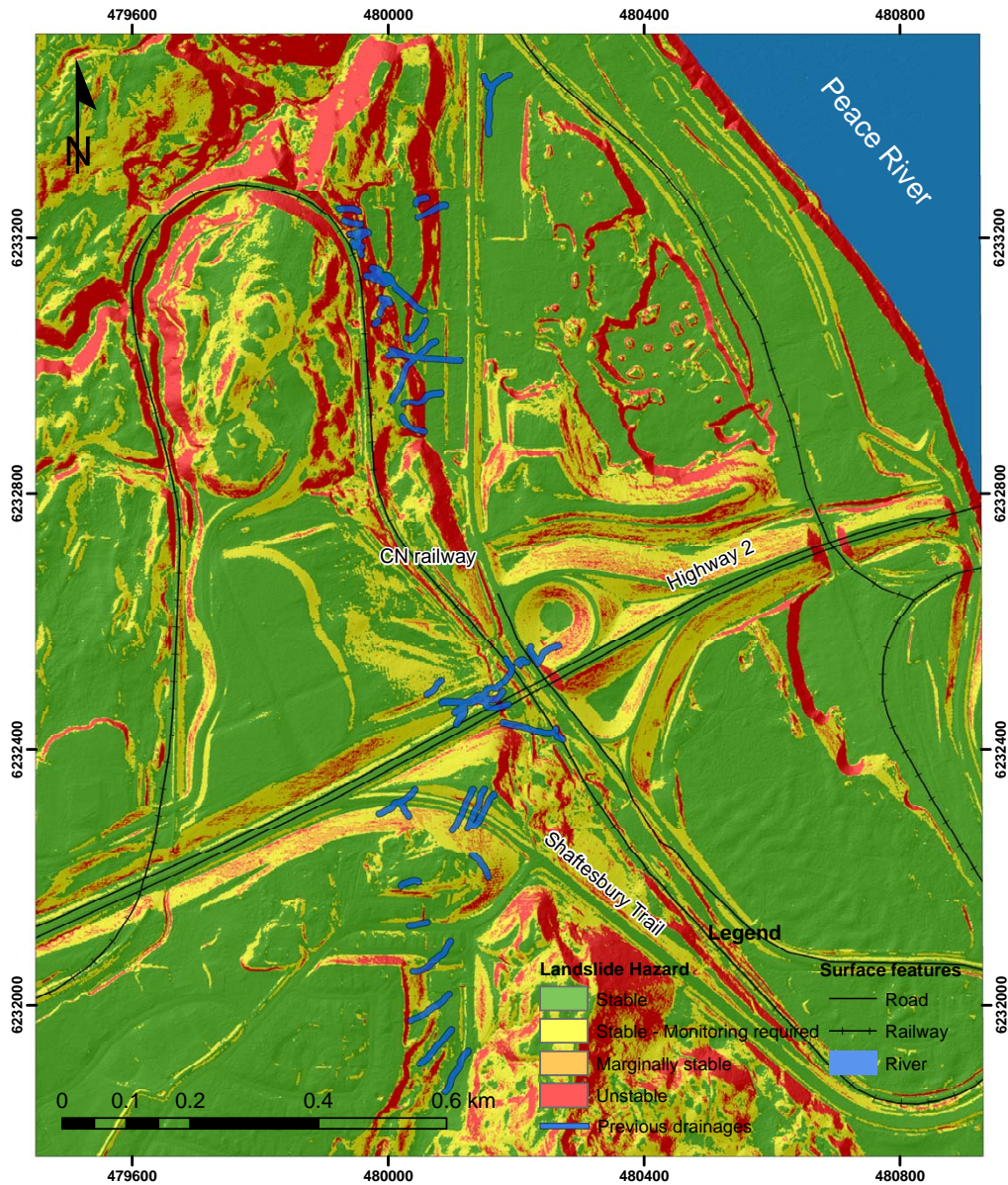


Figure 5.65 Traces of previous drainage systems observed in the west bank of the Peace River and corresponding landslide hazards. Previous drainages are obtained from subsequent geomorphological maps illustrated in Figures 5.51 to 5.61. A five metre buffer is applied around drainages to show the influence of streams. A hillshade imagery presented in the background is obtained from the digital elevation model (Figure 5.4) with the spatial resolution of 0.5 by 0.5 metres

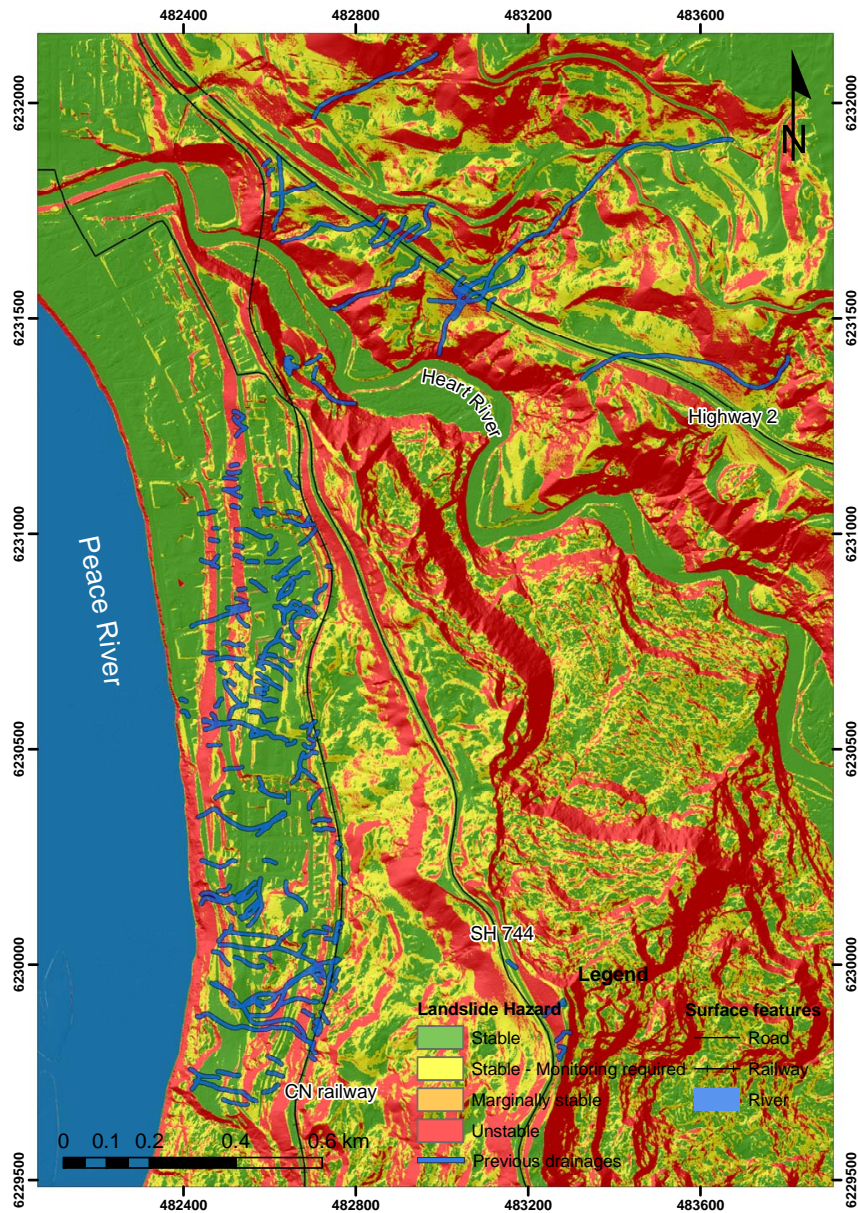


Figure 5.66 Traces of previous drainage systems observed in the east bank of the Peace River and corresponding landslide hazards. Previous drainages are obtained from subsequent geomorphological maps illustrated in Figures 5.51 to 5.61. A five metre buffer is applied around drainages to show the influence of streams. A hillshade imagery presented in the background is obtained from the digital elevation model (Figure 5.4) with the spatial resolution of 0.5 by 0.5 metres

5.4.2.3 Evaluation of the landslide hazard enhanced by using landslide controlled features

In this section, landslide controlled features are used to improve the landslide hazard assessment. Three landslide controlled features (described in Section 5.3) which indicate the degree of the geomorphological evolution are selected and relationships with the slope value are analyzed. Obtained values can be used to determine the different degree of landslide hazards and corresponding activities. Figures 5.67 to 5.69 show results of correlations between these landslide controlled features and the slope value.

In order to determine such relationships the Least Absolute Deviation (LAD) regression is used. This robust method is based on the consideration of the absolute error rather than the squared error and shows an applicability where unusual values (or outliers) are included in the dataset (Carr 2002). Figure 5.67 shows the bivariate distribution of mean texture and slope values from observed landslide deposits. It indicates the increasing trend of mean texture values as slopes are steep. A similar relationship can be found in the distribution between mean vector dispersion and slope values except a relatively flatter slope of their correlation (Figure 5.68). In contrast to these increasing trends, mean eigenvalue ratios show a decreasing trend as slope values increase (Figure 5.69). Figure 5.70 also illustrates various relationships among these landslide controlled features. Because they use the same orientation data, Figure 5.70c, mean vector dispersion and eigenvalue ratio values show a higher bivariate distribution than any other combination.

The degree of the correlation between mean slope and texture values (Figure 5.67) provides two possible speculations. Firstly, texture values are considered to be the dependent variable of the slope. As pointed out in Section 5.3.1.1, the texture analysis uses changes in tone on ground surface. If these tonal variations are influenced by the steepness of ground profiles, obtained results from the texture analysis would be consistent with those from the slope analysis and both methodologies would show a high correlated bivariate distribution (Figure 5.67). It is, therefore, possible that the information which the texture analysis brings to the landslide hazard assessment may be only additional resources, and can support results that the slope analysis finds. This is supported by other relationships shown in Figure 5.70. Two bivariate correlations between mean texture and vector dispersion values (Figure 5.70a), and between mean texture and eigenvalue ratio values (Figure 5.70b) also

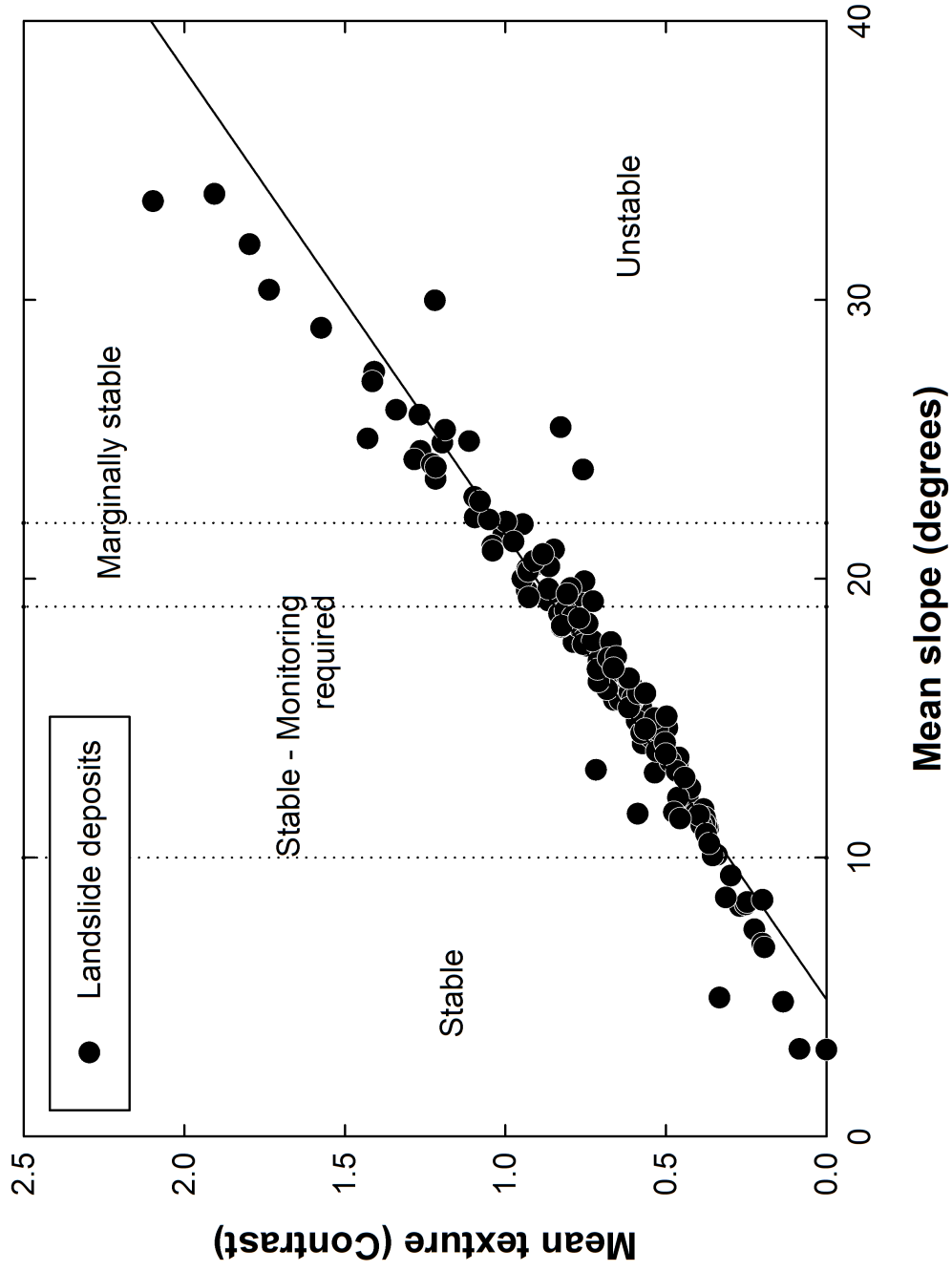


Figure 5.67 Relationship between mean texture and slope values on previous landslide deposits. Values for mean slope and texture shown on the abscissa and ordinate are illustrated in Figures 5.13 and 5.25, respectively. Representative slope values and corresponding states of the landslide hazard described in Table 5.12 are also delineated. The linear regression line is calculated by the Least Absolute Deviation (LAD) method

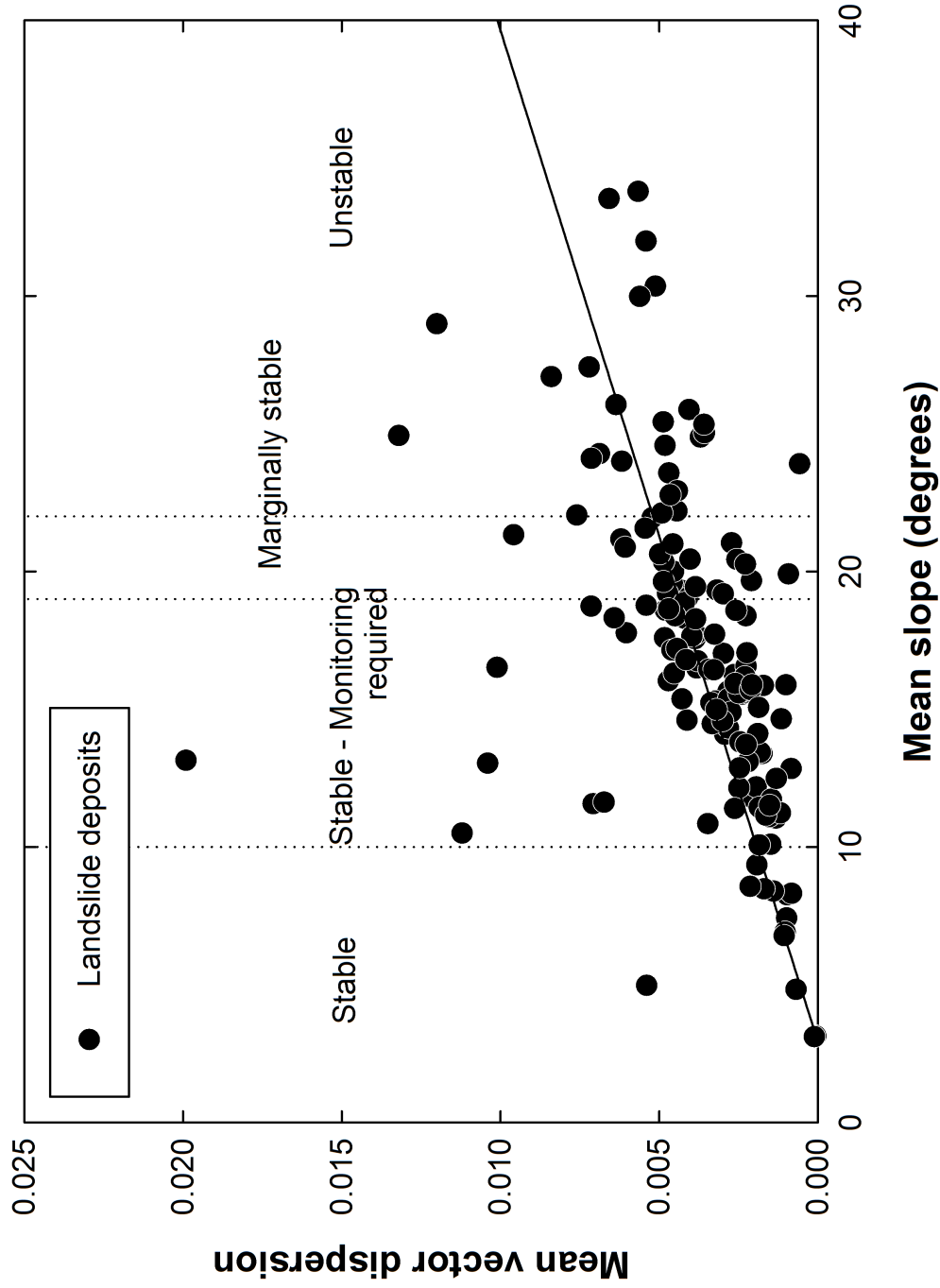


Figure 5.68 Relationship between mean vector dispersion and slope values on previous landslide deposits. Values for mean slope and vector dispersion shown on the abscissa and ordinate are illustrated in Figures 5.13 and 5.35, respectively. Representative slope values and corresponding states of the landslide hazard described in Table 5.12 are also delineated. The linear regression line is calculated by the Least Absolute Deviation (LAD) method

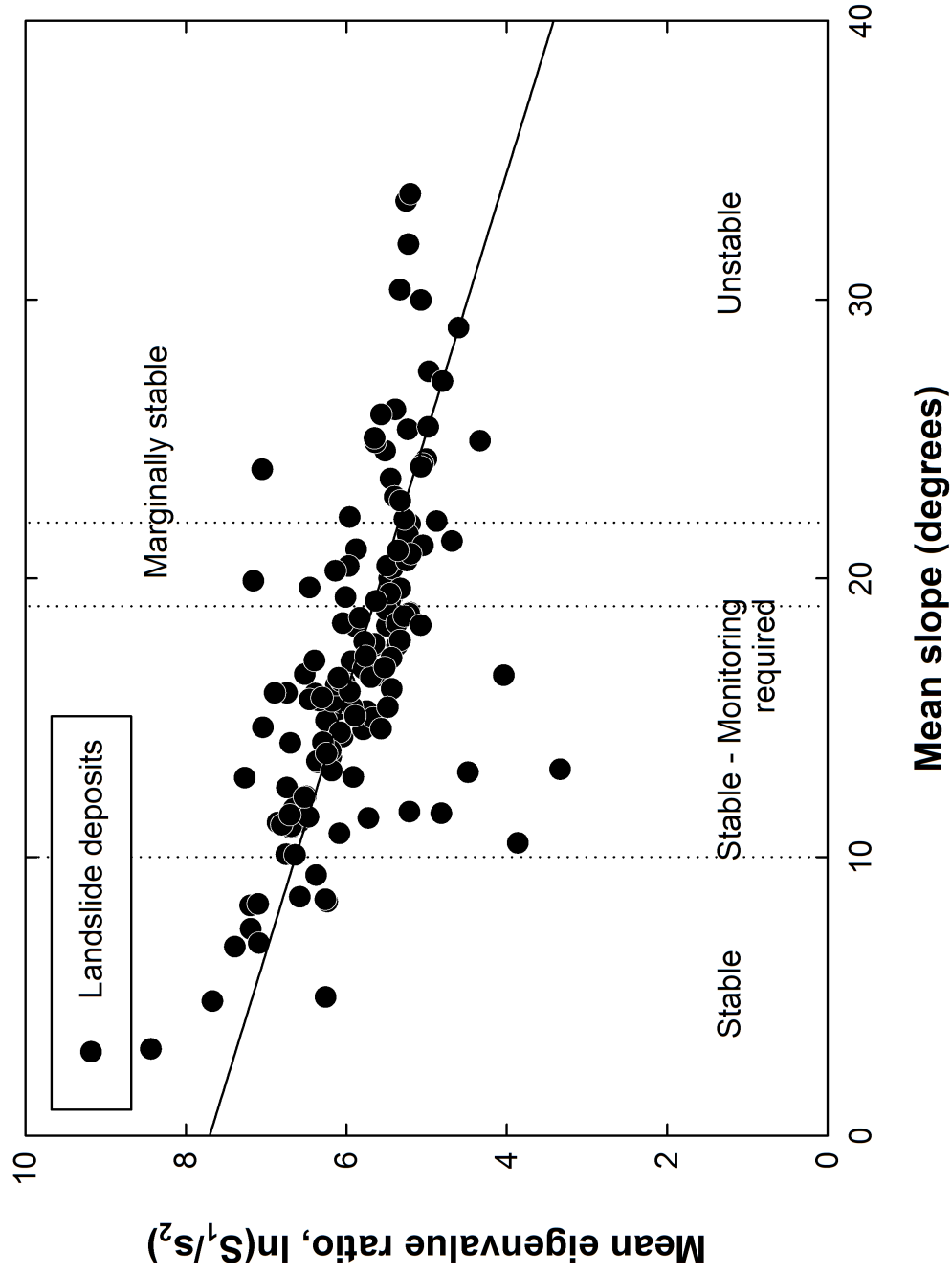
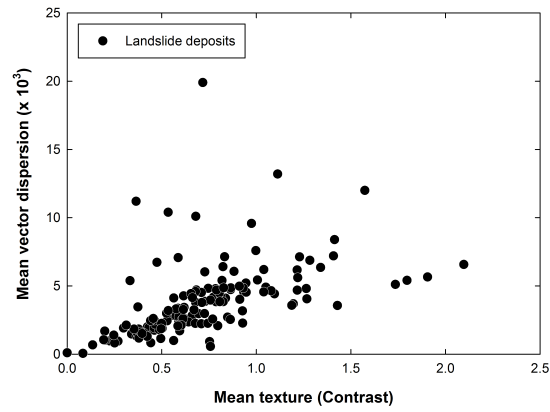
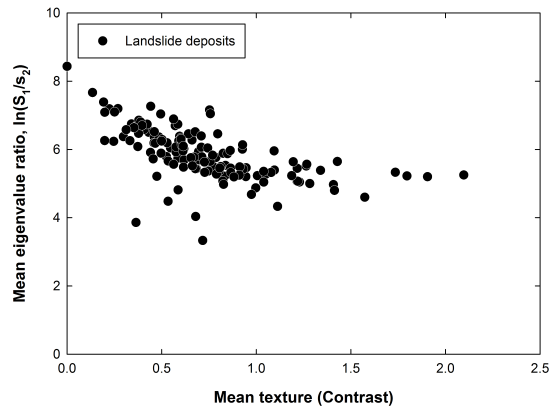


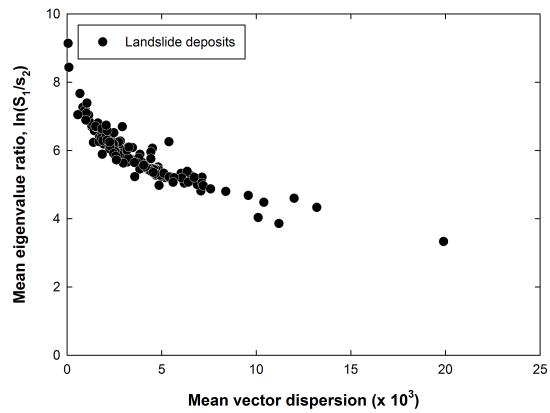
Figure 5.69 Relationship between mean eigenvalue ratio of $\ln(S_1/S_2)$ and slope values on previous landslide deposits. Values for mean slope and eigenvalue ratio shown on the abscissa and ordinate are illustrated in Figures 5.13 and 5.48, respectively. Representative slope values and corresponding states of the landslide hazard described in Table 5.12 are also delineated. The linear regression line is calculated by the Least Absolute Deviation (LAD) method



(a)



(b)



(c)

Figure 5.70 Relationships of mean values of texture, vector dispersion, and eigenvalue ratio. a. Mean texture and vector dispersion values. b. Mean texture and eigenvalue ratio values of $\ln(S_1/S_2)$. c. Mean vector dispersion and eigenvalue ratio values of $\ln(S_1/S_2)$. Mean vector dispersion values are multiplied by 1,000. Mean values for each parameter are shown in Figures 5.25, 5.35, and 5.48, respectively

show similar behaviours in their relationships with mean slope values (Figures 5.68 and 5.69).

If texture values are independent of slope values, the second consideration, it is necessary to explain the physical contributions of texture values to the bivariate distribution with slope values. Unfortunately, tonal changes can be influenced by various factors. Therefore, more physical investigations of texture values are needed to consider them as a significant parameter in the landslide hazard assessment.

One possible explanation on the independent characteristic of the texture analysis is the moisture variation on ground profiles. Generally rougher grounds have little run off in surface drainages. This leads to more infiltration on steep slopes compared to the gentle ground. Large amounts of water which infiltrate into the ground widen the range of moisture contents on the ground surface and this, in turn, reflects the intensity of tonal changes in the texture analysis. Some scatters observed on unstable zone in Figure 5.63 may indicate the effect of the moisture variation on the ground surface, which is detected by the texture analysis as the form of tonal variations.

Relationships between slopes and the orientation data such as vector dispersion values (Figure 5.68) and eigenvalue ratios (Figure 5.69) give some uncertainties in applying those values to the landslide hazard assessment. These uncertainties can be expressed as scatters in the plot when they are related to the slope variation and treated as noise. This noise may be generated at the time when the raw data was obtained. In a LiDAR survey, for example, it might be difficult to achieve accurate data in very steep ground surfaces due to the direction bias of the laser scanner. Although studies have proposed and demonstrated the usefulness of the orientation data in landslide hazard assessments (McKean and Roering 2004; Kasai et al. 2009), they satisfied specific local conditions only. These conditions are closely related to the specific geometry of the geomorphological feature itself such as the presence of preferred directions which are perpendicular to the unit terrain rather than contributions to landslide causal factors. It may be, therefore, necessary to carry out more investigations in order to find physical contributions of the orientation data to other landslide causal factors to make the landslide hazard assessment more comprehensive.

In this study bivariate data analyses on each landslide controlled feature which correlates to slopes can still provide representative values to determine the degree of

landslide hazards and corresponding activities. These values can be considered to improve the landslide hazard assessment, if some considerations which described above are clearly demonstrated. Obtained representative values for each landslide controlled feature and corresponding slope values are described in Table 5.14 and the improved landslide hazard assessment on previous landslide deposits in which results of bivariate correlations from three landslide controlled features are added is shown in Figure 5.71.

Adjusted landslide hazards on identified landslide deposits show changes in the degree of landslide hazards which are based on the degree of geomorphological evolution and the locality of the study area (Figure 5.71). For example, landslide hazards on the west bank of the Peace River are decreased in the adjusted landslide hazard assessment. Major changes in landslide hazards occurred in the stable state (from the 'Stable - Monitoring required' to 'Stable') and these can be found on slopes of Misery Mountain and the south end of the west bank which are relatively old and mature terrains. Changes in landslide hazards observed on the east bank of the Peace River are more complex. Whereas landslide deposits on the north end of the east bank and south end of Heart River decreased their landslide hazards, most valley slopes along tributaries have increased their landslide hazards compared to the landslide hazard assessment shown in Figure 5.62. The most drastic changes can be found in valley slopes on Pat's Creek where landslide hazards have been increased significantly, which are enough to initiate or reactivate landslide movements (from the 'Marginally stable' to 'Unstable'). Other areas such as the east end of study area and valley slopes of the east bank of the Peace River show the increasing landslide hazard from the 'Stable - Monitoring required' to 'Marginally stable.'

5.5 Results and discussions

Figure 5.72 shows the distribution of areas occupied by proposed landslide hazards in this study (Figure 5.63). It indicates that proportions of occupied area generally decrease as landslide hazards become more unfavourable except the occupied area in the 'Unstable' state is greater than that in the 'Marginally stable' state. Small portions of the 'Marginally stable' state can be explained by the narrow slope break between two landslide hazard states (19 to 22 °) compared to other breaks (Table

Table 5.14 Modified states of landslide hazards on landslide deposits identified in the study area which are adjusted by landslide controlled features. Representative values shown in the table are obtained from Figures 5.67 to 5.69. States of landslide hazards and their corresponding activities are presented in Table 5.11

State of landslide hazards	Slope (degrees) [†]	Landslide controlled features		
		Texture	Vector dispersion	Eigenvalue ratio [‡]
Stable	< 10	< 0.305	< 0.0019	> 6.633
Stable - Monitoring required	10-19	0.305-0.845	0.0019-0.0044	5.668-6.633
Marginally stable	19-22	0.845-1.025	0.0044-0.0052	5.346-5.668
Unstable	> 22	> 1.025	> 0.0052	< 5.346

[†] Slope values are shown in Table 5.12.

[‡] $\ln(S_1/S_2)$.

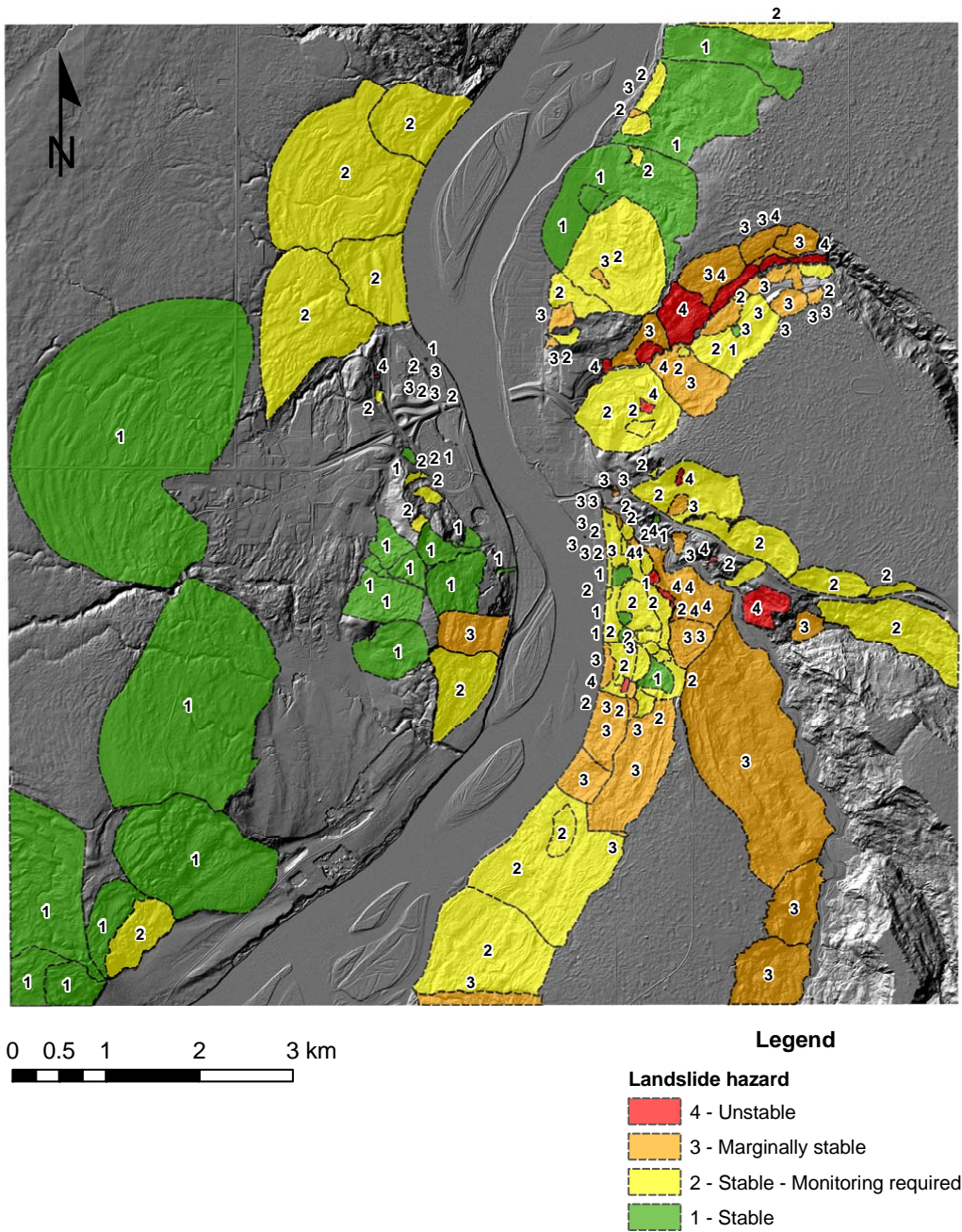


Figure 5.71 Distribution showing modified landslide hazards derived from the addition of landslide controlled features observed on previous landslide deposits in the study area. Representative values for each parameter which determines the state of landslide hazard are shown in Table 5.14. Four levels of landslide hazard are delineated by different colors. A hillshade imagery presented in the background is obtained from the digital elevation model (Figure 5.4) with the spatial resolution of 0.5 by 0.5 metres

5.12). Further examination shows that the 'Stable' state takes the largest portion of the area evaluated, which is equivalent to 68 percent of the entire area (72 km²). In contrast, the smallest area is occupied by the 'Marginally stable' state, which is three percent of the study area evaluated (equivalent to the area of 3 km²). 'Stable - Monitoring required' and 'Unstable' states hold 17 and 12 percent of the total area, which are equivalent to 19 and 12 km², respectively (Figure 5.72).

Although results of the proposed landslide hazard assessment present the appropriate distribution of potential landslide hazards, some areas have the incorrect distribution of landslide hazards. This problem is somewhat exaggerated in areas where 'Stable' and 'Stable - Monitoring required' states co-exist. For example, areas of the 'Stable - Monitoring required' state are occasionally observed in the hummocky terrain, which is the part of flat upland areas and usually present as stable areas. Since the employed landslide hazard assessment methodology is based on the slope variation augmented by the geological property, parts of flat areas which have distinct changes in ground profiles sometimes show higher landslide hazards than those originally evaluated. Similar observations can be found in areas influenced by anthropogenic activities.

The adequacy of the landslide hazard assessment is evaluated by comparing other areas where landslide problems have been reported. Representative areas obtained from numerous geotechnical records are listed in Table 5.15 and their locations are illustrated in Figure 5.73.

The visual observation of the distribution of landslide hazards of listed areas confirms that the proposed landslide hazard assessment is useful to evaluate actual landslide events in the study area. All the listed areas are closely related to the 'Unstable' or 'Marginally Stable' states in the proposed landslide hazard assessment. At least within the given examples, therefore, the possibility of the landslide occurrence in the study area is well represented by the proposed landslide hazard assessment. Figures 5.74 and 5.75 provide a closer look at examples of listed areas in the east and west banks of the Peace River where the proposed landslide hazard correlates to historical landslide incidents.

The feasibility of the proposed landslide hazard assessment is also evaluated by the study previously conducted the landslide susceptibility in the study area (Nilson and McCormick 1978). Figure 5.76 illustrates the result of this comparison. In the

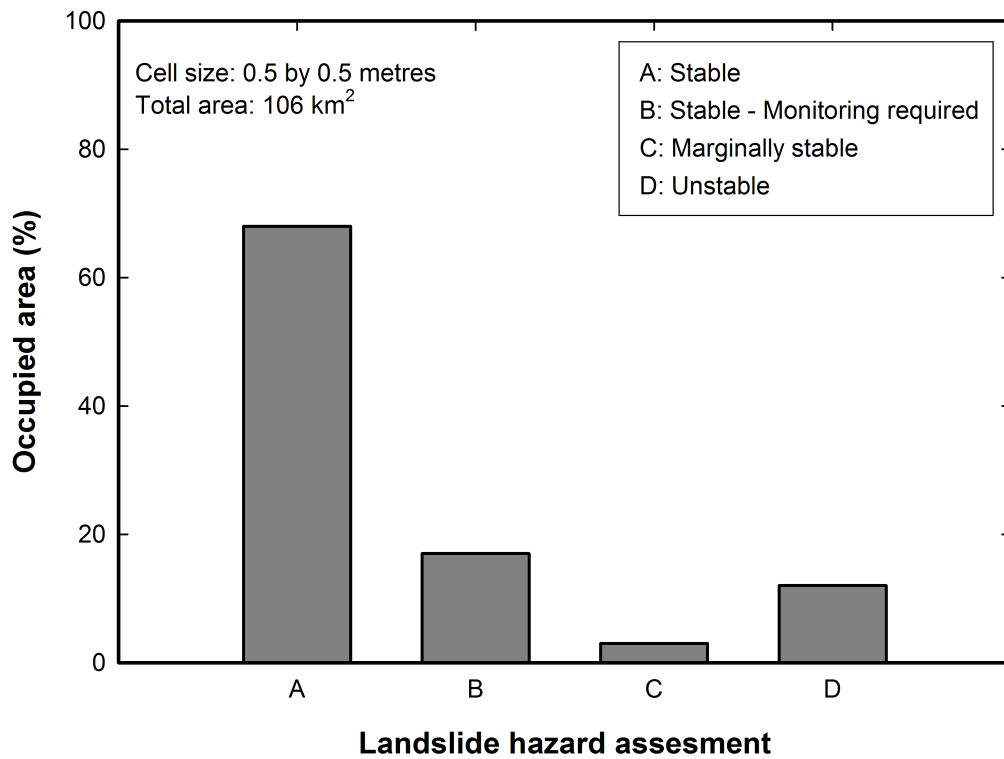


Figure 5.72 Distribution of occupied percentage areas based on the level of landslide hazards. Four states of the landslide hazard proposed in this study are placed in the abscissa. Percentage areas occupied by each state of the landslide hazard are illustrated in the ordinate. The total evaluated area is about 106 km² and the unit cell size of the evaluated area is 0.5 by 0.5 metres

Table 5.15 List of areas where landslide induced problems have been reported. Locations of listed areas are shown in Figure 5.73

Id	Reported area	References
1	3+400 (Retaining wall installed area) [†]	Alberta Transportation 2011
2	2+600 (Site 1) [†]	
3	1+800 (site 2) [†]	
4	1+000 (Site 3) [†]	
5	Grouard Trail Slide (0+000)	Alberta Infrastructure and Transportation 1985 Alberta Transportation 2011
6	Curling Rink Slide	Karall 1992 Little 1992 Karall and Ruban 1994
7	Heart River Slide [‡]	Kjelland et al. 2009 Alberta Transportation 2011
8	Lookout Slid [‡]	
9	Makeout Slide [‡]	
10	Michelin Slide [‡]	
11	Trunk Slide [‡]	
12	Fence Slide [‡]	
13	Mile 46.3 Slide ^{††}	Lindberg and Savigny 1981a
14	Northern Alberta Railway overpass	Harris and Rogers 1979
15	Shaftesbury Trail overpass	Proudfoot and Cullum-Kenyon 2006 Alberta Transportation 2011
16	Northern Alberta Railway overpass	Harris and Rogers 1979
17	Commercial and industrial subdivision	Nilson 1979
18	Peace River landfill	Froese et al. 2002

[†] Peace River east hill (Highway 2). Notations representing each location indicate ‘kilometre + metre’ along the highway from the Grouard Trail (Id 5 in this table) which is designated as 0+000.

[‡] Peace River Judah Hill (Secondary Highway 744).

^{††} Placed on the Canadian National Railway traversing the east bank of the Peace River.

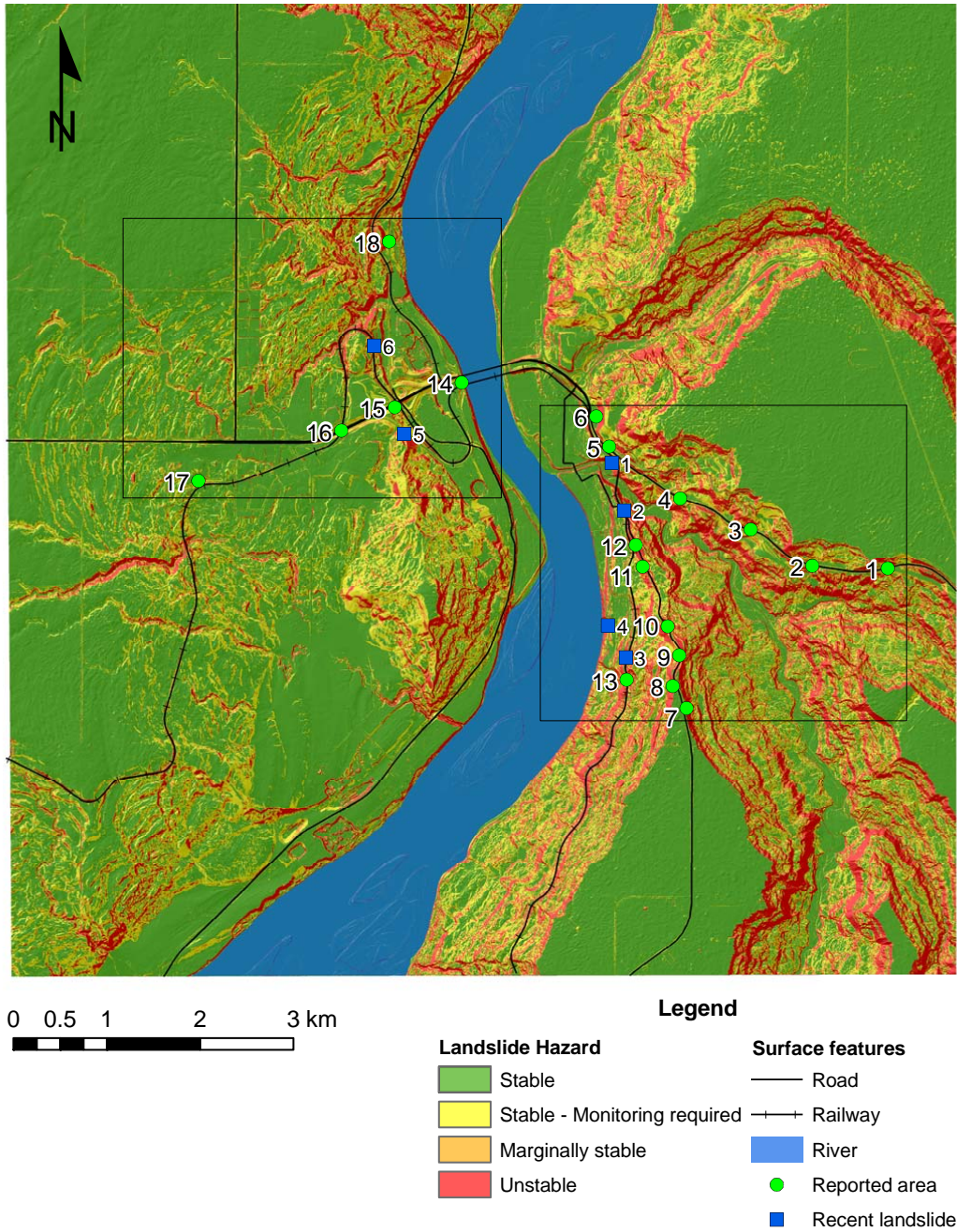


Figure 5.73 Distribution of areas where landslide induced problems have been reported. Numbers represent the location of each reported area noted in Table 5.15. Recent landslides shown in Figure 4.1 are also delineated by using symbols and numbers. Areas outlined by black solid lines indicate a closer look at representative areas in order to validate the feasibility of the generated landslide hazard assessment, which are illustrated in Figures 5.74 and 5.75. The distribution of the landslide hazard which obtained in this study is on the background. A hillshade imagery presented in the background is obtained from the digital elevation model (Figure 5.4) with the spatial resolution of 0.5 by 0.5 metres

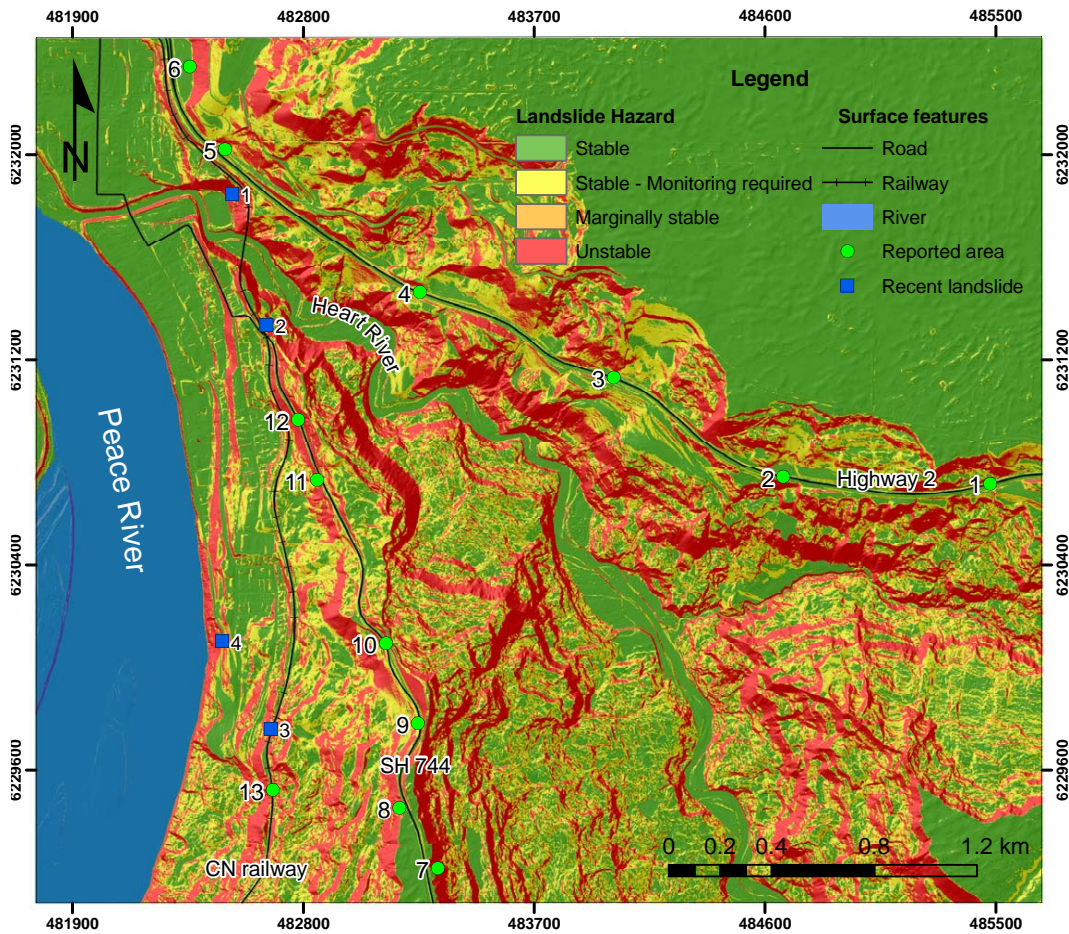


Figure 5.74 Exhaustive examinations for the validation of the proposed landslide hazard assessment with historical landslide evidences in the east bank of the Peace River where Highway 2, Secondary Highway 744, and Canadian National Railway are placed. The location of the figure is presented in Figure 5.73. Specific areas denoted by numbers and symbols are described in Table 5.15. Recent landslides shown in Figure 4.1 are also delineated by using symbols and numbers. A hillshade imagery presented in the background is obtained from the digital elevation model (Figure 5.4) with the spatial resolution of 0.5 by 0.5 metres

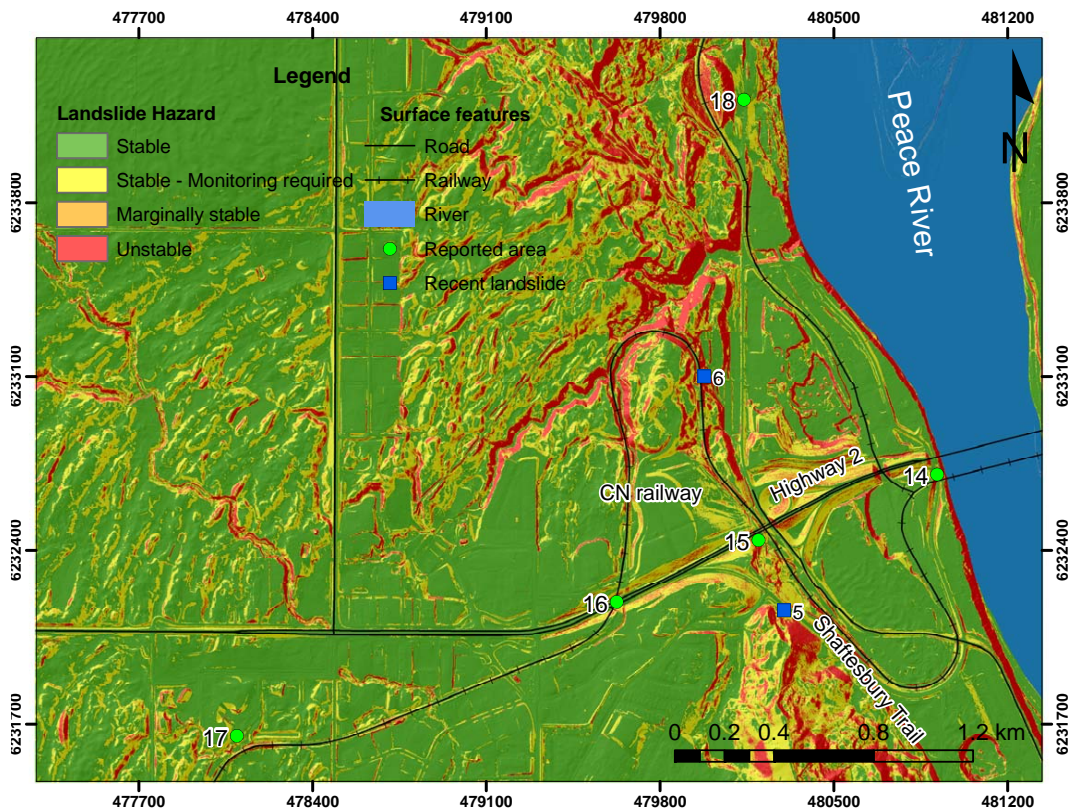


Figure 5.75 Exhaustive examinations for the validation of the proposed landslide hazard assessment with historical landslide evidences in the west bank of the Peace River where Highway 2, Shaftesbury Trail, and Canadian National Railway are placed. The location of the figure is presented in Figure 5.73. Specific areas denoted by numbers and symbols are described in Table 5.15. Recent landslides shown in Figure 4.1 are also delineated by using symbols and numbers. A hillshade imagery presented in the background is obtained from the digital elevation model (Figure 5.4) with the spatial resolution of 0.5 by 0.5 metres

figure each state of landslide hazard denoted by both methods would show consistent locations. For example, unstable areas include southern portions on the east bank of the Peace River, river valleys along the Heart River especially near the Mile 47.8 Slide, west bank of the Peace River adjacent to areas between Shop Slide and Mile 50.9 Slide, and south western parts of study area where the Canadian National Railway traverses the area (Figure 5.76).

The visual representation of the landslide hazard proposed by this study is based on the cell-based analysis, which can describe the state of landslide hazard in each cell (0.5 by 0.5 metres) precisely. This leads to difficulty in generating a simple distribution of states of landslide hazard (as shown by Nilson and McCormick 1978). From the visual inspection, however, it is postulated that the proposed method shows a reasonable agreement (or even provides more specific results) with the previous study in delineating detailed landslide hazards existing in the study area.

Mainly because of various uncertainties in sources of information and subsequent procedures, some limitations have been observed while conducting the landslide hazard assessment. Major issues encountered during procedures of the landslide hazard assessment are as follows:

1. Landslides are the result of multi-interactions between numerous inherent or extrinsic factors. Some of these factors can be relatively easily accessed whereas others are difficult to obtain by conventional methodologies. Even though advances of technology expand choices for those factors, so far a few items are still impossible to capture or are obtained with high uncertainties. In this respect, our selections are too limited to represent the actual mechanism of landslides, which lead to misunderstanding of the hazard state on landslide areas. The reliability of information is, therefore, one of the important considerations before landslide hazard assessments are carried out.

Reliability of sources of information can be damaged by the simplification of data available. For example, the surficial and bedrock information for this study were provided with low precision, especially at the boundary between different units, which leads to a less acceptable analysis. In this case, landslide hazard assessments may have problems especially on a boundary where distinct attributes of information confront each other. The simplification of information used in landslide hazard assessments is closely related to

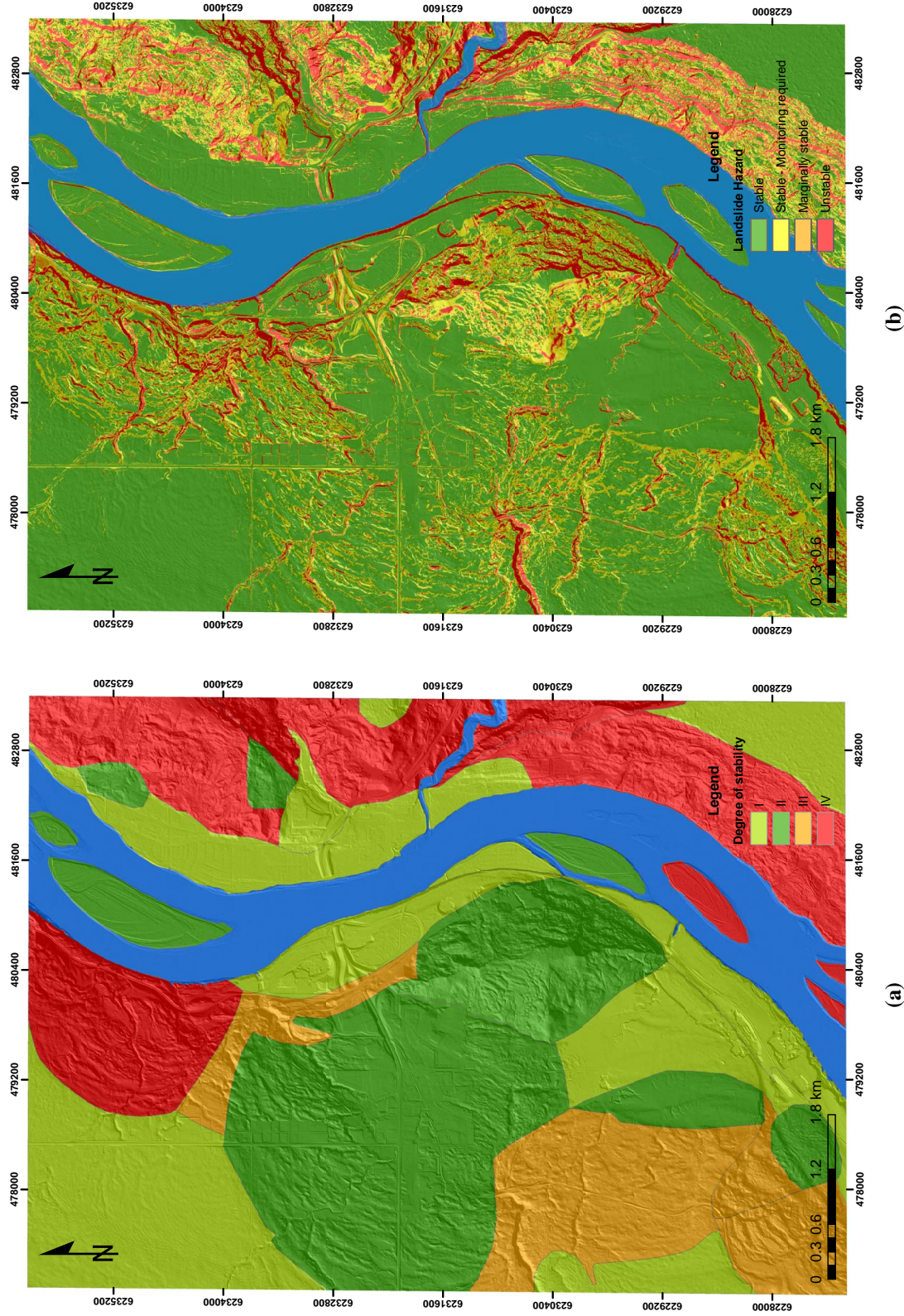


Figure 5.76 Evaluation of the proposed landslide hazard assessment by comparing with the previous study carried out by Nilson and McCormick (1978). a. Landslide susceptibility map showing the degree of slope stability (Nilson and McCormick 1978). b. Landslide hazard map describing a cell-based landslide hazard in the same extent of a. Detailed explanations on the degree of stability class in a are described in Table 5.5. A hillshade imagery presented in the background is obtained from the digital elevation model (Figure 5.4) with the spatial resolution of 0.5 by 0.5 metres

the matter of judgement such as scale and financial issues. The determination of appropriate scales, followed by sound implementations are, therefore, prerequisite processes in all landslide hazard related studies.

2. In this study, relative impacts of triggering factors on landslide hazards are represented through anthropogenic considerations only. Assumptions in delineating the effect of specific landslide triggering causal factors in various perspectives may well simulate actual consequences due to their main causal factors. Correlating rainfall characteristics to hydrological causal factors enhances understanding of the mechanism of landslides by hydrological causes. Anthropogenic impacts are difficult to quantify as impacts on landslide hazards. Urban developments on mountainous areas obviously change the current stability of slopes where large cuts and fills happen. One possible approach which is adaptable to evaluate the influence of anthropogenic factors is the inclusion of regulations or codes. By considering various aspects with regard to slope stabilities, those guidelines can be an indicator for landslide triggering factors which describe the current state of landslide hazards. Incorporating the geotechnical analysis on areas of marginally stable can be useful to determine actions for ongoing or future landslide hazards.
3. High subjectivity built into the landslide hazard assessment can lead an erroneous decision in determining a proper landslide hazard zonation. In this study two main processes may have the subjectivity which might come from experiences of observers: (1) relating relative contribution of landslide causal factors on landslide hazard assessments; and (2) building geomorphological maps based on the aerial photo interpretation. The amount of information derived from geomorphological features of landslides is directly proportional to the depth of knowledge. Various methodologies have been suggested to reduce this problem during implementing landslide hazard assessments. These include statistical methods and exhaustive site investigations in order to determine relative contributions toward landslide hazards. Those approaches require, however, sufficient examples of previous landslides in which landslide causal factors relate to overall landslide hazards based on their frequencies and financial supports. The identification of previous landslides by remote sensing technologies such as the airborne laser altimetry (LiDAR) can be an alternative choice for the proper recognition of existing landslide controlled features by relatively objective and economic manners.

Even though there are several limitations described above, the proposed landslide hazard assessment provides a useful framework to understand different states of the landslide hazard in the study area. Combined with other physical considerations such as geotechnical monitoring for ongoing landslides, estimation of the direction of displaced materials, and identification of the direct relationship between climate characteristics and landslide incidents, the accuracy of landslide hazards can be enhanced and this suggests appropriate mitigation measures.

5.6 Conclusions

In Chapter 5, I focused on three accomplishments. Firstly, I reviewed landslide causal factors which are believed to impact, either directly or indirectly, on landslides in the study area and evaluated their usefulness with respect to relative contributions in landslide hazard perspectives. During this analysis the most influential landslide causal factors in the study area are geologic and geomorphological factors and these can be expressed as slope values and types of surficial deposits. By combining with strength properties of colluvial sediments identified from laboratory tests described in previous chapter (Section 4.2), representative slope values which differentiate each landslide hazard and corresponding activity are determined.

Secondly, I introduced various approaches to identify landslide controlled features which are typical residues after landslides occur such as scarps, cracks, flanks, and displaced materials on the ground and that are distinct from areas without landslide events. These approaches, texture and orientation data analyses, have different theories and corresponding procedures, and are useful to determine potentially unstable areas based on geomorphological characteristics which expressed as tonal changes and the presence of preferred directions on ground profiles.

Finally, the landslide hazard for the study area is evaluated. Correlations between landslide causal factors and controlled features revealed that more investigations explaining physical properties of landslide controlled features and their contributions which influence the mechanism of landslides are needed in order to understand proper relationships even though they provide an insight into characteristics of geomorphological features on ground surfaces. By performing visual observations with landslide records it is postulated that the proposed landslide hazard assess-

ment is useful to evaluate actual landslide events in the study area. I found similar or even more specific results while comparing it with the previous study carried out by Nilson and McCormick (1978).

While evaluating the landslide hazard in the study area I have encountered several limitations related to various causes. Major concerns are the unequal quantity and quality of obtained information, limited applicability in delineating impacts of landslide causal factors, and high subjectivity in determining the landslide hazard. By combining other physical investigations, the landslide hazard assessment proposed in this study will promise a better understanding of landslides and their mechanisms, and provide an enhanced methodology to evaluate their hazards and appropriate actions.

Chapter 6

Summaries and conclusions

This study has provided significant progress in analyzing mechanisms and influences of landslides, either in the present or foreseeable future, in the town of Peace River. This can be readily adaptable to other areas if provided with proper sources of information which the process needs. Results of this study can be used as a basis for assessing landslide risks and their managements. Appropriate actions or decisions and corresponding countermeasures can also be derived from these outcomes.

From a practical point of view, landslide hazard assessments where evidences of previous landslides are prevalent may require a sound understanding of the natural and anthropogenic processes that would control the initiation or reactivation of unstable areas and previous landslide deposits. The estimation of those phenomena might be provided by various landslide causal factors. Linking the relative contribution of these factors to the landslide activity can be an index to identify the priority of our concerns toward the continuity of society within limited resources.

The main idea of this study, therefore, was to identify conditions of local areas and understand processes related to those conditions. The temporal and spatial characteristics including geological and geomorphological histories, meteorological variations, economic developments, and demographic distributions over time were evaluated.

The following summaries and conclusions are derived from the research on the study area, which include desktop studies, field investigations, laboratory tests, and integrated parametric analyses with the Geographical Information Systems (GIS). With these procedures the distribution of landslide hazards in the Town of Peace River is developed. Finally, brief remarks about the future research are presented.

6.1 Summaries

From in-depth reviews of existing literature about landslide related assessments, the general idea of the landslide hazard assessment in the study area had been achieved in Chapter 2. Characteristics and approaches of various landslide hazard analyses were presented. These include definitions, frameworks, essential processes, and typical examples of each landslide hazard assessment. A brief discussion of socio-economic impacts on landslides and some implementations against landslide hazards in urban areas then followed. This also covered various impacts of landslides due to developments, examples of landslide control measures, and roles of landslide hazard assessments against ongoing and future landslide hazards.

Detailed studies on the fundamental information about the study area were discussed in Chapter 3. The general overview, both geographic and economic perspectives, was presented. Town of Peace River, one of the towns on river terraces of the Peace River, has been drastically developed in accordance with the population growth since 1950s. Terraces were fully packed and development commenced on valley slopes to make more spaces for residents. Many valleys in the Peace River Lowland are relatively young, consequently unstable. Even a small disturbance on the valley slope would cause movement. Geological evidence observed in the study area have verified those arguments. Representative geological features are bedrock formations, buried channel deposits, glaciolacustrine and glacial sediments, and fluvial and eolian deposits. The cross sections (Figures 3.7 and 3.9) which I made are useful to delineate the sequence of identified subcrops.

Understanding of major geomorphic events provides an insight into the mechanism of major landslides in the study area. Laminated lacustrine strata created during the ice advance can play a significant role in slope movements. Landslides placed in the Shaftesbury Formation mainly occurred on the pre-sheared layer induced by the movement of glaciers. Valley rebounds due to releases of high pressured loads where river valleys are cut into bedrock by postglacial streams can be an intrinsic factor in the slope stability.

Chapter 3 also covered general reviews on landslides in the Peace River Lowlands, which focused on tributaries located adjacent to the preglacial river channel of the Peace River. Although they are relatively remote from the incorporated area, these regional studies are useful for understanding the mechanisms of the landslides

which occurred in the Peace River Lowland. A temporal distribution of landslides which had occurred in the Town of Peace River over thirty years illustrates that the annual precipitation at the time of the landslide occurrence is above or near the average value of 402 millimetres. From this assumption, it is expected that landslides in the study area were affected by precipitation, a landslide triggering causal factor.

Typical landslide characteristics observed in recent landslides were presented in Chapter 4. Potential rupture surfaces, groundwater distributions, movement behaviours, and possible landslide mechanisms of each recent landslide were analyzed to find general characteristics inherent in landslides observed in the study area.

Landslides which have occurred in the Town of Peace River since the 1970s were collected for the landslide inventory mapping. A total of six landslides on slopes in the Town of Peace River were chosen from various sources. Most landslides were identified as translational block slides and some landslides showed a complex form in which landslides were the combination of or initiated by other forms of the slide. Residences or infrastructures such as roads and railway were observed adjacent to the slide areas. This indicates that developments encroaching on slopes may be a main cause of landslides. The study has also revealed that increasing pore water pressure due to precipitation or melting water may exert landslides on unstable slopes.

In order to understand characteristics of geotechnical properties which control landslide behaviours, laboratory tests were carried out on representative soil samples located at elevations of general rupture surfaces because they usually govern the entire stability of the slope. Representative findings based on index and direct shear tests indicate that colluvial sediments have a large extent on the plasticity chart with similar shear strength parameters to both fully softened and residual values. Advance phase glaciolacustrine sediments show high plasticity with high peak and low residual shear strength values.

Other findings in Chapter 4 were the identification of characteristics in landslide movements. By observing displacement records of landslides they showed a typical relationship between landslides and their causal factors. Obtained information of movements from recent landslides was processed in diverse ways to represent characteristics of landslides. For example, analyzed data would help to understand the existence of a general rupture surface which controls landslides occurred in

the study area. Elevations of general rupture surfaces in the study area are determined around 365 and 386 metres in the west bank, 330, 338, and 370 metres in the east bank, respectively and they are placed in both glacial and colluvial sediments. These general elevations of rupture surfaces can be used in landslide hazards assessments as the form of the landslide preparatory causal factor.

The rate of movements may indicate the state of current landslides and give an intuition in their classification types. Results by analyzing movement rates showed that most movement rates are in the very slow and extremely slow classes. Under these conditions, structures may be undamaged or have manageable damages if cracks occurred by movements. Geomorphological features can also affect these landslide movement displacements. The analysis of the relationship between geomorphological features and movement rates indicated there is a positive correlation between slope angles, either on the ground or at the rupture surface, and movement rates.

Different modes of landslide kinematics were shown by movement patterns. Observations of movement patterns from recent landslides showed distinct movement behaviours which would indicate the evolution of landslide activities. Observed movement characteristics are useful to estimate the future behaviour of unstable slopes and develop a landslide hazard map for the study area.

Results of movement patterns observed from recent landslides in the study area can also provide insights into the formation and propagation of rupture surfaces even though they do not clearly explain kinematics of the rupture or properties of materials which are being deformed. Another possible application derived from observing movement patterns is a warning threshold.

Practical procedures to assess landslide hazards in the study area were presented in Chapter 5. Major considerations of landslide-induced factors for an understanding of the relationship between those factors and landslides were introduced. From thorough reviews of numerous examples, appropriate landslide causal factors were determined and examined for their relative influences on landslides in the study area. These include surficial and bedrock geologies, slope and aspect, hydrologic network, proximity to anthropogenic factors such as roads, railway, and land use. From these various causal factors, I used two most influential landslide causal factors for the evaluation of landslide hazards in the study area. These are geologic and geomorphological factors which represent slope values and colluvial deposits. The

identification of landslide controlled features by using texture values and orientation data was adapted to propose a proper recognition of previous landslide features where landslide hazards are relatively high.

The landslide hazard map I created showed that unstable areas made up either 12 percent of the total evaluated area or 18 percent of landslide deposits identified and can be found in areas on valley slopes along the Heart River and Pats Creek, the eastern entrance to the town, and the small portion of residential areas in the east bank of the Peace River where transportation routes are located nearby. This finding is reasonable as historical records on the occurrence of landslides in the study area have pointed out many landslides which had occurred on and along transportation routes (Kjelland et al. 2009; Alberta Transportation 2011).

Some efforts toward improving the landslide hazard assessment by using consecutive geomorphological maps have been introduced. Two aspects, the identification of the land use adjacent to slopes and previous drainage systems, are closely related to the urban development. By assuming that developing lands for various purposes would inevitably lead to the disturbance of 'Marginally stable' and even 'Stable - Monitoring required' areas and accelerate their instability toward the 'Unstable' condition, land uses near slopes would influence the landslide hazard in areas of concern. Identified land uses which are suitable for the purpose of this study are park, school, or playground, residential areas, and undeveloped or partially developed areas, in that they are relatively less limited to construction on elevated areas than commercial and industrial areas. The consideration of the land use which is located near slopes and susceptible to landslide hazards would make the state of the landslide hazard on those areas more appropriately.

The other consideration is related to temporal geomorphologic changes in previous drainage patterns. Interrupting natural drainages would influence the changes in pore water pressure within slopes and would increase possibilities of future landslides. Causes of this impact seem to be various but the human induced factors represented by developments are considered as a main agent for this geomorphological alteration.

Currently blocked or disappeared drainages were investigated from the subsequent geomorphological maps. Areas where streams had flowed in the past are more susceptible to landslides because of blocking the drainages. Identification of these

areas was then used to raise the level of the landslide hazard following the course of previous drainages. Traces of previous drainage systems that had existed in the past but disappeared at present due to developments are used to improve the landslide hazard mapping on the west and east bank of the Peace River. Distinct changes in previous drainage systems on the west bank of the Peace River are closely related to constructions of major transportations and other nearby structures. These anthropogenic factors affecting previous drainages are also found in the east bank of the Peace River along the current highways and south end of residential areas.

By considering site specific aspects, the landslide hazard assessments can be more precise especially where related information is available. The final product of landslide hazard assessment was evaluated by comparing other areas where landslide problems have been continuously reported. Results showed the feasibility of the landslide hazard assessment generated by this study. Visual observations indicated that listed hazardous areas are closely related to 'Unstable' or 'Marginally stable' states in the proposed landslide hazard assessment. At least within given examples, therefore, the proposed landslide hazard assessment would provide an efficient way to delineate the overall state of the landslide hazard in the study area.

Uncertainties derived from sources of information and subsequent procedures in constructing the landslide hazard assessment may restrict the accurate estimation of unstable areas. Major issues encountered in implementing procedures for landslide hazard assessments are availability of proper landslide causal factors which well represent conditions of the study area, understanding mechanisms of landslide causal factors that explain appropriate impacts on changes in stabilities, and controlling the subjectivity in determining the proper landslide hazard assessment.

In spite of constraints the proposed landslide hazard assessment would provide a useful framework for understanding different states of landslide hazards in the study area. The more accurate landslide hazard model can be generated by combining it with other physical considerations such as the geotechnical monitoring for ongoing landslides, estimation of the direction of displaced materials, and identification of the direct relationship between climate characteristics and landslide incidents. These suggest appropriate mitigation measures against future landslide hazards.

6.2 Conclusions

This study proposes a methodology for conducting the landslide hazard assessment in the Town of Peace River. It considers geomorphologic and geologic aspects, previous and current states of landslides and their geotechnical characteristics, and human-induced attributes presented by temporal observations. All of which might affect the overall condition of landslide hazards in the study area. The major contributions to landslide hazard assessment fields through this study are as follows:

1. Geomorphic and geological characteristics that may impact landslides in the study area are identified. Laboratory tests on representative samples indicate that at least one general rupture surface existed beneath the ground, which would control mechanical behaviours of landslides in the Town of Peace River. By analyzing temporal variations in geomorphologic features, major causes that induced landslides in the past can be identified.
2. Recent landslides observed in the study area are analyzed in order to determine overall landslide characteristics that can be used to quantify the relative contributions on actual landslides. Most observed recent landslides can be identified as translational block slides in which typical behaviours can be caused by the presence of general rupture surfaces. Proximity to residences or infrastructures illustrates that developments on slopes would be a main cause of landslides in the Town of Peace River. Major contributions caused by developments include changes in the geometry and interferences with natural drainage systems due to massive earthworks.
3. Monitoring surface or subsurface movements of landslides explicitly and directly estimate the time intervals to peak landslide velocities. Although this approach does not consider the kinematics of the rupture or the properties of materials which are being deformed, it gives insights to identify future consequences caused by landslides and provides a concept of landslide warning systems.

4. The landslide hazard assessment proposed by this study can well delineate the current state of landslide hazards in the study area by showing that areas where landslide problems have been continuously reported are consistent with the unstable areas designated by the proposed landslide hazard assessment. It also shows a good agreement with results of the previous study carried out by Nilson and McCormick (1978).

6.3 Suggested future research

Specific subjects for the future research in order to improve landslide hazard assessments in the study area can be suggested as follows:

1. Investigation of proper landslide causal factors and their correct relationships to landslide characteristics in order to understand their appropriate contributions to landslides. Studies on the identification of uncertainties in relationships between landslide causal factors and controlled features are also suggested. It is necessary to carry out more investigations to determine a physical contribution of various methodologies on other landslide causal factors in order to make the landslide hazard assessment more accurately.
2. Development of reducing the subjectivity inherent in landslide hazard assessments. Quantitative methodologies such as statistical and physically based approaches can be applied if provided with a clear understanding of mathematical relationships between employed landslide causal factors and easily accessible data for creating a physical model.
3. Development of relevant data accumulation to determine the state of landslides. It is of primary importance to recognize landslide movements by the geotechnical monitoring with surface and subsurface instruments. Proposed landslide hazard assessment provides an appropriate guideline to set up locations where instrumentations are required. Yearly based aerial photographs with a large scale can provide temporal variations in geomorphologic features of landslides. Hourly based precipitation data can give an insight into the determination of a threshold which is useful for the landslide warning system.

4. As pointed out in Chapter 1, the next probable step is to evaluate the landslide risk in the study area. Conducting the landslide risk assessment usually requires processes such as the vulnerability analysis and the identification of elements at risk. From these analyses mitigation and prevention measures against landslides can be established.

Bibliography

- Agriculture and Agri-Food Canada. 2011. Canadian Ecodistrict climate normals 1961-1990, December, 1997 (revised). <http://sis.agr.gc.ca/cansis/nsdb/ecostrat/district/climate.html>. Accessed Jan. 31, 2011.
- Alberta Environment. 2010. Alberta river basins. <http://www.environment.alberta.ca/apps/basins/default.aspx>. Accessed Nov. 9, 2010.
- Alberta Infrastructure and Transportation. 1985. Highway 2:62 Grouard Trail Slide area - Peace River. Technical report, J-07351, Alberta Transportation, Government of Alberta.
- Alberta Study Group. 1954. Lower Cretaceous of the Peace River region. *In* Ralph Leslie Rutherford Memorial Volume, Western Canada Sedimentary Basin Symposium. American Association of Petroleum Geologists. Tulsa, Oklahoma, pp. 268–278.
- Alberta Transportation. 2011. Peace Region (Peace River/High Level) annual landslides assessments. Alberta Transportation, Government of Alberta, <http://www.transportation.alberta.ca/2251.htm>. Accessed May 11, 2011.
- Aleotti, P., and Chowdhury, R. 1999. Landslide hazard assessment: summary review and new perspectives. *Bulletin of Engineering Geology and the Environment*, **58**(1): 21–44.
- Anderson, T.W., and Stephens, M.A. 1972. Tests for randomness of directions against equatorial and bimodal alternatives. *Biometrika*, **59**(3): 613–621.
- Angeli, M.G., Pasuto, A., and Silvano, S. 2000. A critical review of landslide monitoring experiences. *Engineering Geology*, **55**(3): 133–147.
- Antoniol, G., Basco, C., and Ceccarelli, M. 2008. r.texture - Generate images with textural features from a raster map. http://grass.fbk.eu/gdp/html_grass64/r.texture.html. Accessed Mar. 28, 2011.
- Arnould, M. 1976. Geological hazards - Insurance and legal and technical aspects. *Bulletin of Engineering Geology and the Environment*, **13**(1): 263–274.

- ASTM. 2005. Standard test methods for liquid limit, plastic limit, and plasticity index of soils, ASTM Standard D4318. ASTM International, West Conshohocken, PA, doi:10.1520/D4318-05, www.astm.org.
- ASTM. 2007a. Standard test method for consolidated undrained direct simple shear testing of cohesive soils, ASTM Standard D6528. ASTM International, West Conshohocken, PA, doi:10.1520/D6528-07, www.astm.org.
- ASTM. 2007b. Standard test method for particle-size analysis of soils, ASTM Standard D422 (1963). ASTM International, West Conshohocken, PA, doi: 10.1520/D0422-63R07, www.astm.org.
- ASTM. 2010. Standard practice for classification of soils for engineering purposes (Unified Soil Classification System), ASTM Standard D2487. ASTM International, West Conshohocken, PA, doi:10.1520/D2487-10, www.astm.org.
- Atkinson, R.M., and Massari, R. 1998. Generalised linear modelling of susceptibility to landsliding in the central Apennines, Italy. *Computers & Geosciences*, **24**(4): 373–385.
- Australian Geomechanics Society. 2000. Landslide risk management concepts and guidelines. *Australian Geomechanics*, **35**(1): 49–92.
- Australian Geomechanics Society. 2007a. The Australian GeoGuides for slope management and maintenance. *Australian Geomechanics*, **42**(1): 159–182.
- Australian Geomechanics Society. 2007b. Commentary on guideline for landslide susceptibility, hazard and risk zoning for land use management. *Australian Geomechanics*, **42**(1): 37–62.
- Australian Geomechanics Society. 2007c. Commentary on practice note guidelines for landslide risk management 2007. *Australian Geomechanics*, **42**(1): 115–158.
- Australian Geomechanics Society. 2007d. Guideline for landslide susceptibility, hazard and risk zoning for land use management. *Australian Geomechanics*, **42**(1): 13–36.
- Australian Geomechanics Society. 2007e. Practice note guidelines for landslide risk management 2007. *Australian Geomechanics*, **42**(1): 63–114.

- Ayalew, L., and Yamagishi, H. 2005. The application of GIS-based logistic regression for landslide susceptibility mapping in the Kakuda-Yahiko Mountains, Central Japan. *Geomorphology*, **65**(1-2): 15–31.
- Ayalew, L., Yamagishi, H., Marui, H., and Kanno, T. 2005a. Landslides in Sado Island of Japan: Part I. Case studies, monitoring techniques and environmental considerations. *Engineering Geology*, **81**(4): 419–431.
- Ayalew, L., Yamagishi, H., Marui, H., and Kanno, T. 2005b. Landslides in Sado Island of Japan: Part II. GIS-based susceptibility mapping with comparisons of results from two methods and verifications. *Engineering Geology*, **81**(4): 432–445.
- Azimi, C., Biarez, J., Desvarreux, P., and Keime, F. 1988. Pr evision d' boulement en terrain gypseux (Forecasting time of failure for a rockslide in gypsum). *In Proceedings of the 5th International Symposium on Landslides. Edited by C. Bonnard. Vol. 1, A.A. Balkema, pp. 531–536.*
- Badgley, P.C. 1952. Note on the subsurface stratigraphy and oil and gas geology of the Lower Cretaceous series in central Alberta. Geological Survey of Canada Paper 52-11, Geological Survey of Canada.
- Barlow, J.P., and K upper, A.G. 2001. Re: Slope monitoring at Riverview. Technical report, EG07480, AGRA Earth & Environmental Limited.
- Barlow, J.P., and McRoberts, E.C. 1992. Town of Peace River slope stability evaluation south end of 101 Street. Technical report, EG-07480, HBT AGRA Limited.
- Barlow, J.P., and McRoberts, E.C. 1999. Re: 99th/101st Streets slope stabilization project. Technical report, EG07480, AGRA Earth & Environmental Limited.
- Barlow, P., McRoberts, E., and Tenove, R. 1990. Stabilization of urban landslides in Peace River, Alberta. *In Proceedings of the 43rd Canadian Geotechnical Conference. Quebec, pp. 85–90.*
- Barredo, J., Benavidesb, A., Herv as, J., and van Westen, C.J. 2000. Comparing heuristic landslide hazard assessment techniques using GIS in the Tirajana basin, Gran Canaria Island, Spain. *International Journal of Applied Earth Observation and Geoinformation*, **2**(1): 9–23. doi:10.1016/S0303-2434(00)85022-9.

- Beasom, S.L., Wiggers, E.P., and Giardino, J.R. 1983. A technique for assessing land surface ruggedness. *Journal of Wildlife Management*, **47**(4): 1163–1166.
- Bell, R., and Glade, T. 2004. Quantitative risk analysis for landslides - Examples from BÍldudalur, NW-Iceland. *Natural Hazards and Earth System Sciences*, **4**(1): 117–131.
- Bhattacharya, J., and Walker, R.G. 1991a. Allostratigraphic subdivision of the Upper Cretaceous Dunvegan, Shaftesbury, and Kaskapau formations in the subsurface of northwestern Alberta. *Bulletin of Canadian Petroleum Geology*, **39**(2): 145–164.
- Bhattacharya, J., and Walker, R.G. 1991b. River- and wave-dominated depositional systems of the Upper Cretaceous Dunvegan Formation, northwestern Alberta. *Bulletin of Canadian Petroleum Geology*, **39**(2): 165–191.
- Blais-Stevens, A., Couture, R., Page, A., Koch, J., Clague, J.J., and Lipovsky, P.S. 2010. Landslide susceptibility, hazard and risk assessments along pipeline corridors in Canada. *In Proceedings of the 63th Canadian Geotechnical Conference and 6th Canadian Permafrost Conference. Edited by GEO2010 Calgary Organizing Committee. Calgary, Alberta, pp. 878–885.*
- Bonham-Carter, G.F. 1994. *Geographic information systems for geoscientists: Modelling with GIS*. Pergamon.
- Borneuf, D. 1981. *Hydrogeology of the Peace River Area, Alberta*. Alberta Research Council, Earth Sciences Report 81-2, Edmonton, Alberta.
- Borouhaki, S., and Malczewski, J. 2008. Implementing an extension of the analytical hierarchy process using ordered weighted averaging operators with fuzzy quantifiers in ArcGIS. *Computers & Geosciences*, **34**(4): 399–410.
- Boulton, G.S., and Paul, M.A. 1976. The influence of genetic processes on some geotechnical properties of glacial tills. *Quarterly Journal of Engineering Geology*, **9**(3): 159–194.
- Brabb, E.E. 1984. Innovative approaches to landslide hazard and risk mapping. *In Proceedings of the 4th International Symposium of Landslides. Vol. 1, pp. 307–323.*
- Brabb, E.E. 1991. The world landslide problem. *Episodes*, **14**(1): 52–61.

- Brabb, E.E., Pampeyan, E.H., and Bonill, M.G. 1972. Landslide susceptibility in San Mateo County, California. United States Geological Survey, Miscellaneous Filed Studies Map, MF-360.
- Brand, E.W. 1988. Landslide risk assessment in Hong Kong, Special lecture. *In Proceedings of the 5th International Symposium on Landslides. Edited by C. Bonnard.* Vol. 2, Lausanne, Switzerland, pp. 1059–1074.
- Brand, E.W., Premchit, J., and Phillipson, H.B. 1984. Relationship between rainfall and landslides in Hong Kong. *In Proceedings of the 4th International Symposium on Landslides.* Toronto, Canada, pp. 377–384.
- Brardinoni, F., Slaymaker, O., and Hassan, M.A. 2003. Landslide inventory in a rugged forested watershed: a comparison between air-photo and field survey data. *Geomorphology*, **54**(3-4): 179–196.
- Breitenberger, E. 1963. Analogues of the normal distribution on the circle and the sphere. *Biometrika*, **50**(1-2): 81–88.
- Bremananth, R., Nithya, B., and Saipriya, R. 2009. Wood species recognition using GLCM and correlation. *In International Conference on Advances in Recent Technologies in Communication & Computing, ARTCom 2009.* IEEE Computer Society, Kottayam, Kerala, India, pp. 615–619.
- Brown, W.M., Cruden, D.M., and Denison, J.S. 1992. The directory of the World Landslide Inventory. United States Geological Survey, Open-File Report 92-427.
- Bulut, F., Boynukalin, S., Tarhan, F., and Ataoglu, E. 2000. Reliability of landslide isopleth maps. *Bulletin of Engineering Geology and the Environment*, **58**: 95–98.
- Burrough, P.A., and McDonnell, R.A. 1998. Principles of geographic information systems. Oxford University Press.
- Byfield, T. 1984. The Atlas of Alberta: a special project of Alberta Report, the weekly newsmagazine. Interwest Publications, Edmonton.
- Campbell, R.H. 1973. Isopleth map of landslide deposits, Point Dume quadrangle, Los Angeles County, California; an experiment in generalizing and quantifying areal distribution of landslides. United States Geological Survey, Miscellaneous Filed Studies Map, MF-535.

- Canadian Standards Association. 1997. Risk management: Guidelines for decision makers. CAN/CSA-Q850-97(R2009), Canadian Standards Association, Etobicoke, Ontario, Canada.
- Cardinali, M., Reichenbach, P., Guzzetti, F., Ardizzone, F., Antonini, G., Galli, M., Cacciano, M., Castellani, M., and Salvati, P. 2002. A geomorphological approach to the estimation of landslide hazards and risks in Umbria, Central Italy. *Natural Hazards and Earth System Sciences*, **2**(1/2): 57–72.
- Carr, J.R. 2002. Data visualization in the geosciences. Prentice-Hall, Inc., ISBN 0-13-089706-X.
- Carrara, A. 1983. Multivariate models for landslide hazard evaluation. *Mathematical Geology*, **15**(3): 403–426.
- Carrara, A., Cardinali, M., Guzzetti, F., and Reichenbach, P. 1995. GIS technology in mapping landslide hazard. *In Geographical Information Systems in Assessing Natural Hazards. Edited by A. Carrara and F. Guzzetti.* Kluwer Academic Publisher, Dordrecht, The Netherlands, pp. 135–175.
- Carrara, A., Catalano, E., Sorriso Valvo, M., Reali, C., Merenda, L., and Rizzo, V. 1977. Landslide morphometry and typology in two zones, Calabria, Italy. *Bulletin of Engineering Geology and the Environment*, **16**(1): 8–13.
- Carrara, A., Catalano, E., Sorriso Valvo, M., Reali, C., and Osso, T. 1978. Digital terrain analysis for land evaluation. *Geologia Applicata e Idrogeologia*, **13**: 69–127.
- Carrara, A., and Merenda, L. 1974. Metodologia per un censimento degli eventi franosi in Calabria (Methodology for an inventory of slope instability events in Calabria). *Geologia Applicata e Idrogeologia*, **9**: 237–255.
- Carrara, A., and Merenda, L. 1976. Landslide inventory in northern Calabria, southern Italy. *Geological Society of America Bulletin*, **87**(81): 1153–1162.
- Casagrande, A. 1948. Classification and identification of soils. *Transactions of the American Society of Civil Engineers*, **113**: 901–930.
- Cascini, L., and Versace, P. 1988. Relationship between rainfall and landslide in a gneissic cover. *In Proceedings of the 5th International Symposium on Landslides. Edited by C. Bonnard.* Vol. 1, Lausanne, Switzerland, pp. 565–570.

- Catani, F., Farina, P., Moretti, S., Nico, G., and Strozzi, T. 2005. On the application of SAR interferometry to geomorphological studies: Estimation of landform attributes and mass movements. *Geomorphology*, **66**(1-4): 119–131.
- Çevik, E., and Topal, T. 2003. GIS-based landslide susceptibility mapping for a problematic segment of the natural gas pipeline, Hendek (Turkey). *Environmental Geology*, **44**(8): 949–962.
- Chacón, J., Irigaray, C., Fernández, T., and El Hamdouni, R. 2006. Engineering geology maps: landslides and geographical information systems. *Bulletin of Engineering Geology and the Environment*, **65**(4): 341–411.
- Chau, K.T., Sze, Y.L., Fung, M.K., Wong, W.Y., Fong, E.L., and Chan, L.C.P. 2004. Landslide hazard analysis for Hong Kong using landslide inventory and GIS. *Computers & Geosciences*, **30**(4): 429–443.
- Chleborad, A.F. 2000. Preliminary method for anticipating the occurrence of precipitation-induced landslides in Seattle, Washington. United States Geological Survey, Open-File Report 2000-469.
- Chleborad, A.F. 2003. Preliminary evaluation of a precipitation threshold for anticipating the occurrence of landslides in the Seattle, Washington, area. United States Geological Survey, Open-File Report 2003-463.
- Chleborad, A.F., Baum, R.L., and Godt, J.W. 2006. Rainfall thresholds for forecasting landslides in the Seattle, Washington, area - exceedance and probability. United States Geological Survey, Open-File Report 2006-1064.
- Chung, C.F., and Fabbri, A. 1993. The representation of geoscience information for data integration. *Natural Resources Research*, **2**(2): 122–139.
- Chung, C.F., and Fabbri, A. 1999. Probabilistic prediction models for landslide hazard mapping. *Photogrammetric Engineering & Remote Sensing*, **65**: 1389–1399.
- Clerici, A., Perego, S., Tellini, C., and Vescovi, P. 2002. A procedure for landslide susceptibility zonation by the conditional analysis method. *Geomorphology*, **48**(4): 349–364.

- Clerici, A., Perego, S., Tellini, C., and Vescovi, P. 2006. A GIS-based automated procedure for landslide susceptibility mapping by the Conditional Analysis method: the Baganza valley case study (Italian Northern Apennines). *Environmental Geology*, **50**(7): 941–961.
- Clerici, A., Perego, S., Tellini, C., and Vescovi, P. 2010. Landslide failure and runout susceptibility in the upper T. Ceno valley (Northern Apennines, Italy). *Natural Hazards*, **52**(1): 1–29.
- Coe, J.A., Ellis, W.L., Godt, J.W., Savage, W.Z., Savage, J.E., Michael, J.A., Kibler, J.D., Powers, P.S., Lidke, D.J., and Debray, S. 2003. Seasonal movement of the Slumgullion landslide determined from global positioning system surveys and field instrumentation, July 1998-March 2002. *Engineering Geology*, **68**(1-2): 67–101.
- Coe, J.A., Michael, J.A., Crovelli, R.A., Savage, W.Z., Laprade, W.T., and Nashem, W.D. 2004. Probabilistic assessment of precipitation-triggered landslides using historical records of landslide occurrence, Seattle, Washington. *Environmental and Engineering Geoscience*, **10**(2): 103–122.
- Committee on Ground Failure Hazards. 1985. Reducing losses from landsliding in the United States. US National Research Council, Commission on Engineering and Technical Systems, Washington, D.C.
- Committee on the Review of the National Landslide Hazards Mitigation Strategy. 2004. Partnerships for reducing landslide risk: Assessment of the national landslide hazards mitigation strategy. National Academies Press, Washington, D.C.
- Cornelius, R.R., and Scott, P.A. 1993. A materials failure relation of accelerating creep as empirical description of damage accumulation. *Rock Mechanics and Rock Engineering*, **26**(3): 233–252.
- Cornelius, R.R., and Voight, B. 1995. Graphical and PC-software analysis of volcano eruption precursors according to the Materials Failure Forecast Method (FFM). *Journal of Volcanology and Geothermal Research*, **64**(3-4): 295–320.
- Corominas, J., Copons, R., Moya, J., Vilaplana, J., Altimir, J., and Amigó, J. 2005. Quantitative assessment of the residual risk in a rockfall protected area. *Landslides*, **2**(4): 343–357.

- Corominas, J., Leroi, E., and Savage, W.Z. (eds.). 2008. Guidelines for landslide susceptibility, hazard and risk zoning for land use planning. *Engineering Geology*, **102**(3-4): 83–84.
- Corsini, A., Pasuto, A., Soldati, M., and Zannoni, A. 2005. Field monitoring of the Corvara landslide (Dolomites, Italy) and its relevance for hazard assessment. *Geomorphology*, **66**(1-4): 149–165.
- Crosta, G.B., and Agliardi, F. 2002. How to obtain alert velocity thresholds for large rockslides. *Physics and Chemistry of the Earth*, **27**(36): 1557–1565.
- Crosta, G.B., Chen, H., and Lee, C.F. 2004. Replay of the 1987 Val Pola Landslide, Italian Alps. *Geomorphology*, **60**(1-2): 127–146.
- Crozier, M.J. 1986. *Landslides: causes, consequences & environment*. Croom Helm.
- Crozier, M.J., and Glade, T. 2005. Landslide hazard and risk: Issues, concepts and approach. *In Landslide Hazard and Risk. Edited by T. Glade, M. Anderson, and M.J. Crozier*. John Wiley & Sons Ltd, England, pp. 1–40.
- Cruden, D.M. 1991a. The landslide dam on the Saddle River, near Rycroft, Alberta, Canada. *Landslide News*, **5**: 26–27.
- Cruden, D.M. 1991b. A simple definition of a landslide. *Bulletin of the International Association of Engineering Geology*, **43**(1): 27–29.
- Cruden, D.M., Bornhold, B.D., Chagnon, J.-Y., Evans, S.G., Heginbottom, J.A.H., Locat, J., Moran, K., Piper, D.J.W., Powell, R., Prior, D., Quigley, R.M., and Thomson, S. 1989. Landslides: Extent and economic significance in Canada. *In Proceedings of the 28th International Geological Congress: Symposium on Landslides. Edited by E.E. Brabb and B.L. Harrod*. Washington, D.C., pp. 1–23.
- Cruden, D.M., deLugt, J.S., Lindstrom, K., and Thomson, S. 1990a. Landslide incidence in Alberta. Design and Construction Branch, Alberta Environment, Edmonton, Alberta.
- Cruden, D.M., Keegan, T.R., and Thomson, S. 1993. The landslide dam on the Saddle River near Rycroft, Alberta. *Canadian Geotechnical Journal*, **30**(6): 1003–1015.

- Cruden, D.M., Lu, Z.Y., and Thomson, S. 1997. The 1993 Montagneuse River landslide, Alberta. *Canadian Geotechnical Journal*, **34**(5): 799–810.
- Cruden, D.M., and Masoumzadeh, S. 1987. Accelerating creep of the slopes of a coal-mine. *Rock Mechanics and Rock Engineering*, **20**(2): 123–135.
- Cruden, D.M., Ruel, M., and Thomson, S. 1990b. Landslides along the Peace River, Alberta. *In Proceedings of the 43rd Canadian Geotechnical Conference*. Quebec, pp. 61–68.
- Cruden, D.M., and Varnes, D.J. 1996. Landslides types and processes. *In Landslides: Investigation and Mitigation (Special Report 247)*. Edited by A.K. Turner and R.L. Schuster. Transportation Research Board, National Research Council, Washington, D.C., pp. 36–75.
- Dai, F.C., and Lee, C.F. 2003. A spatiotemporal probabilistic modelling of storm-induced shallow landsliding using aerial photographs and logistic regression. *Earth Surface Processes and Landforms*, **28**(5): 527–545.
- Dai, F.C., Lee, C.F., and Nagi, Y.Y. 2002. Landslide risk assessment and management: an overview. *Engineering Geology*, **64**(1): 65–87.
- Davies, M.R., Paulen, R.C., and Hickin, A.S. 2005. Inventory of Holocene landslides, Peace River area, Alberta (NTS 84C). Alberta Energy and Utilities Board, EUB/AGS Geo-Note 2003-43.
- Davis, J.C. 2002. *Statistics and data analysis in geology*. John Wiley & Sons, Inc., Third edition.
- Davis, T.J., and Keller, C.P. 1997. Modelling uncertainty in natural resource analysis using fuzzy sets and Monte Carlo simulation: slope stability prediction. *International Journal of Geographical Information Science*, **11**(5): 409–434.
- Dawson, G.M. 1881. Report on an exploration from Port Simpson on the Pacific coast, to Edmonton on the Saskatchewan, embracing a portion of the northern part of British Columbia and the Peace River Country, 1879. Geological Survey of Canada, Montreal.
- de By, R.A., Knippers, R.A., Sun, Y., Ellis, M.C., Kraak, M.K., Weir, M.J.C., Georgiadou, Y., Radwan, M.M., van Westen, C.J., Kainz, W., and Sides, E.J.

2001. Principles of Geographic Information Systems, an introductory textbook. ITC Educational Textbook Series 1, Enschede, The Netherlands.
- De la Cruz-Reyna, S., and Reyes-Dávila, G. 2001. A model to describe precursory material-failure phenomena: applications to short-term forecasting at Colima volcano, Mexico. *Bulletin of Volcanology*, **63**(5): 297–308.
- Dearman, W.R., Burton, A.N., Cratchley, C.R., Day, J.B.W., Fookes, P.G., Higginbottom, I.E., Hutchinson, J.N., Little, A.L., McKenna, J.M., and Norman, J.W. 1972. The preparation of maps and plans in terms of engineering geology. *Quarterly Journal of Engineering Geology*, **5**(4): 293–382.
- DeGraff, J.V. 1985. Using isopleth maps of landslide deposits as a tool in timber sale planning. *Bulletin of the Association of Engineering Geologists*, **22**(4): 445–453.
- DeGraff, J.V., and Canuti, P. 1988. Using isopleth mapping to evaluate landslide activity in relation to agricultural practices. *Bulletin of the International Association of Engineering Geology*, **38**: 61–71.
- Delacourt, C., Allemand, P., Berthier, E., Raucoules, D., Casson, B., Grandjean, P., Pambrun, C., and Varel, E. 2007. Remote-sensing techniques for analysing landslide kinematics: a review. *Bulletin de la Societe Geologique de France*, **178**(2): 89–100.
- deLugt, J.S., and Cruden, D.M. 1990. The world landslide inventory. *In Proceedings of the annual conference of the Urban and Regional Information Systems Association*, August 12-16. Edmonton, Alberta, pp. 112–124.
- Devonald, D.M., Thompson, J.A., Hencher, S.R., and Sun, H.W. 2009. Geomorphological landslide models for hazard assessment: a case study at Cloudy Hill, Hong Kong. *Quarterly Journal of Engineering Geology and Hydrogeology*, **42**(4): 473–486.
- Diyaljee, V.A. 1992. Stabilization of Judah Hill landslide. *In Proceedings of the 6th International Symposium on Landslides*. Christchurch, New Zealand, pp. 687–692.
- Dow, V., Kienholz, H., Plam, M., and Ives, J.D. 1981. Mountain hazards mapping: the development of a prototype combined hazards map, Monarch Lake Quadrangle, Colorado, USA. *Mountain Research and Development*, **1**(1): 55–64.

- Duncan, J.M., and Wright, S.G. 2005. Soil strength and slope stability. John Wiley & Sons, Inc.
- El-Ramly, H. 2001. Probabilistic analyses of landslide hazards and risks: Bridging theory and practice. Ph.D. thesis, Department of Civil and Environmental Engineering, University of Alberta, Edmonton, Alberta.
- El-Ramly, H., Morgenstern, N.R., and Cruden, D.M. 2002. Probabilistic slope stability analysis for practice. *Canadian Geotechnical Journal*, **39**(3): 665–683.
- El-Ramly, H., Morgenstern, N.R., and Cruden, D.M. 2003. Probabilistic stability analysis of a tailings dyke on presheared clay-shale. *Canadian Geotechnical Journal*, **40**(1): 192–208.
- El-Ramly, H., Morgenstern, N.R., and Cruden, D.M. 2006. Lodalen slide: a probabilistic assessment. *Canadian Geotechnical Journal*, **43**(9): 956–968.
- EM-DAT. 2011. The OFDA/CRED International Disaster Database. Centre for Research on the Epidemiology of Disasters (CRED), Université Catholique de Louvain (UCL), Brussels, Belgium, <http://www.emdat.be/>. Accessed Feb. 18, 2011.
- Energy Resources Conservation Board. 2009. Table of Formations, Alberta. <http://www.ercb.ca/portal/server.pt?>. Accessed Jan. 24, 2011.
- Environment Canada. 2009. National Climate Data and Information Archive. http://www.climate.weatheroffice.ec.gc.ca/climateData/canada_e.html. Accessed Aug. 19, 2009.
- Ercanoglu, M. 2005. Landslide susceptibility assessment of SE Bartin (West Black Sea region, Turkey) by artificial neural networks. *Natural Hazards and Earth System Sciences*, **5**(6): 979–992.
- Ercanoglu, M., Gokceoglu, C., and van Asch, T.W.J. 2004. Landslide susceptibility zoning north of Yenice (NW Turkey) by multivariate statistical techniques. *Natural Hazards*, **32**(1): 1–23.
- Ercanoglu, M., Kasmer, O., and Temiz, N. 2008. Adaptation and comparison of expert opinion to analytical hierarchy process for landslide susceptibility mapping. *Bulletin of Engineering Geology and the Environment*, **67**(4): 565–578.

- Erley, D., and Kockelman, W.J. 1981. Reducing landslide hazards - A guide for planners. American Planning Association, Planning Advisory Service Report 359, Chicago, Illinois.
- Evans, S.G. 1997. Fatal landslide and landslide risk in Canada. *In* Proceedings of the International Workshop on Landslide Risk Assessment. *Edited by* D.M. Cruden and R. Fell. A.A. Balkema, pp. 185–196.
- Evans, S.G. 1999. Landslide disasters in Canada 1840-1998. Geological Survey of Canada, Open File 3712.
- Evans, S.G. 2001. Landslides. *In* A synthesis of geological hazards in Canada. *Edited by* G.R. Brooks. Geological Survey of Canada, Bulletin 548, pp. 43–79.
- Evans, S.G., Couture, R.C., and Raymond, E.L. 2002. Catastrophic landslides and related processes in the southeastern Cordillera: Analysis of impact on lifelines and communities. Public Safety and Emergency Preparedness Canada.
- Evans, S.G., and Savigny, K.W. 1994. Landslides in the Vancouver - Fraser Valley - Whistler region. *In* Geology and Geological Hazards of the Vancouver Region, Southwestern British Columbia. *Edited by* J.W.H. Monger. Geological Survey of Canada, Bulletin 481, pp. 251–286.
- Fara, H.D., and Scheidegger, A.E. 1963. An eigenvalue method for the statistical evaluation of fault plane solutions of earthquakes. Bulletin of the Seismological Society of America, **53**(4): 811–816.
- Federal Geographic Data Committee (FGDC). 2006. FGDC digital cartographic standard for geologic map symbolization. FGDC Document Number FGDC-STD-013-2006, U.S. Geological Survey.
- Fell, R. 1994. Landslide risk assessment and acceptable risk. Canadian Geotechnical Journal, **31**(2): 261–272.
- Fell, R., Corominas, J., Bonnard, C., Cascini, L., Leroi, E., and Savage, W.Z. 2008a. Guidelines for landslide susceptibility, hazard and risk zoning for land use planning. Engineering Geology, **102**(3-4): 85–98.
- Fell, R., Corominas, J., Bonnard, C., Cascini, L., Leroi, E., and Savage, W.Z. 2008b. Guidelines for landslide susceptibility, hazard and risk zoning for land use planning, Commentary. Engineering Geology, **102**(3-4): 99–111.

- Fell, R., Ho, K.K.S., Lacasse, S., and Leroi, E. 2005. A framework for landslide risk assessment and management. *In* Proceedings of the International Conference on Landslide Risk Management. *Edited by* O. Hungr, R. Fell, R. Couture, and E. Eberhardt. Vancouver, B.C., pp. 3–25.
- Fenton, M.M. 1984. Quaternary stratigraphy of the Canadian Prairies. *In* Quaternary stratigraphy of Canada - a Canadian contribution to IGCP project 24. Geological Survey of Canada, pp. 57–68.
- Fenton, M.M., Paulen, R.C., and Pawlowicz, J.G. 2003. Evidence of Pre-late Wisconsin glacial deposits in central and northern Alberta; Program and Abstracts. *In* Canadian Quaternary Association-Canadian Geomorphological Research Group (CANQUA-CGRG) 2003. Halifax, Nova Scotia, p. A28.
- Fisher, N.I., Lewis, T., and Embleton, B.J.J. 1987. Statistical analysis of spherical data. Cambridge University Press.
- Fisher, R. 1953. Dispersion on a sphere. Proceedings of the Royal Society of London. Series A, Mathematical and Physical Sciences, **217**(1130): 295–305.
- Fleming, R.W., Varnes, D.J., and Schuster, R.L. 1979. Landslide hazards and their reduction. Journal of the American Planning Association, **45**(4): 428–439.
- Froese, C.R. 2007. Peace River landslide project: Hazard and risk assessment for urban landsliding. *In* Proceedings of the 60th Canadian Geotechnical Conference and 8th Joint CGS/IAH-CNC Groundwater Conference. Ottawa, pp. 699–704.
- Froese, C.R., Terry, I., Barlow, J.P., and Jackson, R. 2002. Peace River landfill preliminary geotechnical and environmental assessment, Peace River, Alberta. Technical report, EE-30044, AMEC Earth & Environmental Limited.
- Fukuzono, T. 1985. A new method for predicting the failure time of a slope. *In* Proceedings of the 4th International Conference and Field Workshop on Landslides. Tokyo, Japan. Aug. 23-31, pp. 145–150.
- Fukuzono, T. 1990. Recent studies on time prediction of slope failure. Landslide News, **4**: 9–12.
- Fulton, R.J., Fenton, M.M., and Rutter, N.W. 1986. Summary of Quaternary stratigraphy and history, Western Canada. Quaternary Science Reviews, **5**(4): 229–241.

- Galli, M., Ardizzone, F., Cardinali, M., Guzzetti, F., and Reichenbach, P. 2008. Comparing landslide inventory maps. *Geomorphology*, **94**(1-4): 268–289. doi: 10.1016/j.geomorph.2006.09.023.
- Gassen, W.V., and Barlow, J.P. 2003. Re: Geotechnical design washout Brick's Hill, SH684:02 and McAllister Creek. Technical report, EG08628.35, EBA Engineering Consultants Ltd.
- Geotechnical Society of Edmonton. 1996. Risk Assessment in Geotechnical & Geo-Environmental Engineering. The Second Annual One Day Symposium, April 2, Edmonton, Alberta.
- Glade, T., Anderson, M., and Crozier, M.J. 2005. *Landslide Hazard and Risk*. John Wiley and Sons, Ltd.
- Glastonbury, J., and Fell, R. 2002. Report on the analysis of slow, very slow, and extremely slow natural landslides. UNICIV Report No. R-402 January 2002, School of Civil and Environmental Engineering, University of New South Wales, Sydney, Australia.
- Glastonbury, J., and Fell, R. 2008. Geotechnical characteristics of large slow, very slow, and extremely slow landslides. *Canadian Geotechnical Journal*, **45**(7): 984–1005.
- Gleddie, J. 1949. Upper Cretaceous in western Peace River Plains, Alberta. *Bulletin of the American Association of Petroleum Geologists*, **33**(4): 511–532.
- Gleddie, J. 1954. Upper Cretaceous in western Peace River Plains, Alberta. *In* Ralph Leslie Rutherford Memorial Volume, Western Canada Sedimentary Basin Symposium. American Association of Petroleum Geologists. Tulsa, Oklahoma, pp. 486–509.
- Glenn, N.F., Streutker, D.R., Chadwick, D.J., Thackray, G.D., and Dorsch, S.J. 2006. Analysis of LiDAR-derived topographic information for characterizing and differentiating landslide morphology and activity. *Geomorphology*, **73**: 131–148.
- Godt, J.W., Baum, R.L., and Chleborad, A.F. 2006. Rainfall characteristics for shallow landsliding in Seattle, Washington, USA. *Earth Surface Processes and Landforms*, **31**(1): 97–110.

- Godt, J.W., Baum, R.L., Savage, W.Z., Salciarini, D., Schulz, W.H., and Harp, E.L. 2008. Transient deterministic shallow landslide modeling: Requirements for susceptibility and hazard assessments in a GIS framework. *Engineering Geology*, **102**(3-4): 214–226.
- Green, M.R., Forth, R.A., and D. Beaumont, D. 1998. A hazard map of the Magnesian Limestone in County Durham. *Geohazards in Engineering Geology*, Geological Society, London, *Engineering Geology Special Publications*, **15**(1): 239–246.
- Green, R. 1972. Geological map of Alberta. Alberta Geological Survey, Map 27, Edmonton, Alberta.
- Greenlee, D.D. 1987. Raster and vector processing for scanned linework. *Photogrammetric Engineering & Remote Sensing*, **53**(10): 1383–1387.
- Grohmann, C.H., Smith, M.J., and Riccomini, C. 2009. Surface roughness of topography: A multi-scale analysis of landform elements in Midland Valley, Scotland. *In Proceedings of Geomorphometry*. Zurich, Switzerland, pp. 140–148.
- Groshong, Jr., R.H. 2006. *3-D Structural Geology - A practical guide to quantitative surface and subsurface map interpretation*. Springer, second edition.
- Guidicini, G., and Iwasa, O.Y. 1977. Tentative correlation between rainfall and landslides in a humid tropical environment. *Bulletin of Engineering Geology and the Environment*, **16**(1): 3–20.
- Guth, P.L. 2003. Eigenvector analysis of digital elevation models in a GIS: Geomorphometry and quality control. *In Concepts and Modelling in Geomorphology: International Perspectives*. Edited by I.S. Evans, R. Dikau, E. Tokunaga, H. Ohmori, and M. Hirano. Terrapub, Tokyo, pp. 199–220.
- Guzzetti, F., Cardinali, M., and Reichenbach, P. 1994. The AVI Project - A bibliographical and archive inventory of landslides and floods in Italy. *Environmental Management*, **18**(4): 623–633.
- Guzzetti, F., Carrara, A., Cardinali, M., and Reichenbach, P. 1999. Landslide hazard evaluation: a review of current techniques and their application in a multi-scale study, Central Italy. *Geomorphology*, **31**(3-4): 181–216.

- Guzzetti, F., Peruccacci, S., Rossi, M., and Stark, C.P. 2007. Rainfall thresholds for the initiation of landslides in central and southern Europe. *Meteorology and Atmospheric Physics*, **98**(3-4): 239–367. doi:10.1007/s00703-007-0262-7.
- Guzzetti, F., Peruccacci, S., Rossi, M., and Stark, C.P. 2008. The rainfall intensity-duration control of shallow landslides and debris flows: an update. *Landslides*, **5**(1): 3–17.
- Hall-Beyer, M. 2007. The GLCM tutorial home page. <http://www.fp.ucalgary.ca/mhallbey/tutorial.htm>. Accessed Mar. 24, 2011.
- Hamilton, W.N., Price, M.C., Langenberg, C.W., and Chao, D.K. 1999. Geological map of Alberta. Alberta Geological Survey, Map 236, Edmonton, Alberta.
- Hammond, C., Hall, D., Miller, S., and Swetik, P. 1992. Level I Stability Analysis (LISA) documentation for version 2.0, General Technical Report INT-285. United States Department of Agriculture, Forest Service, Intermountain Research Station.
- Hansen, A. 1984. Landslide hazard analysis. *In Slope Instability. Edited by D. Brunsten and D.B. Prior.* John Wiley & Sons, pp. 523–602.
- Haralick, R.M. 1979. Statistical and structural approaches to texture. *Proceedings of the IEEE*, **67**(5): 786–804.
- Haralick, R.M., Shanmugam, K., and Dinstein, I. 1973. Textural features for image classification. *IEEE Transactions on Systems Man and Cybernetics*, **SMC-3**(6): 610–621.
- Hardy, R.M. 1957. Engineering problems involving pre-consolidated clay shale. *Transactions of the Engineering Institute of Canada*, **1**: 5–14.
- Harris, M.C. 1973. Town of Peace River Riverview Subdivision 99 Street road stability. Technical report, E-2738, R. M. HARDY & ASSOCIATES Ltd.
- Harris, M.C., and Rogers, W.G. 1979. Proposed Peace River overpasses Northern Alberta Railways Company geotechnical investigation. Technical report, 17-717-0, Thurber Consultants Ltd.
- Hartlén, J., and Viberg, L. 1988. General report: Evaluation of landslide hazard. *In Proceedings of the 5th International Symposium on Landslides. Edited by C. Bonnard.* Vol. 2, Lausanne, Switzerland, pp. 1037–1057.

- Hasofer, A.M., and Lind, N.C. 1974. Exact and invariant second-moment code format. *Journal of the Engineering Mechanics Division, ASCE*, **100**(EM1): 111–121.
- Hayashi, S., Park, B., Komamura, F., and Yamamori, T. 1988. On the forecast of time to failure of slope (II) - Approximate forecast in the early period of the Tertiary creep -. *Journal of Japanese Landslide Society*, **25**(3): 11–16.
- Heim, A. 1932. *Landslides & human lives (Bergsturz und Menschenleben)*, Translated by N. Skermer. BiTech Publishers, 1989, Vancouver.
- Henderson, E.P. 1959. Surficial geology of Sturgeon Lake map-area, Alberta. *Geological Survey of Canada Memoir 303*, Geological Survey of Canada.
- Hervás, J. 2003. Lessons learnt from landslide disasters in Europe. European Commission Joint Research Centre, European Communities, EUR 20558 EN, http://nedies.jrc.it/doc/Landslides_Final.pdf. Accessed Mar. 24, 2011.
- Hervás, J., and Bobrowsky, P. 2009. Mapping: Inventories, susceptibility, hazard and risk. *In Landslides: Disaster Risk Reduction. Edited by K. Sassa and P. Canuti*. Springer, Berlin, pp. 321–349.
- Hervás, J., and Rosin, P.L. 1996. Landslide mapping by textural analysis of ATM data. *In Proceedings of the 11th Thematic Conference and Workshops on Applied Geologic Remote Sensing. Vol. 2, Las Vegas, Nevada*, pp. 394–402.
- Highland, L.M. 1997. Landslide hazard and risk: Current and future directions for the United States Geological Survey's landslide program. *In Proceedings of the International Workshop on Landslide Risk Assessment. Edited by D.M. Cruden and R. Fell*. Honolulu, Hawaii, pp. 207–213.
- Highland, L.M., and Bobrowsky, P. 2008. *The landslide handbook - A guide to understanding landslides*. Circular 1325. U.S. Geological Survey, Reston, Virginia.
- Hobson, R.D. 1972. Surface roughness in topography: quantitative approach. *In Spatial Analysis in Geomorphology. Edited by R.J. Chorley*. Methuen & Co Ltd., London, Great Britain, pp. 221–245.
- Hodgson, M.E., and Gaile, G.L. 1999. A cartographic modeling approach for surface orientation-related applications. *Photogrammetric Engineering & Remote Sensing*, **65**(1): 85–95.

- Hofmann, B.A., and Barlow, J.P. 1992. Geotechnical investigation 99 Street slope stabilization Lots 4-22, Block 3, Plan 6472NY Peace River, Alberta. Technical report, EG-07480, HBT AGRA Limited.
- Honeycutt, C.E., and Plotnick, R. 2008. Image analysis techniques and gray-level co-occurrence matrices (GLCM) for calculating bioturbation indices and characterizing biogenic sedimentary structures. *Computers & Geosciences*, **34**(1): 1461–1472.
- Hungr, O. 1995. A model for the runout analysis of rapid flow slides, debris flows, and avalanches. *Canadian Geotechnical Journal*, **32**(4): 610–623.
- Hungr, O., Corominas, J., and Eberhardt, E. 2005. Estimating landslide motion mechanism, travel distance and velocity. *In Proceedings of the International Conference on Landslide Risk Management. Edited by O. Hungr, R. Fell, R. Couture, and E. Eberhardt. Vancouver, B.C., pp. 99–128.*
- Hungr, O., Evans, S.G., and Hazzard, J. 1999. Magnitude and frequency of rock falls and rock slides along the main transportation corridors of southwestern British Columbia. *Canadian Geotechnical Journal*, **36**(2): 224–238.
- Hunter, G.J., and Goodchild, M.F. 1997. Modeling the uncertainty of slope and aspect estimates derived from spatial databases. *Geographical Analysis*, **29**(1): 35–49.
- Hutchinson, J.N. 1988. General report: Morphological and geotechnical parameters of landslides in relation to geology and hydrology. *In Proceedings of the 5th International Symposium on Landslides. Edited by C. Bonnard. A.A. Balkema, pp. 3–35.*
- IAEG Commission on Landslides. 1990. Suggested nomenclature for landslides. *Bulletin of the International Association of Engineering Geology*, **41**(1): 13–16.
- Imrie, A.S. 1991. Stress-induced response from both natural and construction-related processes in the deepening of the Peace River valley, B.C. *Canadian Geotechnical Journal*, **28**(5): 719–728.
- IUGS Working Group on Landslides. 1995. A suggested method for describing the rate of movement of a landslide. *Bulletin of the International Association of Engineering Geology*, **52**(1): 75–78.

- IUGS Working Group on Landslides. 2001. A suggested method for reporting landslide remedial measures. *Bulletin of the International Association of Engineering Geology*, **60**(1): 69–74.
- IUGS Working Group on Landslides, Committee on Risk Assessment. 1997. Quantitative risk assessment for slopes and landslides - The state of the art. *In Proceedings of the International Workshop on Landslide Risk Assessment. Edited by D.M. Cruden and R. Fell.* Honolulu, Hawaii, pp. 3–12.
- Ives, J.D., and Bovis, M.J. 1978. Natural hazards maps for land-use planning, San Juan Mountains, Colorado, U.S.A. *Arctic and Alpine Research*, **10**(2): 185–212.
- Jahns, R.H. 1969. Seventeen years of response by the City of Los Angeles to geologic hazards. *In Proceedings of the Geologic Hazards and Public Problems. Edited by R.A. Olson and M.M. Wallace.* Sponsored by Office of Emergency Preparedness, Santa Rosa, California, pp. 283–295.
- Jahns, R.H., 1978. Landslides. *Studies in Geophysics, Geophysical Predictions,* Washington, D.C., National Academy of Science, pp. 58–65.
- Jennings, P.J., and Siddle, H.J. 1998. Use of landslide inventory data to define the spatial location of landslide sites, South Wales, UK. *Geohazards in Engineering Geology, Geological Society, London, Engineering Geology Special Publications*, **15**(1): 199–211.
- Jenson, S.K., and Domingue, J.O. 1988. Extracting topographic structure from digital elevation data for geographic information system analysis. *Photogrammetric Engineering & Remote Sensing*, **54**(1): 1593–1600.
- Jones, J.F. 1966. Geology and groundwater resources of the Peace River district, northernwestern Alberta. *Research Council of Alberta Bulletin 16,* Edmonton, Alberta.
- Kaplan, V. 2006. Using textural information for classification of remote sensing imagery. *In Proceedings of the International Symposium GIS Ostrava 2006.* Ostrava, Czech Republic, http://gis.vsb.cz/GISEngl/Conferences/GIS_Ova/GIS_Ova_2006/Proceedings/Referaty/kaplan.html. Accessed Mar. 24, 2011.
- Karall, D. 1992. Instrumentation of the Curling Rink Slide Highway 2:60 Peace River, Alberta. Technical report, 0106-11088, EBA Engineering Consultants Ltd.

- Karall, D., and Ruban, A.F. 1994. Instrumentation installation Curling Rink Slide Highway 2:60 Peace River, Alberta. Technical report, 0104-20205, EBA Engineering Consultants Ltd.
- Kasai, M., Ikeda, M., Asahina, T., and Fujisawa, K. 2009. LiDAR-derived DEM evaluation of deep-seated landslides in a steep and rocky region of Japan. *Geomorphology*, **113**(1-2): 57–69.
- Keefer, D.K., Wilson, R.C., Mark, R.K., Brabb, E.E., Brown, W.M., Ellen, S.D., Harp, E.L., Wieczorek, G.F., Alger, C.S., and Zatzkin, R.S. 1987. Real-time landslide warning during heavy rainfall. *Science*, **238**(4829): 921–925.
- Keegan, T.R. 1992. The Rycroft landslide dam on the Saddle River, Alberta. M.Sc. thesis, Department of Civil Engineering, University of Alberta, Edmonton, Alberta.
- Keegan, T.R. 2007. Methodology for risk analysis of railway ground hazards. Ph.D. thesis, Department of Civil and Environmental Engineering, University of Alberta, Edmonton, Alberta.
- Keegan, T.R., Cruden, D.M., Martin, C.D., Morgenstern, N.R., Ruel, M., and Pritchard, M. 2007. A railway ground hazard risk management methodology overview. *In* Proceedings of the 60th Canadian Geotechnical Conference and 8th Joint CGS/IAH-CNC Groundwater Conference. Ottawa, pp. 2278–2286.
- Kienholz, H. 1978. Maps of geomorphology and natural hazards of Grindelwald, Switzerland: Scale 1:10,000. *Arctic and Alpine Research*, **10**(2): 169–184.
- Kienholz, H., and Bichsel, M. 1982. The use of air photographs for mapping natural hazards in mountainous areas: A study based on the Colorado Rocky Mountains, U.S.A. *Mountain Research and Development*, **2**(4): 349–358.
- Kienholz, H., Hafner, H., Schneider, G., and Tamrakar, R. 1983. Mountain hazards mapping in Nepal's middle mountains maps of land use and geomorphic damages (Kathmandu-Kakani Area). *Mountain Research and Development*, **3**(3): 195–220.
- Kienholz, H., Schneider, G., Bichsel, M., Grunder, M., and Mool, P. 1984. Mapping of mountain hazards and slope stability. *Mountain Research and Development*, **4**(3): 247–266.

- Kilburn, C.R.J., and Petley, D.N. 2003. Forecasting giant, catastrophic slope collapse: lessons from Vajont, Northern Italy. *Geomorphology*, **54**(1-2): 21–32.
- Kim, T.H., Cruden, D.M., Martin, C.D., and Froese, C.R. 2010a. The 2007 Fox Creek landslide, Peace River Lowland, Alberta, Canada. *Landslides*, **7**(1): 89–98. doi:10.1007/s10346-009-0184-1.
- Kim, T.H., Cruden, D.M., Martin, C.D., Froese, C.R., and Morgan, A.J. 2010b. Landslide movements and their characteristics, Town of Peace River, Alberta. *In Proceedings of the 63th Canadian Geotechnical Conference and 6th Canadian Permafrost Conference. Edited by GEO2010 Calgary Organizing Committee. Calgary, Alberta*, pp. 1622–1629.
- Kimura, H., and Yamaguchi, Y. 2000. Detection of landslide areas using satellite radar interferometry. *Photogrammetric Engineering & Remote Sensing*, **66**(3): 337–344.
- Kjekstad, O., and Highland, L. 2009. Economic and social impacts of landslides. *In Landslides: Disaster Risk Reduction. Edited by K. Sassa and P. Canuti. Springer, Berlin*, pp. 573–587.
- Kjelland, N.H., Skirrow, R.K., Morgan, A.J., and Szmata, E.J. 2009. Slope stabilization efforts along Highway 744:04, Judah Hill Road, Peace River, Alberta. *In Proceedings of the 62th Canadian Geotechnical Conference and 10th Joint CGS/IAH-CNC Groundwater Conference. Halifax, N.S.*, pp. 722–728.
- Klugman, M.A., and Chung, P. 1976. Slope stability study of the regional municipality of Ottawa-Carleton, Ontario, Canada. Ontario Geological Survey, Miscellaneous Paper MP68.
- Kockelman, W.J. 1986. Some techniques for reducing landslide hazards. *Bulletin of the Association of Engineering Geologists*, **23**(1): 29–52.
- Komac, M. 2006. A landslide susceptibility model using the Analytical Hierarchy Process method and multivariate statistics in perialpine Slovenia. *Geomorphology*, **74**(1-4): 17–28.
- Kottek, M., Grieser, J., Beck, C., Rudolf, B., and Rubel, F. 2006. World Map of the Köppen-Geiger climate classification updated. *Meteorologische Zeitschrift*, **15**(3): 259–263. <http://koeppen-geiger.vu-wien.ac.at> or <http://gpcc.dwd.de>. Accessed Mar. 24, 2011.

- Krohn, J.P., and Slosson, J.E. 1976. Landslides potential in the United States. *California Geology*, **29**(10): 224–231.
- Küpper, A.G., Barlow, J.P., and McRoberts, E.C. 1994. 101 Street/99 Street slope stabilization project Peace River, Alberta. Technical report, EG-07480, HBT AGRA Limited.
- Lan, H.X., Zhou, C.H., Wang, L.J., Zhang, H.Y., and Li, R.H. 2004. Landslide hazard spatial analysis and prediction using GIS in the Xiaojiang watershed, Yunnan, China. *Engineering Geology*, **76**(1-2): 109–128.
- Larose, D.T. 2006. *Data mining methods and models*. John Wiley & Sons, Inc.
- Lau, R.K. 1986. Recommendations and preliminary cost estimates for remedial measures Shaftesbury Trail Slide near Peace River, Alberta. Technical report, 0106-4519, EBA Engineering Consultants Ltd.
- Lee, E.M., and Jones, D.K.C. 2004. *Landslide risk assessment*. Thomas Telford.
- Leir, M., and Savigny, K.W. 1996. Ball Park Slide, Mile 47.8, Peace River Subdivision. Technical report, 0034-006-01, Bruce Geotechnical Consultants Inc.
- Leroueil, S. 2001. Natural slopes and cuts: movement and failure mechanism. *Géotechnique*, **51**(3): 197–243.
- Leroueil, S., Vaunat, J., Picarelli, L., Locat, J., Lee, H., and Faure, R. 1996. Geotechnical characterization of slope movements. *In Proceedings of the 7th International Symposium on Landslides. Edited by K. Senneset*. Vol. 1, Trondheim, Norway, pp. 53–74.
- Leslie, L.E., and Fenton, M.M. 2001. Quaternary stratigraphy and surficial geology River River - Final Report. Alberta Geological Survey, Special Report SPE10, Edmonton, Alberta.
- Leventhal, A.R., and Kotze, G.P. 2008. Landslide susceptibility and hazard mapping in Australia for land-use planning - with reference to challenges in metropolitan suburbia. *Engineering Geology*, **102**(3-4): 238–250.
- Leventhal, A.R., and Walker, B.F. 2005. Risky business - development and implementation of a national landslide risk management system. *In Proceedings of the International Conference on Landslide Risk Management. Edited by O. Hungr, R. Fell, R. Couture, and E. Eberhardt*. Vancouver, B.C., pp. 401–109.

- Lindberg, D.A., and Savigny, K.W. 1980. Mile 50.9 Peace River subdivision geotechnical investigation. Technical report, 15-7-30, Thurber Consultants Ltd.
- Lindberg, D.A., and Savigny, K.W. 1981a. Mile 46.3 Peace River Subdivision geotechnical investigation. Technical report, 15-7-31, Thurber Consultants Ltd.
- Lindberg, D.A., and Savigny, K.W. 1981b. Mile 46.5 Peace River Subdivision. Technical report, 15-7-29, Thurber Consultants Ltd.
- Little, P. 1992. 1992 Instrumentation installation Curling Rink Hill Slide Peace River, Alberta. Technical report, GX00527, HBT AGRA Limited.
- Liverman, D.G.E., Catto, N.R., and Rutter, N.W. 1989. Laurentide glaciation in west-central Alberta: a single (Late Wisconsinan) event. *Canadian Journal of Earth Sciences*, **26**(2): 266–274.
- Lu, Z.Y., and Cruden, D.M. 2000. Fluvial processes and landslide activity in the western Peace River Lowland, Alberta, Canada. *In Proceedings of the 8th International Symposium on Landslides*. Cardiff, UK, pp. 955–996.
- Lu, Z.Y., Cruden, D.M., and Thomson, S. 1998. Landslides and preglacial channels in the Western Peace River Lowland, Alberta. *In Proceedings of the 51st Canadian Geotechnical Conference*. Edmonton, Alberta, pp. 267–274.
- Luzi, L., and Pergalani, F. 1999. Slope instability in static and dynamic conditions for urban planning: the ‘Oltre Po Pavese’ case history (Regione Lombardia - Italy). *Natural Hazards*, **20**(1): 57–82.
- Mahr, T., and Malgot, J. 1978. Zoning maps for regional and urban development based on slope stability. *In Proceedings of the 3rd International Congress of Engineering Geology*. Vol. 1, Madrid, Spain, pp. 124–137.
- Mahr, T., and Malgot, J. 1985. Devastation of the environment by landslides activated by construction. *Bulletin of Engineering Geology and the Environment*, **31**(1): 81–88.
- Mardia, K.V. 1972. *Statistics of directional data*. Academic Press.
- Mark, D.M. 1973. Analysis of axial orientation data, including till fabrics. *Geological Society of America Bulletin*, **84**(4): 1369–1374.
- Mark, D.M. 1974. On the interpretation of till fabrics. *Geology*, **2**(2): 101–104.

- Martin, C.D., Tannant, D.D., and Lan, H. 2007. Comparison of terrestrial-based, high resolution, LiDAR and digital photogrammetry surveys of a rock slope. *In* Proceedings of the first Canada - U.S. Rock Mechanics Symposium, Vancouver. *Edited by* E. Eberhardt, D. Stead, and T. Morrison. Taylor and Francis Group, London, pp. 37–44.
- Matheson, D.S., and Thomson, S. 1973. Geological implications of valley rebound. *Canadian Journal of Earth Sciences*, **10**(6): 961–978.
- Mathews, W.H. 1980. Retreat of the last ice sheets in northeastern British Columbia and adjacent Alberta. *Geological Survey Bulletin 331*, Geological Survey of Canada.
- Matula, M. 1979. Regional engineering geological evaluation for planning purposes. *Bulletin of Engineering Geology and the Environment*, **19**(1): 18–24.
- Mayor's Ad Hoc Landslide Committee. 1967. Landslides and attendant problems, a report to the Mayor of the City of Los Angeles. Los Angeles, California.
- McConnell, R.G. 1893. Report on a portion of the district of Athabasca comprising the country between Peace River and Athabasca River north of Lesser Slave Lake. Part D. Annual Report, Vol. 5, 1889-90-91, Geological Survey of Canada, Ottawa, Ontario.
- McKean, J., and Roering, J. 2004. Objective landslide detection and surface morphology mapping using high-resolution airborne laser altimetry. *Geomorphology*, **57**: 331–351.
- McLearn, F.H. 1918. Peace River section, Alberta. Geological Survey of Canada Summary Report, 1917, Part C, Geological Survey of Canada.
- McLearn, F.H. 1919. Cretaceous, Lower Smoky River, Alberta. Geological Survey of Canada Summary Report, 1918, Part C, Geological Survey of Canada.
- McLearn, F.H. 1926. New species from the Coloradoan of lower Smoky and lower Peace Rivers, Alberta. *Geological Survey Bulletin No. 42*, Geological Series, No. 45, Canada Department of Mines, Geological Survey, Ottawa.
- McLearn, F.H. 1932. Problems of the Lower Cretaceous of the Canadian Interior. *In* Proceedings and Transactions of the Royal Society of Canada, Third Series. Vol. 26, The Royal Society of Canada, Ottawa, pp. 157–175.

- McLearn, F.H. 1945. Revision of the Lower Cretaceous of the western interior of Canada (second edition). Geological Survey Paper 44-17, Geological Survey of Canada.
- McLearn, F.H., and Henderson, J.F. 1944. Geology and oil prospects of Lone Mountain area, British Columbia. Geological Survey Paper 44-2, Geological Survey of Canada.
- Mendenhall, W., Beaver, R.J., and Beaver, B.M. 2003. Introduction to probability and statistics. Brooks/Cole, Thomson Learning, Inc., Eleventh edition.
- Meneroud, J.P. 1978. Cartographie des risques dans les alpes - Maritimes (France). *In Proceedings of the 3rd International Congress of Engineering Geology*. Vol. 2, Madrid, Spain, pp. 98–107.
- Mikkelsen, P.E. 1996. Field instrumentation. *In Landslides: Investigation and Mitigation (Special Report 247)*. Edited by A.K. Turner and R.L. Schuster. Transportation Research Board, National Research Council, Washington, D.C., pp. 278–316.
- Miller, B.G.N. 2000. The Spirit and Eureka River landslides, Peace River Lowlands, Alberta. M.Sc. thesis, Department of Earth and Atmospheric Sciences, University of Alberta, Edmonton, Alberta.
- Miller, B.G.N., and Cruden, D.M. 2001. Landslides, landslide dams and the geomorphology of tributaries in the Peace River Lowlands, Alberta. *In Proceedings of the 54th Canadian Geotechnical Conference*, Sept. 16-19. Calgary, Alberta, pp. 363–370.
- Miller, B.G.N., and Cruden, D.M. 2002. The Eureka River landslide and dam, Peace River Lowlands, Alberta. *Canadian Geotechnical Journal*, **39**(4): 863–878.
- Montgomery, D.R., and Dietrich, W.E. 1994. A physically based model for the topographic control on shallow landsliding. *Water Resources Research*, **30**(4): 1153–1171.
- Montgomery, D.R., Schmidt, K.M., Greenberg, H.M., and Dietrich, W.E. 2000. Forest clearing and regional landsliding. *Geology*, **28**(4): 311–314.
- Moon, V., and Blackstock, H. 2004. A methodology for assessing landslide hazard using deterministic stability models. *Natural Hazards*, **32**(1): 111–134.

- Morgan, A.J., Paulen, R.C., and Froese, C.R. 2008. Ancestral buried valleys of the Peace River: Effects on the Town of Peace River. *In* Proceedings of the 61st Canadian Geotechnical Conference, Sept. 21-24. Edmonton, Alberta, pp. 1219–1226.
- Morgan, A.J., Slattery, S.R., and Froese, C.R. 2009. Results of sediment coring at the Town of Peace River, Northwestern Alberta (NTS 84C). Energy Resources Conservation Board, ERCB/AGS Open File Report 2009-18, Edmonton, Alberta.
- Morgan, G.C., Rawlings, G.E., and Sobkowicz, J. 1992. Evaluating total risk to communities from large debris flows. *In* Proceedings of the first Canadian Symposium on Geotechnique and Natural Hazards. Vancouver, B.C., pp. 225–236.
- Morgenstern, N.R., and Martin, C.D. 2008. Landslides: Seeing the ground, Keynote lecture. *In* Proceedings of the 10th International Symposium on Landslides and Engineered Slopes, Xi'an, China. *Edited by* Z. Chen, J. Zhang, Z. Li, F. Wu, and K. Ho. Taylor & Francis Group, London, pp. 3–23.
- Nadim, F., Kjekstad, O., Peduzzi, P., Herold, C., and Jaedicke, C. 2006. Global landslide and avalanche hotspots. *Landslides*, **3**(2): 159–173. doi:10.1007/s10346-006-0036-1.
- Natural Resources Canada. 2010. GeoGratis, an online geospatial data portal, Earth Sciences Sector, Natural Resources Canada. <http://geogratis.cgdi.gc.ca/geogratis/en/index.html>. Accessed Jan. 7, 2011.
- Neuhäuser, B., and Terhorst, B. 2007. Landslide susceptibility assessment using “weights-of-evidence” applied to a study area at the Jurassic escarpment (SW-Germany). *Geomorphology*, **86**(1-2): 12–24.
- Neuland, H. 1976. A prediction model of landslips. *Catena*, **3**(2): 215–230.
- Nguyen, V.U., and Chowdhury, R.N. 1985. Simulation for risk analysis with correlated variables. *Géotechnique*, **35**(1): 47–58.
- Nilsen, T.H., and Turner, B.L. 1975. Influence of rainfall and ancient landslide deposits on recent landslides (1950-71) in urban areas of Contra Costa County, California. United States Geological Survey, Geological Survey Bulletin 1388.
- Nilson, A. 1979. Bradwill Consultants Limited proposed commercial industrial subdivision NE1/4-Sec.26-Twp.83-Rge.22-W5M Peace River, Alberta. Technical report, B-4447, HARDY ASSOCIATES (1978) Ltd.

- Nilson, A., and McCormick, G. 1978. Peace River Regional Planning Commission slope stability assessment Town of Peace River, Peace River, Alberta. Technical report, B-4387, Hardy Associates Ltd.
- Norheim, R.A., Queija, V.R., and Haugerud, R.A. 2002. Comparison of LIDAR and INSAR DEMs with dense ground control. *In* Proceedings of the 22nd Annual ESRI International User Conference. San Diego, California, <http://proceedings.esri.com/library/userconf/proc02/pap0442/p0442.htm>. Accessed Mar. 24, 2011.
- Nossin, J.J. 1975. Multidisciplinary surveys and integration necessary to their fulfillment in development planning. *ITC Journal*, **4**: 429–443.
- O'Brien, F., Cruden, D.M., and Kim, T.H. 2011. Slope movements by blocks sliding on horizontal bedding surfaces. *In* Proceedings of the 5th Canadian Conference on Geotechnique and Natural Hazards. Kelowna, B.C., [Electronic version].
- Ohlmacher, G.C., and Davis, J.C. 2003. Using multiple logistic regression and GIS technology to predict landslide hazard in northeast Kansas, USA. *Engineering Geology*, **69**(3-4): 331–343.
- Olshansky, R.B., and Rogers, J.D. 1987. Unstable ground: Landslide policy in the United States. *Ecology Law Quarterly*, **13**(4): 939–1006.
- Onodera, T., Yoshinaka, R., and Kazama, H. 1988. Slope failures caused by heavy rainfall in Japan. *In* Proceedings of the Second International Congress of the International Association of Engineering Geology. Vol. 2, São Paulo, Brazil, pp. 1–10.
- Ozdemir, A. 2009. Landslide susceptibility mapping of vicinity of Yaka Landslide (Gelendost, Turkey) using conditional probability approach in GIS. *Environmental Geology*, **57**(7): 1675–1686.
- Pack, R.T., Morgan, G.C., and Anderson, L.R. 1987. Philosophy of landslide risk evaluation and acceptance. *In* Proceedings of ICASP5, the fifth International Conference on Applications of Statistics and Probability in Soil and Structural Engineering. Edited by N.C. Lind. Vancouver, B.C., pp. 946–952.
- Pack, R.T., Tarboton, D.G., and Goodwin, C.N. 1998. The SINMAP approach to terrain stability mapping. *In* Proceedings of the 8th Congress of the International Association of Engineering Geology. Edited by D.P. Moore and O. Hungr. Vol. 2, Vancouver, B.C., pp. 1157–1165.

- Pan, X., Nakamura, H., Nozaki, T., and Huang, X. 2008. A GIS-based landslide hazard assessment by multivariate analysis. *Journal of the Japan Landslide Society*, **45**(3): 187–195.
- Paulen, R.C. 2004. Surficial Geology of the Grimshaw Area, (NTS 84C/SW). Alberta Energy and Utilities Board, EUB/AGS Map 291, Scale 1:100,000, Edmonton, Alberta.
- Pašek, J. 1974. Haupttypen und Ursachen der Hangbewegungen. *Z. Geol. Wiss.*, **2**(4): 421–428.
- Pašek, J. 1975. Landslides inventory. *Bulletin of Engineering Geology and the Environment*, **12**(1): 73–74.
- Pawluk, S., and Bayrock, L.A. 1969. Some characteristics and physical properties of Alberta tills. *Research Council of Alberta Bulletin 26*, Research Council of Alberta.
- Peace River Regional Planning Commission. 1971. Central places in the Peace River region of Alberta. Peace River Regional Planning Commission, Grande Prairie, Alberta.
- Peace River Regional Planning Commission. 1980. Town of Peace River general municipal plan, inventory and analysis, 1978-1979. Technical report, Peace River Regional Planning Commission.
- Pestrong, R. 1976. Landslides - The descent of man. *California Geology*, **29**(7): 147–151.
- Peterson, R. 1958. Rebound in the Bearpaw shale, Western Canada. *Geological Society of America Bulletin*, **69**(9): 1113–1124.
- Petley, D.N. 2004. The evolution of slope failures: mechanisms of rupture propagation. *Natural Hazards and Earth System Sciences*, **4**(1): 147–152.
- Petley, D.N. 2008. The global occurrence of fatal landslides in 2007. *Geophysical Research Abstracts*, **10**. EGU General Assembly 2008. SRef-ID: 1607-7962/gra/EGU2008-A-10487.
- Petley, D.N., Bulmer, M.J., and Murphy, W. 2002. Patterns of movement in rotational and translational landslides. *Geology*, **30**(8): 719–722.

- Petley, D.N., Higuchi, T., Petley, D.J., Bulmer, M.H., and Carey, J. 2005. Development of progressive landslide failure in cohesive materials. *Geology*, **33**(3): 201–204.
- Picarelli, L., Oboni, F., Evans, S.G., Mostyn, G., and Fell, R. 2005. Hazard characterization and quantification. *In Proceedings of the International Conference on Landslide Risk Management. Edited by O. Hungr, R. Fell, R. Couture, and E. Eberhardt. Vancouver, B.C., pp. 27–61.*
- Pincus, H.J. 1956. Some vector and arithmetic operations on two-dimensional orientation variates, with applications to geological data. *Journal of Geology*, **64**(6): 533–557.
- Plewes, H.D., and McCormick, G. 1985. Town of Peace River investigation of slide at south end of 99 Street. Technical report, EG-06095, HARDY ASSOCIATES (1978) Ltd.
- Pomeroy, J.S. 1978. Isopleth map of landslide deposits, Washington County, Pennsylvania - A guide to comparative slope stability. United States Geological Survey, Miscellaneous Filed Studies Map, MF-1010.
- Popescu, M.E. 1994. A suggested method for reporting landslide causes. *Bulletin of the International Association of Engineering Geology*, **50**(1): 71–74.
- Popescu, M.E. 1996. From landslide causes to landslide remediation. *In Proceedings of the 7th International Symposium on Landslides. Edited by K. Senneset. Vol. 1, Trondheim, Norway, pp. 75–96.*
- Prandini, L., Guidiini, G., Bottura, J.A., Pançano, W.L., and Santos, A.R. 1977. Behavior of the vegetation in slope stability: A critical review. *Bulletin of Engineering Geology and the Environment*, **16**(1): 51–55.
- Proudfoot, D., and Bijeljanin, V. 2005. Peace Region (Peace River/High Level) geotechnical instrumentation summary, Spring 2005. Technical report, 15-85-14, Thurber Engineering Ltd.
- Proudfoot, D., and Cullum-Kenyon, S. 2006. Peace Region (Peace River - High Level area) geohazard assessment, Shop and Overpass Slides (PH-9), Peace River, 2006 annual inspection report. Technical report, 15-85-37, Thurber Engineering Ltd.

- Reger, J.P. 1979. Discriminant analysis as a possible tool in landslide investigations. *Earth Surface Processes*, **4**(3): 267–273.
- Reichenbach, P., Galli, M., Cardinali, M., Guzzetti, F., and Ardizzone, F. 2005. Geomorphological mapping to assess landslide risk: Concepts, methods and applications in the Umbria Region of Central Italy. *In* *Landslide Hazard and Risk*. Edited by T. Glade, M. Anderson, and M.J. Crozier. John Wiley & Sons Ltd, England, pp. 429–468.
- Remondo, J., Bonachea, J., and Cendrero, A. 2008. Quantitative landslide risk assessment and mapping on the basis of recent occurrences. *Geomorphology*, **94**(3-4): 496–507.
- Rib, H.T., and Liang, T. 1978. Recognition and identification. *In* *Landslides, analysis and control*, Transportation Research Board Special Report 176. Edited by R.L. Schuster and R.J. Krizek. National Academy of Sciences, Washington, D.C., pp. 34–80.
- Riley, S.J., DeGloria, S.D., and Elliot, R. 1999. A terrain ruggedness index that quantifies topographic heterogeneity. *Intermountain Journal of Sciences*, **5**(1-4): 23–27.
- Ritter, P. 1987. A vector-based slope and aspect generation algorithm. *Photogrammetric Engineering & Remote Sensing*, **53**(8): 1109–1111.
- Rodriguez, K.M., Weissel, J.K., and Kim, Y. 2002. Classification of landslide surfaces using fully polarimetric SAR: examples from Taiwan. *In* *Proceedings of the 2002 IEEE International Geoscience and Remote Sensing Symposium (IGARSS '02)*. Vol. 5, pp. 2918–2920.
- Rogers, W.P., Ladwig, L.R., Hornbaker, A.L., Schwochow, S.D., Hart, S.S., Shelton, D.C., Scroggs, D.L., and Soule, J.M. 1974. Guidelines and criteria for identification and land-use controls of geologic hazard and mineral resource areas. Special publication 6, Colorado Geological Survey.
- Rossi, P.H., Wright, J.D., and Weber-burdin, E. 1982. *Natural hazards and public choice, the state and local politics of hazard mitigation*. Academic Press, New York.
- Rott, H., Scheuchl, B., Siegel, A., and Grasemann, B. 1999. Monitoring very slow slope movements by means of SAR interferometry: A case study from a mass

- waste above a reservoir in the Ötztal Alps, Austria. *Geophysical Research Letters*, **26**(11): 1629–1632.
- Rowbotham, D.N., and Dudycha, D. 1998. GIS modelling of slope stability in Phewa Tal watershed, Nepal. *Geomorphology*, **26**(1-3): 151–170.
- Rowlands, K.A., Jones, L.D., and Whitworth, M. 2003. Landslide laser scanning: a new look at an old problem. *Quarterly Journal of Engineering Geology and Hydrogeology*, **36**(2): 155–157.
- Ruel, M.A. 1988. An investigation and analysis of a landslide at Mile 47.6 Peace River Railway subdivision. M.Eng. report, Department of Civil Engineering, University of Alberta, Edmonton, Alberta.
- Rutherford, R.L. 1930. Geology and water resources in parts of the Peace River and Grande Prairie districts, Alberta. Research Council of Alberta Report No. 21, Edmonton, Alberta.
- Rutherford, R.L. 1937. Saskatchewan gravels and sands in central Alberta. *Transactions of the Royal Society of Canada*, **31**(4): 81–95.
- Saaty, T.L. 1990. How to make a decision: The Analytic Hierarchy Process. *European Journal of Operational Research*, **48**(1): 9–26.
- Saito, M. 1965. Forecasting the time of occurrence of a slope failure. *In Proceedings of the 6th International Conference on Soil Mechanics and Foundation Engineering*. Vol. 2, pp. 537–539.
- Saito, M. 1969. Forecasting time of slope failure by Tertiary creep. *In Proceedings of the 7th International Conference on Soil Mechanics and Foundation Engineering*. Vol. 2, pp. 677–683.
- Saito, M. 1970. Estimation of the rupture life of soil based on the shape of the creep curve. *In Proceedings of the 5th International Congress on Rheology*. Vol. 2, University of Tokyo and Park Press, pp. 559–567.
- Saito, M. 1980. Semi-logarithmic representation for forecasting slope failure. *In Proceedings of the International Symposium on Landslides*. New Delhi. Vol. 1, pp. 321–324.

- Saito, M., and Uezawa, H. 1961. Failure of soil due to creep. *In Proceedings of the 5th International Conference on Soil Mechanics and Foundation Engineering*. Vol. 1, pp. 315–318.
- Salciarini, D., Godt, J.W., Savage, W.Z., Baum, R.L., and Conversini, P. 2008. Modeling landslide recurrence in Seattle, Washington, USA. *Engineering Geology*, **102**(3-4): 227–237.
- Salt, G. 1988. Landslide mobility and remedial measures. *In Proceedings of the 5th International Symposium on Landslides*. Edited by C. Bonnard. A.A. Balkema, pp. 757–762.
- Santacana, N., Baeza, B., Corominas, J., Paz, A., De, and Marturia, J. 2003. A GIS-based multivariate statistical analysis for shallow landslide susceptibility mapping in La Pobla de Lillet area (Eastern Pyrenees, Spain). *Natural Hazards*, **30**(3): 281–295.
- Sappington, J.M., Longshore, K.M., and Thompson, D.B. 2007. Quantifying landscape ruggedness for animal habitat analysis: A case study using bighorn sheep in the Mojave Desert. *Journal of Wildlife Management*, **71**(5): 1419–1426.
- Sassa, K., and Picarelli, L. 2010. Preface for the thematic issue “Early Warning of Landslides”. *Landslides*, **7**(3): 217–217. doi:10.1007/s10346-010-0233-9.
- Savigny, K.W., and Harris, M.C. 1988. Geological assessment of the Judah Hill landslide. Technical report, 15-16-34, Thurber Consultants Ltd., Edmonton, Alberta.
- Scheidegger, A.E. 1964. The tectonic stress and tectonic motion direction in Europe and western Asia as calculated from earthquake fault plane solutions. *Bulletin of the Seismological Society of America*, **54**(5A): 1519–1528.
- Scheidegger, A.E. 1965. On the statistics of the orientation of bedding planes, grain axes, and similar sedimentological data. *In Geological Survey Research 1965*, Chapter C. United States Geological Survey Professional Paper 525-C. pp. 164–167.
- Schmid, C.F., and MacCannell, E.H. 1955. Basic Problems, techniques, and theory of isopleth mapping. *Journal of the American Statistical Association*, **50**(269): 220–239.

- Schulz, W.H. 2007. Landslide susceptibility revealed by LIDAR imagery and historical records, Seattle, Washington. *Engineering Geology*, **89**(1-2): 67–87.
- Schuster, R.L. 1991. Landslide hazard management - experience in the United States. *In Proceedings of the International Conference on Slope Stability. Edited by Institution of Civil Engineers. Isle of Wight*, pp. 253–263.
- Schuster, R.L. 1996. Socioeconomic significance of landslides. *In Landslides: Investigation and Mitigation (Special Report 247). Edited by A.K. Turner and R.L. Schuster. Transportation Research Board, National Research Council, Washington, D.C.*, pp. 12–35.
- Schuster, R.L., and Fleming, R.W. 1986. Economic losses and fatalities due to landslides. *Bulletin of the Association of Engineering Geologists*, **23**(1): 11–28.
- Schuster, R.L., and Highland, L.M. 2007. Urban landslides: socioeconomic impacts and overview of mitigative strategies, the third Hans Cloos lecture. *Bulletin of Engineering Geology and the Environment*, **66**(1): 1–27.
- Schuster, R.L., and Kockelman, W.J. 1996. Principles of landslide hazard reduction. *In Landslides: Investigation and Mitigation (Special Report 247). Edited by A.K. Turner and R.L. Schuster. Transportation Research Board, National Research Council, Washington, D.C.*, pp. 91–105.
- Seeley, M.W., and West, D.O. 1990. Approach to geologic hazard zoning for regional planning, Inyo National Forest, California and Nevada. *Bulletin of the Association of Engineering Geologists*, **27**(1): 23–35.
- Sharma, L.M.D. 1970. Geotechnical properties of Peace River glacial lake sediments. M.Sc. thesis, Department of Civil Engineering, University of Alberta, Edmonton, Alberta.
- Shih, E.H.H., and Schowengerdt, R.A. 1983. Classification of arid geomorphic surfaces using Landsat spectral and textural features. *Photogrammetric Engineering & Remote Sensing*, **49**(3): 337–347.
- Singhroy, V. 2005. Remote sensing of landslides. *In Landslide Hazard and Risk. Edited by T. Glade, M. Anderson, and M.J. Crozier. John Wiley and Sons Ltd., West Sussex, England*, pp. 469–492.

- Singhroy, V., and Molch, K. 2004. Characterizing and monitoring rockslides from SAR techniques. *Advances in Space Research*, **33**(3): 290–295. doi:10.1016/S0273-1177(03)00470-8.
- Skempton, A.W., and Delory, F.A. 1957. Stability of natural slopes in London clay. *In Proceedings of the 4th International Conference on Soil Mechanics and Foundation Engineering*. Vol. 2, London, pp. 378–381.
- Slosson, J.E. 1969. The role of engineering geology in urban planning. *In The Governor's Conference on Environmental Geology*. Denver, Colorado. April 30, May 1-2. Colorado Geological Survey, Special Publication No. 1. pp. 8–15.
- Smith, M.J., and Clark, C.D. 2005. Methods for the visualization of digital elevation models for landform mapping. *Earth Surface Processes and Landforms*, **30**(7): 885–900.
- Smith, N., and Salt, G. 1988. Predicting landslide mobility an application to the East Abbotsford Slide, New Zealand. *In Proceedings of the 5th Australia-New Zealand Conference on Geomechanics*. pp. 567–572.
- Smith, R. 1958. Economic and legal aspects. *In Landslides and engineering practice*. Edited by E.B. Eckel. Highway Research Board Special Report 29, Washington, D.C., pp. 6–19.
- Soeters, R., and van Westen, C.J. 1996. Slope instability recognition, analysis and zonation. *In Landslides: Investigation and Mitigation (Special Report 247)*. Edited by A.K. Turner and R.L. Schuster. Transportation Research Board, National Research Council, Washington, D.C., pp. 129–177.
- Spangenberg, M.R. 1993. The Alberta landslide inventory. M.Eng. report, Department of Civil Engineering, University of Alberta, Edmonton, Alberta.
- Spiegelhalter, D.J., and Knill-Jones, R.P. 1984. Statistical and knowledge-based approaches to clinical decision-support systems, with an application in gastroenterology. *Journal of the Royal Statistical Society. Series A (General)*, **147**(1): 35–77.
- Statistics Canada. 2006. Population and dwelling counts, Statistics Canada 2006 Census. <http://www12.statcan.ca/census-recensement/2006/rt-td/pd-pl-eng.cfm>. Accessed Jan. 06, 2010.

- Stephens, M.A. 1974. Axial and bimodal data on a sphere. Technical report, No. 214, Department of Statistics, Stanford University, Stanford, California, <http://statistics.stanford.edu/~ckirby/techreports/ONR/SOL%20ONR%20214.pdf>. Accessed April. 13, 2011.
- Stevenson, P.C. 1977. An empirical method for the evaluation of relative landslide risk. *Bulletin of Engineering Geology and the Environment*, **16**(1): 69–72.
- Styles, K.A., Hansen, A., Dale, M.J., and Burnett, A.D. 1984. Terrain classification methods for development planning and geotechnical appraisal: A Hong Kong case. *In Proceedings of the 4th International Symposium of Landslides*. Vol. 2, Toronto, pp. 561–568.
- Süzen, M.L., and Doyuran, V. 2004a. A comparison of the GIS based landslide susceptibility assessment methods: multivariate versus bivariate. *Environmental Geology*, **45**(5): 665–679.
- Süzen, M.L., and Doyuran, V. 2004b. Data driven bivariate landslide susceptibility assessment using geographical information systems: a method and application to Asarsuyu catchment, Turkey. *Engineering Geology*, **71**(3-4): 303–321.
- Tahir, M.A., Bouridane, A., and Kurugollu, F. 2005. An FPGA based coprocessor for GLCM and Haralick texture features and their application in prostate cancer classification. *Analog Integrated Circuits and Signal Processing*, **43**(2): 205–215.
- Tarboton, D.G., Bras, R.L., and Rodriguez-Iturbe, I. 1991. On the extraction of channel networks from digital elevation data. *Hydrological Processes*, **5**(1): 81–100.
- Taylor, R.S. 1958. Some Pleistocene lakes of northern Alberta and adjacent areas. *Edmonton Geological Society Quarterly*, **2**(4): 1–9.
- Taylor, R.S. 1960. Some Pleistocene lakes of northern Alberta and adjacent areas (Revised). *Journal of the Alberta Society of Petroleum Geologists*, **8**(6): 167–178.
- Teza, G., Pesci, A., Genevois, R., and Galaro, A. 2008. Characterization of landslide ground surface kinematics from terrestrial laser scanning and strain field computation. *Geomorphology*, **97**(3-4): 424–437.

- Thiery, Y., Malet, J.P., Sterlacchini, S., Puissant, A., and Maquaire, O. 2007. Landslide susceptibility assessment by bivariate methods at large scales: Application to a complex mountainous environment. *Geomorphology*, **92**(1-2): 38–59.
- Thomson, S. 1980. Report on slope stability, River Heights Subdivision, Phase III, Town of Peace River, Alberta. Technical report, Peace River Regional Planning Commission.
- Thomson, S., and Hayley, D.W. 1975. The Little Smoky Landslides. *Canadian Geotechnical Journal*, **12**(3): 379–392.
- Tokarsky, O. 1967. Geology and groundwater resources of the Grimshaw-Cardinal lake area, Alberta. M.Sc. thesis, Department of Geology, University of Alberta, Edmonton, Alberta.
- Tokarsky, O. 1971. Hydrogeology of the Grimshaw-Chinook Valley area, Alberta. Research Council of Alberta, Report 71-2, Edmonton, Alberta.
- Trenhaile, A.S. 2004. *Geomorphology: A Canadian perspective*. Oxford University Press.
- Tsurumi, E. 2004. Estimation of the probability of slope disasters along national highways. *Bulletin of the Geographical Survey Institute*, **19**(1): 81–88.
- UNDP. 2004. *Reducing disaster risk: A challenge for development*. United Nations Development Programme, Bureau for Crisis Prevention and Recovery, One United Nations Plaza, New York, NY 10017, USA.
- UNESCO WP/WLI. 1993. A suggested method for describing the activity of a landslide. *Bulletin of the International Association of Engineering Geology*, **47**(1): 53–57.
- UNISDR. 2009. *2009 UNISDR terminology on disaster risk reduction*. United Nations International Strategy for Disaster Reduction Secretariat, Geneva, Switzerland.
- United States Code. 2006a. Identification of flood-prone areas. 42 U.S.C. 4101. 2006 ed., <http://www.gpoaccess.gov/uscode/index.html>. Accessed Mar. 4, 2011.
- United States Code. 2006b. Notice requirements. 42 U.S.C. 4104a. 2006 ed., <http://www.gpoaccess.gov/uscode/index.html>. Accessed Mar. 4, 2011.

- van Asch, T.W.J., Hendriks, M.R., Hessel, R., and Rappange, F.E. 1996. Hydrological triggering conditions of landslides in varved clays in the French Alps. *Engineering Geology*, **42**(4): 239–251.
- van Den Eeckhaut, M., Poesen, J., Verstraeten, G., Vanacker, V., Nyssen, J., Moeyersons, J., van Beek, L.P.H., and Vandekerckhove, L. 2007. Use of LIDAR-derived images for mapping old landslides under forest. *Earth Surface Processes and Landforms*, **32**(5): 754–769.
- van Westen, C.J. 1997. Statistical landslide hazard analysis. *In* Application guide, ILWIS 2.1 for Windows, ITC. Vol. 2, ITC Publication, Enschede, The Netherlands, pp. 73–84.
- van Westen, C.J., Castellanos, E., and Kuriakose, S.L. 2008. Spatial data for landslide susceptibility, hazard, and vulnerability assessment: An overview. *Engineering Geology*, **102**(3-4): 112–131.
- van Westen, C.J., Rengers, N., and Soeters, R. 2003. Use of geomorphological information in indirect landslide susceptibility assessment. *Natural Hazards*, **30**(3): 399–419.
- van Westen, C.J., van Asch, T.W.J., and Soeters, R. 2006. Landslide hazard and risk zonation - why is it still so difficult? *Bulletin of Engineering Geology and the Environment*, **65**(2): 167–184. doi:10.1007/s10064-005-0023-0.
- Varnes, D.J. 1978. Slope movement types and processes. *In* Landslides: Analysis and control (Special Report 176). *Edited by* R.L. Schuster and R.J. Krizek. Transportation Research Board, National Research Council, Washington, D.C., pp. 11–33.
- Varnes, D.J. 1982. Time-deformation relations in creep to failure of earth materials. *In* Proceedings of the 7th Southeast Asian Geotechnical Conference. *Edited by* I. McFeat-Smith and P. Lumb. Vol. 2, Hong Kong, pp. 107–130.
- Varnes, D.J., and IAEG Commission on Landslides and other Mass Movement on Slopes. 1984. Landslide hazard zonation: a review of principles and practice. UNESCO, Paris.
- Vaunat, J., Leroueil, S., and Faure, R.M. 1994. Slope movements: a geotechnical perspective. *In* Proceedings of the 7th International Congress of the International

- Association of Engineering Geology. *Edited by* R. Oliveira, L.F. Rodrigues, A.G. Coelho, and A.P. Cunha. Vol. 3, Lisboa, Portugal, pp. 1637–1646.
- Vecchia, O. 1978. A simple terrain index for the stability of hillsides or scarps. *In* Large Ground Movements and Structures. *Edited by* J.D. Geddes. Halsted Press, John Wiley & Sons, Inc., pp. 449–461.
- Verstappen, H.T. 1995. Aerospace technology and natural disaster reduction. *Advances in Space Research*, **15**(11): 3–15.
- Voight, B. 1988a. Materials science law applies to time forecasts of slope failure. *In* Proceedings of the 5th International Symposium on Landslides. *Edited by* C. Bonnard. Vol. 3, A.A. Balkema, pp. 1471–1472.
- Voight, B. 1988b. A method for prediction of volcanic eruptions. *Nature*, **332** (6160): 125–130.
- Voight, B. 1989. A relation to describe rate-dependent material failure. *Science*, **243**(4888): 200–203.
- Voight, B., and Cornelius, R.R. 1991. Prospects for eruption prediction in near real-time. *Nature*, **350**(6320): 695–698.
- Walker, B.F., Dale, M., Fell, R., Jeffery, R., Leventhal, A., McMahon, M., Mostyn, G., and Phillips, A. 1985. Geotechnical risk associated with hillside development. *Australian Geomechanics News*, **10**: 29–35.
- Ward, T.J., Li, R., and Simons, D.B. 1982. Mapping landslide hazards in forest watersheds. *Journal of the Geotechnical Engineering Division: Proceedings of the American Society of Civil Engineers*, **108**(2): 319–324.
- Watson, G.S. 1956. Analysis of dispersion of a sphere. *Monthly Notices of the Royal Astronomical Society*, **7**(4): 153–159.
- Watson, G.S. 1960. More significance tests on the sphere. *Biometrika*, **47**(1-2): 87–91.
- Watson, G.S. 1965. Equatorial distributions on a sphere. *Biometrika*, **52**(1-2): 193–201.
- Watson, G.S. 1966. The statistics of orientation data. *Journal of Geology*, **74**(5): 786–797.

- Watson, G.S., and Irving, E. 1957. Statistical methods in rock magnetism. *Monthly Notices of the Royal Astronomical Society*, **7**(6): 289–300.
- Whitworth, M., Giles, D., and Murphy, W. 2001. Identification of landslides in clay terrains using Airborne Thematic Mapper (ATM) multispectral imagery. *In Proceedings of the 8th International Symposium on Remote Sensing: Remote Sensing for Environmental Monitoring, GIS Applications and Geology*. Vol. 4545, Society of Photo-Optical Instrumentation Engineers (SPIE), Toulouse, France, p. 9.
- Whitworth, M.C.Z., Giles, D.P., and Murphy, W. 2005. Airborne remote sensing for landslide hazard assessment: a case study on the Jurassic escarpment slopes of Worcestershire, UK. *Quarterly Journal of Engineering Geology and Hydrogeology*, **38**(3): 285–300.
- Whitworth, M.Z., Giles, D., and Anderson, I. 2006. Landslide imaging techniques for urban geoscience reconnaissance. *In Proceedings of the 10th IAEG International Congress, IAEG2006*. The Geological Society of London, Nottingham, United Kingdom, p. 12 (Paper No. 245), <http://iaeg2006.geolsoc.org.uk/cd/>. Accessed Mar. 25, 2011.
- Wickenden, R.T.D. 1951. Some Lower Cretaceous sections on Peace River below the mouth of Smoky River, Alberta. Geological Survey of Canada Paper 51-16, Geological Survey of Canada.
- Wickenden, R.T.D., and Shaw, G. 1943. Stratigraphy and structure in Mount Hulcross-Commotion Creek map-area, British Columbia. Geological Survey Paper 43-13, Geological Survey of Canada.
- Woodcock, N.H. 1976. Structural style in slump sheets: Ludlow Series, Powys, Wales. *Journal of the Geological Society*, **132**(4): 399–415.
- Woodcock, N.H. 1977. Specification of fabric shapes using an eigenvalue method. *Geological Society of America Bulletin*, **88**(9): 1231–1236.
- Woodcock, N.H., and Naylor, M.A. 1983. Randomness testing in three-dimensional orientation data. *Journal of Structural Geology*, **5**(5): 539–548.
- Wright, R.H., Campbell, R.H., and Nilsen, T.H. 1974. Preparation and use of isopleth maps of landslide deposits. *Geology*, **2**(10): 483–485.

- Wright, R.H., and Nilsen, T.H. 1974. Isopleth map of landslide deposits, southern San Francisco Bay region, California. United States Geological Survey, Miscellaneous Filed Studies Map, MF-550.
- Wu, T.H., Tang, W.H., and Einstein, H.H. 1996. Landslide hazard and risk assessment. *In* Landslides: Investigation and Mitigation (Special Report 247). *Edited by* A.K. Turner and R.L. Schuster. Transportation Research Board, National Research Council, Washington, D.C., pp. 106–118.
- Wu, W., and Sidle, R.C. 1995. A distributed slope stability model for steep forested basins. *Water Resources Research*, **31**(8): 2097–2110.
- Yalcin, A. 2008. GIS-based landslide susceptibility mapping using analytical hierarchy process and bivariate statistics in Ardesen (Turkey): Comparisons of results and confirmations. *Catena*, **72**(1): 1–12. doi:10.1016/j.catena.2007.01.003.
- Yalcin, A., and Bulut, F. 2007. Landslide susceptibility mapping using GIS and digital photogrammetric techniques: a case study from Ardesen (NE-Turkey). *Natural Hazards*, **41**(1): 201–226.
- Yamaguchi, Y., Tanaka, S., Odajima, T., Kamai, T., and Tsuchida, S. 2003. Detection of a landslide movement as geometric misregistration in image matching of SPOT HRV data of two different dates. *International Journal of Remote Sensing*, **24**(18): 3523–3534.
- Yin, K.L., and Yan, T.Z. 1988. Statistical prediction models for slope instability of metamorphosed rocks. *In* Proceedings of the 5th International Symposium on Landslides. *Edited by* C. Bonnard. Vol. 2, Lausanne, Switzerland, pp. 1269–1272.
- Yoshimatsu, H., and Abe, S. 2006. A review of landslide hazards in Japan and assessment of their susceptibility using an analytical hierarchic process (AHP) method. *Landslides*, **3**(2): 149–158.
- Zaitchik, B.F., and van Es, H.M. 2003. Applying a GIS slope-stability model to site-specific landslide prevention in Honduras. *Journal of Soil and Water Conservation*, **58**(1): 45–53.
- Zavodni, Z.M., and Broadbent, C.D. 1980. Slope failure kinematics. *Canadian Mining and Metallurgical Bulletin*, **73**(816): 69–74.

- Zevenbergen, L.W., and Thorne, C.R. 1987. Quantitative-analysis of land surface-topography. *Earth Surface Processes and Landforms*, **12**(1): 47–56.
- Zêzere, J.L., Garcia, R.A.C., Oliveira, S.C., and Reis, E. 2008. Probabilistic landslide risk analysis considering direct costs in the area north of Lisbon (Portugal). *Geomorphology*, **94**(3-4): 467–495.
- Zhou, G., Esaki, T., Mitani, Y., Xie, M., and Mori, J. 2003. Spatial probabilistic modeling of slope failure using an integrated GIS Monte Carlo simulation approach. *Engineering Geology*, **68**(3-4): 373–386.
- Zhou, Q., and Liu, X. 2004. Analysis of errors of derived slope and aspect related to DEM data properties. *Computers & Geosciences*, **30**: 369–378.
- Zimmerman, M., Bichsel, M., and Kienholz, H. 1986. Mountain hazards mapping in the Khumbu Himal, Nepal, with prototype map, Scale 1:50,000. *Mountain Research and Development*, **6**(1): 29–40.

Appendix A

Detailed borehole data

Table A.1 Summary of boreholes

Landslide	Landslide type	BHs	Depth / Elevation [†]	Monitoring period [‡]	Ave. / Max. movement rate ^{††}	Max. displacement ^{†††}	M.C. [§]	Point soil type	USCS [¶]
Mile 47.8 Slide	Internal deformation	95-2	2 / 356.62	175	7.75 / 46.95	4	18	Clay (till like)	CI
		95-3	2 / 366.39	175	-4.6 / -22.64	2	-	Silt & sand	SM / SC
	Rotational slide	95-5	4.22 / 340.05	175	99.99 / 756.71	46.9	25	Clay (till like)	CI
		95-7	4.88 / 327.29	175	125.23 / 957.85	41	-	Clay (till like)	CI
Mile 47.6 Slide	Translational block slide	86-20	12.5 / 342.54	69	193.6 / 193.6	17.7	-	Clay	CH
		86-21	11.9 / 338.07	56	58.63 / 446.34	21.4	-	Clay (till like)	CL
	AT-7		2.7 / 342.92	66	41.26 / 41.26	4.8	-	Sand & gravel	CI
			8.2 / 337.42	66	103.82 / 103.82	6.2	25	Clay (till like)	CI
99/101 St. Slides	Translational block slide	86-22	12.5 / 333.12	66	161.7 / 161.7	20.1	22.5	Clay (till like)	CI
			7 / 338.11	56	37.34 / 78.6	3.7	-	Sand & gravel	-
	92-1 (A)		9.4 / 335.71	56	45.12 / 95.46	3.1	-	Sand & gravel	-
			16.7 / 328.41	56	47.43 / 189.93	7	-	Clay (till like)	CI
92-2 (B)	Translational block slide	93-13	23.8 / 338.36	40	320.47 / 343.58	28.7	21	Clay (till like)	CI
			26.3 / 335.86	40	119.27 / 128.95	9.6	-	Clay shale	CH
			22.8 / 338.87	3,253	7.84 / 21.15	50.8	25	Clay shale	CH
			28.8 / 332.86	3,253	0.69 / 7.36	5.2	-	Clay shale	CH
			14.8 / 331.9	2,564	5.47 / 19.13	32.9	-	Clay shale	-

[†] Metre. [‡] Day. ^{††} mm/year. ^{†††} Millimetre. [§] Moisture content (%). [¶] Unified Soil Classification System.

Table A.1 (Cont'd)

Landslide	Landslide type	BHs	Depth / Elevation [†]	Monitoring period [‡]	Ave. / Max. movement rate ^{††}	Max. displacement ^{†††}	M.C. [§]	Point soil type	USCS [¶]
99/101 St. Slides (Cont'd)	Surficial slide	85-1	3.6 / 349.36	2	17,902 / 19,95	54	12	Clay (fill like)	CI
	Translational block slide	85-2	3.6 / 349.66	2,555	2.84 / 34.90	13.3	26	Clay	CI
			7.3 / 345.96	2,555	0.36 / 10.27	9.7	21	Clay (fill like)	CH
			10.9 / 342.36	2,555	1.09 / 5.17	19.9	-	Clay (fill like)	CH
			14.0 / 339.26	2,555	1.17 / 5.76	10.2	-	Sand & gravel	-
			21.3 / 331.96	2,555	5.18 / 14.94	17.2	-	Clay shale	-
	Translational block slide	93-10	2.3 / 338.7	296	129.65 / 295.14	68.8	-	Clay (fill like)	-
			10.3 / 330.7	296	5.47 / 54	3.7	-	Sandstone	-
			9.3 / 345.3	3,376	13.13 / 77.17	79	-	Clay (till like)	-
	Translational block slide	93-11	13.3 / 341.3	3,376	1.76 / 33.73	14.9	-	Clay (till like)	-
			1.8 / 349.7	2,294	10.03 / 134.98	30.4	-	Clay (till like)	-
			0.8 / 350.7	2,294	26.1 / 341.82	25.6	-	Clay (till like)	-
Translational block slide	93-12	13.8 / 337.7	2,294	1.02 / 29.17	15.1	-	Sandstone	-	
		0.3 / 387.29	711	4.99 / 17.32	5.6	-	Clay (fill like)	CI	
		2.74 / 384.85	711	0.58 / 5.37	1.1	19	Clay (till like)	CH	
Shop Slide	Translational block slide	TH05-1	18.54 / 369.1	711	0.67 / 4.28	0.8	25	Clay shale	CH

[†] Metre. [‡] Day. ^{††} mm/year. ^{†††} Millimetre. [§] Moisture content (%). [¶] Unified Soil Classification System.

Table A.1 (Cont'd)

Landslide	Landslide type	BHs	Depth / Elevation [†]	Monitoring period [‡]	Ave. / Max. movement rate ^{††}	Max. displacement ^{†††}	M.C. [§]	Point soil type	USCS [¶]	
Shop Slide (Cont'd)	Translational block slide	TH05-3	1.5 / 383.1	711	0.42 / 5.77	2.2	23	Clay (fill like)	CH	
			8.8 / 375.8	711	2.13 / 3.62	2.3	22	Clay	CH	
			13.1 / 371.5	711	3.13 / 7.9	6.4	20	Clay	CH	
				17.3 / 367.3	711	6.19 / 9.86	11.9	24	Clay	CH
				0.3 / 367.4	711	0.35 / 7.29	3.1	20	Clay (fill like)	CI
				2.7 / 365	711	1.73 / 4.23	1.8	23	Clay	CH
				6.4 / 361.3	711	9.08 / 16.59	11.8	24	Clay	CH
				13.1 / 354.6	711	0.47 / 4.79	1.7	17	Clay (till like)	CI
				15.5 / 352.2	711	0.82 / 6.02	0.8	19	Clay (till like)	CI
Mile 50.9 Slide	Earth flow	80-1	20.4 / 347.3	711	0.45 / 3.09	0.8	15	Clay (till like)	CI	
		80-2	0.3 / 371.7	-	- / -	-	-	Clay	CI	
	Mile 46.5 Slide	Translational block slide	80.8	3.95 / 362.05	-	- / -	-	20	Clay	CI
			80-9	7.6 / 375.2	193	- / -	-	20	Clay (till like)	CI
			12.38 / 370.4	193	- / -	50-60	19	Clay (till like)	CI	
			7.37 / 369.79	193	- / -	50-60	17	Clay (till like)	CI	

[†] Metre. [‡] Day. ^{††} mm/year. ^{†††} Millimetre. [§] Moisture content (%). [¶] Unified Soil Classification System.

Appendix B

Representative borehole stratigraphy¹

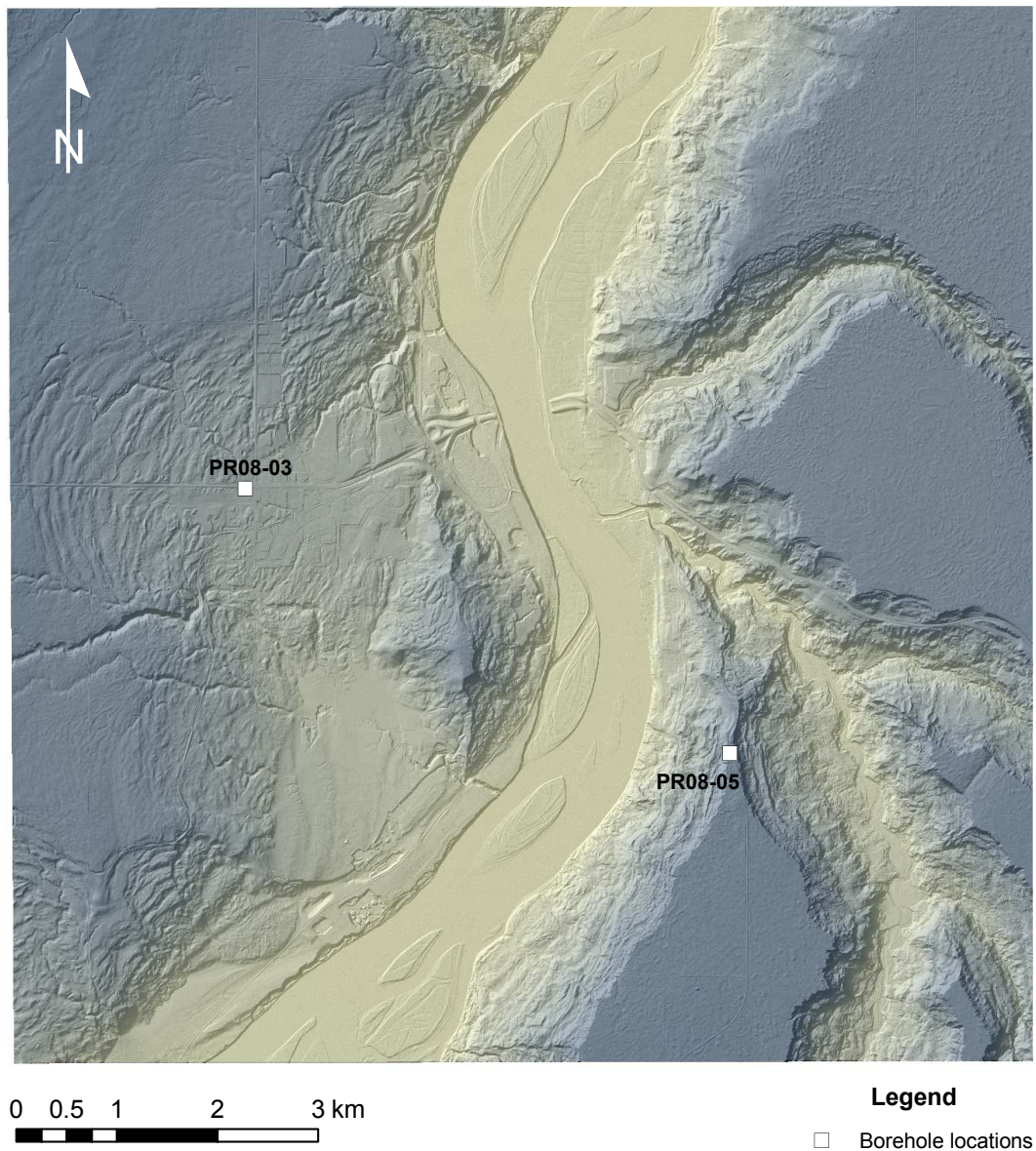


Figure B.1 Location of boreholes

¹Boreholes for soil samplings, which are described in here, were implemented by the Alberta Geological Survey (Morgan et al. 2009).

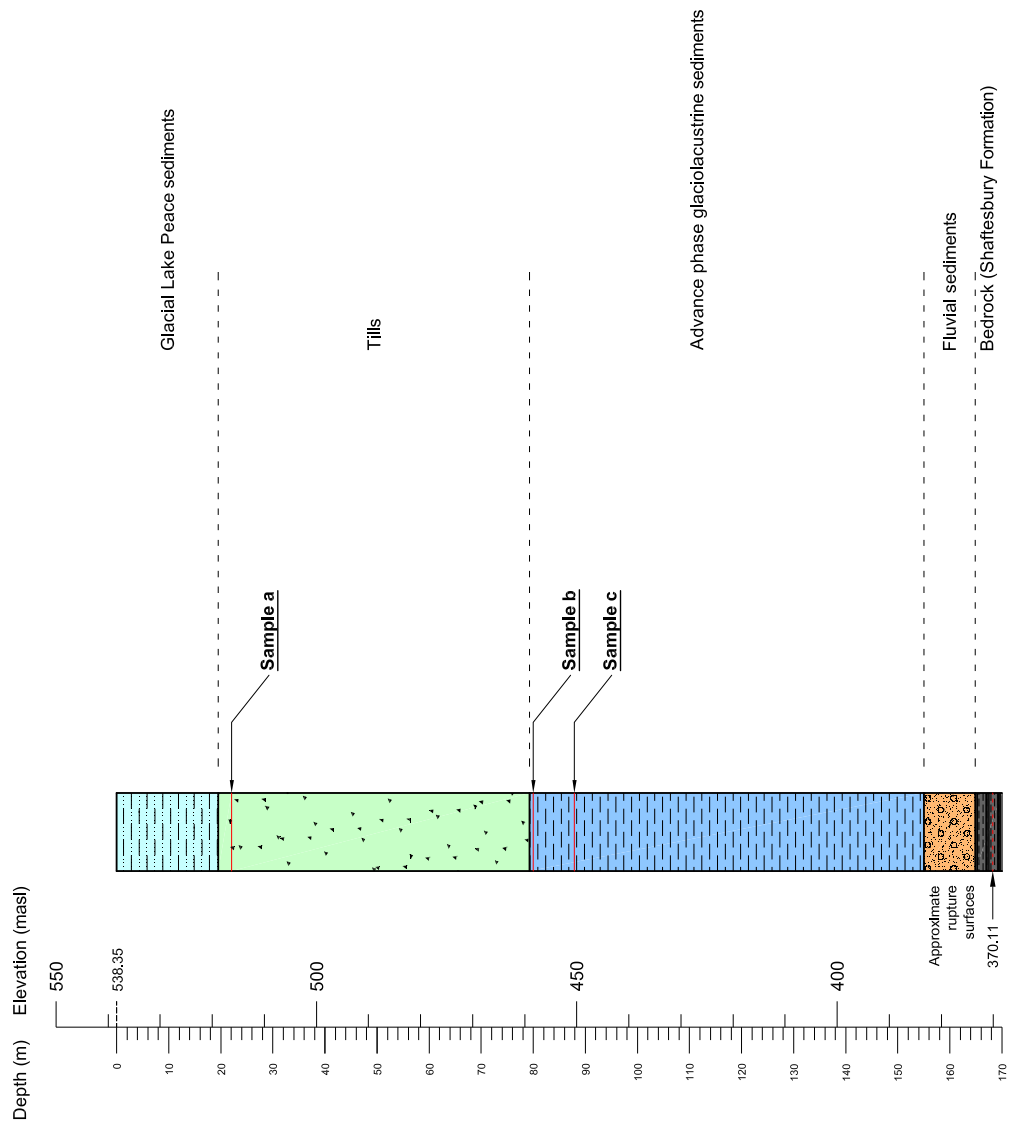


Figure B.2 Representative stratigraphy observed in PR08-05 which is located in the east bank of the Peace River

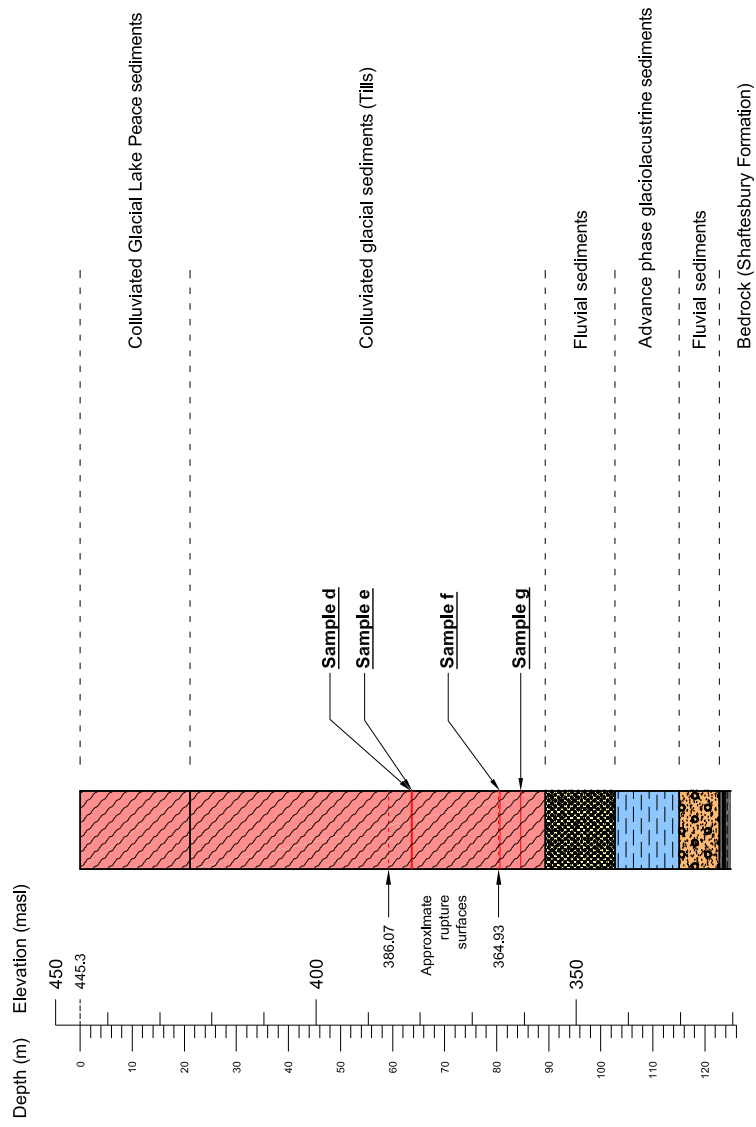


Figure B.3 Representative stratigraphy observed in PR08-03 which is located in the west bank of the Peace River

Appendix C

Laboratory tests summary

(1) Overview of samples used in laboratory tests

Table C.1 Summary of sampling information and brief explanations on samples




Sample	Elevation (m)	Depth (m)	Estimated soil unit [†]	Borehole No. [‡]
a	517.01-515.49	21.34-22.86	Diamicton (Till)	East (PR08-05)
b	459.10-457.58	79.25-80.77	Silt and Clay	
c	450.44	87.91	Silt and Clay	
d	381.75	63.65	Diamicton (Till) ^{††}	West (PR08-03)
e	381.50	63.80	Diamicton (Till) ^{††}	
f	364.71	80.59	Diamicton (Till) ^{††}	
g	360.67	84.63	Silt (Till) ^{††}	

[†] Source: Data from Morgan et al. (2009).

[‡] Representative stratigraphy and corresponding borehole locations are shown in Appendix B.





^{††} Colluviated tills.

Table C.2 General description on soil samples

Sample	Estimated soil unit [†]	Description [†]	Sample appearance
a	Diamicton (Till)	Clayey, very fine to fine grained sandy, silt diamicton (till), very dark gray, clast content ~ 10 %, fracture and shear planes in till	
b	Silt and Clay	Clayey silt to silty clay, interbedded, discontinuous sand lenses/stringers, pseudo-nodules of diamicton noted at 80.6 m. 45 °, slickensided shear plane at base of core through silty clay/clay silt	
c	Silt and Clay	Clayey silt to silty clay, dark gray, laminated, very fine to fine grained sand stringers, slickensided fracture surfaces in clayey silt	

[†] Source: Data from Morgan et al. (2009).

Table C.2 (Cont'd)

Sample	Estimated soil unit [†]	Description [†]	Sample appearance
d	Diamicton (Till)	Silt till with very fine to fine grained sand, minor clay, dark gray, very dense, stone content ~ 5 %	
e	Diamicton (Till)	Silt till with very fine to fine grained sand, minor clay, dark gray, very dense, stone content ~ 5 %, 50 mm thick sandy shear plane	
f	Diamicton (Till)	Silty diamicton interbedded with silty sand, discontinuous stringers/lenses	
g	Silt	Very fine to fine grained sandy silt, dark to olive gray, 45 ° slickensided fracture in strata at 84.7 m	

[†] Source: Data from Morgan et al. (2009).

(2) Results of index tests

Table C.3 Atterberg Limits test results

Location	East (PR08-05)			West (PR08-03)			
	a	b	c	d	e	f	g
Sample							
Moisture content (%)	12.4	26.5	25.5	12.9	5.5	23	17.4
Liquid limit (%)	39	93	59	46	35	69	48
Plastic limit (%)	17	30	21	19	19	26	21
Plasticity Index	22	63	38	27	15	43	27
Soil classification [†]	CL	CH	CH	CL	CL	CH	CL
Clay fraction (%)	33.9	79.7	53	47.3	30.1	72.8	45.8
Activity	0.6	0.8	0.7	0.6	0.5	0.6	0.6

[†] Unified Soil Classification System (USCS) shown in Figure C.1.

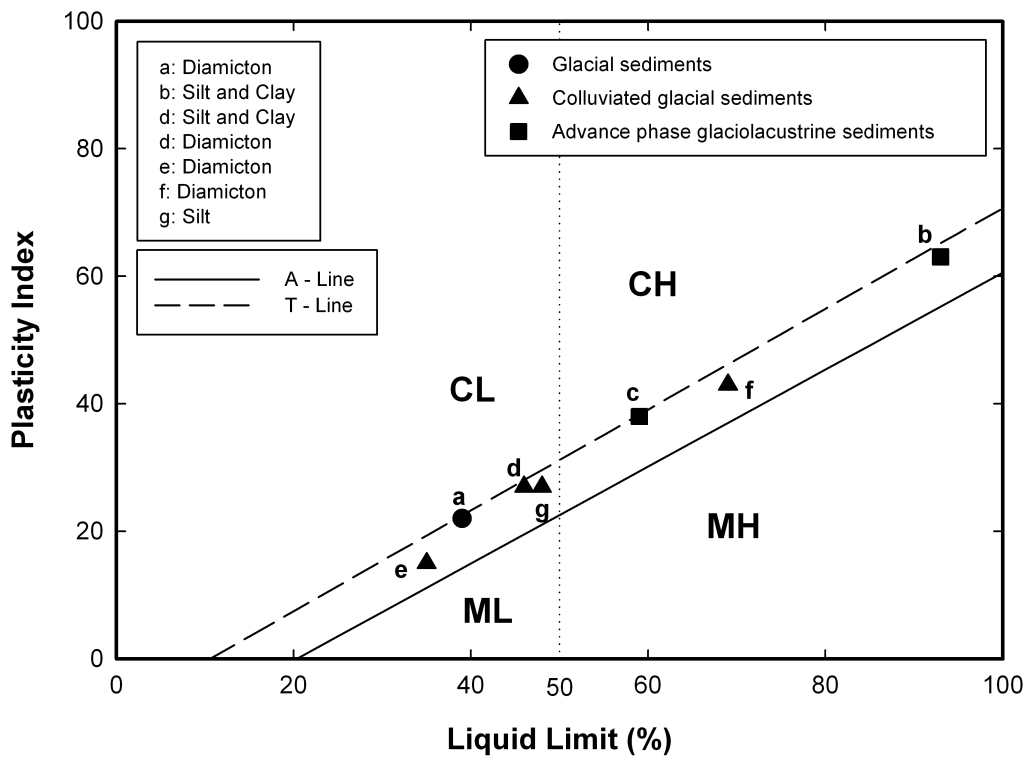


Figure C.1 Plasticity chart for soil samples. Detailed explanations for the figure are illustrated in Figure 4.39

(3) Results of hydrometer tests

Table C.4 Overview of control factors used in the hydrometer analysis

Location	East (PR08-05)			West (PR08-03)			
Sample	a	b	c	d	e	f	g
Hydrometer type	152H						
Zero correction	4.0 (22.5 °C)			3.5 (23 °C)			
Meniscus	1.0						
Dispersing agent	4 % Sodium hexametaphosphate (Na ₆ P ₆ O ₁₈), 125ml						
Control sieve no.	200						
G _s for soil	2.72		2.71	2.68	2.67	2.71	2.68
α factor [†]	0.99				1.0	0.99	
Soil mass (g)	50 (dry)						
% finer	80.3	99.2	97.3	93.6	97.1	99.5	99.6

[†] Correction factor for the unit weight of solids.

Table C.5 Results of Hydrometer tests - Sample a

Date	Time	t ^a	T ^b	C _T ^c	R _a ^d	R _c ^e	Actual % finer	R ^f	L ^g	L/t	K ^h	D ⁱ	Adjusted % finer
Mar. 25, 2009	15:29	2	23.5	0.85	51.0	47.9	94.74	52.0	7.8	3.9000	0.0128	0.0253	76.08
	15:32	5	23.5	0.85	46.0	42.9	84.84	47.0	8.6	1.7200	0.0128	0.0168	68.13
	15:42	15	23.5	0.85	41.0	37.9	74.94	42.0	9.4	0.6267	0.0128	0.0101	60.18
	15:57	30	23.5	0.85	38.0	34.9	69.00	39.0	9.9	0.3300	0.0128	0.0074	55.41
	16:27	60	23.5	0.85	34.0	30.9	61.08	35.0	10.5	0.1750	0.0128	0.0054	49.05
Mar. 26, 2009	19:31	251	23.3	0.79	28.0	24.8	49.08	29.0	11.5	0.0458	0.0129	0.0028	39.41
	15:27	1,440	23.0	0.70	21.0	17.7	35.05	22.0	12.7	0.0088	0.0129	0.0012	28.14

^a Elapsed time, minute.

^b Temperature, degree Celsius.

^c Temperature correction factor.

^d Actual hydrometer reading.

^e Corrected hydrometer reading.

^f Corrected hydrometer reading only for meniscus.

^g Effective depth based on the hydrometer 152H.

^h Constant representing a relationship between the temperature and the specific gravity.

ⁱ Diameter, millimetre.

Table C.5 (Cont'd) - Sample b

Date	Time	t ^a	T ^b	C _T ^c	R _a ^d	R _c ^e	Actual % finer	R ^f	L ^g	L/t	K ^h	D ⁱ	Adjusted % finer
Mar. 25, 2009	16:08	2	23.0	0.70	54.5	51.2	100.00	55.5	7.2	3.6000	0.0129	0.0245	99.20
	16:11	5	23.0	0.70	54.0	50.7	99.02	55.0	7.3	1.4600	0.0129	0.0156	98.23
	16:21	15	23.0	0.70	53.0	49.7	97.07	54.0	7.4	0.4933	0.0129	0.0091	96.29
	16:36	30	23.0	0.70	52.0	48.7	95.12	53.0	7.6	0.2533	0.0129	0.0065	94.36
	17:06	60	23.0	0.70	51.0	47.7	93.16	52.0	7.8	0.1300	0.0129	0.0047	92.42
Mar. 26, 2009	20:16	250	23.0	0.70	47.0	43.7	85.35	48.0	8.4	0.0336	0.0129	0.0024	84.67
	16:06	1,440	22.8	0.64	38.0	34.6	67.66	39.0	9.9	0.0069	0.0129	0.0011	67.12

^a Elapsed time, minute.

^b Temperature, degree Celsius.

^c Temperature correction factor.

^d Actual hydrometer reading.

^e Corrected hydrometer reading.

^f Corrected hydrometer reading only for meniscus.

^g Effective depth based on the hydrometer 152H.

^h Constant representing a relationship between the temperature and the specific gravity.

ⁱ Diametre, millimetre.

Table C.5 (Cont'd) - Sample c

Date	Time	t ^a	T ^b	C _T ^c	R _a ^d	R _c ^e	Actual % finer	R ^f	L ^g	L/t	K ^h	D ⁱ	Adjusted % finer
Mar. 25, 2009	16:40	2	23.5	0.85	48.0	44.9	88.80	49.0	8.3	4.1500	0.0129	0.0263	86.41
	16:43	5	23.5	0.85	45.0	41.9	82.86	46.0	8.8	1.7600	0.0129	0.0171	80.63
	16:53	15	23.5	0.85	41.0	37.9	74.94	42.0	9.4	0.6267	0.0129	0.0102	72.92
	17:08	30	23.5	0.85	39.0	35.9	70.98	40.0	9.7	0.3233	0.0129	0.0073	69.07
	17:38	60	23.5	0.85	36.5	33.4	66.03	37.5	10.2	0.1700	0.0129	0.0053	64.25
Mar. 26, 2009	20:48	250	23.0	0.70	33.0	29.7	58.81	34.0	10.7	0.0428	0.0129	0.0027	57.22
	16:38	1,440	23.0	0.70	28.0	24.7	48.91	29.0	11.5	0.0080	0.0129	0.0012	47.59

^a Elapsed time, minute.

^b Temperature, degree Celsius.

^c Temperature correction factor.

^d Actual hydrometer reading.

^e Corrected hydrometer reading.

^f Corrected hydrometer reading only for meniscus.

^g Effective depth based on the hydrometer 152H.

^h Constant representing a relationship between the temperature and the specific gravity.

ⁱ Diameter, millimetre.

Table C.5 (Cont'd) - Sample d

Date	Time	t ^a	T ^b	C _T ^c	R _a ^d	R _c ^e	Actual % finer	R ^f	L ^g	L/t	K ^h	D ⁱ	Adjusted % finer
Mar. 26, 2009	08:54	2	23.0	0.70	51.0	48.2	95.44	52.0	7.8	3.9000	0.0131	0.0259	89.33
	08:57	5	23.0	0.70	48.0	45.2	89.50	49.0	8.3	1.6600	0.0131	0.0169	83.77
	09:07	15	23.0	0.70	43.0	40.2	79.60	44.0	9.1	0.6067	0.0131	0.0102	74.50
	09:22	30	23.0	0.70	40.0	37.2	73.66	41.0	9.6	0.3200	0.0131	0.0074	68.94
	09:52	60	23.0	0.70	37.0	34.2	67.72	38.0	10.1	0.1683	0.0131	0.0054	63.38
Mar. 27, 2009	13:02	250	23.0	0.70	31.0	28.2	55.84	32.0	11.1	0.0444	0.0131	0.0028	52.26
	08:52	1,440	23.0	0.70	25.5	22.7	44.95	26.5	12.0	0.0083	0.0131	0.0012	42.07

^a Elapsed time, minute.

^b Temperature, degree Celsius.

^c Temperature correction factor.

^d Actual hydrometer reading.

^e Corrected hydrometer reading.

^f Corrected hydrometer reading only for meniscus.

^g Effective depth based on the hydrometer 152H.

^h Constant representing a relationship between the temperature and the specific gravity.

ⁱ Diameter, millimetre.

Table C.5 (Cont'd) - Sample e

Date	Time	t ^a	T ^b	C _T ^c	R _a ^d	R _c ^e	Actual % finer	R ^f	L ^g	L/t	K ^h	D ⁱ	Adjusted % finer
Mar. 26, 2009	09:30	2	23.0	0.70	52.0	49.2	98.40	53.0	7.6	3.8000	0.0131	0.0255	95.55
	09:33	5	23.0	0.70	46.0	43.2	86.40	47.0	8.6	1.7200	0.0131	0.0172	83.89
	09:43	15	23.0	0.70	36.0	33.2	66.40	37.0	10.2	0.6800	0.0131	0.0108	64.47
	09:58	30	23.0	0.70	30.0	27.2	54.40	31.0	11.2	0.3733	0.0131	0.0080	52.82
	10:28	60	23.0	0.70	25.5	22.2	45.40	26.5	12.0	0.1992	0.0131	0.0058	44.08
	13:38	250	23.0	0.79	20.0	17.2	34.40	21.0	12.9	0.0516	0.0131	0.0030	33.40
Mar. 27, 2009	09:28	1,440	23.0	0.70	17.0	14.2	28.40	18.0	13.3	0.0092	0.0131	0.0013	27.58

^a Elapsed time, minute.

^b Temperature, degree Celsius.

^c Temperature correction factor.

^d Actual hydrometer reading.

^e Corrected hydrometer reading.

^f Corrected hydrometer reading only for meniscus.

^g Effective depth based on the hydrometer 152H.

^h Constant representing a relationship between the temperature and the specific gravity.

ⁱ Diameter, millimetre.

Table C.5 (Cont'd) - Sample f

Date	Time	t ^a	T ^b	C _T ^c	R _a ^d	R _c ^e	Actual % finer	R ^f	L ^g	L/t	K ^h	D ⁱ	Adjusted % finer
Mar. 26, 2009	10:17	2	23.0	0.70	56.0	53.7	100.00	57.0	7.0	3.5000	0.0129	0.0241	99.50
	10:20	5	23.0	0.70	56.0	53.7	100.00	57.0	7.0	1.4000	0.0129	0.0153	99.50
	10:30	15	23.0	0.70	54.0	51.7	96.28	55.0	7.3	0.4867	0.0129	0.0090	95.79
	10:45	30	23.0	0.70	53.0	50.7	94.41	54.0	7.4	0.2467	0.0129	0.0064	93.94
	11:15	60	23.0	0.70	51.0	48.7	90.69	52.0	7.8	0.1300	0.0129	0.0047	90.24
Mar. 27, 2009	14:25	250	22.8	0.64	44.5	42.1	78.47	45.5	8.9	0.0354	0.0130	0.0024	78.08
	10:15	1,440	22.5	0.55	36.0	33.6	62.48	37.0	10.2	0.0071	0.0130	0.0011	62.16

^a Elapsed time, minute.

^b Temperature, degree Celsius.

^c Temperature correction factor.

^d Actual hydrometer reading.

^e Corrected hydrometer reading.

^f Corrected hydrometer reading only for meniscus.

^g Effective depth based on the hydrometer 152H.

^h Constant representing a relationship between the temperature and the specific gravity.

ⁱ Diameter, millimetre.

Table C.5 (Cont'd) - Sample g

Date	Time	t ^a	T ^b	C _T ^c	R _a ^d	R _c ^e	Actual % finer	R ^f	L ^g	L/t	K ^h	D ⁱ	Adjusted % finer
Mar. 26, 2009	10:53	2	23.0	0.70	57.0	54.7	100.00	58.0	6.8	3.4000	0.0131	0.0242	99.60
	10:56	5	23.0	0.70	54.0	51.7	94.52	55.0	7.3	1.4600	0.0131	0.0158	94.14
	11:06	15	23.0	0.70	47.0	44.7	81.72	48.0	8.4	0.5600	0.0131	0.0098	81.39
	11:21	30	23.0	0.70	42.0	39.7	72.58	43.0	9.2	0.3067	0.0131	0.0073	72.29
	11:51	60	23.0	0.70	37.0	34.7	63.44	38.0	10.1	0.1683	0.0131	0.0054	63.18
Mar. 27, 2009	15:01	250	22.8	0.64	30.0	27.6	50.53	31.0	11.2	0.0448	0.0131	0.0028	50.33
	10:51	1,440	22.5	0.55	25.0	22.6	41.22	26.0	12.0	0.0083	0.0131	0.0012	41.06

^a Elapsed time, minute.

^b Temperature, degree Celsius.

^c Temperature correction factor.

^d Actual hydrometer reading.

^e Corrected hydrometer reading.

^f Corrected hydrometer reading only for meniscus.

^g Effective depth based on the hydrometer 152H.

^h Constant representing a relationship between the temperature and the specific gravity.

ⁱ Diametre, millimetre.

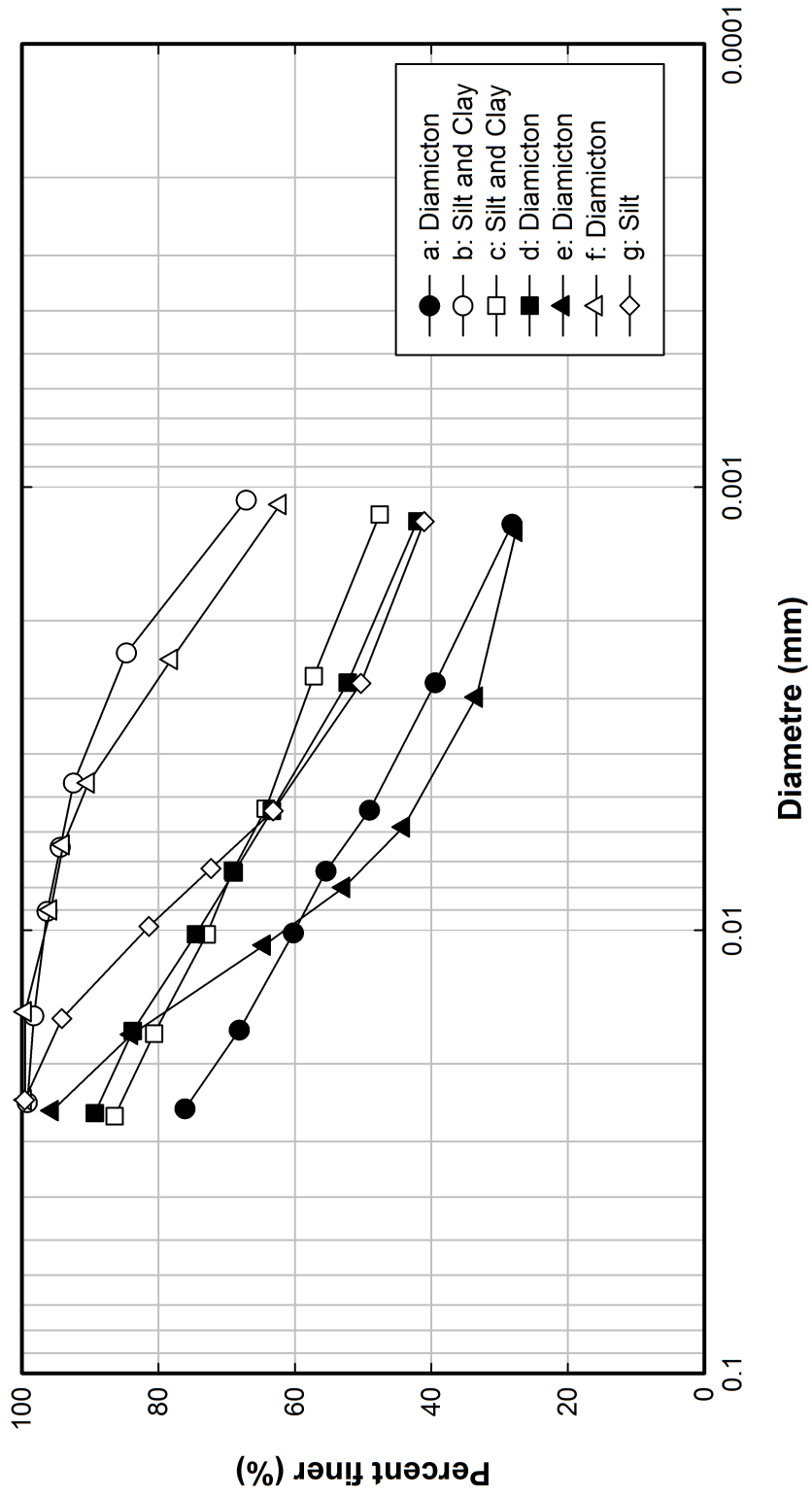


Figure C.2 Particle distributions for soil samples obtained from hydrometer tests

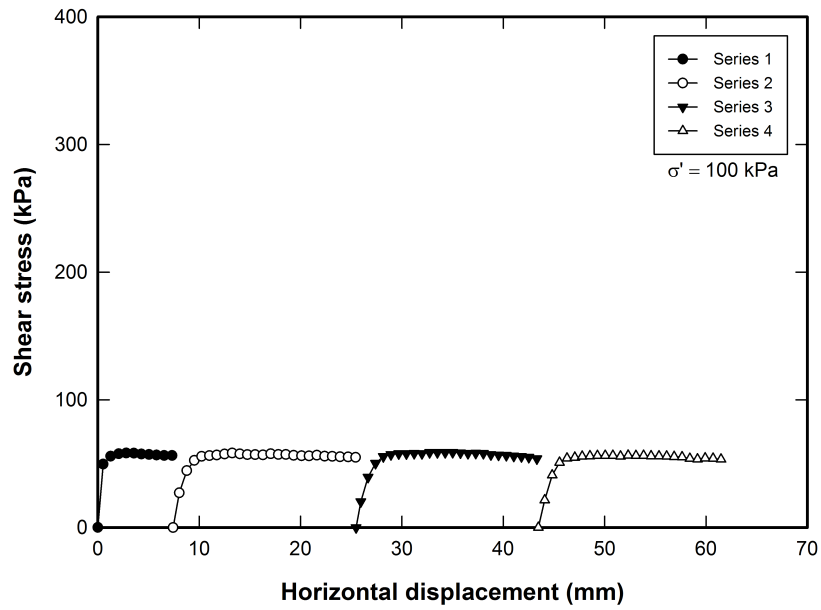
(4) Results of direct shear tests

Table C.6 Summary of samples for the direct shear test

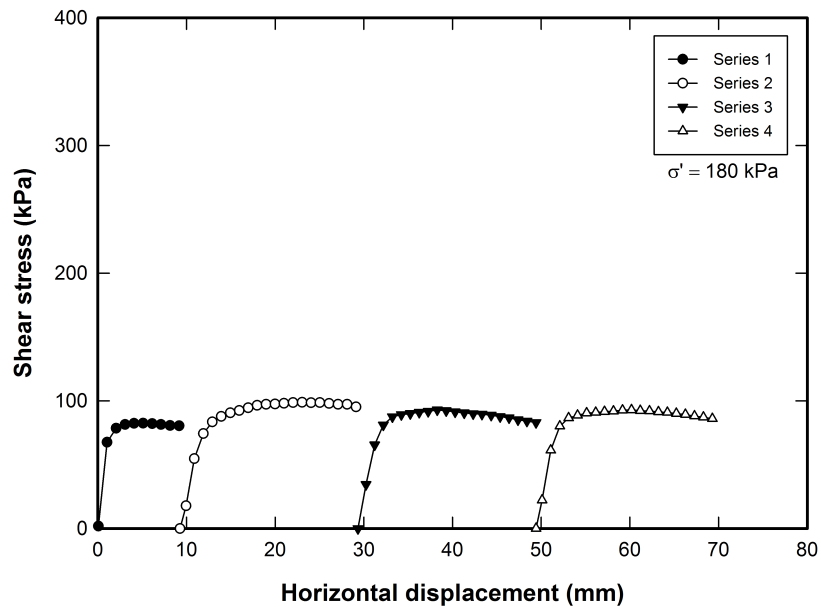
Sample	Estimated soil unit	Applied normal stress (kPa)	Test type [†]
a	Diamicton (Till)	100, 180, 290, 380	<i>fs</i>
b	Silt and Clay	380, 560, 950, 1,120	<i>Peak, fs</i>
e	Diamicton (Till) [‡]	315, 525, 845, 1,020	<i>fs</i>
f	Diamicton (Till) [‡]	430, 640, 1,060, 1,280	<i>Peak, fs</i>

[†] *fs*: Fully softened strengths, *Peak*: Peak strengths.

[‡] Colluviated tills.

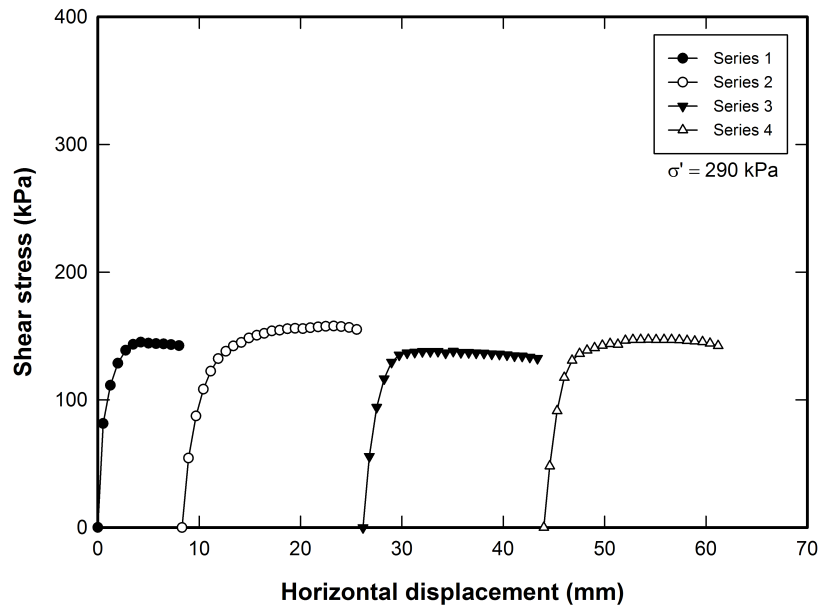


(a) $\sigma' = 100$ kPa

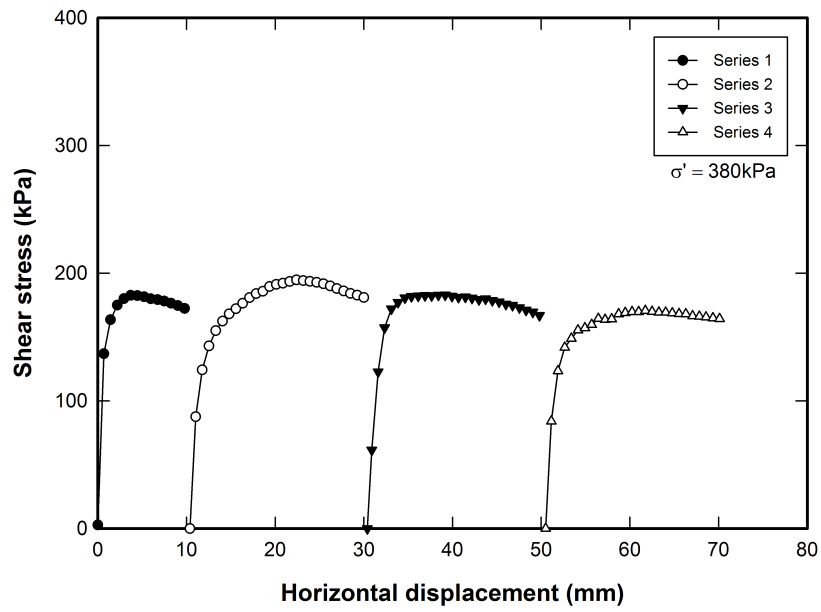


(b) $\sigma' = 180$ kPa

Figure C.3 Direct shear test for sample a (fully softened)

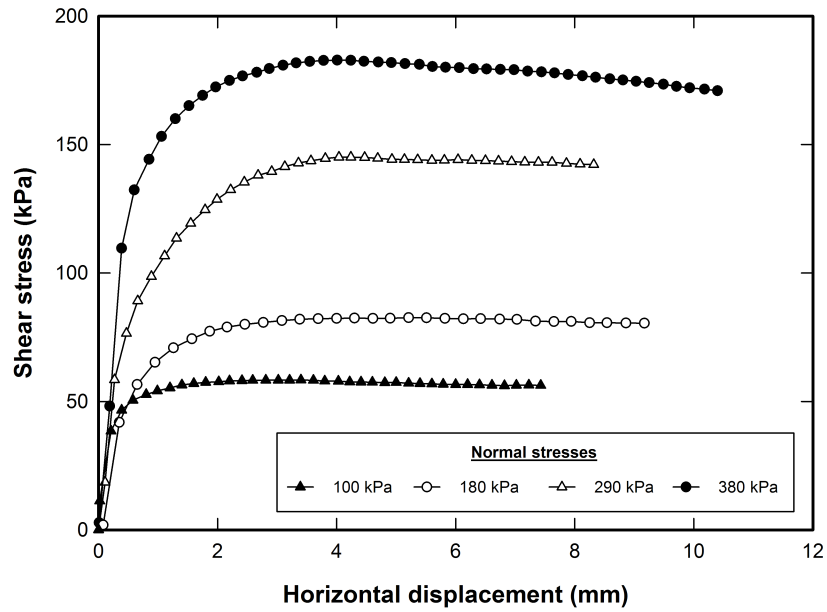


(c) $\sigma' = 290$ kPa

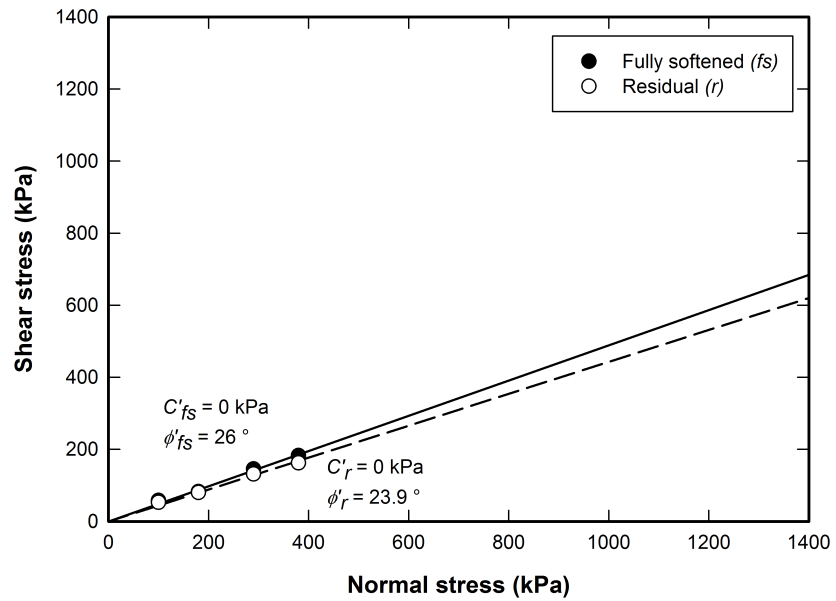


(d) $\sigma' = 380$ kPa

Figure C.3 (Cont'd)



(e) Stress versus displacement curve



(f) Determination of shear strength properties

Figure C.3 (Cont'd)

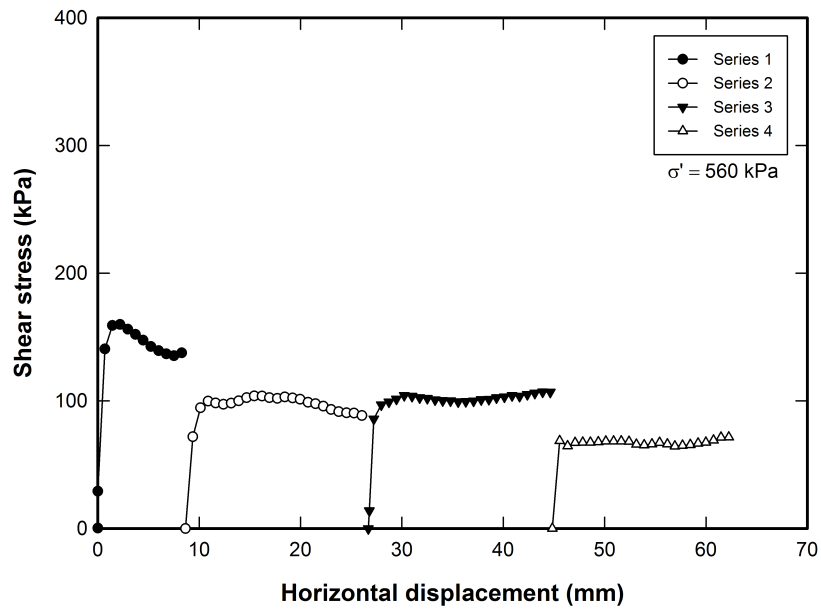
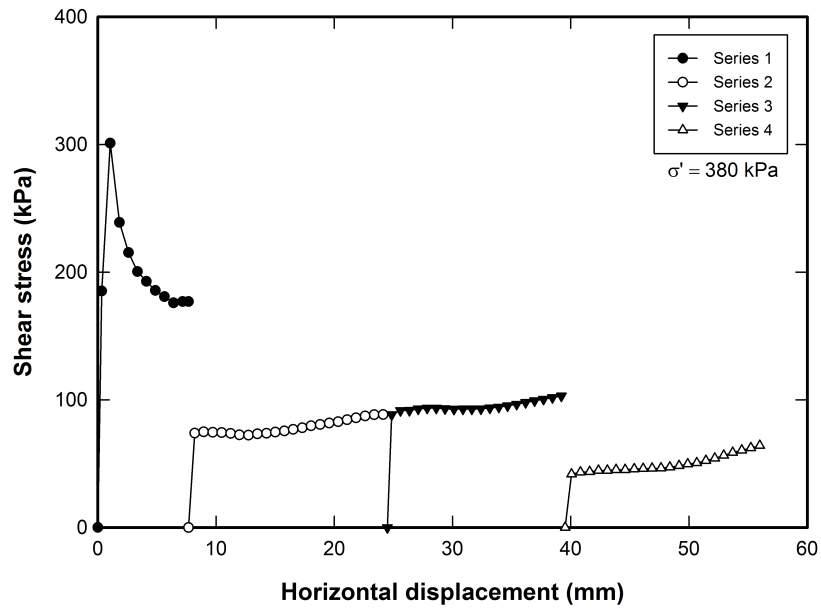
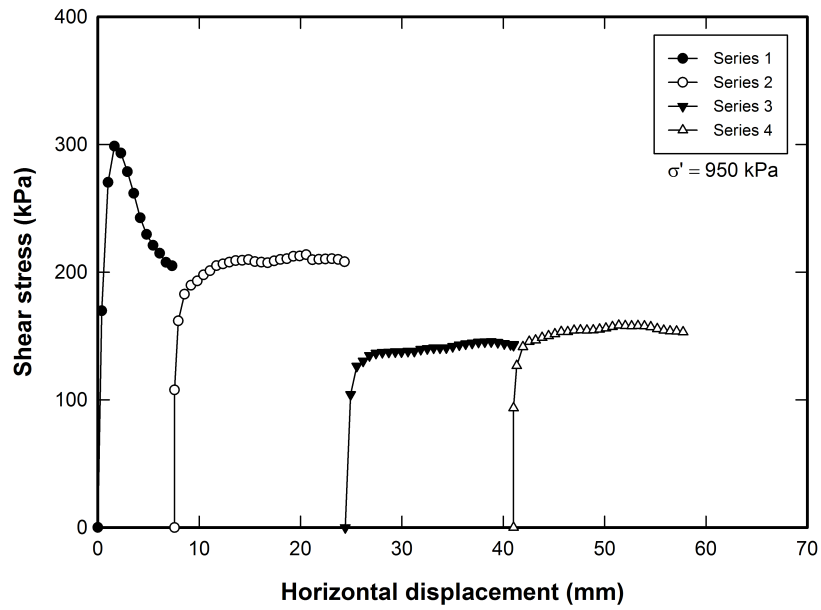
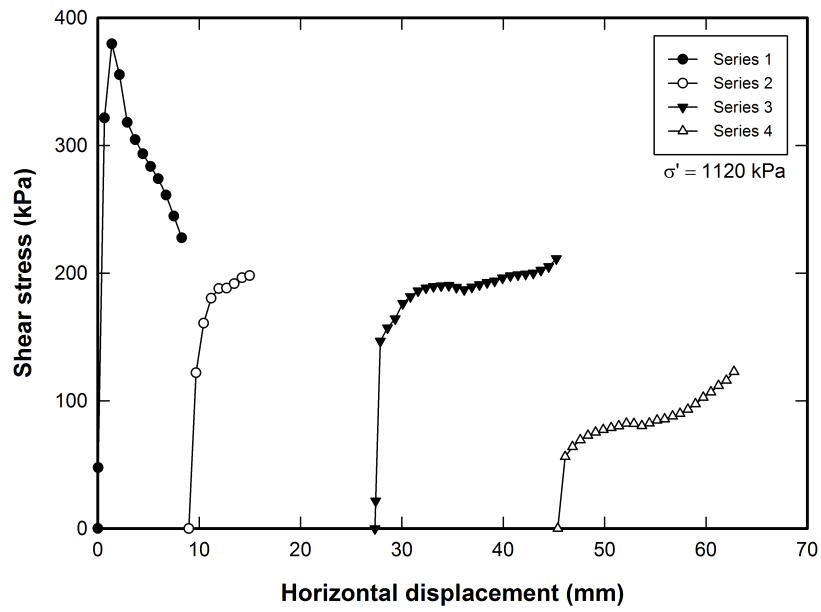


Figure C.4 Direct shear test for sample b (peak)

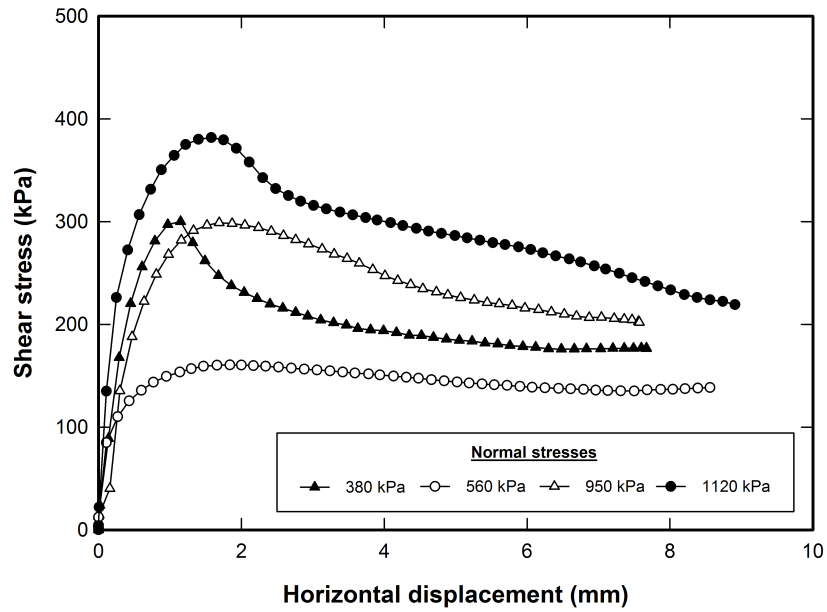


(c) $\sigma' = 950 \text{ kPa}$

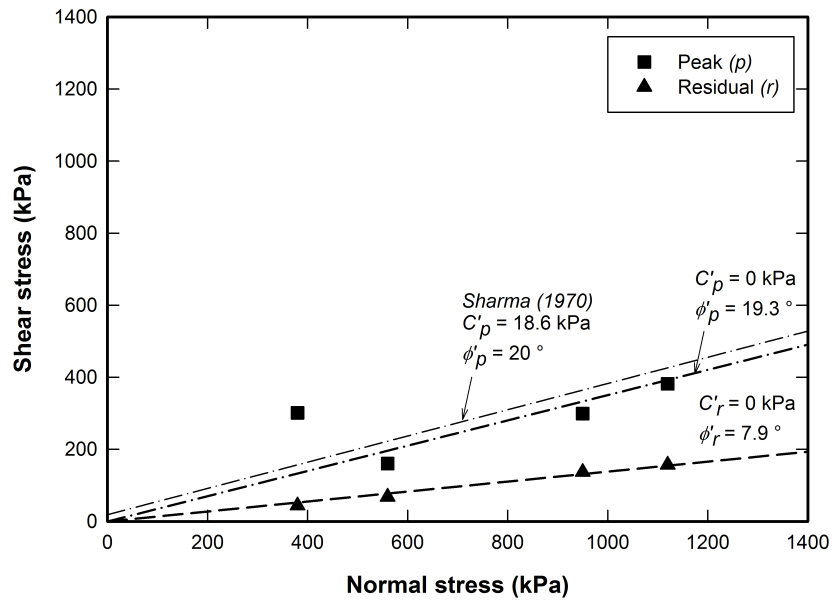


(d) $\sigma' = 1,120 \text{ kPa}$

Figure C.4 (Cont'd)

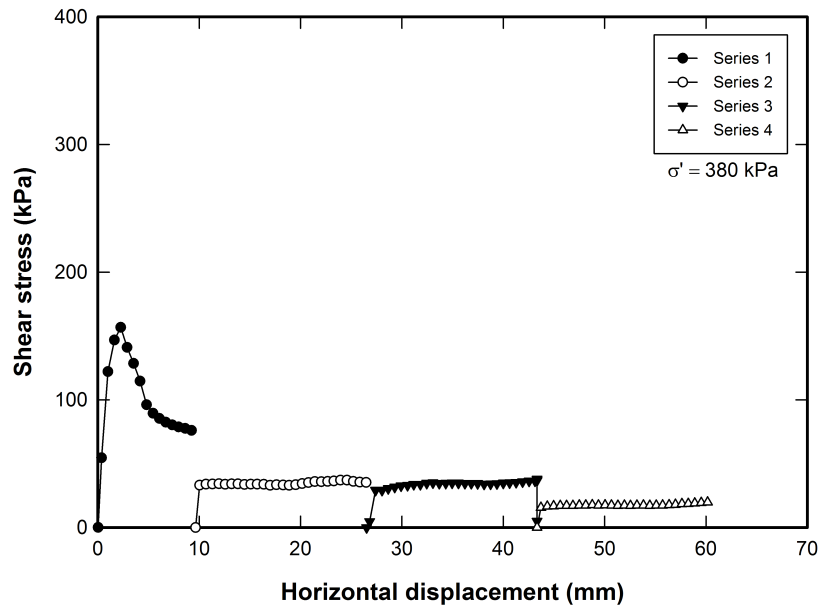


(e) Stress versus displacement curve

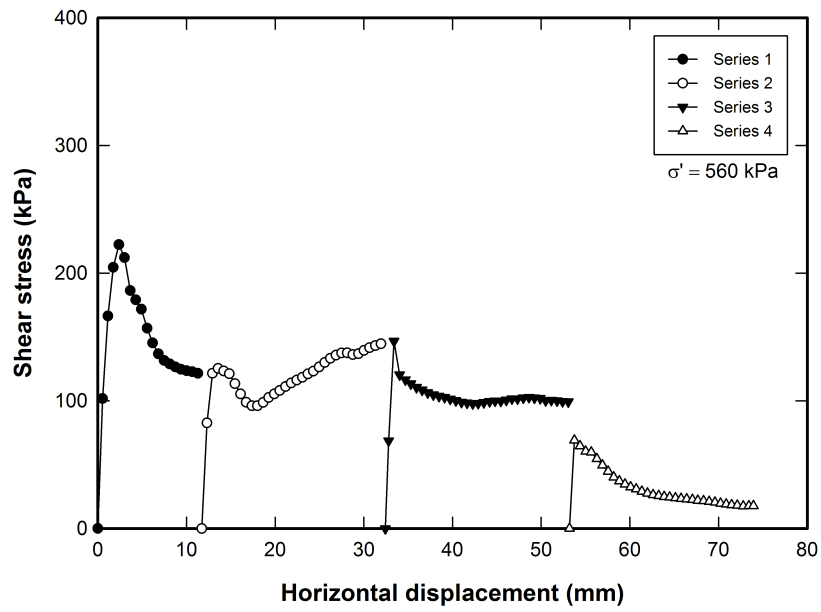


(f) Determination of shear strength properties

Figure C.4 (Cont'd)

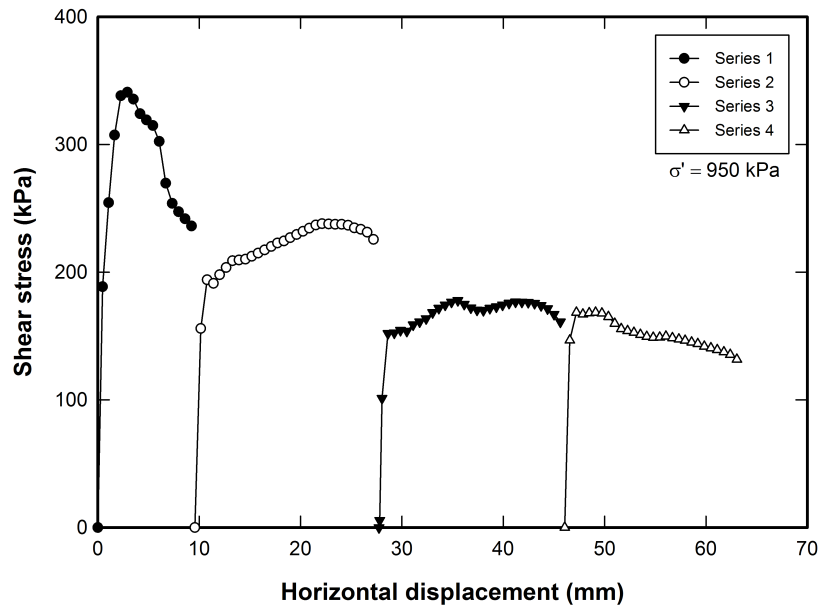


(a) $\sigma' = 380 \text{ kPa}$

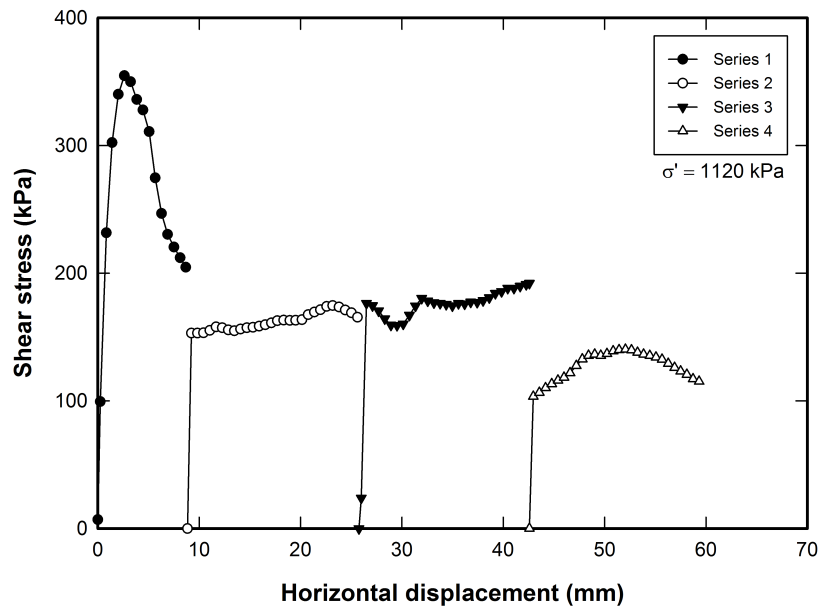


(b) $\sigma' = 560 \text{ kPa}$

Figure C.5 Direct shear test for sample b (fully softened)

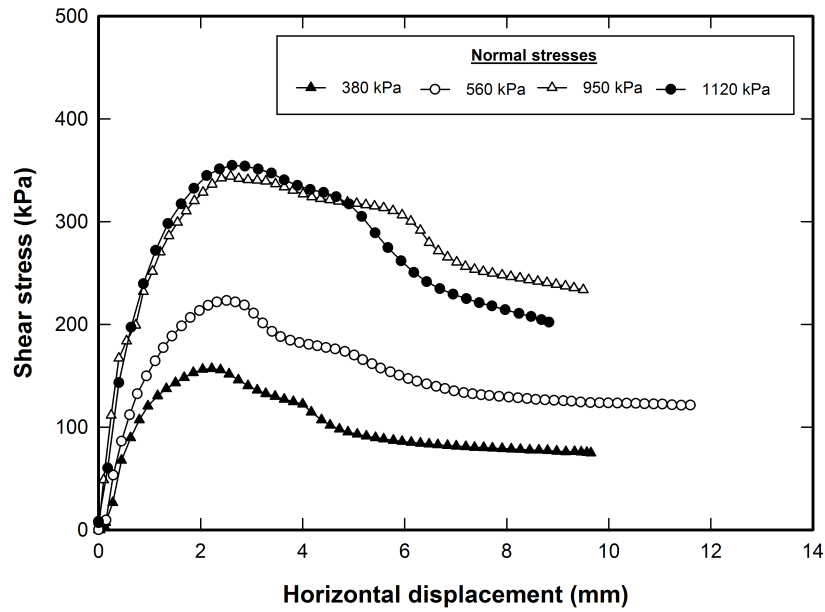


(c) $\sigma' = 950 \text{ kPa}$

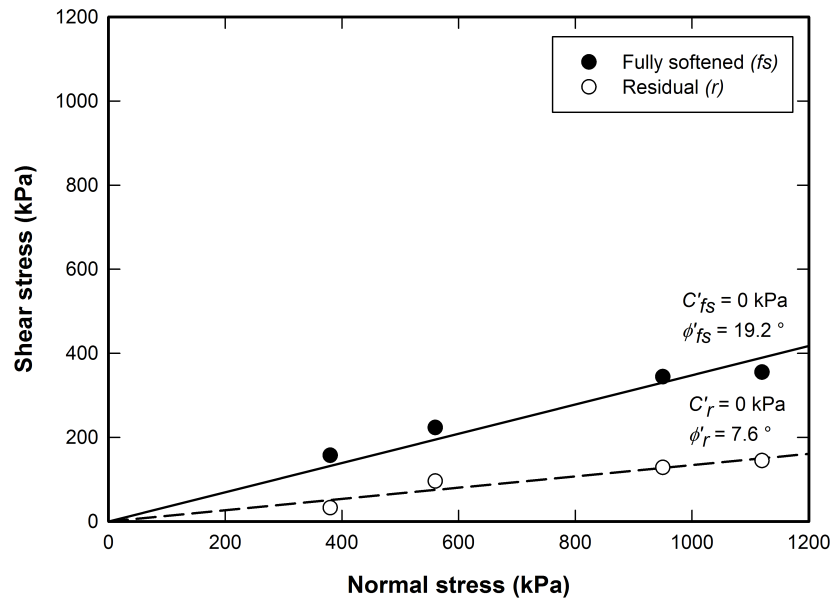


(d) $\sigma' = 1,120 \text{ kPa}$

Figure C.5 (Cont'd)

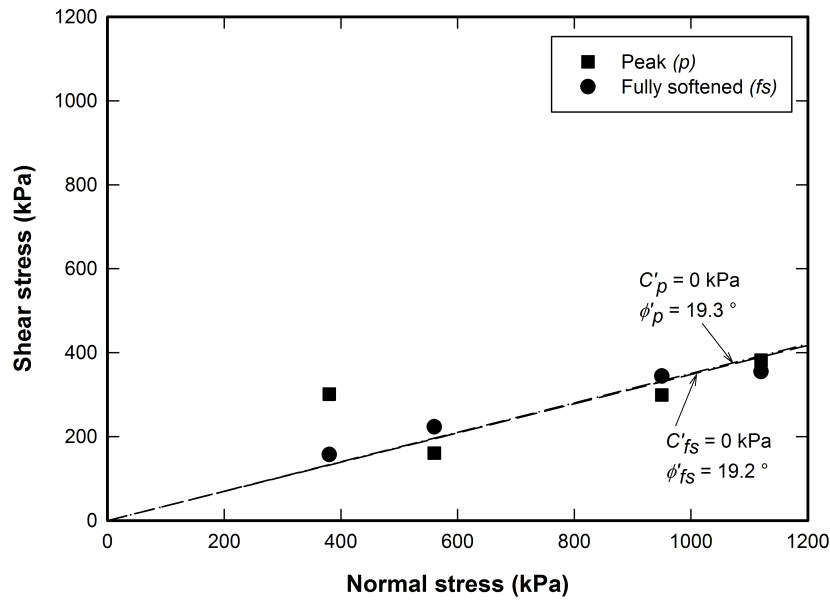


(e) Stress versus displacement curve

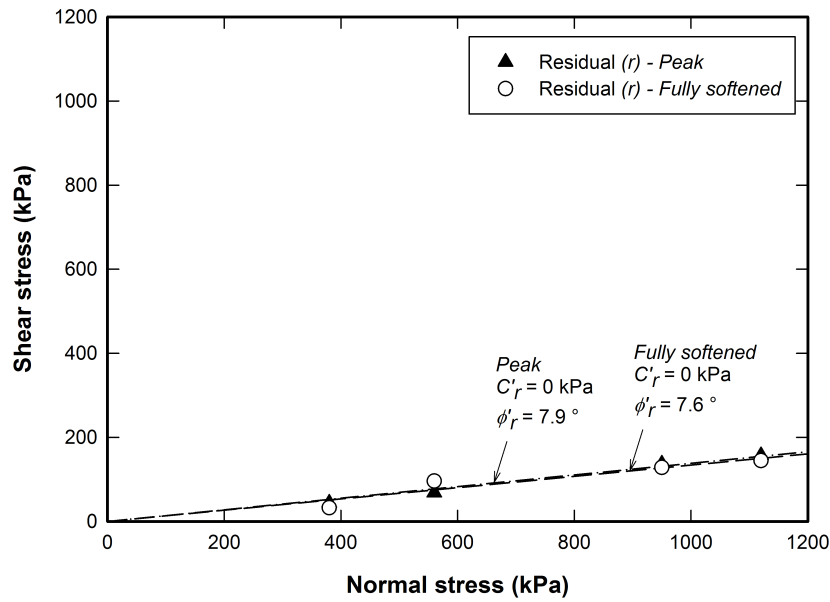


(f) Determination of shear strength properties

Figure C.5 (Cont'd)

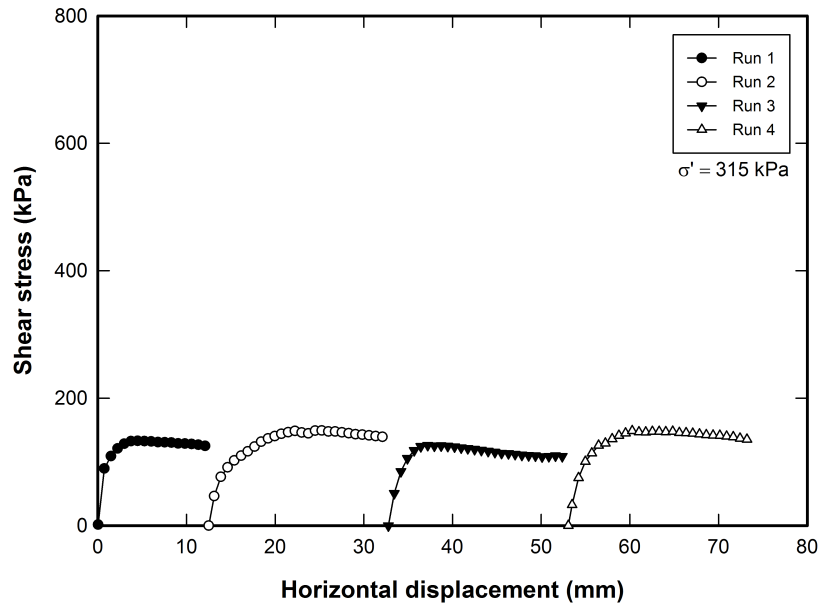


(g) Peak versus fully softened values

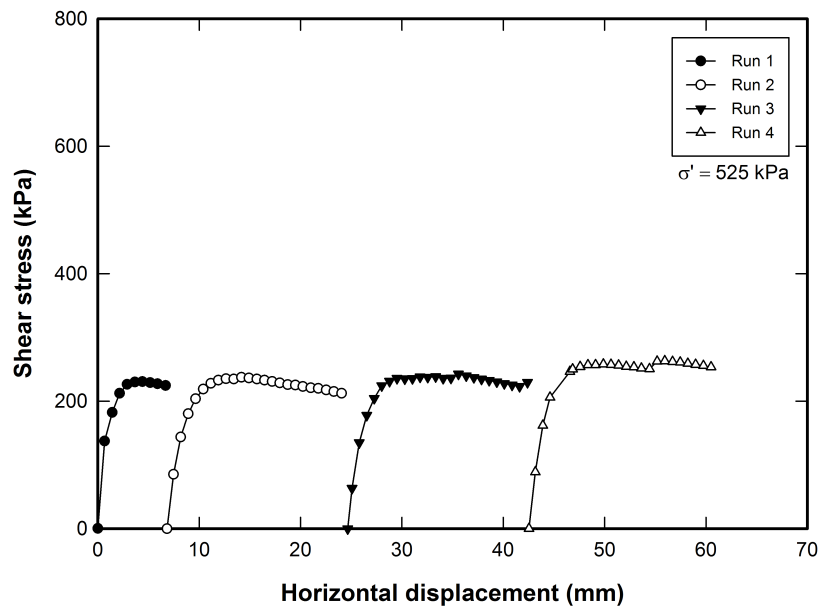


(h) Comparison of residual values

Figure C.5 (Cont'd)

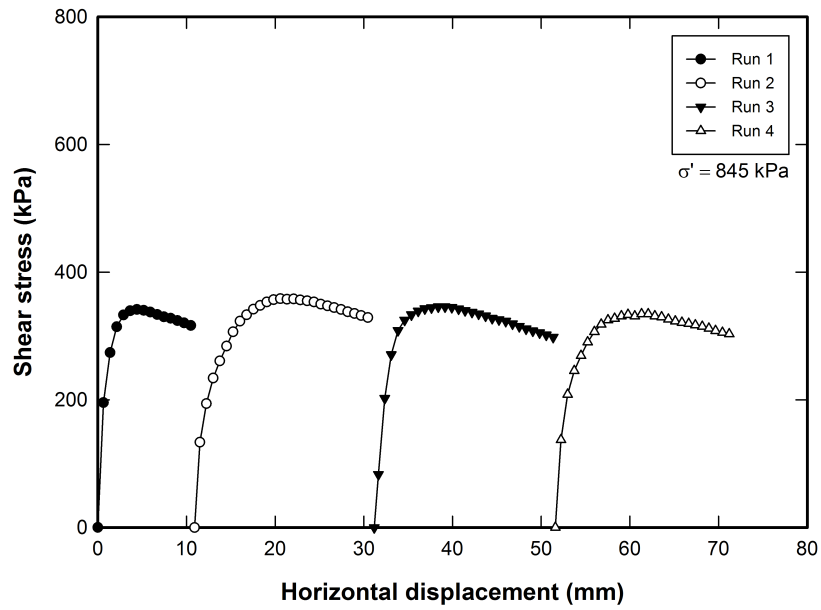


(a) $\sigma' = 315$ kPa

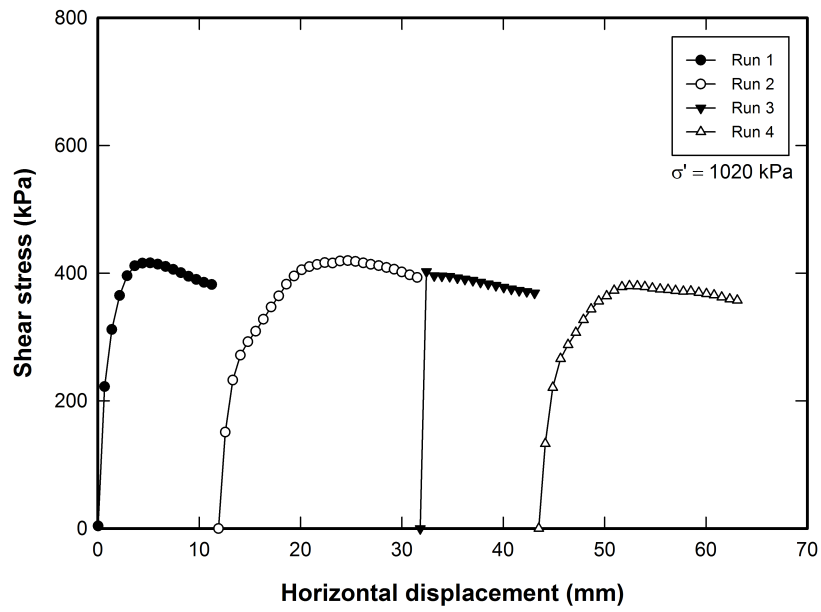


(b) $\sigma' = 525$ kPa

Figure C.6 Direct shear test for sample e (fully softened)

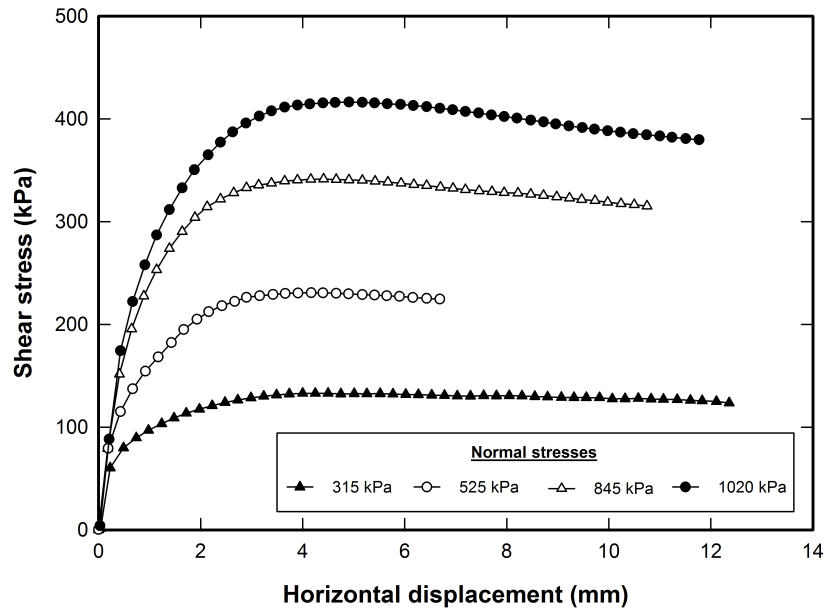


(c) $\sigma' = 845 \text{ kPa}$

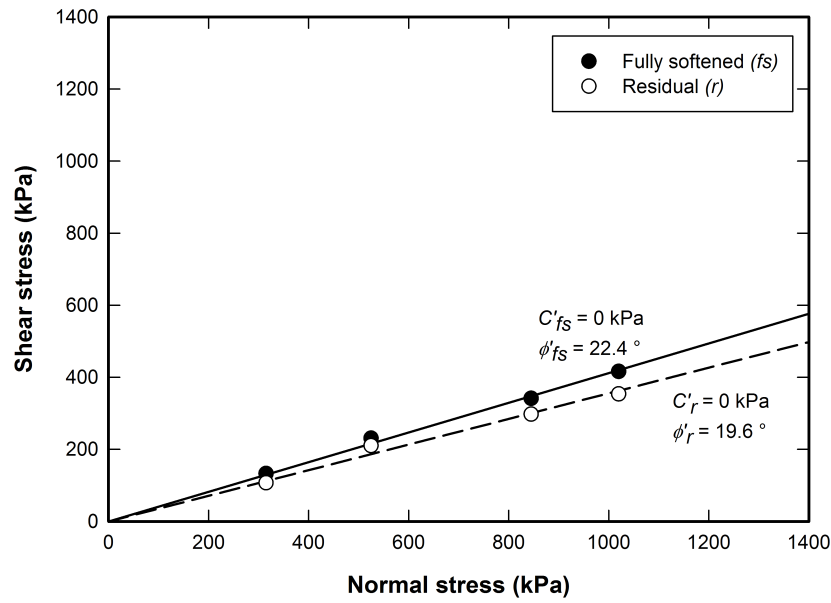


(d) $\sigma' = 1,020 \text{ kPa}$

Figure C.6 (Cont'd)

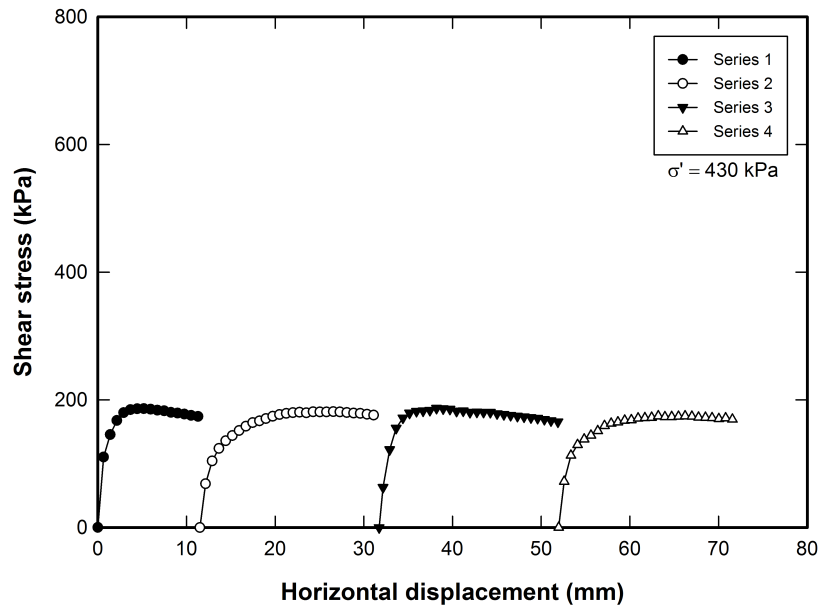


(e) Stress versus displacement curve

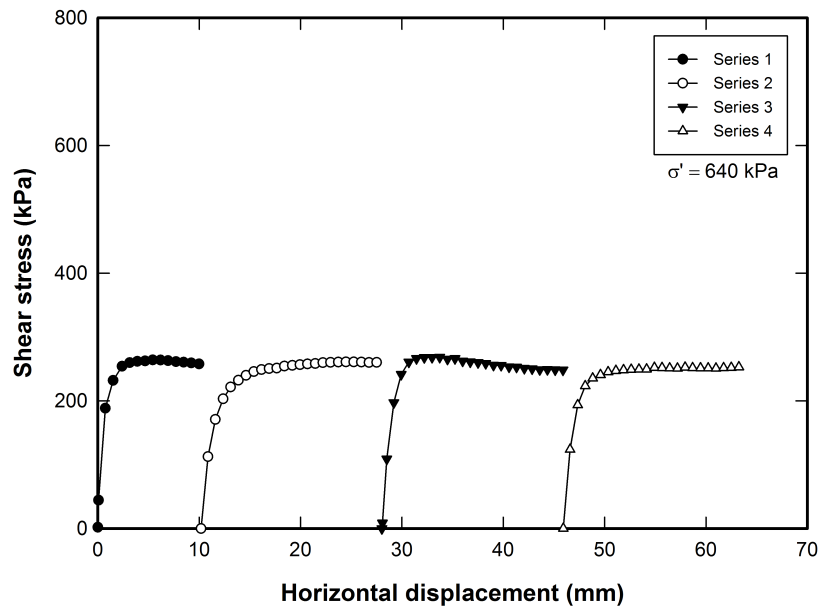


(f) Determination of shear strength properties

Figure C.6 (Cont'd)

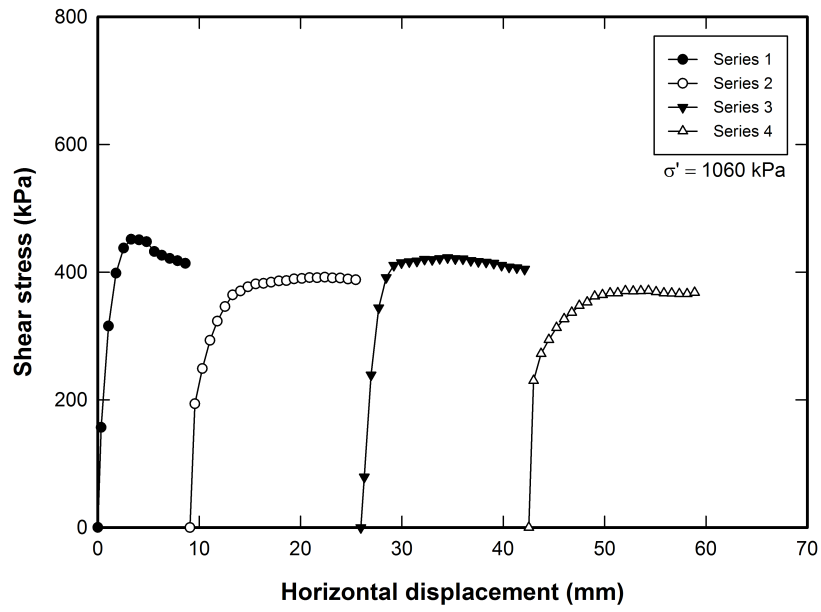


(a) $\sigma' = 430$ kPa

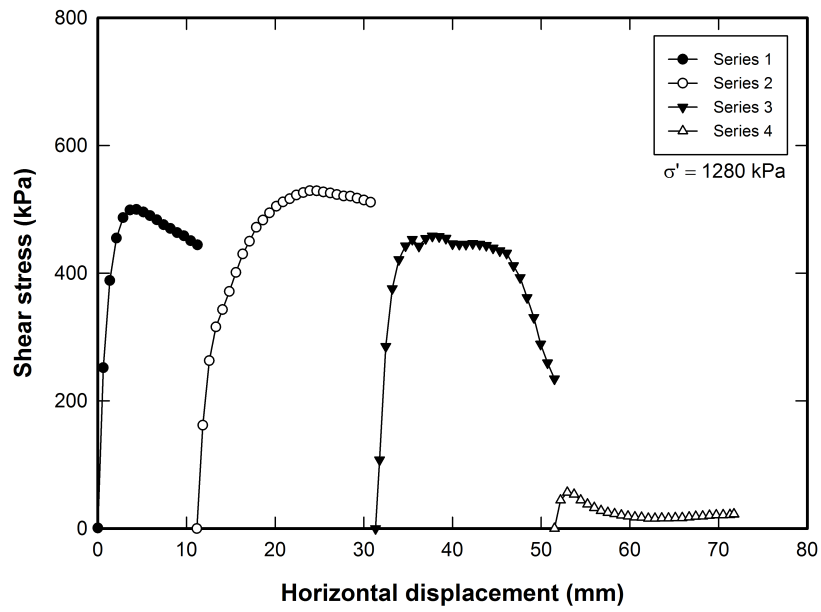


(b) $\sigma' = 640$ kPa

Figure C.7 Direct shear test for sample f (peak and fully softened)

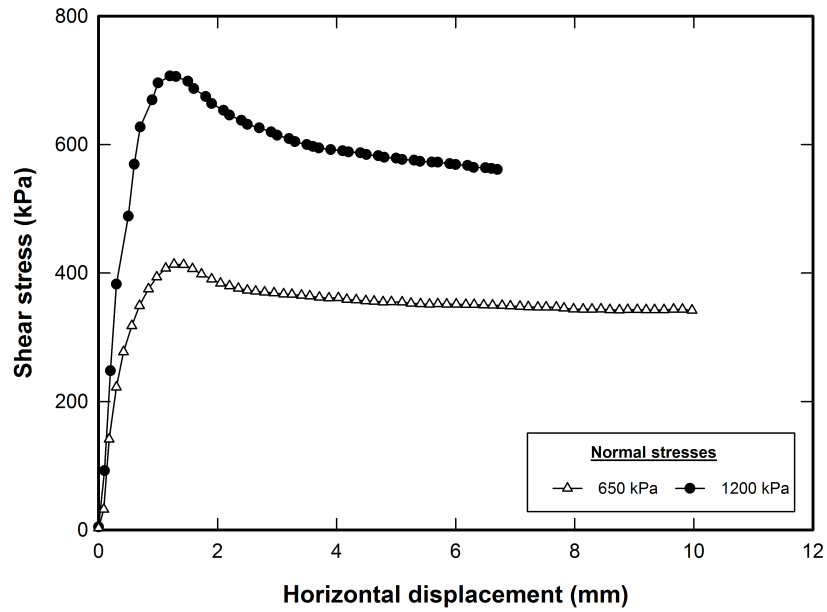


(c) $\sigma' = 1,060 \text{ kPa}$

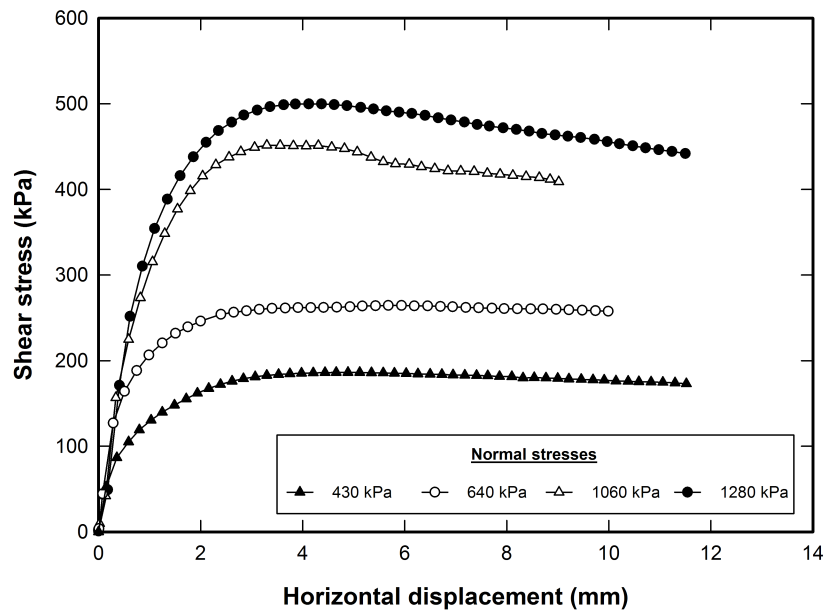


(d) $\sigma' = 1,280 \text{ kPa}$

Figure C.7 (Cont'd)

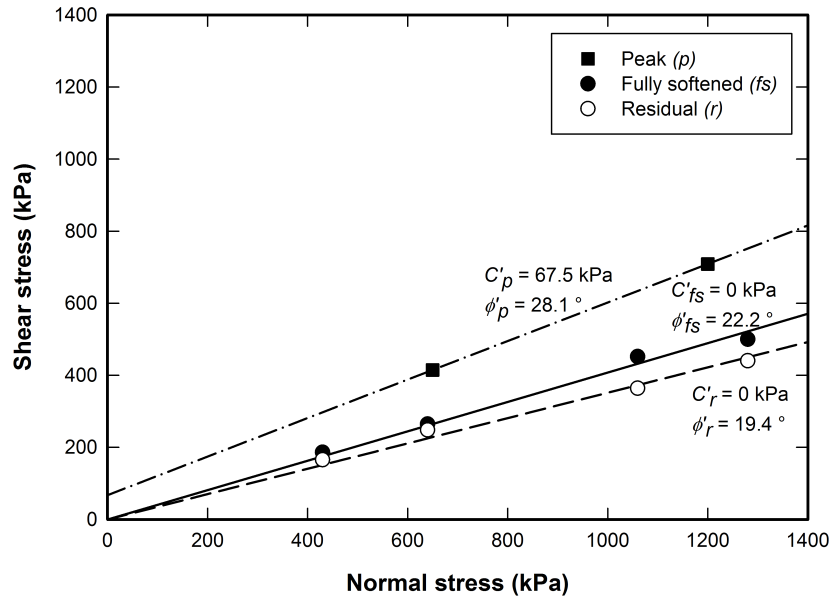


(e) Stress versus displacement curve (peak)



(f) Stress versus displacement curve (fully softened)

Figure C.7 (Cont'd)



(g) Determination of shear strength properties

Figure C.7 (Cont'd)

Appendix D

The 2007 Fox Creek landslide, Peace River Lowland, Alberta, Canada¹

Abstract

Fox Creek is a small tributary of the Saddle River, a tributary of the Peace River in northwestern Alberta. It has several dormant landslides with degraded scarps and grabens. A new, reactivated landslide on the north bank of Fox Creek occurred on 5 May 2007. The landslide formed two major sliding blocks. A rapid translational block slide, it mobilized 47 Mm³ of displaced materials, blocked the creek, and made a natural dam with a maximum height of 19 m at the tips of the displaced blocks. The rupture surfaces of the 2007 landslide were within the advance phase glaciolacustrine sediments. The residual friction angles are about 10 ° similar to those of previous landslides in the Peace River Lowland. Precipitation and snow melt prior to the landslide are likely triggers of the 2007 Fox Creek landslide. The farmlands on the crest of the river valley and timber resources were impacted. The current landslide dam in Fox Creek does not have any evidence of seepage downstream; it may last for many years. Eventually, the creek will overtop and erode the dam. The same cycle of actions, landsliding, damming, and erosion will continue in the foreseeable future.

Introduction

At least five rivers, tributaries of the Peace River, have suffered historic, reactivated, retrogressive, multiple, rapid, translational earth slides (Cruden et al. 1993, 1997; Lu et al. 1998; Miller and Cruden 2001, 2002). These five landslides have occurred in the Late Wisconsin advance phase glaciolacustrine sediments or Late Wisconsin glacial sediments (Morgan et al. 2008). They are the largest historic landslides on the Interior Plains in Canada. They took place on low angle valley slopes, were

¹A modified version of this Appendix has been published as Kim, T.H., Cruden, D.M., Martin, C.D., and Froese, C.R. 2010. The 2007 Fox Creek landslide, Peace River Lowland, Alberta, Canada. *Landslides*, 7(1): 89-98. The electronic article is located at http://www.springerlink.com/openurl.asp?genre=article&id=doi:10.1007/s10346-009-0184-1&sa_campaign=Email/ACE/OF.

tens of millions of cubic meters in volume, and dammed river flow to form landslide lakes (Evans et al. 2005). These major landslides in the Peace River Lowland are documented in Table D.1.

In this paper, we describe a preliminary assessment of the 2007 Fox Creek landslide. Aerial photo interpretation, site reconnaissance, and laboratory tests indicate the landslide mechanism and subsurface stratigraphy. Weather records suggest that the landslide was triggered by rainfall after a record snow accumulation. This sixth landslide of this type is the first on a creek with flow insufficient to overtop the landslide dam.

Fox Creek flows westward to join the Saddle River 4.8 km south of its junction with the eastward-flowing Peace River (Figure D.1). It has several dormant landslides with degraded scarps and grabens. The 2007 Fox Creek landslide occurred on 5 May on the north bank of the Fox Creek. Landslides blocked the creek and created a reservoir upstream. The retrogression of the landslide displaced the farmland on the crown of the slide (Figure D.2).

Site description

The Peace River Lowland is characterized by rolling uplands, flat to undulating plateau areas, and deeply entrenched river valleys (Leslie and Fenton 2001). As the last glaciers retreated, their melt waters rapidly cut the Peace River valley. The valleys of tributary rivers and small streams were cut subsequently and remained in unstable conditions with active downcutting continuing.

Weather records from the nearest meteorological station (Peace River Airport, 50 km NE of Fox Creek, Figure D.1) show that the 30 year average annual temperature and precipitation are 1.2 °C and 402 mm, respectively. The 30 year average snow depth on the ground is 8 cm and usually melts before April. The historical maximum daily precipitation was 53 mm on 4 May 2000 (Table D.2).

Average precipitation recorded from October 2006 to May 2007 indicates precipitation 160 % of the 30 year average (Figure D.3a). Snow had come in mid-November 2006, and over 30 cm had accumulated by April 2007. Very little if any melting occurred during the winter period. Heavy precipitation, in February and March, fell

Table D.1 Major landslides in the Peace River Lowland, Alberta

Year	Location [†]	Landslide type	Location of rupture surface
1939	Montagneuse River ^a	Translational slide	Advance phase glaciolacustrine sediments
1990	Saddle River ^b	Translational slide	Advance phase glaciolacustrine sediments
1990	Hines Creek ^c	Translational slide	Glacial sediments (Tills)
1990	Eureka River ^d	Enlarged earth slide	Advance phase glaciolacustrine sediments
1995	Spirit River ^e	Translational slide	Glacial sediments (Tills)
2007	Fox Creek	Translational slide	Advance phase glaciolacustrine sediments

[†] Location of each landslide is in Figure D.1.

^a Cruden et al. (1997).

^b Cruden et al. (1993).

^c Lu et al. (1998).

^d Miller and Cruden (2002).

^e Miller and Cruden (2001).

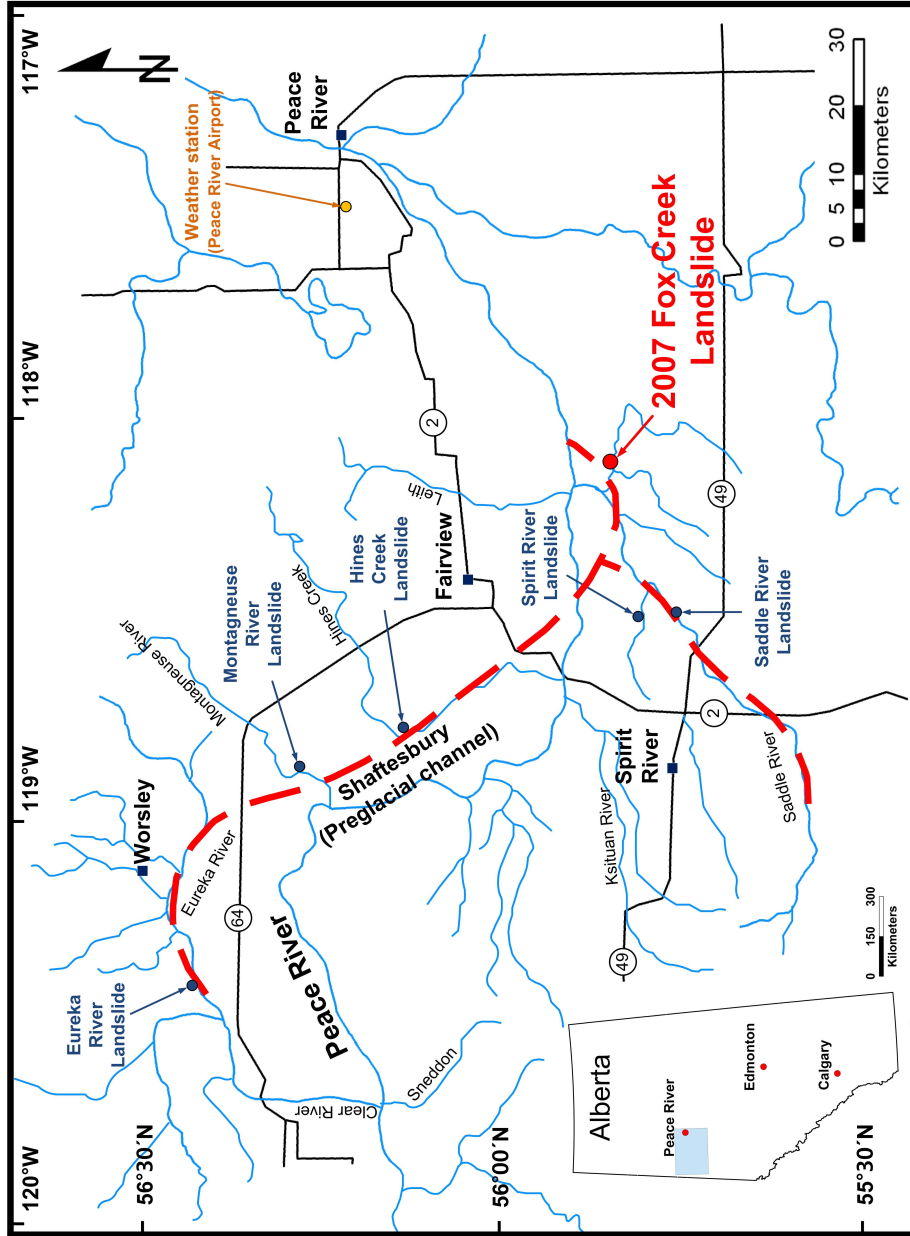


Figure D.1 Location of five historic landslides in the Peace River Lowland. Thalwegs of preglacial valleys and weather station are also indicated (after Miller and Cruden 2002)



(a)



(b)

Figure D.2 Aerial overview of the 2007 Fox Creek landslide. a. High oblique view of the affected area (looking northeast). b. Landslide lake located at the toe of the east sliding block (looking west)

Table D.2 Historical meteorological data in the Peace River, Alberta

Location	Average (1971-2000) [‡]				Extreme (daily) [‡]		
	Temperature (°C)	Precipitation (mm)	Snow depth (cm)	Maximum precipitation (mm)	Maximum temperature (°C)	Minimum temperature (°C)	
Peace River Airport [†] (Elevation: 570.9 m)	1.2	402.3	8	53 (4 May 2000)	36.7 (13 July 1945)	-49.4 (13 Jan. 1950)	

[†] Location of the weather station is illustrated in Figure D.1.

[‡] Source: Data from Environment Canada (2009).

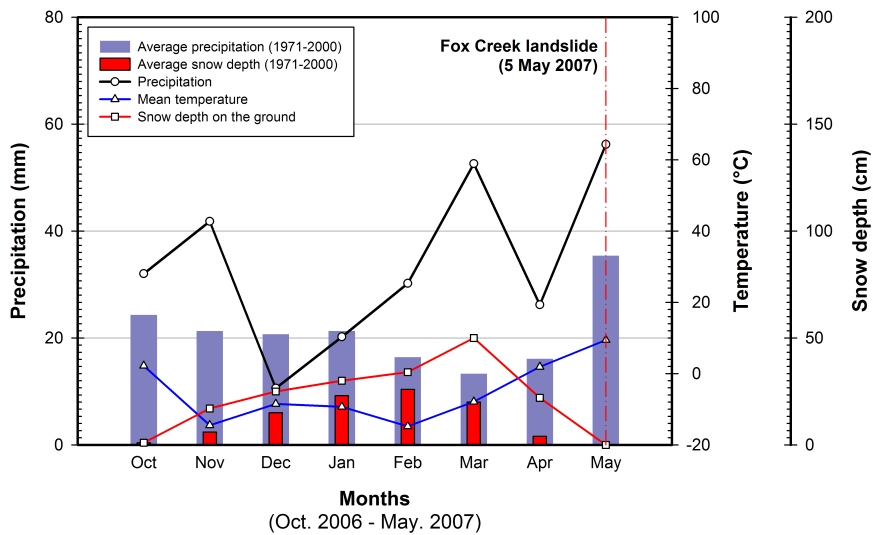
as snow (Figure D.3a). As the mean temperature increased above zero on 8 April (Figure D.3b), the snow melt was relatively rapid. Figure D.3b shows no snow on the ground by mid-April and heavy rainfall on 4 May 2007 just before the landslide occurred. This rainfall together with the melting of the snow and infiltration of the snow melt would likely increase pore water pressure within the soil.

Aerial photo interpretations

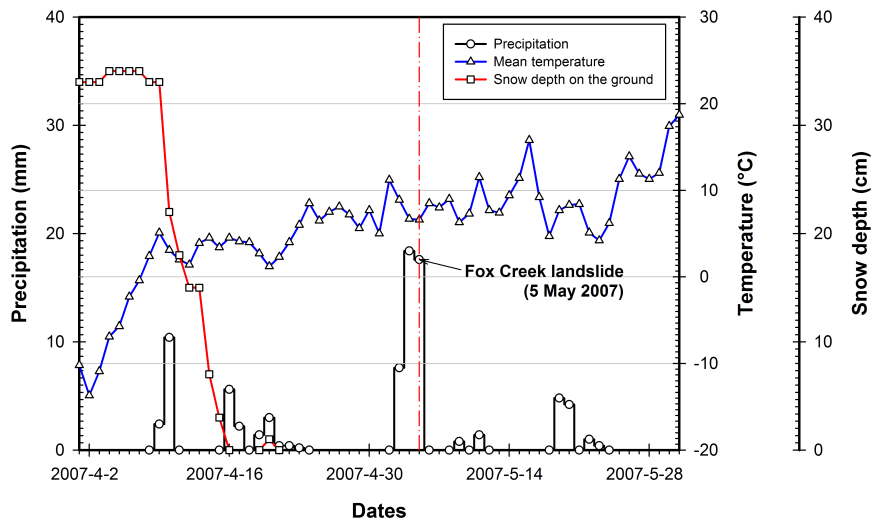
We interpreted six sets of aerial photos: 1952 (1:15,840), 1979 (1:15,000 with false color infrared), 2001 (1:20,000 and 1:30,000), and 2008 (1:10,000 and 1:10,000 with false color infrared). Interpretations focused on the period around the landslide occurrence on 5 May 2007, the 2001 aerial photos (Figure D.4a), those taken in 2008 (Figure D.5a), and their interpretations (Figures D.4b and D.5b). Geomorphological features illustrated in Figures D.4b and D.5b follow the legend used by the Geological Society Engineering Group Working Party (Dearman et al. 1972). We also benefited from a helicopter reconnaissance conducted on 13 August 2008 by the Alberta Geological Survey which provided an aerial overview of the landslide (Figure D.2).

The preslide topography of Fox Creek is shown in Figure D.4. The valley widens westward from 460 m at the east margin of the landslide to 1.2 km at the west margin as the valley side slope decreases from 10 to 9 °. Valley depth increases from 60 to 100 m. Landslide features such as sag ponds and scarps are visible even though they have been degraded over time.

The postslide topography illustrated in Figure D.5 indicates significant differences on the valley crest before and after the landslide. Surface morphology shown by the 2008 aerial photo interpretation indicates that the landslide was composed of two blocks differing in their directions of movement (Figure D.5b). The crown of the east sliding block, on the north bank of Fox Creek, forms a gentle arc 1.1 km across. The slide has a length of 330 to 650 m. Preslide movement may be indicated by the linear dark tone on the 2001 aerial photo (Figure D.4b). The head of the displaced materials is unsupported after cracking, and over time, a rupture within this unsupported, slightly displaced material created a tapering wedge, the active block (Figure D.6), separated from the main body of displaced materials downslope. The active block moved downward to form a graben and uphill-facing scarp. It

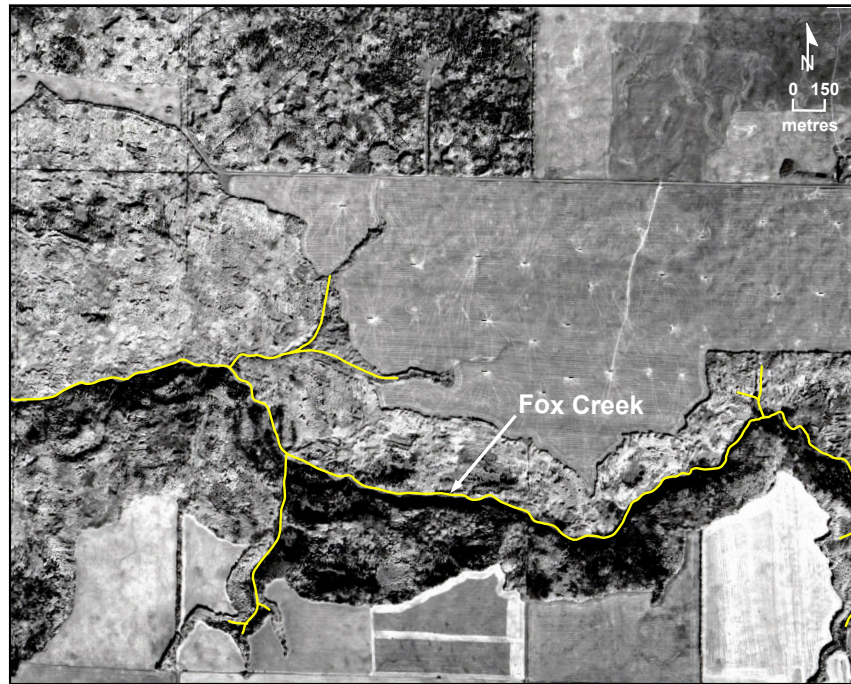


(a)

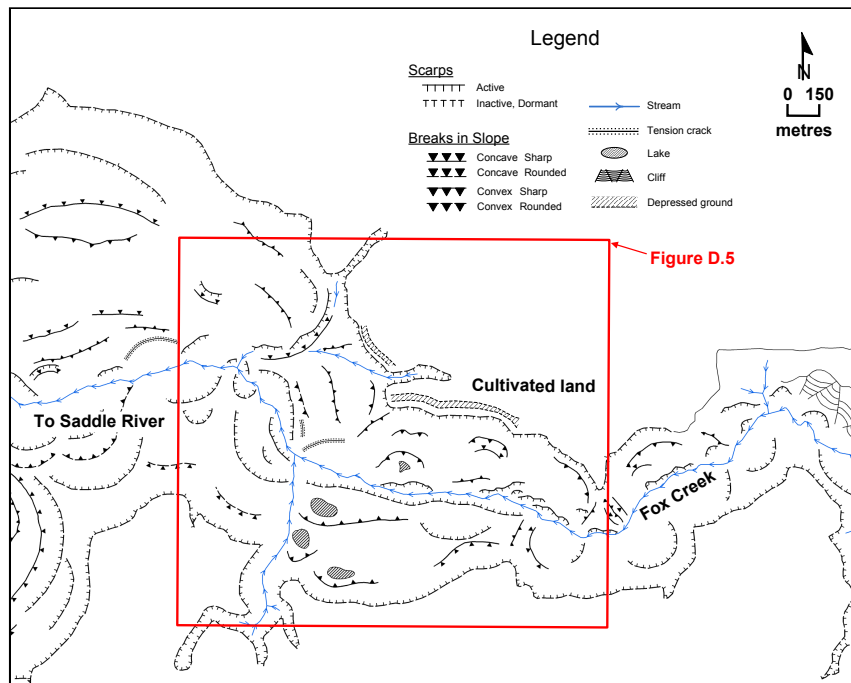


(b)

Figure D.3 Meteorological records measured at the Peace River Airport. a. Monthly records of precipitation (black line with circle), snow depth on the ground (red line with square), and temperature (blue line with triangle) during the October 2006 to May 2007. The 30 year (1971-2000) average precipitation (blue bar) and snow depth (red bar) records are also illustrated. b. Daily records during April to May 2007. Location of the weather station is illustrated in Figure D.1. *Source:* Data from Environment Canada (2009)



(a)



(b)

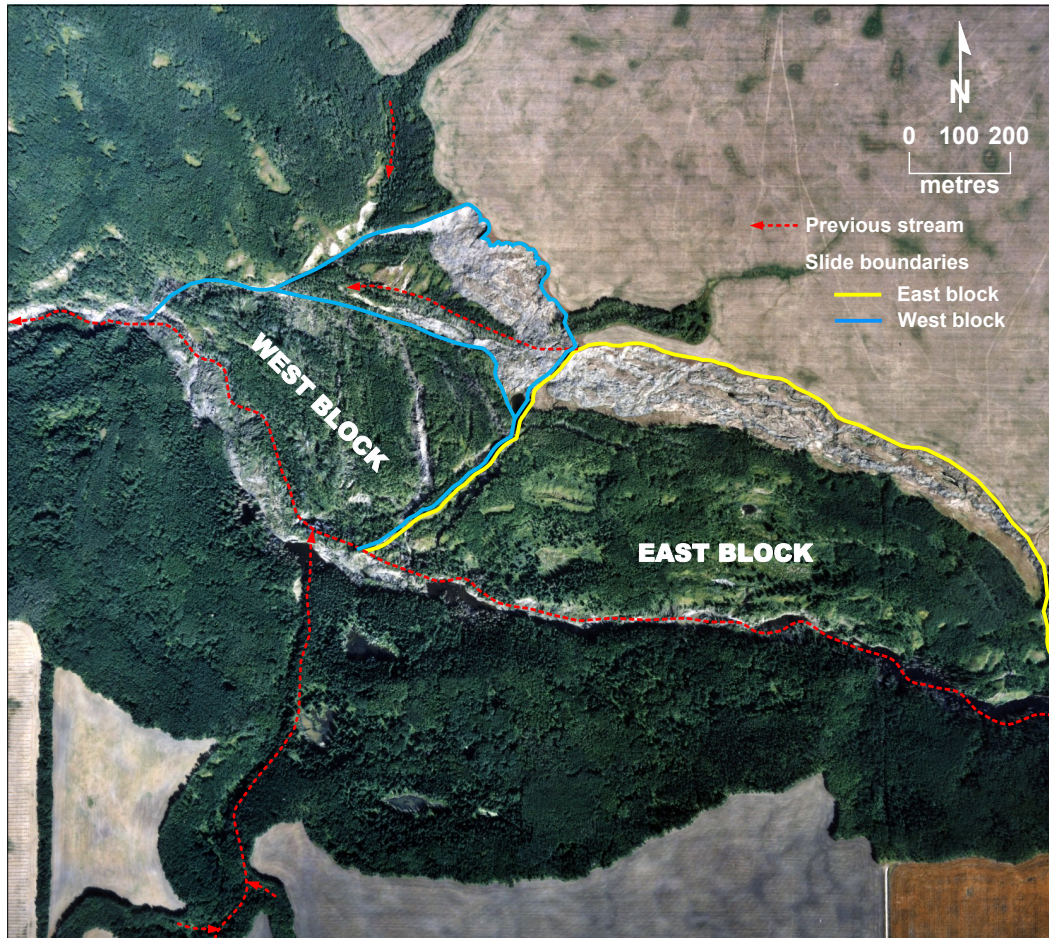
Figure D.4 2001 aerial photo interpretation. a. Aerial photograph of the area in 2001, scale 1:30,000 (Alberta photo: AS5194B-167). b. Interpretation of the aerial photograph AS5194B-167 shown in a. Area outlined in b indicates the 2007 landslide location (Figure D.5)

pushed the downslope passive block southward into the creek. The downstream (west) margin of the east sliding block reactivated the margins of dormant slides to the northwest and to the southeast (Figure D.4b). There was little disturbance of forest on the passive block, which indicated that the movement was a translational block slide on a deep, planar rupture surface. Based on the landslide profile (Figure D.6a), the graben which formed in the east sliding block is 22 m deep.

The west sliding block is 540 m wide and 680 m long. The graben formed on the east sliding block appears to have extended into the west sliding block and been displaced southwestward with the west sliding block. Therefore, the west sliding block slid southwestwards after the movement of the east sliding block. A disturbed zone which showed complex surficial features was found between the two sliding blocks. The graben on the west sliding block is 12 m deeper than the graben formed in the east sliding block indicating a deeper rupture surface (Figure D.6b). The forest is disturbed only at the blocks margins and along the counter scarp.

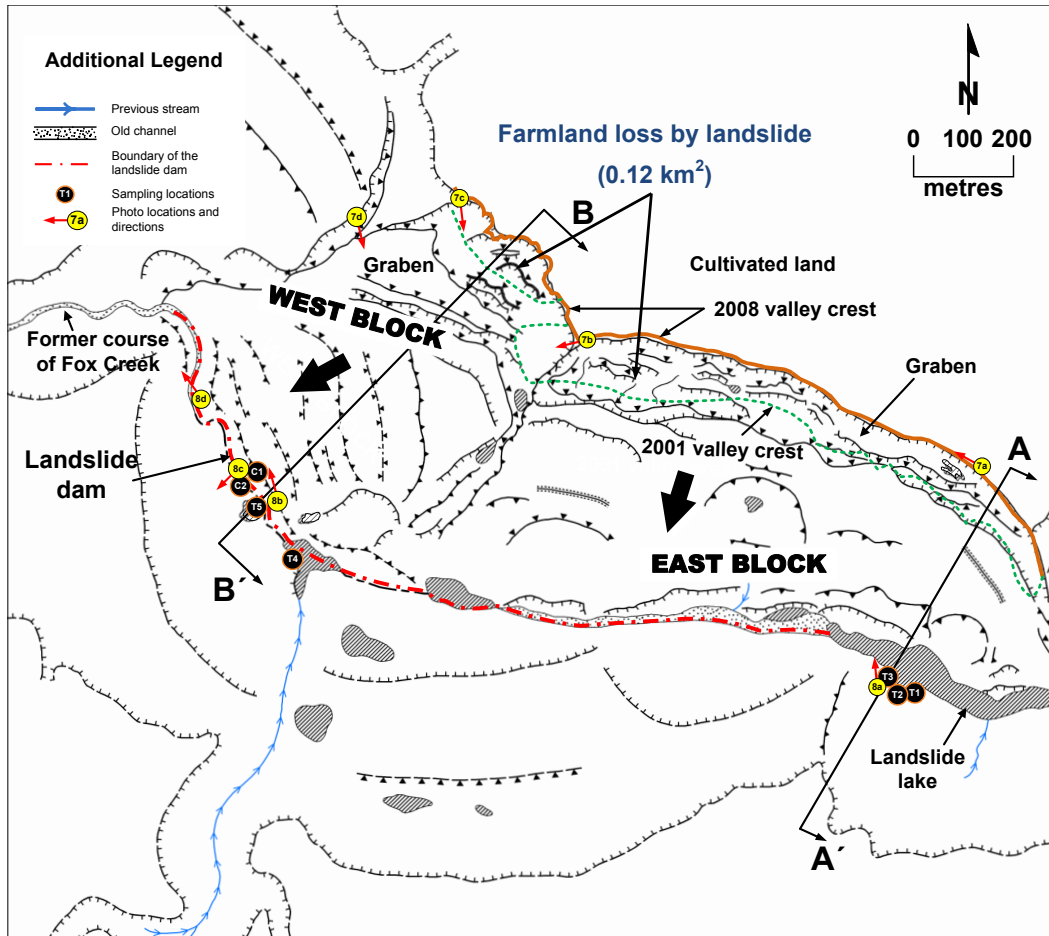
The volume of the 2007 Fox Creek landslide can be estimated by considering the displaced soil mass prior to the landslide as a rigid wedge. The displaced volume is 23.3 Mm³ for the east sliding block and 23.6 Mm³ for the west sliding block. Therefore, the total volume displaced by the 2007 Fox Creek landslide is about 47 Mm³.

Postslide topography had created a natural dam at the toe of the landslide (Figure D.5b). Sliding blocks dammed Fox Creek and generated a lake upstream by heaving the preslide riverbed. The reservoir extends beyond the east flank of the east sliding block for 1.5 km upstream and is up to 70 m wide. The length of the landslide dam is about 1.7 km if several isolated ponds found on the east sliding block are considered to be placed on the landslide dam. Rotated trees at the toe of the west sliding block suggest that the toes of the landslide blocks formed ridges by folding, rupturing, and thrusting. The now abandoned stream bed on the toe of each sliding block was raised from its original level by 13 m on the east sliding block and 19 m on the west sliding block. Therefore, the landslide dams can be classed as type 6 (Costa and Schuster 1988, pp. 1,057-1,058) which “involve one or more failure surfaces that extend under the stream or river valley and emerge on the opposite valley side from the landslide.”



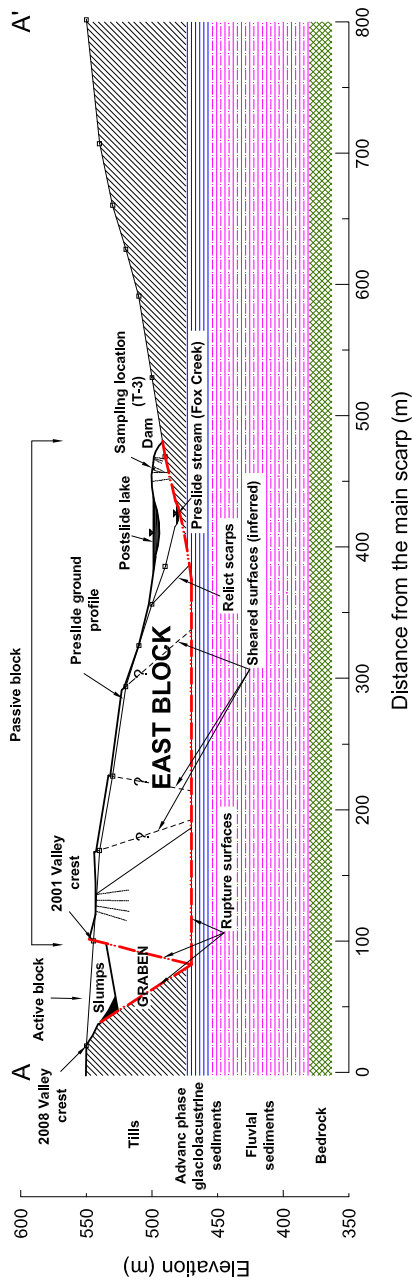
(a)

Figure D.5 2008 aerial photo interpretation. a. Aerial photograph of the area in 2008, scale 1:10,000 (Alberta photo: AS5444N-137). Previous course of the creek and slide boundaries by the 2007 landslide are illustrated. The east and west sliding blocks are reactivations of dormant landslide shown in Figure D.4. b. Interpretation of the aerial photograph AS5444N-137 shown in a. Displaced farmlands due to the retrogression, sampling positions, and locations where photos in Figures D.7 and D.8 are taken are also indicated. Lines ($A - A'$ and $B - B'$) indicate the location of cross sections for each sliding block (Figure D.6)

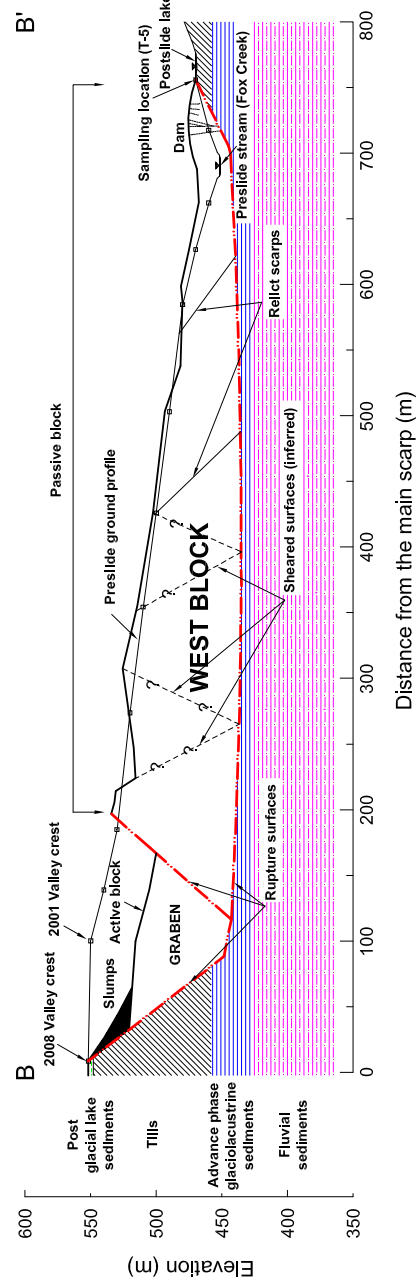


(b)

Figure D.5 (Cont'd)



(a)



(b)

Figure D.6 Hypothetical cross sections (A – A' and B – B' on Figure D.5) of the Fox Creek landslide. a. East sliding block along A – A'. b. West sliding block along B – B'. Approximate subsurface stratigraphy is extrapolated from the previous study at the Saddle River landslide (Figure D.1; Cruden et al. 1993)

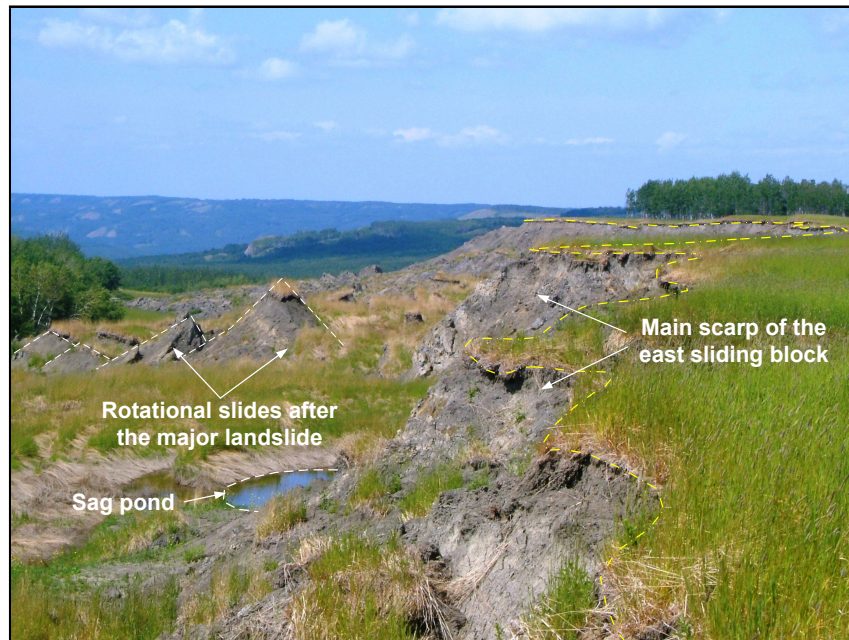
A comparison of the crest of the landslide on 2001 and 2008 aerial photos indicates that the 2007 Fox Creek landslide retrogressed into farmland. The present scarp of the landslide (taken from 2008 aerial photos) is about 90 m behind the valley crest in 2001 (Figure D.5b). The area lost to the 2007 landslide is 0.12 km²; it may extend by further retrogression.

Site reconnaissance

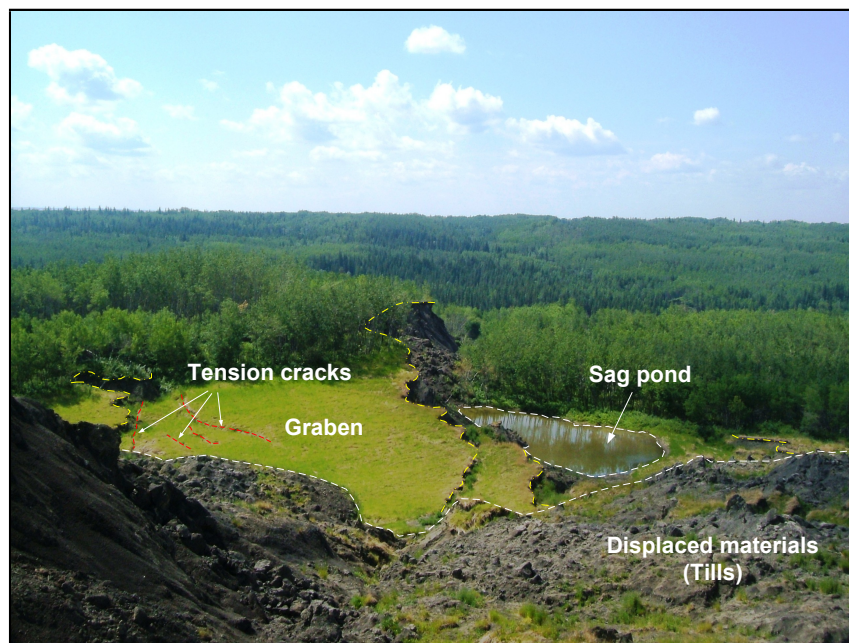
Our two visits were to landslide features which contributed to the 2007 Fox Creek landslide. The first, on 4 and 5 July 2008, focused on the north bank of the creek to identify the main scarps and flanks, which generally outlined the upper part of the slide.

The main scarp was clearly visible at the crest of the valley (Figure D.7a). Some farmland at the crest prior to the landslide had formed rotational slides. The material exposed below the valley crest is mostly tills in the east sliding block while a few meters of postglacial lake sediments were found in the west sliding block (Figures D.7b and D.7c). In Figure D.7c, taken from the main scarp of the west sliding block, boulders were visible within the displaced materials. Tills were deposited in this area by the Late Wisconsinan ice sheet and were characterized by low stone content and clay-rich matrix (Cruden et al. 1993). In Figure D.7d, taken on the west flank of the west sliding block, the graben lies between the main scarp (background) and the uphill-facing counter scarp (foreground).

The second visit on 15 August 2008 concentrated on the toes of sliding blocks and the landslide dam. The lake created by the landslide at the toe of the east sliding block was about 50 m wide (Figure D.8a). Figure D.8b shows landslide dam materials at the toe of the west sliding block. The major deposits forming the dam are tills, rhythmic advance phase glaciolacustrine sediments, and coarse granular sand and gravels which formed the preslide riverbed (Figures D.8c and D.8d). Cruden et al. (1993) showed that the advance phase glaciolacustrine sediments deposited in the Saddle River are highly plastic, stiff, rhythmically laminated, fissured, and slickensided. The proximity of Fox Creek to the Saddle River suggests that the advance phase glaciolacustrine sediments in Fox Creek are similar to those in the Saddle River.

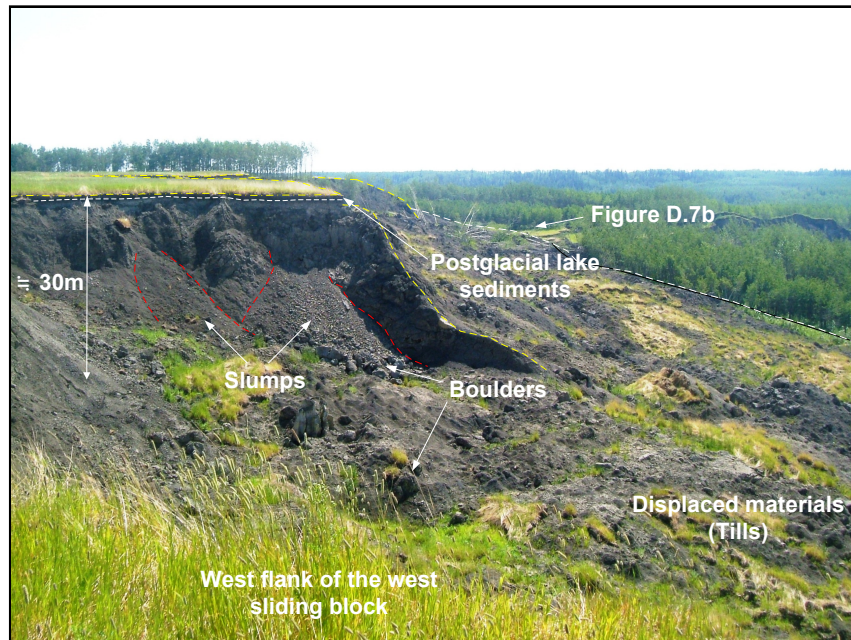


(a)

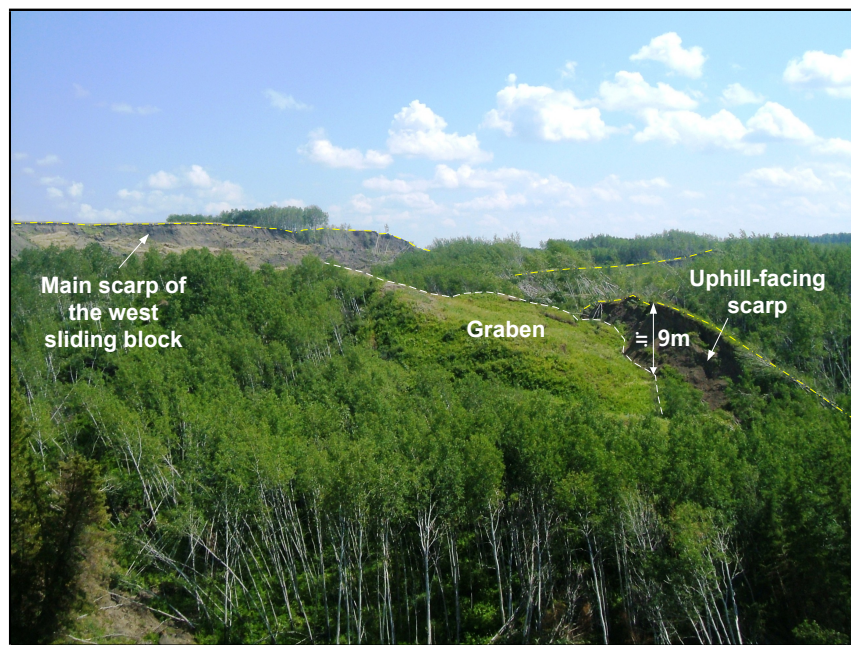


(b)

Figure D.7 Landslide features on the upper part of the sliding blocks. a. Close view of the main scarp with sag pond of the east sliding block. b. Looking south at the west flank of the east sliding block. c. Displaced till materials below the main scarp of the west sliding block. d. Looking southeastward on the west flank of the west sliding block



(c)



(d)

Figure D.7 (Cont'd)

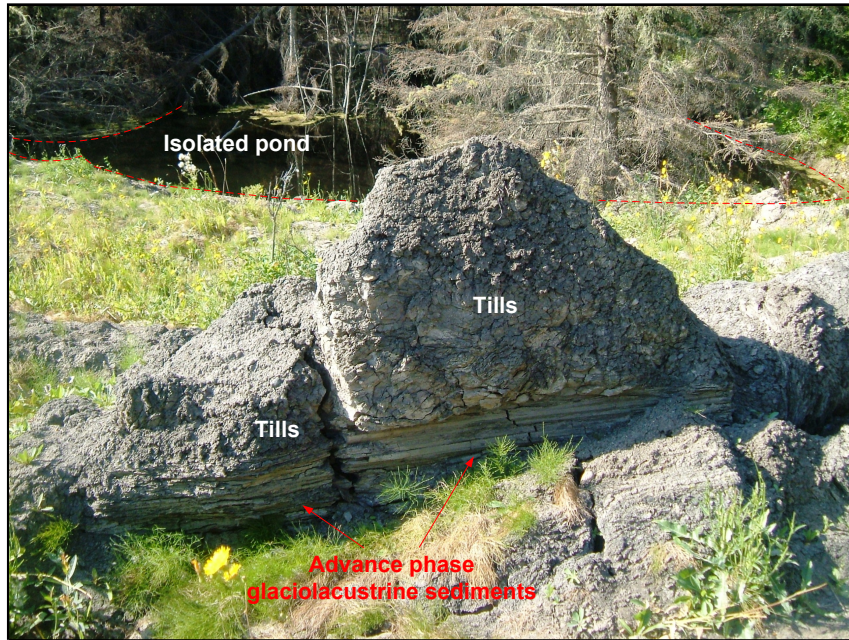


(a)

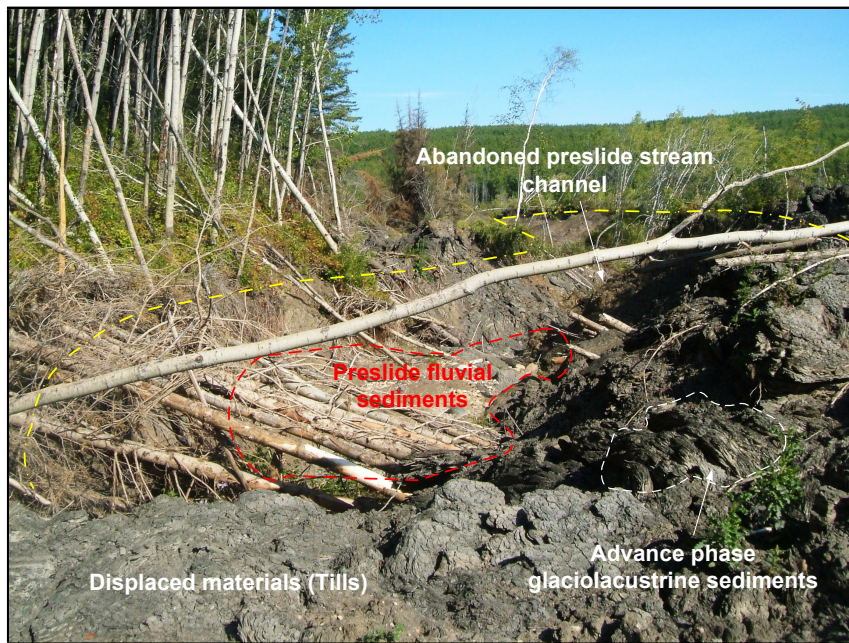


(b)

Figure D.8 Landslide features on the lower part of the sliding blocks and landslide dam. a. Close view of a landslide lake at the toe of the east sliding block. b. Landslide dam materials displaced on the toe of the west sliding block. c. Close view of a typical advance phase glaciolacustrine sediments in the west sliding block showing rhythmic nature. Pebbles are visible in tills and majorities are less than 5 cm. d. Preslide riverbed consisting of sand and gravel underlying the toe of the west sliding block



(c)



(d)

Figure D.8 (Cont'd)

The 2007 Fox Creek landslide is located within the Shaftesbury preglacial valley (Figure D.1; Pawlowicz and Fenton 1995). The stratigraphy in this preglacial valley records the up-drainage advance of the Laurentide ice sheet and the subsequent down-drainage ice front retreat (Miller and Cruden 2002). Hartman and Clague (2008) provide a detailed regional overview of the stratigraphy and glacial history of the ice advance sequence. The preglacial drainage pattern has been described as consisting of mature broad valleys with gentle valley walls (Carlson and Hackbarth 1974). The glaciation deposited tills over advance phase glaciolacustrine sediments which cover preglacial, fluvial channel sediments (Figure D.6).

Laboratory tests

To determine geotechnical properties of the displaced materials, laboratory tests were carried out on tills and advance phase glaciolacustrine sediments. Samples were collected from the landslide dam at the toe of the landslide (Figure D.5b). Atterberg Limits (ASTM 2005) and hydrometer tests (ASTM 2007) were performed to characterize landslide materials.

The results of these tests are given in Table D.3 and also shown in Figure D.9. Atterberg Limits of till samples differ based on the sampling locations. Till samples, T-1, T-2, and T-3, taken near the landslide lake on the east sliding block, are high plasticity, fat clays (CH); the other till samples, T-4 and T-5, taken from the landslide dam in the west sliding block, show medium to high plasticity (CL and OH). The T-line in Figure D.9 suggests that till samples might have experienced sorting processes and characteristic of flow tills or ablation tills (Boulton and Paul 1976).

The advance phase glaciolacustrine sediments are classified as inorganic clays of high plasticity, fat clays (CH). These samples (C-1 and C-2) were divided into different specimens by color to characterize rhythmical sedimentation in the proglacial lake (Figure D.10). The hydrometer tests in Table D.3 show that the dark gray specimen, C-2, has a higher percentage of clay than the light gray one, C-1. Atterberg Limits from the advance phase glaciolacustrine sediments at the historic landslides in the Peace River Lowland presented in Table D.4 indicate that Atterberg Limits at the Fox Creek landslide are close to values taken from the Saddle River landslide and are also within the ranges of values obtained from the Montagneuse River landslide.

Table D.3 Atterberg Limits and hydrometer tests on tills and advance phase glaciolacustrine sediments taken on the toe of the 2007 Fox Creek landslide. Sampling locations are illustrated in Figure D.5 with symbol

Indices	Tills					Advance phase glaciolacustrine sediments	
	T-1	T-2	T-3	T-4	T-5	C-1	C-2
Liquid limit (%)	67	73	74	54	44	64	89
Plastic limit (%)	26	22	28	34	20	26	29
Plasticity index	41	47	45	20	24	37	60
Clay fraction (%)	62	66	69	43	43	62	72
Activity	0.67	0.71	0.66	0.46	0.56	0.60	0.84
USCS classification [†]	CH	CH	CH	OH (MH)	CL	CH	CH

[†] *CH* inorganic clays of high plasticity, fat clays, *CL* inorganic clays of medium plasticity, silty clays (or *CI*), *OH* organic clays of medium to high plasticity, *MH* inorganic silts, micaceous, or diatomaceous fine sandy or silty soils, elastic silts.

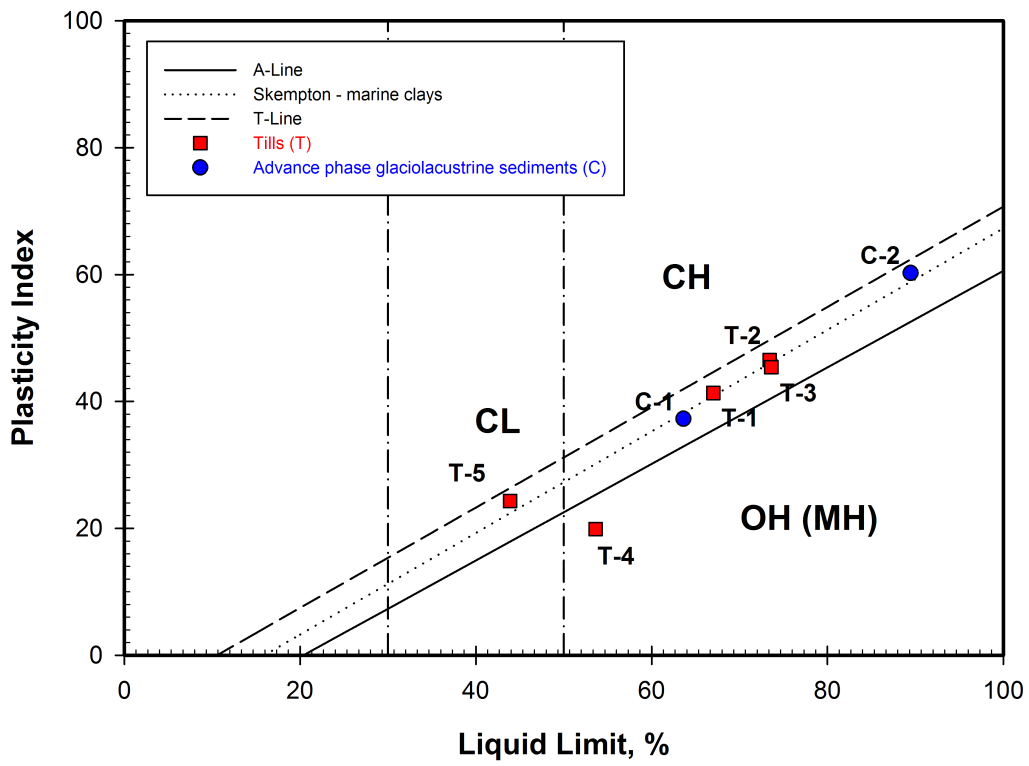
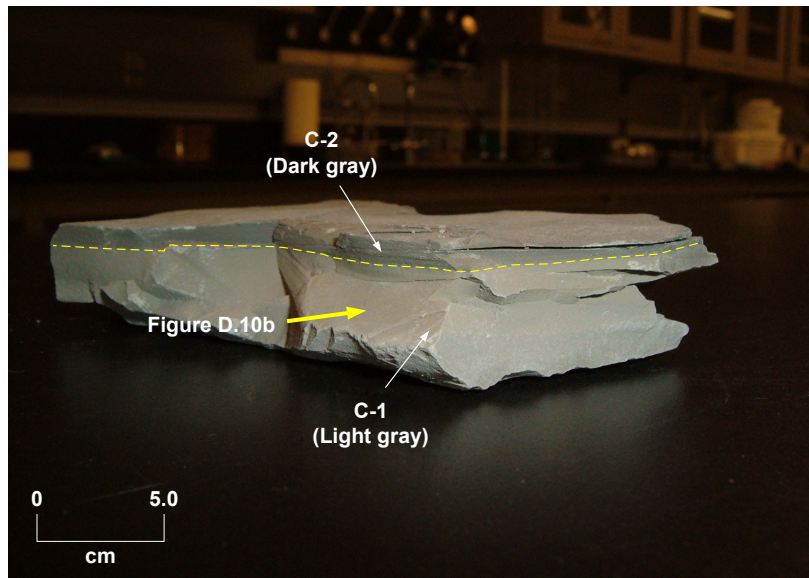
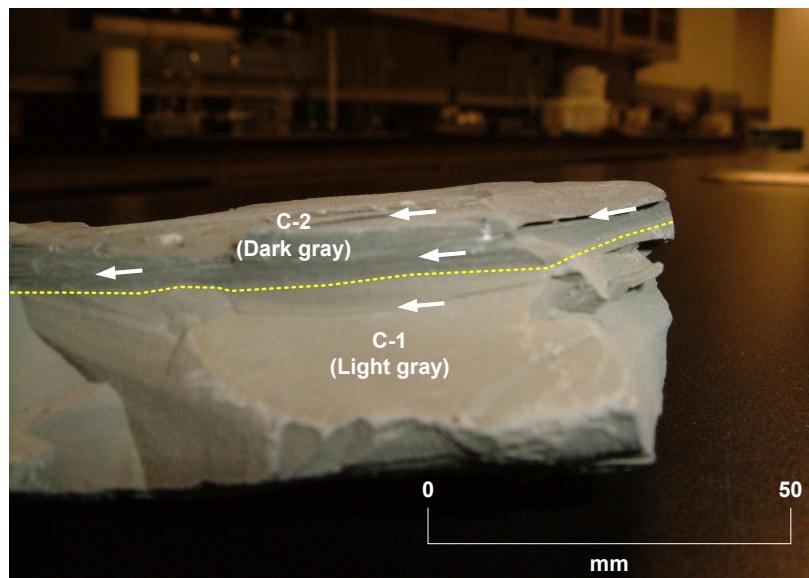


Figure D.9 Plasticity chart for the samples obtained from the 2007 Fox Creek landslide. Sampling points are illustrated in Figure D.5



(a)



(b)

Figure D.10 Typical sample of advance phase glaciolacustrine sediments. a. Sample shown by different tones (dark and light gray). Yellow arrow shows direction of b. b. Close view of a. White arrows indicate rhythmic attributes of the advance phase glaciolacustrine sediments

Table D.4 Atterberg Limits of the advance phase glaciolacustrine sediments at the Saddle River (Cruden et al. 1993), Eureka River (Miller and Cruden 2002), Montagneuse River (Cruden et al. 1997), and Fox Creek landslide

Indices	Saddle River	Eureka River	Montagneuse River	Fox Creek
Liquid limit (%) [†]	73 (69-78)	44	65 (52-74)	77 (64-89)
Plastic limit (%) [†]	25 (22-29)	23	21 (18-24)	28 (26-29)
Plasticity index [†]	48 (44-52)	21	44 (34-53)	49 (37-60)
Activity [†]	0.72	0.53	0.71	0.72 (0.6-0.84)

[†] Values in the table are arithmetic average with ranges given in parentheses.

Preliminary residual friction angles for the advance phase glaciolacustrine sediments were estimated following Skempton (1985). This empirical relationship between the residual friction angle and the clay fraction of the soils suggests residual friction angles between 9 and 13.5 ° for the Fox Creek landslide. Considering the actual effective stresses at the Fox Creek landslide, those values decreased to ranges from 7.4 to 12.6 ° for the east sliding block and from 7.1 to 13.5 ° for the west sliding block, respectively. Estimated friction angles for the Fox Creek landslide show reasonable agreement with those obtained at previous landslides in the Peace River Lowland (Table D.5).

Stability analysis

Only a simple stability analysis could be performed on the 2007 Fox Creek landslide. In the absence of drilling, subsurface stratigraphy, groundwater conditions, and geometry of the displaced materials are assumed or postulated from adjacent studies in the Peace River Lowland (Cruden et al. 1993, 1997; Miller and Cruden 2002). We assume that the displaced materials are single, relatively impermeable wedges of stiff soil with vertical main scarps at the crest of the valley. Water pressure is exerted in the cracks formed at the main scarps which extend down to the horizontal rupture surfaces. Materials on the rupture surfaces have no cohesion and residual friction angles; the cracks are filled with water to the ground surface. These assumptions are supported by the pre- and postlandslide topographies, high precipitation prior to the landslide, and dormant landslide features. With a factor of safety of 1, these premises in a model stability analysis for a block slide developed by Norrish and Wyllie (1996, Eq. 15.3) lead to

$$\tan \Psi_f = \frac{\tan \phi_r (\gamma_r - \gamma_w)}{\gamma_w} = 0.94 \tan \phi_r \quad (\text{D.1})$$

where Ψ_f is the inclination of the valley (east sliding block 10 °; west sliding block 9 °), ϕ_r is the residual friction angle, γ_r is the unit weight of the advance phase glaciolacustrine sediments (19.06 kN/m³, Cruden et al. 1993), and γ_w is the unit weight of water (9.81 kN/m³).

Equation D.1 gives residual friction angles of 10.6 ° for the east sliding block and 9.6 ° for the west sliding block, respectively. These values are within the ranges

Table D.5 Peak and residual friction angles (ϕ_p , ϕ_r) and cohesions (c_p , c_r) of the advance phase glaciolacustrine sediments at the Saddle River (Cruden et al. 1993), Eureka River (Miller and Cruden 2002), Montagneuse River (Cruden et al. 1997), and Fox Creek landslide

Landslide	Location	ϕ_p (°)	c_p (kPa)	ϕ_r (°)	c_r (kPa)
Saddle River	Along bedding	14.4	-	6.7	-
	Across bedding	20.0	-	9.3	-
Eureka River	Along bedding	-	-	8.2-13.1	-
Montagneuse River	Along bedding	14.0	-	6.0	-
	Across bedding	19.0	110	8.0	-
Fox Creek	East block	-	-	7.4-12.6	-
	West block	-	-	7.1-13.5	-

of residual friction angles estimated from Skempton (1985) of 7.4 to 12.6 ° for the east sliding block and 7.1 to 13.5 ° for the west sliding block. More accurate determination of these values requires direct or ring shear tests using undisturbed samples collected from drilling operations.

Geomorphological impact of the landslide

Geomorphological impacts caused by the landslide and its dam include property damage in local communities in the Peace River Lowland. One of the primary effects is farmland loss on the crests of stream valleys. As shown in Figure D.5b, the 2007 Fox Creek landslide affected about 0.12 km² of cultivated area. The retrogressions of landslides in the Peace River Lowland have been threats to local farms cultivated near valley crests. Therefore, slope stability problems in preglacial valleys in the Peace River Lowland may require setbacks for structures or land uses. Damage to forest resources can be another geomorphological impact of landslides. Timber would be destroyed on the landslide margins and drowned in the landslide lake.

A landslide dam failure is also hazardous. Costa and Schuster (1988) indicated that a natural dam by a landslide may cause upstream flooding. This rise of water induces buildup of pore water pressure and consequently decreases stability of slopes. Downstream flooding may result from a breach of the dam. We did not see any evidence of seepage or breach in the current landslide dam. As flow is small in the creek, the landslide dam may last for many years if no overtopping occurs. Over time, however, extreme stream flows may erode the dam materials.

Conclusions

The 2007 Fox Creek landslide occurred within a preglacial valley which contained over 100 m of advance phase glaciolacustrine sediments and tills. The landslide consisted of two major retrogressive translational block slides. These sliding blocks made natural dams on Fox Creek. Based on laboratory tests, the subsurface sediments of this area are similar to those of the Saddle River to which Fox Creek is a tributary. The rupture surface of the 2007 Fox Creek landslide was within the ad-

vance phase glaciolacustrine sediments. The estimated residual friction angles on the rupture surfaces are 7.4 to 12.6 ° for the east sliding block and from 7.1 to 13.5 ° for the west sliding block. These angles are similar to those at previous landslides in the Peace River Lowland. More comprehensive site investigations are necessary to determine the exact location of the rupture surface and the stratigraphy of this study area.

Precipitation and snow melt prior to the landslide are likely trigger mechanisms for the 2007 Fox Creek landslide. Precipitations in the fall of 2006 and the winter of 2007 were above the 30 year average precipitation. Snow on the ground had melted and infiltrated into the ground prior to the landslide. Heavy precipitation and snow melt may have raised pore water pressure within the displaced mass. Increasing pore water pressure, loss of toe support by creek bed incision, and a weak layer within the advance phase glaciolacustrine sediments have worked together to create the landslide in Fox Creek.

The losses of farmland on crests of river valleys and timber resources are impacts which might occur elsewhere in the Peace River Lowland. The 2007 Fox Creek landslide caused about 0.12 km² of cultivated area to slide. Landslide dams cause flooding upstream of the natural dam and downstream if the dam is eroded. The low slopes of the dams make their rapid erosion unlikely.

References

- ASTM. 2005. Standard test methods for liquid limit, plastic limit, and plasticity index of soils, ASTM Standard D4318. ASTM International, West Conshohocken, PA, doi:10.1520/D4318-05, www.astm.org.
- ASTM. 2007. Standard test method for particle-size analysis of soils, ASTM Standard D422 (1963). ASTM International, West Conshohocken, PA, doi: 10.1520/D0422-63R07, www.astm.org.
- Boulton, G.S., and Paul, M.A. 1976. The influence of genetic processes on some geotechnical properties of glacial tills. *Quarterly Journal of Engineering Geology*, **9**(3): 159–194.
- Carlson, V.A., and Hackbarth, P.A. 1974. Bedrock topography of the Grande Prairie area, Alberta, NTS 83M. Alberta Geological Survey, Map 061, Edmonton, Alberta.
- Costa, J.E., and Schuster, R.L. 1988. The formation and failure of natural dams. *Geological Society of America Bulletin*, **100**(7): 1054–1068.
- Cruden, D.M., Keegan, T.R., and Thomson, S. 1993. The landslide dam on the Saddle River near Rycroft, Alberta. *Canadian Geotechnical Journal*, **30**(6): 1003–1015.
- Cruden, D.M., Lu, Z.Y., and Thomson, S. 1997. The 1993 Montagneuse River landslide, Alberta. *Canadian Geotechnical Journal*, **34**(5): 799–810.
- Dearman, W.R., Burton, A.N., Cratchley, C.R., Day, J.B.W., Fookes, P.G., Higginbottom, I.E., Hutchinson, J.N., Little, A.L., McKenna, J.M., and Norman, J.W. 1972. The preparation of maps and plans in terms of engineering geology. *Quarterly Journal of Engineering Geology*, **5**(4): 293–382.
- Environment Canada. 2009. National Climate Data and Information Archive. http://www.climate.weatheroffice.ec.gc.ca/climateData/canada_e.html. Accessed Aug. 19, 2009.
- Evans, S.G, Cruden, D.M., Bobrowsky, P.T., Guthrie, R.H., Keegan, T.R., Liverman, D.G.E., and Perret, D. 2005. Landslide risk assessment in Canada: A review of recent developments. *In Proceedings of the International Conference*

- on Landslide Risk Management. *Edited by* O. Hungr, R. Fell, R. Couture, and E. Eberhardt. Vancouver, B.C., pp. 351–363.
- Hartman, G.M.D., and Clague, J.J. 2008. Quaternary stratigraphy and glacial history of the Peace River valley, northeast British Columbia. *Canadian Journal of Earth Sciences*, **45**(5): 549–564.
- Leslie, L.E., and Fenton, M.M. 2001. Quaternary stratigraphy and surficial geology River River - Final Report. Alberta Geological Survey, Special Report SPE10, Edmonton, Alberta.
- Lu, Z.Y., Cruden, D.M., and Thomson, S. 1998. Landslides and preglacial channels in the Western Peace River Lowland, Alberta. *In Proceedings of the 51st Canadian Geotechnical Conference*. Edmonton, Alberta, pp. 267–274.
- Miller, B.G.N., and Cruden, D.M. 2001. Landslides, landslide dams and the geomorphology of tributaries in the Peace River Lowlands, Alberta. *In Proceedings of the 54th Canadian Geotechnical Conference*, Sept. 16-19. Calgary, Alberta, pp. 363–370.
- Miller, B.G.N., and Cruden, D.M. 2002. The Eureka River landslide and dam, Peace River Lowlands, Alberta. *Canadian Geotechnical Journal*, **39**(4): 863–878.
- Morgan, A.J., Paulen, R.C., and Froese, C.R. 2008. Ancestral buried valleys of the Peace River: Effects on the Town of Peace River. *In Proceedings of the 61st Canadian Geotechnical Conference*, Sept. 21-24. Edmonton, Alberta, pp. 1219–1226.
- Norrish, N.I., and Wyllie, D.C. 1996. Rock slope stability analysis. *In Landslides: Investigation and Mitigation (Special Report 247)*. *Edited by* A.K. Turner and R.L. Schuster. Transportation Research Board, National Research Council, Washington, D.C., pp. 391–425.
- Pawlowicz, J.G., and Fenton, M.M. 1995. Bedrock topography of Alberta. Alberta Geological Survey, Map 226, Edmonton, Alberta.
- Skempton, A.W. 1985. Residual strength of clays in landslides, folded strata and the laboratory. *Géotechnique*, **35**(1): 3–18.

Appendix E

Statistical analyses on identified landslide deposits

Table E.1 Slope analysis for landslide deposits

Deposit ID	Data source	Coordinates [†]		Location	Dimensions		Slope values [‡]				
		Easting	Northing		Length [‡]	Area ^{††}	Min	Max	Range	Mean	STD [§]
1	1949	477,385	6,232,433	West	9,901	5,633,162	0.0	75.3	75.3	7.4	5.4
2	1949	478,007	6,229,564	West	7,476	3,268,749	0.0	62.6	62.6	8.3	6.0
3	LiDAR	484,001	6,229,031	East	7,345	2,497,293	0.0	81.0	81.0	16.5	10.6
4	LiDAR	482,607	6,234,683	East	5,716	2,197,902	0.0	68.5	68.5	11.2	8.8
5	LiDAR	479,599	6,235,167	West	6,101	1,980,880	0.0	85.6	85.6	11.7	8.4
6	1949	476,494	6,227,368	West	6,094	1,755,156	0.0	74.8	74.8	10.1	7.1
7	1949	478,042	6,227,921	West	4,996	1,617,848	0.0	49.7	49.7	11.1	6.5
8	LiDAR	481,849	6,227,839	East	5,313	1,479,106	0.0	72.3	72.3	15.2	9.4
9	LiDAR	479,234	6,233,639	West	5,385	1,309,320	0.0	77.3	77.3	12.2	8.0
10	LiDAR	483,375	6,235,932	East	4,932	1,192,033	0.0	65.3	65.3	13.4	7.9
11	LiDAR	481,150	6,226,949	East	4,468	1,192,017	0.0	79.4	79.4	14.3	9.3
12	LiDAR	482,595	6,234,313	East	3,768	969,270	0.0	56.0	56.0	15.4	8.7
13	LiDAR	482,681	6,232,690	East	3,309	748,926	0.0	75.5	75.5	14.9	10.1
14	LiDAR	482,756	6,228,863	East	4,067	716,868	0.0	69.5	69.5	18.6	10.9
15	LiDAR	485,591	6,230,342	East	4,235	681,791	0.0	81.8	81.8	19.0	10.9
16	LiDAR	483,257	6,230,676	East	5,569	655,255	0.0	84.3	84.3	19.6	13.4
17	LiDAR	477,310	6,227,185	West	3,183	648,433	0.0	48.6	48.6	11.6	7.4
18	LiDAR	482,713	6,230,726	East	4,294	634,726	0.0	70.4	70.4	14.5	11.2
19	1977	480,412	6,235,799	West	3,103	599,440	0.0	85.1	85.1	15.7	10.7
20	1949	479,972	6,234,129	West	3,257	583,427	0.0	63.3	63.3	15.3	9.7

[†] UTM coordinates, NAD83 Datum, UTM Zone 11. [‡] Metre. ^{††} Square metre. ^{‡‡} Degree (°). [§] Standard deviation.

Table E.1 (Cont'd)

Deposit ID	Data source	Coordinates [†]		Location	Dimensions		Slope values [‡]				
		Easting	Northing		Length [‡]	Area ^{††}	Min	Max	Range	Mean	STD [§]
21	LiDAR	483,766	6,236,507	East	3,961	536,559	0.0	70.6	70.6	11.5	7.5
22	LiDAR	483,366	6,231,818	East	3,185	520,900	0.0	60.6	60.6	15.6	9.1
23	LiDAR	484,202	6,226,692	East	2,944	502,635	0.0	73.6	73.6	20.0	12.3
24	1949	476,522	6,226,611	West	2,904	485,915	0.0	73.3	73.3	8.3	5.0
25	LiDAR	482,819	6,229,908	East	2,823	473,886	0.0	75.8	75.8	15.7	10.3
26	1949	480,885	6,229,748	West	3,049	463,151	0.0	59.5	59.5	15.6	8.7
27	LiDAR	483,857	6,233,467	East	3,134	419,623	0.0	67.7	67.7	17.7	11.4
28	LiDAR	484,465	6,227,420	East	2,889	395,106	0.0	76.8	76.8	24.6	12.9
29	LiDAR	483,339	6,233,020	East	2,603	388,250	0.0	74.0	74.0	18.3	10.2
30	1949/1977/2006	480,167	6,230,140	West	2,475	376,455	0.0	44.2	44.2	12.9	6.4
31	1977/2006	484,025	6,231,297	East	3,246	357,093	0.0	65.6	65.6	16.6	9.8
32	LiDAR	480,078	6,230,676	West	2,439	346,265	0.0	37.0	37.0	11.7	5.4
33	1949	477,456	6,227,100	West	2,593	338,850	0.0	57.5	57.5	16.3	8.2
34	LiDAR	480,848	6,230,852	West	2,429	330,131	0.0	51.3	51.3	13.4	6.9
35	LiDAR	481,008	6,230,326	West	2,298	293,811	0.0	56.3	56.3	17.6	10.5
36	1949/1958/2006	482,450	6,229,298	East	2,215	273,890	0.0	74.2	74.2	19.2	11.9
37	LiDAR	483,574	6,234,169	East	2,208	270,652	0.0	60.9	60.9	17.6	10.6
38	LiDAR	483,259	6,233,718	East	2,157	240,652	0.0	68.0	68.0	21.6	11.5
39	1949	476,737	6,226,557	West	2,011	236,711	0.0	60.3	60.3	12.5	6.8
40	LiDAR	484,838	6,230,863	East	2,040	201,788	0.0	62.4	62.4	15.6	9.1

[†] UTM coordinates, NAD83 Datum, UTM Zone 11. [‡] Metre. ^{††} Square metre. ^{‡‡} Degree (°). [§] Standard deviation.

Table E.1 (Cont'd)

Deposit ID	Data source	Coordinates [†]		Location	Dimensions		Slope values [§]				
		Easting	Northing		Length [‡]	Area ^{††}	Min	Max	Range	Mean	STD [§]
41	LiDAR	482,206	6,228,773	East	1,789	193,297	0.0	69.9	69.9	20.4	11.4
42	LiDAR	482,843	6,233,408	East	2,106	187,130	0.0	78.3	78.3	23.6	12.7
43	1958	483,327	6,230,244	East	1,667	182,847	0.0	63.6	63.6	18.8	11.2
44	1958	482,768	6,230,591	East	1,718	178,538	0.0	56.9	56.9	13.8	9.3
45	LiDAR	484,269	6,236,761	East	3,198	177,298	0.0	63.1	63.1	13.1	7.7
46	1949	481,083	6,226,416	East	2,976	170,883	0.0	85.3	85.3	18.7	12.3
47	LiDAR	482,104	6,233,901	East	2,082	162,581	0.0	55.6	55.6	16.2	7.9
48	1949/2006	484,130	6,230,604	East	1,730	160,499	0.0	67.9	67.9	19.6	10.5
49	1949	480,126	6,231,269	West	1,718	142,906	0.0	42.4	42.4	11.3	6.2
50	LiDAR	480,645	6,231,233	West	1,935	134,799	0.0	51.2	51.2	15.9	7.7
51	LiDAR	484,492	6,234,512	East	1,345	113,709	0.0	56.8	56.8	18.9	10.9
52	1949	481,979	6,228,194	East	1,428	111,742	0.0	52.0	52.0	14.6	8.3
53	LiDAR	484,088	6,234,480	East	1,502	107,839	0.0	52.9	52.9	18.4	10.6
54	LiDAR	480,358	6,231,003	West	1,391	101,612	0.0	48.3	48.3	11.1	5.9
55	LiDAR	484,398	6,233,845	East	1,139	87,783	0.0	72.9	72.9	17.7	10.7
56	LiDAR	483,696	6,233,677	East	1,428	86,784	0.0	65.1	65.1	16.0	11.4
57	1958	482,994	6,229,847	East	1,364	85,840	0.0	45.3	45.3	14.1	7.5
58	LiDAR	483,795	6,234,000	East	1,658	82,728	0.0	74.5	74.5	24.3	13.7
59	1977	484,586	6,230,393	East	1,143	81,576	0.0	72.3	72.3	16.3	11.8
60	1977	482,943	6,236,134	East	1,425	78,612	0.0	74.0	74.0	18.3	11.5

[†] UTM coordinates, NAD83 Datum, UTM Zone 11. [‡] Metre. ^{††} Square metre. [§] Degree (°). ^{§§} Standard deviation.

Table E.1 (Cont'd)

Deposit ID	Data source	Coordinates [†]		Location	Dimensions		Slope values [‡]				
		Easting	Northing		Length [‡]	Area ^{††}	Min	Max	Range	Mean	STD [§]
61	2006	483,947	6,230,960	East	1,156	63,524	0.0	64.5	64.5	17.1	10.0
62	1977	482,286	6,234,963	East	974	62,504	0.0	52.0	52.0	6.9	5.4
63	1977	482,772	6,235,743	East	947	58,177	0.0	64.4	64.4	16.8	10.9
64	LiDAR	481,973	6,233,692	East	1,061	56,996	0.0	73.0	73.0	24.9	10.8
65	LiDAR	485,490	6,230,784	East	1,268	53,914	0.0	48.1	48.1	19.7	8.2
66	1958/1977	482,821	6,229,990	East	1,021	49,949	0.0	49.4	49.4	15.9	8.6
67	LiDAR	484,686	6,234,192	East	958	45,466	0.0	63.2	63.2	21.0	7.9
68	1958/2006	482,459	6,229,963	East	1,188	45,452	0.0	80.0	80.0	22.2	15.3
69	1958	482,847	6,229,574	East	1,012	45,458	0.0	49.5	49.5	16.5	9.8
70	LiDAR	482,884	6,233,324	East	933	44,339	0.0	80.0	80.0	24.1	12.7
71	1949	480,043	6,231,008	West	1,665	43,886	0.0	42.2	42.2	11.4	6.3
72	1977	482,811	6,232,514	East	814	38,252	0.0	54.0	54.0	15.7	7.9
73	LiDAR	483,216	6,231,682	East	833	37,868	0.0	57.2	57.2	17.8	10.4
74	1949	480,555	6,231,793	West	813	37,833	0.0	47.2	47.2	13.6	7.0
75	1949	480,992	6,231,319	West	971	35,533	0.0	45.0	45.0	11.2	6.7
76	LiDAR	484,275	6,234,154	East	871	35,336	0.0	63.5	63.5	18.7	10.4
77	1977/2006	484,461	6,234,121	East	1,055	34,471	0.0	57.0	57.0	15.0	8.6
78	1958	482,603	6,230,938	East	775	34,316	0.0	60.9	60.9	10.1	9.7
79	LiDAR	482,033	6,233,480	East	908	34,020	0.0	56.9	56.9	17.7	7.8
80	1958	482,901	6,230,289	East	805	31,530	0.0	46.3	46.3	18.4	8.8

[†] UTM coordinates, NAD83 Datum, UTM Zone 11. [‡] Metre. ^{††} Square metre. ^{‡‡} Degree (°). [§] Standard deviation.

Table E.1 (Cont'd)

Deposit ID	Data source	Coordinates [†]		Location	Dimensions		Slope values [‡]				
		Easting	Northing		Length [‡]	Area ^{††}	Min	Max	Range	Mean	STD [§]
81	LiDAR	484,023	6,234,028	East	740	31,106	0.0	52.8	52.8	17.2	10.1
82	LiDAR	484,241	6,234,352	East	1,317	30,925	0.0	50.1	50.1	15.4	9.8
83	LiDAR	484,613	6,234,314	East	1,025	29,185	0.0	77.4	77.4	33.5	12.2
84	1958	482,873	6,231,069	East	677	27,370	0.2	57.4	57.2	20.5	10.9
85	2006	483,221	6,231,293	East	662	26,812	0.0	78.8	78.8	26.1	13.4
86	LiDAR	484,213	6,234,284	East	884	26,342	0.2	66.4	66.2	27.4	12.1
87	LiDAR	484,673	6,233,912	East	650	22,804	0.0	60.1	60.1	22.9	10.3
88	1977	482,766	6,235,410	East	732	22,784	0.0	50.7	50.7	20.4	9.5
89	1977/2006	480,449	6,231,492	West	725	22,124	0.2	55.3	55.1	19.3	9.6
90	1958	482,577	6,231,107	East	606	21,855	0.0	72.0	72.0	12.2	10.6
91	1949	482,651	6,230,303	East	540	20,236	0.0	43.6	43.6	4.8	4.3
92	2006	482,669	6,231,401	East	525	20,192	0.0	75.8	75.8	19.3	11.4
93	1958	482,722	6,229,527	East	731	19,882	0.0	55.3	55.3	22.1	11.3
94	1958	483,040	6,230,077	East	579	19,414	0.0	46.2	46.2	20.3	10.1
95	1949	482,379	6,234,117	East	643	18,616	0.0	57.8	57.8	17.2	8.8
96	1958	482,640	6,230,486	East	510	16,960	0.0	40.2	40.2	6.8	6.1
97	1977/2006	480,343	6,232,216	West	530	16,470	0.0	44.2	44.2	14.7	5.9
98	1977	483,890	6,233,920	East	509	15,467	0.0	60.3	60.3	13.7	8.6
99	1958	480,376	6,231,980	West	591	15,058	0.2	42.4	42.2	19.9	6.3
100	1977	482,873	6,232,739	East	541	14,983	0.0	52.5	52.5	20.6	10.4

[†] UTM coordinates, NAD83 Datum, UTM Zone 11. [‡] Metre. ^{††} Square metre. ^{‡‡} Degree (°). [§] Standard deviation.

Table E.1 (Cont'd)

Deposit ID	Data source	Coordinates [†]		Location	Dimensions		Slope values [¶]				
		Easting	Northing		Length [‡]	Area ^{††}	Min	Max	Range	Mean	STD [§]
101	1958	482,945	6,230,919	East	459	14,547	0.0	70.9	70.9	24.0	12.1
102	2006	482,715	6,229,712	East	471	14,081	0.0	55.3	55.3	22.1	11.0
103	2006	482,449	6,233,179	East	468	13,325	0.0	56.6	56.6	21.2	12.1
104	1958	483,071	6,230,737	East	682	12,309	0.0	56.1	56.1	21.3	11.0
105	LiDAR	481,858	6,233,430	East	593	12,047	0.0	58.6	58.6	30.4	9.3
106	1977	484,144	6,234,028	East	510	11,231	0.2	57.1	56.9	22.8	10.6
107	2006	480,021	6,232,851	West	409	10,577	0.0	55.3	55.3	17.0	10.1
108	1977	483,272	6,233,326	East	382	10,504	0.0	55.8	55.8	12.9	7.5
109	LiDAR	483,229	6,231,987	East	457	9,518	0.2	57.9	57.7	20.9	10.1
110	1977	482,752	6,235,875	East	431	9,600	0.0	68.6	68.6	18.3	11.4
111	1958	482,634	6,231,249	East	447	9,181	0.0	78.6	78.6	10.9	9.4
112	2006	482,647	6,229,763	East	396	9,065	0.0	61.5	61.5	21.0	12.2
113	1958	482,684	6,230,290	East	365	8,890	0.0	56.3	56.3	8.6	8.7
114	1958/1977	482,976	6,231,502	East	455	8,801	0.2	48.0	47.8	15.9	6.2
115	1977	483,833	6,233,546	East	352	8,477	0.0	43.3	43.3	15.9	6.4
116	1949	481,375	6,230,993	West	505	8,429	0.0	41.8	41.8	14.1	10.5
117	1958	482,710	6,230,181	East	377	8,316	0.0	54.6	54.6	14.6	10.7
118	2006	482,590	6,229,812	East	343	8,039	0.0	58.4	58.4	19.5	11.0
119	LiDAR	482,970	6,232,052	East	558	7,710	0.5	48.0	47.6	19.2	6.7
120	1958	482,472	6,230,744	East	344	7,443	0.0	49.4	49.4	16.4	11.7

[†] UTM coordinates, NAD83 Datum, UTM Zone 11. [‡] Metre. ^{††} Square metre. [¶] Degree (°). [§] Standard deviation.

Table E.1 (Cont'd)

Deposit ID	Data source	Coordinates [†]		Location	Dimensions		Slope values [‡]				
		Easting	Northing		Length [‡]	Area ^{††}	Min	Max	Range	Mean	STD [§]
121	1949	482,595	6,228,180	East	420	6,477	0.0	47.6	47.6	16.8	8.9
122	1977	483,575	6,231,091	East	414	5,272	0.2	66.5	66.3	29.0	14.0
123	1958	482,803	6,231,201	East	278	5,249	1.6	58.1	56.5	32.0	10.0
124	1977	480,498	6,232,002	West	254	3,865	0.0	29.7	29.7	9.4	5.1
125	1958	482,947	6,230,661	East	254	3,712	0.0	44.7	44.7	18.6	9.4
126	1958/2006	482,552	6,231,813	East	246	3,624	0.2	54.7	54.5	25.9	9.1
127	1958	482,537	6,231,864	East	235	3,090	0.0	51.4	51.4	25.0	12.8
128	1958	483,156	6,230,543	East	439	2,695	0.2	50.4	50.2	33.8	7.1
129	1958	483,143	6,230,625	East	194	2,297	0.3	58.9	58.6	27.1	12.4
130	2006	480,000	6,233,056	West	177	1,953	0.2	47.3	47.1	22.0	9.8
131	1958	482,715	6,231,192	East	142	1,174	1.5	55.2	53.7	30.0	9.9
132	1958	482,959	6,231,430	East	121	847	2.6	66.5	63.8	24.9	9.4
133	1958	482,527	6,231,858	East	108	556	4.0	48.1	44.0	25.3	7.9
134	1958	480,524	6,233,254	West	85	526	0.0	12.0	12.0	3.1	1.7
135	1958	480,477	6,233,188	West	77	428	0.2	24.5	24.3	8.4	5.1
136	1958	482,878	6,230,864	East	73	342	4.9	25.6	20.8	15.1	4.0
137	1958	480,513	6,233,129	West	62	268	0.2	41.8	41.6	13.1	13.3
138	1958	482,393	6,231,656	East	60	218	0.3	39.6	39.3	11.6	11.2
139	1958	480,561	6,233,041	West	48	159	0.2	32.4	32.2	5.0	4.7
140	1958	480,538	6,233,082	West	49	139	0.2	43.6	43.4	11.6	12.4

[†] UTM coordinates, NAD83 Datum, UTM Zone 11. [‡] Metre. ^{††} Square metre. ^{‡‡} Degree (°). [§] Standard deviation.

Table E.1 (Cont'd)

Deposit ID	Data source	Coordinates [†]		Location	Dimensions		Slope values [¶]				
		Easting	Northing		Length [‡]	Area ^{††}	Min	Max	Range	Mean	STD [§]
141	1958	480,740	6,232,747	West	45	118	0.2	18.6	18.3	8.5	4.7
142	1958	480,844	6,232,332	West	41	106	0.2	9.5	9.3	3.1	1.8
143	1958	482,722	6,231,569	East	40	101	2.7	25.0	22.3	11.4	5.5
144	1958	480,526	6,233,103	West	39	99	0.0	40.9	40.9	16.5	14.1
145	1958	482,471	6,231,475	East	39	93	1.2	37.1	35.9	25.4	7.2
146	1958	482,219	6,231,343	East	36	86	0.2	46.1	45.9	13.2	13.3
147	1958	482,517	6,231,223	East	36	78	12.5	32.6	20.1	23.9	3.9
148	1958	482,484	6,231,464	East	18	21	1.6	31.6	30.0	10.5	7.1

[†] UTM coordinates, NAD83 Datum, UTM Zone 11. [‡] Metre. ^{††} Square metre. [¶] Degree (°). [§] Standard deviation.

Table E.2 Texture analysis for landslide deposits

Deposit ID	Data source	Coordinates [†]		Location	Dimensions		Texture values (Contrast [‡])			
		Easting	Northing		Length [‡]	Area ^{††}	Min	Max	Range	Mean
1	1949	477,385	6,232,433	West	9,901	5,633,162	0.0	4.6	4.6	0.2
2	1949	478,007	6,229,564	West	7,476	3,268,749	0.0	4.1	4.1	0.3
3	LiDAR	484,001	6,229,031	East	7,345	2,497,293	0.0	7.6	7.6	0.7
4	LiDAR	482,607	6,234,683	East	5,716	2,197,902	0.0	4.9	4.9	0.4
5	LiDAR	479,599	6,235,167	West	6,101	1,980,880	0.0	8.6	8.6	0.4
6	1949	476,494	6,227,368	West	6,094	1,755,156	0.0	7.1	7.1	0.3
7	1949	478,042	6,227,921	West	4,996	1,617,848	0.0	3.8	3.8	0.4
8	LiDAR	481,849	6,227,839	East	5,313	1,479,106	0.0	6.1	6.1	0.6
9	LiDAR	479,234	6,233,639	West	5,385	1,309,320	0.0	7.7	7.7	0.4
10	LiDAR	483,375	6,235,932	East	4,932	1,192,033	0.0	5.7	5.7	0.5
11	LiDAR	481,150	6,226,949	East	4,468	1,192,017	0.0	8.0	8.0	0.6
12	LiDAR	482,595	6,234,313	East	3,768	969,270	0.0	5.3	5.3	0.5
13	LiDAR	482,681	6,232,690	East	3,309	748,926	0.0	5.7	5.7	0.6
14	LiDAR	482,756	6,228,863	East	4,067	716,868	0.0	6.1	6.1	0.8
15	LiDAR	485,591	6,230,342	East	4,235	681,791	0.0	8.3	8.3	0.8
16	LiDAR	483,257	6,230,676	East	5,569	655,255	0.0	8.1	8.1	0.9
17	LiDAR	477,310	6,227,185	West	3,183	648,433	0.0	3.8	3.8	0.4
18	LiDAR	482,713	6,230,726	East	4,294	634,726	0.0	7.5	7.5	0.7
19	1977	480,412	6,235,799	West	3,103	599,440	0.0	8.6	8.6	0.7
20	1949	479,972	6,234,129	West	3,257	583,427	0.0	6.1	6.1	0.6

[†] UTM coordinates, NAD83 Datum, UTM Zone 11.

^{*} Metre.

^{††} Square metre.

[‡] Table 5.7.

[§] Standard deviation.

Table E.2 (Cont'd)

Deposit ID	Data source	Coordinates [†]		Location	Dimensions		Texture values (Contrast [§])				
		Easting	Northing		Length [‡]	Area ^{††}	Min	Max	Range	Mean	STD [§]
21	LiDAR	483,766	6,236,507	East	3,961	536,559	0.0	6.4	6.4	0.4	0.4
22	LiDAR	483,366	6,231,818	East	3,185	520,900	0.0	4.8	4.8	0.6	0.5
23	LiDAR	484,202	6,226,692	East	2,944	502,635	0.0	8.0	8.0	0.9	0.9
24	1949	476,522	6,226,611	West	2,904	485,915	0.0	1.7	1.7	0.3	0.2
25	LiDAR	482,819	6,229,908	East	2,823	473,886	0.0	6.5	6.5	0.6	0.6
26	1949	480,885	6,229,748	West	3,049	463,151	0.0	3.8	3.8	0.6	0.5
27	LiDAR	483,857	6,233,467	East	3,134	419,623	0.0	7.1	7.1	0.8	0.8
28	LiDAR	484,465	6,227,420	East	2,889	395,106	0.0	7.5	7.5	1.3	1.1
29	LiDAR	483,339	6,233,020	East	2,603	388,250	0.0	7.4	7.4	0.8	0.7
30	1949/1977/2006	480,167	6,230,140	West	2,475	376,455	0.0	2.9	2.9	0.4	0.3
31	1977/2006	484,025	6,231,297	East	3,246	357,093	0.0	5.6	5.6	0.7	0.6
32	LiDAR	480,078	6,230,676	West	2,439	346,265	0.0	1.9	1.9	0.4	0.2
33	1949	477,456	6,227,100	West	2,593	338,850	0.0	3.8	3.8	0.6	0.5
34	LiDAR	480,848	6,230,852	West	2,429	330,131	0.0	5.3	5.3	0.5	0.3
35	LiDAR	481,008	6,230,326	West	2,298	293,811	0.0	4.8	4.8	0.7	0.7
36	1949/1958/2006	482,450	6,229,298	East	2,215	273,890	0.0	8.0	8.0	0.9	0.8
37	LiDAR	483,574	6,234,169	East	2,208	270,652	0.0	5.7	5.7	0.7	0.7
38	LiDAR	483,259	6,233,718	East	2,157	240,652	0.0	7.4	7.4	1.0	0.9
39	1949	476,737	6,226,557	West	2,011	236,711	0.0	3.0	3.0	0.4	0.3
40	LiDAR	484,838	6,230,863	East	2,040	201,788	0.0	5.6	5.6	0.6	0.5

[†] UTM coordinates, NAD83 Datum, UTM Zone 11. [‡] Metre. ^{††} Square metre. [§] Standard deviation.

Table E.2 (Cont'd)

Deposit ID	Data source	Coordinates [†]		Location	Dimensions		Texture values (Contrast [‡])				
		Easting	Northing		Length [‡]	Area ^{††}	Min	Max	Range	Mean	STD [§]
41	LiDAR	482,206	6,228,773	East	1,789	193,297	0.0	5.8	5.8	0.9	0.8
42	LiDAR	482,843	6,233,408	East	2,106	187,130	0.0	8.0	8.0	1.2	1.1
43	1958	483,327	6,230,244	East	1,667	182,847	0.0	6.8	6.8	0.8	0.8
44	1958	482,768	6,230,591	East	1,718	178,538	0.0	5.3	5.3	0.5	0.5
45	LiDAR	484,269	6,236,761	East	3,198	177,298	0.0	3.8	3.8	0.5	0.4
46	1949	481,083	6,226,416	East	2,976	170,883	0.0	9.9	9.9	0.8	0.9
47	LiDAR	482,104	6,233,901	East	2,082	162,581	0.0	4.5	4.5	0.6	0.5
48	1949/2006	484,130	6,230,604	East	1,730	160,499	0.0	6.8	6.8	0.9	0.7
49	1949	480,126	6,231,269	West	1,718	142,906	0.0	1.9	1.9	0.4	0.3
50	LiDAR	480,645	6,231,233	West	1,935	134,799	0.0	3.4	3.4	0.6	0.4
51	LiDAR	484,492	6,234,512	East	1,345	113,709	0.0	5.6	5.6	0.8	0.8
52	1949	481,979	6,228,194	East	1,428	111,742	0.0	3.9	3.9	0.5	0.4
53	LiDAR	484,088	6,234,480	East	1,502	107,839	0.0	5.6	5.6	0.8	0.7
54	LiDAR	480,358	6,231,003	West	1,391	101,612	0.0	3.1	3.1	0.4	0.3
55	LiDAR	484,398	6,233,845	East	1,139	87,783	0.0	6.8	6.8	0.8	0.7
56	LiDAR	483,696	6,233,677	East	1,428	86,784	0.0	7.5	7.5	0.7	0.8
57	1958	482,994	6,229,847	East	1,364	85,840	0.0	3.0	3.0	0.5	0.4
58	LiDAR	483,795	6,234,000	East	1,658	82,728	0.0	8.0	8.0	1.3	1.2
59	1977	484,586	6,230,393	East	1,143	81,576	0.0	5.6	5.6	0.7	0.8
60	1977	482,943	6,236,134	East	1,425	78,612	0.0	8.0	8.0	0.8	0.9

[†] UTM coordinates, NAD83 Datum, UTM Zone 11. [‡] Metre. ^{††} Square metre. [§] Standard deviation.

Table E.2 (Cont'd)

Deposit ID	Data source	Coordinates [†]		Location	Dimensions		Texture values (Contrast [‡])				
		Easting	Northing		Length [‡]	Area ^{††}	Min	Max	Range	Mean	STD [§]
61	2006	483,947	6,230,960	East	1,156	63,524	0.0	6.7	6.7	0.7	0.6
62	1977	482,286	6,234,963	East	974	62,504	0.0	2.0	2.0	0.2	0.2
63	1977	482,772	6,235,743	East	947	58,177	0.0	5.3	5.3	0.7	0.7
64	LiDAR	481,973	6,233,692	East	1,061	56,996	0.0	6.1	6.1	1.2	0.9
65	LiDAR	485,490	6,230,784	East	1,268	53,914	0.0	3.5	3.5	0.8	0.5
66	1958/1977	482,821	6,229,990	East	1,021	49,949	0.0	4.4	4.4	0.6	0.5
67	LiDAR	484,686	6,234,192	East	958	45,466	0.0	4.4	4.4	0.8	0.5
68	1958/2006	482,459	6,229,963	East	1,188	45,452	0.0	8.0	8.0	1.1	1.2
69	1958	482,847	6,229,574	East	1,012	45,458	0.0	4.1	4.1	0.6	0.6
70	LiDAR	482,884	6,233,324	East	933	44,339	0.0	8.0	8.0	1.2	1.1
71	1949	480,043	6,231,008	West	1,665	43,886	0.0	1.6	1.6	0.4	0.3
72	1977	482,811	6,232,514	East	814	38,252	0.0	4.1	4.1	0.6	0.5
73	LiDAR	483,216	6,231,682	East	833	37,868	0.0	4.1	4.1	0.7	0.6
74	1949	480,555	6,231,793	West	813	37,833	0.0	3.0	3.0	0.5	0.3
75	1949	480,992	6,231,319	West	971	35,533	0.0	2.6	2.6	0.4	0.3
76	LiDAR	484,275	6,234,154	East	871	35,336	0.0	6.0	6.0	0.8	0.7
77	1977/2006	484,461	6,234,121	East	1,055	34,471	0.0	3.4	3.4	0.5	0.4
78	1958	482,603	6,230,938	East	775	34,316	0.0	3.3	3.3	0.4	0.5
79	LiDAR	482,033	6,233,480	East	908	34,020	0.0	4.3	4.3	0.7	0.4
80	1958	482,901	6,230,289	East	805	31,530	0.0	3.8	3.8	0.7	0.6

[†] UTM coordinates, NAD83 Datum, UTM Zone 11. [‡] Metre. ^{††} Square metre. [§] Standard deviation.

Table E.2 (Cont'd)

Deposit ID	Data source	Coordinates [†]		Location	Dimensions		Texture values (Contrast [‡])				
		Easting	Northing		Length [‡]	Area ^{††}	Min	Max	Range	Mean	STD [§]
81	LiDAR	484,023	6,234,028	East	740	31,106	0.0	4.3	4.3	0.7	0.6
82	LiDAR	484,241	6,234,352	East	1,317	30,925	0.0	3.8	3.8	0.6	0.6
83	LiDAR	484,613	6,234,314	East	1,025	29,185	0.0	7.5	7.5	2.1	1.3
84	1958	482,873	6,231,069	East	677	27,370	0.0	5.6	5.6	0.9	0.8
85	2006	483,221	6,231,293	East	662	26,812	0.0	8.6	8.6	1.3	1.2
86	LiDAR	484,213	6,234,284	East	884	26,342	0.0	7.1	7.1	1.4	1.0
87	LiDAR	484,673	6,233,912	East	650	22,804	0.0	4.2	4.2	1.1	0.7
88	1977	482,766	6,235,410	East	732	22,784	0.0	4.2	4.2	0.9	0.6
89	1977/2006	480,449	6,231,492	West	725	22,124	0.0	4.1	4.1	0.8	0.6
90	1958	482,577	6,231,107	East	606	21,855	0.0	3.3	3.3	0.5	0.5
91	1949	482,651	6,230,303	East	540	20,236	0.0	1.8	1.8	0.1	0.2
92	2006	482,669	6,231,401	East	525	20,192	0.0	8.0	8.0	0.9	0.9
93	1958	482,722	6,229,527	East	731	19,882	0.0	5.0	5.0	1.0	0.8
94	1958	483,040	6,230,077	East	579	19,414	0.0	3.4	3.4	0.9	0.7
95	1949	482,379	6,234,117	East	643	18,616	0.0	4.5	4.5	0.7	0.5
96	1958	482,640	6,230,486	East	510	16,960	0.0	1.3	1.3	0.2	0.2
97	1977/2006	480,343	6,232,216	West	530	16,470	0.0	2.6	2.6	0.5	0.3
98	1977	483,890	6,233,920	East	509	15,467	0.0	4.5	4.5	0.5	0.5
99	1958	480,376	6,231,980	West	591	15,058	0.0	2.0	2.0	0.8	0.4
100	1977	482,873	6,232,739	East	541	14,983	0.0	4.9	4.9	0.9	0.7

[†] UTM coordinates, NAD83 Datum, UTM Zone 11. [‡] Metre. ^{††} Square metre. [§] Standard deviation.

Table E.2 (Cont'd)

Deposit ID	Data source	Coordinates [†]		Location	Dimensions		Texture values (Contrast [§])				
		Easting	Northing		Length [‡]	Area ^{††}	Min	Max	Range	Mean	STD [§]
101	1958	482,945	6,230,919	East	459	14,547	0.0	8.0	8.0	1.2	1.1
102	2006	482,715	6,229,712	East	471	14,081	0.0	6.1	6.1	1.1	0.8
103	2006	482,449	6,233,179	East	468	13,325	0.0	4.9	4.9	1.0	0.9
104	1958	483,071	6,230,737	East	682	12,309	0.0	5.1	5.1	1.0	0.8
105	LiDAR	481,858	6,233,430	East	593	12,047	0.0	6.1	6.1	1.7	1.0
106	1977	484,144	6,234,028	East	510	11,231	0.0	5.6	5.6	1.1	0.8
107	2006	480,021	6,232,851	West	409	10,577	0.0	4.2	4.2	0.7	0.6
108	1977	483,272	6,233,326	East	382	10,504	0.0	2.6	2.6	0.4	0.3
109	LiDAR	483,229	6,231,987	East	457	9,518	0.0	4.9	4.9	0.9	0.7
110	1977	482,752	6,235,875	East	431	9,600	0.0	7.4	7.4	0.8	0.9
111	1958	482,634	6,231,249	East	447	9,181	0.0	6.2	6.2	0.4	0.6
112	2006	482,647	6,229,763	East	396	9,065	0.0	5.6	5.6	1.0	0.9
113	1958	482,684	6,230,290	East	365	8,890	0.0	2.9	2.9	0.3	0.4
114	1958/1977	482,976	6,231,502	East	455	8,801	0.0	4.2	4.2	0.6	0.4
115	1977	483,833	6,233,546	East	352	8,477	0.0	1.6	1.6	0.6	0.3
116	1949	481,375	6,230,993	West	505	8,429	0.0	2.6	2.6	0.6	0.6
117	1958	482,710	6,230,181	East	377	8,316	0.0	4.1	4.1	0.6	0.6
118	2006	482,590	6,229,812	East	343	8,039	0.0	3.8	3.8	0.8	0.7
119	LiDAR	482,970	6,232,052	East	558	7,710	0.0	2.1	2.1	0.7	0.4
120	1958	482,472	6,230,744	East	344	7,443	0.0	2.6	2.6	0.6	0.6

[†] UTM coordinates, NAD83 Datum, UTM Zone 11. [‡] Metre. ^{††} Square metre. [§] Standard deviation.

Table E.2 (Cont'd)

Deposit ID	Data source	Coordinates [†]		Location	Dimensions		Texture values (Contrast [‡])				
		Easting	Northing		Length [‡]	Area ^{††}	Min	Max	Range	Mean	STD [§]
121	1949	482,595	6,228,180	East	420	6,477	0.0	3.1	3.1	0.7	0.5
122	1977	483,575	6,231,091	East	414	5,272	0.0	6.1	6.1	1.6	1.1
123	1958	482,803	6,231,201	East	278	5,249	0.0	6.1	6.1	1.8	1.1
124	1977	480,498	6,232,002	West	254	3,865	0.0	0.8	0.8	0.3	0.2
125	1958	482,947	6,230,661	East	254	3,712	0.0	2.8	2.8	0.8	0.6
126	1958/2006	482,552	6,231,813	East	246	3,624	0.0	4.1	4.1	1.3	0.7
127	1958	482,537	6,231,864	East	235	3,090	0.0	4.3	4.3	1.4	1.0
128	1958	483,156	6,230,543	East	439	2,695	0.3	4.2	3.9	1.9	0.9
129	1958	483,143	6,230,625	East	194	2,297	0.0	5.3	5.3	1.4	1.2
130	2006	480,000	6,233,056	West	177	1,953	0.0	3.1	3.1	0.9	0.6
131	1958	482,715	6,231,192	East	142	1,174	0.0	4.1	4.1	1.2	0.8
132	1958	482,959	6,231,430	East	121	847	0.0	7.5	7.5	1.1	0.9
133	1958	482,527	6,231,858	East	108	556	0.4	2.6	2.2	1.2	0.4
134	1958	480,524	6,233,254	West	85	526	0.0	0.5	0.5	0.1	0.1
135	1958	480,477	6,233,188	West	77	428	0.0	0.8	0.8	0.2	0.2
136	1958	482,878	6,230,864	East	73	342	0.3	0.8	0.5	0.5	0.1
137	1958	480,513	6,233,129	West	62	268	0.0	2.0	2.0	0.5	0.7
138	1958	482,393	6,231,656	East	60	218	0.0	1.6	1.6	0.5	0.5
139	1958	480,561	6,233,041	West	48	159	0.0	1.1	1.1	0.3	0.3
140	1958	480,538	6,233,082	West	49	139	0.0	1.5	1.5	0.6	0.5

[†] UTM coordinates, NAD83 Datum, UTM Zone 1. [‡] Metre. ^{††} Square metre. ^{‡‡} Table 5.7. [§] Standard deviation.

Table E.2 (Cont'd)

Deposit ID	Data source	Coordinates [†]		Location	Dimensions		Texture values (Contrast [§])				
		Easting	Northing		Length [‡]	Area ^{††}	Min	Max	Range	Mean	STD [§]
141	1958	480,740	6,232,747	West	45	118	0.0	0.7	0.7	0.2	0.2
142	1958	480,844	6,232,332	West	41	106	0.0	0.0	0.0	0.0	0.0
143	1958	482,722	6,231,569	East	40	101	0.0	0.9	0.9	0.5	0.3
144	1958	480,526	6,233,103	West	39	99	0.0	1.5	1.5	0.7	0.5
145	1958	482,471	6,231,475	East	39	93	0.4	1.3	0.9	0.8	0.3
146	1958	482,219	6,231,343	East	36	86	0.4	1.1	0.7	0.7	0.2
147	1958	482,517	6,231,223	East	36	78	0.4	1.6	1.2	0.8	0.3
148	1958	482,484	6,231,464	East	18	21	0.0	0.7	0.7	0.4	0.4

[†] UTM coordinates, NAD83 Datum, UTM Zone 11.

[‡] Metre.

^{††} Square metre.

[§] Table 5.7.

[§] Standard deviation.

Table E.3 Vector dispersion analysis for landslide deposits

Deposit ID	Data source	Coordinates [†]		Location	Dimensions		Vector dispersion values [‡]				
		Easting	Northing		Length [‡]	Area ^{††}	Min	Max	Range	Mean	STD [§]
1	1949	477,385	6,232,433	West	9,901	5,633,162	0.00	89.00	89.00	0.98	1.99
2	1949	478,007	6,229,564	West	7,476	3,268,749	0.00	98.88	98.88	0.96	2.13
3	LiDAR	484,001	6,229,031	East	7,345	2,497,293	0.00	105.86	105.86	3.81	4.88
4	LiDAR	482,607	6,234,683	East	5,716	2,197,902	0.00	66.91	66.91	1.63	2.76
5	LiDAR	479,599	6,235,167	West	6,101	1,980,880	0.00	153.46	153.46	2.00	5.01
6	1949	476,494	6,227,368	West	6,094	1,755,156	0.00	156.33	156.33	1.48	3.49
7	1949	478,042	6,227,921	West	4,996	1,617,848	0.00	39.31	39.31	1.31	1.80
8	LiDAR	481,849	6,227,839	East	5,313	1,479,106	0.01	145.13	145.13	3.36	4.28
9	LiDAR	479,234	6,233,639	West	5,385	1,309,320	0.00	135.20	135.20	1.93	4.05
10	LiDAR	483,375	6,235,932	East	4,932	1,192,033	0.00	59.80	59.79	1.81	2.42
11	LiDAR	481,150	6,226,949	East	4,468	1,192,017	0.00	204.44	204.43	2.81	4.53
12	LiDAR	482,595	6,234,313	East	3,768	969,270	0.00	69.63	69.63	2.81	3.63
13	LiDAR	482,681	6,232,690	East	3,309	748,926	0.00	145.09	145.09	2.72	4.54
14	LiDAR	482,756	6,228,863	East	4,067	716,868	0.00	99.57	99.57	4.79	6.39
15	LiDAR	485,591	6,230,342	East	4,235	681,791	0.00	74.96	74.95	4.11	4.93
16	LiDAR	483,257	6,230,676	East	5,569	655,255	0.01	128.52	128.51	4.58	6.69
17	LiDAR	477,310	6,227,185	West	3,183	648,433	0.01	45.38	45.38	1.53	2.37
18	LiDAR	482,713	6,230,726	East	4,294	634,726	0.00	82.25	82.25	3.32	5.59
19	1977	480,412	6,235,799	West	3,103	599,440	0.00	108.46	108.46	2.82	5.69
20	1949	479,972	6,234,129	West	3,257	583,427	0.00	86.71	86.71	3.23	5.27

[†] UTM coordinates, NAD83 Datum, UTM Zone 11. [‡] Metre. ^{††} Square metre. ^{‡‡} Multiplied by 1,000. [§] Standard deviation.

Table E.3 (Cont'd)

Deposit ID	Data source	Coordinates [†]		Location	Dimensions		Vector dispersion values [‡]				
		Easting	Northing		Length [‡]	Area ^{††}	Min	Max	Range	Mean	STD [§]
21	LiDAR	483,766	6,236,507	East	3,961	536,559	0.00	50.22	50.22	1.51	2.52
22	LiDAR	483,366	6,231,818	East	3,185	520,900	0.00	96.10	96.10	2.30	3.81
23	LiDAR	484,202	6,226,692	East	2,944	502,635	0.02	95.84	95.82	4.54	5.91
24	1949	476,522	6,226,611	West	2,904	485,915	0.01	25.83	25.82	0.82	1.18
25	LiDAR	482,819	6,229,908	East	2,823	473,886	0.00	52.86	52.86	2.36	4.27
26	1949	480,885	6,229,748	West	3,049	463,151	0.00	40.83	40.83	2.39	2.87
27	LiDAR	483,857	6,233,467	East	3,134	419,623	0.01	115.27	115.27	3.84	5.39
28	LiDAR	484,465	6,227,420	East	2,889	395,106	0.01	96.25	96.24	4.81	7.06
29	LiDAR	483,339	6,233,020	East	2,603	388,250	0.01	80.84	80.83	4.18	4.94
30	1949/1977/2006	480,167	6,230,140	West	2,475	376,455	0.00	22.22	22.22	0.84	1.44
31	1977/2006	484,025	6,231,297	East	3,246	357,093	0.00	64.49	64.49	2.25	3.71
32	LiDAR	480,078	6,230,676	West	2,439	346,265	0.01	40.46	40.46	1.46	2.28
33	1949	477,456	6,227,100	West	2,593	338,850	0.00	40.82	40.81	2.62	3.23
34	LiDAR	480,848	6,230,852	West	2,429	330,131	0.01	45.84	45.83	1.75	2.26
35	LiDAR	481,008	6,230,326	West	2,298	293,811	0.01	89.06	89.06	3.87	4.82
36	1949/1958/2006	482,450	6,229,298	East	2,215	273,890	0.00	78.28	78.28	4.73	6.33
37	LiDAR	483,574	6,234,169	East	2,208	270,652	0.01	86.31	86.31	4.83	5.80
38	LiDAR	483,259	6,233,718	East	2,157	240,652	0.02	119.82	119.80	5.44	6.64
39	1949	476,737	6,226,557	West	2,011	236,711	0.01	33.44	33.43	1.30	1.96
40	LiDAR	484,838	6,230,863	East	2,040	201,788	0.00	42.21	42.21	2.49	3.41

[†] UTM coordinates, NAD83 Datum, UTM Zone 11. [‡] Metre. ^{††} Square metre. ^{‡‡} Square metre. [§] Standard deviation. ^{§§} Multiplied by 1,000.

Table E.3 (Cont'd)

Deposit ID	Data source	Coordinates [†]		Location	Dimensions		Vector dispersion values [‡]				
		Easting	Northing		Length [‡]	Area ^{††}	Min	Max	Range	Mean	STD [§]
41	LiDAR	482,206	6,228,773	East	1,789	193,297	0.01	109.31	109.30	4.85	6.27
42	LiDAR	482,843	6,233,408	East	2,106	187,130	0.01	102.18	102.17	4.69	6.35
43	1958	483,327	6,230,244	East	1,667	182,847	0.01	79.81	79.80	5.40	6.19
44	1958	482,768	6,230,591	East	1,718	178,538	0.00	75.96	75.95	2.44	4.09
45	LiDAR	484,269	6,236,761	East	3,198	177,298	0.01	50.45	50.44	2.19	3.02
46	1949	481,083	6,226,416	East	2,976	170,883	0.01	167.23	167.22	7.14	13.21
47	LiDAR	482,104	6,233,901	East	2,082	162,581	0.01	49.30	49.29	2.29	3.07
48	1949/2006	484,130	6,230,604	East	1,730	160,499	0.02	69.72	69.70	4.86	5.58
49	1949	480,126	6,231,269	West	1,718	142,906	0.01	25.37	25.36	1.44	2.05
50	LiDAR	480,645	6,231,233	West	1,935	134,799	0.02	31.22	31.21	1.71	2.19
51	LiDAR	484,492	6,234,512	East	1,345	113,709	0.01	61.97	61.95	4.20	4.79
52	1949	481,979	6,228,194	East	1,428	111,742	0.01	35.46	35.45	2.99	3.27
53	LiDAR	484,088	6,234,480	East	1,502	107,839	0.03	48.27	48.24	4.49	4.70
54	LiDAR	480,358	6,231,003	West	1,391	101,612	0.01	24.08	24.07	1.53	2.43
55	LiDAR	484,398	6,233,845	East	1,139	87,783	0.02	80.95	80.93	3.96	4.93
56	LiDAR	483,696	6,233,677	East	1,428	86,784	0.01	69.49	69.48	4.71	5.92
57	1958	482,994	6,229,847	East	1,364	85,840	0.01	35.66	35.65	1.89	2.23
58	LiDAR	483,795	6,234,000	East	1,658	82,728	0.03	90.55	90.52	6.88	7.97
59	1977	484,586	6,230,393	East	1,143	81,576	0.00	135.20	135.20	4.52	9.70
60	1977	482,943	6,236,134	East	1,425	78,612	0.01	69.39	69.38	3.85	6.55

[†] UTM coordinates, NAD83 Datum, UTM Zone 11. [‡] Metre. ^{††} Square metre. ^{‡‡} Square metre. [§] Standard deviation.

Table E.3 (Cont'd)

Deposit ID	Data source	Coordinates [†]		Location	Dimensions		Vector dispersion values [¶]				
		Easting	Northing		Length [‡]	Area ^{††}	Min	Max	Range	Mean	STD [§]
61	2006	483,947	6,230,960	East	1,156	63,524	0.00	59.85	59.85	2.22	3.94
62	1977	482,286	6,234,963	East	974	62,504	0.01	22.29	22.28	1.03	1.78
63	1977	482,772	6,235,743	East	947	58,177	0.02	63.88	63.85	3.79	5.96
64	LiDAR	481,973	6,233,692	East	1,061	56,996	0.02	41.55	41.53	3.69	4.33
65	LiDAR	485,490	6,230,784	East	1,268	53,914	0.00	26.00	25.99	2.09	3.07
66	1958/1977	482,821	6,229,990	East	1,021	49,949	0.04	34.42	34.38	2.60	3.00
67	LiDAR	484,686	6,234,192	East	958	45,466	0.07	44.64	44.58	2.71	3.10
68	1958/2006	482,459	6,229,963	East	1,188	45,452	0.00	81.91	81.91	4.43	8.36
69	1958	482,847	6,229,574	East	1,012	45,458	0.04	41.19	41.16	3.43	4.12
70	LiDAR	482,884	6,233,324	East	933	44,339	0.08	170.29	170.21	7.13	10.22
71	1949	480,043	6,231,008	West	1,665	43,886	0.00	24.54	24.54	1.84	2.71
72	1977	482,811	6,232,514	East	814	38,252	0.01	43.46	43.46	2.12	3.11
73	LiDAR	483,216	6,231,682	East	833	37,868	0.00	93.19	93.19	6.03	8.01
74	1949	480,555	6,231,793	West	813	37,833	0.03	25.80	25.77	1.93	2.08
75	1949	480,992	6,231,319	West	971	35,533	0.00	14.58	14.58	1.18	1.59
76	LiDAR	484,275	6,234,154	East	871	35,336	0.03	42.42	42.39	4.69	4.89
77	1977/2006	484,461	6,234,121	East	1,055	34,471	0.04	29.64	29.60	3.20	3.17
78	1958	482,603	6,230,938	East	775	34,316	0.00	19.95	19.95	1.84	2.84
79	LiDAR	482,033	6,233,480	East	908	34,020	0.03	44.54	44.51	3.25	4.14
80	1958	482,901	6,230,289	East	805	31,530	0.02	21.33	21.32	2.26	2.49

[†] UTM coordinates, NAD83 Datum, UTM Zone 11. [‡] Metre. ^{††} Square metre. [¶] Multiplied by 1,000. [§] Standard deviation.

Table E.3 (Cont'd)

Deposit ID	Data source	Coordinates [†]		Location	Dimensions		Vector dispersion values [¶]				
		Easting	Northing		Length [‡]	Area ^{††}	Min	Max	Range	Mean	STD [§]
81	LiDAR	484,023	6,234,028	East	740	31,106	0.03	76.40	76.37	4.59	5.72
82	LiDAR	484,241	6,234,352	East	1,317	30,925	0.07	50.58	50.50	4.27	5.18
83	LiDAR	484,613	6,234,314	East	1,025	29,185	0.03	81.55	81.52	6.57	8.70
84	1958	482,873	6,231,069	East	677	27,370	0.09	52.52	52.43	4.02	4.97
85	2006	483,221	6,231,293	East	662	26,812	0.01	244.64	244.62	6.35	12.31
86	LiDAR	484,213	6,234,284	East	884	26,342	0.07	95.68	95.62	7.20	8.68
87	LiDAR	484,673	6,233,912	East	650	22,804	0.05	49.63	49.58	4.42	5.11
88	1977	482,766	6,235,410	East	732	22,784	0.02	29.01	28.99	2.54	3.12
89	1977/2006	480,449	6,231,492	West	725	22,124	0.04	42.61	42.57	4.31	4.66
90	1958	482,577	6,231,107	East	606	21,855	0.02	33.92	33.91	2.48	4.37
91	1949	482,651	6,230,303	East	540	20,236	0.00	15.67	15.67	0.68	1.60
92	2006	482,669	6,231,401	East	525	20,192	0.01	46.82	46.81	3.17	4.50
93	1958	482,722	6,229,527	East	731	19,882	0.06	51.09	51.03	7.59	7.78
94	1958	483,040	6,230,077	East	579	19,414	0.03	25.26	25.24	2.28	2.85
95	1949	482,379	6,234,117	East	643	18,616	0.04	113.83	113.79	4.43	9.43
96	1958	482,640	6,230,486	East	510	16,960	0.00	16.46	16.46	1.06	1.80
97	1977/2006	480,343	6,232,216	West	530	16,470	0.01	16.58	16.58	1.15	1.89
98	1977	483,890	6,233,920	East	509	15,467	0.04	41.44	41.39	2.25	3.57
99	1958	480,376	6,231,980	West	591	15,058	0.01	10.59	10.58	0.92	1.39
100	1977	482,873	6,232,739	East	541	14,983	0.04	38.37	38.33	4.98	4.97

[†] UTM coordinates, NAD83 Datum, UTM Zone 11. [‡] Metre. ^{††} Square metre. [¶] Multiplied by 1,000. [§] Standard deviation.

Table E.3 (Cont'd)

Deposit ID	Data source	Coordinates [†]		Location	Dimensions		Vector dispersion values [¶]				
		Easting	Northing		Length [‡]	Area ^{††}	Min	Max	Range	Mean	STD [§]
101	1958	482,945	6,230,919	East	459	14,547	0.20	51.12	50.92	6.17	6.99
102	2006	482,715	6,229,712	East	471	14,081	0.02	40.25	40.23	4.91	5.23
103	2006	482,449	6,233,179	East	468	13,325	0.06	68.17	68.11	6.20	7.32
104	1958	483,071	6,230,737	East	682	12,309	0.15	80.23	80.08	9.58	11.48
105	LiDAR	481,858	6,233,430	East	593	12,047	0.05	48.40	48.35	5.11	6.21
106	1977	484,144	6,234,028	East	510	11,231	0.07	36.78	36.71	4.65	4.74
107	2006	480,021	6,232,851	West	409	10,577	0.01	58.76	58.75	2.97	4.42
108	1977	483,272	6,233,326	East	382	10,504	0.08	21.57	21.50	2.46	2.31
109	LiDAR	483,229	6,231,987	East	457	9,518	0.06	59.64	59.57	6.06	7.91
110	1977	482,752	6,235,875	East	431	9,600	0.05	51.22	51.16	6.41	7.42
111	1958	482,634	6,231,249	East	447	9,181	0.02	50.25	50.23	3.46	6.34
112	2006	482,647	6,229,763	East	396	9,065	0.08	34.60	34.51	4.56	4.84
113	1958	482,684	6,230,290	East	365	8,890	0.01	19.65	19.64	2.13	3.34
114	1958/1977	482,976	6,231,502	East	455	8,801	0.01	48.46	48.46	2.07	4.12
115	1977	483,833	6,233,546	East	352	8,477	0.04	9.02	8.98	1.00	1.25
116	1949	481,375	6,230,993	West	505	8,429	0.01	45.19	45.18	2.93	6.49
117	1958	482,710	6,230,181	East	377	8,316	0.00	30.28	30.27	4.12	4.98
118	2006	482,590	6,229,812	East	343	8,039	0.14	25.47	25.33	3.85	3.84
119	LiDAR	482,970	6,232,052	East	558	7,710	0.14	16.08	15.94	2.97	2.45
120	1958	482,472	6,230,744	East	344	7,443	0.04	31.99	31.95	3.27	5.73

[†] UTM coordinates, NAD83 Datum, UTM Zone 11. [‡] Metre. ^{††} Square metre. [¶] Multiplied by 1,000. [§] Standard deviation.

Table E.3 (Cont'd)

Deposit ID	Data source	Coordinates [†]		Location	Dimensions		Vector dispersion values [¶]				
		Easting	Northing		Length [‡]	Area ^{††}	Min	Max	Range	Mean	STD [§]
121	1949	482,595	6,228,180	East	420	6,477	0.08	51.91	51.83	4.14	4.96
122	1977	483,575	6,231,091	East	414	5,272	0.06	131.38	131.32	12.03	16.20
123	1958	482,803	6,231,201	East	278	5,249	0.04	39.95	39.90	5.41	6.23
124	1977	480,498	6,232,002	West	254	3,865	0.02	13.19	13.17	1.92	2.56
125	1958	482,947	6,230,661	East	254	3,712	0.06	23.64	23.59	2.58	2.70
126	1958/2006	482,552	6,231,813	East	246	3,624	0.09	28.72	28.64	4.05	4.68
127	1958	482,537	6,231,864	East	235	3,090	0.09	36.62	36.53	3.56	4.52
128	1958	483,156	6,230,543	East	439	2,695	0.06	34.02	33.96	5.66	6.16
129	1958	483,143	6,230,625	East	194	2,297	0.58	54.06	53.47	8.39	9.00
130	2006	480,000	6,233,056	West	177	1,953	0.15	34.15	34.01	5.21	5.25
131	1958	482,715	6,231,192	East	142	1,174	0.48	34.33	33.85	5.61	6.15
132	1958	482,959	6,231,430	East	121	847	0.88	62.18	61.30	13.23	15.06
133	1958	482,527	6,231,858	East	108	556	1.16	8.06	6.89	3.58	1.78
134	1958	480,524	6,233,254	West	85	526	0.01	0.29	0.28	0.06	0.04
135	1958	480,477	6,233,188	West	77	428	0.22	4.12	3.90	1.39	0.83
136	1958	482,878	6,230,864	East	73	342	0.47	4.37	3.91	1.86	0.95
137	1958	480,513	6,233,129	West	62	268	0.02	23.68	23.66	10.43	7.16
138	1958	482,393	6,231,656	East	60	218	0.12	19.51	19.39	6.73	6.82
139	1958	480,561	6,233,041	West	48	159	0.02	18.06	18.04	5.39	6.73
140	1958	480,538	6,233,082	West	49	139	0.06	16.37	16.30	7.07	5.51

[†] UTM coordinates, NAD83 Datum, UTM Zone 11. [‡] Metre. ^{††} Square metre. [¶] Multiplied by 1,000. [§] Standard deviation.

Table E.3 (Cont'd)

Deposit ID	Data source	Coordinates [†]		Location	Dimensions		Vector dispersion values [¶]				
		Easting	Northing		Length [‡]	Area ^{††}	Min	Max	Range	Mean	STD [§]
141	1958	480,740	6,232,747	West	45	118	0.00	3.48	3.48	1.69	1.21
142	1958	480,844	6,232,332	West	41	106	0.03	0.19	0.16	0.10	0.05
143	1958	482,722	6,231,569	East	40	101	0.35	8.06	7.71	2.61	1.92
144	1958	480,526	6,233,103	West	39	99	1.56	15.68	14.13	10.11	4.30
145	1958	482,471	6,231,475	East	39	93	0.63	11.11	10.47	4.87	3.44
146	1958	482,219	6,231,343	East	36	86	6.50	32.17	25.66	19.86	7.77
147	1958	482,517	6,231,223	East	36	78	0.22	1.14	0.93	0.57	0.31
148	1958	482,484	6,231,464	East	18	21	7.32	15.17	7.85	11.25	3.93

[†] UTM coordinates, NAD83 Datum, UTM Zone 11. [‡] Metre. ^{††} Square metre. [¶] Multiplied by 1,000. [§] Standard deviation.

Table E.4 Eigenvalue analysis for landslide deposits

Deposit ID	Data source	Coordinates [†]		Location	Dimensions		Eigenvalue ratio [¶]				
		Easting	Northing		Length [‡]	Area ^{††}	Min	Max	Range	Mean	STD [§]
1	1949	477,385	6,232,433	West	9,901	5,633,162	1.63	16.75	15.12	7.19	1.34
2	1949	478,007	6,229,564	West	7,476	3,268,749	1.50	13.21	11.71	7.20	1.28
3	LiDAR	484,001	6,229,031	East	7,345	2,497,293	1.44	12.48	11.04	5.62	1.16
4	LiDAR	482,607	6,234,683	East	5,716	2,197,902	1.95	16.75	14.80	6.80	1.57
5	LiDAR	479,599	6,235,167	West	6,101	1,980,880	1.00	12.54	11.54	6.61	1.40
6	1949	476,494	6,227,368	West	6,094	1,755,156	1.02	11.71	10.69	6.75	1.26
7	1949	478,042	6,227,921	West	4,996	1,617,848	2.50	12.05	9.55	6.69	1.18
8	LiDAR	481,849	6,227,839	East	5,313	1,479,106	1.06	11.11	10.05	5.74	1.17
9	LiDAR	479,234	6,233,639	West	5,385	1,309,320	1.17	16.75	15.58	6.50	1.32
10	LiDAR	483,375	6,235,932	East	4,932	1,192,033	2.05	11.11	9.06	6.36	1.14
11	LiDAR	481,150	6,226,949	East	4,468	1,192,017	0.68	13.09	12.41	6.05	1.25
12	LiDAR	482,595	6,234,313	East	3,768	969,270	1.89	11.50	9.61	5.93	1.16
13	LiDAR	482,681	6,232,690	East	3,309	748,926	1.32	11.80	10.47	6.25	1.53
14	LiDAR	482,756	6,228,863	East	4,067	716,868	1.53	12.61	11.08	5.38	1.14
15	LiDAR	485,591	6,230,342	East	4,235	681,791	1.81	11.69	9.88	5.53	1.16
16	LiDAR	483,257	6,230,676	East	5,569	655,255	1.18	10.94	9.75	5.45	1.12
17	LiDAR	477,310	6,227,185	West	3,183	648,433	2.39	11.18	8.79	6.58	1.20
18	LiDAR	482,713	6,230,726	East	4,294	634,726	1.71	12.01	10.30	6.08	1.51
19	1977	480,412	6,235,799	West	3,103	599,440	1.42	13.98	12.56	6.28	1.51
20	1949	479,972	6,234,129	West	3,257	583,427	1.65	15.25	13.60	6.10	1.58

[†] UTM coordinates, NAD83 Datum, UTM Zone 11. [‡] Metre. ^{††} Square metre. [¶] $\ln(S_1/S_2)$. [§] Standard deviation.

Table E.4 (Cont'd)

Deposit ID	Data source	Coordinates [†]		Location	Dimensions		Eigenvalue ratio [¶]				
		Easting	Northing		Length [‡]	Area ^{††}	Min	Max	Range	Mean	STD [§]
21	LiDAR	483,766	6,236,507	East	3,961	536,559	2.26	11.50	9.24	6.70	1.29
22	LiDAR	483,366	6,231,818	East	3,185	520,900	1.53	12.50	10.97	6.34	1.41
23	LiDAR	484,202	6,226,692	East	2,944	502,635	1.56	10.30	8.75	5.46	1.15
24	1949	476,522	6,226,611	West	2,904	485,915	2.94	11.05	8.11	7.10	1.10
25	LiDAR	482,819	6,229,908	East	2,823	473,886	2.18	11.98	9.80	6.46	1.54
26	1949	480,885	6,229,748	West	3,049	463,151	2.46	11.72	9.26	6.07	1.19
27	LiDAR	483,857	6,233,467	East	3,134	419,623	1.32	11.25	9.93	5.76	1.36
28	LiDAR	484,465	6,227,420	East	2,889	395,106	1.53	10.47	8.94	5.51	1.27
29	LiDAR	483,339	6,233,020	East	2,603	388,250	1.76	10.81	9.05	5.49	1.13
30	1949/1977/2006	480,167	6,230,140	West	2,475	376,455	3.17	12.86	9.69	7.26	1.31
31	1977/2006	484,025	6,231,297	East	3,246	357,093	1.99	12.24	10.25	6.52	1.57
32	LiDAR	480,078	6,230,676	West	2,439	346,265	2.47	11.22	8.75	6.65	1.21
33	1949	477,456	6,227,100	West	2,593	338,850	2.46	11.36	8.90	6.02	1.19
34	LiDAR	480,848	6,230,852	West	2,429	330,131	2.34	10.83	8.49	6.35	1.09
35	LiDAR	481,008	6,230,326	West	2,298	293,811	1.62	11.17	9.55	5.66	1.26
36	1949/1958/2006	482,450	6,229,298	East	2,215	273,890	1.89	11.66	9.77	5.45	1.21
37	LiDAR	483,574	6,234,169	East	2,208	270,652	1.68	10.97	9.29	5.36	1.14
38	LiDAR	483,259	6,233,718	East	2,157	240,652	1.34	9.54	8.20	5.23	1.10
39	1949	476,737	6,226,557	West	2,011	236,711	2.67	11.08	8.42	6.74	1.20
40	LiDAR	484,838	6,230,863	East	2,040	201,788	2.43	12.43	10.00	6.17	1.37

[†] UTM coordinates, NAD83 Datum, UTM Zone 11. [‡] Metre. ^{††} Square metre. [¶] $\ln(S_1/S_2)$. [§] Standard deviation.

Table E.4 (Cont'd)

Deposit ID	Data source	Coordinates [†]		Location	Dimensions		Eigenvalue ratio [¶]				
		Easting	Northing		Length [‡]	Area ^{††}	Min	Max	Range	Mean	STD [§]
41	LiDAR	482,206	6,228,773	East	1,789	193,297	1.63	10.26	8.63	5.42	1.23
42	LiDAR	482,843	6,233,408	East	2,106	187,130	1.47	10.08	8.61	5.45	1.20
43	1958	483,327	6,230,244	East	1,667	182,847	1.76	10.41	8.65	5.21	1.08
44	1958	482,768	6,230,591	East	1,718	178,538	1.80	11.67	9.87	6.19	1.31
45	LiDAR	484,269	6,236,761	East	3,198	177,298	2.23	10.56	8.33	6.18	1.15
46	1949	481,083	6,226,416	East	2,976	170,883	0.89	10.93	10.04	5.21	1.33
47	LiDAR	482,104	6,233,901	East	2,082	162,581	2.27	10.27	8.00	6.13	1.14
48	1949/2006	484,130	6,230,604	East	1,730	160,499	1.89	9.56	7.67	5.33	1.11
49	1949	480,126	6,231,269	West	1,718	142,906	2.96	11.16	8.21	6.58	1.14
50	LiDAR	480,645	6,231,233	West	1,935	134,799	2.76	10.37	7.61	6.39	1.12
51	LiDAR	484,492	6,234,512	East	1,345	113,709	2.01	10.47	8.46	5.50	1.15
52	1949	481,979	6,228,194	East	1,428	111,742	2.69	10.68	7.99	5.79	1.09
53	LiDAR	484,088	6,234,480	East	1,502	107,839	2.28	9.54	7.25	5.37	1.09
54	LiDAR	480,358	6,231,003	West	1,391	101,612	3.01	10.75	7.75	6.69	1.33
55	LiDAR	484,398	6,233,845	East	1,139	87,783	1.76	9.76	8.00	5.65	1.26
56	LiDAR	483,696	6,233,677	East	1,428	86,784	1.90	10.09	8.18	5.43	1.18
57	1958	482,994	6,229,847	East	1,364	85,840	2.60	10.99	8.39	6.29	1.12
58	LiDAR	483,795	6,234,000	East	1,658	82,728	1.62	9.77	8.15	5.00	1.10
59	1977	484,586	6,230,393	East	1,143	81,576	1.14	11.58	10.44	6.06	1.73
60	1977	482,943	6,236,134	East	1,425	78,612	1.89	10.78	8.88	5.88	1.36

[†] UTM coordinates, NAD83 Datum, UTM Zone 11. [‡] Metre. ^{††} Square metre. [¶] $\ln(S_1/S_2)$. [§] Standard deviation.

Table E.4 (Cont'd)

Deposit ID	Data source	Coordinates [†]		Location	Dimensions		Eigenvalue ratio [¶]				
		Easting	Northing		Length [‡]	Area ^{††}	Min	Max	Range	Mean	STD [§]
61	2006	483,947	6,230,960	East	1,156	63,524	2.07	11.87	9.79	6.39	1.37
62	1977	482,286	6,234,963	East	974	62,504	3.33	11.04	7.71	7.09	1.28
63	1977	482,772	6,235,743	East	947	58,177	1.99	9.85	7.86	5.78	1.28
64	LiDAR	481,973	6,233,692	East	1,061	56,996	2.45	9.84	7.39	5.64	1.16
65	LiDAR	485,490	6,230,784	East	1,268	53,914	2.93	11.68	8.76	6.46	1.47
66	1958/1977	482,821	6,229,990	East	1,021	49,949	2.98	9.55	6.57	5.95	1.09
67	LiDAR	484,686	6,234,192	East	958	45,466	2.36	9.03	6.67	5.88	1.03
68	1958/2006	482,459	6,229,963	East	1,188	45,452	1.72	11.37	9.65	5.96	1.75
69	1958	482,847	6,229,574	East	1,012	45,458	2.45	9.46	7.01	5.69	1.11
70	LiDAR	482,884	6,233,324	East	933	44,339	1.14	9.12	7.98	5.05	1.18
71	1949	480,043	6,231,008	West	1,665	43,886	2.99	11.60	8.61	6.47	1.35
72	1977	482,811	6,232,514	East	814	38,252	2.41	10.87	8.46	6.30	1.20
73	LiDAR	483,216	6,231,682	East	833	37,868	1.61	11.24	9.63	5.33	1.49
74	1949	480,555	6,231,793	West	813	37,833	2.94	9.75	6.81	6.19	1.05
75	1949	480,992	6,231,319	West	971	35,533	3.54	11.51	7.97	6.85	1.25
76	LiDAR	484,275	6,234,154	East	871	35,336	2.43	9.78	7.35	5.28	0.98
77	1977/2006	484,461	6,234,121	East	1,055	34,471	2.87	9.02	6.15	5.66	1.00
78	1958	482,603	6,230,938	East	775	34,316	3.20	12.28	9.07	6.64	1.50
79	LiDAR	482,033	6,233,480	East	908	34,020	2.38	9.15	6.77	5.77	1.12
80	1958	482,901	6,230,289	East	805	31,530	3.13	9.76	6.63	6.04	1.06

[†] UTM coordinates, NAD83 Datum, UTM Zone 11. [‡] Metre. ^{††} Square metre. [¶] $\ln(S_1/S_2)$. [§] Standard deviation.

Table E.4 (Cont'd)

Deposit ID	Data source	Coordinates [†]		Location	Dimensions		Eigenvalue ratio [¶]				
		Easting	Northing		Length [‡]	Area ^{††}	Min	Max	Range	Mean	STD [§]
81	LiDAR	484,023	6,234,028	East	740	31,106	1.85	9.66	7.81	5.43	1.14
82	LiDAR	484,241	6,234,352	East	1,317	30,925	2.24	9.08	6.84	5.48	1.11
83	LiDAR	484,613	6,234,314	East	1,025	29,185	1.75	9.49	7.74	5.25	1.42
84	1958	482,873	6,231,069	East	677	27,370	2.19	9.00	6.81	5.49	1.04
85	2006	483,221	6,231,293	East	662	26,812	0.44	9.90	9.46	5.39	1.43
86	LiDAR	484,213	6,234,284	East	884	26,342	1.60	9.01	7.42	4.97	1.16
87	LiDAR	484,673	6,233,912	East	650	22,804	2.27	8.59	6.32	5.40	1.02
88	1977	482,766	6,235,410	East	732	22,784	2.82	9.59	6.77	5.97	1.10
89	1977/2006	480,449	6,231,492	West	725	22,124	2.42	9.32	6.90	5.43	1.09
90	1958	482,577	6,231,107	East	606	21,855	2.75	10.31	7.55	6.52	1.59
91	1949	482,651	6,230,303	East	540	20,236	3.45	11.77	8.32	7.67	1.37
92	2006	482,669	6,231,401	East	525	20,192	2.37	10.54	8.17	6.01	1.43
93	1958	482,722	6,229,527	East	731	19,882	2.22	9.38	7.16	4.87	1.19
94	1958	483,040	6,230,077	East	579	19,414	2.96	9.73	6.77	6.14	1.20
95	1949	482,379	6,234,117	East	643	18,616	1.35	9.21	7.86	5.76	1.25
96	1958	482,640	6,230,486	East	510	16,960	3.44	12.00	8.55	7.39	1.79
97	1977/2006	480,343	6,232,216	West	530	16,470	3.39	10.93	7.54	7.04	1.44
98	1977	483,890	6,233,920	East	509	15,467	2.50	9.52	7.02	6.25	1.16
99	1958	480,376	6,231,980	West	591	15,058	3.92	10.45	6.53	7.16	1.25
100	1977	482,873	6,232,739	East	541	14,983	2.67	9.25	6.57	5.25	1.10

[†] UTM coordinates, NAD83 Datum, UTM Zone 11. [‡] Metre. ^{††} Square metre. [¶] $\ln(S_1/S_2)$. [§] Standard deviation.

Table E.4 (Cont'd)

Deposit ID	Data source	Coordinates [†]		Location	Dimensions		Eigenvalue ratio [¶]				
		Easting	Northing		Length [‡]	Area ^{††}	Min	Max	Range	Mean	STD [§]
101	1958	482,945	6,230,919	East	459	14,547	2.23	8.11	5.88	5.07	1.07
102	2006	482,715	6,229,712	East	471	14,081	2.48	9.34	6.86	5.27	1.10
103	2006	482,449	6,233,179	East	468	13,325	1.91	9.28	7.37	5.04	1.13
104	1958	483,071	6,230,737	East	682	12,309	1.76	8.49	6.73	4.68	1.16
105	LiDAR	481,858	6,233,430	East	593	12,047	2.28	9.38	7.10	5.33	1.23
106	1977	484,144	6,234,028	East	510	11,231	2.63	9.03	6.39	5.33	1.09
107	2006	480,021	6,232,851	West	409	10,577	2.14	10.01	7.87	5.93	1.28
108	1977	483,272	6,233,326	East	382	10,504	3.34	8.90	5.56	5.91	0.98
109	LiDAR	483,229	6,231,987	East	457	9,518	2.06	9.21	7.15	5.19	1.17
110	1977	482,752	6,235,875	East	431	9,600	2.22	9.15	6.93	5.07	1.15
111	1958	482,634	6,231,249	East	447	9,181	2.25	10.26	8.01	6.08	1.53
112	2006	482,647	6,229,763	East	396	9,065	2.73	8.82	6.09	5.36	1.13
113	1958	482,684	6,230,290	East	365	8,890	3.22	10.75	7.53	6.58	1.56
114	1958/1977	482,976	6,231,502	East	455	8,801	2.39	11.18	8.79	6.74	1.71
115	1977	483,833	6,233,546	East	352	8,477	4.01	9.47	5.46	6.89	1.06
116	1949	481,375	6,230,993	West	505	8,429	2.36	10.38	8.03	6.70	1.73
117	1958	482,710	6,230,181	East	377	8,316	2.78	11.51	8.74	5.56	1.27
118	2006	482,590	6,229,812	East	343	8,039	2.97	8.61	5.64	5.45	0.98
119	LiDAR	482,970	6,232,052	East	558	7,710	3.42	8.42	5.00	5.63	0.89
120	1958	482,472	6,230,744	East	344	7,443	2.71	9.28	6.57	6.09	1.36

[†] UTM coordinates, NAD83 Datum, UTM Zone 11. [‡] Metre. ^{††} Square metre. [¶] $\ln(S_1/S_2)$. [§] Standard deviation.

Table E.4 (Cont'd)

Deposit ID	Data source	Coordinates [†]		Location	Dimensions		Eigenvalue ratio [¶]				
		Easting	Northing		Length [‡]	Area ^{††}	Min	Max	Range	Mean	STD [§]
121	1949	482,595	6,228,180	East	420	6,477	2.22	9.05	6.84	5.52	1.12
122	1977	483,575	6,231,091	East	414	5,272	1.19	9.13	7.94	4.60	1.45
123	1958	482,803	6,231,201	East	278	5,249	2.48	9.41	6.94	5.22	1.12
124	1977	480,498	6,232,002	West	254	3,865	3.63	10.15	6.52	6.37	1.47
125	1958	482,947	6,230,661	East	254	3,712	3.02	8.90	5.88	5.83	0.97
126	1958/2006	482,552	6,231,813	East	246	3,624	2.83	8.94	6.11	5.56	1.21
127	1958	482,537	6,231,864	East	235	3,090	2.58	8.86	6.28	5.65	1.18
128	1958	483,156	6,230,543	East	439	2,695	2.73	9.25	6.52	5.20	1.18
129	1958	483,143	6,230,625	East	194	2,297	2.17	7.16	4.98	4.80	1.06
130	2006	480,000	6,233,056	West	177	1,953	2.71	8.23	5.52	5.20	1.15
131	1958	482,715	6,231,192	East	142	1,174	2.64	7.37	4.74	5.07	1.01
132	1958	482,959	6,231,430	East	121	847	2.08	6.66	4.58	4.33	1.16
133	1958	482,527	6,231,858	East	108	556	4.16	6.64	2.48	5.23	0.61
134	1958	480,524	6,233,254	West	85	526	7.52	10.96	3.44	9.14	0.59
135	1958	480,477	6,233,188	West	77	428	4.83	7.80	2.97	6.23	0.63
136	1958	482,878	6,230,864	East	73	342	4.76	7.19	2.43	5.89	0.62
137	1958	480,513	6,233,129	West	62	268	3.02	9.15	6.12	4.48	1.69
138	1958	482,393	6,231,656	East	60	218	3.22	8.40	5.18	5.21	1.63
139	1958	480,561	6,233,041	West	48	159	3.30	9.68	6.38	6.25	2.53
140	1958	480,538	6,233,082	West	49	139	3.40	8.92	5.52	4.81	1.65

[†] UTM coordinates, NAD83 Datum, UTM Zone 11. [‡] Metre. ^{††} Square metre. [¶] $\ln(S_1/S_2)$. [§] Standard deviation.

Table E.4 (Cont'd)

Deposit ID	Data source	Coordinates [†]		Location	Dimensions		Eigenvalue ratio [¶]				
		Easting	Northing		Length [‡]	Area ^{††}	Min	Max	Range	Mean	STD [§]
141	1958	480,740	6,232,747	West	45	118	4.96	9.80	4.84	6.26	1.39
142	1958	480,844	6,232,332	West	41	106	7.86	9.20	1.34	8.43	0.38
143	1958	482,722	6,231,569	East	40	101	4.17	7.36	3.20	5.72	0.81
144	1958	480,526	6,233,103	West	39	99	3.45	5.78	2.34	4.04	0.61
145	1958	482,471	6,231,475	East	39	93	3.79	6.71	2.91	4.98	0.92
146	1958	482,219	6,231,343	East	36	86	2.71	4.35	1.64	3.33	0.53
147	1958	482,517	6,231,223	East	36	78	6.13	8.14	2.01	7.05	0.68
148	1958	482,484	6,231,464	East	18	21	3.49	4.23	0.74	3.86	0.37

[†] UTM coordinates, NAD83 Datum, UTM Zone 11.

[‡] Metre.

^{††} Square metre.

[¶] $\ln(S_1/S_2)$.

[§] Standard deviation.